Faculdade de Engenharia, Universidade do Porto

Departamento de Engenharia Mecânica

Analysis of laminated and functionally graded plates and shells by a Unified Formulation and Collocation with Radial Basis Functions

by

Ana Maria Azevedo Neves

A thesis submitted for the Doctoral Degree in Mechanical Engineering

Supervisor:

António Joaquim Mendes Ferreira

Full Professor, Faculdade de Engenharia, Universidade do Porto

Co-Supervisors:

Cristóvão Manuel Mota Soares

Associate Professor, Instituto Superior Técnino, Universidade Técnica de Lisboa

Renato Manuel Natal Jorge

Associate Professor, Faculdade de Engenharia, Universidade do Porto

2012

Abstract

Nowadays, most of numerical methods are based on the well-known finite element method. However, innovative and alternative formulations have been recently developed, based on meshless methods, using just a nodal grid, and keeping the quality of the numerical solution.

In the last decades, structures formed by plates and shells and using composite materials such as laminated and functionally graded materials, have experienced very high rates of development. This work intends to apply a meshless method to analyze the mechanical behavior of those structures. For this purpose, differential governing equations from several theories of plates and shells are presented.

The global radial basis function collocation method is chosen to interpolate the differential equations and boundary conditions. The method has an easy implementation and it has been applied successfully in several areas. It proved to be excellent for solving differential equations. However, its application in mechanical engineering problems has been kept limited. In order to demonstrate the performance of the method, the present work shows some applications related with that area.

The method proved to be excellent to perform the analysis of plates and shells. It is known that one of the problems of the present method is due to a bad choice of the shape parameter. For that reason the shape parameter is obtained by an optimization technique.

New shear deformation plate and shell theories were developed within present thesis. The differential governing equations and boundary conditions of the new shear deformation theories are obtained by a unified formulation by Carrera and further interpolated via global collocation with radial basis functions. The combination of Carrera's Unified formulation and meshless methods proved to be good for modeling the mechanical behavior of such structures.

Resumo

Actualmente, a maior parte dos métodos numéricos para a resolução de problemas de estruturas baseia-se em formulações de elementos finitos. Contudo, têm surgido recentemente formulações inovadoras e alternativas, baseadas em métodos sem malha, considerando apenas uma rede de nós e mantendo a qualidade da solução.

Nas últimas décadas, estruturas formadas por placas e cascas feitas em materiais compósitos tipo laminados e gradativos funcionais atingiram elevados níveis de desenvolvimento. Nesta tese, pretende-se aplicar um método sem malha para analisar o comportamento mecânico de tais estruturas. Para tal, apresenta-se equações diferenciais de diversas teorias de placa e casca.

O método de colocação global com funções de base radial é usado para interpolar as equações diferenciais e as condições de fronteira. Este método é de implementação simples e tem sido aplicado com sucesso em diversas áreas. O método revelou-se excelente para a resolução de equações diferenciais. Todavia, a sua aplicação em problemas de engenharia mecânica continua a ser escassa. A presente tese mostra algumas aplicações nesta área, de forma a demonstrar a eficácia do método.

O método revelou-se excelente para a análise de placas e cascas. Um dos problemas conhecidos deste método tem origem na má escolha do valor do parâmetro de forma e, por este motivo, este é escolhido com base numa técnica de optimização.

Novas teorias de deformação de placas e cascas foram desenvolvidas na tese. As equações diferenciais dos problemas e respectivas condições de fronteira são obtidas através da formulação unificada de Carrera e posteriormente interpoladas através do método de colocação global com funções de base radial. A combinação da formulação unificada de Carrera com métodos sem malha revelou-se boa na modelagem do comportamento mecânico das estruturas em estudo.

Résumé

Actuellement, la plupart des méthodes numériques sont basées sur la procédée bien connu des éléments finis. Toutefois, des formulations alternatives et innovantes ont été récemment développées, basés sur des méthodes sans maillage, qui utilisent simplement une grille nodale et conservent la qualité de la solution numérique.

Dans les dernières décennies, les structures composées par des plaques ou des coques, usant des matériaux composites ou des matériaux à gradient fonctionnel, ont connu des développements très significatifs. LŠobjectif principal de ce travail est lŠapplication dŠune méthode meshless à lŠanalyse du comportement mécanique de ces structures. A cet effet, les équations différentielles régissant plusieurs théories de plaques et coques sont présentés.

La méthode globale de colocalisation avec des fonctions de base radiales a été choisie pour interpoler les équations différentielles et les conditions aux frontières. La méthode á une mise en IJuvre facile et elle a été appliquée avec succès sur plusieurs domaines. Elle s'est avérée excellente pour résoudre des équations différentielles. Cependant, son application aux problèmes de génie mécanique a été maintenue limitée. De façon de démontrer la performance de la méthode, ce travail montre certaines applications dans ce domaine.

La méthode est excellente pour effectuer l'analyse des plaques et coques. Il est connu que l'un des problèmes de la méthode actuelle est dû à un mauvais choix du paramètre de forme. Pour cette raison, le paramètre de forme est obtenu par une technique d'optimisation.

Des nouvelles théories de déformation des plaques et des coques ont été développées dans cette thèse. Les équations différentielles à dérivées partielles et les conditions aux frontières qui gouverne ces nouvelles théories de déformation par cisaillement ont été

obtenues, usant une formulation unifiée par Carrera, et encore interpolées par l'intermédiaire de colocalisation globale avec des fonctions de base radiales. La combinaison de la formulation unifiée Carrera avec les méthodes sans maillage, á montrée être excellente pour la modélisation du comportement mécanique de ces structures.

Acknowledgements

I thank the supervisors of this thesis, Professores António Joaquim Mendes Ferreira, Cristóvão Manuel Mota Soares, and Renato Manuel Natal Jorge for their orientation and support.

I thank Professor Erasmo Carrera and Dr. Maria Cinefra for their contribution and support with the Unified Formulation.

I also thank the collaboration of Professor Tobin A. Driscoll, Professor Alfa R. H. Heryudono, Professor J. N. Reddy, Professor Greg Fasshauer, Professor K. M. Liew, and Dr. C. M. C. Roque.

I acknowledge the financial support received from Fundação para a Ciência e a Tecnologia, under the grant SFRH / BD / 45554 / 2008.

Contents

List of Figures

List of Tables

1

Introduction and objectives

1.1 Short overview of the thesis

This thesis presents a numerical study for the analysis of laminated and functionally graded plates and shells. The numerical technique is based on global collocation with radial basis functions, as a strong-form type of meshless methods.

The analysis of plates and shells considers several higher-order shear deformation theories, in particular polynomial, sinusoidal, and hyperbolic sine theories as well as zig-zag theories, allowing for thickness-stretching. Given the strong-form meshless technique, the governing equation and boundary conditions are derived by a Unified Formulation by Carrera [2, 3] (CUF). The governing equations are then interpolated and a global system of equations is obtained.

The radial basis functions global collocation technique is presented in 1.3. In 1.4 Carrera's Unified Formulation and its application to the analysis of functionally graded plates and shells is presented. This chapter also presents the new theories implemented using CUF. This part of the thesis emphasizes functionally graded structures because studies on the combination of carrera's Unified Formulation and meshless methods were performed for the first time for such structures in this thesis.

Several numerical examples for laminated and functionally graded plates and shells are presented and discussed, in the various journal papers shown in the following chapters. The first set has the purpose of showing the potential of the chosen meshless method and the second set to study its combination with CUF.

1.2 Objectives

The thesis has several objectives, in order to fill the gap of knowledge:

- to use the Carrera's Unified Formulation for the (meshless) analysis of laminated and functionally graded plates and shells
- to implement several higher-order shear deformation theories, namely polynomial, sinusoidal, hyperbolic sine and zig-zag theories
- to investigate the effects of $\epsilon_{zz} \neq 0$ in the behaviour of such theories
- to investigate the accuracy of such theories and its meshless implementation in the static, free vibration and buckling analysis of laminated and functionally graded plates and shells
- to implement some new oscillatory radial basis functions and strategies for improving the shape parameter issue

1.3 Modelling with Radial basis functions

1.3.1 Introduction

Finding the analytical solution of an engineering problem is not always possible. In most of the cases, solutions can only be obtained numerically and, in practice, a good approximation is all that we need.

Numerical methods can give approximations to the correct or exact mathematical solution and have been extensively used in the past several decades due to advances in computing power.

Computational simulation techniques are often used to analyse the static and dynamic analysis of structures such as plates and shells. It implies solving a set of partial differential equations in a domain and boundary conditions on the boundary. Solving it by finite element method (FEM) is now fully established.

Although this method is robust and widely used in engineering, the complexity of computacional mechanical problems have shown the limitation of the FEM and other convencional computational methods as the finite volume (FVM) or finite difference methods (FDM). While traditional methods are often based on (piecewise) polynomials and frequently require a fairly simple geometry and a certain amount of regularity of the associated discretization of the problem, meshless methods share the advantage of being able to deal with complex geometries and irregular discretizations. Furthermore, traditional methods such as finite elements and splines are defined on an underlying computational mesh. Studying problems involving large deformations or simulate crack growth with arbitrary and complex paths, and adaptive methods that require mesh actualization [4, 5, 1] are examples of the limitations of finite element method. Many of these problems are due to the fact that FEM needs a mesh, that is a set of nodes connected in a predefined manner. Other terminologies as *grids* (FDM), *elements* (FEM), *volumes* or *cells* (FVM) can be termed mesh-related according to the above definition of mesh.

The use of alternative methods such as the strong-form meshless (or mesh free) methods is attractive due to the absence of a mesh and the ease of collocation methods.

1.3.2 Meshless methods

As the name implies, the objective of meshless methods is to eliminate the process of mesh generation in the sense of conventional computational methods such as the FEM. According to Liu [6], the ideal meshless method does not need a mesh at all throughout the process of solving the problem of given arbitrary geometry governed by a partial differential system of equations subject to all kinds of boundary conditions. Nonetheless, meshless methods developed so far are not really ideal.

First references to meshless numerical methods appear in the 1930's decade, related to collocation methods [7, 8]. The first meshless method presented consistently was the smooth particle hydronamics (SPH) for modeling an astrophysical problems, just in the 1970's [9, 10, 11]. Not before 1990's meshless methods get regular attention, specially methods based on weak formulations.

Table 1.1 classifies meshless methods based on three criteria: the formulation procedures, the function approximation schemes, and the domain representation [12].

According to the formulation procedures:
strong formulation
weak formulation
weak-strong formulation
According to the function approximation schemes:
moving least squares
integral representation
point interpolation method
other
According to the domain representation:
domain-type
boundary-type

Table 1.1: Meshless methods classification, by Liu [1]

Meshless methods based on weak formulation of governing equations:

In meshfree weak-forms methods, the governing partial differential equations with derivative boundary conditions are first transformed to a set of weak-form integral equations and are then used to derive a set of algebraic system of equations. Examples of these methods are the diffuse element method (DEM) [13], the element free-Galerkin (EFG) [14], radial point interpolation method (RPIM) [15, 16], the meshless local Petrov-Galerkin method (MLPG) [17], and the local radial point interpolation method (LRPIM) [18], etc.

Meshless methods based on strong formulation of governing equations:

Meshless methods based on collocation techniques is another group of meshless techniques. In these methods, the governing equations and equations for boundary conditions are directly discretized at the field nodes using simple collocation techniques to obtain a set of discretized system of equations. Strong form equations are for example those given in the form of PDEs for solid mechanics problems. The general finite difference method (GFDM) [19], the finite point method (FPM) [20], and the meshless collocation method [21, 22] are examples of these methods.

Meshless methods based on weak-strong formulation of governing equations:

The key idea of the meshless methods based on the combination of weak-form and collocation techniques is that in establishing the discretized system of equations, both the strong-form and the weak-form are used for the same problem, but for different group of nodes that carries different types of equations/conditions. Examples are the meshless weak-strong form method (MWS) [23], and the smooth particle hydronamics (SPH) [11].

Meshless methods based on the moving least squares (MLS) approximation:

The interpolation techniques used in these methods are series representation generated by a moving least squares method. The meshless local Petrov-Galerkin method (MLPG) [17], the element free-Galerkin (EFG) [14], and the boundary node method (BNM) [24] are included in this group.

Meshless methods based on the integral representation method for the function approximation:
These methods represent the function using its information in a local domain [6] via an integral form [6, 12]. Examples of methods in this group are the smooth particle hydronamics (SPH) [11], and the reproducing kernel particle method (RKPM) [25, 26].

Meshless methods using point interpolation method:
These interpolation techniques use nodes distributed locally to formulate weak-form methods [12]. The aproximation is obtained by letting the interpolation function pass throught the function values at each scattered node within the support domain [6]. The basis functions can be polynomials or radial basis functions (RBFs). The radial point interpolation method (RPIM) [15], and the local radial point interpolation method (LRPIM) [18], among others examples.

Meshless methods based on other interpolation schemes:
All meshless methods not using point interpolation, neither based on the moving least squares approximation, nor on the integral representation method for the function approximation, are in this category. Examples of these methods are the hp-cloud method [27], the partition of unity method (PU) [28], and the moving kriging interpolation (MK)[29].

Meshless methods based on the domain:
In these methods, both the problem domain and boundaries are represented by nodes to discretize the system of equations. Some examples are the element free-Galerkin (EFG) [14], the meshless local Petrov-Galerkin method (MLPG) [17], the smooth particle hydronamics (SPH) [11], the radial point interpolation method (RPIM) [15], and the local radial point interpolation method (LRPIM) [18].

Meshless methods based on the boundary:
In these methods, only the boundary of the problem domain is represented by a set of nodes to obtain the discretized system of equations. Examples are the boundary node method (BNM) [24], the boundary point interpolation method (BPIM) [30], etc.

Combination of meshless methods and those that need a mesh is also possible, for example EFG/FEM [31], EFG/BEM [32], MLPG/FEM/BEM [33], moving least squares approximation augmented with the enriched basis functions/FEM [34].

1.3.3 Radial Basis Functions and collocation

Although most of work to date on radial basis functions relates to scattered data approximation and in general to interpolation theory, there has recently been as increased interest in their use for solving partial differential equations.

The solution of a set of ordinary (ODE) or partial differential equations (PDE) can be approximated in an average form or totally satisfied in a set of chosen points distributed in the domain. In collocation techniques we seek the last option [12].

When using collocation with radial basis functions (RBFs) this is obtained by a point interpolation method (PIM) using radial basis functions. The approximation is obtained by a series representation with interpolation function passing through the function values at each scattered node within the support domain [6].

Collocation methods seem to be first used in the decade of 1930's [8], with early development and applications, for example in [7].

Advantages of collocation methods are a simple algorithm, computational efficiency and the fact of being *truly* meshless [12]. Unfortunately, these methods are often unstable, not robust, and inaccurate, especially for problems with derivative boundary counditions.

Interest on radial basis functions increased after Franke's paper [35]. He compares methods available in the early 1980's for scattered data interpolation in terms of timing, storage, accuracy, visual pleasantness of the surface, and ease of implementation, and concludes that multiquadrics and thin plate splines were the best methods available at that time.

A radial function is a real-valued function whose value depends only on the distance from a point $\mathbf{x_i}$ so that $\phi(\mathbf{x}, \mathbf{x_i}) = \phi(\|\mathbf{x} - \mathbf{x_i}\|)$. Point $\mathbf{x_i}$ is tradicionally called a center because our basis functions will be radially symmetric about these points [36, 37, 38]. The distance is usually the Euclidean distance, although others can be used.

Radial basis functions can also depend on a shape parameter c, replacing $\phi(\|\mathbf{x}-\mathbf{x_i}\|)$ by $\phi(\|\mathbf{x}-\mathbf{x_i}\|, c)$. This is a user-defined parameter and has a big influence on the accuracy of the solution. Finding the optimal shape parameter is still an open discussion.

Radial basis functions (RBF) approximations are grid-free numerical schemes that can exploit accurate representations of the boundary, are easy to implement and can be spectrally accurate [39, 40]. It also has the advantage of being insensitive to spatial dimension [36, 37, 38].

Recently in literature the unsymmetric global collocation method with radial basis functions is also called RBF-Direct method [41, 42] to be distinguished from other methods that derive from or are combined with RBF, such as the RBF-QR (based on QR decomposition) and the RBF-PS (RBF in a pseudospectral framework). We will now present the formulation of the global unsymmetrical collocation RBF-based method used in this thesis.

Radial basis functions

The radial basis function (ϕ) approximation of a function ($\mathbf{u}$) is given by

$$\widetilde{\mathbf{u}}(\mathbf{x}) = \sum_{i=1}^{N} \alpha_i \phi\left(\|x - y_i\|_2\right), \mathbf{x} \in \mathbb{R}^n \tag{1.1}$$

where $y_i, i = 1, .., N$ is a finite set of distinct points (centers) in $\mathbb{R}^n$. The coefficients

α_i are chosen so that $\widetilde{\mathbf{u}}$ satisfies some boundary conditions. Some common RBFs are

$$\phi(r) = r^3, \quad \text{cubic} \tag{1.2}$$

$$\phi(r) = r^2 \log(r), \quad \text{thin plate splines} \tag{1.3}$$

$$\phi(r) = (1-r)_+^m p(r), \quad \text{Wendland functions} \tag{1.4}$$

$$\phi(r) = e^{-(cr)^2}, \quad \text{Gaussian} \tag{1.5}$$

$$\phi(r) = \sqrt{c^2 + r^2}, \quad \text{Multiquadric} \tag{1.6}$$

$$\phi(r) = (c^2 + r^2)^{-1/2}, \quad \text{Inverse Multiquadric} \tag{1.7}$$

where r is the euclidean norm between grid points of coordinates $(x,\ y)$, a, b are the length of the plate along x and y axis, respectively and c is a user defined shape parameter. In the present thesis, three different formulations for the shape parameter were used:

- *Fixed shape parameter:* The value of the shape parameter was chosen by trial and error for the shape parameter. For example in paper presented in 3.1.4 the value $\sqrt{2/N}$ (where N is the number of nodes per side of the plate) is used and in paper 3.2.3 a different fixed value is used. The radial basis function considers the same shape parameter for all the points.

- *Optimized shape parameter:* The shape parameter is obtained by an optimization procedure as detailed in Ferreira and Fasshauer [43]. All points have the same shape parameter. This formulation was used in paper presented in 2.4, for example.

- *Adaptive shape parameter:* At each iteration, the shape parameter is automatically adapted. The radial basis function may use different shape parameter values for different points. This adaptive technique was used in paper presented in 3.1.1.

Other RBFs not so typical in literature are

$$\phi(r) = r^q, \qquad \text{Radial Powers} \tag{1.8}$$

$$\phi(r) = (c^2 + r^2)^q, \qquad \text{Generalized Multiquadrics} \tag{1.9}$$

$$\phi(r) = r^{2q}\log(r), \qquad \text{Thin Plate Splines} \tag{1.10}$$

$$\phi(r) = \sqrt{\frac{2}{\pi}}\cos(cr), \qquad \text{Poisson with } d = 1 \tag{1.11}$$

$$\phi(r) = \sqrt{\frac{2}{\pi}}\frac{\sin(cr)}{cr}, \qquad \text{Poisson with } d = 3 \tag{1.12}$$

$$\phi(r) = \sqrt{\frac{2}{\pi}}\frac{\sin(cr) - cr\cos(cr)}{(cr)^3}, \qquad \text{Poisson with } d = 5 \tag{1.13}$$

$$\phi(r) = 1/\sqrt{1 + c^2\left((x_i - x_j)^2 + \frac{(y_i - y_j)^2}{(b/a)^2}\right)}, \qquad \text{Anisotropic Inverse Multiquadrics} \tag{1.14}$$

In (1.9), $q = 1/2$ and $q = -1/2$ leads to (1.6) and (1.7).

Local functions, such as the Wendland functions (1.4) are denoted as $\varphi_{s,k}$ and a detailed exposition can be found in [44]. Some of the most commomly used Wendland functions in $\mathbb{R}^3$ are:

$$\varphi_{3,0}(r) = (1 - \epsilon r)_+^2 \tag{1.15}$$

$$\varphi_{3,1}(r) = (1 - \epsilon r)_+^4(4\epsilon r + 1) \tag{1.16}$$

$$\varphi_{3,2}(r) = (1 - \epsilon r)_+^6\left(35(\epsilon r)^2 + 18\epsilon r + 3\right) \tag{1.17}$$

$$\varphi_{3,3}(r) = (1 - \epsilon r)_+^8\left(32(\epsilon r)^3 + 25(\epsilon r)^2 + 8\epsilon r + 1\right) \tag{1.18}$$

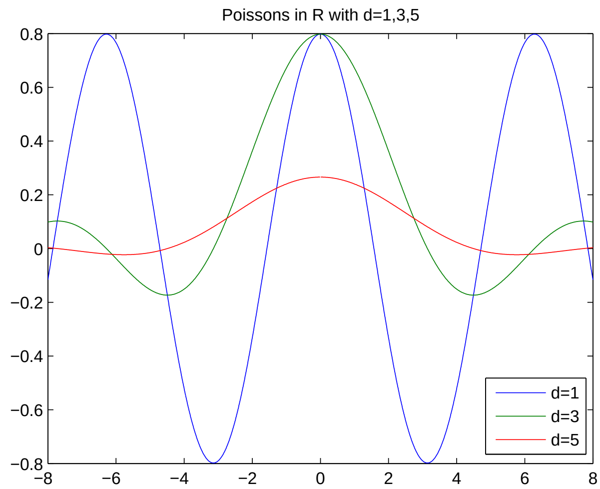

Figure 1.1: Poisson functions in $\mathbb{R}$

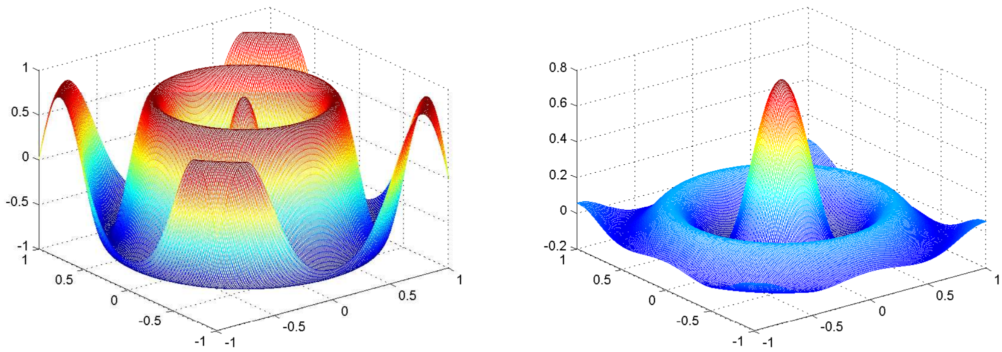

Figure 1.2: Poisson functions in $\mathbb{R}^2$ with $d = 1$ on the left and $d = 3$ on the right

The definition of the Poisson functions family is based on the Bessel function of order d. Poisson functions (1.11) to (1.13) centered at the origin are displayed in figures 1.1 to 1.3 both in $\mathbb{R}$ and $\mathbb{R}^2$. A shape parameter $c = 10$ was used in $\mathbb{R}^2$.

In (1.14) the radial basis function depends on the direction it is being computed and is sometimes called anisotropic radial basis function [45].

Other RBFs also not so typically found in literature are the Laguerre-Gaussians listed in table 1.2 and displayed in figures 1.4 and 1.5 in $\mathbb{R}$ and $\mathbb{R}^2$ respectively and centered at the origin. In $\mathbb{R}^2$ a shape parameter $c = 3$ was used. The definition of Laguerre-Gaussians functions family comes from the generalized Laguerre polynomials of degree n and order $s/2$.

Another family of radial basis functions are the Matérn functions also known as Sobolev

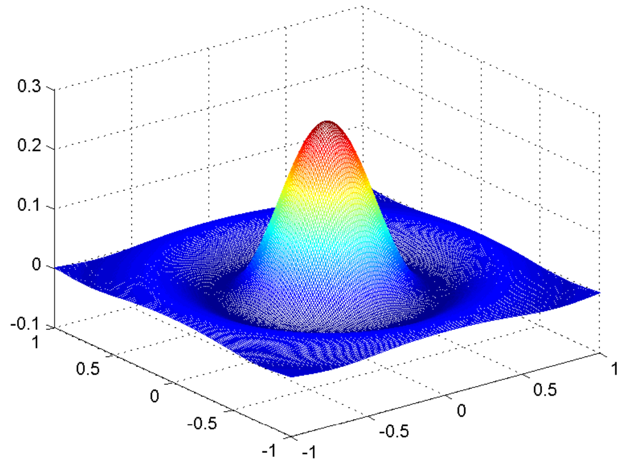

Figure 1.3: Poisson function in $\mathbb{R}^2$ with $d = 5$

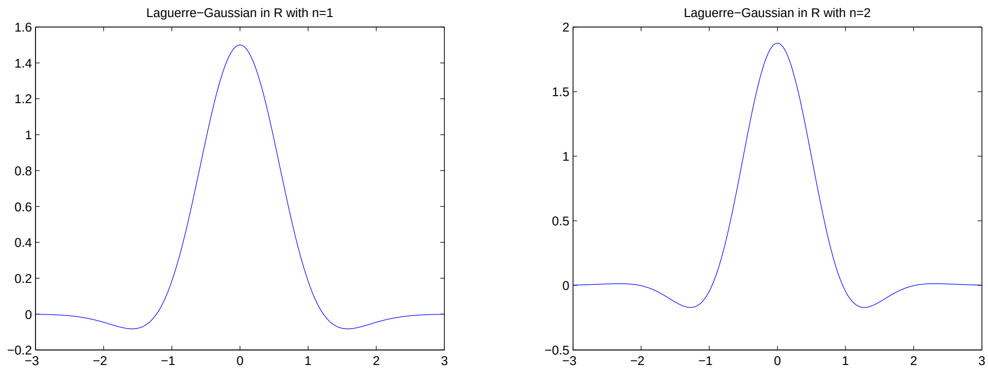

Figure 1.4: Laguerre-Gaussians functions in $\mathbb{R}$ with $n = 1$ on the left and $n = 2$ on the right

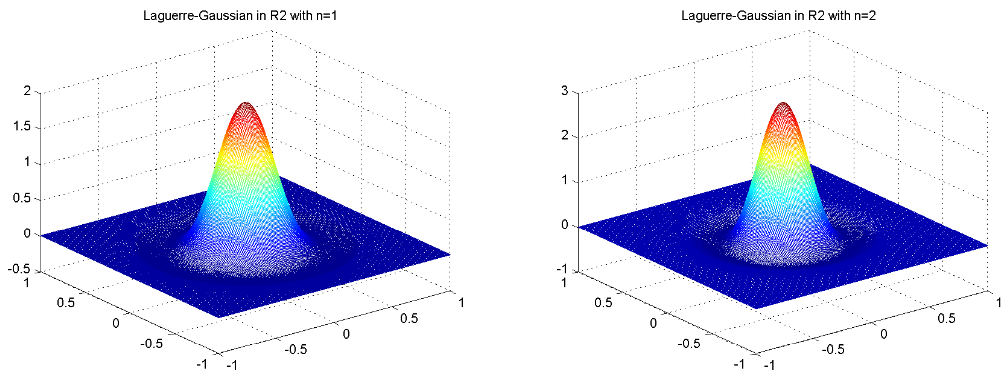

Figure 1.5: Laguerre-Gaussians functions in $\mathbb{R}^2$ with $n = 1$ on the left and $n = 2$ on the right

s \ n	1	2
1	$\phi(r) = \left(\frac{3}{2} - (cr)^2\right) e^{-(cr)^2}$	$\phi(r) = \left(\frac{15}{8} - \frac{5}{2}(cr)^2 + \frac{1}{2}(cr)^4\right) e^{-(cr)^2}$
2	$\phi(r) = \left(2 - (cr)^2\right) e^{-(cr)^2}$	$\phi(r) = \left(3 - 3(cr)^2 + \frac{1}{2}(cr)^4\right) e^{-(cr)^2}$
3	$\phi(r) = \left(\frac{5}{2} - (cr)^2\right) e^{-(cr)^2}$	$\phi(r) = \left(\frac{35}{8} - \frac{7}{2}(cr)^2 + \frac{1}{2}(cr)^4\right) e^{-(cr)^2}$

Table 1.2: Laguerre-Gaussians radial functions

splines. Examples are listed in table 1.3.

name	matern function
basic	$\phi(r) = e^{-cr}$
linear	$\phi(r) = (1 + cr)e^{-cr}$
quadratic	$\phi(r) = (1 + cr + \frac{(cr)^2}{3})e^{-cr}$
cubic	$\phi(r) = (15 + 15cr + 6(cr)^2 + (cr)^3)e^{-cr}$

Table 1.3: Matérn functions for several choices of β

More recently Gneiting [46] introduced a new family of radial functions $\tau_{s,l}(r)$. Some of them with $s = 2$ are listed bellow:

$$\tau_{2,\frac{7}{2}}(r) = (1 - \epsilon r)_+^{\frac{7}{2}} \left(1 + \frac{7}{2}\epsilon r - \frac{135}{8}(\epsilon r)^2\right) \tag{1.19}$$

$$\tau_{2,5}(r) = (1 - \epsilon r)_+^5 \left(1 + 5\epsilon r - 27(\epsilon r)^2\right) \tag{1.20}$$

$$\tau_{2,\frac{15}{2}}(r) = (1 - \epsilon r)_+^{\frac{15}{2}} \left(1 + \frac{15}{2}\epsilon r - \frac{391}{8}(\epsilon r)^2\right) \tag{1.21}$$

$$\tau_{2,12}(r) = (1 - \epsilon r)_+^{12} \left(1 + 12\epsilon r - 104(\epsilon r)^2\right) \tag{1.22}$$

The radial basis functions used in the present thesis are the Gaussian (1.5) in paper here presented in 3.1.2, the Multiquadric (1.6) in 3.2.3, the Inverse Multiquadric (1.7) in 3.2.2, the Gaussian-Laguerre (see table 1.2) in 3.1.2, the Matérn cubic (see table 1.3) in 3.2.1, and the Wendland (1.18) in 2.1.

An overview of some properties of radial basis functions and some important results are now presented.

positive semi-definite matrix:

A real symmetric matrix A is called positive semi-definite if its associated quadratic form is non-negative [38], i.e.,

$$\sum_{j=1}^{N}\sum_{k=1}^{N} c_j c_k A_{jk} \geq 0 \tag{1.23}$$

for $\mathbf{c}= [c_1, ..., c_N]^T \in \mathbb{R}^N$.

positive definite matrix:

A real symmetric matrix A is called positive definite if its associated quadratic (1.23) form is zero only for $\mathbf{c}\equiv 0$ [38], i.e.,

$$\sum_{j=1}^{N}\sum_{k=1}^{N} c_j c_k A_{jk} = 0 \Leftrightarrow \mathbf{c} \equiv 0 \tag{1.24}$$

for $\mathbf{c}= [c_1, ..., c_N]^T \in \mathbb{R}^N$.

These terminologies for matrices are connected with the following for functions, as we define a matrix A with entries $A_{jk} = \phi(\mathbf{x}_j - \mathbf{x}_k)$ from a function $\Phi(r)$.

positive definite functions:

A complex-valued continuos function ϕ: $\mathbb{R}^s \to \mathbb{C}$ is called positive definite on $\mathbb{R}^s$ if [38]

$$\sum_{j=1}^{N}\sum_{k=1}^{N} c_j \bar{c}_k \phi(\mathbf{x}_j - \mathbf{x}_k) \geq 0 \tag{1.25}$$

for any N pairwise different points $\mathbf{x}_1, ..., \mathbf{x}_N \in \mathbb{R}^s$, and $\mathbf{c}= [c_1, ..., c_N]^T \in \mathbb{C}^N$.

strictly positive definite functions:

A complex-valued continuos function ϕ: $\mathbb{R}^s \to \mathbb{C}$ is called strictly positive definite on $\mathbb{R}^s$ if the associated quadratic form (1.25) is zero only for $\mathbf{c}\equiv 0$ [38], i.e.,

$$\sum_{j=1}^{N}\sum_{k=1}^{N} c_j \bar{c}_k \phi(\mathbf{x}_j - \mathbf{x}_k) = 0 \Leftrightarrow \mathbf{c} \equiv 0 \tag{1.26}$$

Examples of strictly positive definite radial functions are the Gaussian (1.5), the Inverse Multiquadric (1.7), the Generalized Multiquadrics (1.9) with $q = 1$ or $q = 2$, and the Matérn in table 1.3. The Wendlands $\varphi_{s,k}$ (1.4) and (1.15)-(1.18), the Laguerre-Gaussians listed in table 1.2, and the Poissons (1.11)-(1.12) are strictly positive definite radial functions in $\mathbb{R}^s$. The Gneiting functions $\tau_{s,l}(r)$ (1.19)-(1.22) are strictly positive definite radial functions in $\mathbb{R}^s$ provided $l \geq \frac{s+5}{2}$.

completely monotonic or ***completely monotone:***
A function ϕ with domain $(0, \infty)$ is said to be completely monotonic [37, 47] or completely monotone [38] if it possesses derivatives $\phi^{(n)}(r)$ for all $n = 0, 1, 2, 3, ...$ and if $(-1)^n \phi^{(n)}(r) \geq 0$ for all $r > 0$.

The Gaussian is an example of a completely monotonic radial basis function.

A first remark is that if $\phi = \Phi(\|\cdot\|)$ is (strictly) positive definite and radial on $\mathbb{R}^n$ then ϕ is also (strictly) positive and definite and radial on $\mathbb{R}^m$ for any $m \leq n$.

Next results connect the concepts described so far and are due to Schoenberg [48]:

Theorem 1.3.1: A function Φ is completely monotone on $[0, \infty)$ if and only if $\phi = \Phi(\|\cdot\|^2)$ is positive definite and radial on $\mathbb{R}^n$ for all n.

Theorem 1.3.2: A function $\Phi : [0, \infty) \to \mathbb{R}$ is completely monotone but not constant if and only if $\Phi(\|\cdot\|^2)$ is strictly positive definite and radial on $\mathbb{R}^n$ for any n.

These results are important in the context of interpolation problems, related to the nonsingularity and invertibility of interpolation matrices. A discussion on the subject can be found in [38], and proofs in [37, 49].

The next two definitios are the generalized version to complex-valued functions [38] from Michelli's [50] definitions for real-valued. Buhmann [37] uses the real-valued definition.

Conditionally positive definite functions:

A complex-valued continuos function ϕ is called conditionally positive definite of order m on $\mathbb{R}^n$ if (1.25) holds for any N pairwise different points $\mathbf{x}_1, ..., \mathbf{x}_N \in \mathbb{R}^n$, and $\mathbf{c}= [c_1, ..., c_N]^T \in \mathbb{C}^N$ satisfying

$$\sum c_j p(\mathbf{x}_j) = 0, \tag{1.27}$$

for any complex-valued polynomial p of degree at most $m-1$.

Strictly conditionally positive definite functions:

Analogous to previous definitions, a complex-valued continuos function ϕ is called conditionally positive definite of order m on $\mathbb{R}^n$ if (1.25) holds for any N pairwise different points $\mathbf{x}_1, ..., \mathbf{x}_N \in \mathbb{R}^n$, and $\mathbf{c}= [c_1, ..., c_N]^T \in \mathbb{C}^N$ satisfying

$$\sum c_j p(\mathbf{x}_j) = 0, \tag{1.28}$$

for any complex-valued polynomial p of degree at most $m-1$ and if the quadratic form (1.25) is zero only for $\mathbf{c}\equiv 0$.

Examples of strictly conditionally positive definite radial functions of order 1 are the Multiquadric (1.6) and the Radial Power (1.8) with $q = 1$. Examples of strictly conditionally positive definite radial functions of order 2 are the Cubic (1.2) which corresponds to the Radial Power (1.8) with $q = 3$ and the Thin Plate Splines (1.3). The Radial Power (1.8) with $q = 5$ and the Thin Plate Spline (1.10) with $q = 2$ are examples of strictly conditionally positive definite radial functions of order 3.

As observation to be made is that a function which is (strictly) conditionally positive definite of order m on $\mathbb{R}^n$ is also (strictly) conditionally positive definite of any higher order. In particular, a (strictly) positive definite function is always (strictly) conditionally positive definite of any order [38].

As before, we now present results connecting strictly conditionally positive definite radial functions to completely monotone functions.

Theorem 1.3.3: Let $\Phi \in C[0,\infty) \cap C^{\infty}(0,\infty)$. Then the function $\phi = \Phi(\|\cdot\|^2)$ is conditionally positive definite of order m and radial on $\mathbb{R}^n$ for all n if and only if $(-1)^m \Phi^{(m)}$ is completely monotone on $(0,\infty)$.

For $m = 0$ this is Schoenberg's theorem 1.3.1. Micchelli in 1986 [50] proves that complete monotonicity implies conditional positive definiteness and Guo et al. [51] prove the remaining.

Theorem 1.3.4: If $\Phi \in C[0,\infty) \cap C^{\infty}(0,\infty)$ is not a polynomial of degree at most m then the function $\phi = \Phi(\|\cdot\|^2)$ is strictly conditionally positive definite of order m and radial on $\mathbb{R}^n$ for all n.

A proof of this theorem can be found in [49].

For the interpolation problem, we have the following result:

Theorem 1.3.5: Let ϕ be a strictly conditionally positive definite of order one with $\phi(\mathbf{0}) = 0$. Then for any distinct points $\mathbf{x}_1, ..., \mathbf{x}_N \in \mathbb{R}^n$ the matrix A with entries $A_{jk} = \phi(\mathbf{x}_j - \mathbf{x}_k)$ has $N-1$ positive eigenvalues and one negative, and is therefore non-singular.

This was first proved in 1986 [50] motivated by Hardy's earlier work [52] and Franke's conjecture [35].

Compactly supported functions:

The support of the function ϕ with domain Ω is the closure of the set of points $\mathbf{x} \in \Omega$ for which $\phi(\mathbf{x}) \neq \mathbf{0}$. A function of compact support in Ω is a function defined on Ω such that its support is a closed bounded set located at a distance from the boundary of the domain by a number greater than $\delta > 0$.

This means that the function has compact support if it takes the value zero outside a compact set.

Compactly supported radial functions were introduced by Schaback [53]. Examples are the Wendland's functions (1.4), consisting of a univariate polynomial within their support. They can be scaled so that the size of local support changes from $\delta = 1$ presented in (1.4) and (1.15)-(1.18) to another δ [37, 12]. Another example of functions with compact support are those of Gneiting (1.19)-(1.22).

Buhmann [36] and Wu [54] constructed other radial functions with compact support. Such functions have the advantage of leading to a sparse interpolation matrix.

Unlike these functions, most of radial functions have global support, such as the Gaussian (1.5), the Multiquadric (1.6), the Cubic (1.2), the Thin Plate Splines (1.3), and the family of Laguerre-Gaussians, some listed in table 1.2.

Infinitely smooth radial functions are, for example, the Gaussian (1.5), the Multiquadric (1.6), and the Inverse Multiquadric (1.7).

Examples of piecewise smooth radial functions are the family of Wendland functions (1.4) and the Thin Plate Splines (1.3).

Examples of oscillating radial functions, also called in the literature oscillatory radial functions, are the Laguerre-Gaussians, some of them listed in table 1.2, the family of Poisson functions, including 1.11 to 1.13, and the Gneiting functions family (1.19)-(1.22).

Solution of the interpolation problem

Hardy [52] introduced multiquadrics in the analysis of scattered geographical data. In the 1990's Kansa [21] used multiquadrics for the solution of partial differential equations.

Considering N distinct interpolations, and knowing $u(x_j), j = 1, 2, ..., N$, we find α_i by the solution of a $N \times N$ linear system

$$\mathbf{A}\underline{\alpha} = \mathbf{u} \tag{1.29}$$

where $\mathbf{A} = [\phi(\|x - y_i\|_2)]_{N\times N}$, $\underline{\alpha} = [\alpha_1, \alpha_2, ..., \alpha_N]^T$ and $\mathbf{u} = [u(x_1), u(x_2), ..., u(x_N)]^T$. The RBF interpolation matrix A is positive definite for some RBFs [36], but in general provides ill-conditioned systems.

The static problem

Consider a linear elliptic partial differential operator $\mathcal{L}$ acting in a bounded region Ω in $\mathbb{R}^n$ and another operator $\mathcal{L}_B$ acting on a boundary $\partial\Omega$. We seek the computation of displacements ($\mathbf{u}$) from the global system of equations

$$\mathcal{L}\mathbf{u} = \mathbf{f} \text{ in } \Omega; \qquad \mathcal{L}_B\mathbf{u} = \mathbf{g} \text{ on } \partial\Omega \tag{1.30}$$

The external forces applied on the plate and the boundary conditions applied along the perimeter of the plate, respectively, are at the right-hand side of (1.30). The PDE problem defined in (1.30) will be replaced by a finite problem, defined by an algebraic system of equations, after the radial basis expansions.

Solution of the static problem

The solution of a static problem by radial basis functions considers N_I nodes in the domain and N_B nodes on the boundary, with a total number of nodes $N = N_I + N_B$. In the present thesis three different grids of points are used:

Figure 1.6: $\mathbb{R}^2$ grids with 11^2 points: equally spaced (left) and Chebyshev (right).

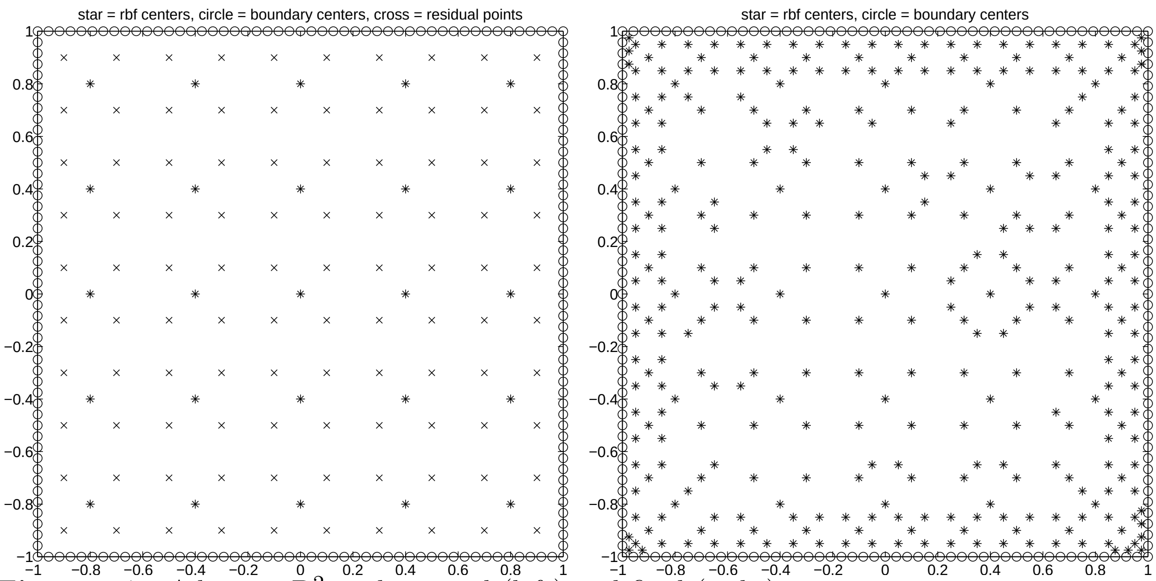

Figure 1.7: Adaptive $\mathbb{R}^2$ grids: initial (left) and final (right).

- *Equally spaced points* The points are equally spaced. Such grid was used in paper in 3.2.4 for example. An illustration of a $2D$ grid with 11^2 points is in figure 1.6.

- *Chebyshev points* For a given number of nodes per side $(N+1)$ they are generated by MATLAB code as:

  ```
  x = cos(pi*(0:N)/N)'; y=x;
  ```

  One advantage of such mesh is the concentration of points near the boundary. This grid was used for example in paper presented in 2.3.

- *Adaptive points* Nodes can be added to or removed from the set of centers based on a residual. Figure 1.7 shows an example of an initial and a final grid. It refers to a square simply-suppported isotropic plate, with side to thickness ratio $a/h = 100$. This example was taken from 3.1.1.

We denote the sampling points by $x_i \in \Omega, i = 1, ..., N_I$ and $x_i \in \partial\Omega, i = N_I + 1, ..., N$. At the points in the domain $(x_i \in \Omega, i = 1, ..., N_I)$ we solve the following system of equations

$$\sum_{i=1}^{N} \alpha_i \mathcal{L}\phi\left(\|x - y_i\|_2\right) = \mathbf{f}(x_j), j = 1, 2, ..., N_I \tag{1.31}$$

or

$$\mathcal{L}^I \boldsymbol{\alpha} = \mathbf{F} \tag{1.32}$$

where

$$\mathcal{L}^I = \left[\mathcal{L}\phi\left(\|x - y_i\|_2\right)\right]_{N_I \times N} \tag{1.33}$$

At the points on the boundary $(x_i \in \partial\Omega, i = N_I + 1, ..., N)$, we impose boundary conditions as

$$\sum_{i=1}^{N} \alpha_i \mathcal{L}_B\phi\left(\|x - y_i\|_2\right) = \mathbf{g}(x_j), j = N_I + 1, ..., N \tag{1.34}$$

or

$$\mathbf{B}\boldsymbol{\alpha} = \mathbf{G} \tag{1.35}$$

where

$$\mathbf{B} = \mathcal{L}_B\phi\left[\left(\|x_{N_I+1} - y_j\|_2\right)\right]_{N_B \times N}$$

Therefore, we can write a finite-dimensional static problem as

$$\begin{bmatrix} \mathcal{L}^I \\ \mathbf{B} \end{bmatrix} \boldsymbol{\alpha} = \begin{bmatrix} \mathbf{F} \\ \mathbf{G} \end{bmatrix} \tag{1.36}$$

By inverting the system (1.36), we obtain the vector $\boldsymbol{\alpha}$. We then obtain the solution $\mathbf{u}$ using the interpolation equation (1.1).

The eigenproblem

The eigenproblem looks for eigenvalues (λ) and eigenvectors ($\mathbf{u}$) that satisfy

$$\mathcal{L}\mathbf{u} + \lambda\mathbf{u} = 0 \text{ in } \Omega; \qquad \mathcal{L}_B\mathbf{u} = 0 \text{ on } \partial\Omega \tag{1.37}$$

As in the static problem, the eigenproblem defined in (1.37) is replaced by a finite-dimensional eigenvalue problem, based on RBF approximations.

Solution of the eigenproblem

We consider N_I nodes in the interior of the domain and N_B nodes on the boundary, with $N = N_I + N_B$. We denote interpolation points by $x_i \in \Omega, i = 1, ..., N_I$ and $x_i \in \partial\Omega, i = N_I + 1, ..., N$. At the points in the domain, we define the eigenproblem as

$$\sum_{i=1}^{N} \alpha_i \mathcal{L}\phi\left(\|x - y_i\|_2\right) = \lambda\widetilde{\mathbf{u}}(x_j), j = 1, 2, ..., N_I \tag{1.38}$$

or

$$\mathcal{L}^I\boldsymbol{\alpha} = \lambda\widetilde{\mathbf{u}}^I \tag{1.39}$$

where

$$\mathcal{L}^I = \left[\mathcal{L}\phi\left(\|x - y_i\|_2\right)\right]_{N_I \times N} \tag{1.40}$$

At the points on the boundary, we enforce the boundary conditions as

$$\sum_{i=1}^{N} \alpha_i \mathcal{L}_B \phi \left(\|x - y_i\|_2 \right) = 0, j = N_I + 1, ..., N \tag{1.41}$$

or

$$\mathbf{B}\boldsymbol{\alpha} = 0 \tag{1.42}$$

Equations (1.39) and (1.42) can now be solved as a generalized eigenvalue problem

$$\begin{bmatrix} \mathcal{L}^I \\ \mathbf{B} \end{bmatrix} \boldsymbol{\alpha} = \lambda \begin{bmatrix} \mathbf{A}^I \\ \mathbf{0} \end{bmatrix} \boldsymbol{\alpha} \tag{1.43}$$

where

$$\mathbf{A}^I = \phi \left[\left(\|x_{N_I} - y_j\|_2 \right) \right]_{N_I \times N}$$

Discretization of the governing equations and boundary conditions

The radial basis collocation method follows a simple implementation procedure. Taking equation (1.36), we compute

$$\boldsymbol{\alpha} = \begin{bmatrix} L^I \\ \mathbf{B} \end{bmatrix}^{-1} \begin{bmatrix} \mathbf{F} \\ \mathbf{G} \end{bmatrix} \tag{1.44}$$

This $\boldsymbol{\alpha}$ vector is then used to obtain solution $\tilde{\mathbf{u}}$, by using (1.1). If derivatives of $\tilde{\mathbf{u}}$ are needed, such derivatives are computed as

$$\frac{\partial \tilde{\mathbf{u}}}{\partial x} = \sum_{j=1}^{N} \alpha_j \frac{\partial \phi_j}{\partial x}; \qquad \frac{\partial^2 \tilde{\mathbf{u}}}{\partial x^2} = \sum_{j=1}^{N} \alpha_j \frac{\partial^2 \phi_j}{\partial x^2}, \text{etc} \tag{1.45}$$

In the present collocation approach, we need to impose essential and natural boundary conditions. Consider, for example, the condition $w_0 = 0$, on a simply supported or clamped edge. We enforce the conditions by interpolating as

$$w_0 = 0 \rightarrow \sum_{j=1}^{N} \alpha_j^{W_0} \phi_j = 0 \tag{1.46}$$

Other boundary conditions are interpolated in a similar way.

Free vibrations problems

For free vibration problems we set the external force to zero, and assume harmonic solution in terms of displacements u_j as

$$u_j = U_j(w, y) e^{i\omega t}; \tag{1.47}$$

and analogous for v_j and w_j, where j may be $j = 0, 1, 2, 3, Z$ depending on the deformation theory, and ω is the frequency of natural vibration. Substituting the harmonic expansion into equations (1.43) in terms of the amplitudes U_j, V_j, W_j, we may obtain the natural frequencies and vibration modes for the plate problem, by solving the eigenproblem

$$\left[\mathcal{L} - \omega^2 \mathcal{G}\right] \mathbf{X} = \mathbf{0} \tag{1.48}$$

where $\mathcal{L}$ collects all stiffness terms and $\mathcal{G}$ collects all terms related to the inertial terms. In (1.48) $\mathbf{X}$ are the modes of vibration associated with the natural frequencies defined as ω.

Buckling problems

The eigenproblem associated to the governing equations is defined as

$$[\mathcal{L} - \lambda\mathcal{G}]\,\mathbf{X} = \mathbf{0} \tag{1.49}$$

where $\mathcal{L}$ collects all stiffness terms and $\mathcal{G}$ collects all terms related to the in-plane forces. In (1.49) $\mathbf{X}$ are the buckling modes associated with the buckling loads defined as λ.

1.3.4 Combining collocation with Radial Basis Functions and Pseudospectral methods

Polynomial pseudospectral (PS) methods (also called spectral methods) are known as highly accurate solvers for PDEs [55, 56]. Generally speaking, one represents the spatial part of the approximate solution of a given PDE by a linear combination of certain smooth basis functions, (i, j represents the N grid points).

$$u^h(x_i) = \sum_{j=1}^{N} \alpha_j \phi_j(x_i), i = 1, ..., N \tag{1.50}$$

or in matrix-vector notation

$$\mathbf{u} = \mathbf{A}\alpha \tag{1.51}$$

with $\alpha = [\alpha_1, ..., \alpha_x]$ and $A_{i,i} = \phi_i(x_i)$

Traditionally, polynomial basis functions are used. When we are using the radial basis functions collocation technique in a pseudospectral framework, however, we use any of the radial basis functions (RBFs) in 1.2 to 1.14.

The derivatives of are easily computed. For example,

$$\mathbf{u}' = \mathbf{A_x}\alpha = \mathbf{Du} \tag{1.52}$$

with $A_x = \frac{d}{dx}\phi_j(x_i)$ where matrix is the differentiation matrix.

The use of PS and RBF combined for the analysis of structures was first presented by Ferreira and Fasshauer [57]. Its application for laminated structures was then presented by Ferreira et al. [58].

One advantage in using RBF-PS is that it provides an faster framework for dynamic analysis due to the fact that we obtain directly solutions at points and not just some parameters for interpolation of solution. Although this advantage is not noticeable in free vibration analysis when compared to regular RBFs, it is quite relevant in transient dynamics where interpolation with RBFs would have to be established in each time step.

1.4 The Carrera's Unified Formulation for the analysis of functionally graded plates and shells

1.4.1 Carrera's Unified Formulation

The Unified Formulation proposed by Carrera (further denoted as CUF) method [2, 3] is employed to obtain the algebraic equations of motion and boundary conditions. Such equations of motion and corresponding boundary conditions are then interpolated by radial basis functions to obtain an algebraic system of equations.

The CUF method has been applied in several finite element analysis, either using the Principle of Virtual Displacements, or by using the Reissner's Mixed Variational theorem. The stiffness matrix components, the external force terms or the inertia terms can be obtained directly with this unified formulation, irrespective of the shear deformation theory being considered.

Carrera's Unified Formulation (CUF) was proposed in [59, 3, 60] for laminated plates and shells and extended to FGM plates in [61, 62, 63]. It is possible to implement any C_z^0 theory under CUF, using layer-wise as well as equivalent single-layer descriptions, and the Principle of Virtual Displacements, as is the case in present thesis, or the Reissner mixed variational theorem. CUF allows a systematic assessment of a large number of plate models.

The combination of CUF and meshless methods has been performed in [64, 65, 66, 67] for laminated plates and in [68, 69] for laminated shells. In the present thesis the combination of CUF and meshless methods is generalized for FG plates and shells.

Furthermore, the deformation theories used in the present thesis demand for a generalization of the original CUF, by introducing different displacement fields for in-plane and out-of-plane displacements.

Moreover, a novel application of CUF is proposed in this thesis. The explicit governing equations and boundary conditions in terms of displacements of the static, free vibration or buckling problems are obtained using symbolic computation. The combination of CUF and the symbolic calculations performed in MATLAB can be seen as a time-saving and error reducer.

1.4.2 Shear deformation theories

The classical plate theory (CLPT) yields acceptable results only for the analysis of thin plates. The accuracy of the first-order shear deformation theory (FSDT) depends on the shear correction factor which may be difficult to compute. Higher-order shear deformation theories (HSDT) provide better accuracy for transverse shear stresses without the need of a shear correction factor.

Examples of HSDT were proposed by Reddy [70], Kant [71, 72, 73, 74, 75, 76] and Batra [77, 78].

The use of a sinusoidal shear deformation theory for composite laminated plates and shells was first presented by Touratier [79, 80] [81] in the early 1990's. Later Vidal and Polit [82] used a sinusoidal shear deformation theory for composite laminated beams. The use of sinusoidal plate theories for functionally graded plates was first presented by Zenkour [83], where a $\epsilon_{zz} = 0$ approach was used.

To the best of authors' knowledge, plate theories involving hyperbolic functions are quite rare in literature. Soldatos [84] used a displacement field involving the hyperbolic function

$$f(z) = h \sinh\left(\frac{z}{h}\right) - z \cosh\left(\frac{1}{2}\right). \tag{1.53}$$

In [85, 86] two displacement fields are presented both considering a hyperbolic function:

$$f(z) = \frac{3\pi}{2} h \tanh\left(\frac{z}{h}\right) - \frac{3\pi}{2} z \,\mathrm{sech}^2\left(\frac{1}{2}\right) \tag{1.54}$$

and

$$f(z) = z \,\mathrm{sech}\left(\frac{\pi z^2}{h^2}\right) - z \,\mathrm{sech}\left(\frac{\pi}{4}\right)\left[1 - \frac{\pi}{2}\tanh\left(\frac{\pi}{4}\right)\right]. \tag{1.55}$$

These hyperbolic functions were used in the study of laminated composite plates. Noureddine et al. [87] consider the hyperbolic function

$$f(z) = \frac{\frac{h}{\pi}\sinh\left(\frac{\pi z}{h}\right) - z}{\cosh\left(\frac{\pi}{2}\right) - 1}. \tag{1.56}$$

in the study of functionally graded plates. In all cases the hyperbolic functions are used for the in-plane expansions only, while the transverse displacement is kept constant ($w = w_0$).

The zig-zag effect is produced by the strong difference of mechanical properties between faces and core in sandwich structures. A discontinuity of the deformed core-faces planes at the interfaces is introduced and makes difficult the use of classical theories such as Kirchhoff [88] or Reissner-Mindlin [89, 90] type theories. This thesis focus on equivalent single layer models and in this framework Murakami [91] proposed a zig-zag function that is able to reproduce the slope discontinuity.

Two major topics arise from the literature revision: the warping and the zig-zag effects on the analyis of the structures behaviour. Most of studies on functionally graded plates are performed with theories not accounting for transverse extensibility by neglecting the σ_{zz} effects, considering the transverse displacement to be independent of the thickness coordinates.

In this thesis several novel higher-order shear deformation theories are implemented using the Principle of Virtual Displacements under Carrera's Unified Formulation, all based on an assumed displacement field. They are here categorized based on the expansion of the displacement in the $x-$ direction:

- Higher-order (polynomial) shear deformation theories

- Sinusoidal shear deformation theories

- Hyperbolic sine shear deformation theories

Higher-order (polynomial) shear deformation theories:

In-plane displacements are considered to be cubic across the thickness coordinate. The transverse displacement may be defined as constant if warping is not allowed, or as parabolic in the thickness direction if warping is allowed.

$$\begin{cases} u = u_0 + zu_1 + z^3u_3 \\ v = v_0 + zv_1 + z^3v_3 \\ w = w_0 + zw_1 + z^2w_2 \end{cases} \tag{1.57}$$

Here and in the following $u = u(x, y, z, t)$, $v = v(x, y, z, t)$, and $w = w(x, y, z, t)$ are the displacements in the $x-$, $y-$, and $z-$ directions, respectively. $u_i = u(x, y, t)$ and $v_i = v_i(x, y, t)$, with $i = 0, 1, 3$, and $w_i = w_i(x, y, t)$, with $i = 0, 1, 2$, are functions to be determined.

$$\begin{cases} u = u_0 + zu_1 + z^3u_3 \\ v = v_0 + zv_1 + z^3v_3 \\ w = w_0 \end{cases} \tag{1.58}$$

Sinusoidal shear deformation theories:

The use of trigonometric shear deformation theories accounting for thickness-stretching or the zig-zag effects for the analysis of plates has not been performed before. In this thesis quasi-3D sinusoidal shear deformation theories are introduced. In-plane displacements are considered to be of sinusoidal type across the thickness coordinate and may include or not the terms to account for the zig-zag effect. The transverse displacement may be defined as constant if warping is not allowed, or as parabolic in the thickness direction if warping is allowed.

$$\begin{cases} u = u_0 + z u_1 + \sin\left(\frac{\pi z}{h}\right) u_s \\ v = v_0 + z v_1 + \sin\left(\frac{\pi z}{h}\right) v_s \\ w = w_0 + z w_1 + z^2 w_2 \end{cases} \tag{1.59}$$

$$\begin{cases} u = u_0 + z u_1 + \sin\left(\frac{\pi z}{h}\right) u_s \\ v = v_0 + z v_1 + \sin\left(\frac{\pi z}{h}\right) v_s \\ w = w_0 \end{cases} \tag{1.60}$$

$$\begin{cases} u = u_0 + z u_1 + \sin\left(\frac{\pi z}{h}\right) u_s + (-1)^k \frac{2}{h_k}\left(z - \frac{1}{2}\left(z_k + z_{k+1}\right)\right) u_Z \\ v = v_0 + z v_1 + \sin\left(\frac{\pi z}{h}\right) v_s + (-1)^k \frac{2}{h_k}\left(z - \frac{1}{2}\left(z_k + z_{k+1}\right)\right) v_Z \\ w = w_0 + z w_1 + z^2 w_2 \end{cases} \tag{1.61}$$

$$\begin{cases} u = u_0 + zu_1 + \sin\left(\frac{\pi z}{h}\right) u_s + (-1)^k \frac{2}{h_k} \left(z - \frac{1}{2}\left(z_k + z_{k+1}\right)\right) u_Z \\ v = v_0 + zv_1 + \sin\left(\frac{\pi z}{h}\right) v_s + (-1)^k \frac{2}{h_k} \left(z - \frac{1}{2}\left(z_k + z_{k+1}\right)\right) v_Z \\ w = w_0 \end{cases} \tag{1.62}$$

Hyperbolic sine shear deformation theories:

In all previous investigations with hyperbolic functions, the transverse displacement is considered as constant resulting in shear deformation theories that neglect the thickness stretching ($\epsilon_{zz} = 0$) and the zig-zag effect is not taken in account. In the present thesis new hyperbolic sine theories accounting for thickness stretching and zig-zag effects are introduced for the analysis of functionally graded plates.

$$\begin{cases} u = u_0 + zu_1 + \sinh\left(\frac{\pi z}{h}\right) u_Z \\ v = v_0 + zv_1 + \sinh\left(\frac{\pi z}{h}\right) v_Z \\ w = w_0 + zw_1 + z^2 w_2 \end{cases} \tag{1.63}$$

$$\begin{cases} u = u_0 + zu_1 + \sinh\left(\frac{\pi z}{h}\right) u_Z \\ v = v_0 + zv_1 + \sinh\left(\frac{\pi z}{h}\right) v_Z \\ w = w_0 \end{cases} \tag{1.64}$$

$$\begin{cases} u = u_0 + zu_1 + sinh\left(\frac{\pi z}{h}\right) u_3 + (-1)^k \frac{2}{h_k} \left(z - \frac{1}{2}\left(z_k + z_{k+1}\right)\right) u_Z \\ v = v_0 + zv_1 + sinh\left(\frac{\pi z}{h}\right) v_3 + (-1)^k \frac{2}{h_k} \left(z - \frac{1}{2}\left(z_k + z_{k+1}\right)\right) v_Z \\ w = w_0 + zw_1 + z^2 w_2 \end{cases} \tag{1.65}$$

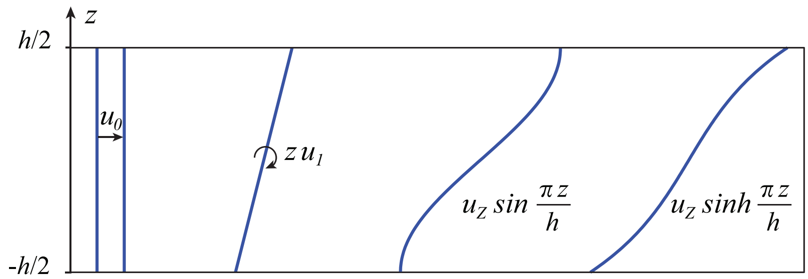

Figure 1.8: Scheme of the expansions involved in the displacement fields.

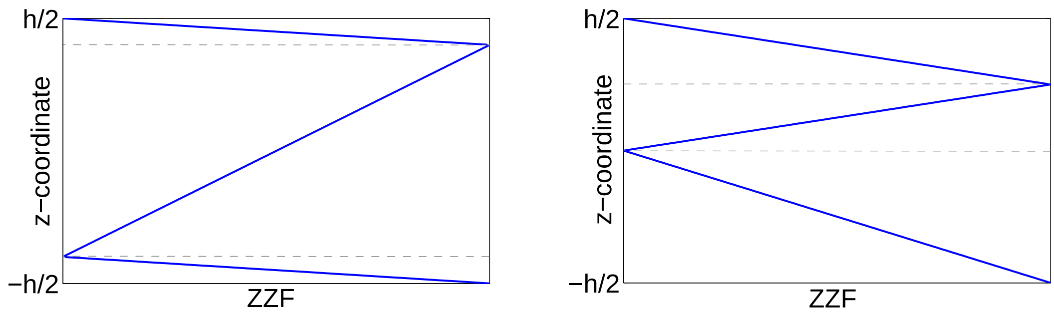

Figure 1.9: Zig-zag effect for two different sandwich configurations.

$$\begin{cases} u = u_0 + zu_1 + sinh\left(\frac{\pi z}{h}\right) u_3 + (-1)^k \frac{2}{h_k}\left(z - \frac{1}{2}\left(z_k + z_{k+1}\right)\right) u_Z \\ v = v_0 + zv_1 + sinh\left(\frac{\pi z}{h}\right) v_3 + (-1)^k \frac{2}{h_k}\left(z - \frac{1}{2}\left(z_k + z_{k+1}\right)\right) v_Z \\ w = w_0 \end{cases} \tag{1.66}$$

In (1.57) to (1.66) the unknowns are u_i, v_i, and w_i (where i can take the values $i = 0, 1, 2, 3, Z$ depending on the shear deformation theory). The expansion of the degrees of freedom u_0, u_1, u_3, v_0, v_1, v_3, w_0, w_1, and w_2 are functions of the thickness coordinate only as well as the u_Z and v_Z that comes with the sinusoidal or the hyperbolic sine expansion. These are layer-independent, unlike those of u_Z and v_Z associated to the $(-1)^k$ expansion, as illustrated in figures 1.8 and 1.9. These last terms introduce the zig-zag effect and can be seen in this context as a generalization of the Murakami's original work [91]. Figure 1.8 shows the meaning of the unknowns in the in-plane displacements expansion in present theories: u_0, v_0 are translations; u_1, v_1, u_3, and v_3 are rotations. In figure 1.9 one can visualize that this zig-zag function corresponds to a rotation per layer.

theory	considers zig-zag effect	allows thichness-stretching	requires shear correction factor
z^3 (1.57)	no	yes	no
$z^3 0$ (1.58)	no	no	no
sinus (1.59)	no	yes	no
sinus0 (1.60)	no	no	no
sinusZZ (1.61)	yes	yes	no
sinusZZ0 (1.62)	yes	no	no
sinh (1.63)	no	yes	no
sinh0 (1.64)	no	no	no
sinhZZ (1.65)	yes	yes	no
sinhZZ0 (1.66)	yes	no	no

Table 1.4: Overview on the present theories.

Table 1.4 presents an overview on the characteristics of the new theories implemented in present thesis. They all require no shear correction factors and the higher-order terms are odd functions. Some theories allow thickness-stretching by considering a parabolic expansion for the out-of-plane displacement, and some consider the zig-zag effect. Studies on the influence of the warping effect in the thickness direction and the zig-zag effects were carried out with this theories.

1.4.3 Functionally graded materials

Functionally graded (FG) materials (FGM) are a class of composite materials that were first proposed in 1972 by Bever and colleagues [92, 93] but investigation on such materials started only in the 1980s. In a typical FGM plate the material properties continuously vary over the thickness direction by mixing two different materials [94]. The computational modelling of FGM is an important tool to the understanding of the structures behavior, and has been the target of intense research [94, 95, 96, 97, 98, 99, 100].

The concept of functionally graded materials (FGM) was introduced to satisfy the demand of ultra-high-temperature environment and to eliminate the stress singularities [101]. Due to the continuous change in material properties of an FGM, the interfaces between two materials disappear but the characteristics of two or more different materials of the composite are preserved. Interested readers on FGM application fields

Figure 1.10: Isotropic FGM plate.

can refer to [100] or [94]. A review of the main developments in FGM can be found in Birman and Byrd [99].

In a conventional FGM plate a continuous variation of material properties over the thickness direction is obtained by mixing two different materials [94]. The material properties of the FGM plate are assumed to change continuously throughout the thickness of the plate, according to the volume fraction of the constituent materials.

Functionally graded materials (FGM) are a class of composites in which the properties of the material gradually change over one or more cartesian direction. A typical FGM plate considers a continuous variation of material properties over the thickness direction by mixing two different materials [94]. The gradual variation of properties avoids the delamination failure that are common in laminated composites. The FGM concept has applications in several fields such as aerospace and civil [94].

Three different types of functionally graded plates are studied in this thesis:

- isotropic FGM plates and shells;
- sandwich plates with FGM core;
- sandwich plates with FGM skins.

The isotropic FGM plate or shell is graded from metal (bottom) to ceramic (top) (see figure 1.10).

Figure 1.11: Sandwich plate with FGM core and isotropic skins.

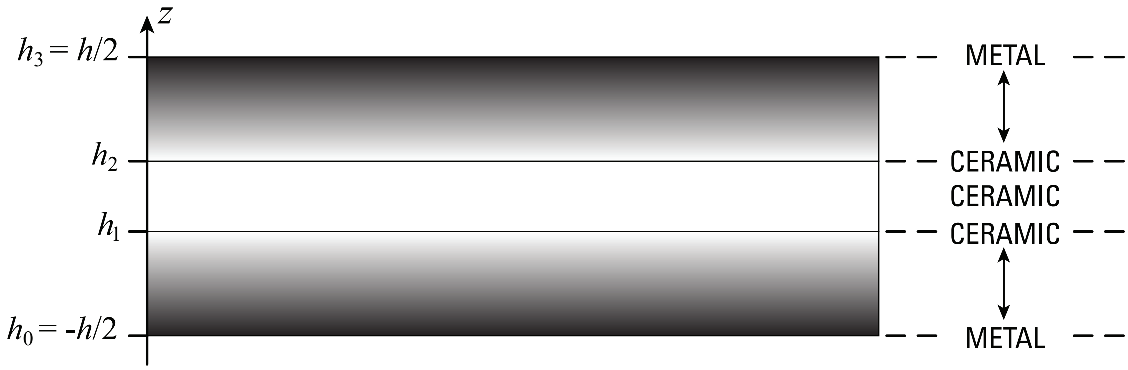

Figure 1.12: Sandwich plate with isotropic core and FGM skins.

In a sandwich plate with FGM core, the bottom skin is isotropic (fully metal) and the top skin is isotropic (fully ceramic). The core layer is graded from metal to ceramic so that there are no interfaces between core and skins, as illustrated in figure 1.11.

In sandwich plates with FGM skins, the core is isotropic (fully ceramic) and skins are composed of a functionally graded material across the thickness direction. The bottom skin varies from a metal-rich surface ($z = -h/2$) to a ceramic-rich surface while the top skin face varies from a ceramic-rich surface to a metal-rich surface ($z = h/2$), as illustrated in figure 1.12. There are no interfaces between core and skins.

A conventional FG plate considers a continuous variation of material properties over the thickness direction by mixing two different materials [94]. The material properties of the FG plate are assumed to change continuously throughout the thickness of the plate, according to the volume fraction of the constituent materials. Although one can use CUF for one-layer, isotropic plate, we consider a multi-layered plate. In fact, the sandwiches in study present 3 physical layers, $kp = 1, 2, 3$, and depending on the considered theory may have different displacement fields. Nevertheless, we are dealing with functionally graded materials and becomes mandatory to model the continuos variation of properties across the thickness direction. A considerable number of layers is needed for both isotropic FG and FG sandwich plates or shells to ensure correct computation of material properties at each thickness position, and for that reason we consider $N_l = 91$ virtual (mathematical) layers of constant thickness. In the following, kp refers to physical layers and $k = 1, ..., 91$ refers to virtual layers.

The CUF procedure applied to FG materials starts by evaluating the volume fraction of the two constituents for each layer. To describe the volume fractions an exponential function can be used as in [102], or the sigmoid function as proposed in [103]. In the present work a power-law function is used as most researchers do [104] [105, 106, 83]. In the typical FG plate the power-law function defines the volume fraction of the constituints as:

$$\begin{cases} V_c = \left(0.5 + \frac{z}{h}\right)^p; & \text{for the ceramic phase} \\ V_m = 1 - V_c & \text{for the metal phase} \end{cases} \tag{1.67}$$

where $z \in [-h/2, h/2]$, h is the thickness of the plate, and p is a scalar parameter that allows the user to define gradation of material properties across the thickness direction. The volume fraction of the constituints are computed for each layer

$$\begin{cases} V_c^k = \left(0.5 + \frac{\tilde{z}}{h}\right)^p; & \text{for the ceramic phase} \\ V_m^k = 1 - V_c^k & \text{for the metal phase} \end{cases} \tag{1.68}$$

where $\tilde{z}$ is the thickness coordinate of a point of each (virtual) layer. In the sandwich plate with functionally graded core or skins, the volume fraction of the ceramic phase of the FG layers are obtained by adapting the typical power-law. Furthermore, for both FG sandwich plates, one needs to compute the volume fraction for each layer. In the case of the sandwich plate with FG skins one has:

$$\begin{cases} V_c^k = \left(\frac{\tilde{z}-h_0}{h_1-h_0}\right)^p, \quad z \in [h_0, h_1] \\ V_c^k = 1, \quad z \in [h_1, h_2] \\ V_c^k = \left(\frac{\tilde{z}-h_3}{h_2-h_3}\right)^p, \quad z \in [h_2, h_3] \end{cases} \tag{1.69}$$

where $\tilde{z}$ is the thickness coordinate of a point of each (virtual) skin layer, h_0, h_1, h_2, and h_3 are the z-coordinates of the interfaces of the layers as visualized in figure 1.12, and $p \geq 0$ is a scalar parameter that allows the user to define gradation of material properties across the thickness direction of the skins.

Once having the volume fraction of each constituent, a homogenization procedure is employed to find the values of the modulus of elasticity, E^k, and Poisson's ratio, ν^k, of each layer. A possible homogenization technique is the Mori-Tanaka one [107, 108], and other possibility is the law-of-mixtures.

The law-of-mixtures states that:

$$E^k(z) = E_m V_m^k + E_c V_c^k; \qquad \nu^k(z) = \nu_m V_m^k + \nu_c V_c^k \tag{1.70}$$

The Mori-Tanaka homogenization procedure [107, 108] starts by finding the bulk modulus, K, and the effective shear modulus, G, of the composite equivalent layer as

$$\frac{K - K_m}{K_c - K_m} = \frac{V_c}{1 + V_m \frac{K_c - K_m}{K_m + 4/3 G_m}}; \quad \frac{G - G_m}{G_c - G_m} = \frac{V_c}{1 + V_m \frac{G_c - G_m}{G_m + f_m}} \tag{1.71}$$

where

$$f_m = \frac{G_m(9K_m + 8G_m)}{6(K_m + 2G_m)} \tag{1.72}$$

The effective values of Young's modulus, E^k, and Poisson's ratio, ν^k, are then found from

$$E^k = \frac{9KG}{3K+G}; \quad \nu^k = \frac{3K-2G}{2(3K+G)} \tag{1.73}$$

1.4.4 Displacements

According to the Unified Formulation by Carrera, the three displacement components u_x, $u_y(=v)$ and $u_z(=w)$ and their relative variations are modeled as:

$$(u_x, u_y, u_z) = F_\tau \; (u_{x\tau}, u_{y\tau}, u_{z\tau}) \qquad (\delta u_x, \delta u_y, \delta u_z) = F_s \; (\delta u_{xs}, \delta u_{ys}, \delta u_{zs}) \tag{1.74}$$

The vectors are chosen by resorting to the displacement field. For example, when considering the displacement field in (1.59), the thickness functions are as follows

$$\begin{cases} F_{sux} = F_{suy} = F_{\tau ux} = F_{\tau uy} = \left[1 \quad z \quad \sin\left(\frac{\pi z}{h}\right)\right] \\ F_{suz} = F_{\tau uz} = [1 \quad z \quad z^2] \end{cases} \tag{1.75}$$

and for displacement field in (1.66) are

$$\begin{cases} F_{sux} = F_{suy} = F_{\tau ux} = F_{\tau uy} = \left[1 \quad z \quad \sinh\left(\frac{\pi z}{h}\right) \quad (-1)^{kp} \frac{2}{h_{kp}} \left(z - \frac{1}{2}\left(z_{kp} + z_{kp+1}\right)\right)\right] \\ F_{suz} = F_{\tau uz} = [1] \end{cases} \tag{1.76}$$

Combining CUF and global collocation with RBFs allowed to implement a new theory just by changing this vectors. We then automatically obtained the governing equations and boundary conditions in terms of displacements of the chosen theory and the analysis of the plate or shell behaviour based on that theory.

1.4.5 Plates

Strains

Strains are separated into in-plane and normal components, denoted respectively by the subscripts p and n.

The geometrical relations (G) between the mechanical strains in the kth layer and the displacement field $\mathbf{u}^k = \{u_x^k, u_y^k, u_z^k\}$ depend on the option of considering or not the warping in thickness direction.

If warping is allowed (i.e., $\epsilon_{zz} \neq 0$), G can be stated as follows:

$$\epsilon_{pG}^k = [\epsilon_{xx}, \epsilon_{yy}, \gamma_{xy}]^{kT} = \mathbf{D}_p^{k(nl)} \mathbf{u}^k \ , \tag{1.77}$$

$$\epsilon_{nG}^k = [\gamma_{xz}, \gamma_{yz}, \epsilon_{zz}]^{kT} = (\mathbf{D}_{np}^k + \mathbf{D}_{nz}^k)\ \mathbf{u}^k \ ,$$

wherein the differential operator arrays are defined as follows:

$$\mathbf{D}_p^{k(nl)} = \begin{bmatrix} \partial_x & 0 & \partial_x^2/2 \\ 0 & \partial_y & \partial_y^2/2 \\ \partial_y & \partial_x & \partial_x \partial_y \end{bmatrix} , \quad \mathbf{D}_{np}^k = \begin{bmatrix} 0 & 0 & \partial_x \\ 0 & 0 & \partial_y \\ 0 & 0 & 0 \end{bmatrix} , \quad \mathbf{D}_{nz}^k = \begin{bmatrix} \partial_z & 0 & 0 \\ 0 & \partial_z & 0 \\ 0 & 0 & \partial_z \end{bmatrix} , \tag{1.78}$$

Although one needs to account for the nonliner contributions for the buckling analysis, we can use the linear version of CUF as the non-linear terms will only influence the equation refering to δw_0. In fact, the compressive in-plane forces and distributed shear forces only actuate on the mid-plane ($z = 0$) and the nonlinear terms are reduced to $\frac{1}{2}\left(\frac{\partial w_0}{\partial x}\right)^2$, $\frac{1}{2}\left(\frac{\partial w_0}{\partial y}\right)^2$, and $\frac{\partial w_0}{\partial x}\frac{\partial w_0}{\partial y}$.

Irrespective of the nature of the problem (static, free vibration or buckling) when warping is allowed we use

$$\mathbf{D}_p^k = \begin{bmatrix} \partial_x & 0 & 0 \\ 0 & \partial_y & 0 \\ \partial_y & \partial_x & 0 \end{bmatrix} \tag{1.79}$$

instead of $\mathbf{D}_p^{k(nl)}$ and just add the terms in referred equation.

When warping is not allowed (i.e. $\epsilon_{zz} = 0$), ϵ_{pG}^k and the differential operator array $\mathbf{D}_p^k$ remain as before, but the other strains are reduced to

$$\epsilon_{nG}^k = [\gamma_{xz}, \gamma_{yz}]^{kT} = (\mathbf{D}_{np}^k + \mathbf{D}_{nz}^k)\ \mathbf{u}^k\ , \tag{1.80}$$

wherein the differential operator arrays are defined as:

$$\mathbf{D}_{np}^k = \begin{bmatrix} 0 & 0 & \partial_x \\ 0 & 0 & \partial_y \end{bmatrix}\ , \quad \mathbf{D}_{nz}^k = \begin{bmatrix} \partial_z & 0 & 0 \\ 0 & \partial_z & 0 \end{bmatrix}\ , \tag{1.81}$$

Elastic stress-strain relations

To define the constitutive equations (C), stresses are separated into in-plane and normal components as well. The elastic stress-strain relations depend on which assumption of ϵ_{zz} we consider.

For the $\epsilon_{zz} \neq 0$ case, the 3D constitutive equations are used:

$$\begin{aligned} \sigma^k_{pC} &= [\sigma_{xx}, \sigma_{yy}, \sigma_{xy}]^{kT} = \mathbf{C}^k_{pp}\, \epsilon^k_{pG} + \mathbf{C}^k_{pn}\, \epsilon^k_{nG} \\ \sigma^k_{nC} &= [\sigma_{xz}, \sigma_{yz}, \sigma_{zz}]^{kT} = \mathbf{C}^k_{np}\, \epsilon^k_{pG} + \mathbf{C}^k_{nn}\, \epsilon^k_{nG} \end{aligned} \tag{1.82}$$

with

$$\begin{aligned} \mathbf{C}^k_{pp} &= \begin{bmatrix} C^k_{11} & C^k_{12} & 0 \\ C^k_{12} & C^k_{11} & 0 \\ 0 & 0 & C^k_{44} \end{bmatrix} \qquad \mathbf{C}^k_{pn} = \begin{bmatrix} 0 & 0 & C^k_{12} \\ 0 & 0 & C^k_{12} \\ 0 & 0 & 0 \end{bmatrix} \\ \mathbf{C}^k_{np} &= \begin{bmatrix} 0 & 0 & 0 \\ 0 & 0 & 0 \\ C^k_{12} & C^k_{12} & 0 \end{bmatrix} \qquad \mathbf{C}^k_{nn} = \begin{bmatrix} C^k_{44} & 0 & 0 \\ 0 & C^k_{44} & 0 \\ 0 & 0 & C^k_{11} \end{bmatrix} \end{aligned} \tag{1.83}$$

and the C^k_{ij} are the three-dimensional elastic constants

$$C^k_{11} = \frac{E^k(1-(\nu^k)^2)}{1-3(\nu^k)^2-2(\nu^k)^3}; \quad C^k_{12} = \frac{E^k(\nu^k+(\nu^k)^2)}{1-3(\nu^k)^2-2(\nu^k)^3}; \quad C^k_{44} = \frac{E^k}{2(1+\nu^k)} \tag{1.84}$$

where the modulus of elasticity and Poisson's ratio were defined in (1.70) or (1.73).

For the $\epsilon_{zz} = 0$ case, the plane-stress case is used:

$$\begin{aligned} \sigma^k_{pC} &= [\sigma_{xx}, \sigma_{yy}, \sigma_{xy}]^{kT} = \mathbf{C}^k_{pp}\, \epsilon^k_{pG} \\ \sigma^k_{nC} &= [\sigma_{xz}, \sigma_{yz}]^{kT} = \mathbf{C}^k_{nn}\, \epsilon^k_{nG} \end{aligned} \tag{1.85}$$

with $\mathbf{C}^k_{pp}$ and ϵ^k_{pG} as before, $\epsilon^k_{nG} = [\gamma_{xz}, \gamma_{yz}]^{kT}$ and

$$\mathbf{C}^k_{nn} = \begin{bmatrix} C^k_{44} & 0 \\ 0 & C^k_{44} \end{bmatrix} \tag{1.86}$$

and C_{ij}^k are the plane-stress reduced elastic constants:

$$C_{11}^k = \frac{E^k}{1-(\nu^k)^2}; \quad C_{12}^k = \nu^k \frac{E^k}{1-(\nu^k)^2}; \quad C_{44}^k = \frac{E^k}{2(1+\nu^k)} \tag{1.87}$$

Principle of virtual displacements

In the framework of the Unified Formulation, the Principle of Virtual Displacements (PVD) for the pure-mechanical case is written as:

$$\sum_{k=1}^{N_l} \int_{\Omega_k} \int_{A_k} \left\{ \delta\epsilon_{pG}^{k\ T} \sigma_{pC}^k + \delta\epsilon_{nG}^{k\ T} \sigma_{nC}^k \right\} d\Omega_k dz = \sum_{k=1}^{N_l} \delta L_e^k \tag{1.88}$$

where Ω_k and A_k are the integration domains in plane (x,y) and z direction, respectively. As stated before, G means geometrical relations and C constitutive equations, and k indicates the virtual layer. T is the transpose operator and δL_e^k is the external work for the kth layer.

Substituting the geometrical relations (G), the constitutive equations (C), and the modeled displacement field (F_τ and F_s), all for the kth layer, (1.88) becomes:

$$\begin{aligned} \int_{\Omega_k} \int_{A_k} \Big[& (\mathbf{D}_p^k\ F_s \delta \mathbf{u}_s^k)^T (\mathbf{C}_{pp}^k \mathbf{D}_p^k\ F_\tau \mathbf{u}_\tau^k + \mathbf{C}_{pn}^k (\mathbf{D}_{n\Omega}^k + \mathbf{D}_{nz}^k) F_\tau \mathbf{u}_\tau^k) \\ & + ((\mathbf{D}_{n\Omega}^k + \mathbf{D}_{nz}^k) F_s \delta \mathbf{u}_s^k)^T (\mathbf{C}_{np}^k \mathbf{D}_p^k\ F_\tau \mathbf{u}_\tau^k + \mathbf{C}_{nn}^k (\mathbf{D}_{n\Omega}^k + \mathbf{D}_{nz}^k) F_\tau \mathbf{u}_\tau^k) \Big] d\Omega_k dz = \delta L_e^k \end{aligned} \tag{1.89}$$

At this point, the formula of integration by parts is applied:

$$\int_{\Omega_k} \left((\mathbf{D}_\Omega) \delta \mathbf{a}^k \right)^T \mathbf{a}^k d\Omega_k = -\int_{\Omega_k} \delta \mathbf{a}^{k^T} \left((\mathbf{D}_\Omega^T) \mathbf{a}^k \right) d\Omega_k + \int_{\Gamma_k} \delta \mathbf{a}^{k^T} \left((\mathbf{I}_\Omega) \mathbf{a}^k \right) d\Gamma_k \tag{1.90}$$

where $\mathbf{I}_\Omega$ matrix is obtained applying the *Gradient theorem*:

$$\int_\Omega \frac{\partial \psi}{\partial x_i} dv = \oint_\Gamma n_i \psi ds \tag{1.91}$$

being n_i the components of the normal $\widehat{n}$ to the boundary along the direction i. After integration by parts, the governing equations and boundary conditions for the plate in the mechanical case are obtained:

$$\begin{aligned}
&\int_{\Omega_k}\int_{A_k} (\delta \mathbf{u}_s^k)^T \Big[\Big(\big(-\mathbf{D}_p^k \big)^T \big(\mathbf{C}_{pp}^k (\mathbf{D}_p^k) + \mathbf{C}_{pn}^k (\mathbf{D}_{n\Omega}^k + \mathbf{D}_{nz}^k \big) \\
&+ \big(-\mathbf{D}_{n\Omega}^k + \mathbf{D}_{nz}^k \big)^T \big(\mathbf{C}_{np}^k (\mathbf{D}_p^k) + \mathbf{C}_{nn}^k (\mathbf{D}_{n\Omega}^k + \mathbf{D}_{nz}^k)\big)\Big) \mathbf{F}_\tau \mathbf{F}_s \mathbf{u}_\tau^k \Big] dxdydz \\
&+ \int_{\Omega_k}\int_{A_k} (\delta \mathbf{u}_s^k)^T \Big[\Big(\mathbf{I}_p^{kT} \big(\mathbf{C}_{pp}^k (\mathbf{D}_p^k) + \mathbf{C}_{pn}^k (\mathbf{D}_{n\Omega}^k + \mathbf{D}_{nz}^k)\big) \\
&+ \mathbf{I}_{np}^{kT} \big(\mathbf{C}_{np}^k (\mathbf{D}_p^k) + \mathbf{C}_{nn}^k (\mathbf{D}_{n\Omega}^k + \mathbf{D}_{nz}^k)\big)\Big) \mathbf{F}_\tau \mathbf{F}_s \mathbf{u}_\tau^k \Big] dxdydz = \int_{\Omega_k} \delta \mathbf{u}_s^{kT} F_s \mathbf{p}_u^k d\Omega_k \ .
\end{aligned} \tag{1.92}$$

where $\mathbf{I}_p^k$ and $\mathbf{I}_{np}^k$ depend on the boundary geometry:

$$\mathbf{I}_p^k = \begin{bmatrix} n_x & 0 & 0 \\ 0 & n_y & 0 \\ n_y & n_x & 0 \end{bmatrix}, \quad \mathbf{I}_{np}^k = \begin{bmatrix} 0 & 0 & n_x \\ 0 & 0 & n_y \\ 0 & 0 & 0 \end{bmatrix}. \tag{1.93}$$

The normal to the boundary of domain Ω is:

$$\widehat{\mathbf{n}} = \begin{bmatrix} n_x \\ n_y \end{bmatrix} = \begin{bmatrix} cos(\varphi_x) \\ cos(\varphi_y) \end{bmatrix} \tag{1.94}$$

where φ_x and φ_y are the angles between the normal $\widehat{n}$ and the direction x and y respectively.

Governing equations and boundary conditions

The governing equations for a multi-layered plate subjected to mechanical loadings are:

$$\delta \mathbf{u}_s^{kT} : \qquad \mathbf{K}_{uu}^{k\tau s}\, \mathbf{u}_\tau^k \;=\; \mathbf{P}_{u\tau}^k \tag{1.95}$$

where the fundamental nucleus $\mathbf{K}_{uu}^{k\tau s}$ is obtained as:

$$\begin{aligned}\mathbf{K}_{uu}^{k\tau s} = &\Big[\big(-\mathbf{D}_p^k\big)^T\big(\mathbf{C}_{pp}^k(\mathbf{D}_p^k)\ + \mathbf{C}_{pn}^k(\mathbf{D}_{n\Omega}^k + \mathbf{D}_{nz}^k\big)\\ &+ \big(-\mathbf{D}_{n\Omega}^k + \mathbf{D}_{nz}^k\big)^T\big(\mathbf{C}_{np}^k(\mathbf{D}_p^k) + \mathbf{C}_{nn}^k(\mathbf{D}_{n\Omega}^k + \mathbf{D}_{nz}^k)\big)\Big]\mathbf{F}_\tau \mathbf{F}_s\end{aligned} \tag{1.96}$$

and the corresponding Neumann-type boundary conditions on Γ_k are:

$$\mathbf{\Pi}_d^{k\tau s}\, \mathbf{u}_\tau^k \;=\; \mathbf{\Pi}_d^{k\tau s}\, \bar{\mathbf{u}}_\tau^k\ , \tag{1.97}$$

where:

$$\begin{aligned}\mathbf{\Pi}_d^{k\tau s} = &\Big[\mathbf{I}_p^{kT}\big(\mathbf{C}_{pp}^k(\mathbf{D}_p^k)\ + \mathbf{C}_{pn}^k(\mathbf{D}_{n\Omega}^k + \mathbf{D}_{nz}^k)\big) +\\ &\mathbf{I}_{np}^{kT}\big(\mathbf{C}_{np}^k(\mathbf{D}_p^k)\ + \mathbf{C}_{nn}^k(\mathbf{D}_{n\Omega}^k + \mathbf{D}_{nz}^k)\big)\Big]\mathbf{F}_\tau \mathbf{F}_s\end{aligned} \tag{1.98}$$

and $\mathbf{P}_{u\tau}^k$ are variationally consistent loads with applied pressure.

Fundamental nuclei

For FG materials, the fundamental nuclei in explicit form becomes:

$$
\begin{aligned}
K^{k\tau s}_{uu_{11}} =& (-\partial^{\tau}_{x}\partial^{s}_{x}C_{11} + \partial^{\tau}_{z}\partial^{s}_{z}C_{55} - \partial^{\tau}_{y}\partial^{s}_{y}C_{66})F_{\tau}F_{s} \\
K^{k\tau s}_{uu_{12}} =& (-\partial^{\tau}_{x}\partial^{s}_{y}C_{12} - \partial^{\tau}_{y}\partial^{s}_{x}C_{66})F_{\tau}F_{s} \\
K^{k\tau s}_{uu_{13}} =& (-\partial^{\tau}_{x}\partial^{s}_{z}C_{13} + \partial^{\tau}_{z}\partial^{s}_{x}C_{55})F_{\tau}F_{s} \\
K^{k\tau s}_{uu_{21}} =& (-\partial^{\tau}_{y}\partial^{s}_{x}C_{12} - \partial^{\tau}_{x}\partial^{s}_{y}C_{66})F_{\tau}F_{s} \\
K^{k\tau s}_{uu_{22}} =& (-\partial^{\tau}_{y}\partial^{s}_{y}C_{22} + \partial^{\tau}_{z}\partial^{s}_{z}C_{44} - \partial^{\tau}_{x}\partial^{s}_{x}C_{66})F_{\tau}F_{s} \qquad (1.99) \\
K^{k\tau s}_{uu_{23}} =& (-\partial^{\tau}_{y}\partial^{s}_{z}C_{23} + \partial^{\tau}_{z}\partial^{s}_{y}C_{44})F_{\tau}F_{s} \\
K^{k\tau s}_{uu_{31}} =& (\partial^{\tau}_{z}\partial^{s}_{x}C_{13} - \partial^{\tau}_{x}\partial^{s}_{z}C_{55})F_{\tau}F_{s} \\
K^{k\tau s}_{uu_{32}} =& (\partial^{\tau}_{z}\partial^{s}_{y}C_{23} - \partial^{\tau}_{y}\partial^{s}_{z}C_{44})F_{\tau}F_{s} \\
K^{k\tau s}_{uu_{33}} =& (\partial^{\tau}_{z}\partial^{s}_{z}C_{33} - \partial^{\tau}_{y}\partial^{s}_{y}C_{44} - \partial^{\tau}_{x}\partial^{s}_{x}C_{55})F_{\tau}F_{s}
\end{aligned}
$$

$$
\begin{aligned}
\Pi_{11}^{k\tau s} =&(n_x\partial_x^s C_{11} + n_y\partial_y^s C_{66})F_\tau F_s \\
\Pi_{12}^{k\tau s} =&(n_x\partial_y^s C_{12} + n_y\partial_x^s C_{66})F_\tau F_s \\
\Pi_{13}^{k\tau s} =&(n_x\partial_z^s C_{13})F_\tau F_s \\
\Pi_{21}^{k\tau s} =&(n_y\partial_x^s C_{12} + n_x\partial_y^s C_{66})F_\tau F_s \\
\Pi_{22}^{k\tau s} =&(n_y\partial_y^s C_{22} + n_x\partial_x^s C_{66})F_\tau F_s \\
\Pi_{23}^{k\tau s} =&(n_y\partial_z^s C_{23})F_\tau F_s \\
\Pi_{31}^{k\tau s} =&(n_x\partial_z^s C_{55})F_\tau F_s \\
\Pi_{32}^{k\tau s} =&(n_y\partial_z^s C_{44})F_\tau F_s \\
\Pi_{33}^{k\tau s} =&(n_y\partial_y^s C_{44} + n_x\partial_x^s C_{55})F_\tau F_s
\end{aligned}
\tag{1.100}
$$

Dynamic governing equations

In the framework of the Unified Formulation, the PVD for the dynamic case reads:

$$
\sum_{k=1}^{N_l}\int_{\Omega_k}\int_{A_k}\left\{\delta\boldsymbol{\epsilon}_{pG}^{k}{}^{T}\boldsymbol{\sigma}_{pC}^{k} + \delta\boldsymbol{\epsilon}_{nG}^{k}{}^{T}\boldsymbol{\sigma}_{nC}^{k}\right\}d\Omega_k dz = \sum_{k=1}^{N_l}\int_{\Omega_k}\int_{A_k}\rho^k\delta\boldsymbol{u}^{kT}\ddot{\boldsymbol{u}}^k d\Omega_k dz + \sum_{k=1}^{N_l}\delta L_e^k
\tag{1.101}
$$

where ρ^k is the mass density of the k-th layer and double dots denote acceleration. The remainings are as in (1.88).

As for the static case, we obtain the following governing equations:

$$\delta \boldsymbol{u}_s^{k^T} : \qquad \boldsymbol{K}_{uu}^{k\tau s}\, \boldsymbol{u}_\tau^k = \boldsymbol{M}^{k\tau s} \ddot{\boldsymbol{u}}_\tau^k + \boldsymbol{P}_{u\tau}^k \tag{1.102}$$

where $\boldsymbol{M}^{k\tau s}$ is the fundamental nucleus for the inertial term with explicit form as:

$$\begin{cases} M_{ij}^{k\tau s} = & \rho^k F_\tau F_s \quad \text{for } i = j \\ M_{ij}^{k\tau s} = & 0 \quad \text{for } i \neq j \end{cases} \tag{1.103}$$

The geometrical and mechanical boundary conditions are the same of the static case.

Governing equations and boundary conditions in terms of displacements

In order to discretize the governing equations by radial basis functions, we need the explicit terms of that equations and the corresponding boundary conditions as well in terms of the generalized displacements. The explicit governing equations and corresponding boundary conditions in terms of generalized displacements for the static, free vibration and buckling analysis of functionally graded plates of some theories can be found in papers presented in this thesis in 2.2, 2.3, 2.4, and 2.5. For the sake of completeness we present here the equation of the buckling problem of *sinus* theory (1.59) that corresponds to the w_0 variable for the buckling problems.

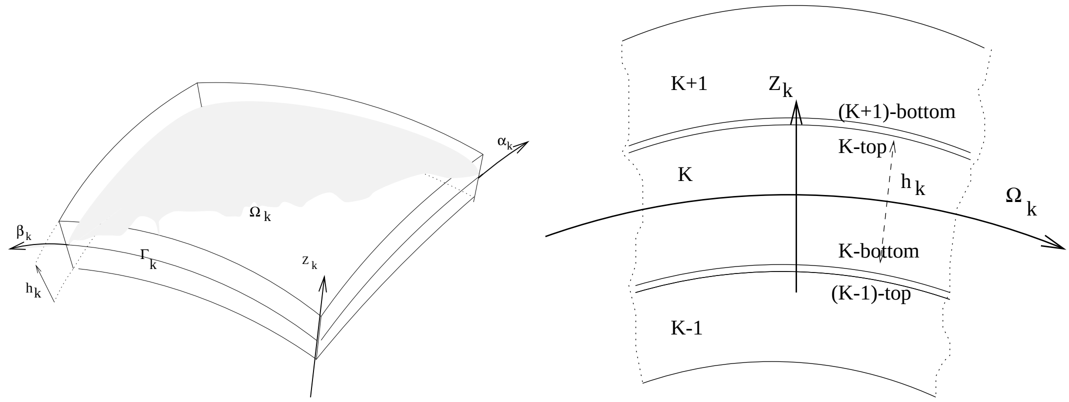

Figure 1.13: Geometry and notations for a multilayered shell (doubly curved).

$$
\begin{aligned}
\delta w_0 :& A_{13}\frac{\partial u_1}{\partial x} + 2B_{13}\frac{\partial u_Z}{\partial x} + A_{23}\frac{\partial v_1}{\partial y} + 2B_{23}\frac{\partial v_Z}{\partial y} - A_{55}\frac{\partial^2 w_0}{\partial x^2} - A_{44}\frac{\partial^2 w_0}{\partial y^2} \\
& - B_{55}\frac{\partial^2 w_1}{\partial x^2} - B_{44}\frac{\partial^2 w_1}{\partial y^2} - D_{55}\frac{\partial^2 w_Z}{\partial x^2} - D_{44}\frac{\partial^2 w_Z}{\partial y^2} \\
& + \bar{N}_{xx}\frac{\partial^2 w_0}{\partial x^2} + 2\bar{N}_{xy}\frac{\partial^2 w_0}{\partial x \partial y} + \bar{N}_{yy}\frac{\partial^2 w_0}{\partial y^2} = 0
\end{aligned}
\tag{1.104}
$$

The stiffness components of this equation can be computed as follows:

$$
A_{ij} = \sum_{k=1}^{N_l} c_{ij}^k \left(z_{k+1} - z_k\right); \quad B_{ij} = \frac{1}{2}\sum_{k=1}^{N_l} c_{ij}^k \left(z_{k+1}^2 - z_k^2\right); \quad D_{ij} = \frac{1}{3}\sum_{k=1}^{N_l} c_{ij}^k \left(z_{k+1}^3 - z_k^3\right)
\tag{1.105}
$$

where N_l is the number of mathematical layers across the thickness direction, h_k is the thickness of each layer, and z_k, z_{k+1} are the lower and upper z coordinate for each layer k. $\bar{N}_{xx}$, $\bar{N}_{xy}$, and $\bar{N}_{yy}$ denote the in-plane applied loads.

1.4.6 Shells

The geometry and the reference system are indicated in Fig. (1.13).

The functionally graded shell is divided into a number (N_l) of uniform thickness (virtual) layers. The square of an infinitesimal linear segment in the k-th layer, the associated infinitesimal area and volume are given by:

$$
\begin{aligned}
ds_k^2 = &\quad H_\alpha^{k^2}\, d\alpha^2 \;+\; H_\beta^{k^2}\, d\beta^2 + H_z^{k^2}\, dz^2 \;, \\
d\Omega_k = &\quad H_\alpha^k H_\beta^k \, d\alpha \, d\beta \;, \\
dV_k = &\quad H_\alpha^k \; H_\beta^k \; H_z^k \; d\alpha \; d\beta \; dz \;,
\end{aligned}
\tag{1.106}
$$

where the metric coefficients are:

$$
H_\alpha^k = A^k(1 + z/R_\alpha^k), \quad H_\beta^k = B^k(1 + z/R_\beta^k), \quad H_z^k = 1 \; . \tag{1.107}
$$

k denotes the k-layer of the multilayered shell; R_α^k and R_β^k are the principal radii of curvature along the coordinates α and β respectively. A^k and B^k are the coefficients of the first fundamental form of Ω_k (Γ_k is the Ω_k boundary). In this work, the attention has been restricted to shells with constant radii of curvature (cylindrical, spherical, toroidal geometries) for which $A^k = B^k = 1$.

Strains

As for the plates, strains are separated into in-plane and normal components, denoted respectively by the subscripts p and n.

When considering stretching in the thickness direction the mechanical strains in the kth layer can be related to the displacement field $\boldsymbol{u}^k = \{u_\alpha^k, u_\beta^k, u_z^k\}$ via the geometrical relations:

$$
\epsilon_{pG}^k = [\epsilon_{\alpha\alpha}^k, \epsilon_{\beta\beta}^k, \epsilon_{\alpha\beta}^k]^T = (\boldsymbol{D}_p^k + \boldsymbol{A}_p^k) \; \boldsymbol{u}^k \;, \; \epsilon_{nG}^k = [\epsilon_{\alpha z}^k, \epsilon_{\beta z}^k, \epsilon_{zz}^k]^T = (\boldsymbol{D}_{n\Omega}^k + \boldsymbol{D}_{nz}^k - \boldsymbol{A}_n^k) \; \boldsymbol{u}^k
\tag{1.108}
$$

The explicit form of the introduced arrays follows:

$$\boldsymbol{D}_p^k = \begin{bmatrix} \frac{\partial_\alpha}{H_\alpha^k} & 0 & 0 \\ 0 & \frac{\partial_\beta}{H_\beta^k} & 0 \\ \frac{\partial_\beta}{H_\beta^k} & \frac{\partial_\alpha}{H_\alpha^k} & 0 \end{bmatrix}, \quad \boldsymbol{D}_{n\Omega}^k = \begin{bmatrix} 0 & 0 & \frac{\partial_\alpha}{H_\alpha^k} \\ 0 & 0 & \frac{\partial_\beta}{H_\beta^k} \\ 0 & 0 & 0 \end{bmatrix}, \quad \boldsymbol{D}_{nz}^k = \begin{bmatrix} \partial_z & 0 & 0 \\ 0 & \partial_z & 0 \\ 0 & 0 & \partial_z \end{bmatrix}, \tag{1.109}$$

$$\boldsymbol{A}_p^k = \begin{bmatrix} 0 & 0 & \frac{1}{H_\alpha^k R_\alpha^k} \\ 0 & 0 & \frac{1}{H_\beta^k R_\beta^k} \\ 0 & 0 & 0 \end{bmatrix}, \boldsymbol{A}_n^k = \begin{bmatrix} \frac{1}{H_\alpha^k R_\alpha^k} & 0 & 0 \\ 0 & \frac{1}{H_\beta^k R_\beta^k} & 0 \\ 0 & 0 & 0 \end{bmatrix}. \tag{1.110}$$

Elastic stress-strain relations

As before, strains are separated into in-plane (p) and normal (n) components. The constitutive equations still

$$\begin{aligned} \sigma_{pC}^k &= \mathbf{C}_{pp}^k\, \epsilon_{pG}^k + \mathbf{C}_{pn}^k\, \epsilon_{nG}^k \\ \sigma_{nC}^k &= \mathbf{C}_{np}^k\, \epsilon_{pG}^k + \mathbf{C}_{nn}^k\, \epsilon_{nG}^k \end{aligned} \tag{1.111}$$

and depending on the assumption on considering or not thickness-stretch effects, 3D or reduced plane-tress constitutive equations are chosen as for the plates. The matrices $\mathbf{C}_{pp}^k$, $\mathbf{C}_{pn}^k$, $\mathbf{C}_{np}^k$, and $\mathbf{C}_{nn}^k$ are as before and the computation of elastic constants C_{ij}^k for each layer, considers the same steps:

1. 1^{st} Computation of volume fraction of the ceramic V_c^k and metal V_m^k phases, in the present thesis by the power-law formulation (1.67);

2. 2^{nd} Computation of elastic properties E^k and ν^k, either by the Mori-Tanaka homogeneization technique (1.73) or the law-of-mistures (1.70).

3. 3^{rd} Computation of elastic constants C_{ij}^k as in (1.83) or (1.86) depending on the assumption of ϵ_{zz}.

Principle of virtual displacements

The Principle of Virtual Displacements (PVD) remains as in (1.88) and the steps to obtain the governing equations are as for the plates:

- Substitution of the geometrical relations (subscript G);
- Substitution of the appropriate constitutive equations (subscript C);
- Modeling of the displacement field by defining F_{sux}, F_{suy}, $F_{\tau ux}$, $F_{\tau uy}$, F_{suz}, and $F_{\tau uz}$.

Substituting the geometrical relations, the constitutive equations and the displacement field modeled by the unified formulation into the variational statement PVD (1.88), for the kth layer, one obtains for the shell:

$$\sum_{k=1}^{N_l}\{\int_{\Omega_k}\int_{A_k}\{((\boldsymbol{D}_p+\boldsymbol{A}_p)\delta\boldsymbol{u}^k)^T(\boldsymbol{C}^k_{pp}(\boldsymbol{D}_p+\boldsymbol{A}_p)\boldsymbol{u}^k+\boldsymbol{C}^k_{pn}(\boldsymbol{D}_{n\Omega}+\boldsymbol{D}_{nz}-\boldsymbol{A}_n)\boldsymbol{u}^k)+$$

$$((\boldsymbol{D}_{n\Omega}+\boldsymbol{D}_{nz}-\boldsymbol{A}_n)\delta\boldsymbol{u}^k)^T(\boldsymbol{C}^k_{np}(\boldsymbol{D}_p+\boldsymbol{A}_p)\boldsymbol{u}^k+\boldsymbol{C}^k_{nn}(\boldsymbol{D}_{n\Omega}+\boldsymbol{D}_{nz}-\boldsymbol{A}_n)\boldsymbol{u}^k)\}d\Omega_k dz_k\}$$

$$=\sum_{k=1}^{N_l}\delta L^k_e \tag{1.112}$$

As for the plates, after integration by parts (see (1.90) and (1.91)) and the substitution of CUF, the governing equations and boundary conditions for the shell in the mechanical case are obtained:

$$
\begin{aligned}
&\sum_{k=1}^{N_l}\{\int_{\Omega_k}\int_{A_k}\{\delta\boldsymbol{u}_s^{kT}[(-\boldsymbol{D}_p+\boldsymbol{A}_p)^T F_s(\boldsymbol{C}_{pp}^k(\boldsymbol{D}_p+\boldsymbol{A}_p)F_\tau\boldsymbol{u}_\tau^k+\boldsymbol{C}_{pn}^k(\boldsymbol{D}_{n\Omega}+\boldsymbol{D}_{nz}-\boldsymbol{A}_n)F_\tau\boldsymbol{u}_\tau^k)]+\\
&\delta\boldsymbol{u}_s^{kT}[(-\boldsymbol{D}_{n\Omega}+\boldsymbol{D}_{nz}-\boldsymbol{A}_n)^T F_s(\boldsymbol{C}_{np}^k(\boldsymbol{D}_p+\boldsymbol{A}_p)F_\tau\boldsymbol{u}_\tau^k+\boldsymbol{C}_{nn}^k(\boldsymbol{D}_{n\Omega}+\boldsymbol{D}_{nz}-\boldsymbol{A}_n)F_\tau\boldsymbol{u}_\tau^k)]\}d\Omega_k dz_k\}\\
&+\sum_{k=1}^{N_l}\{\int_{\Gamma_k}\int_{A_k}\{\delta\boldsymbol{u}_s^{kT}[\boldsymbol{I}_p^T F_s(\boldsymbol{C}_{pp}^k(\boldsymbol{D}_p+\boldsymbol{A}_p)F_\tau\boldsymbol{u}_\tau^k+\boldsymbol{C}_{pn}^k(\boldsymbol{D}_{n\Omega}+\boldsymbol{D}_{nz}-\boldsymbol{A}_n)F_\tau\boldsymbol{u}_\tau^k)]+\\
&\delta\boldsymbol{u}_s^{kT}[\boldsymbol{I}_{np}^T F_s(\boldsymbol{C}_{np}^k(\boldsymbol{D}_p-\boldsymbol{A}_p)F_\tau\boldsymbol{u}_\tau^k+\boldsymbol{C}_{nn}^k(\boldsymbol{D}_{n\Omega}+\boldsymbol{D}_{nz}-\boldsymbol{A}_n)F_\tau\boldsymbol{u}_\tau^k)]\}d\Gamma_k dz_k\}\\
&=\sum_{k=1}^{N_l}\{\int_{\Omega_k}\delta\boldsymbol{u}_s^{kT}F_s\boldsymbol{p}_u^k\}\ .
\end{aligned}
\tag{1.113}
$$

where $\mathbf{I}_p^k$ and $\mathbf{I}_{np}^k$ depend on the boundary geometry:

$$
\mathbf{I}_p=\begin{bmatrix}\frac{n_\alpha}{H_\alpha} & 0 & 0\\ 0 & \frac{n_\beta}{H_\beta} & 0\\ \frac{n_\beta}{H_\beta} & \frac{n_\alpha}{H_\alpha} & 0\end{bmatrix};\mathbf{I}_{np}=\begin{bmatrix}0 & 0 & \frac{n_\alpha}{H_\alpha}\\ 0 & 0 & \frac{n_\beta}{H_\beta}\\ 0 & 0 & 0\end{bmatrix}. \tag{1.114}
$$

The normal to the boundary of domain Ω is:

$$
\widehat{\boldsymbol{n}}=\begin{bmatrix}n_\alpha\\ n_\beta\end{bmatrix}=\begin{bmatrix}cos(\varphi_\alpha)\\ cos(\varphi_\beta)\end{bmatrix} \tag{1.115}
$$

where φ_α and φ_β are the angles between the normal $\widehat{n}$ and the direction α and β respectively.

Governing equations and boundary conditions

The governing equations for a multilayered shell subjected to mechanical loadings are:

$$\delta \mathbf{u}_s^{kT} : \qquad \mathbf{K}_{uu}^{k\tau s}\, \mathbf{u}_\tau^k \;=\; \mathbf{P}_{u\tau}^k \tag{1.116}$$

where the fundamental nucleus $\mathbf{K}_{uu}^{k\tau s}$ is obtained as:

$$\begin{aligned}
&\boldsymbol{K}_{uu}^{k\tau s} = \int_{A_k} \Big[[-\boldsymbol{D}_p + \boldsymbol{A}_p]^T\ \boldsymbol{C}_{pp}^k[\boldsymbol{D}_p + \boldsymbol{A}_p] + [-\boldsymbol{D}_p + \boldsymbol{A}_p]^T\ \boldsymbol{C}_{pn}^k[\boldsymbol{D}_{n\Omega} + \boldsymbol{D}_{nz} - \boldsymbol{A}_n] + \\
&[-\boldsymbol{D}_{n\Omega} + \boldsymbol{D}_{nz} - \boldsymbol{A}_n]^T\ \boldsymbol{C}_{np}^k[\boldsymbol{D}_p + \boldsymbol{A}_p] + [-\boldsymbol{D}_{n\Omega} + \boldsymbol{D}_{nz} - \boldsymbol{A}_n]^T\ \boldsymbol{C}_{nn}^k[\boldsymbol{D}_{n\Omega} + \boldsymbol{D}_{nz} - \boldsymbol{A}_n]\Big] \\
&F_\tau F_s H_\alpha^k H_\beta^k\ dz\ .
\end{aligned} \tag{1.117}$$

and the corresponding Neumann-type boundary conditions on Γ_k are:

$$\mathbf{\Pi}_d^{k\tau s}\, \mathbf{u}_\tau^k \;=\; \mathbf{\Pi}_d^{k\tau s}\, \bar{\mathbf{u}}_\tau^k\ , \tag{1.118}$$

where:

$$\begin{aligned}
&\mathbf{\Pi}_d^{k\tau s} = \int_{A_k} \Big[\boldsymbol{I}_p^T\ \boldsymbol{C}_{pp}^k[\boldsymbol{D}_p + \boldsymbol{A}_p^\tau] + \boldsymbol{I}_p^T\ \boldsymbol{C}_{pn}^k[\boldsymbol{D}_{n\Omega} + \boldsymbol{D}_{nz} - \boldsymbol{A}_n^\tau] + \\
&\qquad \boldsymbol{I}_{np}^T \boldsymbol{C}_{np}^k[\boldsymbol{D}_p + \boldsymbol{A}_p^\tau] + \boldsymbol{I}_{np}^T\ \boldsymbol{C}_{nn}^k[\boldsymbol{D}_{n\Omega} + \boldsymbol{D}_{nz} - \boldsymbol{A}_n^\tau]\Big] F_\tau F_s H_\alpha^k H_\beta^k\ dz\ .
\end{aligned} \tag{1.119}$$

and $\mathbf{P}_{u\tau}^k$ are variationally consistent loads with applied pressure.

Fundamental nuclei

The fundamental nuclei $\mathbf{K}_{uu}^{k\tau s}$ is reported for functionally graded doubly curved shells (radii of curvature in both α and β directions (see Fig.1.13)):

$$\left(\mathbf{K}_{uu}^{\tau sk}\right)_{11} = -C_{11}^{k} J_{\beta/\alpha}^{k\tau s} \partial_{\alpha}^{s} \partial_{\alpha}^{\tau} - C_{44}^{k} J_{\alpha/\beta}^{k\tau s} \partial_{\beta}^{s} \partial_{\beta}^{\tau}$$

$$+ C_{44}^{k} \left(J_{\alpha\beta}^{k\tau_z s_z} - \frac{1}{R_{\alpha_k}} J_{\beta}^{k\tau_z s} - \frac{1}{R_{\alpha_k}} J_{\beta}^{k\tau s_z} + \frac{1}{R_{\alpha_k}^{2}} J_{\beta/\alpha}^{k\tau s} \right)$$

$$\left(\mathbf{K}_{uu}^{\tau sk}\right)_{12} = -C_{12}^{k} J^{k\tau s} \partial_{\alpha}^{\tau} \partial_{\beta}^{s} - C_{44}^{k} J^{k\tau s} \partial_{\alpha}^{s} \partial_{\beta}^{\tau}$$

$$\left(\mathbf{K}_{uu}^{\tau sk}\right)_{13} = -C_{11}^{k} \frac{1}{R_{\alpha_k}} J_{\beta/\alpha}^{k\tau s} \partial_{\alpha}^{\tau} - C_{12}^{k} \frac{1}{R_{\beta_k}} J^{k\tau s} \partial_{\alpha}^{\tau} - C_{12}^{k} J_{\beta}^{k\tau s_z} \partial_{\alpha}^{\tau}$$

$$+ C_{44}^{k} \left(J_{\beta}^{k\tau_z s} \partial_{\alpha}^{s} - \frac{1}{R_{\alpha_k}} J_{\beta/\alpha}^{k\tau s} \partial_{\alpha}^{s} \right)$$

$$\left(\mathbf{K}_{uu}^{\tau sk}\right)_{21} = -C_{12}^{k} J^{k\tau s} \partial_{\alpha}^{s} \partial_{\beta}^{\tau} - C_{44}^{k} J^{k\tau s} \partial_{\alpha}^{\tau} \partial_{\beta}^{s}$$

$$\left(\mathbf{K}_{uu}^{\tau sk}\right)_{22} = -C_{22}^{k} J_{\alpha/\beta}^{k\tau s} \partial_{\beta}^{s} \partial_{\beta}^{\tau} - C_{26}^{k} J^{k\tau s} \partial_{\alpha}^{s} \partial_{\beta}^{\tau} - C_{26}^{k} J^{k\tau s} \partial_{\alpha}^{\tau} \partial_{\beta}^{s} - C_{44}^{k} J_{\beta/\alpha}^{k\tau s} \partial_{\alpha}^{s} \partial_{\alpha}^{\tau}$$

$$+ C_{44}^{k} \left(J_{\alpha\beta}^{k\tau_z s_z} - \frac{1}{R_{\beta_k}} J_{\alpha}^{k\tau_z s} - \frac{1}{R_{\beta_k}} J_{\alpha}^{k\tau s_z} + \frac{1}{R_{\beta_k}^{2}} J_{\alpha/\beta}^{k\tau s} \right)$$

$$\left(\mathbf{K}_{uu}^{\tau sk}\right)_{23} = -C_{12}^{k} \frac{1}{R_{\alpha_k}} J^{k\tau s} \partial_{\beta}^{\tau} - C_{22}^{k} \frac{1}{R_{\beta_k}} J_{\alpha/\beta}^{k\tau s} \partial_{\beta}^{\tau} - C_{12}^{k} J_{\alpha}^{k\tau s_z} \partial_{\beta}^{\tau}$$

$$+ C_{44}^{k} \left(J_{\alpha}^{k\tau_z s} \partial_{\beta}^{s} - \frac{1}{R_{\beta_k}} J_{\alpha/\beta}^{k\tau s} \partial_{\beta}^{s} \right)$$

$$\left(\mathbf{K}_{uu}^{\tau sk}\right)_{31} = C_{11}^{k} \frac{1}{R_{\alpha_k}} J_{\beta/\alpha}^{k\tau s} \partial_{\alpha}^{s} + C_{12}^{k} \frac{1}{R_{\beta_k}} J^{k\tau s} \partial_{\alpha}^{s} + C_{12}^{k} J_{\beta}^{k\tau_z s} \partial_{\alpha}^{s}$$

$$- C_{44}^{k} \left(J_{\beta}^{k\tau s_z} \partial_{\alpha}^{\tau} - \frac{1}{R_{\alpha_k}} J_{\beta/\alpha}^{k\tau s} \partial_{\alpha}^{\tau} \right)$$

$$\left(\mathbf{K}_{uu}^{\tau sk}\right)_{32} = C_{12}^{k}\frac{1}{R_{\alpha_k}}J^{k\tau s}\partial_{\beta}^{s} + C_{22}^{k}\frac{1}{R_{\beta_k}}J_{\alpha/\beta}^{k\tau s}\partial_{\beta}^{s} + C_{12}^{k}J_{\alpha}^{k\tau_z s}\partial_{\beta}^{s}$$

$$- C_{44}^{k}\left(J_{\alpha}^{k\tau s_z}\partial_{\beta}^{\tau} - \frac{1}{R_{\beta_k}}J_{\alpha/\beta}^{k\tau s}\partial_{\beta}^{\tau}\right)$$

$$\left(\mathbf{K}_{uu}^{\tau sk}\right)_{33} = C_{11}^{k}\frac{1}{R_{\alpha_k}^2}J_{\beta/\alpha}^{k\tau s} + C_{22}^{k}\frac{1}{R_{\beta_k}^2}J_{\alpha/\beta}^{k\tau s} + C_{33}^{k}J_{\alpha\beta}^{k\tau_z s_z}$$

$$+ 2C_{12}^{k}\frac{1}{R_{\alpha_k}}\frac{1}{R_{\beta_k}}J^{k\tau s} + C_{12}^{k}\frac{1}{R_{\alpha_k}}\left(J_{\beta}^{k\tau_z s} + J_{\beta}^{k\tau s_z}\right) + C_{12}^{k}\frac{1}{R_{\beta_k}}\left(J_{\alpha}^{k\tau_z s} + J_{\alpha}^{k\tau s_z}\right)$$

$$- C_{44}^{k}J_{\alpha/\beta}^{k\tau s}\partial_{\beta}^{s}\partial_{\beta}^{\tau} - C_{44}^{k}J_{\beta/\alpha}^{k\tau s}\partial_{\alpha}^{s}\partial_{\alpha}^{\tau} \tag{1.120}$$

where

$$(J^{k\tau s}, J_{\alpha}^{k\tau s}, J_{\beta}^{k\tau s}, J_{\frac{\alpha}{\beta}}^{k\tau s}, J_{\frac{\beta}{\alpha}}^{k\tau s}, J_{\alpha\beta}^{k\tau s}) = \int_{A_k} F_{\tau}F_{s}(1, H_{\alpha}, H_{\beta}, \frac{H_{\alpha}}{H_{\beta}}, \frac{H_{\beta}}{H_{\alpha}}, H_{\alpha}H_{\beta})\ dz$$

$$(J^{k\tau_z s}, J_{\alpha}^{k\tau_z s}, J_{\beta}^{k\tau_z s}, J_{\frac{\alpha}{\beta}}^{k\tau_z s}, J_{\frac{\beta}{\alpha}}^{k\tau_z s}, J_{\alpha\beta}^{k\tau_z s}) = \int_{A_k} \frac{\partial F_{\tau}}{\partial z}F_{s}(1, H_{\alpha}, H_{\beta}, \frac{H_{\alpha}}{H_{\beta}}, \frac{H_{\beta}}{H_{\alpha}}, H_{\alpha}H_{\beta})\ dz$$

$$(J^{k\tau s_z}, J_{\alpha}^{k\tau s_z}, J_{\beta}^{k\tau s_z}, J_{\frac{\alpha}{\beta}}^{k\tau s_z}, J_{\frac{\beta}{\alpha}}^{k\tau s_z}, J_{\alpha\beta}^{k\tau s_z}) = \int_{A_k} F_{\tau}\frac{\partial F_{s}}{\partial z}(1, H_{\alpha}, H_{\beta}, \frac{H_{\alpha}}{H_{\beta}}, \frac{H_{\beta}}{H_{\alpha}}, H_{\alpha}H_{\beta})\ dz$$

$$(J^{k\tau_z s_z}, J_{\alpha}^{k\tau_z s_z}, J_{\beta}^{k\tau_z s_z}, J_{\frac{\alpha}{\beta}}^{k\tau_z s_z}, J_{\frac{\beta}{\alpha}}^{k\tau_z s_z}, J_{\alpha\beta}^{k\tau_z s_z}) = \int_{A_k} \frac{\partial F_{\tau}}{\partial z}\frac{\partial F_{s}}{\partial z}(1, H_{\alpha}, H_{\beta}, \frac{H_{\alpha}}{H_{\beta}}, \frac{H_{\beta}}{H_{\alpha}}, H_{\alpha}H_{\beta})\ dz \tag{1.121}$$

The application of boundary conditions makes use of the fundamental nuclei $\mathbf{\Pi}_d$ in the form:

$$\left(\mathbf{\Pi}_{uu}^{\tau sk}\right)_{11} = n_{\alpha}C_{11}^{k}J_{\beta/\alpha}^{k\tau s}\partial_{\alpha}^{s} + n_{\beta}C_{44}^{k}J_{\alpha/\beta}^{k\tau s}\partial_{\beta}^{s}$$

$$\left(\mathbf{\Pi}_{uu}^{\tau sk}\right)_{12} = n_{\alpha}C_{12}^{k}J^{k\tau s}\partial_{\beta}^{s} + n_{\beta}C_{44}^{k}J^{k\tau s}\partial_{\alpha}^{s}$$

$$\left(\mathbf{\Pi}_{uu}^{\tau sk}\right)_{13} = n_\alpha \frac{1}{R_{\alpha k}} C_{11}^k J_{\beta/\alpha}^{k\tau s} + n_\alpha \frac{1}{R_{\beta k}} C_{12}^k J^{k\tau s} + n_\alpha C_{12}^k J_\beta^{k\tau s_z}$$

$$\left(\mathbf{\Pi}_{uu}^{\tau sk}\right)_{21} = n_\beta C_{12}^k J^{k\tau s} \partial_\alpha^s + n_\alpha C_{44}^k J^{k\tau s} \partial_\beta^s$$

$$\left(\mathbf{\Pi}_{uu}^{\tau sk}\right)_{22} = n_\alpha C_{44}^k J_{\beta/\alpha}^{k\tau s} \partial_\alpha^s + n_\beta C_{22}^k J_{\alpha/\beta}^{k\tau s} \partial_\beta^s + n_\beta C_{26}^k J^{k\tau s} \partial_\alpha^s + n_\alpha C_{26}^k J^{k\tau s} \partial_\beta^s$$

$$\left(\mathbf{\Pi}_{uu}^{\tau sk}\right)_{23} = n_\beta \frac{1}{R_{\alpha k}} C_{12}^k J^{k\tau s} + n_\beta \frac{1}{R_{\beta k}} C_{22}^k J_{\alpha/\beta}^{k\tau s} + n_\beta C_{12}^k J_\alpha^{k\tau s_z}$$

$$\left(\mathbf{\Pi}_{uu}^{\tau sk}\right)_{31} = -n_\alpha \frac{1}{R_{\alpha k}} C_{44}^k J_{\beta/\alpha}^{k\tau s} + n_\alpha C_{44}^k J_\beta^{k\tau s_z}$$

$$\left(\mathbf{\Pi}_{uu}^{\tau sk}\right)_{32} = -n_\beta \frac{1}{R_{\beta k}} C_{44}^k J_{\alpha/\beta}^{k\tau s} + n_\beta C_{44}^k J_\alpha^{k\tau s_z}$$

$$\left(\mathbf{\Pi}_{uu}^{\tau sk}\right)_{33} = n_\alpha C_{44}^k J_{\beta/\alpha}^{k\tau s} \partial_\alpha^s + n_\beta C_{44}^k J_{\alpha/\beta}^{k\tau s} \partial_\beta^s \tag{1.122}$$

Note that all the equations written for the shell degenerate in those for the plate when $\frac{1}{R_{\alpha k}} = \frac{1}{R_{\beta k}} = 0$. In practice, the radii of curvature are set to 10^9 for analysis of plates with the present formulation.

Dynamic governing equations

The PVD for the shell dynamic case is expressed as for the plate dynamic case as in (1.101). Substituting the geometrical relations and the constitutive equations, one obtains the following governing equations:

$$\delta \mathbf{u}_s^{kT} : \qquad \mathbf{K}_{uu}^{k\tau s}\, \mathbf{u}_\tau^k = \mathbf{M}^{k\tau s} \ddot{\mathbf{u}}_\tau^k + \mathbf{P}_{u\tau}^k \tag{1.123}$$

In the case of free vibrations one has:

$$\delta \mathbf{u}_s^{kT} : \qquad \mathbf{K}_{uu}^{k\tau s}\, \mathbf{u}_\tau^k = \mathbf{M}^{k\tau s} \ddot{\mathbf{u}}_\tau^k \tag{1.124}$$

where $\mathbf{M}^{k\tau s}$ is the fundamental nucleus for the inertial term, given by

$$\mathbf{M}_{ij}^{k\tau s} = \rho^k J_{\alpha\beta}^{k\tau s}, \quad i = j$$
$$\mathbf{M}_{ij}^{k\tau s} = 0, \quad i \neq j \tag{1.125}$$

The meaning of the integral $J_{\alpha\beta}^{k\tau s}$ has been illustrated in eq. (1.121). The geometrical and mechanical boundary conditions are the same of the static case.

1.5 Organization of the thesis

After a short introduction, we present the papers published in international journals. In the end of the thesis we formulate some conclusions.

The list of papers presented are as follows:

Title: Dynamic Analysis of Functionally Graded Plates and Shells by Radial Basis Functions

On Carrera's Unified Formulation

Title: Bending of FGM plates by a sinusoidal plate formulation and collocation with radial basis functions

Title: A quasi-3D sinusoidal shear deformation theory for the static and free vibration analysis of functionally graded plates

Title: A quasi-3D hyperbolic shear deformation theory for the static and free vibration analysis of functionally graded plates

Title: Static, free vibration and buckling analysis of isotropic and sandwich functionally graded plates using a quasi-3D higher-order shear deformation theory and a meshless technique

Title: Buckling analysis of sandwich plates with functionally graded skins using a new quasi-3D hyperbolic sine shear deformation theory and collocation with radial basis functions

Title: Static analysis of functionally graded sandwich plates according to a hyperbolic theory considering Zig-Zag and warping effects

Title: Influence of Zig-Zag and warping effects on buckling of functionally graded sandwich plates according to sinusoidal shear deformation theories

Title: Free vibration analysis of functionally graded shells by a higher-order shear deformation theory and radial basis functions collocation, accounting for through-the-thickness deformations

Title: Buckling behavior of cross-ply laminated plates by a higher-order shear deformation theory

On the radial basis function collocation technique

On the RBF-Direct method

Title: Adaptive Methods for analysis of Composite Plates with Radial Basis Functions

Title: Vibration and buckling of composite structures using oscillatory radial basis functions

Title: Analysis of plates on Pasternak foundations by radial basis functions

Title: Buckling and vibration analysis of isotropic and laminated plates by radial basis functions

Title: Buckling analysis of isotropic and laminated plates by radial basis functions according to a higher-order shear deformation theory

On the RBF-PS method

Title: Solving time-dependent problems by an RBF-PS method with an optimal shape parameter

Title: Transient analysis of composite plates by radial basis functions in a pseudospectral framework

Title: Transient analysis of composite and sandwich plates by radial basis functions

References

[1] Y T Gu. Meshfree methods and their comparisons. *International Journal of Computational Methods*, 2(4):477–515, 2005.

[2] E. Carrera. C^0 reissner-mindlin multilayered plate elements including zig-zag and interlaminar stress continuity. *International Journal of Numerical Methods in Engineering*, 39:1797–1820, 1996.

[3] E. Carrera. Developments, ideas, and evaluations based upon reissner's mixed variational theorem in the modelling of multilayered plates and shells. *Appl. Mech. Rev.*, 54:301–329, 2001.

[4] T. Belytschko, Y. Krongauz, D. Organ, M. Fleming, and P. Krysl. Meshless methods: An overview and recent developments. *Computer Methods in Applied Mechanics and Engineering*, 139(1-4):3–47, December 1996.

[5] G. R. Liu. *Mesh Free Methods. Moving Beyond the Finite Element Method.* CRC Press, 2003.

[6] G. R. Liu. *Mesh Free Methods. Moving Beyond the Finite Element Method.* CRC Press, 2009.

[7] A Frazer, W P Jones, and S W Skan. Approximation to functions and to the solutions of differential equations. *Great Britain Aeronautical Research Council, Reports and Memoranda*, No 1799, 1937.

[8] J C Slater. Electronic energy bands in metals. *Physical Review*, 45:794–801, 1934.

[9] L. B. Lucy. A numerical approach to the testing of the fission hypothesis. *Astronomical Journal*, 82:1013–1024, 1977.

[10] R A Gingold and J J Monaghan. Smoothed particle hydrodynamicstheory and application to non-spherical stars. *Monthly Notices Of The Royal Astronomical Society*, 181(2):375–389, 1977.

[11] J. J. Monaghan. Smoothed particle hydrodynamics. *Annual Review of Astronomy and Astrophysics*, 30:543–574, 1992.

[12] G R Liu and Y T Gu. *An introduction to meshfree methods and their programming*. Springer, 2005.

[13] B. Nayroles, G. Touzot, and P. Villon. Generalizing the finite element method: Diffuse approximation and diffuse elements. *Computational Mechanics*, 10(5):307–318, 1992.

[14] T. Belytschko, Y. Y. Lu, and L. Gu. Element-free galerkin methods. *International Journal for Numerical Methods in Engineering*, 37(2):229–256, 1994.

[15] G. R. Liu and Y. T. Gu. A point interpolation method for two-dimensional solids. *International Journal for Numerical Methods in Engineering*, 50(4):937–951, 2001.

[16] J. G. Wang and G. R. Liu. A point interpolation meshless method based on radial basis functions. *International Journal for Numerical Methods in Engineering*, 54(11):1623–1648, 2002.

[17] S. N. Atluri and T. Zhu. A new meshless local petrov-galerkin (mlpg) approach in computational mechanics. *Computational Mechanics*, 22(2):117–127, 1998.

[18] G. R. Liu and Y. T. Gu. A local radial point interpolation method (lrpim) for free vibration analyses of 2-d solids. *Journal of Sound and Vibration*, 246(1):29–46, September 2001.

[19] T. Liszka and J. Orkisz. Finite difference method at arbitrary irregular grids and its application in applied mechanics. *Computers and Structures*, 11(1-2):83–95, 1980.

[20] E. Oñate, S. Idelsohn, O. C. Zienkiewicz, and R. L. Taylor. A finite point method in computational mechanics. applications to convective transport and fluid flow. *International Journal for Numerical Methods in Engineering*, 39(22):3839–3866, 1996.

[21] E. J. Kansa. Multiquadrics. a scattered data approximation scheme with applications to computational fluid-dynamics. i. surface approximations and partial derivative estimates. *Computers & mathematics with applications*, 19(8-9):127–145, 1990.

[22] E. J. Kansa. Multiquadrics. a scattered data approximation scheme with applications to computational fluid-dynamics. ii. solutions to parabolic, hyperbolic and elliptic partial differential equations. *Computers & mathematics with applications*, 19(8-9):147–161, 1990.

[23] G. R. Liu and Y. T. Gu. A meshfree method: Meshfree weak-strong (mws) form method, for 2-d solids. *Computational Mechanics*, 33(1):2–14, 2003.

[24] V. S. Kothnur, S. Mukherjee, and Y. X. Mukherjee. Two-dimensional linear elasticity by the boundary node method. *International Journal of Solids and Structures*, 36(8):1129–1147, 1999.

[25] W. K. Liu, S. Jun, and Y. F. Zhang. Reproducing kernel particle methods. *International Journal for Numerical Methods in Fluids*, 20(8-9):1081–1106, 1995.

[26] N R Aluru. A point collocation method based on reproducing kernel approxima-

tions. *International Journal for Numerical Methods in Engineering*, 47(6):1083–1121, 2000.

[27] O Garcia, E A Fancello, C S Barcellos, and C A Duarte. hp-Clouds in Mindlin's thick plate model. *International Journal for Numerical Methods in Engineering*, 47(8):1381–1400, 2000.

[28] A Meshfree Method based on the Local Partition of Unity for Cohesive Cracks. *Computational Mechanics*, 39(6):743–760, 2007.

[29] P Tongsuk and W Kanok-Nukulchai. Further investigation of element-free galerkin method using moving kriging interpolation. *International Journal of Computational Methods*, 1:345–365, 2004.

[30] Y T Gu and G R Liu. A boundary point interpolation method for stress analysis of solids. *Computational Mechanics*, 28:47–54, 2002.

[31] T Belytschko, D Organ, and Y Krongauz. Coupled finite element-element-free Galerkin method. *Computational Mechanics*, 17(3):186–195, 1995.

[32] Y T Gu and G R Liu. A coupled element free Galerkin/boundary element method for stress analysis of tow-dimensional solids. *Computer Methods in Applied Mechanics and Engineering*, 190(34):4405–4419, 2001.

[33] Y T Gu and G R Liu. Hybrid boundary point interpolation methods and their coupling with the element free Galerkin method. *Engineering Analysis with Boundary Elements*, 27(9):905–917, 2003.

[34] Y. T. Gu and L.C. Zhang. Coupling of the meshfree and finite element methods for determination of the crack tip fields. *Engineering Fracture Mechanics*, 75(5):986–1004, March 2008.

[35] R Franke. Scattered data interpolation: tests of some methods. *Mathematics of Computation*, 38(157):181–200, 1982.

[36] M. D. Buhmann. Radial basis functions. *Acta numerica*, 9:1–38, 2000.

[37] M. D. Buhmann. *Radial Basis Functions: Theory and Implementations.* Cambridge University Press, 2003.

[38] G. E. Fasshauer. *Meshfree Approximations Methods with Matlab*. World Scientific, 2007.

[39] W. R. Madich and S. A. Nelson. Multivariate interpolation and conditionally positive definite functions. ii. *Math. Comp.*, 54(189):211–230, 1990.

[40] J. Yoon. Spectral approximation orders of radial basis function interpolation on the sobolev space. *SIAM J. Math. Anal.*, 33(4):946–958, 2001.

[41] Natasha Flyer and Bengt Fornberg. Radial basis functions: Developments and applications to planetary scale flows. *Computers & Fluids*, 46(1):23–32, 2011.

[42] B Fornberg, E Larsson, and N Flyer. Stable Computations with Gaussian Radial Basis Functions. *SIAM J. SCI. COMPUT.*, 33(2):869–892, 2011.

[43] A. J. M. Ferreira and G. E. Fasshauer. Computation of natural frequencies of shear deformable beams and plates by a rbf-pseudospectral method. *Computer Methods in Applied Mechanics and Engineering*, 196:134–146, 2006.

[44] Holger Wendland. Piecewise polynomial, positive definite and compactly supported radial functions of minimal degree. *Advances in Computational Mathematics*, V4(1):389–396, December 1995.

[45] G. Casciola, D. Lazzaro, L.B. Montefusco, and S. Morigi. Shape preserving surface reconstruction using locally anisotropic radial basis function interpolants. *Computers & Mathematics with Applications*, 51(8):1185–1198, April 2006.

[46] T Gneiting. Compactly Supported Correlation Functions. *Journal of Multivariate Analysis*, 83(2):493–508, 2002.

[47] S G Miller K. S.; Samko. Completely monotonic functions. *Integral Transforms and Special Functions*, 12(4):389–402, 2001.

[48] I J Schoenberg. Metric spaces and completely monotone functions. *Annals of Mathematics*, 39(4):811–841, 1938.

[49] H Wendland. *Scattered Data Approximation.* Combridge University Press, 2005.

[50] C. A. Micchelli. Interpolation of scattered data distance matrices and conditionally positive definite functions. *Constructive Approximation*, 2(1):11–22, 1986.

[51] S.; Sun X Guo K.; Hu. Conditionally Positive Definite Functions and Laplace-Stieltjes Integrals. *Journal of Approximation Theory*, 74(2):249–265, 1993.

[52] R. L. Hardy. Multiquadric equations of topography and other irregular surfaces. *Geophys. Res.*, 176:1905–1915, 1971.

[53] R Schaback. Creating surfaces from scattered data using radial basis functions, in Mathematical Models for Curves and Surfaces. Daehlen, M.; Lyche, T.; and Schumaker, L. L. (eds.). *Vanderbilt University Press, Nashville, TN.*

[54] Z Wu. Compactly supported positive definite radial functions. *Advances in Computational Mathematics*, 4:283–292, 1995.

[55] B Fornberg. *A Practical Guide to Pseudospectral Methods.* Cambridge University Press, 1998.

[56] L N Trefethen. *Spectral Methods in Matlab.* SIAM, 2000.

[57] A. J. M. Ferreira and G. E. Fasshauer. Computation of natural frequencies of shear deformable beams and plates by a rbf-pseudospectral method. *Computer Methods in Applied Mechanics and Engineering*, 196:134–146, 2006.

[58] A J M Ferreira, G E Fasshauer, R C Batra, and J D Rodrigues. Static deforma-

tions and vibrations analysis of composite and sandwich plates using a layerwise theory and RBF-PS discretizations with optimal shape parameters. *Composite Structures*, 86:328–343, 2008.

[59] E. Carrera. Evaluation of layer-wise mixed theories for laminated plate analysis. *AIAA Journal*, (36):830–839, 1998.

[60] Erasmo Carrera. Theories and finite elements for multilayered plates and shells: A unified compact formulation with numerical assessment and benchmarking. *Archives of Computational Methods in Engineering*, 10:215–296, 2003.

[61] S. Brischetto and E. Carrera. Advanced mixed theories for bending analysis of functionally graded plates. *Computers and Structures*, 88(23-24):1474 – 1483, 2010.

[62] S. Brischetto. Classical and mixed advanced models for sandwich plates embedding functionally graded cores. *J Mech Mater Struct*, 4:13–33, 2009.

[63] E. Carrera, S. Brischetto, and A. Robaldo. Variable kinematic model for the analysis of functionally graded material plates. *AIAA Journal*, 46:194–203, 2008.

[64] A.J.M. Ferreira, C.M.C. Roque, E. Carrera, M. Cinefra, and O. Polit. Radial basis functions collocation and a unified formulation for bending, vibration and buckling analysis of laminated plates, according to a variation of murakami's zigzag theory. *European Journal of Mechanics - A/Solids*, 30(4):559 – 570, 2011.

[65] J.D. Rodrigues, C.M.C. Roque, A.J.M. Ferreira, E. Carrera, and M. Cinefra. Radial basis functions-finite differences collocation and a unified formulation for bending, vibration and buckling analysis of laminated plates, according to murakami's zig-zag theory. *Composite Structures*, 93(7):1613 – 1620, 2011.

[66] A.J.M. Ferreira, C.M.C. Roque, E. Carrera, and M. Cinefra. Analysis of thick isotropic and cross-ply laminated plates by radial basis functions and a unified formulation. *Journal of Sound and Vibration*, 330(4):771 – 787, 2011.

[67] A. J.M. Ferreira, C. M.C. Roque, E. Carrera, M. Cinefra, and O. Polit. Two higher order zig-zag theories for the accurate analysis of bending, vibration and buckling response of laminated plates by radial basis functions collocation and a unified formulation. *Journal of Composite Materials*, 2011.

[68] A. Ferreira, E. Carrera, M. Cinefra, and C. Roque. Analysis of laminated doubly-curved shells by a layerwise theory and radial basis functions collocation, accounting for through-the-thickness deformations. *Computational Mechanics*, 48:13–25, 2011. 10.1007/s00466-011-0579-4.

[69] A.J.M. Ferreira, E. Carrera, M. Cinefra, C.M.C. Roque, and O. Polit. Analysis of laminated shells by a sinusoidal shear deformation theory and radial basis functions collocation, accounting for through-the-thickness deformations. *Composites Part B: Engineering*, 42(5):1276 – 1284, 2011.

[70] J. N. Reddy. Analysis of functionally graded plates. *International Journal for Numerical Methods in Engineering*, 47:663–684, 2000.

[71] Kant T., Owen D. R. J., and O C Zienkiewicz. A refined higher-order Cˆo plate element. *Computers and Structures*, 15(2):177–183, 1982.

[72] B. N. Pandya and T. Kant. Higher-order shear deformable theories for flexure of sandwich plates–finite element evaluations. *International Journal of Solids and Structures*, 24(12):1267–1286, 1988.

[73] B. N. Pandya and T. Kant. Finite element analysis of laminated composite plates using a higher-order displacement model. *Composites Science and Technology*, 32(2):137–155, 1988.

[74] T. Kant and K. Swaminathan. Analytical solutions for the static analysis of laminated composite and sandwich plates based on a higher order refined theory. *Composite Structures*, 56(4):329 – 344, 2002.

[75] T. Kant and K. Swaminathan. Analytical solutions for free vibration of laminated

composite and sandwich plates based on a higher-order refined theory. *Composite Structures*, 53(1):73 – 85, 2001.

[76] Ajay Kumar Garg, Rakesh Kumar Khare, and Tarun Kant. Higher-order closed-form solutions for free vibration of laminated composite and sandwich shells. *Journal of Sandwich Structures and Materials*, 8(3):205–235, 2006.

[77] R. C. Batra and S. Vidoli. Higher-order piezoelectric plate theory derived from a three-dimensional variational principle. *AIAA Journal*, 40:91–104, 2002.

[78] R. C. Batra, S. Vidoli, and F. Vestroni. Plane wave solutions and modal analysis in higher order shear and normal deformable plate theories. *Journal of Sound and Vibration*, 257(1):63–88, 2002.

[79] M. Touratier. A generalization of shear deformation theories for axisymmetric multilayered shells. *International Journal of Solids and Structures*, 29:1379–1399, 1992.

[80] M. Touratier. An efficient standard plate theory. *International Journal of Engineering Science*, 29:901–916, 1991.

[81] M. Touratier. A refined theory of laminated shallow shells. *International Journal of Solids and Structures*, 29(11):1401–1415, 1992.

[82] P. Vidal and O. Polit. A family of sinus finite elements for the analysis of rectangular laminated beams. *Composite Structures*, 84:56–72, 2008.

[83] A. M. Zenkour. Generalized shear deformation theory for bending analysis of functionally graded plates. *Appl Math Modell*, 30:67–84, 2006.

[84] K. Soldatos. A transverse shear deformation theory for homogeneous monoclinic plates. *Acta Mechanica*, 94:195–220, 1992. 10.1007/BF01176650.

[85] S. Akavci. Two new hyperbolic shear displacement models for orthotropic lam-

inated composite plates. *Mechanics of Composite Materials*, 46:215–226, 2010. 10.1007/s11029-010-9140-3.

[86] S. Akavci and A. Tanrikulu. Buckling and free vibration analyses of laminated composite plates by using two new hyperbolic shear-deformation theories. *Mechanics of Composite Materials*, 44:145–154, 2008. 10.1007/s11029-008-9004-2.

[87] Noureddine El Meiche, Abdelouahed Tounsi, Noureddine Ziane, Ismail Mechab, and El Abbes Adda.Bedia. A new hyperbolic shear deformation theory for buckling and vibration of functionally graded sandwich plate. *International Journal of Mechanical Sciences*, 53(4):237 – 247, 2011.

[88] G. Kirchhoff. Uber das gleichgewicht und die bewegung einer elastischen scheibe. *J. Angew. Math.*, 40:51–88, 1850.

[89] E. Reissner. The effect of transverse shear deformations on the bending of elastic plates. *J. Appl. Mech.*, 12:A69–A77, 1945.

[90] R. D. Mindlin. Influence of rotary inertia and shear in flexural motions of isotropic elastic plates. *J. Appl. Mech.*, 18:31–38, 1951.

[91] H. Murakami. Laminated composite plate theory with improved in-plane responses. *Journal of Applied Mechanics*, 53:661–666, 1986.

[92] M.B. Bever and P.E. Duwez. Gradients in composite materials. *Materials Science and Engineering*, 10(0):1 – 8, 1972.

[93] M. Shen and M. B. Bever. Gradients in polymeric materials. *Journal of Materials Science*, 7:741–746, 1972. 10.1007/BF00549902.

[94] Y Miyamoto, W A Kaysser, B H Rabin, A Kawasaki, and R G Ford. *Functionally Graded Materials: Design, Processing and Applications*. Kluwer Academic Publishers, 1999.

[95] F.J. Ferrante and L.L. Graham-Brady. Stochastic simulation of non-gaussian/non-stationary properties in a functionally graded plate. *Computer Methods in Applied Mechanics and Engineering*, 194(12-16):1675 – 1692, 2005.

[96] H.M Yin, L.Z Sun, and G.H Paulino. Micromechanics-based elastic model for functionally graded materials with particle interactions. *Acta Materialia*, 52(12):3535 – 3543, 2004.

[97] Zheng Zhong and Ertao Shang. Closed-form solutions of three-dimensional functionally graded plates. *Mechanics of Advanced Materials and Structures*, 15(5):355–363, 2008.

[98] T. K. Nguyen, K. Sab, and G. Bonnet. Shear correction factors for functionally graded plates. *Mechanics of Advanced Materials and Structures*, 14(8):567–575, 2007.

[99] Victor Birman and Larry W. Byrd. Modeling and analysis of functionally graded materials and structures. *Applied Mechanics Reviews*, 60(5):195–216, 2007.

[100] M. Koizumi. Fgm activities in japan. *Composites Part B: Engineering*, 28(1-2):1 – 4, 1997. Use of Composites Multi-Phased and Functionally Graded Materials.

[101] M. Niino and S. Maeda. Recent development status of functionally gradient materials. *ISIJ International*, 30(9):699–703, 1990.

[102] Z. H. Jin and R. C. Batra. Stress intensity relaxation at the tip of an edge crack in a functionally graded material subjected to a thermal shock. *Journal of Thermal Stresses*, 19:317–339, 1996.

[103] Y.L. Chung and S.H. Chi. The residual stress of functionally graded materials. *Journal of the Chinese Institute of Civil and Hydraulic Engineering*, 13:1–9, 2001.

[104] G. N. Praveen and J. N. Reddy. Nonlinear transient thermoelastic analysis of functionally graded ceramic-metal plates. *International Journal of Solids and*

Structures, 35(33):4457 – 4476, 1998.

[105] M. M. Najafizadeh and M. R. Eslami. Buckling analysis of circular plates of functionally graded materials under uniform radial compression. *International Journal of Mechanical Sciences*, 44(12):2479 – 2493, 2002.

[106] A.M. Zenkour. A comprehensive analysis of functionally graded sandwich plates: Part 1–deflection and stresses. *International Journal of Solids and Structures*, 42(18-19):5224 – 5242, 2005.

[107] T Mori and K Tanaka. Average stress in matrix and average elastic energy of materials with misfitting inclusions. *Acta Metallurgica*, 21(5):571 – 574, 1973.

[108] Y. and Benveniste. A new approach to the application of mori-tanaka's theory in composite materials. *Mechanics of Materials*, 6(2):147 – 157, 1987.

2

Papers on Carrera's Unified Formulation

2.1 Bending of FGM plates by a sinusoidal plate formulation and collocation with radial basis functions

Ana M. A. Neves, A. J. M. Ferreira, E. Carrera, C. M. C. Roque, M. Cinefra, R. M. N. Jorge, C. M. M. Soares, Bending of FGM plates by a sinusoidal plate formulation and collocation with radial basis functions, Mechanics Research Communications, Volume 38, 2011, pages 368-371.

Mechanics Research Communications 38 (2011) 368–371

Contents lists available at ScienceDirect

Mechanics Research Communications

journal homepage: www.elsevier.com/locate/mechrescom

Bending of FGM plates by a sinusoidal plate formulation and collocation with radial basis functions

A.M.A. Neves[a], A.J.M. Ferreira[a,*], E. Carrera[c], C.M.C. Roque[b], M. Cinefra[c], R.M.N. Jorge[a], C.M.M. Soares[d]

[a] Departamento de Engenharia Mecânica, Faculdade de Engenharia, Universidade do Porto, Rua Dr. Roberto Frias, 4200-465 Porto, Portugal
[b] INEGI, Faculdade de Engenharia, Universidade do Porto, Rua Dr. Roberto Frias, 4200-465 Porto, Portugal
[c] Department of Aeronautics and Aerospace Engineering, Politecnico di Torino, Corso Duca degli Abruzzi, 24, 10129 Torino, Italy
[d] Instituto Superior Técnico, Av. Rovisco Pais, Lisboa, Portugal

ARTICLE INFO

Article history:
Received 15 March 2011
Available online 7 May 2011

ABSTRACT

This paper addresses the static deformations analysis of functionally graded plates by collocation with radial basis functions, according to a sinusoidal shear deformation formulation for plates. The present plate theory approach accounts for through-the-thickness deformations. The equations of motion and the boundary conditions are obtained by the Carrera's Unified Formulation, and further interpolated by collocation with radial basis functions.

1. Introduction

Functionally graded plates (FGP) are obtained from gradual and continuous variation of material properties across the thickness direction. One advantage of FGP compared to laminated plates is that the material properties continuously vary in the thickness direction, as opposed to being discontinuous across adjoining layers as they are in laminated plates. This gradual variation avoids the delamination issues in laminated plates.

Typically FGP have been analysed neglecting the thickness stretching ϵ_{zz}, being the transverse displacement considered independent by thickness coordinates. Some recent work on the analysis of functionally graded plates was presented (Zenkour, 2006; Cheng and Batra, 2000; Loy et al., 1999; Reddy, 2000; Ferreira et al., 2005, 2006, 2007; Viola and Tornabene, 2009).

The effect of thickness stretching in FG plates has been investigated by Carrera et al. (2011), using finite elements.

The present paper addresses for the first time, the thickness stretching issue on FG plates, by a meshless technique based on collocation with radial basis functions. The technique is combined with the Carrera's Unified Formulation (CUF) (Carrera, 1996, 2001), in order to obtain the relevant equations of motion and natural boundary condition in strong form.

In recent years, radial basis functions (RBFs) proved to be an accurate technique for interpolating data and functions. A radial basis function, $\phi(||x-x_j||)$ depends on the Euclidian distance between distinct data centers $x_j, j=1,2,\ldots,N \in \mathbb{R}^n$, also called collocation points. Kansa (1990) introduced the concept of solving PDEs by an unsymmetric RBF collocation method based upon the MQ interpolation functions. The use of alternative methods to the Finite Element Methods for the analysis of plates, such as the meshless methods based on radial basis functions is attractive due to the absence of a mesh and the ease of collocation methods. The authors have recently applied the RBF collocation to the static deformations of composite beams and plates (Ferreira, 2003a,b; Ferreira et al., 2003).

The use of sinusoidal shear deformation plate theory was first presented by Touratier (1992, 1991, 1992), and later by Vidal and Polit (2008). The use of sinusoidal plate theories for functionally graded plates was presented by Zenkour (2006), where a $\epsilon_{zz}=0$ approach was used. The use of trigonometric shear deformation theory accounting for $\epsilon_{zz}\neq 0$ for the analysis of plates has not been used before. In this paper we consider an hybrid quasi-3D sinusoidal shear deformation theory. The expansion of both inplane displacements is defined as:

$$u = u_0 + z u_1 + \sin\left(\frac{\pi z}{h}\right) u_Z; \quad v = v_0 + z v_1 + \sin\left(\frac{\pi z}{h}\right) v_Z \tag{1}$$

while the transverse displacement is defined as:

$$w = w_0 + z w_1 + z^2 w_2 \tag{2}$$

It is relevant to notice that the application of applied loads is now possible at the top (or bottom) surfaces.

2. Numerical examples

In this example, an isotropic FGM square plate with a polynomial material law, as given by Zenkour (2006) is considered. The plate is

* Corresponding author. Tel.: +35 1225081705.
E-mail address: ferreira@fe.up.pt (A.J.M. Ferreira).

0093-6413/$ – see front matter © 2011 Elsevier Ltd. All rights reserved.
doi:10.1016/j.mechrescom.2011.04.011

Table 1
FGM isotropic plate with polynomial material law (Zenkour, 2006). Effect of transverse normal strain ϵ_{zz} for a bending problem.

k	a/h	ϵ_{zz}	$\bar{\sigma}_{xx}(h/3)$			$\bar{u}_z(0,0)$		
			4	10	100	4	10	100
1	Carrera et al. (2008)	$\neq 0$	0.6221	1.5064	14.969	0.7171	0.5875	0.5625
	CLT	0	0.8060	2.0150	20.150	0.5623	0.5623	0.5623
	FSDT (k = 5/6)	0	0.8060	2.0150	20.150	0.7291	0.5889	0.5625
	GSDT (Zenkour, 2006)	0		1.4894			0.5889	
	Carrera (N = 4) (Carrera et al., 2011)	0	0.7856	2.0068	20.149	0.7289	0.5890	0.5625
	Carrera (N = 4) (Carrera et al., 2011)	$\neq 0$	0.6221	1.5064	14.969	0.7171	0.5875	0.5625
	Present 13 × 13 grid	$\neq 0$	0.5925	1.4939	14.901	0.6997	0.5844	0.5596
	Present 17 × 17 grid	$\neq 0$	0.5925	1.4945	14.957	0.6998	0.5845	0.5622
	Present 21 × 21 grid	$\neq 0$	0.5925	1.4945	14.969	0.6997	0.5845	0.5624
4	Carrera et al. (2008)	$\neq 0$	0.4877	1.1971	11.923	1.1585	0.8821	0.8286
	CLT	0	0.6420	1.6049	16.049	0.8281	0.8281	0.8281
	FSDT (k = 5/6)	0	0.6420	1.6049	16.049	1.1125	0.8736	0.828
	GSDT (Zenkour, 2006)	0		1.1783			0.8651	
	Carrera (N = 4) (Carrera et al., 2011)	0	0.5986	1.5874	16.047	1.1673	0.8828	0.8286
	Carrera (N = 4) (Carrera et al., 2011)	$\neq 0$	0.4877	1.1971	11.923	1.1585	0.8821	0.8286
	Present 13 × 13 grid	$\neq 0$	0.4404	1.1780	11.894	1.1178	0.8749	0.8251
	Present 17 × 17 grid	$\neq 0$	0.4404	1.1783	11.923	1.1178	0.8750	0.8284
	Present 21 × 21 grid	$\neq 0$	0.4404	1.1783	11.932	1.1178	0.8750	0.8286
10	Carrera et al. (2008)	$\neq 0$	0.3695	0.8965	8.9077	1.3745	1.0072	0.9361
	CLT	0	0.4796	1.1990	11.990	0.9354	0.9354	0.9354
	FSDT (k = 5/6)	0	0.4796	1.1990	11.990	1.3178	0.9966	0.9360
	GSDT (Zenkour, 2006)	0		0.8775			1.0089	
	Carrera (N = 4) (Carrera et al., 2011)	0	0.4345	1.1807	11.989	1.3925	1.0090	0.9361
	Carrera (N = 4) (Carrera et al., 2011)	$\neq 0$	0.1478	0.8965	8.9077	1.3745	1.0072	0.9361
	Present 13 × 13 grid	$\neq 0$	0.3227	1.1780	11.894	1.3490	0.8749	0.8251
	Present 17 × 17 grid	$\neq 0$	0.3227	1.1783	11.923	1.3490	0.8750	0.8284
	Present 21 × 21 grid	$\neq 0$	0.3227	1.1783	11.932	1.3490	0.8750	0.8286

simply supported with a bi-sinusoidal transverse mechanical load, of amplitude load $p_z = \bar{p}_z \sin(\pi x/a)\sin(\pi y/a)$ applied at the top of the plate, $z = h/2$, $\bar{p}_z = 1$.

The considered thickness ratios a/h are 4, 10 and 100, which means thickness h equals 0.25, 0.1 and 0.01, respectively. The plate is graded from aluminum (bottom) to alumina (top). The following functional relationship is considered for Young's modulus $E(z)$ in the thickness direction z (Zenkour, 2006):

$$E(z) = E_m + (E_c - E_m)\left(\frac{2z+h}{2h}\right)^k \tag{3}$$

where E_m = 70 GPa and E_c = 380 GPa are the corresponding properties of the metal and ceramic, respectively; k is the (positive number) volume fraction exponent. The Poisson ratio is considered constant (ν = 0.3).

The in-plane displacements, the transverse displacements, the normal stresses and the in-plane and transverse shear stresses are

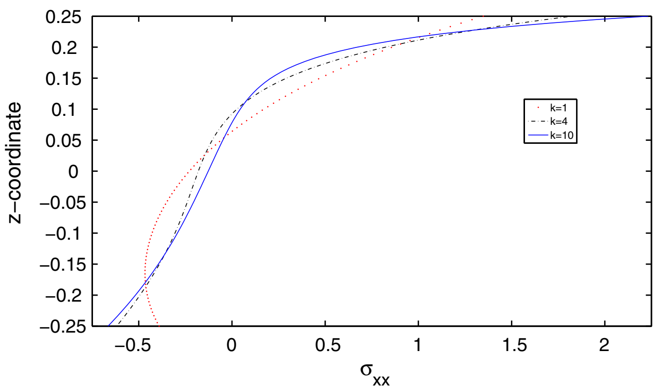

Fig. 2. FGM square plate subjected to sinusoidal load at the top, with a/h = 4. σ_{xx} through the thickness direction for different values of k.

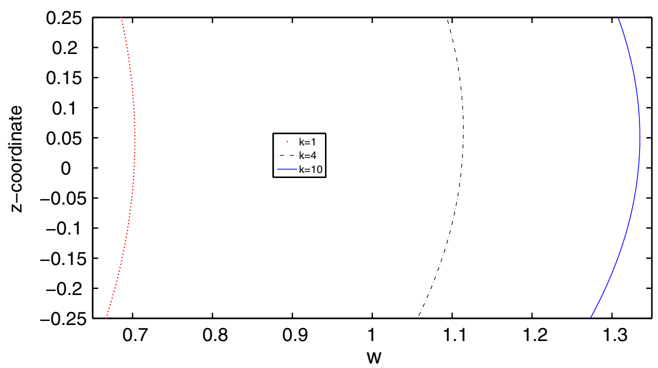

Fig. 1. FGM square plate subjected to sinusoidal load at the top, with a/h = 4. Displacement through the thickness direction for different values of k.

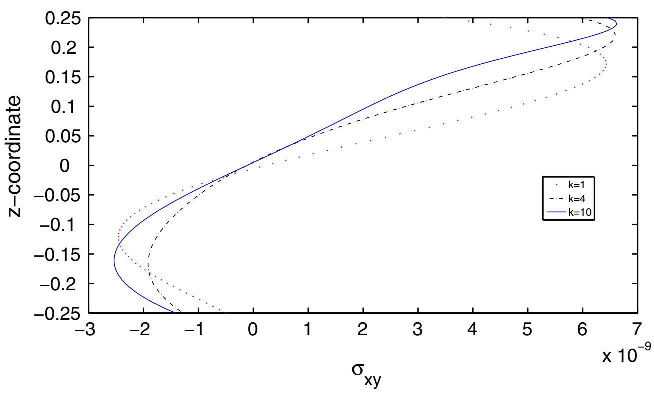

Fig. 3. FGM square plate subjected to sinusoidal load at the top, with a/h = 4. σ_{xy} through the thickness direction for different values of k.

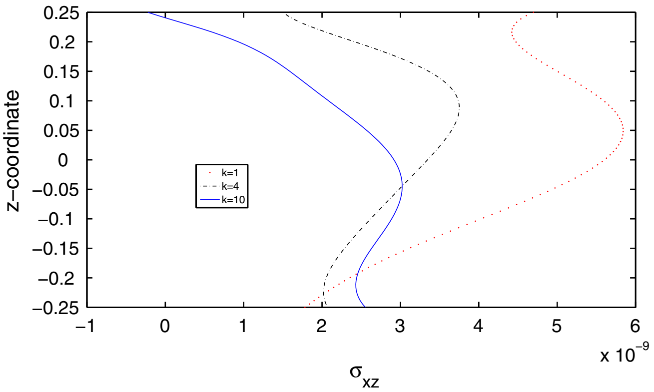

Fig. 4. FGM square plate subjected to sinusoidal load at the top, with $a/h = 4$. σ_{xz} through the thickness direction for different values of k.

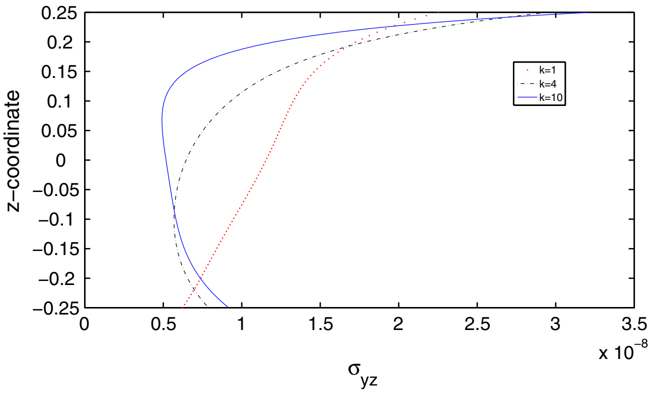

Fig. 5. FGM square plate subjected to sinusoidal load at the top, with $a/h = 4$. σ_{yz} through the thickness direction for different values of k.

presented in normalized form as:

$$\bar{u}_z = \frac{10h^3 E_c}{a^4 \bar{p}_z} u_z, \quad \bar{\sigma}_{xx} = \frac{h}{a\bar{p}_z}\sigma_{xx}, \quad \bar{\sigma}_{xz} = \frac{h}{a\bar{p}_z}\sigma_{xz}, \quad \bar{\sigma}_{zz} = \sigma_{zz} \qquad (4)$$

In Table 1 we analyse a FGM plate. We consider 90 mathematical layers, in order to model the continuous variation of properties across the thickness direction. We consider a Wendland C6 radial function, and a Chebyshev grid (see Ferreira and Fasshauer, 2006, for details). It is important to note that the load is applied at the top surface ($z = h/2$), which is not only physically correct as it makes all the difference in terms of the displacement and stresses evolution.

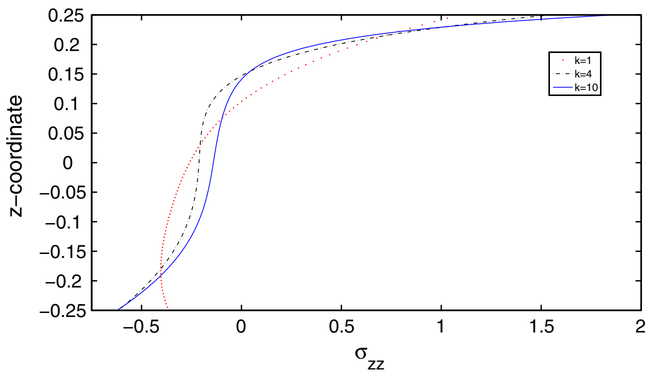

Fig. 6. FGM square plate subjected to sinusoidal load at the top, with $a/h = 4$. σ_{zz} through the thickness direction for different values of k.

In Figs. 1–6 we present the evolution of the displacement and stresses across the thickness direction for various values of the exponent k, using a 21×21 grid.

It should be noted that the present numerical method presents very close results to those of Carrera et al. (2011) for a $N = 4$ expansion. The consideration of a non-zero ϵ_{zz} strain produces a significant change in the transverse displacement as well as in the normal stress. This becomes evident when we compare the present approach with that of Zenkour (2006) who neglected the ϵ_{zz} strain in the formulation.

3. Conclusions

In this paper we presented a study using the radial basis function collocation method to analyse static deformations of functionally graded plates using a sinusoidal shear deformation plate formulation, allowing for through-the-thickness deformations. This has not been done before and serves to fill the gap of knowledge in this area.

The Unified Formulation by Carrera was used to generate the algebraic equations of equilibrium, later collocated with radial basis.

We analysed a square functionally graded plate in bending. The present results were compared with existing analytical solutions or competitive finite element solutions and excellent agreement was observed in all cases. It is relevant to notice the strong effect of considering the non-zero transverse normal deformations ϵ_{zz}.

References

Carrera, E., 1996. C^0 reissner-mindlin multilayered plate elements including zig-zag and interlaminar stress continuity. International Journal of Numerical Methods in Engineering 39, 1797–1820.
Carrera, E., 2001. Developments, ideas, and evaluations based upon reissner's mixed variational theorem in the modelling of multilayered plates and shells. Applied Mechanics Reviews 54, 301–329.
Carrera, E., Brischetto, S., Robaldo, A., 2008. Variable kinematic model for the analysis of functionally graded material plates. AIAA Journal 46, 194–203.
Carrera, E., Brischetto, S., Cinefra, M., Soave, M., 2011. Effects of thickness stretching in functionally graded plates and shells. Composites Part B: Engineering 42, 123–133.
Cheng, Z.Q., Batra, R.C., 2000. Deflection relationships between the homogeneous kirchhoff plate theory and different functionally graded plate theories. Archive of Mechanics 52, 143–158.
Ferreira, A.J.M., 2003a. A formulation of the multiquadric radial basis function method for the analysis of laminated composite plates. Composite Structures 59, 385–392.
Ferreira, A.J.M., 2003b. Thick composite beam analysis using a global meshless approximation based on radial basis functions. Mechanics of Advanced Materials and Structures 10, 271–284.
Ferreira, A.J.M., Fasshauer, G.E., 2006. Computation of natural frequencies of shear deformable beams and plates by a rbf-pseudospectral method. Computer Methods in Applied Mechanics and Engineering 196, 134–146.
Ferreira, A.J.M., Roque, C.M.C., Martins, P.A.L.S., 2003. Analysis of composite plates using higher-order shear deformation theory and a finite point formulation based on the multiquadric radial basis function method. Composites: Part B 34, 627–636.
Ferreira, A.J.M., Batra, R.C., Roque, C.M.C., Qian, L.F., Martins, P.A.L.S., 2005. Static analysis of functionally graded plates using third-order shear deformation theory and a meshless method. Composite Structures 69 (4), 449–457.
Ferreira, A.J.M., Batra, R.C., Roque, C.M.C., Qian, L.F., Jorge, R.M.N., September 2006. Natural frequencies of functionally graded plates by a meshless method. Composite Structures 75 (1–4), 593–600.
Ferreira, A.J.M., Roque, C.M.C., Jorge, R.M.N., Fasshauer, G.E., Batra, R.C., 2007. Analysis of functionally graded plates by a robust meshless method. Mechanics of Advanced Materials and Structures 14 (8), 577–587.
Kansa, E.J., 1990. Multiquadrics – a scattered data approximation scheme with applications to computational fluid dynamics. i: surface approximations and partial derivative estimates. Computers and Mathematics with Applications 19 (8/9), 127–145.
Loy, C.T., Reddy, J.N., Lam, K.Y., 1999. Vibration of functionally graded cylindrical shells. International Journal of Mechanical Sciences 41, 309–324.
Reddy, J.N., 2000. Analysis of functionally graded plates. International Journal for Numerical Methods in Engineering 47, 663–684.
Touratier, M., 1992. A generalization of shear deformation theories for axisymmetric multilayered shells. International Journal of Solids and Structures 29, 1379–1399.

Touratier, M., 1991. An efficient standard plate theory. International Journal of Engineering Science 29, 901–916.
Touratier, M., 1992. A refined theory of laminated shallow shells. International Journal of Solids and Structures 29 (11), 1401–1415.
Vidal, P., Polit, O., 2008. A family of sinus finite elements for the analysis of rectangular laminated beams. Composite Structures 84, 56–72.
Viola, E., Tornabene, F., 2009. Free vibrations of three parameter functionally graded parabolic panels of revolution. Mechanics Research Communications 35 (5), 587–594.
Zenkour, A.M., 2006. Generalized shear deformation theory for bending analysis of functionally graded plates. Applied Mathematical Modelling 30, 67–84.

2.2 A quasi-3D sinusoidal shear deformation theory for the static and free vibration analysis of functionally graded plates

A. M. A. Neves, A. J. M. Ferreira, E. Carrera, C. M. C. Roque, M. Cinefra, R. M. N. Jorge, C. M. M. Soares, A quasi-3D sinusoidal shear deformation theory for the static and free vibration analysis of functionally graded plates, Composites Part B, Volume 43, 2012, pages 711-725.

Composites: Part B 43 (2012) 711–725

Contents lists available at SciVerse ScienceDirect

Composites: Part B

journal homepage: www.elsevier.com/locate/compositesb

A quasi-3D sinusoidal shear deformation theory for the static and free vibration analysis of functionally graded plates

A.M.A. Neves [a], A.J.M. Ferreira [a,*], E. Carrera [c], C.M.C. Roque [b], M. Cinefra [c], R.M.N. Jorge [a], C.M.M. Soares [d]

[a] Departamento de Engenharia Mecânica, Faculdade de Engenharia, Universidade do Porto, Rua Dr. Roberto Frias, 4200-465 Porto, Portugal
[b] INEGI, Faculdade de Engenharia, Universidade do Porto, Rua Dr. Roberto Frias, 4200-465 Porto, Portugal
[c] Departament of Aeronautics and Aerospace Engineering, Politecnico di Torino, Corso Duca degli Abruzzi, 24, 10129 Torino, Italy
[d] Instituto Superior Técnico, Av. Rovisco Pais, Lisboa, Portugal

ARTICLE INFO

Article history:
Received 16 July 2011
Accepted 14 August 2011
Available online 25 August 2011

Keywords:
A. Layered structures
C. Computational modelling

ABSTRACT

In this paper we present a new application for Carrera's unified Formulation (CUF) to analyse functionally graded plates.

In this paper the authors present explicit governing equations of a sinusoidal shear deformation theory for functionally graded plates. It addresses the bending and free vibration analysis and accounts for through-the-thickness deformations.

The equations of motion are interpolated by collocation with radial basis functions. Numerical examples demonstrate the efficiency of the present approach.

1. Introduction

Functionally graded materials (FGM) are a class of composites in which the properties of the material gradually change over one or more cartesian direction. A typical FGM plate considers a continuous variation of material properties over the thickness direction by mixing two different materials [1]. The gradual variation of properties avoids the delamination failure that are common in laminated composites. The FGM concept has applications in several fields such as aerospace and civil [1]. The increase of FGM applications requires accurate plate theories. Typically, the analysis of FGM plates is performed using the first-order shear deformation theory (FSDT) [2–5] or higher-order shear deformation theories (HSDT) [3,5–8]. The FSDT gives acceptable results but depends on the shear correction factor which is hard to find as it depends on many parameters. There is no need of a shear correction factor when using a HSDT but equations of motion are more complicated than those of the FSDT. Carrera's Unified Formulation (CUF) made the implementation of such theories easier.

Typically functionally graded plates have been analysed with shear deformation theories that neglect the thickness stretching ϵ_{zz}, being the transverse displacement considered to be independent of thickness coordinates. The effect of thickness stretching in FGM plates has been recently investigated by Carrera et al. [9], using finite element approximations.

The use of alternative methods to the finite element methods for the analysis of plates, such as the meshless methods based on collocation with radial basis functions is atractive due to the absence of a mesh and the ease of collocation methods. In recent years, radial basis functions (RBFs) showed excellent accuracy in the interpolation of data and functions. Kansa [10] introduced the concept of solving partial differential equations by an unsymmetric RBF collocation method based upon the multiquadric interpolation functions. The authors have recently applied the RBF collocation to the static deformations and free vibrations of composite beams and plates [11–18].

The present paper addresses the thickness stretching issue on the static and free vibration analysis of FGM plates, by a meshless technique based on collocation with radial basis functions. The CUF method [19,20] is employed to obtain the algebraic equations of motion and boundary conditions. Such equations of motion and corresponding boundary conditions are then interpolated by radial basis functions to obtain an algebraic system of equations.

2. Governing equations and boundary conditions in the framework of unified formulation

The unified formulation proposed by Carrera [19,20] (further denoted as CUF) has been applied in several finite element analysis, either using the Principle of Virtual Displacements, or by using the Reissner's Mixed Variational theorem. The stiffness matrix components, the external force terms or the inertia terms can be obtained directly with this unified formulation, irrespective of the shear deformation theory being considered.

* Corresponding author.
E-mail address: ferreira@fe.up.pt (A.J.M. Ferreira).

1359-8368/$ - see front matter © 2011 Elsevier Ltd. All rights reserved.
doi:10.1016/j.compositesb.2011.08.009

For the sake of completeness, the meshless version of Carrera's unified formulation [19,20] is briefly reviewed. It is shown how to obtain the fundamental nuclei, which allows the derivation of the equations of motion and boundary conditions, for the present collocation with RBFs.

The use of sinusoidal shear deformation plate theory was first presented by Touratier [21–23], later by Vidal and Polit [24], and recently by Neves et al. [25]. The use of sinusoidal plate theories for functionally graded plates was presented by Zenkour [2], where a $\epsilon_{zz} = 0$ approach was used. The use of trigonometric shear deformation theory accounting for $\epsilon_{zz} \neq 0$ for the analysis of plates has not been used before. In this paper we consider an hybrid quasi-3D sinusoidal shear deformation theory, with different expansion for the in-plane displacements (u, v) and the out-of-plane displacement (w).

Consider a rectangular plate of plan-form dimensions a and b and uniform thickness h. The co-ordinate system is taken such that the x–y plane coincides with the midplane of the plate. The plate is composed of a functionally graded material across the thickness direction.

2.1. Displacement field

A generalization of the CUF concepts is introduced here by considering different expansions for every displacement component as function of the thickness variable. In-plane displacements are considered to be of sinusoidal type across the thickness coordinate,

$$u = u_0 + zu_1 + \sin\left(\frac{\pi z}{h}\right) u_Z \tag{1}$$

$$v = v_0 + zv_1 + \sin\left(\frac{\pi z}{h}\right) v_Z \tag{2}$$

while the transverse displacement is defined as quadratic in the thickness direction

$$w = w_0 + zw_1 + z^2 w_Z \tag{3}$$

It turns out that the present formulation can be seen as a generalization of the original CUF, by introducing different displacement fields for in-plane and out-of-plane displacements.

2.2. Strains

Stresses and strains are separated into in-plane and normal components, denoted respectively by the subscripts p and n. The mechanical strains in the kth layer can be related to the displacement field $\mathbf{u}^k = \left\{u_x^k, u_y^k, u_z^k\right\}$ via the geometrical relations:

$$\begin{aligned} \epsilon_{pG}^k &= [\epsilon_{xx}, \epsilon_{yy}, \gamma_{xy}]^{kT} = \mathbf{D}_p^k \mathbf{u}^k \\ \epsilon_{nG}^k &= [\gamma_{xz}, \gamma_{yz}, \epsilon_{zz}]^{kT} = \left(\mathbf{D}_{np}^k + \mathbf{D}_{nz}^k\right) \mathbf{u}^k \end{aligned} \tag{4}$$

wherein the differential operator arrays are defined as follows:

$$\mathbf{D}_p^k = \begin{bmatrix} \partial_x & 0 & 0 \\ 0 & \partial_y & 0 \\ \partial_y & \partial_x & 0 \end{bmatrix} \quad \mathbf{D}_{np}^k = \begin{bmatrix} 0 & 0 & \partial_x \\ 0 & 0 & \partial_y \\ 0 & 0 & 0 \end{bmatrix} \quad \mathbf{D}_{nz}^k = \begin{bmatrix} \partial_z & 0 & 0 \\ 0 & \partial_z & 0 \\ 0 & 0 & \partial_z \end{bmatrix} \tag{5}$$

2.3. Elastic stress–strain relations

The 3D constitutive equations in each layer k are given as:

$$\begin{aligned} \sigma_{pC}^k &= \mathbf{C}_{pp}^k \epsilon_{pG}^k + \mathbf{C}_{pn}^k \epsilon_{nG}^k \\ \sigma_{nC}^k &= \mathbf{C}_{np}^k \epsilon_{pG}^k + \mathbf{C}_{nn}^k \epsilon_{nG}^k \end{aligned} \tag{6}$$

with

$$\begin{aligned} \mathbf{C}_{pp}^k &= \begin{bmatrix} C_{11} & C_{12} & 0 \\ C_{12} & C_{22} & 0 \\ 0 & 0 & C_{66} \end{bmatrix} \quad \mathbf{C}_{pn}^k = \begin{bmatrix} 0 & 0 & C_{13} \\ 0 & 0 & C_{23} \\ 0 & 0 & 0 \end{bmatrix} \\ \mathbf{C}_{np}^k &= \begin{bmatrix} 0 & 0 & 0 \\ 0 & 0 & 0 \\ C_{13} & C_{23} & 0 \end{bmatrix} \quad \mathbf{C}_{nn}^k = \begin{bmatrix} C_{55} & 0 & 0 \\ 0 & C_{44} & 0 \\ 0 & 0 & C_{33} \end{bmatrix} \end{aligned} \tag{7}$$

The functionally graded plate is divided into a number of uniform thickness layers. For every layer, we define the volume fraction of the ceramic phase as:

$$V_c = \left(0.5 + \frac{z}{h}\right)^p \tag{8}$$

where $z \in [-h/2, h/2]$, and p is a scalar parameter that allows the user to define gradation of material properties across the thickness direction. The volume fraction for the metal phase is given as $V_m = 1 - V_c$.

The computation of the elastic constants C_{ij}^k depends on which assumption of ϵ_{zz} we consider. If $\epsilon_{zz} = 0$, then C_{ij}^k are the plane-stress reduced elastic constants:

$$C_{11}^k = \frac{E^k}{1 - (\nu^k)^2}, \quad C_{12}^k = \nu^k \frac{E^k}{1 - (\nu^k)^2}, \quad C_{22}^k = \frac{E^k}{1 - (\nu^k)^2} \tag{9}$$

$$C_{44}^k = G^k, \quad C_{55}^k = G^k, \quad C_{66}^k = G^k, \quad C_{33}^k = 0 \tag{10}$$

where E^k is the modulus of elasticity, ν^k is the Poisson's ratio, and G^k is the shear modulus $G^k = \frac{E^k}{2(1+\nu^k)}$ for each layer.

It is interesting to note that the present theory does not consider the use of shear-correction factors, as would be the case of the first-order shear deformation theory (FSDT).

If $\epsilon_{zz} \neq 0$ (thickness stretching), then C_{ij}^k are the three-dimensional elastic constants, given by

$$C_{11}^k = \frac{E^k(1 - (\nu^k)^2)}{1 - 3(\nu^k)^2 - 2(\nu^k)^3}, \quad C_{12}^k = \frac{E^k(\nu^k + (\nu^k)^2)}{1 - 3(\nu^k)^2 - 2(\nu^k)^3}, \quad C_{22}^k = \frac{E^k(1 - (\nu^k)^2)}{1 - 3(\nu^k)^2 - 2(\nu^k)^3} \tag{11}$$

$$C_{44}^k = G^k, \quad C_{55}^k = G^k, \quad C_{66}^k = G^k, \quad C_{33}^k = \frac{E^k(1 - (\nu^k)^2)}{1 - 3(\nu^k)^2 - 2(\nu^k)^3} \tag{12}$$

In the CUF formulation we consider virtual (mathematical) layers of constant thickness, each containing a homogeneized modulus of elasticity, E^k, and a homogeneized Poisson's ratio, ν^k.

For each virtual layer, the elastic properties E^k and ν^k can be computed in two ways. First, we may consider the the law-of-mistures:

$$E^k(z) = E_m V_m + E_c V_c \quad \nu^k(z) = \nu_m V_m + \nu_c V_c \tag{13}$$

Second, and perhaps more interesting, we may consider the Mori–Tanaka homogenization procedure. In this homogenization method, we find the bulk modulus, K, and the effective shear modulus, G, of the composite equivalent layer as

$$\frac{K - K_1}{K_2 - K_1} = \frac{V_2}{1 + (1 - V_2)\frac{K_2 - K_1}{K_1 + 4/3G_1}} \quad \frac{G - G_1}{G_2 - G_1} = \frac{V_2}{1 + (1 - V_2)\frac{G_2 - G_1}{G_1 + f_1}} \tag{14}$$

where

$$f_1 = \frac{G_1(9K_1 + 8G_1)}{6(K_1 + 2G_1)} \tag{15}$$

The effective values of Young's modulus, E^k, and Poisson's ratio, ν^k, are found from

$$E^k = \frac{9KG}{3K + G}; \quad \nu^k = \frac{3K - 2G}{2(3K + G)} \tag{16}$$

2.4. Governing equations

The three displacement components u_x, u_y and u_z (given in (1)–(3)) and their relative variations can be modelled as:

$$(u_x, u_y, u_z) = F_\tau(u_{x\tau}, u_{y\tau}, u_{z\tau}) \quad (\delta u_x, \delta u_y, \delta u_z) = F_s(\delta u_{xs}, \delta u_{ys}, \delta u_{zs}) \tag{17}$$

In the present formulation the thickness functions are

$$F_{sux} = F_{suy} = F_{\tau ux} = F_{\tau uy} = \left[1 \quad z \quad \sin\left(\frac{\pi z}{h}\right)\right] \tag{18}$$

for inplane displacements u, v and

$$F_{suz} = F_{\tau uz} = [1 \quad z \quad z^2] \tag{19}$$

for transverse displacement w. We then obtain all terms of the equations of motion by integrating through the thickness direction.

It is interesting to note that under this combination of the unified formulation and RBF collocation, the collocation code depends only on the choice of F_τ, F_s, in order to solve this type of problems. We designed a MATLAB code that just by changing F_τ, F_s can analyse static deformations and free vibrations for any type of C_z^0 shear deformation theory.

A multi-layered functionally graded plate with N_l layers is considered. The Principle of Virtual Displacements (PVD) for the mechanical case is defined as:

$$\sum_{k=1}^{N_l} \int_{\Omega_k} \int_{A_k} \left\{ \delta\epsilon_{pG}^{k\;T} \sigma_{pC}^k + \delta\epsilon_{nG}^{k\;T} \sigma_{nC}^k \right\} d\Omega_k\, dz = \sum_{k=1}^{N_l} \delta L_e^k \tag{20}$$

where Ω_k and A_k are the integration domains in plane (x,y) and z direction, respectively. Here, k indicates the layer and T the transpose of a vector, and δL_e^k is the external work for the kth layer. G means geometrical relations and C constitutive equations.

Substituting the geometrical relations, the constitutive equations and the unified formulation into the variational statement PVD, for the kth layer, one has:

$$\int_{\Omega_k} \int_{A_k} \left[\left(\mathbf{D}_p^k F_s \delta \mathbf{u}_s^k\right)^T \left(\mathbf{C}_{pp}^k \mathbf{D}_p^k F_\tau \mathbf{u}_\tau^k + \mathbf{C}_{pn}^k \left(\mathbf{D}_{n\Omega}^k + \mathbf{D}_{nz}^k\right) F_\tau \mathbf{u}_\tau^k\right) + \left(\left(\mathbf{D}_{n\Omega}^k + \mathbf{D}_{nz}^k\right) F_s \delta \mathbf{u}_s^k\right)^T \left(\mathbf{C}_{np}^k \mathbf{D}_p^k F_\tau \mathbf{u}_\tau^k + \mathbf{C}_{nn}^k \left(\mathbf{D}_{n\Omega}^k + \mathbf{D}_{nz}^k\right) F_\tau \mathbf{u}_\tau^k\right) \right] d\Omega_k\, dz = \delta L_e^k \tag{21}$$

At this point, the formula of integration by parts is applied:

$$\int_{\Omega_k} ((\mathbf{D}_\Omega)\delta \mathbf{a}^k)^T \mathbf{a}^k\, d\Omega_k = -\int_{\Omega_k} \delta \mathbf{a}^{k^T} ((\mathbf{D}_\Omega^T)\mathbf{a}^k) d\Omega_k + \int_{\Gamma_k} \delta \mathbf{a}^{k^T} ((\mathbf{I}_\Omega)\mathbf{a}^k) d\Gamma_k \tag{22}$$

where $\mathbf{I}_\Omega$ matrix is obtained applying the *Gradient theorem*:

$$\int_\Omega \frac{\partial \psi}{\partial x_i} d\upsilon = \oint_\Gamma n_i \psi\, ds \tag{23}$$

being n_i the components of the normal $\hat{n}$ to the boundary along the direction i. After integration by parts, the governing equations and boundary conditions for the plate in the mechanical case are obtained:

$$\begin{aligned}
&\int_{\Omega_k} \int_{A_k} (\delta \mathbf{u}_s^k)^T \Big[\Big(\left(-\mathbf{D}_p^k\right)^T \left(\mathbf{C}_{pp}^k (\mathbf{D}_p^k) + \mathbf{C}_{pn}^k \left(\mathbf{D}_{n\Omega}^k + \mathbf{D}_{nz}^k\right)\right) \\
&+ \left(-\mathbf{D}_{n\Omega}^k + \mathbf{D}_{nz}^k\right)^T \left(\mathbf{C}_{np}^k (\mathbf{D}_p^k) + \mathbf{C}_{nn}^k (\mathbf{D}_{n\Omega}^k + \mathbf{D}_{nz}^k)\right)\Big) F_\tau F_s \mathbf{u}_\tau^k \Big] dx\, dy\, dz \\
&+ \int_{\Omega_k} \int_{A_k} (\delta \mathbf{u}_s^k)^T \Big[\left(\mathbf{I}_p^{kT} \left(\mathbf{C}_{pp}^k (\mathbf{D}_p^k) + \mathbf{C}_{pn}^k (\mathbf{D}_{n\Omega}^k + \mathbf{D}_{nz}^k)\right)\right. \\
&\left.+ \mathbf{I}_{np}^{kT} \left(\mathbf{C}_{np}^k (\mathbf{D}_p^k) + \mathbf{C}_{nn}^k (\mathbf{D}_{n\Omega}^k + \mathbf{D}_{nz}^k)\right)\right) F_\tau F_s \mathbf{u}_\tau^k \Big] dx\, dy\, dz \\
&= \int_{\Omega_k} \delta \mathbf{u}_s^{kT} F_s \mathbf{p}^k\, d\Omega_k
\end{aligned} \tag{24}$$

where $\mathbf{I}_p^k$ and $\mathbf{I}_{np}^k$ depend on the boundary geometry:

$$\mathbf{I}_p^k = \begin{bmatrix} n_x & 0 & 0 \\ 0 & n_y & 0 \\ n_y & n_x & 0 \end{bmatrix} \quad \mathbf{I}_{np}^k = \begin{bmatrix} 0 & 0 & n_x \\ 0 & 0 & n_y \\ 0 & 0 & 0 \end{bmatrix} \tag{25}$$

The normal to the boundary of domain Ω is:

$$\hat{\mathbf{n}} = \begin{bmatrix} n_x \\ n_y \end{bmatrix} = \begin{bmatrix} cos(\varphi_x) \\ cos(\varphi_y) \end{bmatrix} \tag{26}$$

where φ_x and φ_y are the angles between the normal $\hat{n}$ and the direction x and y respectively.

The governing equations for a multi-layered plate subjected to mechanical loadings are:

$$\delta \mathbf{u}_s^{k^T} : \mathbf{K}_{uu}^{k\tau s} \mathbf{u}_\tau^k = \mathbf{P}_{u\tau}^k \tag{27}$$

where the fundamental nucleus $\mathbf{K}_{uu}^{k\tau s}$ is obtained as:

$$\begin{aligned}
\mathbf{K}_{uu}^{k\tau s} = \Big[&\left(-\mathbf{D}_p^k\right)^T \left(\mathbf{C}_{pp}^k (\mathbf{D}_p^k) + \mathbf{C}_{pn}^k (\mathbf{D}_{n\Omega}^k + \mathbf{D}_{nz}^k)\right) \\
&+ \left(-\mathbf{D}_{n\Omega}^k + \mathbf{D}_{nz}^k\right)^T \left(\mathbf{C}_{np}^k (\mathbf{D}_p^k) + \mathbf{C}_{nn}^k (\mathbf{D}_{n\Omega}^k + \mathbf{D}_{nz}^k)\right)\Big] F_\tau F_s
\end{aligned} \tag{28}$$

and the corresponding Neumann-type boundary conditions on Γ_k are:

$$\mathbf{\Pi}_d^{k\tau s} \mathbf{u}_\tau^k = \mathbf{\Pi}_d^{k\tau s} \bar{\mathbf{u}}_\tau^k \tag{29}$$

where

$$\begin{aligned}
\mathbf{\Pi}_d^{k\tau s} = \Big[&\mathbf{I}_p^{kT} \left(\mathbf{C}_{pp}^k \left(\mathbf{D}_p^k\right) + \mathbf{C}_{pn}^k (\mathbf{D}_{n\Omega}^k + \mathbf{D}_{nz}^k)\right) + \mathbf{I}_{np}^{kT} \Big(\mathbf{C}_{np}^k \left(\mathbf{D}_p^k\right) \\
&+ \mathbf{C}_{nn}^k \left(\mathbf{D}_{n\Omega}^k + \mathbf{D}_{nz}^k\right)\Big)\Big] F_\tau F_s
\end{aligned} \tag{30}$$

and $\mathbf{P}_{u\tau}^k$ are variationally consistent loads with applied pressure.

2.5. Dynamic governing equations

The PVD for the dynamic case is expressed as:

$$\begin{aligned}
&\sum_{k=1}^{N_l} \int_{\Omega_k} \int_{A_k} \left\{ \delta\epsilon_{pG}^{k\;T} \sigma_{pC}^k + \delta\epsilon_{nG}^{k\;T} \sigma_{nC}^k \right\} d\Omega_k\, dz \\
&= \sum_{k=1}^{N_l} \int_{\Omega_k} \int_{A_k} \rho^k \delta \mathbf{u}^{kT} \ddot{\mathbf{u}}^k d\Omega_k\, dz + \sum_{k=1}^{N_l} \delta L_e^k
\end{aligned} \tag{31}$$

where ρ^k is the mass density of the k-th layer and double dots denote acceleration.

By substituting the geometrical relations, the constitutive equations and the unified formulation, we obtain the following governing equations:

$$\delta \mathbf{u}_s^{k^T} : \mathbf{K}_{uu}^{k\tau s} \mathbf{u}_\tau^k = \mathbf{M}^{k\tau s} \ddot{\mathbf{u}}_\tau^k + \mathbf{P}_{u\tau}^k \tag{32}$$

In the case of free vibrations one has:

$$\delta \mathbf{u}_s^{k^T} : \mathbf{K}_{uu}^{k\tau s} \mathbf{u}_\tau^k = \mathbf{M}^{k\tau s} \ddot{\mathbf{u}}_\tau^k \tag{33}$$

where $\mathbf{M}^{k\tau s}$ is the fundamental nucleus for the inertial term. The explicit form of the inertial terms is

$$\begin{aligned}
M_{ij}^{k\tau s} &= \sum_{k=1}^{N_l} \int_{z_k}^{z_{k+1}} \rho^k F_\tau F_s\, dz, \quad i = j = 1,2,3 \\
M_{ij}^{k\tau s} &= 0, \quad i \neq j
\end{aligned} \tag{34}$$

The geometrical and mechanical boundary conditions are the same of the static case.

2.6. Equations of motion and boundary conditions in terms of resultants

The following stress layer-resultants are defined:

$$\left(\boldsymbol{R}_p^{ks}, \boldsymbol{R}_n^{ks}\right) = \int_{A_k} \left(F_s \boldsymbol{\sigma}_p^k, F_s \boldsymbol{\sigma}_n^k\right) dz \tag{35}$$

where $\boldsymbol{R}_p^{ks} = \left\{R_{xx}^{ks}, R_{yy}^{ks}, R_{xy}^{ks}\right\}$ and $\boldsymbol{R}_n^{ks} = \left\{R_{xz}^{ks}, R_{yz}^{ks}, R_{zz}^{ks}\right\}$.

Substituting in (31), that includes the inertial term, and performing the integration by parts, one obtains:

$$\sum_{k=1}^{N_l} \left(\int_{\Omega^k} \delta \boldsymbol{u}_s^{kT} \left(-\boldsymbol{D}_p^{sT} \boldsymbol{R}_p^{ks} + \left(-\boldsymbol{D}_{n\Omega}^s + \boldsymbol{D}_{nz}^s\right)^T \boldsymbol{R}_n^{ks}\right) d\Omega^k + \int_{\Gamma^k} \delta \boldsymbol{u}_s^{kT} \left(\boldsymbol{I}_p^T \boldsymbol{R}_p^{ks} + \boldsymbol{I}_{np}^T \boldsymbol{R}_n^{ks}\right) d\Gamma^k \right) = \sum_{k=1}^{N_l} \int_{\Omega^k} \delta \boldsymbol{u}_s^{kT} \left(\rho^k E_{\tau s} \boldsymbol{I} \ddot{\boldsymbol{u}}_\tau^k + \boldsymbol{p}_s^k\right) d\Omega^k \tag{36}$$

where $E_{\tau s} = \int_{A^k} F_\tau F_s \, dz$ and $\boldsymbol{I}$ is the identity matrix.

By imposing the definition of virtual variations for the unknown displacements, the differential system of governing equations and related boundary conditions are derived in terms of the introduced stress resultants. For the k-layer, the equilibrium equations on Ω^k are:

$$\delta \boldsymbol{u}_s^{kT} : -\boldsymbol{D}_p^{sT} \boldsymbol{R}_p^{ks} + \left(-\boldsymbol{D}_{n\Omega}^s + \boldsymbol{D}_{nz}^s\right)^T \boldsymbol{R}_n^{ks} = E_{\tau s} \boldsymbol{I} \ddot{\boldsymbol{u}}_\tau^k + \boldsymbol{p}_s^k \tag{37}$$

while the boundary conditions on Γ^k are:

$$\boldsymbol{u}_s^k = \bar{\boldsymbol{u}}_s^k \quad \text{geometrical} \tag{38}$$

$$\boldsymbol{I}_p^T \boldsymbol{R}_p^{ks} + \boldsymbol{I}_{np}^T \boldsymbol{R}_n^{ks} = \boldsymbol{I}_p^T \overline{\boldsymbol{R}}_p^{ks} + \boldsymbol{I}_{np}^T \overline{\boldsymbol{R}}_n^{ks} \quad \text{mechanical} \tag{39}$$

We rename the resultants as follows:

$$\begin{aligned} &\boldsymbol{R}_{xx}^0 = \int_A 1 \cdot \boldsymbol{\sigma}_{xx} = N_{xx}; \quad \boldsymbol{R}_{yy}^0 = N_{yy}; \quad \boldsymbol{R}_{xy}^0 = N_{xy} \\ &\boldsymbol{R}_{xz}^0 = Q_{xz}; \quad \boldsymbol{R}_{yz}^0 = Q_{yz}; \quad \boldsymbol{R}_{zz}^0 = Q_{zz} \quad (\text{for } s = 0) \end{aligned} \tag{40}$$

$$\begin{aligned} &\boldsymbol{R}_{xx}^1 = M_{xx}; \quad \boldsymbol{R}_{yy}^1 = M_{yy}; \quad \boldsymbol{R}_{xy}^1 = M_{xy} \\ &\boldsymbol{R}_{xz}^1 = M_{xz}; \quad \boldsymbol{R}_{yz}^1 = M_{yz}; \quad \boldsymbol{R}_{zz}^1 = M_{zz} \quad (\text{for } s = 1) \end{aligned} \tag{41}$$

The name of resultants does not change for $s = Z$.

Substituting in the equilibrium Eqs. (37) and performing the products, one obtains the following equations of motion:

$$\begin{aligned}
\delta \boldsymbol{u}_0 &: -\partial_x N_{xx} - \partial_y N_{xy} + \partial_z Q_{xz} = \sum_{k=1}^{N_l} \int_{A_k} \rho^k (\ddot{u}_0 + z\ddot{u}_1 + \sin(z)\ddot{u}_Z) dz + (p_x + zp_x + \sin(z)p_x) \\
\delta \boldsymbol{v}_0 &: -\partial_x N_{xy} - \partial_y N_{yy} + \partial_z Q_{yz} = \sum_{k=1}^{N_l} \int_{A_k} \rho^k (\ddot{v}_0 + z\ddot{v}_1 + \sin(z)\ddot{v}_Z) dz + (p_y + zp_y + \sin(z)p_y) \\
\delta \boldsymbol{w}_0 &: -\partial_x Q_{xz} - \partial_y Q_{yz} + \partial_z Q_{zz} = \sum_{k=1}^{N_l} \int_{A_k} \rho^k (\ddot{w}_0 + z\ddot{w}_1 + z^2\ddot{w}_Z) dz + (p_z + zp_z + z^2 p_z) \\
\delta \boldsymbol{u}_1 &: -\partial_x M_{xx} - \partial_y M_{xy} + \partial_z M_{xz} = \sum_{k=1}^{N_l} \int_{A_k} \rho^k z (\ddot{u}_0 + z\ddot{u}_1 + \sin(z)\ddot{u}_Z) dz + (p_x + zp_x + \sin(z)p_x) \\
\delta \boldsymbol{v}_1 &: -\partial_x M_{xy} - \partial_y M_{yy} + \partial_z M_{yz} = \sum_{k=1}^{N_l} \int_{A_k} \rho^k z (\ddot{v}_0 + z\ddot{v}_1 + \sin(z)\ddot{v}_Z) dz + (p_y + zp_y + \sin(z)p_y) \\
\delta \boldsymbol{w}_1 &: -\partial_x M_{xz} - \partial_y M_{yz} + \partial_z M_{zz} = \sum_{k=1}^{N_l} \int_{A_k} \rho^k z (\ddot{w}_0 + z\ddot{w}_1 + z^2\ddot{w}_Z) dz + (p_z + zp_z + z^2 p_z) \\
\boldsymbol{u}_Z &: -\partial_x R_{xx}^Z - \partial_y R_{xy}^Z + \partial_z R_{xz}^Z = \sum_{k=1}^{N_l} \int_{A_k} \rho^k \sin(z) (\ddot{u}_0 + z\ddot{u}_1 + \sin(z)\ddot{u}_Z) dz + (p_x + zp_x + \sin(z)p_x) \\
\delta \boldsymbol{v}_Z &: -\partial_x R_{xy}^Z - \partial_y R_{yy}^Z + \partial_z R_{yz}^Z = \sum_{k=1}^{N_l} \int_{A_k} \rho^k \sin(z) (\ddot{v}_0 + z\ddot{v}_1 + \sin(z)\ddot{v}_Z) dz + (p_y + zp_y + \sin(z)p_y) \\
\delta \boldsymbol{w}_Z &: -\partial_x R_{xz}^Z - \partial_y R_{yz}^Z + \partial_z R_{zz}^Z = \sum_{k=1}^{N_l} \int_{A_k} \rho^k z^2 (\ddot{w}_0 + z\ddot{w}_1 + z^2\ddot{w}_Z) dz + (p_z + zp_z + z^2 p_z)
\end{aligned} \tag{42}$$

and the mechanical boundary conditions:

$$\begin{aligned}
\delta \boldsymbol{u}_0 &: n_x N_{xx} + n_y N_{xy} = n_x \overline{N}_{xx} + n_y \overline{N}_{xy} \\
\delta \boldsymbol{v}_0 &: n_x N_{xy} + n_y N_{yy} = n_x \overline{N}_{xy} + n_y \overline{N}_{yy} \\
\delta \boldsymbol{w}_0 &: n_x Q_{xz} + n_y Q_{yz} = n_x \overline{Q}_{xz} + n_y \overline{Q}_{yz} \\
\delta \boldsymbol{u}_1 &: n_x M_{xx} + n_y M_{xy} = n_x \overline{M}_{xx} + n_y \overline{M}_{xy} \\
\delta \boldsymbol{v}_1 &: n_x M_{xy} + n_y M_{yy} = n_x \overline{M}_{xy} + n_y \overline{M}_{yy} \\
\delta \boldsymbol{w}_1 &: n_x M_{xz} + n_y M_{yz} = n_x \overline{M}_{xz} + n_y \overline{M}_{yz} \\
\delta \boldsymbol{u}_Z &: n_x R_{xx}^Z + n_y R_{xy}^Z = n_x \overline{R}_{xx}^Z + n_y \overline{R}_{xy}^Z \\
\delta \boldsymbol{v}_Z &: n_x R_{xy}^Z + n_y R_{yy}^Z = n_x \overline{R}_{xy}^Z + n_y \overline{R}_{yy}^Z \\
\delta \boldsymbol{w}_Z &: n_x R_{xz}^Z + n_y R_{yz}^Z = n_x \overline{R}_{xz}^Z + n_y \overline{R}_{yz}^Z
\end{aligned} \tag{43}$$

2.7. Equations of motion and boundary conditions in terms of displacements

In order to discretize the equations of motion by radial basis functions, we present in the following the explicit terms of the equations of motion and the boundary conditions in terms of the generalized displacements.

$$\begin{aligned}
\delta u_0 :& -A_{11} \frac{\partial^2 u_0}{\partial x^2} - A_{66} \frac{\partial^2 u_0}{\partial y^2} - B_{11} \frac{\partial^2 u_1}{\partial x^2} - B_{66} \frac{\partial^2 u_1}{\partial y^2} + G_{11} \frac{\partial^2 u_Z}{\partial x^2} \\
&+ G_{66} \frac{\partial^2 u_Z}{\partial y^2} - (A_{12} + A_{66}) \frac{\partial^2 v_0}{\partial x \partial y} - (B_{12} + B_{66}) \frac{\partial^2 v_1}{\partial x \partial y} \\
&+ (G_{12} + G_{66}) \frac{\partial^2 v_Z}{\partial x \partial y} + A_{55} \frac{\partial w_1}{\partial x} + H_{55} \frac{\partial w_Z}{\partial x} = I_0 \ddot{u}_0 + I_1 \ddot{u}_1 + I_5 \ddot{u}_Z
\end{aligned} \tag{44}$$

$$\begin{aligned}
\delta v_0 :& -(A_{12} + A_{66}) \frac{\partial^2 u_0}{\partial x \partial y} - (B_{12} + B_{66}) \frac{\partial^2 u_1}{\partial x \partial y} + (G_{12} + G_{66}) \frac{\partial^2 u_Z}{\partial x \partial y} \\
&- A_{22} \frac{\partial^2 v_0}{\partial y^2} - A_{66} \frac{\partial^2 v_0}{\partial x^2} - B_{22} \frac{\partial^2 v_1}{\partial y^2} - B_{66} \frac{\partial^2 v_1}{\partial x^2} + G_{22} \frac{\partial^2 v_Z}{\partial y^2} \\
&+ G_{66} \frac{\partial^2 v_Z}{\partial x^2} + A_{44} \frac{\partial w_1}{\partial y} + H_{44} \frac{\partial w_Z}{\partial y} = I_0 \ddot{v}_0 + I_1 \ddot{v}_1 + I_5 \ddot{v}_Z
\end{aligned} \tag{45}$$

$$\begin{aligned}
\delta w_0 :& A_{13} \frac{\partial u_1}{\partial x} + 2B_{13} \frac{\partial u_Z}{\partial x} + A_{23} \frac{\partial v_1}{\partial y} + 2B_{23} \frac{\partial v_Z}{\partial y} - A_{55} \frac{\partial^2 w_0}{\partial x^2} \\
&- A_{44} \frac{\partial^2 w_0}{\partial y^2} - B_{55} \frac{\partial^2 w_1}{\partial x^2} - B_{44} \frac{\partial^2 w_1}{\partial y^2} - D_{55} \frac{\partial^2 w_Z}{\partial x^2} \\
&- D_{44} \frac{\partial^2 w_Z}{\partial y^2} + q_0 = I_0 \ddot{w}_0 + I_1 \ddot{w}_1 + I_2 \ddot{w}_Z
\end{aligned} \tag{46}$$

$$\begin{aligned}\delta u_1 :& -B_{11}\frac{\partial^2 u_0}{\partial x^2} - B_{66}\frac{\partial^2 u_0}{\partial y^2} - D_{11}\frac{\partial^2 u_1}{\partial x^2} + A_{55}u_1 - D_{66}\frac{\partial^2 u_1}{\partial y^2}\\ & - N_{11}\frac{\partial^2 u_Z}{\partial x^2} + H_{55}u_Z + N_{66}\frac{\partial^2 u_Z}{\partial y^2} - (B_{12}+B_{66})\frac{\partial^2 v_0}{\partial x\partial y}\\ & - (D_{12}+D_{66})\frac{\partial^2 v_1}{\partial x\partial y} - (N_{12}+N_{66})\frac{\partial^2 v_Z}{\partial x\partial y} - A_{13}\frac{\partial w_0}{\partial x}\\ & + (-B_{13}+B_{55})\frac{\partial w_1}{\partial x} + (G_{55}+O_{55}+G_{13})\frac{\partial w_Z}{\partial x}\\ & = I_1\ddot{u}_0 + I_2\ddot{u}_1 + I_7\ddot{u}_Z \end{aligned} \tag{47}$$

$$\begin{aligned}\delta v_1 :& -(B_{12}+B_{66})\frac{\partial^2 u_0}{\partial x\partial y} - (D_{12}+D_{66})\frac{\partial^2 u_1}{\partial x\partial y}\\ & - (N_{12}+N_{66})\frac{\partial^2 u_Z}{\partial x\partial y} - B_{22}\frac{\partial^2 v_0}{\partial y^2} - B_{66}\frac{\partial^2 v_0}{\partial x^2} - D_{22}\frac{\partial^2 v_1}{\partial y^2}\\ & + A_{44}v_1 - D_{66}\frac{\partial^2 v_1}{\partial x^2} - N_{22}\frac{\partial^2 v_Z}{\partial y^2} + H_{44}v_Z - N_{66}\frac{\partial^2 v_Z}{\partial x^2}\\ & - A_{23}\frac{\partial w_0}{\partial y} + (-B_{23}+B_{44})\frac{\partial w_1}{\partial y} + (G_{44}+O_{44}+G_{23})\frac{\partial w_Z}{\partial y}\\ & = I_1\ddot{v}_0 + I_2\ddot{v}_1 + I_7\ddot{v}_Z \end{aligned} \tag{48}$$

$$\begin{aligned}\delta w_1 :& -A_{55}\frac{\partial u_0}{\partial x} + (-B_{55}+B_{13})\frac{\partial u_1}{\partial x} + (-D_{55}+2D_{13})\frac{\partial u_Z}{\partial x}\\ & - A_{44}\frac{\partial v_0}{\partial y} + (-B_{44}+B_{23})\frac{\partial v_1}{\partial y} + (-D_{44}+2D_{23})\frac{\partial v_Z}{\partial y}\\ & - B_{55}\frac{\partial^2 w_0}{\partial x^2} - B_{44}\frac{\partial^2 w_0}{\partial y^2} - D_{55}\frac{\partial^2 w_1}{\partial x^2} + A_{33}w_1 - D_{44}\frac{\partial^2 w_1}{\partial y^2}\\ & - E_{55}\frac{\partial^2 w_Z}{\partial x^2} + B_{33}w_Z - E_{44}\frac{\partial^2 w_Z}{\partial y^2} = I_1\ddot{w}_0 + I_2\ddot{w}_1 + I_3\ddot{w}_Z \end{aligned} \tag{49}$$

$$\begin{aligned}\delta u_Z :& G_{11}\frac{\partial^2 u_0}{\partial x^2} + G_{66}\frac{\partial^2 u_0}{\partial y^2} - N_{11}\frac{\partial^2 u_1}{\partial x^2} + H_{55}u_1 - N_{66}\frac{\partial^2 u_1}{\partial y^2} + R_{55}u_Z\\ & + (J_{11}+J_{66})\frac{\partial^2 u_Z}{\partial x^2} + (G_{12}+G_{66})\frac{\partial^2 v_0}{\partial x\partial y} - (N_{12}+N_{66})\frac{\partial^2 v_1}{\partial x\partial y}\\ & + (J_{12}+J_{66})\frac{\partial^2 v_Z}{\partial x\partial y} - 2B_{13}\frac{\partial w_0}{\partial x} + (-2D_{13}+D_{55})\frac{\partial w_1}{\partial x}\\ & + (P_{55}-2N_{55}-2N_{13})\frac{\partial w_Z}{\partial x} = I_5\ddot{u}_0 + I_7\ddot{u}_1 + I_6\ddot{u}_Z \end{aligned} \tag{50}$$

$$\begin{aligned}\delta v_Z :& (G_{12}+G_{66})\frac{\partial^2 u_0}{\partial x\partial y} - (N_{12}+N_{66})\frac{\partial^2 u_1}{\partial x\partial y} + (J_{12}+J_{66})\frac{\partial^2 u_Z}{\partial x\partial y}\\ & + G_{22}\frac{\partial^2 v_0}{\partial y^2} + G_{66}\frac{\partial^2 v_0}{\partial x^2} - N_{22}\frac{\partial^2 v_1}{\partial y^2} + H_{44}v_1 - N_{66}\frac{\partial^2 v_1}{\partial x^2} + R_{44}v_Z\\ & + J_{22}\frac{\partial^2 v_Z}{\partial y^2} + J_{66}\frac{\partial^2 v_Z}{\partial x^2} - 2B_{23}\frac{\partial w_0}{\partial y} + (-2D_{23}+D_{44})\frac{\partial w_1}{\partial y}\\ & + (P_{44}-2N_{44}-2N_{23})\frac{\partial w_Z}{\partial y} = I_5\ddot{v}_0 + I_7\ddot{v}_1 + I_6\ddot{v}_Z \end{aligned} \tag{51}$$

$$\begin{aligned}\delta w_Z :& -H_{55}\frac{\partial u_0}{\partial x} - (G_{55}+O_{55}+G_{13})\frac{\partial u_1}{\partial x} - (P_{55}-2N_{55}-2N_{13})\frac{\partial u_Z}{\partial x}\\ & - H_{44}\frac{\partial v_0}{\partial y} - (G_{44}+O_{44}+G_{23})\frac{\partial v_1}{\partial y} - (P_{44}-2N_{44}-2N_{23})\frac{\partial v_Z}{\partial y}\\ & - D_{55}\frac{\partial^2 w_0}{\partial x^2} - D_{44}\frac{\partial^2 w_0}{\partial y^2} - E_{55}\frac{\partial^2 w_1}{\partial x^2} + 2B_{33}w_1 - E_{44}\frac{\partial^2 w_1}{\partial y^2}\\ & - F_{55}\frac{\partial^2 w_Z}{\partial x^2} + 4D_{33}w_Z - F_{44}\frac{\partial^2 w_Z}{\partial y^2} + q_2 = I_2\ddot{w}_0 + I_3\ddot{w}_1 + I_4\ddot{w}_Z \end{aligned} \tag{52}$$

Nothing N_l as the number of mathematical layers across the thickness direction, the stiffness components can be computed as follows.

$$\begin{aligned}
A_{ij} &= \sum_{k=1}^{NL} c_{ij}^k (z_{k+1} - z_k)\\
B_{ij} &= \frac{1}{2}\sum_{k=1}^{NL} c_{ij}^k (z_{k+1}^2 - z_k^2)\\
D_{ij} &= \frac{1}{3}\sum_{k=1}^{NL} c_{ij}^k (z_{k+1}^3 - z_k^3)\\
E_{ij} &= \frac{1}{4}\sum_{k=1}^{NL} c_{ij}^k (z_{k+1}^4 - z_k^4)\\
F_{ij} &= \frac{1}{5}\sum_{k=1}^{NL} c_{ij}^k (z_{k+1}^5 - z_k^5)\\
G_{ij} &= \sum_{k=1}^{NL} c_{ij}^k \frac{h_k}{\pi}\left[\cos\left(\frac{\pi z_{k+1}}{h_k}\right) - \cos\left(\frac{\pi z_k}{h_k}\right)\right]\\
H_{ij} &= \sum_{k=1}^{NL} c_{ij}^k \left[\sin\left(\frac{\pi z_{k+1}}{h_k}\right) - \sin\left(\frac{\pi z_k}{h_k}\right)\right]\\
J_{ij} &= \sum_{k=1}^{NL} c_{ij}^k \left[\frac{h_k}{4\pi}\left[\sin\left(\frac{2\pi z_{k+1}}{h_k}\right) - \sin\left(\frac{2\pi z_k}{h_k}\right)\right]\right.\\
&\quad \left. -\frac{1}{2}(z_{k+1} - z_k)\right]\\
N_{ij} &= \sum_{k=1}^{NL} c_{ij}^k \left[\left(\frac{h_k}{\pi}\right)^2\left(\sin\left(\frac{\pi z_{k+1}}{h_k}\right) - \sin\left(\frac{\pi z_k}{h_k}\right)\right)\right.\\
&\quad \left. -\frac{h_k}{\pi}\left(z_{k+1}\cos\left(\frac{\pi z_{k+1}}{h_k}\right) - z_k\cos\left(\frac{\pi z_k}{h_k}\right)\right)\right]\\
O_{ij} &= \sum_{k=1}^{NL} c_{ij}^k \left[z_{k+1}\sin\left(\frac{\pi z_{k+1}}{h_k}\right) - z_k\sin\left(\frac{\pi z_k}{h_k}\right)\right]\\
P_{ij} &= \sum_{k=1}^{NL} c_{ij}^k \left[z_{k+1}^2\sin\left(\frac{\pi z_{k+1}}{h_k}\right) - z_k^2\sin\left(\frac{\pi z_k}{h_k}\right)\right]\\
R_{ij} &= \sum_{k=1}^{NL} c_{ij}^k \left[\frac{\pi}{4h_k}\left[\sin\left(\frac{2\pi z_{k+1}}{h_k}\right) - \sin\left(\frac{2\pi z_k}{h_k}\right)\right]\right.\\
&\quad \left. +\frac{1}{2}\left(\frac{\pi}{h_k}\right)^2 (z_{k+1} - z_k)\right]
\end{aligned} \tag{53}$$

and

$$\begin{aligned}
I_0 &= \sum_{k=1}^{NL} \rho^k (z_{k+1} - z_k)\\
I_1 &= \frac{1}{2}\sum_{k=1}^{NL} \rho^k (z_{k+1}^2 - z_k^2)\\
I_2 &= \frac{1}{3}\sum_{k=1}^{NL} \rho^k (z_{k+1}^3 - z_k^3)\\
I_3 &= \frac{1}{4}\sum_{k=1}^{NL} \rho^k (z_{k+1}^4 - z_k^4)\\
I_4 &= \frac{1}{5}\sum_{k=1}^{NL} \rho^k (z_{k+1}^5 - z_k^5)\\
I_5 &= -\sum_{k=1}^{NL} \rho^k \frac{h_k}{\pi}\left[\cos\left(\frac{\pi z_{k+1}}{h_k}\right) - \cos\left(\frac{\pi z_k}{h_k}\right)\right]\\
I_6 &= \sum_{k=1}^{NL} \rho^k \left[\frac{1}{2}(z_{k+1} - z_k) - \frac{h_k}{4\pi}\left[\sin\left(\frac{2\pi z_{k+1}}{h_k}\right) - \sin\left(\frac{2\pi z_k}{h_k}\right)\right]\right]\\
I_7 &= \sum_{k=1}^{NL} \rho^k \left[\left(\frac{h_k}{\pi}\right)^2\left(\sin\left(\frac{\pi z_{k+1}}{h_k}\right) - \sin\left(\frac{\pi z_k}{h_k}\right)\right)\right.\\
&\quad \left. -\frac{h_k}{\pi}\left(z_{k+1}\cos\left(\frac{\pi z_{k+1}}{h_k}\right) - z_k\cos\left(\frac{\pi z_k}{h_k}\right)\right)\right]
\end{aligned} \tag{54}$$

where h_k is the thickness of each layer and z_k,z_{k+1} are the lower and upper z coordinate for each layer k.

2.8. Natural boundary conditions

This meshless method based on collocation with radial basis functions needs the imposition of essential (e.g. $w = 0$) and mechanical (e.g. $M_{xx} = 0$) boundary conditions. Assuming a rectangular plate (for the sake of simplicity) Eqs. (30) are expressed as follows.

Given the number of degrees of freedom, at each boundary point at edges $x = min$ or $x = max$ we impose:

$$M_{xx1} = A_{11}\frac{\partial u_0}{\partial x} + B_{11}\frac{\partial u_1}{\partial x} - G_{11}\frac{\partial u_Z}{\partial x} + A_{12}\frac{\partial v_0}{\partial y} + B_{12}\frac{\partial v_1}{\partial y} - G_{12}\frac{\partial v_Z}{\partial y} \tag{55}$$

$$M_{xx2} = B_{11}\frac{\partial u_0}{\partial x} + D_{11}\frac{\partial u_1}{\partial x} + N_{11}\frac{\partial u_Z}{\partial x} + B_{12}\frac{\partial v_0}{\partial y} + D_{12}\frac{\partial v_1}{\partial y} + N_{12}\frac{\partial v_Z}{\partial y} + A_{13}w_0 + B_{13}w_1 - G_{13}w_Z \tag{56}$$

$$M_{xx3} = -G_{11}\frac{\partial u_0}{\partial x} + N_{11}\frac{\partial u_1}{\partial x} - J_{11}\frac{\partial u_Z}{\partial x} - G_{12}\frac{\partial v_0}{\partial y} + N_{12}\frac{\partial v_1}{\partial y} - J_{12}\frac{\partial v_Z}{\partial y} + 2B_{13}w_0 + 2D_{13}w_1 + 2N_{13}w_Z \tag{57}$$

$$M_{xx4} = A_{66}\frac{\partial u_0}{\partial y} + B_{66}\frac{\partial u_1}{\partial y} - G_{66}\frac{\partial u_Z}{\partial y} + A_{66}\frac{\partial v_0}{\partial x} + B_{66}\frac{\partial v_1}{\partial x} - G_{66}\frac{\partial v_Z}{\partial x} \tag{58}$$

$$M_{xx5} = B_{66}\frac{\partial u_0}{\partial y} + D_{66}\frac{\partial u_1}{\partial y} + N_{66}\frac{\partial u_Z}{\partial y} + B_{66}\frac{\partial v_0}{\partial x} + D_{66}\frac{\partial v_1}{\partial x} + N_{66}\frac{\partial v_Z}{\partial x} \tag{59}$$

$$M_{xx6} = -G_{66}\frac{\partial u_0}{\partial y} + N_{66}\frac{\partial u_1}{\partial y} - J_{66}\frac{\partial u_Z}{\partial y} - G_{66}\frac{\partial v_0}{\partial x} + N_{66}\frac{\partial v_1}{\partial x} - J_{66}\frac{\partial v_Z}{\partial x} \tag{60}$$

$$M_{xx7} = A_{55}\frac{\partial w_0}{\partial x} + B_{55}\frac{\partial w_1}{\partial x} + D_{55}\frac{\partial w_Z}{\partial x} \tag{61}$$

$$M_{xx8} = A_{55}u_0 + B_{55}u_1 + D_{55}u_Z + B_{55}\frac{\partial w_0}{\partial x} + D_{55}\frac{\partial w_1}{\partial x} + E_{55}\frac{\partial w_Z}{\partial x} \tag{62}$$

$$M_{xx9} = H_{55}u_0 + (G_{55} + O_{55})u_1 + (P_{55} - 2N_{55})u_Z + D_{55}\frac{\partial w_0}{\partial x} + E_{55}\frac{\partial w_1}{\partial x} + F_{55}\frac{\partial w_Z}{\partial x} \tag{63}$$

Similarly, given the number of degrees of freedom, at each boundary point at edges $y = min$ or $y = max$ we impose:

$$M_{yy1} = A_{66}\frac{\partial u_0}{\partial y} + B_{66}\frac{\partial u_1}{\partial y} - G_{66}\frac{\partial u_Z}{\partial y} + A_{66}\frac{\partial v_0}{\partial x} + B_{66}\frac{\partial v_1}{\partial x} - G_{66}\frac{\partial v_Z}{\partial x} \tag{64}$$

$$M_{yy2} = B_{66}\frac{\partial u_0}{\partial y} + D_{66}\frac{\partial u_1}{\partial y} + N_{66}\frac{\partial u_Z}{\partial y} + B_{66}\frac{\partial v_0}{\partial x} + D_{66}\frac{\partial v_1}{\partial x} + N_{66}\frac{\partial v_Z}{\partial x} \tag{65}$$

$$M_{yy3} = -G_{66}\frac{\partial u_0}{\partial y} + N_{66}\frac{\partial u_1}{\partial y} - J_{66}\frac{\partial u_Z}{\partial y} - G_{66}\frac{\partial v_0}{\partial x} + N_{66}\frac{\partial v_1}{\partial x} - J_{66}\frac{\partial v_Z}{\partial x} \tag{66}$$

$$M_{yy4} = A_{12}\frac{\partial u_0}{\partial x} + B_{12}\frac{\partial u_1}{\partial x} - G_{12}\frac{\partial u_Z}{\partial x} + A_{22}\frac{\partial v_0}{\partial y} + B_{22}\frac{\partial v_1}{\partial y} - G_{22}\frac{\partial v_Z}{\partial y} \tag{67}$$

$$M_{yy5} = B_{12}\frac{\partial u_0}{\partial x} + D_{12}\frac{\partial u_1}{\partial x} + N_{12}\frac{\partial u_Z}{\partial x} + B_{22}\frac{\partial v_0}{\partial y} + D_{22}\frac{\partial v_1}{\partial y} + N_{22}\frac{\partial v_Z}{\partial y} \tag{68}$$

$$M_{yy6} = -G_{12}\frac{\partial u_0}{\partial x} + N_{12}\frac{\partial u_1}{\partial x} - J_{12}\frac{\partial u_Z}{\partial x} - G_{22}\frac{\partial v_0}{\partial y} + N_{22}\frac{\partial v_1}{\partial y} - J_{22}\frac{\partial v_Z}{\partial y} \tag{69}$$

$$M_{yy7} = A_{44}\frac{\partial w_0}{\partial y} + B_{44}\frac{\partial w_1}{\partial y} + D_{44}\frac{\partial w_Z}{\partial y} \tag{70}$$

$$M_{yy8} = A_{44}v_0 + B_{44}v_1 + D_{44}v_Z + B_{44}\frac{\partial w_0}{\partial y} + D_{44}\frac{\partial w_1}{\partial y} + E_{44}\frac{\partial w_Z}{\partial y} \tag{71}$$

$$M_{yy9} = H_{44}v_0 + (G_{44} + O_{44})v_1 + (P_{44} - 2N_{44})v_Z + D_{44}\frac{\partial w_0}{\partial y} + E_{44}\frac{\partial w_1}{\partial y} + F_{44}\frac{\partial w_Z}{\partial y} \tag{72}$$

with A_{ij}, B_{ij}, D_{ij}, E_{ij}, F_{ij}, G_{ij}, H_{ij}, J_{ij}, N_{ij}, O_{ij}, P_{ij}, R_{ij} already given in (53).

3. The radial basis function method

For the sake of completeness we present here the basics of collocation with radial basis functions for static and vibrations problems.

3.1. The static problem

In this section the formulation of a global unsymmetrical collocation RBF-based method to compute elliptic operators is presented. Consider a linear elliptic partial differential operator L and a bounded region Ω in $\mathbb{R}^n$ with some boundary $\partial\Omega$. In the static problems we seek the computation of displacements (u) from the global system of equations

$$\mathcal{L}\mathbf{u} = \mathbf{f} \text{ in } \Omega; \quad \mathcal{L}_B\mathbf{u} = \mathbf{g} \text{ on } \partial\Omega \tag{73}$$

where $\mathcal{L}$, $\mathcal{L}_B$ are linear operators in the domain and on the boundary, respectively. The right-hand sides in (73) represent the external forces applied on the plate and the boundary conditions applied along the perimeter of the plate, respectively. The PDE problem defined in (73) will be replaced by a finite problem, defined by an algebraic system of equations, after the radial basis expansions.

3.2. The eigenproblem

The eigenproblem looks for eigenvalues (λ) and eigenvectors ($\mathbf{u}$) that satisfy

$$\mathcal{L}\mathbf{u} + \lambda\mathbf{u} = 0 \text{ in } \Omega; \quad \mathcal{L}_B\mathbf{u} = 0 \text{ on } \partial\Omega \tag{74}$$

As in the static problem, the eigenproblem defined in (74) is replaced by a finite-dimensional eigenvalue problem, based on RBF approximations.

3.3. Radial basis functions approximations

The radial basis function (ϕ) approximation of a function (u) is given by

$$\tilde{\mathbf{u}}(\mathbf{x}) = \sum_{i=1}^{N} \alpha_i \phi(\|x - y_i\|_2), \quad \mathbf{x} \in \mathbb{R}^n \tag{75}$$

where y_i, $i = 1, \ldots, N$ is a finite set of distinct points (centers) in $\mathbb{R}^n$. Although we can use many RBFs, in this paper we restrict to the Wendland function, defined as

$$\phi(r) = (1 - c\, r)_+^8 (32(c\, r)^3 + 25(c\, r)^2 + 8c\, r + 1) \tag{76}$$

where the Euclidian distance r is real and non-negative and c is a positive shape parameter. The shape parameter (c) was obtained by an optimization procedure, as detailed in Ferreira and Fasshauer [26].

Considering N distinct interpolations, and knowing $u(x_j)$, $j = 1, 2, \ldots, N$, we find α_i by the solution of a $N \times N$ linear system

$$\mathbf{A}\boldsymbol{\alpha} = \mathbf{u} \tag{77}$$

where $\mathbf{A} = [\phi(\|x - y_i\|_2)]_{N\times N}$, $\boldsymbol{\alpha} = [\alpha_1, \alpha_2, \ldots, \alpha_N]^T$ and $\mathbf{u} = [u(x_1), u(x_2), \ldots, u(x_N)]^T$.

3.4. Solution of the static problem

The solution of a static problem by radial basis functions considers N_I nodes in the domain and N_B nodes on the boundary, with a total number of nodes $N = N_I + N_B$. We denote the sampling points by $x_i \in \Omega$, $i = 1, \ldots, N_I$ and $x_i \in \partial\Omega$, $i = N_I + 1, \ldots, N$. At the points in the domain we solve the following system of equations

$$\sum_{i=1}^{N} \alpha_i \mathcal{L}\phi(\|x - y_i\|_2) = \mathbf{f}(x_j), \quad j = 1, 2, \ldots, N_I \tag{78}$$

or

$$\mathcal{L}^I \boldsymbol{\alpha} = \mathbf{F} \tag{79}$$

where

$$\mathcal{L}^I = [\mathcal{L}\phi(\|x - y_i\|_2)]_{N_I \times N} \tag{80}$$

At the points on the boundary, we impose boundary conditions as

$$\sum_{i=1}^{N} \alpha_i \mathcal{L}_B \phi(\|x - y_i\|_2) = \mathbf{g}(x_j), \quad j = N_I + 1, \ldots, N \tag{81}$$

or

$$\mathbf{B}\boldsymbol{\alpha} = \mathbf{G} \tag{82}$$

where

$$\mathbf{B} = \mathcal{L}_B \phi[(\|x_{N_I+1} - y_j\|_2)]_{N_B \times N}$$

Therefore, we can write a finite-dimensional static problem as

$$\begin{bmatrix} \mathcal{L}^I \\ \mathbf{B} \end{bmatrix} \boldsymbol{\alpha} = \begin{bmatrix} \mathbf{F} \\ \mathbf{G} \end{bmatrix} \tag{83}$$

By inverting the system (83), we obtain the vector $\boldsymbol{\alpha}$. We then obtain the solution $\mathbf{u}$ using the interpolation Eq. (75).

3.5. Solution of the eigenproblem

We consider N_I nodes in the interior of the domain and N_B nodes on the boundary, with $N = N_I + N_B$. We denote interpolation points by $x_i \in \Omega$, $i = 1, \ldots, N_I$ and $x_i \in \partial\Omega$, $i = N_I + 1, \ldots, N$. At the points in the domain, we define the eigenproblem as

$$\sum_{i=1}^{N} \alpha_i \mathcal{L}\phi(\|x - y_i\|_2) = \lambda \tilde{\mathbf{u}}(x_j), \quad j = 1, 2, \ldots, N_I \tag{84}$$

or

$$\mathcal{L}^I \boldsymbol{\alpha} = \lambda \tilde{\mathbf{u}}^I \tag{85}$$

where

$$\mathcal{L}^I = [\mathcal{L}\phi(\|x - y_i\|_2)]_{N_I \times N} \tag{86}$$

At the points on the boundary, we enforce the boundary conditions as

$$\sum_{i=1}^{N} \alpha_i \mathcal{L}_B \phi(\|x - y_i\|_2) = 0, \quad j = N_I + 1, \ldots, N \tag{87}$$

or

$$\mathbf{B}\boldsymbol{\alpha} = 0 \tag{88}$$

Eqs. (85) and (88) can now be solved as a generalized eigenvalue problem

$$\begin{bmatrix} \mathcal{L}^I \\ \mathbf{B} \end{bmatrix} \boldsymbol{\alpha} = \lambda \begin{bmatrix} \mathbf{A}^I \\ \mathbf{0} \end{bmatrix} \boldsymbol{\alpha} \tag{89}$$

where

$$\mathbf{A}^I = \phi[(\|x_{N_I} - y_j\|_2)]_{N_I \times N}$$

3.6. Discretization of the equations of motion and boundary conditions

The radial basis collocation method follows a simple implementation procedure. Taking Eq. (83), we compute

$$\boldsymbol{\alpha} = \begin{bmatrix} L^I \\ \mathbf{B} \end{bmatrix}^{-1} \begin{bmatrix} \mathbf{F} \\ \mathbf{G} \end{bmatrix} \tag{90}$$

This $\boldsymbol{\alpha}$ vector is then used to obtain solution $\tilde{\mathbf{u}}$, by using (75). If derivatives of $\tilde{\mathbf{u}}$ are needed, such derivatives are computed as

$$\frac{\partial \tilde{\mathbf{u}}}{\partial x} = \sum_{j=1}^{N} \alpha_j \frac{\partial \phi_j}{\partial x}; \quad \frac{\partial^2 \tilde{\mathbf{u}}}{\partial x^2} = \sum_{j=1}^{N} \alpha_j \frac{\partial^2 \phi_j}{\partial x^2}, \quad \text{etc.} \tag{91}$$

In the present collocation approach, we need to impose essential and natural boundary conditions. Consider, for example, the condition $w_0 = 0$, on a simply supported or clamped edge. We enforce the conditions by interpolating as

$$w_0 = 0 \rightarrow \sum_{j=1}^{N} \alpha_j^{W_0} \phi_j = 0 \tag{92}$$

Other boundary conditions are interpolated in a similar way.

3.7. Free vibrations problems

For free vibration problems we set the external force to zero, and assume harmonic solution in terms of displacements u_0, u_1, u_Z, v_0, v_1, v_Z, w_0, w_1, w_Z as

$$\begin{aligned} &u_0 = U_0(w,y)e^{i\omega t}; \quad u_1 = U_1(w,y)e^{i\omega t}; \quad u_Z = U_Z(w,y)e^{i\omega t}; \\ &v_0 = V_0(w,y)e^{i\omega t}; \quad v_1 = V_1(w,y)e^{i\omega t}; \quad v_Z = V_Z(w,y)e^{i\omega t}; \\ &w_0 = W_0(w,y)e^{i\omega t}; \quad w_1 = W_1(w,y)e^{i\omega t}; \quad w_Z = W_Z(w,y)e^{i\omega t} \end{aligned} \tag{93}$$

where ω is the frequency of natural vibration. Substituting the harmonic expansion into Eqs. (89) in terms of the amplitudes U_0, U_1, U_Z, V_0, V_1, V_Z, W_0, W_1, W_Z, we may obtain the natural frequencies and vibration modes for the plate problem, by solving the eigenproblem

$$[\mathcal{L} - \omega^2 \mathcal{G}]\mathbf{X} = \mathbf{0} \tag{94}$$

where $\mathcal{L}$ collects all stiffness terms and $\mathcal{G}$ collects all terms related to the inertial terms. In (94) $\mathbf{X}$ are the modes of vibration associated with the natural frequencies defined as ω.

Table 1
FGM isotropic plate with polynomial material law [2]. Effect of transverse normal strain ϵ_{zz} for a bending problem.

p		ϵ_{zz}	$\bar{\sigma}_{xx}(h/3)$			$\bar{u}_z(0,0)$		
			$a/h = 4$	$a/h = 10$	$a/h = 100$	$a/h = 4$	$a/h = 10$	$a/h = 100$
1	Ref. [27]	≠0	0.6221	1.5064	14.969	0.7171	0.5875	0.5625
	CLT	0	0.8060	2.0150	20.150	0.5623	0.5623	0.5623
	FSDT (k = 5/6)	0	0.8060	2.0150	20.150	0.7291	0.5889	0.5625
	GSDT [2]	0		1.4894			0.5889	
	Ref. [9] N = 4	0	0.7856	2.0068	20.149	0.7289	0.5890	0.5625
	Ref. [9] N = 4	≠0	0.6221	1.5064	14.969	0.7171	0.5875	0.5625
	Present 13^2 grid	≠0	0.5925	1.4939	14.901	0.6997	0.5844	0.5596
	Present 17^2 grid	≠0	0.5925	1.4945	14.957	0.6998	0.5845	0.5622
	Present 21^2 grid	≠0	0.5925	1.4945	14.969	0.6997	0.5845	0.5624
4	Ref. [27]	≠0	0.4877	1.1971	11.923	1.1585	0.8821	0.8286
	CLT	0	0.6420	1.6049	16.049	0.8281	0.8281	0.8281
	FSDT (k = 5/6)	0	0.6420	1.6049	16.049	1.1125	0.8736	0.828
	GSDT [2]	0		1.1783			0.8651	
	Ref. [9] N = 4	0	0.5986	1.5874	16.047	1.1673	0.8828	0.8286
	Ref. [9] N = 4	≠0	0.4877	1.1971	11.923	1.1585	0.8821	0.8286
	Present 13^2 grid	≠0	0.4404	1.1780	11.894	1.1178	0.8749	0.8251
	Present 17^2 grid	≠0	0.4404	1.1783	11.923	1.1178	0.8750	0.8284
	Present 21^2 grid	≠0	0.4404	1.1783	11.932	1.1178	0.8750	0.8286
10	Ref. [27]	≠0	0.3695	0.8965	8.9077	1.3745	1.0072	0.9361
	CLT	0	0.4796	1.1990	11.990	0.9354	0.9354	0.9354
	FSDT (k = 5/6)	0	0.4796	1.1990	11.990	1.3178	0.9966	0.9360
	GSDT [2]	0		0.8775			1.0089	
	Ref. [9] N = 4	0	0.4345	1.1807	11.989	1.3925	1.0090	0.9361
	Ref. [9] N = 4	≠0	0.1478	0.8965	8.9077	1.3745	1.0072	0.9361
	Present 13^2 grid	≠0	0.3227	1.1780	11.894	1.3490	0.8749	0.8251
	Present 17^2 grid	≠0	0.3227	1.1783	11.923	1.3490	0.8750	0.8284
	Present 21^2 grid	≠0	0.3227	1.1783	11.932	1.3490	0.8750	0.8286

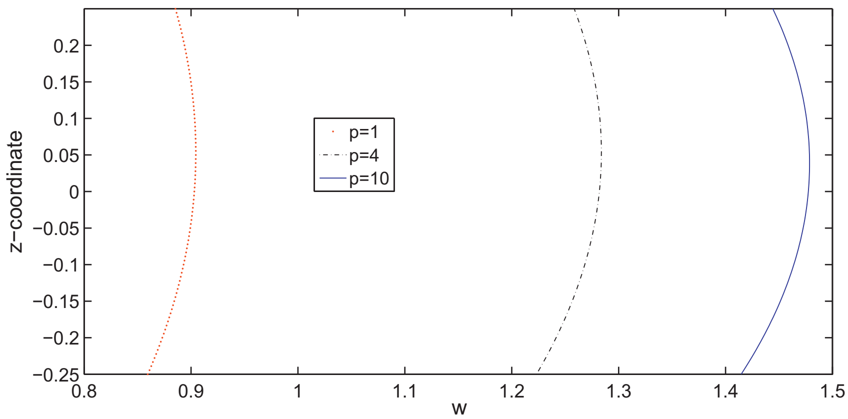

Fig. 1. FGM square plate subjected to sinusoidal load at the top, with a/h = 4. Displacement through the thickness direction for different values of p at the center of the plate $(\frac{a}{2}, \frac{b}{2})$.

4. Numerical examples

4.1. Bending problems

In the next examples we use the sinusoidal plate theory to analyse simply supported square (side lengths $a = b$) plates subjected to a bi-sinusoidal transverse mechanical load, of amplitude load $p_z = \bar{p}_z sin(\frac{\pi x}{a}) sin(\frac{\pi y}{b})$ applied at the top plate surface, $z = h/2$, $\bar{p}_z = 1$. Three side-to-thickness ratios (a/h) are considered 4, 10 and 100.

We consider 91 mathematical layers, in order to model the continuous variation of properties across the thickness direction.[1] We consider a Wendland C6 radial function as in (76), and a Chebyshev grid (see [26] for details).

4.1.1. Isotropic functionally graded plate

In this example, an isotropic FGM square plate with a polynomial material law, as given by Zenkour [2] is considered. The plate is graded from aluminum (bottom surface) to alumina (top surface) materials. The following functional relationship is considered for modulus of elasticity $E(z)$ in the thickness direction (z) [2]:

$$E(z) = E_m + (E_c - E_m)\left(\frac{2z + h}{2h}\right)^p \qquad (95)$$

where E_m = 70 GPa and E_c = 380 GPa are the corresponding modulus of elasticity of the metal and ceramic phases, respectively; p is the (positive number) volume fraction exponent. The Poisson's ratio is considered constant (ν = 0.3).

[1] A significant number of mathematical layers is needed to ensure correct material properties at each thickness position.

The in-plane displacements, the transverse displacements, the normal stresses and the in-plane and transverse shear stresses are respectively presented in normalized form as

$$\bar{u}_z = \frac{10h^3 E_c}{a^4 \bar{p}_z} u_z, \quad \bar{\sigma}_{xx} = \frac{h}{a\bar{p}_z}\sigma_{xx}, \quad \bar{\sigma}_{xz} = \frac{h}{a\bar{p}_z}\sigma_{xz}, \quad \bar{\sigma}_{zz} = \sigma_{zz} \tag{96}$$

The present approach with $\epsilon_{zz} \neq 0$ is compared with analytical solutions by Carrera et al. [27], the classical plate theory (CLT), the first-order shear deformation theory (FSDT), a generalized shear deformation theory by Zenkour [2] (who considered $\epsilon_{zz} = 0$), and finite element solutions by Carrera et al. [9]. We consider Chebyschev grids with 13^2,17^2 and 21^2 points. Three FGM configurations are considered by using different p exponents ($p = 1,4,10$). Thick ($a/h = 4$) down to thin ($a/h = 100$) plates are analysed. Normalized transverse displacements ($\bar{u}_z$) and normal stresses ($\bar{\sigma}_{xx}$) at selected points are shown in Table 1. Our approach presents very close re-

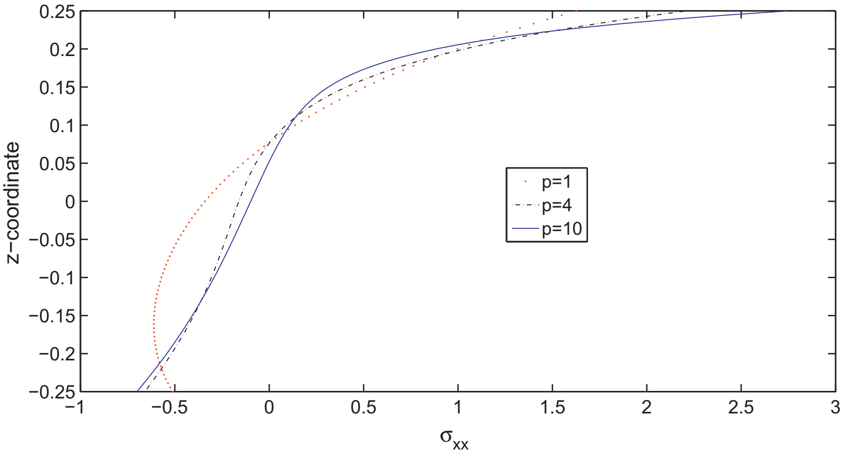

Fig. 2. FGM square plate subjected to sinusoidal load at the top, with $a/h = 4$. σ_{xx} through the thickness direction for different values of p at the center of the plate $(\frac{a}{2}, \frac{b}{2})$.

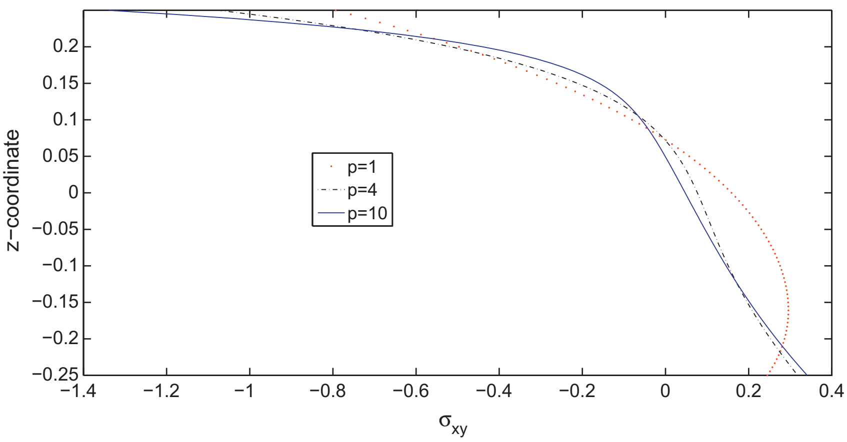

Fig. 3. FGM square plate subjected to sinusoidal load at the top, with $a/h = 4$. σ_{xy} through the thickness direction at the corner of the plate (0,0) for different values of p.

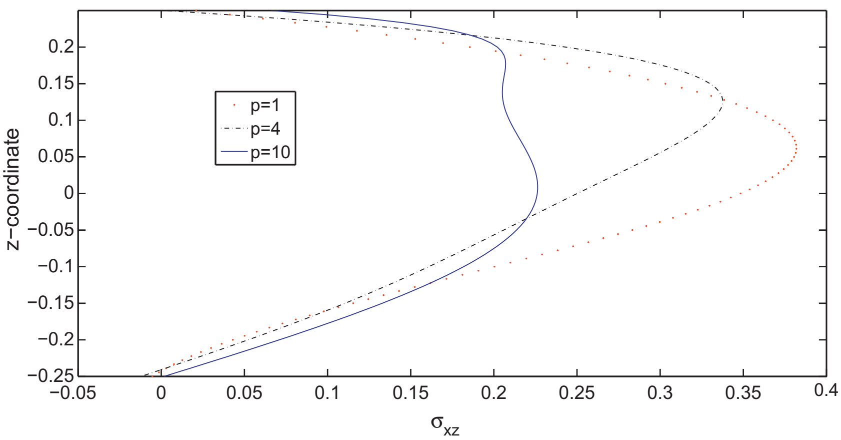

Fig. 4. FGM square plate subjected to sinusoidal load at the top, with $a/h = 4$. σ_{xz} through the thickness direction at the center of the plate $(0, \frac{b}{2})$ for different values of p.

sults to those theories that consider thickness stretching, and clearly deviates from those theories that neglect ϵ_{zz}, in particular for thicker plates. The present approach presents very close results to Carrera's analytical solution [27].

In Figs. 1–6 we present the evolution of the displacement and stresses across the thickness direction for various values of the exponent p, using a 21^2 grid. As can be seen in Fig. 6, the transverse normal component σ_{zz} cannot be neglected for the present problem.

4.1.2. Sandwich square plate with FGM core

In this example we consider a sandwich plate with total thickness h, by using a polynomial material law for the core, as given by Zenkour [2]. The bottom skin is aluminium ($E_m = 70$ GPa) with thickness $h_b = 0.1h$ and the top skin is alumina ($E_c = 380$ GPa) with thickness $h_t = 0.1h$. The core is a FGM with the following functional relationship for modulus of elasticity $E(z)$ in the thickness direction z [2]:

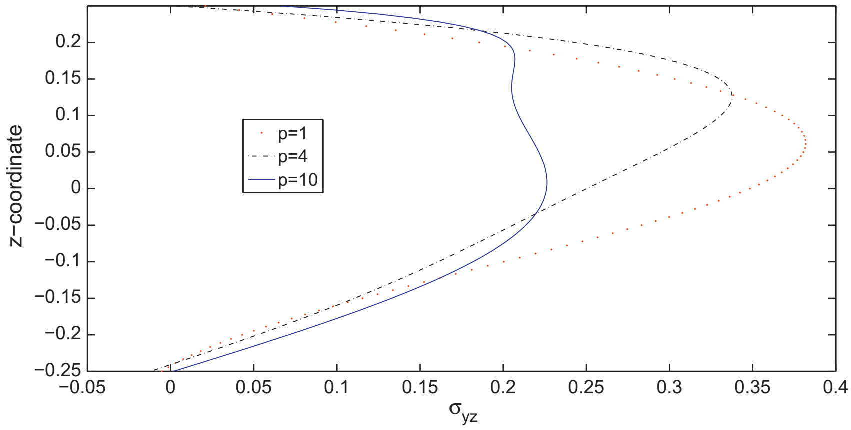

Fig. 5. FGM square plate subjected to sinusoidal load at the top, with $a/h = 4$. σ_{yz} through the thickness direction at the point $(\frac{a}{2}, 0)$ for different values of p.

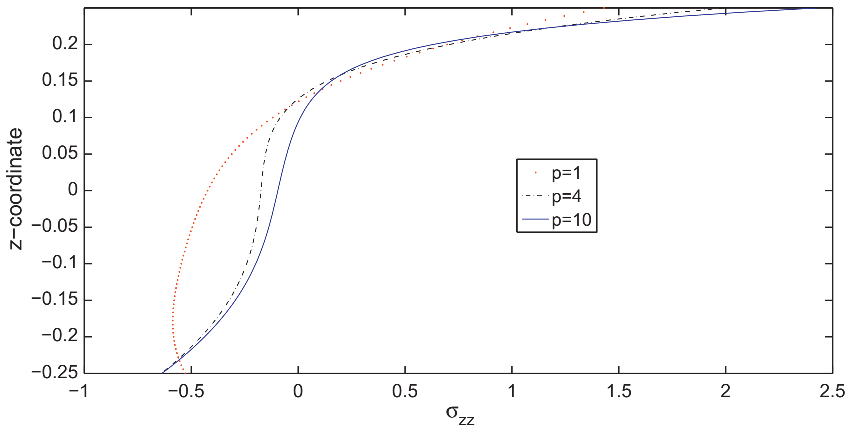

Fig. 6. FGM square plate subjected to sinusoidal load at the top, with $a/h = 4$. σ_{zz} through the thickness direction for different values of p at the center of the plate $(\frac{a}{2}, \frac{b}{2})$.

Table 2
Sandwich simply supported square plate with FGM core with polynomial material law [2] using a 19^2 grid. Effect of transverse normal strain ϵ_{zz} on σ_{xz} and transverse displacement for a bending problem.

p		ϵ_{zz}	$\bar{\sigma}_{xz}(0, \frac{b}{2}, \frac{h}{3})$			$\bar{w}(0,0,0)$		
			$a/h = 4$	$a/h = 10$	$a/h = 100$	$a/h = 4$	$a/h = 10$	$a/h = 100$
1	Ref. [9] $N = 4$	0	0.2604	0.2594	0.2593	0.7628	0.6324	0.6072
	Ref. [9] $N = 4$	$\neq 0$	0.2596	0.2593	0.2593	0.7735	0.6337	0.6072
	Present	0	0.2703	0.2718	0.2720	0.7744	0.6356	0.6092
	Present	$\neq 0$	0.2742	0.2788	0.2793	0.7416	0.6305	0.6092
4	Ref. [9] $N = 4$	0	0.2400	0.2398	0.2398	1.0930	0.8307	0.7797
	Ref. [9] $N = 4$	$\neq 0$	0.2400	0.2398	0.2398	1.0977	0.8308	0.7797
	Present	0	0.2699	0.2726	0.2728	1.0847	0.8276	0.7785
	Present	$\neq 0$	0.2723	0.2778	0.2785	1.0391	0.8202	0.7784
10	Ref. [9] $N = 4$	0	0.1932	0.1944	0.1946	1.2172	0.8740	0.8077
	Ref. [9] $N = 4$	$\neq 0$	0.1935	0.1944	0.1946	1.2240	0.8743	0.8077
	Present	0	0.1998	0.2021	0.2022	1.2212	0.8718	0.8050
	Present	$\neq 0$	0.2016	0.2059	0.2064	1.1780	0.8650	0.8050

$$E(z) = E_m + (E_c - E_m)\left(\frac{2z+h}{2h}\right)^p \quad (97)$$

where p is the (positive number) volume fraction exponent. The Poisson's ratio is considered constant $\nu = 0.3$.

The transverse displacement and the normal stresses are computed in normalized form as

$$\bar{u}_z = \frac{10h^3E_c}{a^4\bar{p}_z}u_z\left(\frac{a}{2},\frac{b}{2}\right) \quad \bar{\sigma}_{xx} = \frac{h}{a\bar{p}_z}\sigma_{xx}\left(\frac{a}{2},\frac{b}{2}\right)$$
$$\bar{\sigma}_{yy} = \frac{h}{a\bar{p}_z}\sigma_{yy}\left(\frac{a}{2},\frac{b}{2}\right) \quad \bar{\sigma}_{zz} = \sigma_{zz}\left(\frac{a}{2},\frac{b}{2}\right) \quad (98)$$

The shear stresses are normalized according to

Table 3
Sandwich simply supported square plate with FGM core with polynomial material law [2] using a 19^2 grid. Effect of transverse normal strain ϵ_{zz} on σ_{xy} and σ_{zz} for a bending problem. $\bar{\sigma}_{zz} = \sigma_{zz}\frac{h}{a\bar{p}_z}$.

p		ϵ_{zz}	$\bar{\sigma}_{xy}(0,0,\frac{h}{3})$		$\bar{\sigma}_{zz}(\frac{a}{2},\frac{b}{2},0)$	
			$a/h = 4$	$a/h = 100$	$a/h = 4$	$a/h = 100$
1	Ref. LD4 [28]	0	0.3007	8.4968	0.0922	0.0038
	Ref. LM4 [28]	≠0	0.3007	8.4968	0.0922	0.0038
	Present	0	0.3303	8.4882	0.1276	3.1987
	Present	≠0	0.3167	8.4911	0.0827	0.0034
5	Ref. LD4 [28]	0	0.1999	6.4942	0.0911	0.0037
	Ref. LM4 [28]	≠0	0.1996	6.4942	0.0924	0.0037
	Present	0	0.2317	6.4454	0.0777	1.9535
	Present	≠0	0.2248	6.4441	0.0522	0.0022
10	Ref. LD4 [28]	0	0.1412	5.1402	0.1064	0.0043
	Ref. LM4 [28]	≠0	0.1403	5.1401	0.1067	0.0042
	Present	0	0.1745	5.0745	0.0685	1.6978
	Present	≠0	0.1687	5.0754	0.0443	0.0018

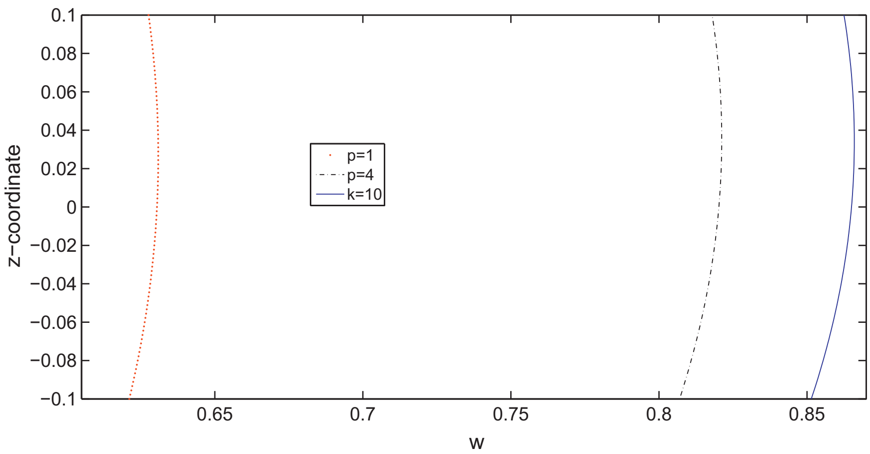

Fig. 7. Sandwich square plate with FGM core subjected to sinusoidal load at the top, with $a/h = 10$. Displacement through the thickness direction at the center of the plate $(\frac{a}{2},\frac{b}{2})$ for different values of p.

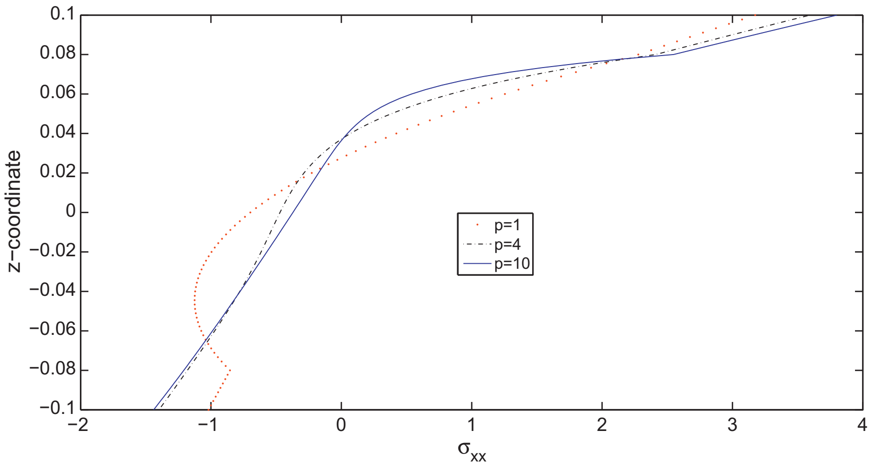

Fig. 8. Sandwich square plate with FGM core subjected to sinusoidal load at the top, with $a/h = 10$. σ_{xx} through the thickness direction at the center of the plate $(\frac{a}{2},\frac{b}{2})$ for different values of p.

$$\bar{\sigma}_{xy} = \frac{h}{a\bar{p}_z}\sigma_{xy}(0,0); \quad \bar{\sigma}_{xz} = \frac{h}{a\bar{p}_z}\sigma_{xz}\left(0,\frac{b}{2}\right);$$
$$\bar{\sigma}_{yz} = \frac{h}{a\bar{p}_z}\sigma_{yz}\left(\frac{a}{2},0\right) \tag{99}$$

In Table 2 we present the normalized transverse displacement ($\bar{w}$) and the normalized transverse shear stress ($\bar{\sigma}_{xz}$) at selected locations. In Table 3 we present the normalized in-plane shear stress ($\bar{\sigma}_{xy}$) and the normalized transverse normal stress ($\bar{\sigma}_{zz}$) at selected

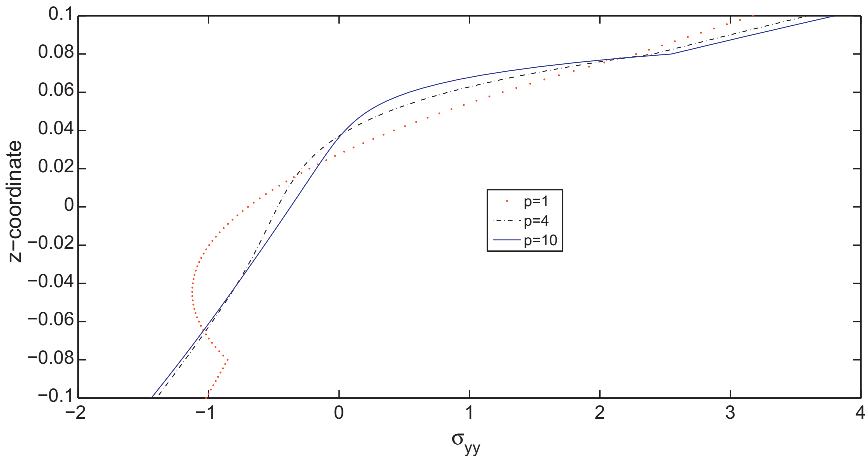

Fig. 9. Sandwich square plate with FGM core subjected to sinusoidal load at the top, with $a/h = 10$. σ_{yy} through the thickness direction at the center of the plate $(\frac{a}{2},\frac{b}{2})$ for different values of p.

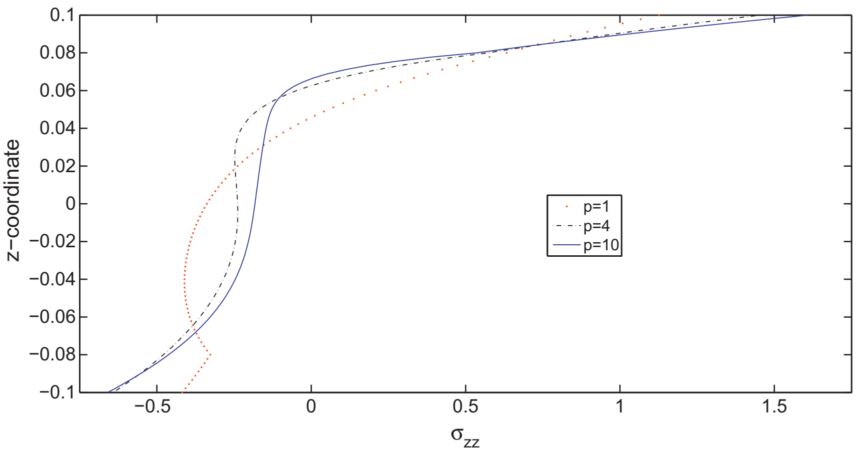

Fig. 10. Sandwich square plate with FGM core subjected to sinusoidal load at the top, with $a/h = 10$. σ_{zz} through the thickness direction at the center of the plate $(\frac{a}{2},\frac{b}{2})$ for different values of p.

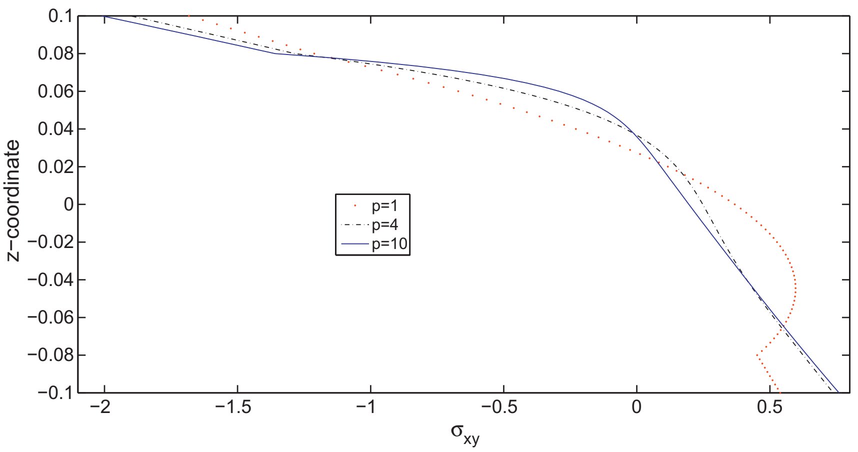

Fig. 11. Sandwich square plate with FGM core subjected to sinusoidal load at the top, with $a/h = 10$. σ_{xy} through the thickness direction at the point (0,0) for different values of p.

locations. In both tables we consider three a/h ratios (4, 10 and 100), and three power-law exponents (p = 1, 4 and 10). We use a 19^2 Chebyshev grid and consider both $\epsilon_{zz} = 0$ and $\epsilon_{zz} \neq 0$ approaches. Our meshless results are compared in Table 2 with finite element results by Carrera et al. [9], and compare quite well for all cases. In Table 3 we compare the present approach with FEM results by Brischetto [28] and again the comparison is quite good.

n Figs. 7–13 we present the evolution of the displacement and stresses across the thickness direction for various values of the exponent p of a plate with side to thickness ratio $a/h = 10$, using a 19^2 grid.

The present numerical method presents very close results to those of Carrera et al. [9] for a $N = 4$ expansion.

The consideration of a non-zero ϵ_{zz} strain produces a significant change in the transverse displacement as well as in the normal stress. This becomes evident when we compare the present approch with that of Zenkour [2] who neglected the ϵ_{zz} strain in the formulation.

4.2. Free vibration problems

In this example, we study the free vibration behavior of simply-supported isotropic FGM plates. We consider both the $\epsilon_{zz} = 0$ and the $\epsilon_{zz} \neq 0$ cases. We compare results with an exact (analytical) solution by Vel and Batra [29], and another meshless technique by Qian et al. [8]. In order to compare results, we use the Mori–Tanaka scheme for obtaing equivalent material properties.

In Table 4 we consider thin and thick plates, with $p = 1$, and using 13^2 Chebishev points. The ϵ_{zz} effect is significant. In fact, the exact solution by Vel and Batra [29] is achieved for all cases, by allowing $\epsilon_{zz} \neq 0$. In Table 5 we compare with the same sources, varying the p exponent, for $a/h = 5$ and using 13^2 points. Our present formulation with $\epsilon_{zz} \neq 0$ matches the exact solution.

In Fig. 14 the first four frequencies are presented for $p = 1$ and using 17^2 points. In Table 6 we present the first ten frequencies for the same exponent p and compare results with those from [8] for different side-to-thickness ratios and different number of Chebishev points.

Table 4
Fundamental frequency $\bar{\omega} = \omega h\sqrt{\rho_m/E_m}$ of a SSSS isotropic functionally graded plate (Al/ZrO_2), $p = 1$, using 13^2 points.

Source	a/h		
	20	10	5
Ref. [8]	0.0149	0.0584	0.2152
Exact [29]	0.0153	0.0596	0.2192
Present, Sinus ($\epsilon_{zz} = 0$)	0.0153	0.0595	0.2184
Present, Sinus ($\epsilon_{zz} \neq 0$)	0.0153	0.0596	0.2193

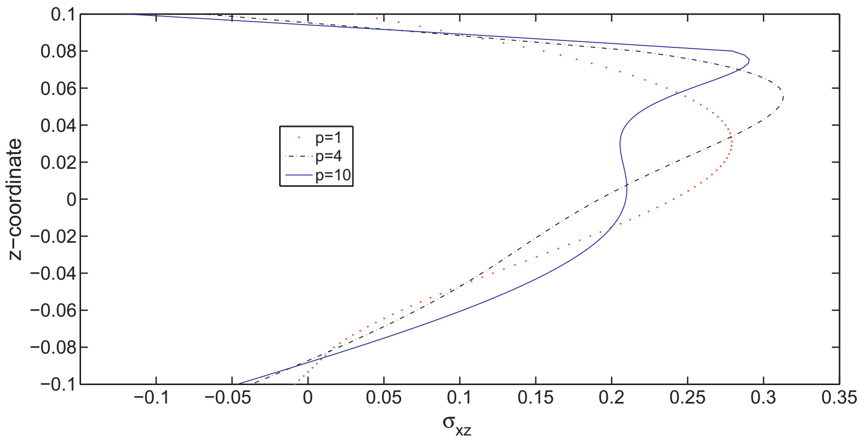

Fig. 12. Sandwich square plate with FGM core subjected to sinusoidal load at the top, with $a/h = 10$. σ_{xz} through the thickness direction at the point $(0, \frac{b}{2})$ for different values of p.

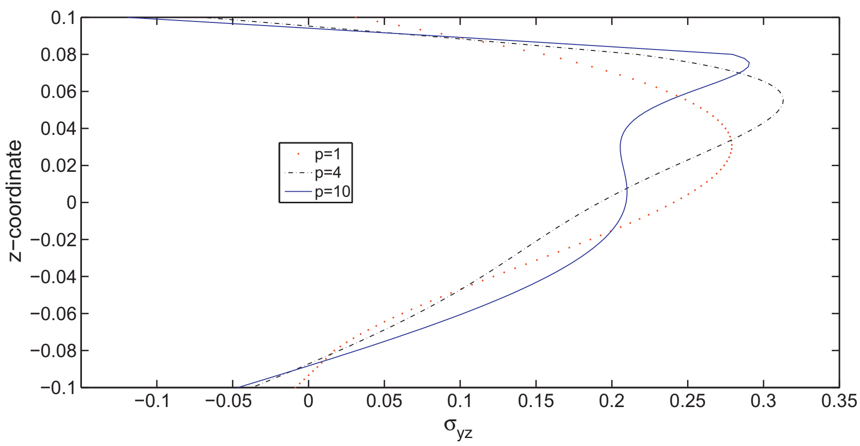

Fig. 13. Sandwich square plate with FGM core subjected to sinusoidal load at the top, with $a/h = 10$. σ_{yz} through the thickness direction at the point $(\frac{a}{2}, 0)$ for different values of p.

Table 5
Fundamental frequency $\bar{\omega} = \omega h \sqrt{\rho_m/E_m}$ of a SSSS isotropic functionally graded plate (Al/ZrO_2), $a/h = 5$, and using 13^2 points.

Source	$p = 2$	$p = 3$	$p = 5$
Ref. [8]	0.2153	0.2172	0.2194
Exact [29]	0.2197	0.2211	0.2225
Present, Sinus ($\epsilon_{zz} = 0$)	0.2189	0.2202	0.2215
Present, Sinus ($\epsilon_{zz} \neq 0$)	0.2198	0.2212	0.2225

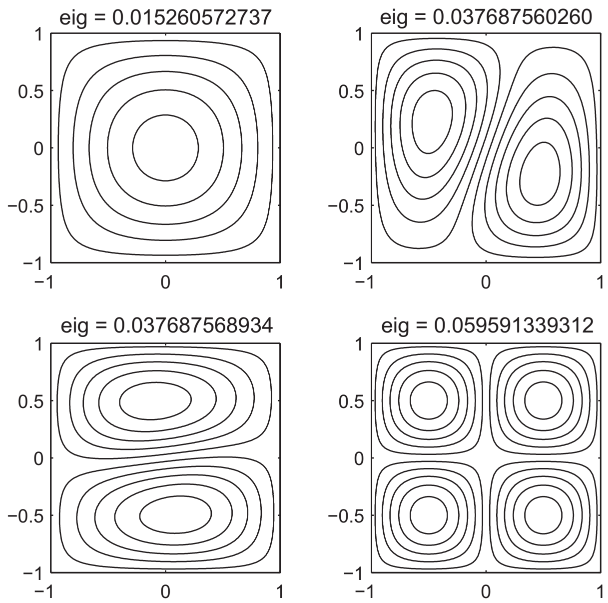

Fig. 14. First 4 frequencies $\bar{\omega} = \omega h \sqrt{\rho_m/E_m}$ of a SSSS isotropic functionally graded plate (Al/ZrO_2), with $a/h = 20$, $p = 1$, and using 17^2 points.

Table 6
First 10 frequencies $\bar{\omega} = \omega h \sqrt{\rho_m/E_m}$ of a SSSS isotropic functionally graded plate (Al/ZrO_2), $p = 1$.

$a/h = 20$				$a/h = 10$			
Present 13^2	17^2	21^2	Ref. [8]	13^2	17^2	21^2	Ref. [8]
0.0153	0.0153	0.0153	0.0149	0.0596	0.0596	0.0596	0.0584
0.0377	0.0377	0.0377	0.0377	0.1426	0.1426	0.1426	0.1410
0.0377	0.0377	0.0377	0.0377	0.1426	0.1426	0.1426	0.1410
0.0596	0.0596	0.0596	0.0593	0.2058	0.2058	0.2058	0.2058
0.0741	0.0739	0.0739	0.0747	0.2058	0.2058	0.2058	0.2058
0.0741	0.0739	0.0739	0.0747	0.2193	0.2193	0.2193	0.2164
0.0953	0.0950	0.0950	0.0769	0.2677	0.2676	0.2676	0.2646
0.0953	0.0950	0.0950	0.0912	0.2677	0.2676	0.2676	0.2677
0.1029	0.1029	0.1029	0.0913	0.2911	0.2910	0.2910	0.2913
0.1029	0.1029	0.1029	0.1029	0.3366	0.3363	0.3363	0.3264

5. Conclusions

A novel application of a unified formulation by a meshless discretization is proposed. A thickness-stretching sinusoidal shear deformation theory was implemented for the static and free vibration analysis of functionally graded plates.

The present formulation was compared with analytical, meshless or finite element methods and proved very accurate in both static and vibration problems. The effect of $\epsilon_{zz} \neq 0$ showed significance in thicker plates. Even for a thinner functionally graded plate, the σ_{zz} shoud always be considered in the formulation.

For the first time, the complete equations of motion and boundary conditions are present to help readers to implement it successfully with this or other strong-form techniques.

Appendix A. Fundamental nuclei

The stress–strain relations for functionally graded materials assume isotropic behavior at each layer k. Therefore, many terms are cancelled due to absence of membrane-bending coupling, etc. For a functionally graded plate the fundamental nuclei in explicit form are then obtained as:

$$\begin{aligned}
K_{uu_{11}}^{k\tau s} &= \left(-\partial_x^\tau \partial_x^s C_{11} + \partial_z^\tau \partial_z^s C_{55} - \partial_y^\tau \partial_y^s C_{66}\right) F_\tau F_s \\
K_{uu_{12}}^{k\tau s} &= \left(-\partial_x^\tau \partial_y^s C_{12} - \partial_y^\tau \partial_x^s C_{66}\right) F_\tau F_s \\
K_{uu_{13}}^{k\tau s} &= \left(-\partial_x^\tau \partial_z^s C_{13} + \partial_z^\tau \partial_x^s C_{55}\right) F_\tau F_s \\
K_{uu_{21}}^{k\tau s} &= \left(-\partial_y^\tau \partial_x^s C_{12} - \partial_x^\tau \partial_y^s C_{66}\right) F_\tau F_s \\
K_{uu_{22}}^{k\tau s} &= \left(-\partial_y^\tau \partial_y^s C_{22} + \partial_z^\tau \partial_z^s C_{44} - \partial_x^\tau \partial_x^s C_{66}\right) F_\tau F_s \\
K_{uu_{23}}^{k\tau s} &= \left(-\partial_y^\tau \partial_z^s C_{23} + \partial_z^\tau \partial_y^s C_{44}\right) F_\tau F_s \\
K_{uu_{31}}^{k\tau s} &= \left(\partial_z^\tau \partial_x^s C_{13} - \partial_x^\tau \partial_z^s C_{55}\right) F_\tau F_s \\
K_{uu_{32}}^{k\tau s} &= \left(\partial_z^\tau \partial_y^s C_{23} - \partial_y^\tau \partial_z^s C_{44}\right) F_\tau F_s \\
K_{uu_{33}}^{k\tau s} &= \left(\partial_z^\tau \partial_z^s C_{33} - \partial_y^\tau \partial_y^s C_{44} - \partial_x^\tau \partial_x^s C_{55}\right) F_\tau F_s
\end{aligned} \tag{A.1}$$

$$\begin{aligned}
\Pi_{11}^{k\tau s} &= \left(n_x \partial_x^s C_{11} + n_y \partial_y^s C_{66}\right) F_\tau F_s \\
\Pi_{12}^{k\tau s} &= \left(n_x \partial_y^s C_{12} + n_y \partial_x^s C_{66}\right) F_\tau F_s \\
\Pi_{13}^{k\tau s} &= n_x \partial_z^s C_{13} F_\tau F_s \\
\Pi_{21}^{k\tau s} &= \left(n_y \partial_x^s C_{12} + n_x \partial_y^s C_{66}\right) F_\tau F_s \\
\Pi_{22}^{k\tau s} &= \left(n_y \partial_y^s C_{22} + n_x \partial_x^s C_{66}\right) F_\tau F_s \\
\Pi_{23}^{k\tau s} &= n_y \partial_z^s C_{23} F_\tau F_s \\
\Pi_{31}^{k\tau s} &= n_x \partial_z^s C_{55} F_\tau F_s \\
\Pi_{32}^{k\tau s} &= n_y \partial_z^s C_{44} F_\tau F_s \\
\Pi_{33}^{k\tau s} &= \left(n_y \partial_y^s C_{44} + n_x \partial_x^s C_{55}\right) F_\tau F_s
\end{aligned} \tag{A.2}$$

References

[1] Miyamoto Y, Kaysser WA, Rabin BH, Kawasaki A, Ford RG. Functionally graded materials: design, processing and applications. Kluwer Academic Publishers; 1999.
[2] Zenkour AM. Generalized shear deformation theory for bending analysis of functionally graded plates. Appl Math Modell 2006;30.
[3] Cheng ZQ, Batra RC. Deflection relationships between the homogeneous kirchhoff plate theory and different functionally graded plate theories. Arch Mech 2000;52:143–58.
[4] Batra RC, Jin J. Natural frequencies of a functionally graded anisotropic rectangular plate. J Sound Vib 2005;282(1–2):509–16.
[5] Ferreira AJM, Batra RC, Roque CMC, Qian LF, Jorge RMN. Natural frequencies of functionally graded plates by a meshless method. Compos Struct 2006;75(1–4):593–600.
[6] Reddy JN. Analysis of functionally graded plates. Int J Numer Methods Eng 2000;47:663–84.
[7] Ferreira AJM, Batra RC, Roque CMC, Qian LF, Martins PALS. Static analysis of functionally graded plates using third-order shear deformation theory and a meshless method. Compos Struct 2005;69(4):449–57.
[8] Qian LF, Batra RC, Chen LM. Static and dynamic deformations of thick functionally graded elastic plate by using higher-order shear and normal deformable plate theory and meshless local Petrov-Galerkin method. Composites: Part B 2004;35:685–97.
[9] Carrera E, Brischetto S, Cinefra M, Soave M. Effects of thickness stretching in functionally graded plates and shells. Compos Part B: Engineering 2011;42:123–33.

[10] Kansa EJ. Multiquadrics – a scattered data approximation scheme with applications to computational fluid dynamics. I: surface approximations and partial derivative estimates. Comput Math Appl 1990;19(8/9):127–45.
[11] Ferreira AJM. A formulation of the multiquadric radial basis function method for the analysis of laminated composite plates. Compos Struct 2003;59:385–92.
[12] Ferreira AJM. Thick composite beam analysis using a global meshless approximation based on radial basis functions. Mech Adv Mater Struct 2003;10:271–84.
[13] Ferreira AJM, Roque CMC, Martins PALS. Analysis of composite plates using higher-order shear deformation theory and a finite point formulation based on the multiquadric radial basis function method. Composites: Part B 2003;34:627–36.
[14] Ferreira AJM, Roque CMC, Jorge RMN, Kansa EJ. Static deformations and vibration analysis of composite and sandwich plates using a layerwise theory and multiquadrics discretizations. Eng Anal Bound Elem 2005;29(12):1104–14.
[15] Ferreira AJM, Roque CMC, Jorge RMN. Analysis of composite plates by trigonometric shear deformation theory and multiquadrics. Comput Struct 2005;83(27):2225–37.
[16] Ferreira AJM, Batra RC, Roque CMC, Qian LF, Jorge RMN. Natural frequencies of functionally graded plates by a meshless method. Compos Struct 2006;75(1–4):593–600. Thirteenth International Conference on Composite Structures – ICCS/13.
[17] Ferreira AJM, Roque CMC, Jorge RMN. Free vibration analysis of symmetric laminated composite plates by fsdt and radial basis functions. Comput Methods Appl Mech Eng 2005;194(39–41):4265–78.
[18] Ferreira AJM, Roque CMC, Martins PALS. Radial basis functions and higher-order shear deformation theories in the analysis of laminated composite beams and plates. Compos Struct 2004;66(1–4):287–93. Twelfth International Conference on Composite Structures.
[19] Carrera E. C^0 Reissner–Mindlin multilayered plate elements including zig-zag and interlaminar stress continuity. Int J Numer Methods Eng 1996;39:1797–820.
[20] Carrera E. Developments, ideas, and evaluations based upon Reissner's mixed variational theorem in the modelling of multilayered plates and shells. Appl Mech Rev 2001;54:301–29.
[21] Touratier M. A generalization of shear deformation theories for axisymmetric multilayered shells. Int J Solids Struct 1992;29:1379–99.
[22] Touratier M. An efficient standard plate theory. Int J Eng Sci 1991;29:901–16.
[23] Touratier M. A refined theory of laminated shallow shells. Int J Solids Struct 1992;29(11):1401–15.
[24] Vidal P, Polit O. A family of sinus finite elements for the analysis of rectangular laminated beams. Compos Struct 2008;84:56–72.
[25] Neves AMA, Ferreira AJM, Carrera E, Roque CMC, Cinefra M, Jorge RMN, et al. Bending of fgm plates by a sinusoidal plate formulation and collocation with radial basis functions. Mech Res Commun, in press.
[26] Ferreira AJM, Fasshauer GE. Computation of natural frequencies of shear deformable beams and plates by a rbf-pseudospectral method. Comput Methods Appl Mech Eng 2006;196:134–46.
[27] Carrera E, Brischetto S, Robaldo A. Variable kinematic model for the analysis of functionally graded material plates. AIAA J 2008;46:194–203.
[28] Brischetto S. Classical and mixed advanced models for sandwich plates embedding functionally graded cores. J Mech Mater Struct 2009;4:13–33.
[29] Vel SS, Batra RC. Three-dimensional exact solution for the vibration of functionally graded rectangular plates. J Sound Vib 2004;272:703–30.

2.3 A quasi-3D hyperbolic shear deformation theory for the static and free vibration analysis of functionally graded plates

A. M. A. Neves, A. J. M. Ferreira, E. Carrera, M. Cinefra, C. M. C. Roque, R. M. N. Jorge, C. M. M. Soares, A quasi-3D hyperbolic shear deformation theory for the static and free vibration analysis of functionally graded plates, Composites Structures, Volume 94, 2012, pages 1814-1825.

Composite Structures 94 (2012) 1814–1825

Contents lists available at SciVerse ScienceDirect

Composite Structures

journal homepage: www.elsevier.com/locate/compstruct

A quasi-3D hyperbolic shear deformation theory for the static and free vibration analysis of functionally graded plates

A.M.A. Neves [a], A.J.M. Ferreira [a,*], E. Carrera [c], M. Cinefra [c], C.M.C. Roque [b], R.M.N. Jorge [a], C.M.M. Soares [d]

[a] Departamento de Engenharia Mecânica, Faculdade de Engenharia, Universidade do Porto, Rua Dr. Roberto Frias, 4200-465 Porto, Portugal
[b] INEGI, Faculdade de Engenharia, Universidade do Porto, Rua Dr. Roberto Frias, 4200-465 Porto, Portugal
[c] Departament of Aeronautics and Aerospace Engineering, Politecnico di Torino, Corso Duca degli Abruzzi, 24, 10129 Torino, Italy
[d] Instituto Superior Técnico, Technical University of Lisbon, Av. Rovisco Pais, 1049-001 Lisboa, Portugal

ARTICLE INFO

Article history:
Available online 29 December 2011

Keywords:
Functionally graded materials
Meshless methods
Plates and shells

ABSTRACT

This paper presents an original hyperbolic sine shear deformation theory for the bending and free vibration analysis of functionally graded plates. The theory accounts for through-the-thickness deformations.

Equations of motion and boundary conditions are obtained using Carrera's Unified Formulation and further interpolated by collocation with radial basis functions.

The efficiency of the present approach combining the new theory with this meshless technique is demonstrated in several numerical examples, for the static and free vibration analysis of functionally graded plates. Excellent agreement for simply-supported plates with other literature results has been found.

1. Introduction

Functionally graded materials (FGM) are a class of composites in which the properties change gradually over one or more directions. A typical FGM plate presents a continuous variation of material properties over the thickness direction by mixing two different materials [1]. The gradual variation of properties avoids the delamination failure that is common in laminated composites.

Typically, the analysis of FGM plates is performed using the first-order shear deformation theory (FSDT) [2–5] or higher-order shear deformation theories (HSDT) [3,5–8]. The FSDT gives acceptable results but depends on a shear correction factor which is difficult to find as it depends on many parameters. There is no need of a shear correction factor when using a HSDT but equations of motion are more complicated to obtain than those of the FSDT.

Typically functionally graded plates have been analysed with shear deformation theories that neglect the thickness stretching ϵ_{zz}, considering the transverse displacement independent of the thickness coordinate. The effect of thickness stretching in FGM plates has been recently investigated by Carrera et al. [9], using finite element approximations.

The use of alternative methods to the Finite Element Methods for the analysis of plates, such as the meshless methods based on collocation with radial basis functions (RBFs) is atractive due to the absence of a mesh and the ease of collocation methods. In recent years, radial basis functions showed excellent accuracy in the interpolation of data and functions. Kansa [10] introduced the concept of solving partial differential equations by an unsymmetric RBF collocation method based upon the multiquadric interpolation functions. The authors have recently applied the RBF collocation to the static deformations and free vibrations of composite beams and plates [11–18].

The present paper addresses the thickness stretching effect on the static and free vibration analysis of FGM plates, by a meshless technique based on collocation with radial basis functions. The Unified Formulation proposed by Carrera (further denoted as CUF) method [19,20] is employed to obtain the algebraic equations of motion and boundary conditions. Such equations of motion and corresponding boundary conditions are then interpolated by radial basis functions to obtain an algebraic system of equations. The CUF method has been applied in several finite element analysis, either using the Principle of Virtual Displacements, or by using the Reissner's Mixed Variational theorem. The stiffness matrix components, the external force terms or the inertia terms can be obtained directly with this unified formulation, irrespective of the shear deformation theory being considered.

To the best of authors' knowledge, plate theories involving hyperbolic functions are quite rare in literature. Soldatos [21] used a displacement field involving the hyperbolic function

$$f(z) = h \sinh\left(\frac{z}{h}\right) - z \cosh\left(\frac{1}{2}\right). \quad (1)$$

* Corresponding author.
E-mail address: ferreira@fe.up.pt (A.J.M. Ferreira).

0263-8223/$ - see front matter © 2011 Elsevier Ltd. All rights reserved.
doi:10.1016/j.compstruct.2011.12.005

In [22,23] two displacement fields are presented both considering a hyperbolic function:

$$f(z) = \frac{3\pi}{2} h \tanh\left(\frac{z}{h}\right) - \frac{3\pi}{2} z \operatorname{sech}^2\left(\frac{1}{2}\right) \tag{2}$$

and

$$f(z) = z \operatorname{sech}\left(\frac{\pi z^2}{h^2}\right) - z \operatorname{sech}\left(\frac{\pi}{4}\right)\left[1 - \frac{\pi}{2}\tanh\left(\frac{\pi}{4}\right)\right]. \tag{3}$$

In [24] the considered hyperbolic function is

$$f(z) = \frac{\frac{h}{\pi}\sinh\left(\frac{\pi z}{h}\right) - z}{\cosh\left(\frac{\pi}{2}\right) - 1}. \tag{4}$$

In all cases the hyperbolic functions are used for the in-plane expansions only, while the transverse displacement is kept constant ($w = w_0$).

The use of hyperbolic shear deformation theory accounting for $\epsilon_{zz} \neq 0$ for the static and free vibration analysis of plates has not been done yet. In this paper an hybrid quasi-3D hyperbolic shear deformation theory, with different expansion for the in-plane and the out-of-plane displacement is proposed. In-plane displacements are considered to be of hyperbolic sine type across the thickness coordinate and the out-of-plane displacement is defined as quadratic in the thickness direction. The present formulation can be seen as a enhancement of the original CUF in the sense that different displacement fields for in-plane and out-of-plane displacements are introduced.

2. Governing equations and boundary conditions

A rectangular plate of in-plane dimensions a and b and uniform thickness h is considered. The co-ordinate system is such that the x–y plane coincides with the midplane of the plate. The plate is made of a material graded across the thickness direction.

2.1. Displacement field

The following displacement field is assumed:

$$u(x,y,z,t) = u_0(x,y,t) + z u_1(x,y,t) + \sinh\left(\frac{\pi z}{h}\right) u_Z(x,y,t) \tag{5}$$

$$v(x,y,z,t) = v_0(x,y,t) + z v_1(x,y,t) + \sinh\left(\frac{\pi z}{h}\right) v_Z(x,y,t) \tag{6}$$

$$w(x,y,z,t) = w_0(x,y,t) + z w_1(x,y,t) + z^2 w_2(x,y,t) \tag{7}$$

where u, v, and w are the displacements in the x-, y-, and z-directions, respectively. u_0, u_1, u_Z, v_0, v_1, v_Z, w_0, w_1, and w_2 are functions to be determined.

2.2. Strains

The strain–displacement relationships are:

$$\begin{Bmatrix} \epsilon_{xx} \\ \epsilon_{yy} \\ \gamma_{xy} \end{Bmatrix} = \begin{Bmatrix} \frac{\partial u}{\partial x} \\ \frac{\partial v}{\partial y} \\ \frac{\partial u}{\partial y} + \frac{\partial v}{\partial x} \end{Bmatrix}, \quad \begin{Bmatrix} \gamma_{xz} \\ \gamma_{yz} \\ \epsilon_{zz} \end{Bmatrix} = \begin{Bmatrix} \frac{\partial u}{\partial z} + \frac{\partial w}{\partial x} \\ \frac{\partial v}{\partial z} + \frac{\partial w}{\partial y} \\ \frac{\partial w}{\partial z} \end{Bmatrix} \tag{8}$$

By substitution of the displacement field in (8), the strains are obtained in terms of the proposed model unknowns:

$$\begin{Bmatrix} \epsilon_{xx} \\ \epsilon_{yy} \\ \gamma_{xy} \end{Bmatrix} = \begin{Bmatrix} \frac{\partial u_0}{\partial x} \\ \frac{\partial v_0}{\partial y} \\ \frac{\partial u_0}{\partial y} + \frac{\partial v_0}{\partial x} \end{Bmatrix} + z \begin{Bmatrix} \frac{\partial u_1}{\partial x} \\ \frac{\partial v_1}{\partial y} \\ \frac{\partial u_1}{\partial y} + \frac{\partial v_1}{\partial x} \end{Bmatrix} + \sinh\left(\frac{\pi z}{h}\right) \begin{Bmatrix} \frac{\partial u_Z}{\partial x} \\ \frac{\partial v_Z}{\partial y} \\ \frac{\partial u_Z}{\partial y} + \frac{\partial v_Z}{\partial x} \end{Bmatrix} \tag{9}$$

$$\begin{Bmatrix} \gamma_{xz} \\ \gamma_{yz} \end{Bmatrix} = \begin{Bmatrix} u_1 \\ v_1 \end{Bmatrix} + \cosh\left(\frac{\pi z}{h}\right)\frac{\pi}{h} \begin{Bmatrix} u_Z \\ v_Z \end{Bmatrix} + \begin{Bmatrix} \frac{\partial w_0}{\partial x} \\ \frac{\partial w_0}{\partial y} \end{Bmatrix} + z \begin{Bmatrix} \frac{\partial w_1}{\partial x} \\ \frac{\partial w_1}{\partial y} \end{Bmatrix} + z^2 \begin{Bmatrix} \frac{\partial w_2}{\partial x} \\ \frac{\partial w_2}{\partial y} \end{Bmatrix} \tag{10}$$

$$\epsilon_{zz} = w_1 + 2 z w_2 \tag{11}$$

2.3. Elastic stress–strain relations

The elastic stress–strain relations depends on which assumption of ϵ_{zz} we consider. If $\epsilon_{zz} \neq 0$, i.e., thickness stretching is allowed, then the 3D model is used and the constitutive equations can be written as:

$$\begin{Bmatrix} \sigma_{xx} \\ \sigma_{yy} \\ \tau_{xy} \\ \tau_{xz} \\ \tau_{yz} \\ \sigma_{zz} \end{Bmatrix} = \begin{Bmatrix} C_{11} & C_{12} & 0 & 0 & 0 & C_{13} \\ C_{12} & C_{22} & 0 & 0 & 0 & C_{23} \\ 0 & 0 & C_{66} & 0 & 0 & 0 \\ 0 & 0 & 0 & C_{55} & 0 & 0 \\ 0 & 0 & 0 & 0 & C_{44} & 0 \\ C_{13} & C_{23} & 0 & 0 & 0 & C_{33} \end{Bmatrix} \begin{Bmatrix} \epsilon_{xx} \\ \epsilon_{yy} \\ \gamma_{xy} \\ \gamma_{xz} \\ \gamma_{yz} \\ \epsilon_{zz} \end{Bmatrix} \tag{12}$$

The C_{ij} are the three-dimensional elastic constants, given by

$$C_{11} = \frac{E(1-\nu^2)}{1-3\nu^2-2\nu^3}, \quad C_{12} = \frac{E(\nu+\nu^2)}{1-3\nu^2-2\nu^3}, \quad C_{22} = \frac{E(1-\nu^2)}{1-3\nu^2-2\nu^3},$$

$$C_{13} = \frac{E(\nu+\nu^2)}{1-3\nu^2-2\nu^3}, \quad C_{23} = \frac{E(\nu+\nu^2)}{1-3\nu^2-2\nu^3}, \tag{14}$$

$$C_{44} = G, \quad C_{55} = G, \quad C_{66} = G, \quad C_{33} = \frac{E(1-\nu^2)}{1-3\nu^2-2\nu^3} \tag{15}$$

where E is the modulus of elasticity, ν is Poisson's ratio, and G is the shear modulus $G = \frac{E}{2(1+\nu)}$.

If $\epsilon_{zz} = 0$, then the plane-stress case is used

$$\begin{Bmatrix} \sigma_{xx} \\ \sigma_{yy} \\ \tau_{xy} \\ \tau_{xz} \\ \tau_{yz} \end{Bmatrix} = \begin{Bmatrix} C_{11} & C_{12} & 0 & 0 & 0 \\ C_{12} & C_{22} & 0 & 0 & 0 \\ 0 & 0 & C_{66} & 0 & 0 \\ 0 & 0 & 0 & C_{55} & 0 \\ 0 & 0 & 0 & 0 & C_{44} \end{Bmatrix} \begin{Bmatrix} \epsilon_{xx} \\ \epsilon_{yy} \\ \gamma_{xy} \\ \gamma_{xz} \\ \gamma_{yz} \end{Bmatrix} \tag{16}$$

The C_{ij} are the plane-stress reduced elastic constants:

$$C_{11} = \frac{E}{1-\nu^2}, \quad C_{12} = \nu\frac{E}{1-\nu^2}, \quad C_{22} = \frac{E}{1-\nu^2}, \tag{17}$$

$$C_{44} = G, \quad C_{55} = G, \quad C_{66} = G \tag{18}$$

It is interesting to note that the use of shear-correction factors is not considered, as would be the case of the first-order shear deformation theory.

We consider virtual (mathematical) layers of constant thickness, each containing a homogeneized modulus of elasticity, E^k, and a homogeneized Poisson's ratio, ν^k. The functionally graded plate is divided into a NL layers of equal thickness. For each layer the volume fraction of the ceramic phase is defined as:

$$V_c^k = \left(0.5 + \frac{\tilde{z}}{h}\right)^p \tag{19}$$

where $\tilde{z}$ is the thickness coordinate of a point of each layer, and p is the polynomial gradation law exponent. The volume fraction for the metal phase is given as $V_m^k = 1 - V_c^k$.

For each virtual layer, the elastic properties E^k and ν^k can be computed in two ways. First, we consider the law-of-mistures:

$$E^k(z) = E_m V_m + E_c V_c; \quad \nu^k(z) = \nu_m V_m + \nu_c V_c \tag{20}$$

Second, we consider the Mori–Tanaka homogenization procedure [25,26]. In this homogenization method, we find the bulk modulus, K, and the effective shear modulus, G, of the composite equivalent layer as

$$\frac{K-K_m}{K_c-K_m}=\frac{V_c}{1+(1-V_c)\frac{K_c-K_m}{K_m+4/3G_m}};\quad \frac{G-G_m}{G_c-G_m}=\frac{V_c}{1+(1-V_c)\frac{G_c-G_m}{G_m+f_m}} \tag{21}$$

where

$$f_m=\frac{G_m(9K_m+8G_m)}{6(K_m+2G_m)} \tag{22}$$

The effective values of Young's modulus, E^k, and Poisson's ratio, ν^k, are found from

$$E^k=\frac{9K^kG^k}{3K^k+G^k};\quad \nu^k=\frac{3K^k-2G^k}{2(3K^k+G^k)} \tag{23}$$

After using the law-of-mixtures or the Mori–Tanaka homogenization procedure, the computation of the elastic constants C_{ij}^k is performed for each layer based on ν^k and E^k. For example,

$$C_{12}^k=\frac{E^k(\nu^k+(\nu^k)^2)}{1-3(\nu^k)^2-2(\nu^k)^3} \tag{24}$$

Other C_{ij}^k terms follow a similar procedure.

2.4. Governing equations

The equations of motion of the hyperbolic sine theory are derived from the Principle of Virtual Displacements (PVD). In analytical form, it can be stated as:

$$\int_\Omega\left\{\delta\boldsymbol{\epsilon}_p^T\boldsymbol{\sigma}_p+\delta\boldsymbol{\epsilon}_n^T\boldsymbol{\sigma}_n\right\}d\Omega=\int_\Omega\left\{\rho\,\delta\mathbf{u}^T\ddot{\mathbf{u}}+\delta\mathbf{u}^T\mathbf{p}\right\}d\Omega \tag{25}$$

where (p) indicates in-plane components (xx), (yy) and (xy), and (n) the transverse components (xz), (yz) and (zz). Ω is the volume of the plate, δ denotes a virtual variation and T indicates the transpose operator. ρ is the density of the material and double dots denote acceleration. $\mathbf{p}=\{p_x,p_y,p_z\}$ is the external load applied to the structure. For the considered functionally graded plate, the PVD can be written as:

$$\sum_{k=1}^{NL}\int_{\Omega_k}\int_{A_k}\left(\delta\boldsymbol{\epsilon}_p^T\boldsymbol{\sigma}_p^k+\delta\boldsymbol{\epsilon}_n^T\boldsymbol{\sigma}_n^k\right)dz\,d\Omega_k=\sum_{k=1}^{NL}\int_{\Omega_k}\int_{A_k}\left(\rho^k\,\delta\mathbf{u}^T\ddot{\mathbf{u}}+\delta\mathbf{u}^T\mathbf{p}\right)dz\,d\Omega_k \tag{26}$$

where Ω_k is the in-plane integration domain (x,y) and A_k is the integration domains in z direction of the k-th layer. Integrating through the thickness and summing on the index k, integrating by parts with respect to x and y and collecting the coefficients of δu_0, δv_0, δw_0, δu_1, δv_1, δw_1, δu_Z, δv_Z, and δw_2, the following equations of motion are obtained:

$$\begin{aligned}
\delta u_0:&\ \sum_{k=1}^{NL}\left(-\frac{\partial N_{xx}^k}{\partial x}-\frac{\partial N_{xy}^k}{\partial y}\right)=\sum_{k=1}^{NL}\int_{A_k}\left\{\rho^k\left(\ddot{u}_0+z\ddot{u}_1+\sinh\left(\frac{\pi z}{h}\right)\ddot{u}_Z\right)+p_x\right\}dz\\
\delta v_0:&\ \sum_{k=1}^{NL}\left(-\frac{\partial N_{xy}^k}{\partial x}-\frac{\partial N_{yy}^k}{\partial y}\right)=\sum_{k=1}^{NL}\int_{A_k}\left\{\rho^k\left(\ddot{v}_0+z\ddot{v}_1+\sinh\left(\frac{\pi z}{h}\right)\ddot{v}_Z\right)+p_y\right\}dz\\
\delta w_0:&\ \sum_{k=1}^{NL}\left(-\frac{\partial Q_{xz}^k}{\partial x}-\frac{\partial Q_{yz}^k}{\partial y}\right)=\sum_{k=1}^{NL}\int_{A_k}\left\{\rho^k(\ddot{w}_0+z\ddot{w}_1+z^2\ddot{w}_2)+p_z\right\}dz\\
\delta u_1:&\ \sum_{k=1}^{NL}\left(-\frac{\partial M_{xx}^k}{\partial x}-\frac{\partial M_{xy}^k}{\partial y}+Q_{xz}^k\right)=\sum_{k=1}^{NL}\int_{A_k}\left\{\rho^kz\left(\ddot{u}_0+z\ddot{u}_1+\sinh\left(\frac{\pi z}{h}\right)\ddot{u}_Z\right)+zp_x\right\}dz\\
\delta v_1:&\ \sum_{k=1}^{NL}\left(-\frac{\partial M_{xy}^k}{\partial x}-\frac{\partial M_{yy}^k}{\partial y}+Q_{yz}^k\right)=\sum_{k=1}^{NL}\int_{A_k}\left\{\rho^kz\left(\ddot{v}_0+z\ddot{v}_1+\sinh\left(\frac{\pi z}{h}\right)\ddot{v}_Z\right)+zp_y\right\}dz\\
\delta w_1:&\ \sum_{k=1}^{NL}\left(-\frac{\partial M_{xz}^k}{\partial x}-\frac{\partial M_{yz}^k}{\partial y}+Q_{zz}^k\right)=\sum_{k=1}^{NL}\int_{A_k}\left\{\rho^kz(\ddot{w}_0+z\ddot{w}_1+z^2\ddot{w}_2)+zp_z\right\}dz\\
\delta u_Z:&\ \sum_{k=1}^{NL}\left(-\frac{\partial R_{xx}^{kZ}}{\partial x}-\frac{\partial R_{xy}^{kZ}}{\partial y}+R_{xz}^{kZ}\right)=\sum_{k=1}^{NL}\int_{A_k}\left\{\rho^k\sinh\left(\frac{\pi z}{h}\right)\left(\ddot{u}_0+z\ddot{u}_1+\sinh\left(\frac{\pi z}{h}\right)\ddot{u}_Z\right)+\sinh\left(\frac{\pi z}{h}\right)p_x\right\}dz\\
\delta v_Z:&\ \sum_{k=1}^{NL}\left(-\frac{\partial R_{xy}^{kZ}}{\partial x}-\frac{\partial R_{yy}^{kZ}}{\partial y}+R_{yz}^{kZ}\right)=\sum_{k=1}^{NL}\int_{A_k}\left\{\rho^k\sinh\left(\frac{\pi z}{h}\right)\left(\ddot{v}_0+z\ddot{v}_1+\sinh\left(\frac{\pi z}{h}\right)\ddot{v}_Z\right)+\sinh\left(\frac{\pi z}{h}\right)p_y\right\}dz\\
\delta w_2:&\ \sum_{k=1}^{NL}\left(-\frac{\partial R_{xz}^{k2}}{\partial x}-\frac{\partial R_{yz}^{k2}}{\partial y}+2M_{zz}^k\right)=\sum_{k=1}^{NL}\int_{A_k}\left\{\rho^kz^2(\ddot{w}_0+z\ddot{w}_1+z^2\ddot{w}_2)+z^2p_z\right\}dz
\end{aligned} \tag{27}$$

The following stress resultants for each fictitious layer are considered:

$$\begin{Bmatrix}N_{xx}^k\\N_{yy}^k\\N_{xy}^k\end{Bmatrix}=\int_{A_k}\begin{Bmatrix}\sigma_{xx}^k\\\sigma_{yy}^k\\\tau_{xy}^k\end{Bmatrix}dz,\quad \begin{Bmatrix}Q_{xz}^k\\Q_{yz}^k\\Q_{zz}^k\end{Bmatrix}=\int_{A_k}\begin{Bmatrix}\tau_{xz}^k\\\tau_{yz}^k\\\sigma_{zz}^k\end{Bmatrix}dz \tag{28}$$

$$\begin{Bmatrix}M_{xx}^k\\M_{yy}^k\\M_{xy}^k\end{Bmatrix}=\int_{A_k}z\begin{Bmatrix}\sigma_{xx}^k\\\sigma_{yy}^k\\\tau_{xy}^k\end{Bmatrix}dz,\quad \begin{Bmatrix}M_{xz}^k\\M_{yz}^k\\M_{zz}^k\end{Bmatrix}=\int_{A_k}z\begin{Bmatrix}\tau_{xz}^k\\\tau_{yz}^k\\\sigma_{zz}^k\end{Bmatrix}dz \tag{29}$$

$$\begin{Bmatrix}R_{xx}^{kZ}\\R_{yy}^{kZ}\\R_{xy}^{kZ}\end{Bmatrix}=\int_{A_k}\sinh\left(\frac{\pi z}{h}\right)\begin{Bmatrix}\sigma_{xx}^k\\\sigma_{yy}^k\\\tau_{xy}^k\end{Bmatrix}dz,\quad \begin{Bmatrix}R_{xz}^{kZ}\\R_{yz}^{kZ}\end{Bmatrix}=\frac{\pi}{h}\int_{A_k}\cosh\left(\frac{\pi z}{h}\right)\begin{Bmatrix}\tau_{xz}^k\\\tau_{yz}^k\end{Bmatrix}dz \tag{30}$$

$$\begin{Bmatrix}R_{xz}^{k2}\\R_{yz}^{k2}\end{Bmatrix}=\int_{A_k}z^2\begin{Bmatrix}\tau_{xz}^k\\\tau_{yz}^k\end{Bmatrix}dz \tag{31}$$

The corresponding mechanical boundary conditions are defined as:

$$\begin{aligned}
\delta u_0&:\ n_xN_{xx}^k+n_yN_{xy}^k=n_x\overline{N}_{xx}^k+n_y\overline{N}_{xy}^k\\
\delta v_0&:\ n_xN_{xy}^k+n_yN_{yy}^k=n_x\overline{N}_{xy}^k+n_y\overline{N}_{yy}^k\\
\delta w_0&:\ n_xQ_{xz}^k+n_yQ_{yz}^k=n_x\overline{Q}_{xz}^k+n_y\overline{Q}_{yz}^k
\end{aligned}$$

$$
\begin{aligned}
&\delta u_1 : n_x M_{xx}^k + n_y M_{xy}^k = n_x \overline{M}_{xx}^k + n_y \overline{M}_{xy}^k \\
&\delta v_1 : n_x M_{xy}^k + n_y M_{yy}^k = n_x \overline{M}_{xy}^k + n_y \overline{M}_{yy}^k \\
&\delta w_1 : n_x M_{xz}^k + n_y M_{yz}^k = n_x \overline{M}_{xz}^k + n_y \overline{M}_{yz}^k \\
&\delta u_Z : n_x R_{xx}^{kZ} + n_y R_{xy}^{kZ} = n_x \overline{R}_{xx}^{kZ} + n_y \overline{R}_{xy}^{kZ} \\
&\delta v_Z : n_x R_{xy}^{kZ} + n_y R_{yy}^{kZ} = n_x \overline{R}_{xy}^{kZ} + n_y \overline{R}_{yy}^{kZ} \\
&\delta w_2 : n_x R_{xz}^{k2} + n_y R_{yz}^{k2} = n_x \overline{R}_{xz}^{k2} + n_y \overline{R}_{yz}^{k2}
\end{aligned} \tag{32}
$$

where (n_x, n_y) denotes the unit normal-to-boundary vector and over-lined terms are the imposed resultants.

2.5. Equations of motion and boundary conditions in terms of displacements

In order to discretize the equations of motion by radial basis functions, we present in the following the explicit terms of the equations of motion and the boundary conditions in terms of the generalized displacements. The following equations are derived considering that the plate is subjected to a transverse external load p_z applied at the top of the plate $z = h/2$.

$$
\begin{aligned}
\delta u_0 : & -\left(G_{11}\frac{\partial^2 u_Z}{\partial x^2} + G_{66}\frac{\partial^2 u_Z}{\partial y^2}\right) - (G_{12}+G_{66})\frac{\partial^2 v_Z}{\partial x \partial y} \\
& -\left(A_{11}\frac{\partial^2 u_0}{\partial x^2} + A_{66}\frac{\partial^2 u_0}{\partial y^2}\right) - (A_{12}+A_{66})\frac{\partial^2 v_0}{\partial x \partial y} \\
& -\left(B_{11}\frac{\partial^2 u_1}{\partial x^2} + B_{66}\frac{\partial^2 u_1}{\partial y^2}\right) - (B_{12}+B_{66})\frac{\partial^2 v_1}{\partial x \partial y} - A_{13}\frac{\partial w_1}{\partial x} - 2B_{13}\frac{\partial w_2}{\partial x} \\
& = I_1 \ddot{u}_1 + I_0 \ddot{u}_0 + I_5 \ddot{u}_Z
\end{aligned} \tag{33}
$$

$$
\begin{aligned}
\delta u_1 : & \left(-D_{11}\frac{\partial^2 u_1}{\partial x^2} + A_{55}u_1 - D_{66}\frac{\partial^2 u_1}{\partial y^2}\right) \\
& + \left(H_{55}u_Z + N_{11}\frac{\partial^2 u_Z}{\partial x^2} + N_{66}\frac{\partial^2 u_Z}{\partial y^2}\right) + (N_{12}+N_{66})\frac{\partial^2 v_Z}{\partial x \partial y} \\
& - \left(B_{11}\frac{\partial^2 u_0}{\partial x^2} + B_{66}\frac{\partial^2 u_0}{\partial y^2}\right) - (B_{12}+B_{66})\frac{\partial^2 v_0}{\partial x \partial y} \\
& - (D_{12}+D_{66})\frac{\partial^2 v_1}{\partial x \partial y} + (B_{55}-B_{13})\frac{\partial w_1}{\partial x} \\
& + (D_{55}-2D_{13})\frac{\partial w_2}{\partial x} + A_{55}\frac{\partial w_0}{\partial x} \\
& = I_7 \ddot{u}_Z + I_1 \ddot{u}_0 + I_2 \ddot{u}_1
\end{aligned} \tag{34}
$$

$$
\begin{aligned}
\delta u_Z : & -\left(G_{11}\frac{\partial^2 u_0}{\partial x^2} + G_{66}\frac{\partial^2 u_0}{\partial y^2}\right) + (O_{55}-G_{55}-G_{13})\frac{\partial w_1}{\partial x} \\
& + \left(H_{55}u_1 + N_{11}\frac{\partial^2 u_1}{\partial x^2} + N_{66}\frac{\partial^2 u_1}{\partial y^2}\right) - (G_{12}+G_{66})\frac{\partial^2 v_0}{\partial x \partial y} \\
& + \left(-J_{11}\frac{\partial^2 u_Z}{\partial x^2} + R_{55}u_Z - J_{66}\frac{\partial^2 u_Z}{\partial y^2}\right) + (P_{55}+2N_{55}+2N_{13})\frac{\partial w_2}{\partial x} \\
& + (N_{12}+N_{66})\frac{\partial^2 v_1}{\partial x \partial y} - (J_{12}+J_{66})\frac{\partial^2 v_Z}{\partial x \partial y} + H_{55}\frac{\partial w_0}{\partial x} \\
& = I_7 \ddot{u}_1 + I_6 \ddot{u}_Z + I_5 \ddot{u}_0
\end{aligned} \tag{35}
$$

$$
\begin{aligned}
\delta v_0 : & -(G_{12}+G_{66})\frac{\partial^2 u_Z}{\partial x \partial y} - \left(G_{22}\frac{\partial^2 v_Z}{\partial y^2} + G_{66}\frac{\partial^2 v_Z}{\partial x^2}\right) - (A_{12}+A_{66})\frac{\partial^2 u_0}{\partial x \partial y} \\
& - \left(A_{22}\frac{\partial^2 v_0}{\partial y^2} + A_{66}\frac{\partial^2 v_0}{\partial x^2}\right) - (B_{12}+B_{66})\frac{\partial^2 u_1}{\partial x \partial y} \\
& - \left(B_{22}\frac{\partial^2 v_1}{\partial y^2} + B_{66}\frac{\partial^2 v_1}{\partial x^2}\right) - A_{23}\frac{\partial w_1}{\partial y} - 2B_{23}\frac{\partial w_2}{\partial y} \\
& = I_1 \ddot{v}_1 + I_0 \ddot{v}_0 + I_5 \ddot{v}_Z
\end{aligned} \tag{36}
$$

$$
\begin{aligned}
\delta v_1 : & \left(-D_{22}\frac{\partial^2 v_1}{\partial y^2} + A_{44}v_1 - D_{66}\frac{\partial^2 v_1}{\partial x^2}\right) \\
& + \left(H_{44}v_Z + N_{22}\frac{\partial^2 v_Z}{\partial y^2} + N_{66}\frac{\partial^2 v_Z}{\partial x^2}\right) + (N_{12}+N_{66})\frac{\partial^2 u_Z}{\partial x \partial y} \\
& - (B_{12}+B_{66})\frac{\partial^2 u_0}{\partial x \partial y} - (D_{12}+D_{66})\frac{\partial^2 u_1}{\partial x \partial y} - \left(B_{22}\frac{\partial^2 v_0}{\partial y^2} + B_{66}\frac{\partial^2 v_0}{\partial x^2}\right) \\
& + (B_{44}-B_{23})\frac{\partial w_1}{\partial y} + (D_{44}-2D_{23})\frac{\partial w_2}{\partial y} + A_{44}\frac{\partial w_0}{\partial y} \\
& = I_7 \ddot{v}_Z + I_1 \ddot{v}_0 + I_2 \ddot{v}_1
\end{aligned} \tag{37}
$$

$$
\begin{aligned}
\delta v_Z : & -(G_{12}+G_{66})\frac{\partial^2 u_0}{\partial x \partial y} + (O_{44}-G_{44}-G_{23})\frac{\partial w_1}{\partial y} \\
& + \left(H_{44}v_1 + N_{22}\frac{\partial^2 v_1}{\partial y^2} + N_{66}\frac{\partial^2 v_1}{\partial x^2}\right) - \left(G_{22}\frac{\partial^2 v_0}{\partial y^2} + G_{66}\frac{\partial^2 v_0}{\partial x^2}\right) \\
& + \left(-J_{22}\frac{\partial^2 v_Z}{\partial y^2} + R_{44}v_Z - J_{66}\frac{\partial^2 v_Z}{\partial x^2}\right) + (P_{44}+2N_{44}+2N_{23})\frac{\partial w_2}{\partial y} \\
& + (N_{12}+N_{66})\frac{\partial^2 u_1}{\partial x \partial y} - (J_{12}+J_{66})\frac{\partial^2 u_Z}{\partial x \partial y} + H_{44}\frac{\partial w_0}{\partial y} \\
& = I_7 \ddot{v}_1 + I_6 \ddot{v}_Z + I_5 \ddot{v}_0
\end{aligned} \tag{38}
$$

$$
\begin{aligned}
\delta w_0 : & -\left(A_{55}\frac{\partial^2 w_0}{\partial x^2} + A_{44}\frac{\partial^2 w_0}{\partial y^2}\right) - \left(B_{55}\frac{\partial^2 w_1}{\partial x^2} + B_{44}\frac{\partial^2 w_1}{\partial y^2}\right) \\
& - \left(D_{55}\frac{\partial^2 w_2}{\partial x^2} + D_{44}\frac{\partial^2 w_2}{\partial y^2}\right) - H_{55}\frac{\partial u_Z}{\partial x} - H_{44}\frac{\partial v_Z}{\partial y} - A_{55}\frac{\partial u_1}{\partial x} \\
& - A_{44}\frac{\partial v_1}{\partial y} + p_z \\
& = I_1 \ddot{w}_1 + I_2 \ddot{w}_2 + I_0 \ddot{w}_0
\end{aligned} \tag{39}
$$

$$
\begin{aligned}
\delta w_1 : & \left(-E_{55}\frac{\partial^2 w_2}{\partial x^2} + 2B_{33}w_2 - E_{44}\frac{\partial^2 w_2}{\partial y^2}\right) + (-O_{55}+G_{55}+G_{13})\frac{\partial u_Z}{\partial x} \\
& + (-O_{44}+G_{44}+G_{23})\frac{\partial v_Z}{\partial y} + \left(-D_{55}\frac{\partial^2 w_1}{\partial x^2} + A_{33}w_1 - D_{44}\frac{\partial^2 w_1}{\partial y^2}\right) \\
& + (B_{13}-B_{55})\frac{\partial u_1}{\partial x} + (B_{23}-B_{44})\frac{\partial v_1}{\partial y} - \left(B_{55}\frac{\partial^2 w_0}{\partial x^2} + B_{44}\frac{\partial^2 w_0}{\partial y^2}\right) \\
& + A_{13}\frac{\partial u_0}{\partial x} + A_{23}\frac{\partial v_0}{\partial y} \\
& = I_1 \ddot{w}_0 + I_2 \ddot{w}_1 + I_3 \ddot{w}_2
\end{aligned} \tag{40}
$$

$$
\begin{aligned}
\delta w_2 : & \left(-E_{55}\frac{\partial^2 w_1}{\partial x^2} + 2B_{33}w_1 - E_{44}\frac{\partial^2 w_1}{\partial y^2}\right) \\
& + \left(-F_{55}\frac{\partial^2 w_2}{\partial x^2} + 4D_{33}w_2 - F_{44}\frac{\partial^2 w_2}{\partial y^2}\right) \\
& - (P_{55}+2N_{55}+2N_{13})\frac{\partial u_Z}{\partial x} - (P_{44}+2N_{44}+2N_{23})\frac{\partial v_Z}{\partial y} \\
& + (2D_{13}-D_{55})\frac{\partial u_1}{\partial x} + (2D_{23}-D_{44})\frac{\partial v_1}{\partial y} \\
& - \left(D_{55}\frac{\partial^2 w_0}{\partial x^2} + D_{44}\frac{\partial^2 w_0}{\partial y^2}\right) + 2B_{13}\frac{\partial u_0}{\partial x} + 2B_{23}\frac{\partial v_0}{\partial y} + \left(\frac{h}{2}\right)^2 p_z \\
& = I_2 \ddot{w}_0 + I_3 \ddot{w}_1 + I_4 \ddot{w}_2
\end{aligned} \tag{41}
$$

The laminate stiffness components can be computed as

$$
\begin{aligned}
A_{ij} &= \sum_{k=1}^{NL} c_{ij}^k (z_{k+1} - z_k); \quad B_{ij} = \frac{1}{2} \sum_{k=1}^{NL} c_{ij}^k (z_{k+1}^2 - z_k^2) \\
D_{ij} &= \frac{1}{3} \sum_{k=1}^{NL} c_{ij}^k (z_{k+1}^3 - z_k^3); \quad E_{ij} = \frac{1}{4} \sum_{k=1}^{NL} c_{ij}^k (z_{k+1}^4 - z_k^4) \\
F_{ij} &= \frac{1}{5} \sum_{k=1}^{NL} c_{ij}^k (z_{k+1}^5 - z_k^5) \\
G_{ij} &= \sum_{k=1}^{NL} c_{ij}^k \frac{h_k}{\pi} \left[\cosh\left(\frac{\pi z_{k+1}}{h_k}\right) - \cosh\left(\frac{\pi z_k}{h_k}\right) \right] \\
H_{ij} &= \sum_{k=1}^{NL} c_{ij}^k \left[\sinh\left(\frac{\pi z_{k+1}}{h_k}\right) - \sinh\left(\frac{\pi z_k}{h_k}\right) \right] \\
J_{ij} &= \sum_{k=1}^{NL} c_{ij}^k \left[\frac{h_k}{4\pi} \left[\sinh\left(\frac{2\pi z_{k+1}}{h_k}\right) - \sinh\left(\frac{2\pi z_k}{h_k}\right) \right] - \frac{1}{2}(z_{k+1} - z_k) \right] \\
N_{ij} &= \sum_{k=1}^{NL} c_{ij}^k \left[\left(\frac{h_k}{\pi}\right)^2 \left(\sinh\left(\frac{\pi z_{k+1}}{h_k}\right) - \sinh\left(\frac{\pi z_k}{h_k}\right) \right) \right. \\
&\quad \left. - \frac{h_k}{\pi} \left(z_{k+1} \cosh\left(\frac{\pi z_{k+1}}{h_k}\right) - z_k \cosh\left(\frac{\pi z_k}{h_k}\right) \right) \right] \\
O_{ij} &= \sum_{k=1}^{NL} c_{ij}^k \left[z_{k+1} \sinh\left(\frac{\pi z_{k+1}}{h_k}\right) - z_k \sinh\left(\frac{\pi z_k}{h_k}\right) \right] \\
P_{ij} &= \sum_{k=1}^{NL} c_{ij}^k \left[z_{k+1}^2 \sinh\left(\frac{\pi z_{k+1}}{h_k}\right) - z_k^2 \sinh\left(\frac{\pi z_k}{h_k}\right) \right] \\
R_{ij} &= \sum_{k=1}^{NL} c_{ij}^k \left[\frac{\pi}{4h_k} \left[\sinh\left(\frac{2\pi z_{k+1}}{h_k}\right) - \sinh\left(\frac{2\pi z_k}{h_k}\right) \right] \right. \\
&\quad \left. + \frac{1}{2} \left(\frac{\pi}{h_k}\right)^2 (z_{k+1} - z_k) \right]
\end{aligned} \tag{42}
$$

The mass moments of inertia are defined by

$$
\begin{aligned}
I_0 &= \sum_{k=1}^{NL} \rho^k (z_{k+1} - z_k); \quad I_1 = \frac{1}{2} \sum_{k=1}^{NL} \rho^k (z_{k+1}^2 - z_k^2) \\
I_2 &= \frac{1}{3} \sum_{k=1}^{NL} \rho^k (z_{k+1}^3 - z_k^3); \quad I_3 = \frac{1}{4} \sum_{k=1}^{NL} \rho^k (z_{k+1}^4 - z_k^4) \\
I_4 &= \frac{1}{5} \sum_{k=1}^{NL} \rho^k (z_{k+1}^5 - z_k^5); \\
I_5 &= \sum_{k=1}^{NL} \rho^k \frac{h_k}{\pi} \left[\cosh\left(\frac{\pi z_{k+1}}{h_k}\right) - \cosh\left(\frac{\pi z_k}{h_k}\right) \right] \\
I_6 &= \sum_{k=1}^{NL} \rho^k \left[\frac{h_k}{4\pi} \left[\sin\left(\frac{2\pi z_{k+1}}{h_k}\right) - \sin\left(\frac{2\pi z_k}{h_k}\right) \right] - \frac{1}{2}(z_{k+1} - z_k) \right] \\
I_7 &= -\sum_{k=1}^{NL} \rho^k \left[\left(\frac{h_k}{\pi}\right)^2 \left(\sinh\left(\frac{\pi z_{k+1}}{h_k}\right) - \sinh\left(\frac{\pi z_k}{h_k}\right) \right) \right. \\
&\quad \left. - \frac{h_k}{\pi} \left(z_{k+1} \cosh\left(\frac{\pi z_{k+1}}{h_k}\right) - z_k \cosh\left(\frac{\pi z_k}{h_k}\right) \right) \right]
\end{aligned} \tag{43}
$$

where h_k is the thickness of each layer, z_k,z_{k+1} are the bottom and top z coordinate for each layer k, and ρ^k is the material density of the k-th layer.

2.5.1. Boundary conditions in terms of displacements

This meshless method based on collocation with radial basis functions needs the imposition of essential (e.g. $w = 0$) and mechanical (e.g. $M_{xx} = 0$) boundary conditions. Assuming a rectangular plate (for the sake of simplicity), Eq. (32) are expressed as follows: given the number of degrees of freedom, at each boundary point at edges $x = min$ or $x = max$ we impose

$$
\begin{aligned}
M_{xxu0} =& 2B_{13}w_2 + A_{13}w_1 + A_{11}\frac{\partial u_0}{\partial x} + A_{12}\frac{\partial v_0}{\partial y} + B_{11}\frac{\partial u_1}{\partial x} + B_{12}\frac{\partial v_1}{\partial y} \\
&+ G_{11}\frac{\partial u_Z}{\partial x} + G_{12}\frac{\partial v_Z}{\partial y}
\end{aligned} \tag{44}
$$

$$
\begin{aligned}
M_{xxu1} =& -N_{11}\frac{\partial u_Z}{\partial x} + 2D_{13}w_2 + B_{13}w_1 - N_{12}\frac{\partial v_Z}{\partial y} + B_{11}\frac{\partial u_0}{\partial x} \\
&+ D_{11}\frac{\partial u_1}{\partial x} + B_{12}\frac{\partial v_0}{\partial y} + D_{12}\frac{\partial v_1}{\partial y}
\end{aligned} \tag{45}
$$

$$
\begin{aligned}
M_{xxu2} =& -2N_{13}w_2 - N_{11}\frac{\partial u_1}{\partial x} - N_{12}\frac{\partial v_1}{\partial y} + J_{11}\frac{\partial u_Z}{\partial x} + J_{12}\frac{\partial v_Z}{\partial y} \\
&+ G_{13}w_1 + G_{11}\frac{\partial u_0}{\partial x} + G_{12}\frac{\partial v_0}{\partial y}
\end{aligned} \tag{46}
$$

$$
M_{xxv0} = A_{66}\frac{\partial u_0}{\partial y} + A_{66}\frac{\partial v_0}{\partial x} + B_{66}\frac{\partial u_1}{\partial y} + B_{66}\frac{\partial v_1}{\partial x} + G_{66}\frac{\partial u_Z}{\partial y} + G_{66}\frac{\partial v_Z}{\partial x} \tag{47}
$$

$$
M_{xxv1} = -N_{66}\frac{\partial u_Z}{\partial y} - N_{66}\frac{\partial v_Z}{\partial x} + B_{66}\frac{\partial u_0}{\partial y} + D_{66}\frac{\partial u_1}{\partial y} + B_{66}\frac{\partial v_0}{\partial x} + D_{66}\frac{\partial v_1}{\partial x} \tag{48}
$$

$$
M_{xxv2} = -N_{66}\frac{\partial u_1}{\partial y} - N_{66}\frac{\partial v_1}{\partial x} + J_{66}\frac{\partial u_Z}{\partial y} + J_{66}\frac{\partial v_Z}{\partial x} + G_{66}\frac{\partial u_0}{\partial y} + G_{66}\frac{\partial v_0}{\partial x} \tag{49}
$$

$$
M_{xxw0} = H_{55}u_Z + A_{55}u_1 + A_{55}\frac{\partial w_0}{\partial x} + B_{55}\frac{\partial w_1}{\partial x} + D_{55}\frac{\partial w_2}{\partial x} \tag{50}
$$

$$
M_{xxw1} = B_{55}u_1 + (O_{55} - G_{55})u_Z + B_{55}\frac{\partial w_0}{\partial x} + D_{55}\frac{\partial w_1}{\partial x} + E_{55}\frac{\partial w_2}{\partial x} \tag{51}
$$

$$
M_{xxw2} = D_{55}u_1 + (P_{55} + 2N_{55})u_Z + D_{55}\frac{\partial w_0}{\partial x} + E_{55}\frac{\partial w_1}{\partial x} + F_{55}\frac{\partial w_2}{\partial x} \tag{52}
$$

Similarly, given the number of degrees of freedom, at each boundary point at edges $y = min$ or $y = max$ we impose:

$$
M_{yyu0} = A_{66}\frac{\partial u_0}{\partial y} + A_{66}\frac{\partial v_0}{\partial x} + B_{66}\frac{\partial u_1}{\partial y} + B_{66}\frac{\partial v_1}{\partial x} + G_{66}\frac{\partial u_Z}{\partial y} + G_{66}\frac{\partial v_Z}{\partial x} \tag{53}
$$

$$
M_{yyu1} = -N_{66}\frac{\partial u_Z}{\partial y} - N_{66}\frac{\partial v_Z}{\partial x} + B_{66}\frac{\partial u_0}{\partial y} + D_{66}\frac{\partial u_1}{\partial y} + B_{66}\frac{\partial v_0}{\partial x} + D_{66}\frac{\partial v_1}{\partial x} \tag{54}
$$

$$
M_{yyu2} = -N_{66}\frac{\partial u_1}{\partial y} - N_{66}\frac{\partial v_1}{\partial x} + J_{66}\frac{\partial u_Z}{\partial y} + J_{66}\frac{\partial v_Z}{\partial x} + G_{66}\frac{\partial u_0}{\partial y} + G_{66}\frac{\partial v_0}{\partial x} \tag{55}
$$

$$
M_{yyv0} = A_{12}\frac{\partial u_0}{\partial x} + A_{22}\frac{\partial v_0}{\partial y} + B_{12}\frac{\partial u_1}{\partial x} + B_{22}\frac{\partial v_1}{\partial y} + G_{12}\frac{\partial u_Z}{\partial x} + G_{22}\frac{\partial v_Z}{\partial y} \tag{56}
$$

$$
M_{yyv1} = -N_{12}\frac{\partial u_Z}{\partial x} - N_{22}\frac{\partial v_Z}{\partial y} + B_{12}\frac{\partial u_0}{\partial x} + D_{12}\frac{\partial u_1}{\partial x} + B_{22}\frac{\partial v_0}{\partial y} + D_{22}\frac{\partial v_1}{\partial y} \tag{57}
$$

$$
M_{yyv2} = -N_{12}\frac{\partial u_1}{\partial x} - N_{22}\frac{\partial v_1}{\partial y} + J_{12}\frac{\partial u_Z}{\partial x} + J_{22}\frac{\partial v_Z}{\partial y} + G_{12}\frac{\partial u_0}{\partial x} + G_{22}\frac{\partial v_0}{\partial y} \tag{58}
$$

$$M_{yyw0} = H_{44}v_Z + A_{44}v_1 + A_{44}\frac{\partial w_0}{\partial y} + B_{44}\frac{\partial w_1}{\partial y} + D_{44}\frac{\partial w_2}{\partial y} \quad (59)$$

$$M_{yyw1} = B_{44}v_1 + (O_{44} - G_{44})v_Z + B_{44}\frac{\partial w_0}{\partial y} + D_{44}\frac{\partial w_1}{\partial y} + E_{44}\frac{\partial w_2}{\partial y} \quad (60)$$

$$M_{yyw2} = D_{44}v_1 + (P_{44} + 2N_{44})v_Z + D_{44}\frac{\partial w_0}{\partial y} + E_{44}\frac{\partial w_1}{\partial y} + F_{44}\frac{\partial w_2}{\partial y} \quad (61)$$

with A_{ij}, B_{ij}, D_{ij}, E_{ij}, F_{ij}, G_{ij}, H_{ij}, J_{ij}, N_{ij}, O_{ij}, P_{ij}, R_{ij} already described in (42).

3. The radial basis function method

For the sake of completeness we present here the basics of collocation with radial basis functions for static and vibrations problems.

3.1. The static problem

In this section the formulation of a global unsymmetrical collocation RBF-based method to compute elliptic operators is presented. Consider a linear elliptic partial differential operator L and a bounded region Ω in $\mathbb{R}^n$ with boundary $\partial\Omega$. In the static problems we seek the computation of displacements ($\mathbf{u}$) from the global system of equations

$$\mathcal{L}\mathbf{u} = \mathbf{f} \text{ in } \Omega; \quad \mathcal{L}_B\mathbf{u} = \mathbf{g} \text{ on } \partial\Omega \quad (62)$$

where $\mathcal{L}$, $\mathcal{L}_B$ are linear operators in the domain and on the boundary, respectively. The right-hand sides in (62) represent the external forces applied on the plate and the boundary conditions applied along the perimeter of the plate, respectively. The PDE problem defined in (62) will be replaced by a finite problem, defined by an algebraic system of equations, after the radial basis expansions.

3.2. The eigenproblem

The eigenproblem looks for eigenvalues (λ) and eigenvectors ($\mathbf{u}$) that satisfy

$$\mathcal{L}\mathbf{u} + \lambda\mathbf{u} = 0 \text{ in } \Omega; \quad \mathcal{L}_B\mathbf{u} = 0 \text{ on } \partial\Omega \quad (63)$$

As in the static problem, the eigenproblem defined in (63) is replaced by a finite-dimensional eigenvalue problem, based on RBF approximations.

3.3. Radial basis functions approximations

The radial basis function (ϕ) approximation of a function ($\mathbf{u}$) is given by

$$\tilde{\mathbf{u}}(\mathbf{x}) = \sum_{i=1}^{N} \alpha_i \phi(\|x - y_i\|_2), \quad \mathbf{x} \in \mathbb{R}^n \quad (64)$$

where y_i, $i = 1, \ldots, N$ is a finite set of distinct points (centers) in $\mathbb{R}^n$. Although we can use many RBFs, in this paper we restrict to the Wendland function, defined as

$$\phi(r) = (1 - c\,r)_+^8 \left(32(c\,r)^3 + 25(c\,r)^2 + 8c\,r + 1\right) \quad (65)$$

where the Euclidian distance r is real and non-negative and c is a positive shape parameter. The shape parameter (c) was obtained by an optimization procedure, as detailed in Ferreira and Fasshauer [27].

Considering N distinct interpolations, and knowing $u(x_j)$, $j = 1, 2, \ldots, N$, we find α_i by the solution of a $N \times N$ linear system

$$\mathbf{A}\boldsymbol{\alpha} = \mathbf{u} \quad (66)$$

where $\mathbf{A} = [\phi(\|x - y_i\|_2)]_{N\times N}$, $\boldsymbol{\alpha} = [\alpha_1, \alpha_2, \ldots, \alpha_N]^T$ and $\mathbf{u} = [u(x_1), u(x_2), \ldots, u(x_N)]^T$.

3.4. Solution of the static problem

The solution of a static problem by radial basis functions considers N_I nodes in the domain and N_B nodes on the boundary, with a total number of nodes $N = N_I + N_B$. We denote the sampling points by $x_i \in \Omega$, $i = 1, \ldots, N_I$ and $x_i \in \partial\Omega$, $i = N_I + 1, \ldots, N$. At the points in the domain we solve the following system of equations

$$\sum_{i=1}^{N} \alpha_i \mathcal{L}\phi(\|x - y_i\|_2) = \mathbf{f}(x_j), \quad j = 1, 2, \ldots, N_I \quad (67)$$

or

$$\mathcal{L}^I\boldsymbol{\alpha} = \mathbf{F} \quad (68)$$

where

$$\mathcal{L}^I = [\mathcal{L}\phi(\|x - y_i\|_2)]_{N_I\times N} \quad (69)$$

At the points on the boundary, we impose boundary conditions as

$$\sum_{i=1}^{N} \alpha_i \mathcal{L}_B\phi(\|x - y_i\|_2) = \mathbf{g}(x_j), \quad j = N_I + 1, \ldots, N \quad (70)$$

or

$$\mathbf{B}\boldsymbol{\alpha} = \mathbf{G} \quad (71)$$

where

$$\mathbf{B} = \mathcal{L}_B\phi\left[(\|x_{N_I+1} - y_j\|_2)\right]_{N_B\times N}$$

Therefore, we can write a finite-dimensional static problem as

$$\begin{bmatrix} \mathcal{L}^I \\ \mathbf{B} \end{bmatrix} \boldsymbol{\alpha} = \begin{bmatrix} \mathbf{F} \\ \mathbf{G} \end{bmatrix} \quad (72)$$

By inverting the system (72), we obtain the vector $\boldsymbol{\alpha}$. We then obtain the solution $\mathbf{u}$ using the interpolation Eq. (64).

3.5. Solution of the eigenproblem

As in the solution of the static problem, we consider N_I nodes in the interior of the domain and N_B nodes on the boundary. For $x_i \in \Omega$, $i = 1, \ldots, N_I$, we define the eigenproblem as

$$\sum_{i=1}^{N} \alpha_i \mathcal{L}\phi(\|x - y_i\|_2) = \lambda\tilde{\mathbf{u}}(x_j), \quad j = 1, 2, \ldots, N_I \quad (73)$$

or

$$\mathcal{L}^I\boldsymbol{\alpha} = \lambda\tilde{\mathbf{u}}^I \quad (74)$$

where

$$\mathcal{L}^I = [\mathcal{L}\phi(\|x - y_i\|_2)]_{N_I\times N} \quad (75)$$

For $x_i \in \partial\Omega$, $i = N_I + 1, \ldots, N$, we enforce the boundary conditions as

$$\sum_{i=1}^{N} \alpha_i \mathcal{L}_B\phi(\|x - y_i\|_2) = 0, \quad j = N_I + 1, \ldots, N \quad (76)$$

or

$$\mathbf{B}\boldsymbol{\alpha} = 0 \quad (77)$$

Eqs. (74) and (77) can now be solved as a generalized eigenvalue problem

$$\begin{bmatrix} \mathcal{L}^I \\ \mathbf{B} \end{bmatrix} \boldsymbol{\alpha} = \lambda \begin{bmatrix} \mathbf{A}^I \\ \mathbf{0} \end{bmatrix} \boldsymbol{\alpha} \tag{78}$$

where

$$\mathbf{A}^I = \phi\left[\left(\|x_{N_I} - y_j\|_2\right)\right]_{N_I \times N}$$

3.6. Discretization of the equations of motion and boundary conditions

The radial basis collocation method follows a simple implementation procedure. Taking Eq. (72), we compute

$$\boldsymbol{\alpha} = \begin{bmatrix} L^I \\ \mathbf{B} \end{bmatrix}^{-1} \begin{bmatrix} \mathbf{F} \\ \mathbf{G} \end{bmatrix} \tag{79}$$

This $\boldsymbol{\alpha}$ vector is then used to obtain solution $\tilde{\mathbf{u}}$, by using (64). If derivatives of $\tilde{\mathbf{u}}$ are needed, such derivatives are computed as

$$\frac{\partial \tilde{\mathbf{u}}}{\partial x} = \sum_{j=1}^{N} \alpha_j \frac{\partial \phi_j}{\partial x}; \quad \frac{\partial^2 \tilde{\mathbf{u}}}{\partial x^2} = \sum_{j=1}^{N} \alpha_j \frac{\partial^2 \phi_j}{\partial x^2}, \text{ etc.} \tag{80}$$

In the present collocation approach, we need to impose essential and natural boundary conditions. Consider, for example, the condition $w_0 = 0$, on a simply supported or clamped edge. We enforce the conditions by interpolating as

$$w_0 = 0 \rightarrow \sum_{j=1}^{N} \alpha_j^{W_0} \phi_j = 0 \tag{81}$$

Other boundary conditions are interpolated in a similar way.

3.7. Free vibrations problems

For free vibration problems we set the external force to zero, and assume harmonic solution in terms of displacements u_0, u_1, u_Z, v_0, v_1, v_Z, w_0, w_1, w_2 as

$$\begin{aligned} u_0 &= U_0(w,y)e^{i\omega t}; \quad u_1 = U_1(w,y)e^{i\omega t}; \quad u_Z = U_Z(w,y)e^{i\omega t}; \\ v_0 &= V_0(w,y)e^{i\omega t}; \quad v_1 = V_1(w,y)e^{i\omega t}; \quad v_Z = V_Z(w,y)e^{i\omega t}; \\ w_0 &= W_0(w,y)e^{i\omega t}; \quad w_1 = W_1(w,y)e^{i\omega t}; \quad w_2 = W_2(w,y)e^{i\omega t} \end{aligned} \tag{82}$$

where ω is the frequency of natural vibration. Substituting the harmonic expansion into Eq. (78) in terms of the amplitudes U_0, U_1, U_Z, V_0, V_1, V_Z, W_0, W_1, W_2, we may obtain the natural frequencies and vibration modes for the plate problem, by solving the eigenproblem

$$\left[\mathcal{L} - \omega^2 \mathcal{G}\right]\mathbf{X} = \mathbf{0} \tag{83}$$

where $\mathcal{L}$ collects all stiffness terms and $\mathcal{G}$ collects all terms related to the inertial terms. In (83) $\mathbf{X}$ are the modes of vibration associated with the natural frequencies defined as ω.

4. Numerical examples

4.1. Bending problems

In the next examples we use the hyperbolic sine plate theory to analyse simply supported (SSSS) square (side lengths $a = b$) plates subjected to a bi-sinusoidal transverse mechanical load, of bi-sinusoidal load $p_z = \bar{p}_z sin(\frac{\pi x}{a}) sin(\frac{\pi y}{b})$ applied at the top plate surface, $z = h/2$, $\bar{p}_z = 1$. Three side-to-thickness ratios (a/h) are considered 4, 10 and 100.

We consider 91 mathematical layers, in order to model the continuous variation of properties across the thickness direction.[1] We consider a Wendland C6 radial function as in (65), and a Chebyshev grid (see [27] for details).

4.1.1. Isotropic functionally graded plate

In this example, an isotropic FGM square plate with a polynomial material law, as given by Zenkour [2] is considered. The plate is graded from aluminum (bottom surface) to alumina (top surface) materials. The following functional relationship is considered for modulus of elasticity $E(z)$ in the thickness direction (z) [2]:

$$E(z) = E_m + (E_c - E_m)\left(\frac{2z + h}{2h}\right)^p \tag{84}$$

where $E_m = 70$ GPa and $E_c = 380$ GPa are the corresponding modulus of elasticity of the metal and ceramic phases, respectively; p is the (positive number) volume fraction exponent. The Poisson's ratio is considered constant ($\nu = 0.3$).

The transverse displacement and the normal stresses are computed in normalized form as

$$\begin{aligned} \bar{u}_z &= \frac{10h^3 E_c}{a^4 \bar{p}_z} u_z\left(\frac{a}{2}, \frac{b}{2}\right) \qquad \bar{\sigma}_{xx} = \frac{h}{a\bar{p}_z} \sigma_{xx}\left(\frac{a}{2}, \frac{b}{2}\right) \\ \bar{\sigma}_{yy} &= \frac{h}{a\bar{p}_z} \sigma_{yy}\left(\frac{a}{2}, \frac{b}{2}\right) \qquad \bar{\sigma}_{zz} = \sigma_{zz}\left(\frac{a}{2}, \frac{b}{2}\right) \end{aligned} \tag{85}$$

The shear stresses are normalized according to

$$\bar{\sigma}_{xy} = \frac{h}{a\bar{p}_z} \sigma_{xy}(0,0); \quad \bar{\sigma}_{xz} = \frac{h}{a\bar{p}_z} \sigma_{xz}\left(0, \frac{b}{2}\right); \quad \bar{\sigma}_{yz} = \frac{h}{a\bar{p}_z} \sigma_{yz}\left(\frac{a}{2}, 0\right) \tag{86}$$

$(\frac{a}{2}, \frac{b}{2})$ is the center of the plate, $(0, \frac{b}{2})$ and $(\frac{a}{2}, 0)$ are the midpoints of the sides, and $(0,0)$ is the corner of the plate.

The present approach with $\epsilon_{zz} \neq 0$ is compared with analytical solutions by Carrera et al. [28], the classical plate theory (CLT), the first-order shear deformation theory (FSDT), a generalized shear deformation theory by Zenkour [2] (who considered $\epsilon_{zz} = 0$), and finite element solutions by Carrera et al. [9]. We consider Chebyschev grids with 13^2, 17^2 and 21^2 points. Three FGM configurations are considered by using different p exponents ($p = 1,4,10$). Thick ($a/h = 4$) down to thin ($a/h = 100$) plates are analysed. Normalized transverse displacements ($\bar{u}_z$) and normal stresses ($\bar{\sigma}_{xx}$) at the central point of the plate and selected thickness coordinate are shown in Table 1. Our approach presents very close results to those theories that consider thickness stretching, and clearly deviates from those theories that neglect ϵ_{zz}, in particular for thicker plates. The present approach presents very close results to Carrera's analytical solution [28].

In Figs. 1–6 we present the evolution of the displacement and stresses across the thickness direction for various values of the exponent p, using a 21^2 grid. As can be seen in Fig. 6, the transverse normal component σ_{zz} cannot be neglected for the present problem.

4.1.2. Sandwich square plate with FGM core

In this example we consider a sandwich plate with total thickness h, by using a polynomial material law for the core, as described in Zenkour [2]. The bottom skin is aluminium ($E_m = 70$ GPa) with thickness $h_b = 0.1h$ and the top skin is alumina ($E_c = 380$ GPa) with thickness $h_t = 0.1h$. The core is a FGM layer with the following functional relationship for modulus of elasticity $E(z)$ in the thickness direction z as in (84). The Poisson's ratio is considered constant $\nu = 0.3$.

[1] A significant number of mathematical layers is needed to ensure correct computation of material properties at each thickness position.

Table 1
FGM isotropic plate with polynomial material law [2]. Effect of transverse normal strain ϵ_{zz} for a bending problem.

	a/h		$\bar{\sigma}_{xx}(h/3)$			$\bar{u}_z(0)$		
p		ϵ_{zz}	4	10	100	4	10	100
1	Ref. [28]	≠0	0.6221	1.5064	14.969	0.7171	0.5875	0.5625
	CLT	0	0.8060	2.0150	20.150	0.5623	0.5623	0.5623
	FSDT (k = 5/6)	0	0.8060	2.0150	20.150	0.7291	0.5889	0.5625
	GSDT [2]	0		1.4894			0.5889	
	Ref. [9] N = 4	0	0.7856	2.0068	20.149	0.7289	0.5890	0.5625
	Ref. [9] N = 4	≠0	0.6221	1.5064	14.969	0.7171	0.5875	0.5625
	Ref. [29]	≠0	0.5925	1.4945	14.969	0.6997	0.5845	0.5624
	Present 13^2 grid	≠0	0.5910	1.4911	14.873	0.7020	0.5868	0.5620
	Present 17^2 grid	≠0	0.5910	1.4916	14.930	0.7020	0.5868	0.5646
	Present 21^2 grid	≠0	0.5910	1.4917	14.944	0.7020	0.5868	0.5648
4	Ref. [28]	≠0	0.4877	1.1971	11.923	1.1585	0.8821	0.8286
	CLT	0	0.6420	1.6049	16.049	0.8281	0.8281	0.8281
	FSDT (k = 5/6)	0	0.6420	1.6049	16.049	1.1125	0.8736	0.828
	GSDT [2]	0		1.1783			0.8651	
	Ref. [9] N = 4	0	0.5986	1.5874	16.047	1.1673	0.8828	0.8286
	Ref. [9] N = 4	≠0	0.4877	1.1971	11.923	1.1585	0.8821	0.8286
	Ref. [29]	≠0	0.4404	1.1783	11.932	1.1178	0.8750	0.8286
	Present 13^2 grid	≠0	0.4341	1.1590	11.698	1.1094	0.8697	0.8205
	Present 17^2 grid	≠0	0.4340	1.1593	11.727	1.1095	0.8698	0.8238
	Present 21^2 grid	≠0	0.4340	1.1593	11.738	1.1095	0.8698	0.8241
10	Ref. [28]	≠0	0.3695	0.8965	8.9077	1.3745	1.0072	0.9361
	CLT	0	0.4796	1.1990	11.990	0.9354	0.9354	0.9354
	FSDT (k = 5/6)	0	0.4796	1.1990	11.990	1.3178	0.9966	0.9360
	GSDT [2]	0		0.8775			1.0089	
	Ref. [9] N = 4	0	0.4345	1.1807	11.989	1.3925	1.0090	0.9361
	Ref. [9] N = 4	≠0	0.1478	0.8965	8.9077	1.3745	1.0072	0.9361
	Ref. [29]	≠0	0.3227	1.1783	11.932	1.3490	0.8750	0.8286
	Present 13^2 grid	≠0	0.3108	0.8465	8.5844	1.3327	0.9886	0.9194
	Present 17^2 grid	≠0	0.3108	0.8467	8.5948	1.3327	0.9886	0.9225
	Present 21^2 grid	≠0	0.3108	0.8467	8.6013	1.3327	0.9886	0.9228

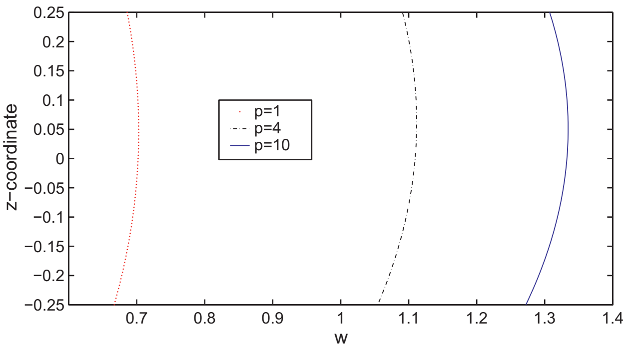

Fig. 1. FGM square plate subjected to sinusoidal load at the top, with $a/h = 4$. Displacement through the thickness direction for different values of p at the center of the plate $(\frac{a}{2},\frac{b}{2})$ according to the hyperbolic sine theory.

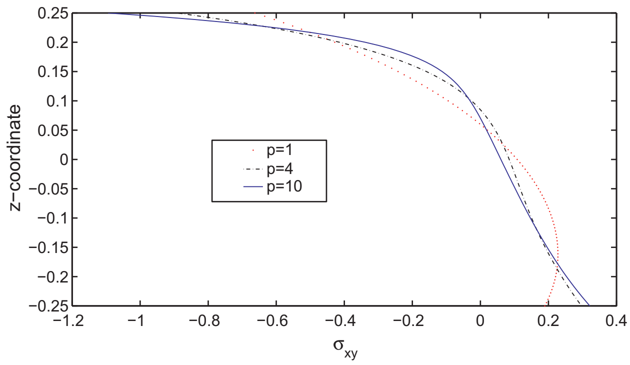

Fig. 3. FGM square plate subjected to sinusoidal load at the top, with $a/h = 4$. $\bar{\sigma}_{xy}$ through the thickness direction at the corner of the plate $(0,0)$ for different values of p according to the hyperbolic sine theory.

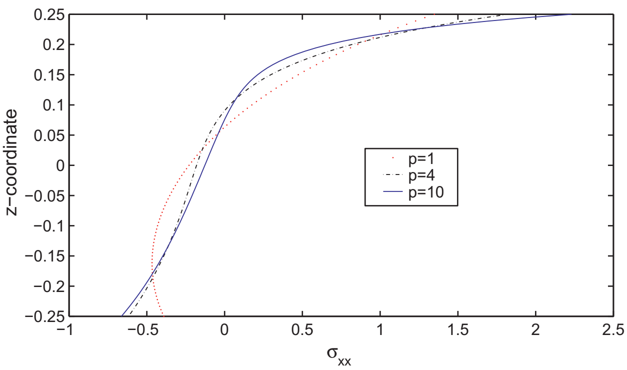

Fig. 2. FGM square plate subjected to sinusoidal load at the top, with $a/h = 4$. $\bar{\sigma}_{xx}$ through the thickness direction for different values of p at the center of the plate $(\frac{a}{2},\frac{b}{2})$ according to the hyperbolic sine theory.

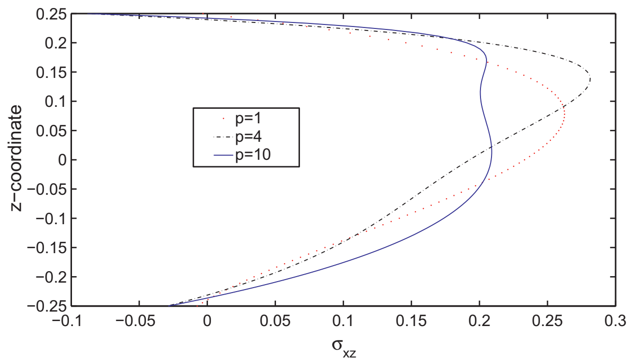

Fig. 4. FGM square plate subjected to sinusoidal load at the top, with $a/h = 4$. $\bar{\sigma}_{xz}$ through the thickness direction at the center of the plate $(0,\frac{b}{2})$ for different values of p according to the hyperbolic sine theory.

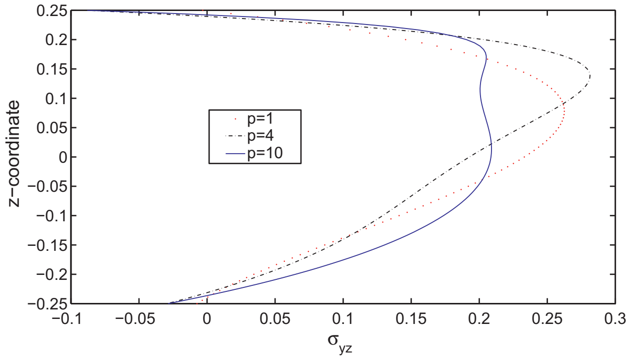

Fig. 5. FGM square plate subjected to sinusoidal load at the top, with $a/h = 4$. $\bar{\sigma}_{yz}$ through the thickness direction at the point $(\frac{a}{2}, 0)$ for different values of p according to the hyperbolic sine theory.

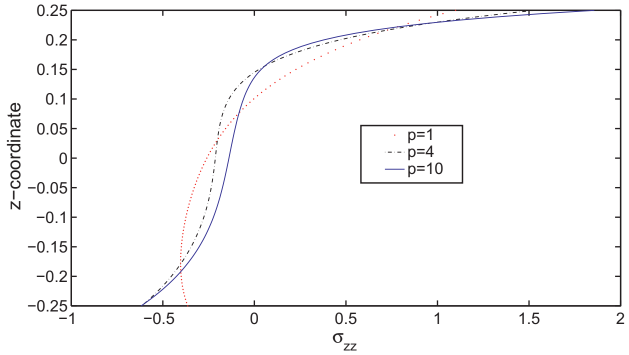

Fig. 6. FGM square plate subjected to sinusoidal load at the top, with $a/h = 4$. σ_{zz} through the thickness direction for different values of p at the center of the plate $(\frac{a}{2}, \frac{b}{2})$ according to the hyperbolic sine theory.

The same dimensionless forms as in (85) and (86) are used.

In Table 2 we present the normalized transverse displacement ($\bar{w}$) and the normalized transverse shear stress ($\bar{\sigma}_{xz}$) at selected locations. In Table 3 we present the normalized in-plane shear stress ($\bar{\sigma}_{xy}$) and the normalized transverse normal stress ($\bar{\sigma}_{zz}$) at selected locations. In both tables we consider three a/h ratios (4, 10 and 100), and three power-law exponents ($p = 1$, 4 and 10). We use a 21^2 Chebyshev grid and consider both $\epsilon_{zz} = 0$ and $\epsilon_{zz} \neq 0$ approaches. Our meshless results are compared in Table 2 with finite element results by Carrera et al. [9], and compare quite well for all cases. In Table 3 we compare the present approach with FEM results by Brischetto [30] and again the comparison is quite good.

In Figs. 7–13 we present the evolution of the displacement and stresses across the thickness direction for various values of the exponent p of a plate with side to thickness ratio $a/h = 10$, using a 21^2 grid.

The present numerical method presents very close results to those of Carrera et al. [9] for a $N = 4$ expansion.

The consideration of a non-zero ϵ_{zz} strain produces a significant change in the transverse displacement as well as in the normal stress. This becomes evident when we compare the present approch with that of Zenkour [2] who neglected the ϵ_{zz} strain in the formulation.

4.2. Free vibration problems

In this example, we study the free vibration behavior of simply-supported (SSSS) isotropic FGM Al/ZrO_2 plates. The modulus of elasticity are $E_m = 70$ GPa and $E_c = 380$ GPa, the mass densities are $\rho_m = 2702$ kg/m^3 and $\rho_c = 5700$ kg/m^3, and the Poisson's ratio is $\nu = 0.3$. We consider both the $\epsilon_{zz} = 0$ and the $\epsilon_{zz} \neq 0$ cases. We compare results with an exact (analytical) solution by Vel and Batra [31], and another meshless technique by Qian et al. [8]. In order to compare results, we use the Mori–Tanaka scheme for obtaining equivalent material properties.

In Table 4 we consider thin and thick plates, with $p = 1$, and using 21^2 Chebishev points. The ϵ_{zz} effect is significant. In fact, the exact solution by Vel and Batra [31] is achieved for all cases, by allowing $\epsilon_{zz} \neq 0$. In Table 5 we compare with the same sources, varying the p exponent, for $a/h = 5$ and using 21^2 points. Our present formulation with $\epsilon_{zz} \neq 0$ matches the exact solution.

In Fig. 14 the first four frequencies are presented for $p = 1$ and using 21^2 points. In Tables 6 and 7 we present the first ten frequencies for the same exponent p and compare results with those from Qian et al. [8] for different side-to-thickness ratios and different number of Chebishev points.

Table 2
Sandwich simply supported square plate with FGM core with polynomial material law [2] using a 21^2 grid. Effect of transverse normal strain ϵ_{zz} on σ_{xz} and transverse displacement for a bending problem using the hyperbolic sine theory.

	a/h		$\bar{\sigma}_{xz}(0, \frac{b}{2}, \frac{h}{3})$			$\bar{w}(0,0,0)$		
p		ϵ_{zz}	4	10	100	4	10	100
1	Ref. [9] $N = 4$	0	0.2604	0.2594	0.2593	0.7628	0.6324	0.6072
	Ref. [9] $N = 4$	≠0	0.2596	0.2593	0.2593	0.7735	0.6337	0.6072
	Ref. [29]	0	0.2703	0.2718	0.2720	0.7744	0.6356	0.6092
	Ref. [29]	≠0	0.2742	0.2788	0.2793	0.7416	0.6305	0.6092
	Present	0	0.2028	0.2017	0.2015	0.7744	0.6356	0.6093
	Present	≠0	0.2233	0.2271	0.2274	0.7417	0.6305	0.6093
4	Ref. [9] $N = 4$	0	0.2400	0.2398	0.2398	1.0930	0.8307	0.7797
	Ref. [9] $N = 4$	≠0	0.2400	0.2398	0.2398	1.0977	0.8308	0.7797
	Ref. [29]	0	0.2699	0.2726	0.2728	1.0847	0.8276	0.7785
	Ref. [29]	≠0	0.2723	0.2778	0.2785	1.0391	0.8202	0.7784
	Present	0	0.2813	0.2808	0.2806	1.0847	0.8276	0.7786
	Present	≠0	0.3154	0.3219	0.3230	1.0349	0.8195	0.7785
10	Ref. [9] $N = 4$	0	0.1932	0.1944	0.1946	1.2172	0.8740	0.8077
	Ref. [9] $N = 4$	≠0	0.1935	0.1944	0.1946	1.2240	0.8743	0.8077
	Ref. [29]	0	0.1998	0.2021	0.2022	1.2212	0.8718	0.8050
	Ref. [29]	≠0	0.2016	0.2059	0.2064	1.1780	0.8650	0.8050
	Present	0	0.2623	0.2624	0.2623	1.2212	0.8718	0.8051
	Present	≠0	0.2945	0.3000	0.3004	1.1720	0.8639	0.8050

Table 3
Sandwich simply supported square plate with FGM core with polynomial material law [2] using a 19^2 grid. Effect of transverse normal strain ϵ_{zz} on $\bar{\sigma}_{xy}$ and $\bar{\sigma}_{zz}$ for a bending problem $\bar{\sigma}_{zz} = \sigma_{zz}\frac{h}{ap_z}$.

	a/h		$\bar{\sigma}_{xy}(0,0,\frac{h}{3})$		$\bar{\sigma}_{zz}(\frac{a}{2},\frac{b}{2},0)$	
p		ϵ_{zz}	4	100	4	100
1	Ref. LD4 [30]	0	0.3007	8.4968	0.0922	0.0038
	Ref. LM4 [30]	≠0	0.3007	8.4968	0.0922	0.0038
	Ref. [29]	0	0.3303	8.4882	0.1276	3.1987
	Ref. [29]	≠0	0.3167	8.4911	0.0827	0.0034
	Present	0	0.3303	8.4903	0.1276	3.1983
	Present	≠0	0.3165	8.5056	0.0828	0.0034
5	Ref. LD4 [30]	0	0.1999	6.4942	0.0911	0.0037
	Ref. LM4 [30]	≠0	0.1996	6.4942	0.0924	0.0037
	Ref. [29]	0	0.2317	6.4454	0.0777	1.9535
	Ref. [29]	≠0	0.2248	6.4441	0.0522	0.0022
	Present	0	0.2317	6.4463	0.0777	1.9532
	Present	≠0	0.2247	6.4458	0.0522	0.0022
10	Ref. LD4 [30]	0	0.1412	5.1402	0.1064	0.0043
	Ref. LM4 [30]	≠0	0.1403	5.1401	0.1067	0.0042
	Ref. [29]	0	0.1745	5.0745	0.0685	1.6978
	Ref. [29]	≠0	0.1687	5.0754	0.0443	0.0018
	Present	0	0.1745	5.0752	0.0685	1.6975
	Present	≠0	0.1708	5.0784	0.0444	0.0018

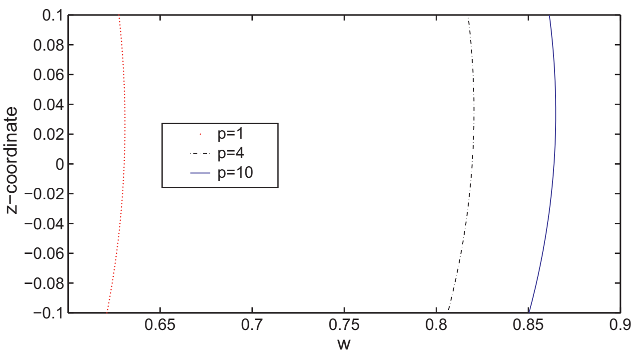

Fig. 7. Sandwich square plate with FGM core subjected to sinusoidal load at the top, with $a/h = 10$. Displacement through the thickness direction at the center of the plate $(\frac{a}{2},\frac{b}{2})$ for different values of p according to the hyperbolic sine theory.

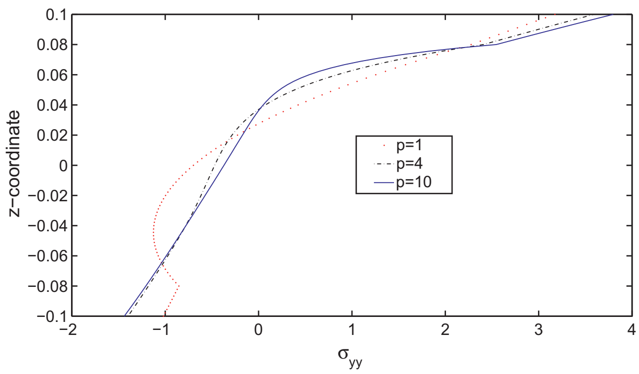

Fig. 9. Sandwich square plate with FGM core subjected to sinusoidal load at the top, with $a/h = 10$. $\bar{\sigma}_{yy}$ through the thickness direction at the center of the plate $(\frac{a}{2},\frac{b}{2})$ for different values of p according to the hyperbolic sine theory.

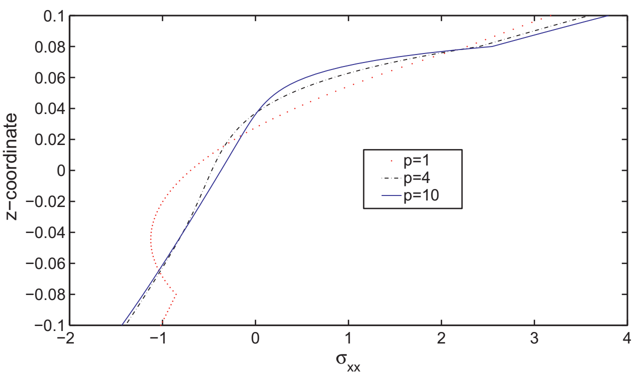

Fig. 8. Sandwich square plate with FGM core subjected to sinusoidal load at the top, with $a/h = 10$. $\bar{\sigma}_{xx}$ through the thickness direction at the center of the plate $(\frac{a}{2},\frac{b}{2})$ for different values of p according to the hyperbolic sine theory.

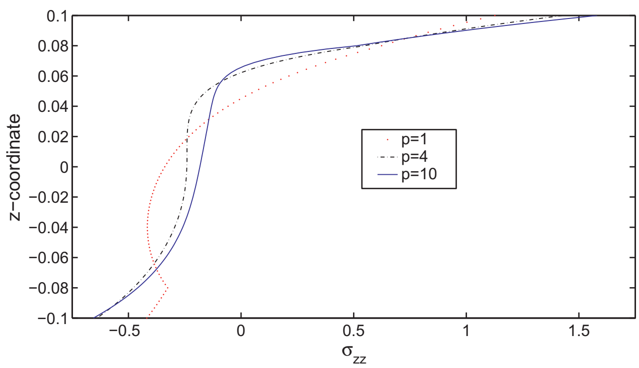

Fig. 10. Sandwich square plate with FGM core subjected to sinusoidal load at the top, with $a/h = 10$. σ_{zz} through the thickness direction at the center of the plate $(\frac{a}{2},\frac{b}{2})$ for different values of p according to the hyperbolic sine theory.

5. Conclusions

In this paper a new hyperbolic sine shear deformation theory accounting for through-the-thickness deformations was presented. Bending deformations and free vibrations of functionally graded plates were analysed. The equations of motion in terms of resultants and generalized displacements are obtained by the Carrera's Unified Formulation (CUF).

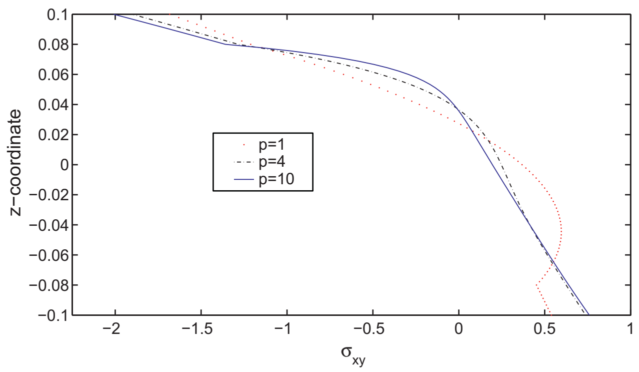

Fig. 11. Sandwich square plate with FGM core subjected to sinusoidal load at the top, with $a/h = 10$. $\bar{\sigma}_{xy}$ through the thickness direction at the point $(0, 0)$ for different values of p according to the hyperbolic sine theory.

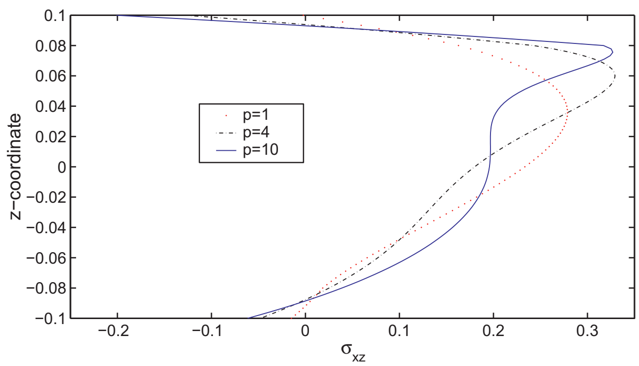

Fig. 12. Sandwich square plate with FGM core subjected to sinusoidal load at the top, with $a/h = 10$. $\bar{\sigma}_{xz}$ through the thickness direction at the point $(0, \frac{b}{2})$ for different values of p according to the hyperbolic sine theory.

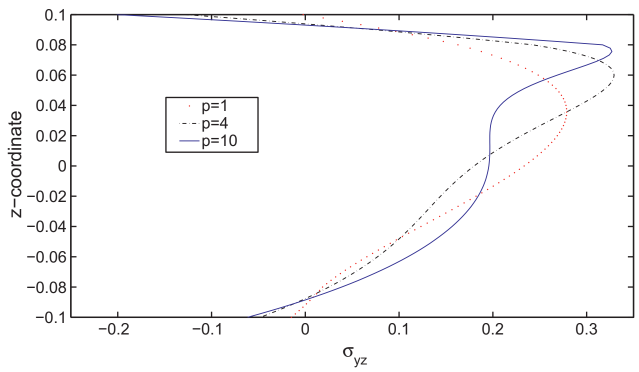

Fig. 13. Sandwich square plate with FGM core subjected to sinusoidal load at the top, with $a/h = 10$. $\bar{\sigma}_{yz}$ through the thickness direction at the point $(\frac{a}{2}, 0)$ for different values of p according to the hyperbolic sine theory.

Table 4
Fundamental frequency $\bar{\omega} = \omega h\sqrt{\rho_m/E_m}$ of a SSSS isotropic functionally graded plate (Al/ZrO_2), $p = 1$, using 21^2 points.

Source	a/h		
	20	10	5
Ref. [8]	0.0149	0.0584	0.2152
Exact [31]	0.0153	0.0596	0.2192
Ref. [29] ($\epsilon_{zz} = 0$)	0.0153	0.0595	0.2184
Ref. [29] ($\epsilon_{zz} \neq 0$)	0.0153	0.0596	0.2193
Present ($\epsilon_{zz} = 0$)	0.0153	0.0595	0.2184
Present ($\epsilon_{zz} \neq 0$)	0.0153	0.0596	0.2193

Table 5
Fundamental frequency $\bar{\omega} = \omega h\sqrt{\rho_m/E_m}$ of a SSSS isotropic functionally graded plate (Al/ZrO_2), $a/h = 5$, using 21^2 points and the hyperbolic sine theory.

Source	$p = 2$	$p = 3$	$p = 5$
Ref. [8]	0.2153	0.2172	0.2194
Exact [31]	0.2197	0.2211	0.2225
Ref. [29] ($\epsilon_{zz} = 0$)	0.2189	0.2202	0.2215
Ref. [29] ($\epsilon_{zz} \neq 0$)	0.2198	0.2212	0.2225
Present ($\epsilon_{zz} = 0$)	0.2191	0.2205	0.2220
Present ($\epsilon_{zz} \neq 0$)	0.2201	0.2216	0.2230

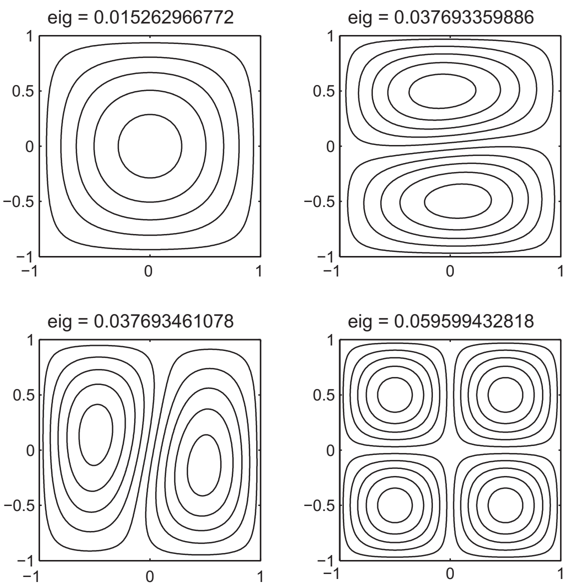

Fig. 14. First 4 frequencies $\bar{\omega} = \omega h\sqrt{\rho_m/E_m}$ of a SSSS isotropic functionally graded plate (Al/ZrO_2), with $a/h = 20$, $p = 1$, using 21^2 points and the hyperbolic sine theory.

Table 6
First 10 frequencies $\bar{\omega} = \omega h\sqrt{\rho_m/E_m}$ of a SSSS isotropic functionally graded plate (Al/ZrO_2), $p = 1$, $a/h = 20$, with the hyperbolic sine theory.

Present 13^2	17^2	21^2	Ref. [8]	Ref. [29]
0.0153	0.0153	0.0153	0.0149	0.0153
0.0377	0.0377	0.0377	0.0377	0.0377
0.0377	0.0377	0.0377	0.0377	0.0377
0.0596	0.0596	0.0596	0.0593	0.0596
0.0741	0.0739	0.0739	0.0747	0.0739
0.0741	0.0739	0.0739	0.0747	0.0739
0.0953	0.0950	0.0950	0.0769	0.0950
0.0953	0.0950	0.0950	0.0912	0.0950
0.1030	0.1030	0.1030	0.0913	0.1029
0.1030	0.1030	0.1030	0.1029	0.1029

Table 7
First 10 frequencies $\bar{\omega} = \omega h\sqrt{\rho_m/E_m}$ of a SSSS isotropic functionally graded plate (Al/ZrO_2), $p = 1$, $a/h = 10$, with the hyperbolic sine theory.

Present 13^2	17^2	21^2	Ref. [8]	Ref. [29]
0.0596	0.0596	0.0596	0.0584	0.0596
0.1426	0.1426	0.1426	0.1410	0.1426
0.1426	0.1426	0.1426	0.1410	0.1426
0.2059	0.2059	0.2059	0.2058	0.2058
0.2059	0.2059	0.2059	0.2058	0.2058
0.2194	0.2193	0.2193	0.2164	0.2193
0.2678	0.2676	0.2676	0.2646	0.2676
0.2678	0.2676	0.2676	0.2677	0.2676
0.2912	0.2912	0.2912	0.2913	0.2910
0.3367	0.3364	0.3364	0.3264	0.3363

Examples include an isotropic functionally graded plate and a sandwich plate with functionally graded core. Equations were interpolated by collocation with radial basis functions.

The present formulation produces highly accurate solutions for both bending deformations and free vibrations. The use of this hyperbolic sine theory and its meshless implementation are novel and serves to fill the gap of knowledge in this area.

Acknowledgment

The first author acknowledges support from FCT Grant SFRH/BD/45554/2008.

References

[1] Miyamoto Y, Kaysser WA, Rabin BH, Kawasaki A, Ford RG. Functionally graded materials: design, processing and applications. Kluwer Academic Publishers.; 1999.
[2] Zenkour AM. Generalized shear deformation theory for bending analysis of functionally graded plates. Appl Math Modell 2006;30.
[3] Cheng ZQ, Batra RC. Deflection relationships between the homogeneous kirchhoff plate theory and different functionally graded plate theories. Arch Mech 2000;52:143–58.
[4] Batra RC, Jin J. Natural frequencies of a functionally graded anisotropic rectangular plate. J Sound Vib 2005;282(1–2):509–16.
[5] Ferreira AJM, Batra RC, Roque CMC, Qian LF, Jorge RMN. Natural frequencies of functionally graded plates by a meshless method. Compos Struct 2006;75(1–4): 593–600.
[6] Reddy JN. Analysis of functionally graded plates. Int J Numer Methods Eng 2000;47:663–84.
[7] Ferreira AJM, Batra RC, Roque CMC, Qian LF, Martins PALS. Static analysis of functionally graded plates using third-order shear deformation theory and a meshless method. Compos Struct 2005;69(4):449–57.
[8] Qian LF, Batra RC, Chen LM. Static and dynamic deformations of thick functionally graded elastic plate by using higher-order shear and normal deformable plate theory and meshless local Petrov–Galerkin method. Composites: Part B 2004;35:685–97.
[9] Carrera E, Brischetto S, Cinefra M, Soave M. Effects of thickness stretching in functionally graded plates and shells. Compos Part B: Eng 2011;42:123–33.
[10] Kansa EJ. Multiquadrics – a scattered data approximation scheme with applications to computational fluid dynamics. Part i: surface approximations and partial derivative estimates. Comput Math Appl 1990;19(8/9):127–45.
[11] Ferreira AJM. A formulation of the multiquadric radial basis function method for the analysis of laminated composite plates. Compos Struct 2003;59: 385–92.
[12] Ferreira AJM. Thick composite beam analysis using a global meshless approximation based on radial basis functions. Mech Adv Mater Struct 2003; 10:271–84.
[13] Ferreira AJM, Roque CMC, Martins PALS. Analysis of composite plates using higher-order shear deformation theory and a finite point formulation based on the multiquadric radial basis function method. Composites: Part B 2003;34:627–36.
[14] Ferreira AJM, Roque CMC, Jorge RMN, Kansa EJ. Static deformations and vibration analysis of composite and sandwich plates using a layerwise theory and multiquadrics discretizations. Eng Anal Bound Elem 2005;29(12): 1104–14.
[15] Ferreira AJM, Roque CMC, Jorge RMN. Analysis of composite plates by trigonometric shear deformation theory and multiquadrics. Comput Struct 2005;83(27):2225–37.
[16] Ferreira AJM, Batra RC, Roque CMC, Qian LF, Jorge RMN. Natural frequencies of functionally graded plates by a meshless method. Compos Struct 2006; 75(1–4):593–600.
[17] Ferreira AJM, Roque CMC, Jorge RMN. Free vibration analysis of symmetric laminated composite plates by fsdt and radial basis functions. Comput Methods Appl Mech Eng 2005;194(39–41):4265–78.
[18] Ferreira AJM, Roque CMC, Martins PALS. Radial basis functions and higher-order shear deformation theories in the analysis of laminated composite beams and plates. Compos Struct 2004;66(1–4):287–93.
[19] Carrera E. C^0 Reissner–Mindlin multilayered plate elements including zig–zag and interlaminar stress continuity. Int J Numer Methods Eng 1996;39: 1797–820.
[20] Carrera E. Developments, ideas, and evaluations based upon Reissner's mixed variational theorem in the modelling of multilayered plates and shells. Appl Mech Rev 2001;54:301–29.
[21] Soldatos K. A transverse shear deformation theory for homogeneous monoclinic plates. Acta Mech 1992;94:195–220. doi:10.1007/BF01176650.
[22] Akavci S. Two new hyperbolic shear displacement models for orthotropic laminated composite plates. Mech Compos Mater 2010;46:215–26. doi:10.1007/s11029-010-9140-3.
[23] Akavci S, Tanrikulu A. Buckling and free vibration analyses of laminated composite plates by using two new hyperbolic shear-deformation theories. Mech Compos Mater 2008;44:145–54. doi:10.1007/s11029-008-9004-2.
[24] Meiche Noureddine El, Tounsi Abdelouahed, Ziane Noureddine, Mechab Ismail, Bedia El Abbes Adda. A new hyperbolic shear deformation theory for buckling and vibration of functionally graded sandwich plate. Int J Mech Sci 2011;53(4):237–47.
[25] Mori T, Tanaka K. Average stress in matrix and average elastic energy of materials with misfitting inclusions. Acta Metall 1973;21(5):571–4.
[26] Benveniste Y. A new approach to the application of Mori–Tanaka's theory in composite materials. Mech Mater 1987;6(2):147–57.
[27] Ferreira AJM, Fasshauer GE. Computation of natural frequencies of shear deformable beams and plates by a rbf-pseudospectral method. Comput Methods Appl Mech Eng 2006;196:134–46.
[28] Carrera E, Brischetto S, Robaldo A. Variable kinematic model for the analysis of functionally graded material plates. AIAA J 2008;46:194–203.
[29] Neves AMA, Ferreira AJM, Carrera E, Roque CMC, Cinefra M, Jorge RMN, Soares CMM. A quasi-3d sinusoidal shear deformation theory for the static and free vibration analysis of functionally graded plates. Composites Part B, in press.
[30] Brischetto S. Classical and mixed advanced models for sandwich plates embedding functionally graded cores. J Mech Mater Struct 2009;4: 13–33.
[31] Vel SS, Batra RC. Three-dimensional exact solution for the vibration of functionally graded rectangular plates. J Sound Vib 2004;272:703–30.

2.4 Static, free vibration and buckling analysis of functionally graded plates using a quasi-3D higher-order shear deformation theory and a meshless technique

A. M. A. Neves, A. J. M. Ferreira, E. Carrera, M. Cinefra, C. M. C. Roque, R. M. N. Jorge, C. M. M. Soares, Static, free vibration and buckling analysis of functionally graded plates using a quasi-3D higher-order shear deformation theory and a meshless technique, Composites Part B: Engineering, 2012, in press.

ARTICLE IN PRESS

Composites: Part B xxx (2012) xxx–xxx

Contents lists available at SciVerse ScienceDirect

Composites: Part B

journal homepage: www.elsevier.com/locate/compositesb

Static, free vibration and buckling analysis of isotropic and sandwich functionally graded plates using a quasi-3D higher-order shear deformation theory and a meshless technique

A.M.A. Neves [a], A.J.M. Ferreira [a,*], E. Carrera [b], M. Cinefra [b], C.M.C. Roque [c], R.M.N. Jorge [a], C.M.M. Soares [d]

[a] Departamento de Engenharia Mecânica, Faculdade de Engenharia, Universidade do Porto, Rua Dr. Roberto Frias, 4200-465 Porto, Portugal
[b] Departamento of Aeronautics and Aerospace Engineering, Politecnico di Torino, Corso Duca degli Abruzzi, 24, 10129 Torino, Italy
[c] INEGI, Faculdade de Engenharia, Universidade do Porto, Rua Dr. Roberto Frias, 4200-465 Porto, Portugal
[d] Instituto Superior Técnico, Av. Rovisco Pais, Lisboa, Portugal

ARTICLE INFO

Article history:
Received 5 November 2011
Received in revised form 30 January 2012
Accepted 31 January 2012
Available online xxxx

Keywords:
A. Plates
B. Buckling
B. Vibration
C. Computational modeling
Functionally graded materials

ABSTRACT

In this paper the authors derive a higher-order shear deformation theory for modeling functionally graded plates accounting for extensibility in the thickness direction.

The explicit governing equations and boundary conditions are obtained using the principle of virtual displacements under Carrera's Unified Formulation. The static and eigenproblems are solved by collocation with radial basis functions.

The efficiency of the present approach is assessed with numerical results including deflection, stresses, free vibration, and buckling of functionally graded isotropic plates and functionally graded sandwich plates.

1. Introduction

Functionally graded materials (FGM) are a class of composite materials that were first proposed by Bever and Duwez [1] in 1972. In a typical FGM plate the material properties continuously vary over the thickness direction by mixing two different materials [2]. The computational modeling of FGM is an important tool to the understanding of the structures behavior, and has been the target of intense research [2–8].

When compared to isotropic and laminated plates, the literature on FGM plates is relatively scarce. Because of FGM applications in high temperature environments most of the studies on the behavior of FGM plates focus on the thermo-mechanical response of FGM plates: Reddy and Chin [9], Reddy [10], Vel and Batra [11,12], Cheng and Batra [13], and Javaheri and Eslami [14]. Studies on the mechanical behavior of FGM plates include the static analysis of FGM plates performed by Kashtalyan [15], Kashtalyan and Menshykova [16], Qian et al. [17], Zenkour [18,19], Ramirez et al. [20], Ferreira et al. [21,22], Chi and Chung [23,24], and Cheng and Batra [25]. Vibrations problems of FGM plates can be found in Batra and Jin [26], Ferreira et al. [27], Vel and Batra [28], Zenkour [29], Roque et al. [30], and Cheng and Batra [31]. Mechanical buckling of FGM plates can be found in Najafizadeh and Eslami [32], Zenkour [29], Cheng and Batra [31], Birman [33], and Javaheri and Eslami [34].

The Classical Plate Theory (CLPT) yields acceptable results only for the analysis of thin plates. The accuracy of the first-order shear deformation theory (FSDT) depends on the shear correction factor which may be difficult to compute. Higher-order shear deformation theories (HSDT) provide better accuracy for transverse shear stresses without the need of a shear correction factor. Examples of HSDT were proposed by Reddy [10], Kant and co-workers [35–40] and Batra and co-workers [17,41–52]. Most of these theories do not account for transverse extensibility by neglecting the σ_{zz} effects. This paper proposes a higher-order theory that accounts for such transverse effects, by using the Unified Formulation proposed by Carrera. The effect of thickness stretching in FGM plates was recently investigated by Carrera et al. [53] using Carrera's Unified Formulation and finite element approximations.

Carrera's Unified Formulation (CUF) was proposed in [54–56] for laminated plates and shells and extended to FGM plates in [57–59]. It is possible to implement any C_z^0 theory under CUF, using layer-wise as well as equivalent single-layer descriptions, and the Principle of Virtual Displacements, as is the case in present formulation, or the Reissner mixed variational theorem. CUF allows a

* Corresponding author.
E-mail address: ferreira@fe.up.pt (A.J.M. Ferreira).

1359-8368/$ - see front matter © 2012 Elsevier Ltd. All rights reserved.
doi:10.1016/j.compositesb.2012.01.089

systematic assessment of a large number of plate models. The present formulation can be seen as a generalization of the original CUF, by introducing different displacement fields for in-plane and out-of-plane displacements. Another form of Generalized Unified Formulation (GUF) was proposed by Demasi [60] and Luciano and Demasi [61] based on CUF. GUF has been applied in the study of laminated plates using the finite element method and has been extended to Layerwise, zig-zag and mixed theories [62–66]. It allows to independently choose the expansions of each displacement (as in present formulation) but it also allows to independently choose the expansion of each stress σ_{xz}, σ_{yz}, and σ_{zz}.

Another higher-order concept for quasi-3D FGM plates problems was proposed by Batra and Vidoli [41] and Batra et al. [42] who also consider thickness-stretching effects in FGM plates. The plate theory is derived using three-dimensional mixed variational principle. CUF has been applied either using the Principle of Virtual Displacements or by using the Reissner's Mixed Variational theorem. The stiffness matrix components, the external force terms or the inertia terms can be obtained directly with CUF irrespective of the shear deformation theory being considered. In Batra and Vidoli's approach the transverse shear and normal stresses are expanded as polynomials in z of degree 2 higher than the displacements. CUF has the advantage of being not restricted to polynomials (see [67–69], for example, where a sinusoidal and a hyperbolic expansion has been considered). On the other hand, the constitutive relations in Batra and Vidoli's approach explicitly present the tractions and the charge density applied on the top and the bottom surfaces of the plate which is not the case in CUF. Such loads may be considered at any point of the plate, not restricted to the top or bottom surfaces, but CUF does not present them explicitly.

Williams and co-workers [70–75] also proposed another unified formulation. Williams' unified plate theory is a displacement based theory and uses a generalized two length scale displacement field by superposition of global and local arbitrary displacement fields. The global field spans the thickness of the plate; the set of local fields must be consistent with the layering thickness and may be activated only in chosen regions. Williams' unified plate theory may address the non-linear analysis of laminated plates in the presence of delaminations.

The use of alternative methods to the Finite Element Methods for the analysis of plates, such as the meshless methods based on collocation with radial basis functions is atractive due to the absence of a mesh and the ease of collocation methods. In recent years, radial basis functions (RBFs) showed excellent accuracy in the interpolation of data and functions. The authors have applied the RBF collocation to the static deformations and free vibrations of composite beams and plates [76–83]. The combination of CUF and meshless methods has been performed in [84–87] for laminated plates and in [67,68] for FGM plates. Furthermore, a generalized form of the CUF method is here applied for the first time to the static, free vibration and buckling analysis of FGM plates, owing to collocation with radial basis functions.

This paper presents explicit governing equations and boundary conditions of the HSDT and focus on the thickness stretching issue on the static, free vibration, and buckling analysis of FGM plates by a meshless technique. The CUF method is employed to obtain the algebraic governing equations and boundary conditions which are then interpolated by radial basis functions to obtain an algebraic system of equations.

2. Problem formulation

Consider a rectangular plate of plan-form dimensions a and b and uniform thickness h. The co-ordinate system is taken such that the x–y plane ($z = 0$) coincides with the midplane of the plate ($z \in [-h/2, h/2]$).

For static bending analysis, the plate may be subjected to a transverse mechanical load applied at the top of the plate.

For buckling analysis, the plate may be subjected to compressive in-plane forces acting on the mid-plane of the plate and distributed shear force (see Fig. 1). $\overline{N}_{xx}$ and $\overline{N}_{yy}$ denote the in-plane loads perpendicular to the edges $x = 0$ and $y = 0$ respectively, and $\overline{N}_{xy}$ denote the distributed shear force parallel to the edges $x = 0$ and $y = 0$ respectively.

Three different types of functionally graded plates are studied: (A) isotropic FGM plates; (B) sandwich plates with FGM core; (C) sandwich plates with FGM skins.

2.1. Plate A: isotropic FGM plate

The plate of type A is graded from metal (bottom) to ceramic (top) (see Fig. 2). The volume fraction of the ceramic phase is defined as in [19]:

$$V_c = \left(0.5 + \frac{z}{h}\right)^p \qquad (1)$$

where $z \in [-h/2, h/2]$, h is the thickness of the plate, and p is a scalar parameter that allows the user to define gradation of material properties across the thickness direction.

2.2. Plate B: sandwich plate with FGM core

In this type of sandwich plates the bottom skin is isotropic (fully metal) and the top skin is isotropic (fully ceramic). The core layer is graded from metal to ceramic so that there are no interfaces between core and skins, as illustrated in Fig. 3.

The volume fraction of the ceramic phase in the core is obtained by adapting the polynomial material law in [19]:

$$V_c = \left(\frac{z_c - h_1}{h_c}\right)^p \qquad (2)$$

where $z_c \in [h_1, h_2]$, $h_c = h_2 - h_1$ is the thickness of the core, and p is the power-law exponent that defines the gradation of material properties across the thickness direction.

2.3. Plate C: sandwich plate with FGM skins

In C-type plates the sandwich core is isotropic (fully ceramic) and skins are composed of a functionally graded material across the thickness direction. The bottom skin varies from a metal-rich surface ($z = -h/2$) to a ceramic-rich surface while the top skin face varies from a ceramic-rich surface to a metal-rich surface ($z = h/2$),

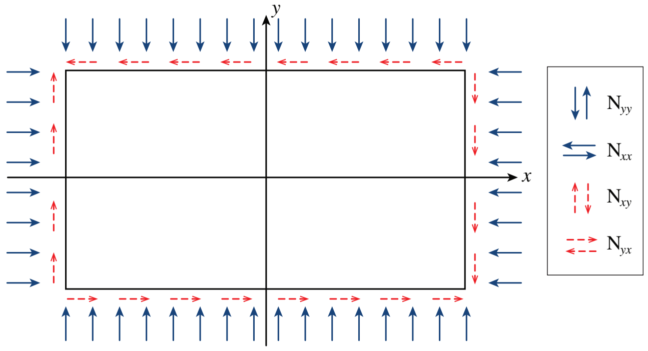

Fig. 1. Rectangular plate subjected to compressive in-plane forces and distributed shear forces.

Fig. 2. Plate *A*: isotropic FGM plate.

Fig. 3. Plate *B*: sandwich plate with FGM core and isotropic skins.

Fig. 4. Plate *C*: sandwich with isotropic core and FGM skins.

as illustrated in Fig. 4. There are no interfaces between core and skins. The volume fraction of the ceramic phase is obtained as:

$$\begin{aligned} &V_c = \left(\frac{z-h_0}{h_1-h_0}\right)^p, \quad z \in [-h/2, h_1], \quad \text{bottom skin} \\ &V_c = 1, \quad z \in [h_1, h_2], \quad \text{core} \\ &V_c = \left(\frac{z-h_3}{h_2-h_3}\right)^p, \quad z \in [h_2, h/2], \quad \text{top skin} \end{aligned} \tag{3}$$

where $z \in [-h/2, h/2]$, and p is a scalar parameter that allows the user to define gradation of material properties across the thickness direction of the skins.

The sandwich plate *C*-type may be symmetric or non-symmetric about the mid-plane as we may vary the thickness of each face.

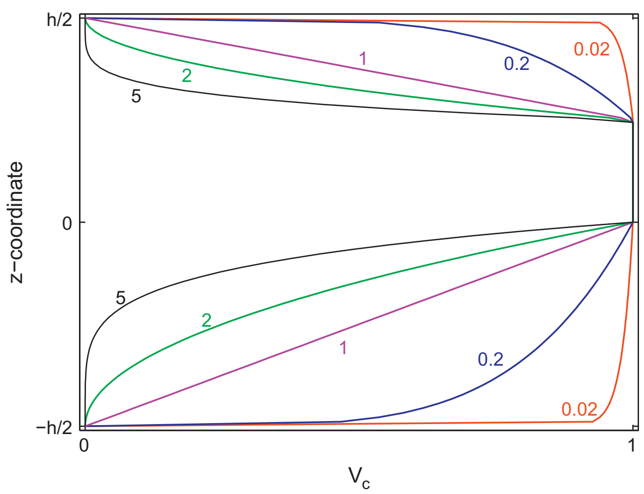

Fig. 5. A 2-1-1 *C*-type plate for several exponents of the power law in (3).

Fig. 5 shows a non-symmetric sandwich with volume fraction defined by the power-law (3) for various exponents p, in which top skin thickness is the same as the core thickness and the bottom skin thickness is twice the core thickness. Such thickness relation is denoted as 2-1-1. A bottom-core-top notation is being used. 1-1-1 means that skins and core have the same thickness.

For the three types of plates, *A*, *B*, and *C*, the volume fraction for the metal phase is given as $V_m = 1 - V_c$. The isotropic fully ceramic plate can be seen as a particular case of plates *A*, *B*, and *C*, by setting to zero the exponent p of the power law in (1)–(3).

3. A quasi-3D higher-order plate theory

3.1. Displacement field

The present theory is based on the following displacement field:

$$u(x,y,z,t) = u_0(x,y,t) + zu_1(x,y,t) + z^3 u_3(x,y,t) \tag{4}$$

$$v(x,y,z,t) = v_0(x,y,t) + zv_1(x,y,t) + z^3 v_3(x,y,t) \tag{5}$$

$$w(x,y,z,t) = w_0(x,y,t) + zw_1(x,y,t) + z^2 w_2(x,y,t) \tag{6}$$

where u, v, and w are the displacements in the x-, y-, and z-directions, respectively. u_0, u_1, u_3, v_0, v_1, v_3, w_0, w_1, and w_2 are functions to be determined.

3.2. Strains

The strain–displacement relationships are given as:

$$\begin{Bmatrix} \epsilon_{xx} \\ \epsilon_{yy} \\ \gamma_{xy} \end{Bmatrix} = \begin{Bmatrix} \frac{\partial u}{\partial x} + \frac{1}{2}\left(\frac{\partial w_0}{\partial x}\right)^2 \\ \frac{\partial v}{\partial y} + \frac{1}{2}\left(\frac{\partial w_0}{\partial y}\right)^2 \\ \frac{\partial u}{\partial y} + \frac{\partial v}{\partial x} + \frac{\partial w_0}{\partial x}\frac{\partial w_0}{\partial y} \end{Bmatrix}, \quad \begin{Bmatrix} \gamma_{xz} \\ \gamma_{yz} \\ \epsilon_{zz} \end{Bmatrix} = \begin{Bmatrix} \frac{\partial u}{\partial z} + \frac{\partial w}{\partial x} \\ \frac{\partial v}{\partial z} + \frac{\partial w}{\partial y} \\ \frac{\partial w}{\partial z} \end{Bmatrix} \tag{7}$$

By substitution of the displacement field in (7), the strains are obtained:

$$\begin{Bmatrix} \epsilon_{xx} \\ \epsilon_{yy} \\ \gamma_{xy} \end{Bmatrix} = \begin{Bmatrix} \epsilon_{xx}^{(0)} \\ \epsilon_{yy}^{(0)} \\ \gamma_{xy}^{(0)} \end{Bmatrix} + \begin{Bmatrix} \epsilon_{xx}^{(nl)} \\ \epsilon_{yy}^{(nl)} \\ \gamma_{xy}^{(nl)} \end{Bmatrix} + z \begin{Bmatrix} \epsilon_{xx}^{(1)} \\ \epsilon_{yy}^{(1)} \\ \gamma_{xy}^{(1)} \end{Bmatrix} + z^3 \begin{Bmatrix} \epsilon_{xx}^{(3)} \\ \epsilon_{yy}^{(3)} \\ \gamma_{xy}^{(3)} \end{Bmatrix} \tag{8}$$

$$\begin{Bmatrix} \gamma_{xz} \\ \gamma_{yz} \\ \epsilon_{zz} \end{Bmatrix} = \begin{Bmatrix} \gamma_{xz}^{(0)} \\ \gamma_{yz}^{(0)} \\ \epsilon_{zz}^{(0)} \end{Bmatrix} + z \begin{Bmatrix} \gamma_{xz}^{(1)} \\ \gamma_{yz}^{(1)} \\ \epsilon_{zz}^{(1)} \end{Bmatrix} + z^2 \begin{Bmatrix} \gamma_{xz}^{(2)} \\ \gamma_{yz}^{(2)} \\ \epsilon_{zz}^{(2)} \end{Bmatrix} \tag{9}$$

being the strain components obtained as

$$\begin{Bmatrix} \epsilon_{xx}^{(0)} \\ \epsilon_{yy}^{(0)} \\ \gamma_{xy}^{(0)} \end{Bmatrix} = \begin{Bmatrix} \frac{\partial u_0}{\partial x} \\ \frac{\partial v_0}{\partial y} \\ \frac{\partial u_0}{\partial y} + \frac{\partial v_0}{\partial x} \end{Bmatrix}; \quad \begin{Bmatrix} \epsilon_{xx}^{(nl)} \\ \epsilon_{yy}^{(nl)} \\ \gamma_{xy}^{(nl)} \end{Bmatrix} = \begin{Bmatrix} \frac{1}{2}\left(\frac{\partial w_0}{\partial x}\right)^2 \\ \frac{1}{2}\left(\frac{\partial w_0}{\partial y}\right)^2 \\ \frac{\partial w_0}{\partial x}\frac{\partial w_0}{\partial y} \end{Bmatrix} \tag{10}$$

$$\begin{Bmatrix} \epsilon_{xx}^{(1)} \\ \epsilon_{yy}^{(1)} \\ \gamma_{xy}^{(1)} \end{Bmatrix} = \begin{Bmatrix} \frac{\partial u_1}{\partial x} \\ \frac{\partial v_1}{\partial y} \\ \frac{\partial u_1}{\partial y} + \frac{\partial v_1}{\partial x} \end{Bmatrix}; \quad \begin{Bmatrix} \epsilon_{xx}^{(3)} \\ \epsilon_{yy}^{(3)} \\ \gamma_{xy}^{(3)} \end{Bmatrix} = \begin{Bmatrix} \frac{\partial u_3}{\partial x} \\ \frac{\partial v_3}{\partial y} \\ \frac{\partial u_3}{\partial y} + \frac{\partial v_3}{\partial x} \end{Bmatrix} \tag{11}$$

$$\begin{Bmatrix} \gamma_{xz}^{(0)} \\ \gamma_{yz}^{(0)} \\ \epsilon_{zz}^{(0)} \end{Bmatrix} = \begin{Bmatrix} u_1 + \frac{\partial w_0}{\partial x} \\ v_1 + \frac{\partial w_0}{\partial y} \\ w_1 \end{Bmatrix}; \quad \begin{Bmatrix} \gamma_{xz}^{(1)} \\ \gamma_{yz}^{(1)} \\ \epsilon_{zz}^{(1)} \end{Bmatrix} = \begin{Bmatrix} \frac{\partial w_1}{\partial x} \\ \frac{\partial w_1}{\partial y} \\ 2w_2 \end{Bmatrix}; \quad \begin{Bmatrix} \gamma_{xz}^{(2)} \\ \gamma_{yz}^{(2)} \\ \epsilon_{zz}^{(2)} \end{Bmatrix} = \begin{Bmatrix} 3u_3 + \frac{\partial w_2}{\partial x} \\ 3v_3 + \frac{\partial w_2}{\partial y} \\ 0 \end{Bmatrix} \tag{12}$$

where $\epsilon_{\alpha\beta}^{(nl)}$ contains the non-linear terms that will originate the linearized buckling equation.

Please cite this article in press as: Neves AMA et al. Static, free vibration and buckling analysis of isotropic and sandwich functionally graded plates using a quasi-3D higher-order shear deformation theory and a meshless technique. Composites: Part B (2012), doi:10.1016/j.compositesb.2012.01.089

3.3. Elastic stress–strain relations

The elastic stress–strain relations depends on which assumption of ϵ_{zz} we consider.

If $\epsilon_{zz} \neq 0$, i.e., thickness stretching is allowed, then the 3D model is used. In the case of functionally graded materials, the constitutive equations can be written as:

$$\begin{Bmatrix} \sigma_{xx} \\ \sigma_{yy} \\ \tau_{xy} \\ \tau_{xz} \\ \tau_{yz} \\ \sigma_{zz} \end{Bmatrix} = \begin{Bmatrix} C_{11} & C_{12} & 0 & 0 & 0 & C_{12} \\ C_{12} & C_{11} & 0 & 0 & 0 & C_{12} \\ 0 & 0 & C_{44} & 0 & 0 & 0 \\ 0 & 0 & 0 & C_{44} & 0 & 0 \\ 0 & 0 & 0 & 0 & C_{44} & 0 \\ C_{12} & C_{12} & 0 & 0 & 0 & C_{33} \end{Bmatrix} \begin{Bmatrix} \epsilon_{xx} \\ \epsilon_{yy} \\ \gamma_{xy} \\ \gamma_{xz} \\ \gamma_{yz} \\ \epsilon_{zz} \end{Bmatrix} \tag{13}$$

where the C_{ij} are the three-dimensional elastic constants, given by

$$C_{11} = \frac{E(1-v^2)}{1-3v^2-2v^3}, \quad C_{12} = \frac{E(v+v^2)}{1-3v^2-2v^3} \tag{14}$$

$$C_{44} = G, \quad C_{33} = \frac{E(1-v^2)}{1-3v^2-2v^3} \tag{15}$$

where E is the modulus of elasticity, v is Poisson's ratio, and G is the shear modulus $G = \frac{E}{2(1+v)}$.

If $\epsilon_{zz} = 0$, then the plane-stress case is used

$$\begin{Bmatrix} \sigma_{xx} \\ \sigma_{yy} \\ \tau_{xy} \\ \tau_{xz} \\ \tau_{yz} \end{Bmatrix} = \begin{Bmatrix} C_{11} & C_{12} & 0 & 0 & 0 \\ C_{12} & C_{11} & 0 & 0 & 0 \\ 0 & 0 & C_{44} & 0 & 0 \\ 0 & 0 & 0 & C_{44} & 0 \\ 0 & 0 & 0 & 0 & C_{44} \end{Bmatrix} \begin{Bmatrix} \epsilon_{xx} \\ \epsilon_{yy} \\ \gamma_{xy} \\ \gamma_{xz} \\ \gamma_{yz} \end{Bmatrix} \tag{16}$$

where C_{ij} are the plane-stress reduced elastic constants:

$$C_{11} = \frac{E}{1-v^2}; \quad C_{12} = v\frac{E}{1-v^2}; \quad C_{44} = G \tag{17}$$

It is interesting to note that the use of shear-correction factors is not considered, as would be the case of the first-order shear deformation theory.

3.4. Governing equations and boundary conditions

The governing equations of present theory are derived from the dynamic version of the Principle of Virtual Displacements. The internal virtual work is initially defined as

$$\begin{aligned} \delta U = \int_{\Omega_0} \Big\{ \int_{-h/2}^{h/2} \big[& \sigma_{xx}\big(\delta\epsilon_{xx}^{(0)} + z\delta\epsilon_{xx}^{(1)} + z^3\delta\epsilon_{xx}^{(3)}\big) \\ & + \sigma_{yy}\Big(\delta\epsilon_{yy}^{(0)} + z\delta\epsilon_{yy}^{(1)} + z^3\delta\epsilon_{yy}^{(3)} + \sigma_{xy}\Big(\delta\gamma_{xy}^{(0)} + z\delta\gamma_{xy}^{(1)} + z^3\delta\gamma_{xy}^{(3)}\Big) \\ & + \sigma_{xz}\big(\delta\gamma_{xz}^{(0)} + z\delta\gamma_{xz}^{(1)} + z^2\delta\gamma_{xz}^{(2)}\big) + \sigma_{yz}\Big(\delta\gamma_{yz}^{(0)} + z\delta\gamma_{yz}^{(1)} + z^2\delta\gamma_{yz}^{(2)}\Big) \\ & + \sigma_{zz}\big(\delta\epsilon_{zz}^{(0)} + z\delta\epsilon_{zz}^{(1)}\big)\big]dz\Big\}dx\,dy \end{aligned} \tag{18}$$

By performing the integrals in the thickness direction, the internal virtual work becomes

$$\begin{aligned} \delta U = \int_{\Omega_0} \Big(& N_{xx}\delta\epsilon_{xx}^{(0)} + M_{xx}\delta\epsilon_{xx}^{(1)} + R_{xx}\delta\epsilon_{xx}^{(3)} + N_{yy}\delta\epsilon_{yy}^{(0)} + M_{yy}\delta\epsilon_{yy}^{(1)} \\ & + R_{yy}\delta\epsilon_{yy}^{(3)} + N_{xy}\delta\gamma_{xy}^{(0)} + M_{xy}\delta\gamma_{xy}^{(1)} + R_{xy}\delta\gamma_{xy}^{(3)} + Q_{xz}\delta\gamma_{xz}^{(0)} \\ & + M_{xz}\delta\gamma_{xz}^{(1)} + R_{xz}\delta\gamma_{xz}^{(2)} + Q_{yz}\delta\gamma_{yz}^{(0)} + M_{yz}\delta\gamma_{yz}^{(1)} + R_{yz}\delta\gamma_{yz}^{(2)} \\ & + Q_{zz}\delta\epsilon_{zz}^{(0)} + M_{zz}\delta\epsilon_{zz}^{(1)}\big)dx\,dy \end{aligned} \tag{19}$$

where Ω_0 is the integration domain in plane (x,y) and the resultants are computed as

$$\begin{Bmatrix} N_{xx} \\ N_{yy} \\ N_{xy} \end{Bmatrix} = \int_{-h/2}^{h/2} \begin{Bmatrix} \sigma_{xx} \\ \sigma_{yy} \\ \sigma_{xy} \end{Bmatrix} dz, \quad \begin{Bmatrix} Q_{xz} \\ Q_{yz} \\ Q_{zz} \end{Bmatrix} = \int_{-h/2}^{h/2} \begin{Bmatrix} \sigma_{xz} \\ \sigma_{yz} \\ \sigma_{zz} \end{Bmatrix} dz \tag{20}$$

$$\begin{Bmatrix} M_{xx} \\ M_{yy} \\ M_{xy} \end{Bmatrix} = \int_{-h/2}^{h/2} z \begin{Bmatrix} \sigma_{xx} \\ \sigma_{yy} \\ \sigma_{xy} \end{Bmatrix} dz, \quad \begin{Bmatrix} M_{xz} \\ M_{yz} \\ M_{zz} \end{Bmatrix} = \int_{-h/2}^{h/2} z \begin{Bmatrix} \sigma_{xz} \\ \sigma_{yz} \\ \sigma_{zz} \end{Bmatrix} dz \tag{21}$$

$$\begin{Bmatrix} R_{xx} \\ R_{yy} \\ R_{xy} \end{Bmatrix} = \int_{-h/2}^{h/2} z^3 \begin{Bmatrix} \sigma_{xx} \\ \sigma_{yy} \\ \sigma_{xy} \end{Bmatrix} dz, \quad \begin{Bmatrix} R_{xz} \\ R_{yz} \end{Bmatrix} = \int_{-h/2}^{h/2} z^2 \begin{Bmatrix} \sigma_{xz} \\ \sigma_{yz} \end{Bmatrix} dz. \tag{22}$$

The external virtual work due to an external load (p_z) applied to the plate is given as:

$$\delta V = -\int_{\Omega_0} p_z \delta w dx\, dy = -\int_{\Omega_0} p_z\big(\delta w_0 + z^2\delta w_2\big)dx\, dy \tag{23}$$

The external virtual work due to in-plane forces and shear forces applied to the plate is given as:

$$\begin{aligned} \delta V = -\int_{\Omega_0} \Big[& \overline{N}_{xx}\frac{\partial w_0}{\partial x}\frac{\delta\partial w_0}{\partial x} + \overline{N}_{xy}\frac{\partial w_0}{\partial y}\frac{\delta\partial w_0}{\partial x} + \overline{N}_{yx}\frac{\partial w_0}{\partial x}\frac{\delta\partial w_0}{\partial y} \\ & + \overline{N}_{yy}\frac{\partial w_0}{\partial y}\frac{\delta\partial w_0}{\partial y}\Big]dx\, dy \end{aligned} \tag{24}$$

being $\overline{N}_{xx}$ and $\overline{N}_{yy}$ the in-plane loads perpendicular to the edges $x = 0$ and $y = 0$ respectively, and $\overline{N}_{xy}$ and $\overline{N}_{yx}$ the distributed shear forces parallel to the edges $x = 0$ and $y = 0$ respectively.

The virtual kinetic energy is given as:

$$\begin{aligned} \delta K &= \int_{\Omega_0} \Big\{ \int_{-h/2}^{h/2} \rho(\dot{u}\delta\dot{u} + \dot{v}\delta\dot{v} + \dot{w}\delta\dot{w})dz \Big\}dx\, dy \\ &= \int_{\Omega_0} \Big\{ \int_{-h/2}^{h/2} \rho\Big[(\dot{u}_0\delta\dot{u}_0 + \dot{v}_0\delta\dot{v}_0 + \dot{w}_0\delta\dot{w}_0) + z(\dot{u}_0\delta\dot{u}_1 + \dot{u}_1\delta\dot{u}_0 \\ &\quad + \dot{v}_0\delta\dot{v}_1 + \dot{v}_1\delta\dot{v}_0 + \dot{w}_0\delta\dot{w}_1 + \dot{w}_1\delta\dot{w}_0) + z^2(\dot{u}_1\delta\dot{u}_1 + \dot{v}_1\delta\dot{v}_1 \\ &\quad + \dot{w}_0\delta\dot{w}_2 + \dot{w}_1\delta\dot{w}_1 + \dot{w}_2\delta\dot{w}_0) + z^3(\dot{u}_0\delta\dot{u}_3 + \dot{u}_3\delta\dot{u}_0 + \dot{v}_0\delta\dot{v}_3 \\ &\quad + \dot{v}_3\delta\dot{v}_0 + \dot{w}_1\delta\dot{w}_2 + \dot{w}_2\delta\dot{w}_1) + z^4(\dot{u}_1\delta\dot{u}_3 + \dot{u}_3\delta\dot{u}_1 + \dot{v}_3\delta\dot{v}_1 \\ &\quad + \dot{v}_1\delta\dot{v}_3 + \dot{w}_2\delta\dot{w}_2) + z^6(\dot{u}_3\delta\dot{u}_3 + \dot{v}_3\delta\dot{v}_3)\Big]dz\Big\}dx\, dy \end{aligned} \tag{25}$$

By performing the integrals in the thickness direction, the virtual kinetic energy is now obtained as

$$\begin{aligned} \delta K = \int_{\Omega_0} [& I_0(\dot{u}_0\delta\dot{u}_0 + \dot{v}_0\delta\dot{v}_0 + \dot{w}_0\delta\dot{w}_0) + I_1(\dot{u}_0\delta\dot{u}_1 + \dot{u}_1\delta\dot{u}_0 + \dot{v}_0\delta\dot{v}_1 \\ & + \dot{v}_1\delta\dot{v}_0 + \dot{w}_0\delta\dot{w}_1 + \dot{w}_1\delta\dot{w}_0) + I_2(\dot{u}_1\delta\dot{u}_1 + \dot{v}_1\delta\dot{v}_1 + \dot{w}_0\delta\dot{w}_2 \\ & + \dot{w}_1\delta\dot{w}_1 + \dot{w}_2\delta\dot{w}_0) + I_3(\dot{u}_0\delta\dot{u}_3 + \dot{u}_3\delta\dot{u}_0 + \dot{v}_0\delta\dot{v}_3 + \dot{v}_3\delta\dot{v}_0 \\ & + \dot{w}_1\delta\dot{w}_2 + \dot{w}_2\delta\dot{w}_1) + I_4(\dot{u}_1\delta\dot{u}_3 + \dot{u}_3\delta\dot{u}_1 + \dot{v}_3\delta\dot{v}_1 + \dot{v}_1\delta\dot{v}_3 \\ & + \dot{w}_2\delta\dot{w}_2) + I_6(\dot{u}_3\delta\dot{u}_3 + \dot{v}_3\delta\dot{v}_3)]dx\, dy \end{aligned} \tag{26}$$

where the dots denote the derivative with respect to time t and the inertia terms are computed as

$$I_i = \int_{-h/2}^{h/2} \rho z^i dz \quad i = 1, 2, 3, 4, 6 \tag{27}$$

Substituting δU, δV, and δK in the virtual work statement, integrating through the thickness, integrating by parts with respect to x and y, and collecting the coefficients of δu_0, δu_1, δu_3, δv_0, δv_1, δv_3, δw_0, δw_1, δw_2, the following governing equations are obtained:

$$\delta u_0:-\frac{\partial N_{xx}}{\partial x}-\frac{\partial N_{xy}}{\partial y}=\int_{-h/2}^{h/2}\rho(\ddot{u}_0+z\ddot{u}_1+z^3\ddot{u}_3)dz$$
$$\delta v_0:-\frac{\partial N_{xy}}{\partial x}-\frac{\partial N_{yy}}{\partial y}=\int_{-h/2}^{h/2}\rho(\ddot{v}_0+z\ddot{v}_1+z^3\ddot{v}_3)dz$$
$$\delta w_0:-\frac{\partial Q_{xz}}{\partial x}-\frac{\partial Q_{yz}}{\partial y}+\overline{N}_{xx}\frac{\partial^2 w_0}{\partial x^2}+\overline{N}_{xy}\frac{\partial^2 w_0}{\partial y\partial x}+\overline{N}_{yx}\frac{\partial^2 w_0}{\partial x\partial y}+\overline{N}_{yy}\frac{\partial^2 w_0}{\partial y^2}=\int_{-h/2}^{h/2}\{\rho(\ddot{w}_0+z\ddot{w}_1+z^2\ddot{w}_2)+p_z\}dz$$
$$\delta u_1:-\frac{\partial M_{xx}}{\partial x}-\frac{\partial M_{xy}}{\partial y}+Q_{xz}=\int_{-h/2}^{h/2}\rho z(\ddot{u}_0+z\ddot{u}_1+z^3\ddot{u}_3)dz$$
$$\delta v_1:-\frac{\partial M_{xy}}{\partial x}-\frac{\partial M_{yy}}{\partial y}+Q_{yz}=\int_{-h/2}^{h/2}\rho z(\ddot{v}_0+z\ddot{v}_1+z^3\ddot{v}_3)dz$$
$$\delta w_1:-\frac{\partial M_{xz}}{\partial x}-\frac{\partial M_{yz}}{\partial y}+Q_{zz}=\int_{-h/2}^{h/2}\rho z(\ddot{w}_0+z\ddot{w}_1+z^2\ddot{w}_2)dz$$
$$\delta u_3:-\frac{\partial R_{xx}}{\partial x}-\frac{\partial R_{xy}}{\partial y}+3R_{xz}=\int_{-h/2}^{h/2}\rho z^3(\ddot{u}_0+z\ddot{u}_1+z^3\ddot{u}_3)dz$$
$$\delta v_3:-\frac{\partial R_{xy}}{\partial x}-\frac{\partial R_{yy}}{\partial y}+3R_{yz}=\int_{-h/2}^{h/2}\rho z^3(\ddot{v}_0+z\ddot{v}_1+z^3\ddot{v}_3)dz$$
$$\delta w_2:-\frac{\partial R_{xz}}{\partial x}-\frac{\partial R_{yz}}{\partial y}+2M_{zz}=\int_{-h/2}^{h/2}\rho z^2(\ddot{w}_0+z\ddot{w}_1+z^2\ddot{w}_2)\,dz+\left(\frac{h}{2}\right)^2 p_z \quad (28)$$

The mechanical boundary conditions are defined as:

$$\begin{aligned}
&\delta u_0: n_xN_{xx}+n_yN_{xy}=n_x\overline{N}_{xx}+n_y\overline{N}_{xy}\\
&\delta v_0: n_xN_{xy}+n_yN_{yy}=n_x\overline{N}_{xy}+n_y\overline{N}_{yy}\\
&\delta w_0: n_xQ_{xz}+n_yQ_{yz}=n_x\overline{Q}_{xz}+n_y\overline{Q}_{yz}\\
&\delta u_1: n_xM_{xx}+n_yM_{xy}=n_x\overline{M}_{xx}+n_y\overline{M}_{xy}\\
&\delta v_1: n_xM_{xy}+n_yM_{yy}=n_x\overline{M}_{xy}+n_y\overline{M}_{yy}\\
&\delta w_1: n_xM_{xz}+n_yM_{yz}=n_x\overline{M}_{xz}+n_y\overline{M}_{yz}\\
&\delta u_3: n_xR_{xx}+n_yR_{xy}=n_x\overline{R}_{xx}+n_y\overline{R}_{xy}\\
&\delta v_3: n_xR_{xy}+n_yR_{yy}=n_x\overline{R}_{xy}+n_y\overline{R}_{yy}\\
&\delta w_2: n_xR_{xz}+n_yR_{yz}=n_x\overline{R}_{xz}+n_y\overline{R}_{yz}
\end{aligned} \quad (29)$$

where (n_x, n_y) denotes the unit normal-to-boundary vector and the bar $(\bar{\cdot})$ denotes the prescribed values of the resultants.

4. Governing equations and boundary conditions in the framework of Unified Formulation

The Unified Formulation proposed by Carrera [88,55] (further denoted as CUF) has been applied, using the Principle of Virtual Displacements, to obtain the equations of the present theory (see Eq. (28)). The stiffness matrix components, the external force terms or the inertia terms can be obtained directly with this unified formulation, irrespective of the shear deformation theory being considered.

The three displacement components u_x, u_y and u_z (given in (4)–(6)) and their variations can be modeled as:

$$(u_x,u_y,u_z)=F_\tau\ (u_{x\tau},u_{y\tau},u_{z\tau})\qquad (\delta u_x,\delta u_y,\delta u_z)=F_s\ (\delta u_{xs},\delta u_{ys},\delta u_{zs}) \quad (30)$$

In the present formulation the thickness functions are

$$F_{sux}=F_{suy}=F_{\tau ux}=F_{\tau uy}=[1\quad z\quad z^3] \quad (31)$$

for in-plane displacements u, v and

$$F_{suz}=F_{\tau uz}=[1\quad z\quad z^2] \quad (32)$$

for transverse displacement w.

The CUF formulation applied to FGM plates considers virtual (mathematical) layers of constant thickness, each containing a homogeneized modulus of elasticity, E^k, and a homogeneized Poisson's ratio, ν^k. The functionally graded plate is divided into a number (NL) of uniform thickness layers and for each layer the volume fraction of the ceramic phase is defined according to (1), (2) or (3). The volume fraction for the metal phase is given as $V_m = 1 - V_c$.

For each virtual layer, the elastic properties E^k and ν^k can be computed by the law-of-mixtures or by the Mori–Tanaka homogeneization method. According to the law-of-mixtures, the Young's modulus and Poisson's ratio are defined as

$$E^k(z)=E_mV_m+E_cV_c;\qquad \nu^k(z)=\nu_mV_m+\nu_cV_c \quad (33)$$

When considering the Mori–Tanaka homogenization procedure [89,90], we start by finding the bulk modulus, K, and the effective shear modulus, G, of the composite equivalent layer as

$$\frac{K-K_m}{K_c-K_m}=\frac{V_c}{1+V_m\frac{K_c-K_m}{K_m+4/3G_m}};\quad \frac{G-G_m}{G_c-G_m}=\frac{V_c}{1+V_m\frac{G_c-G_m}{G_m+f_m}} \quad (34)$$

where

$$f_m=\frac{G_m(9K_m+8G_m)}{6(K_m+2G_m)} \quad (35)$$

The effective values of Young's modulus, E^k, and Poisson's ratio, ν^k, are then found from

$$E^k=\frac{9KG}{3K+G};\quad \nu^k=\frac{3K-2G}{2(3K+G)} \quad (36)$$

After using the law-of-mixtures or the Mori–Tanaka homogenization procedure, the computation of the elastic constants C_{ij}^k is performed for each layer based on the values of ν^k and E^k. For example,

$$C_{12}^k=\frac{E^k(\nu^k+(\nu^k)^2)}{1-3(\nu^k)^2-2(\nu^k)^3}. \quad (37)$$

The procedure for the other C_{ij}^k is analogous.

Under CUF formulation the PVD is expressed considering a sumatoria over the layers:

$$\sum_{k=1}^{NL}\int_{\Omega_k}\int_{A_k}\left(\delta\boldsymbol{\epsilon}_p^T\boldsymbol{\sigma}_p^k+\delta\boldsymbol{\epsilon}_n^T\boldsymbol{\sigma}_n^k\right)dz\,d\Omega_k=\sum_{k=1}^{NL}\int_{\Omega_k}\int_{A_k}(\rho^k\,\delta\mathbf{u}^T\ddot{\mathbf{u}})dz\ +\delta w_0p_z+\delta w_2p_zd\Omega_k \quad (38)$$

Here, k indicates the layer and Ω_k and A_k are the integration domains in plane (x,y) and z direction, respectively, and ρ^k is the mass density of the kth layer. Subscript p indicates in-plane components (xx,yy,xy) and subscript n the transverse components (xz, yz, and zz). $\boldsymbol{p} = \{p_x, p_y, p_z\}$ is the external load applied to the structure. T denotes the transpose of a vector, δ denotes the variational symbol, and double dots acceleration.

Eq. (38) considers the 9 variationals δu_0, δv_0, δw_0, δu_1, δv_1, δw_1, δu_Z, δv_Z, and δw_2 disregarding the the in-plane loads and the shear forces. These external forces just imply addicional terms on the variational $\delta\boldsymbol{w}_0$:

$$\int_{\Omega_0}\overline{N}_{\alpha\beta}w_{0,\alpha}\delta w_{0,\beta}d\Omega_0 \quad (39)$$

where Ω_0 is the integration domain in plane (x,y) and α and β take the symbols x, y.

Considering that the mechanical external load is a transverse $\boldsymbol{p} = \{0, 0, p_z\}$ load applied at the top (coordinate $z = h/2$), equations in (28) become:

Please cite this article in press as: Neves AMA et al. Static, free vibration and buckling analysis of isotropic and sandwich functionally graded plates using a quasi-3D higher-order shear deformation theory and a meshless technique. Composites: Part B (2012), doi:10.1016/j.compositesb.2012.01.089

$$\delta u_0 : \sum_{k=1}^{NL}\left(-\frac{\partial N^k_{xx}}{\partial x}-\frac{\partial N^k_{xy}}{\partial y}\right)=\sum_{k=1}^{NL}\int_{A_k}\rho^k(\ddot{u}_0+z\ddot{u}_1+z^3\ddot{u}_3)dz$$
$$\delta v_0 : \sum_{k=1}^{NL}\left(-\frac{\partial N^k_{xy}}{\partial x}-\frac{\partial N^k_{yy}}{\partial y}\right)=\sum_{k=1}^{NL}\int_{A_k}\rho^k(\ddot{v}_0+z\ddot{v}_1+z^3\ddot{v}_3)dz$$
$$\delta w_0 : \sum_{k=1}^{NL}\left(-\frac{\partial Q^k_{xz}}{\partial x}-\frac{\partial Q^k_{yz}}{\partial y}\right)+\overline{N}_{xx}\frac{\partial^2 w_0}{\partial x^2}+2\overline{N}_{xy}\frac{\partial^2 w_0}{\partial x\partial y}+\overline{N}_{yy}\frac{\partial^2 w_0}{\partial y^2}$$
$$=\sum_{k=1}^{NL}\int_{A_k}\rho^k(\ddot{w}_0+z\ddot{w}_1+z^2\ddot{w}_2)dz+p_z$$
$$\delta u_1 : \sum_{k=1}^{NL}\left(-\frac{\partial M^k_{xx}}{\partial x}-\frac{\partial M^k_{xy}}{\partial y}+Q^k_{xz}\right)=\sum_{k=1}^{NL}\int_{A_k}\rho^k z(\ddot{u}_0+z\ddot{u}_1+z^3\ddot{u}_3)dz$$
$$\delta v_1 : \sum_{k=1}^{NL}\left(-\frac{\partial M^k_{xy}}{\partial x}-\frac{\partial M^k_{yy}}{\partial y}+Q^k_{yz}\right)=\sum_{k=1}^{NL}\int_{A_k}\rho^k z(\ddot{v}_0+z\ddot{v}_1+z^3\ddot{v}_3)dz$$
$$\delta w_1 : \sum_{k=1}^{NL}\left(-\frac{\partial M^k_{xz}}{\partial x}-\frac{\partial M^k_{yz}}{\partial y}+Q^k_{zz}\right)=\sum_{k=1}^{NL}\int_{A_k}\rho^k z(\ddot{w}_0+z\ddot{w}_1+z^2\ddot{w}_2)dz$$
$$\delta u_3 : \sum_{k=1}^{NL}\left(-\frac{\partial R^k_{xx}}{\partial x}-\frac{\partial R^k_{xy}}{\partial y}+3R^k_{xz}\right)=\sum_{k=1}^{NL}\int_{A_k}\rho^k z^3(\ddot{u}_0+z\ddot{u}_1+z^3\ddot{u}_3)dz$$
$$\delta v_3 : \sum_{k=1}^{NL}\left(-\frac{\partial R^k_{xy}}{\partial x}-\frac{\partial R^k_{yy}}{\partial y}+3R^k_{yz}\right)=\sum_{k=1}^{NL}\int_{A_k}\rho^k z^3(\ddot{v}_0+z\ddot{v}_1+z^3\ddot{v}_3)dz$$
$$\delta w_2 : \sum_{k=1}^{NL}\left(-\frac{\partial R^k_{xz}}{\partial x}-\frac{\partial R^k_{yz}}{\partial y}+2M^k_{zz}\right)=\sum_{k=1}^{NL}\int_{A_k}\rho^k z^2(\ddot{w}_0+z\ddot{w}_1+z^2\ddot{w}_2)dz$$
$$+\left(\frac{h}{2}\right)^2 p_z \tag{40}$$

where $N^k_{xx}=\int_{A_k}\sigma^k_{xx}dz,\ R^k_{xz}=\int_{A_k}z^2\sigma^k_{xz}dz$ and analogous procedure for other resultants.

In (40), for static problems, the ρ^k and the $\overline{N}_{\alpha\beta}$ terms are set to zero; for the free vibration problems, the $\overline{N}_{\alpha\beta}$ and the p_z terms are set to zero; and for buckling problems the p_z and the ρ^k terms are set to zero.

4.1. Governing equations and boundary conditions in terms of displacements

In order to discretize the governing equations by radial basis functions, we present in the following the explicit terms of the governing equations and the boundary conditions in terms of the generalized displacements.

$$\delta u_0 : -\left(A_{11}\frac{\partial^2 u_0}{\partial x^2}+A_{66}\frac{\partial^2 u_0}{\partial y^2}\right)-(A_{12}+A_{66})\frac{\partial^2 v_0}{\partial x\partial y}$$
$$-\left(B_{11}\frac{\partial^2 u_1}{\partial x^2}+B_{66}\frac{\partial^2 u_1}{\partial y^2}\right)-\left(E_{11}\frac{\partial^2 u_3}{\partial x^2}+E_{66}\frac{\partial^2 u_3}{\partial y^2}\right)$$
$$-(B_{12}+B_{66})\frac{\partial^2 v_1}{\partial x\partial y}-(E_{12}+E_{66})\frac{\partial^2 v_3}{\partial x\partial y}$$
$$-A_{13}\frac{\partial w_1}{\partial x}-2B_{13}\frac{\partial w_2}{\partial x}=I_0\frac{\partial^2 u_0}{\partial t^2}+I_1\frac{\partial^2 u_1}{\partial t^2}+I_3\frac{\partial^2 u_3}{\partial t^2} \tag{41}$$

$$\delta u_1 : \left(-F_{11}\frac{\partial^2 u_3}{\partial x^2}+3D_{55}u_3-F_{66}\frac{\partial^2 u_3}{\partial y^2}\right)$$
$$+\left(-D_{11}\frac{\partial^2 u_1}{\partial x^2}+A_{55}u_1-D_{66}\frac{\partial^2 u_1}{\partial y^2}\right)-\left(B_{11}\frac{\partial^2 u_0}{\partial x^2}+B_{66}\frac{\partial^2 u_0}{\partial y^2}\right)$$
$$-(B_{12}+B_{66})\frac{\partial^2 v_0}{\partial x\partial y}-(D_{12}+D_{66})\frac{\partial^2 v_1}{\partial x\partial y}-(F_{12}+F_{66})\frac{\partial^2 v_3}{\partial x\partial y}$$
$$+(-B_{13}+B_{55})\frac{\partial w_1}{\partial x}+(-2D_{13}+D_{55})\frac{\partial w_2}{\partial x}+A_{55}\frac{\partial w_0}{\partial x}=I_1\frac{\partial^2 u_0}{\partial t^2}$$
$$+I_2\frac{\partial^2 u_1}{\partial t^2}+I_4\frac{\partial^2 u_3}{\partial t^2} \tag{42}$$

$$\delta u_3 : \left(-F_{11}\frac{\partial^2 u_1}{\partial x^2}+3D_{55}u_1-F_{66}\frac{\partial^2 u_1}{\partial y^2}\right)$$
$$+\left(-G_{11}\frac{\partial^2 u_3}{\partial x^2}+9F_{55}u_3-G_{66}\frac{\partial^2 u_3}{\partial y^2}\right)$$
$$-\left(E_{11}\frac{\partial^2 u_0}{\partial x^2}+E_{66}\frac{\partial^2 u_0}{\partial y^2}\right)-(E_{12}+E_{66})\frac{\partial^2 v_0}{\partial x\partial y}-(F_{12}$$
$$+F_{66})\frac{\partial^2 v_1}{\partial x\partial y}-(G_{12}+G_{66})\frac{\partial^2 v_3}{\partial x\partial y}+(-E_{13}+3E_{55})\frac{\partial w_1}{\partial x}$$
$$+(-2F_{13}+3F_{55})\frac{\partial w_2}{\partial x}+3D_{55}\frac{\partial w_0}{\partial x}$$
$$=I_3\frac{\partial^2 u_0}{\partial t^2}+I_4\frac{\partial^2 u_1}{\partial t^2}+I_6\frac{\partial^2 u_3}{\partial t^2} \tag{43}$$

$$\delta v_0 : -(A_{12}+A_{66})\frac{\partial^2 u_0}{\partial x\partial y}-\left(A_{22}\frac{\partial^2 v_0}{\partial y^2}+A_{66}\frac{\partial^2 v_0}{\partial x^2}\right)-(B_{12}$$
$$+B_{66})\frac{\partial^2 u_1}{\partial x\partial y}-(E_{12}+E_{66})\frac{\partial^2 u_3}{\partial x\partial y}-\left(B_{22}\frac{\partial^2 v_1}{\partial y^2}+B_{66}\frac{\partial^2 v_1}{\partial x^2}\right)$$
$$-\left(E_{22}\frac{\partial^2 v_3}{\partial y^2}+E_{66}\frac{\partial^2 v_3}{\partial x^2}\right)-A_{23}\frac{\partial w_1}{\partial y}-2B_{23}\frac{\partial w_2}{\partial y}$$
$$=I_0\frac{\partial^2 v_0}{\partial t^2}+I_1\frac{\partial^2 v_1}{\partial t^2}+I_3\frac{\partial^2 v_3}{\partial t^2} \tag{44}$$

$$\delta v_1 : \left(-F_{22}\frac{\partial^2 v_3}{\partial y^2}+3D_{44}v_3-F_{66}\frac{\partial^2 v_3}{\partial x^2}\right)$$
$$+\left(-D_{22}\frac{\partial^2 v_1}{\partial y^2}+A_{44}v_1-D_{66}\frac{\partial^2 v_1}{\partial x^2}\right)-(B_{12}+B_{66})\frac{\partial^2 u_0}{\partial x\partial y}$$
$$-(D_{12}+D_{66})\frac{\partial^2 u_1}{\partial x\partial y}-(F_{12}+F_{66})\frac{\partial^2 u_3}{\partial x\partial y}$$
$$-\left(B_{22}\frac{\partial^2 v_0}{\partial y^2}+B_{66}\frac{\partial^2 v_0}{\partial x^2}\right)+(-B_{23}+B_{44})\frac{\partial w_1}{\partial y}+(-2D_{23}$$
$$+D_{44})\frac{\partial w_2}{\partial y}+A_{44}\frac{\partial w_0}{\partial y}$$
$$=I_1\frac{\partial^2 v_0}{\partial t^2}+I_2\frac{\partial^2 v_1}{\partial t^2}+I_4\frac{\partial^2 v_3}{\partial t^2} \tag{45}$$

$$\delta v_3 : \left(-F_{22}\frac{\partial^2 v_1}{\partial y^2}+3D_{44}v_1-F_{66}\frac{\partial^2 v_1}{\partial x^2}\right)$$
$$+\left(-G_{22}\frac{\partial^2 v_3}{\partial y^2}+9F_{44}v_3-G_{66}\frac{\partial^2 v_3}{\partial x^2}\right)-(E_{12}+E_{66})\frac{\partial^2 u_0}{\partial x\partial y}$$
$$-(F_{12}+F_{66})\frac{\partial^2 u_1}{\partial x\partial y}-(G_{12}+G_{66})\frac{\partial^2 u_3}{\partial x\partial y}$$
$$-\left(E_{22}\frac{\partial^2 v_0}{\partial y^2}+E_{66}\frac{\partial^2 v_0}{\partial x^2}\right)+(-E_{23}+3E_{44})\frac{\partial w_1}{\partial y}+(-2F_{23}$$
$$+3F_{44})\frac{\partial w_2}{\partial y}+3D_{44}\frac{\partial w_0}{\partial y}$$
$$=I_3\frac{\partial^2 v_0}{\partial t^2}+I_4\frac{\partial^2 v_1}{\partial t^2}+I_6\frac{\partial^2 v_3}{\partial t^2} \tag{46}$$

$$\delta w_0 : -\left(A_{55}\frac{\partial^2 w_0}{\partial x^2} + A_{44}\frac{\partial^2 w_0}{\partial y^2}\right) - \left(B_{55}\frac{\partial^2 w_1}{\partial x^2} + B_{44}\frac{\partial^2 w_1}{\partial y^2}\right) - \left(D_{55}\frac{\partial^2 w_2}{\partial x^2} + D_{44}\frac{\partial^2 w_2}{\partial y^2}\right) - A_{55}\frac{\partial u_1}{\partial x} - A_{44}\frac{\partial v_1}{\partial y} - 3D_{55} \times \frac{\partial u_3}{\partial x} - 3D_{44}\frac{\partial v_3}{\partial y} + \overline{N}_{xx}\frac{\partial^2 w_0}{\partial x^2} + 2\overline{N}_{xy}\frac{\partial^2 w_0}{\partial x \partial y} + \overline{N}_{yy}\frac{\partial^2 w_0}{\partial y^2} = I_0\frac{\partial^2 w_0}{\partial t^2} + I_1\frac{\partial^2 w_1}{\partial t^2} + I_2\frac{\partial^2 w_2}{\partial t^2} + p_z \quad (47)$$

$$\delta w_1 : \left(-E_{55}\frac{\partial^2 w_2}{\partial x^2} + 2B_{33}w_2 - E_{44}\frac{\partial^2 w_2}{\partial y^2 w_2}\right) + \left(-D_{55}\frac{\partial^2 w_1}{\partial x^2} + A_{33}w_1 - D_{44}\frac{\partial^2 w_1}{\partial y^2}\right) + (B_{13} - B_{55})\frac{\partial u_1}{\partial x} + (E_{13} - 3E_{55})\frac{\partial u_3}{\partial x} + (B_{23} - B_{44})\frac{\partial v_1}{\partial y} + (E_{23} - 3E_{44})\frac{\partial v_3}{\partial y} - \left(B_{55}\frac{\partial^2 w_0}{\partial x^2} + B_{44}\frac{\partial^2 w_0}{\partial y^2}\right) + A_{13}\frac{\partial u_0}{\partial x} + A_{23}\frac{\partial v_0}{\partial y} = I_1\frac{\partial^2 w_0}{\partial t^2} + I_2\frac{\partial^2 w_1}{\partial t^2} + I_3\frac{\partial^2 w_2}{\partial t^2} \quad (48)$$

$$\delta w_2 : \left(-E_{55}\frac{\partial^2 w_1}{\partial x^2} + 2B_{33}w_1 - E_{44}\frac{\partial^2 w_1}{\partial y^2}\right) + \left(-F_{55}\frac{\partial^2 w_2}{\partial x^2} + 4D_{33}w_2 - F_{44}\frac{\partial^2 w_2}{\partial y^2}\right) + (2D_{13} - D_{55}) \times \frac{\partial u_1}{\partial x} + (2F_{13} - 3F_{55})\frac{\partial u_3}{\partial x} + (2D_{23} - D_{44})\frac{\partial v_1}{\partial y} + (2F_{23} - 3F_{44})\frac{\partial v_3}{\partial y} - \left(D_{55}\frac{\partial^2 w_0}{\partial x^2} + D_{44}\frac{\partial^2 w_0}{\partial y^2}\right) + 2B_{13}\frac{\partial u_0}{\partial x} + 2B_{23}\frac{\partial v_0}{\partial y} = I_2\frac{\partial^2 w_0}{\partial t^2} + I_3\frac{\partial^2 w_1}{\partial t^2} + I_4\frac{\partial^2 w_2}{\partial t^2} + \left(\frac{h}{2}\right)^2 p_z \quad (49)$$

Being NL the number of mathematical layers across the thickness direction, the stiffness components can be computed as follows.

$$A_{ij} = \sum_{k=1}^{NL} C_{ij}^k (z_{k+1} - z_k); \qquad B_{ij} = \frac{1}{2}\sum_{k=1}^{NL} C_{ij}^k (z_{k+1}^2 - z_k^2) \quad (50)$$

$$D_{ij} = \frac{1}{3}\sum_{k=1}^{NL} C_{ij}^k (z_{k+1}^3 - z_k^3); \qquad E_{ij} = \frac{1}{4}\sum_{k=1}^{NL} C_{ij}^k (z_{k+1}^4 - z_k^4) \quad (51)$$

$$F_{ij} = \frac{1}{5}\sum_{k=1}^{NL} C_{ij}^k (z_{k+1}^5 - z_k^5); \qquad G_{ij} = \frac{1}{7}\sum_{k=1}^{NL} C_{ij}^k (z_{k+1}^7 - z_k^7) \quad (52)$$

The inertia terms are defined by

$$I_i = \frac{1}{i+1}\sum_{k=1}^{NL} \rho^{(k)} (z_{k+1}^{i+1} - z_k^{i+1}) \quad (53)$$

where $\rho^{(k)}$ is the material density, h_k is the thickness, and z_k, z_{k+1} are the lower and upper z coordinate for each layer k.

4.2. Natural boundary conditions

This meshless method based on collocation with radial basis functions needs the imposition of essential (e.g. $w = 0$) and mechanical (e.g. $M_{xx} = 0$) boundary conditions. Assuming a rectangular plate (for the sake of simplicity) Eq. (29) are expressed as follows.

Given the number of degrees of freedom, at each boundary point at edges $x = min$ or $x = max$ we impose:

$$M_{xxu0} = 2B_{13}w_2 + A_{13}w_1 + A_{11}\frac{\partial u_0}{\partial x} + A_{12}\frac{\partial v_0}{\partial y} + B_{11}\frac{\partial u_1}{\partial x} + E_{11} \times \frac{\partial u_3}{\partial x} + B_{12}\frac{\partial v_1}{\partial y} + E_{12}\frac{\partial v_3}{\partial y} \quad (54)$$

$$M_{xxu1} = B_{13}w_1 + 2D_{13}w_2 + B_{11}\frac{\partial u_0}{\partial x} + D_{11}\frac{\partial u_1}{\partial x} + F_{11}\frac{\partial u_3}{\partial x} + B_{12} \times \frac{\partial v_0}{\partial y} + D_{12}\frac{\partial v_1}{\partial y} + F_{12}\frac{\partial v_3}{\partial y} \quad (55)$$

$$M_{xxu3} = E_{13}w_1 + 2F_{13}w_2 + E_{11}\frac{\partial u_0}{\partial x} + F_{11}\frac{\partial u_1}{\partial x} + G_{11}\frac{\partial u_3}{\partial x} + E_{12} \times \frac{\partial v_0}{\partial y} + F_{12}\frac{\partial v_1}{\partial y} + G_{12}\frac{\partial v_3}{\partial y} \quad (56)$$

$$M_{xxv0} = A_{66}\frac{\partial u_0}{\partial y} + A_{66}\frac{\partial v_0}{\partial x} + B_{66}\frac{\partial u_1}{\partial y} + E_{66}\frac{\partial u_3}{\partial y} + B_{66}\frac{\partial v_1}{\partial x} + E_{66} \times \frac{\partial v_3}{\partial x} \quad (57)$$

$$M_{xxv1} = B_{66}\frac{\partial u_0}{\partial y} + D_{66}\frac{\partial u_1}{\partial y} + F_{66}\frac{\partial u_3}{\partial y} + B_{66}\frac{\partial v_0}{\partial x} + D_{66}\frac{\partial v_1}{\partial x} + F_{66}\frac{\partial v_3}{\partial x} \quad (58)$$

$$M_{xxv3} = E_{66}\frac{\partial u_0}{\partial y} + F_{66}\frac{\partial u_1}{\partial y} + G_{66}\frac{\partial u_3}{\partial y} + E_{66}\frac{\partial v_0}{\partial x} + F_{66}\frac{\partial v_1}{\partial x} + G_{66} \times \frac{\partial v_3}{\partial x} \quad (59)$$

$$M_{xxw0} = 3D_{55}u_3 + A_{55}u_1 + A_{55}\frac{\partial w_0}{\partial x} + B_{55}\frac{\partial w_1}{\partial x} + D_{55}\frac{\partial w_2}{\partial x} \quad (60)$$

$$M_{xxw1} = B_{55}u_1 + 3E_{55}u_3 + B_{55}\frac{\partial w_0}{\partial x} + D_{55}\frac{\partial w_1}{\partial x} + E_{55}\frac{\partial w_2}{\partial x} \quad (61)$$

$$M_{xxw2} = D_{55}u_1 + 3F_{55}u_3 + D_{55}\frac{\partial w_0}{\partial x} + E_{55}\frac{\partial w_1}{\partial x} + F_{55}\frac{\partial w_2}{\partial x} \quad (62)$$

Similarly, given the number of degrees of freedom, at each boundary point at edges $y = min$ or $y = max$ we impose:

$$M_{yyu0} = A_{66}\frac{\partial u_0}{\partial y} + A_{66}\frac{\partial v_0}{\partial x} + B_{66}\frac{\partial u_1}{\partial y} + E_{66}\frac{\partial u_3}{\partial y} + B_{66}\frac{\partial v_1}{\partial x} + E_{66} \times \frac{\partial v_3}{\partial x} \quad (63)$$

$$M_{yyu1} = B_{66}\frac{\partial u_0}{\partial y} + D_{66}\frac{\partial u_1}{\partial y} + F_{66}\frac{\partial u_3}{\partial y} + B_{66}\frac{\partial v_0}{\partial x} + D_{66}\frac{\partial v_1}{\partial x} + F_{66}\frac{\partial v_3}{\partial x} \quad (64)$$

$$M_{yyu3} = E_{66}\frac{\partial u_0}{\partial y} + F_{66}\frac{\partial u_1}{\partial y} + G_{66}\frac{\partial u_3}{\partial y} + E_{66}\frac{\partial v_0}{\partial x} + F_{66}\frac{\partial v_1}{\partial x} + G_{66} \times \frac{\partial v_3}{\partial x} \quad (65)$$

$$M_{yyv0} = A_{12}\frac{\partial u_0}{\partial x} + A_{22}\frac{\partial v_0}{\partial y} + B_{12}\frac{\partial u_1}{\partial x} + E_{12}\frac{\partial u_3}{\partial x} + B_{22}\frac{\partial v_1}{\partial y} + E_{22} \times \frac{\partial v_3}{\partial y} \quad (66)$$

$$M_{yyv1} = B_{12}\frac{\partial u_0}{\partial x} + D_{12}\frac{\partial u_1}{\partial x} + F_{12}\frac{\partial u_3}{\partial x} + B_{22}\frac{\partial v_0}{\partial y} + D_{22}\frac{\partial v_1}{\partial y} + F_{22}\frac{\partial v_3}{\partial y} \quad (67)$$

$$M_{yyv3} = E_{12}\frac{\partial u_0}{\partial x} + F_{12}\frac{\partial u_1}{\partial x} + G_{12}\frac{\partial u_3}{\partial x} + E_{22}\frac{\partial v_0}{\partial y} + F_{22}\frac{\partial v_1}{\partial y} + G_{22}\frac{\partial v_3}{\partial y} \quad (68)$$

$$M_{yyw0} = 3D_{44}v_3 + A_{44}v_1 + A_{44}\frac{\partial w_0}{\partial y} + B_{44}\frac{\partial w_1}{\partial y} + D_{44}\frac{\partial w_2}{\partial y} \tag{69}$$

$$M_{yyw1} = B_{44}v_1 + 3E_{44}v_3 + B_{44}\frac{\partial w_0}{\partial y} + D_{44}\frac{\partial w_1}{\partial y} + E_{44}\frac{\partial w_2}{\partial y} \tag{70}$$

$$M_{yyw2} = D_{44}v_1 + 3F_{44}v_3 + D_{44}\frac{\partial w_0}{\partial y} + E_{44}\frac{\partial w_1}{\partial y} + F_{44}\frac{\partial w_2}{\partial y} \tag{71}$$

with A_{ij}, B_{ij}, D_{ij}, E_{ij}, F_{ij}, G_{ij} as in (52).

5. The radial basis function method

The governing equations are interpolated by radial basis function method. This meshless method was first used by Hardy [91] in the early 1970s for the interpolation of geographical data. Kansa [92,93] introduced in 1990 the concept of solving partial differential equations (PDE) by an unsymmetric RBF collocation method based upon the multiquadric interpolation functions. Nowadays this technique is well known for solving systems of partial differential equations with excellent accuracy [94–97]. For the sake of completeness we present in the following the basics of collocation with radial basis functions for static, vibrations, and buckling problems.

5.1. Radial basis functions approximations

The radial basis function (ϕ) approximation of a function (u) is given by

$$\tilde{\mathbf{u}}(\mathbf{x}) = \sum_{i=1}^{N} \alpha_i \phi(\|x - y_i\|_2), \mathbf{x} \in \mathbb{R}^n \tag{72}$$

where y_i, $i = 1, \ldots, N$ is a finite set of distinct points (centers) in $\mathbb{R}^n$. Examples of the many RBFs that can be used are

$$\phi(r) = r^3, \quad \text{cubic} \tag{73}$$

$$\phi(r) = e^{-(cr)^2}, \quad \text{Gaussian} \tag{74}$$

$$\phi(r) = \sqrt{c^2 + r^2}, \quad \text{Multiquadric} \tag{75}$$

where the Euclidean distance r is real and non-negative and c is a positive user defined shape parameter.

Considering N distinct interpolations, and knowing $u(x_j)$,$j = 1,2,\ldots,N$, we find α_i by the solution of a $N \times N$ linear system

$$\mathbf{A}\boldsymbol{\alpha} = \mathbf{u} \tag{76}$$

where $\mathbf{A} = [\phi(\|x - y_i\|_2)]_{N\times N}$, $\boldsymbol{\alpha} = [\alpha_1, \alpha_2, \ldots, \alpha_N]^T$ and $\mathbf{u} = [u(x_1), u(x_2), \ldots, u(x_N)]^T$.

5.2. The static problem

Consider a linear elliptic partial differential operator $\mathcal{L}$ acting in a bounded region Ω in $\mathbb{R}^n$ and another operator $\mathcal{L}_B$ acting on a boundary $\partial\Omega$. We seek the computation of displacements (u) from the global system of equations

$$\mathcal{L}\mathbf{u} = \mathbf{f} \text{ in } \Omega; \qquad \mathcal{L}_B\mathbf{u} = \mathbf{g} \text{on} \partial\Omega \tag{77}$$

The external forces applied on the plate and the boundary conditions applied along the perimeter of the plate, respectively, are at the right-hand side of (77). The PDE problem defined in (77) will be replaced by a finite problem, defined by an algebraic system of equations, after the radial basis expansions.

5.3. Solution of the static problem

The solution of a static problem by radial basis functions considers N_I nodes in the domain and N_B nodes on the boundary, with a total number of nodes $N = N_I + N_B$. We denote the sampling points by $x_i \in \Omega$, $i = 1, \ldots, N_I$ and $x_i \in \partial\Omega$, $i = N_I + 1, \ldots, N$. At the points in the domain we solve the following system of equations

$$\sum_{i=1}^{N} \alpha_i \mathcal{L}\phi(\|x - y_i\|_2) = \mathbf{f}(x_j), \quad j = 1, 2, \ldots, N_I \tag{78}$$

or

$$\mathcal{L}^I \boldsymbol{\alpha} = \mathbf{F} \tag{79}$$

where

$$\mathcal{L}^I = [\mathcal{L}\phi(\|x - y_i\|_2)]_{N_I \times N} \tag{80}$$

At the points on the boundary, we impose boundary conditions as

$$\sum_{i=1}^{N} \alpha_i \mathcal{L}_B\phi(\|x - y_i\|_2) = \mathbf{g}(x_j), j = N_I + 1, \ldots, N \tag{81}$$

or

$$\mathbf{B}\boldsymbol{\alpha} = \mathbf{G} \tag{82}$$

where

$$\mathbf{B} = \mathcal{L}_B\phi[(\|x_{N_I+1} - y_j\|_2)]_{N_B\times N}$$

Therefore, we can write a finite-dimensional static problem as

$$\begin{bmatrix} \mathcal{L}^I \\ \mathbf{B} \end{bmatrix} \boldsymbol{\alpha} = \begin{bmatrix} \mathbf{F} \\ \mathbf{G} \end{bmatrix} \tag{83}$$

By inverting the system (83), we obtain the vector $\boldsymbol{\alpha}$. We then obtain the solution $\boldsymbol{u}$ using the interpolation Eq. (72).

5.4. The eigenproblem

The eigenproblem looks for eigenvalues (λ) and eigenvectors ($\mathbf{u}$) that satisfy

$$\mathcal{L}\mathbf{u} + \lambda\mathbf{u} = 0 \text{ in } \Omega; \qquad \mathcal{L}_B\mathbf{u} = 0 \text{ on } \partial\Omega \tag{84}$$

As in the static problem, the eigenproblem defined in (84) is replaced by a finite-dimensional eigenvalue problem, based on RBF approximations.

5.5. Solution of the eigenproblem

We consider N_I nodes in the interior of the domain and N_B nodes on the boundary, with $N = N_I + N_B$. We denote interpolation points by $x_i \in \Omega$, $i = 1, \ldots, N_I$ and $x_i \in \partial\Omega$, $i = N_I + 1, \ldots, N$. At the points in the domain, we define the eigenproblem as

$$\sum_{i=1}^{N} \alpha_i \mathcal{L}\phi(\|x - y_i\|_2) = \lambda\tilde{\mathbf{u}}(x_j), \quad j = 1, 2, \ldots, N_I \tag{85}$$

or

$$\mathcal{L}^I \boldsymbol{\alpha} = \lambda\tilde{\mathbf{u}}^I \tag{86}$$

where

$$\mathcal{L}^I = [\mathcal{L}\phi(\|x - y_i\|_2)]_{N_I \times N} \tag{87}$$

At the points on the boundary, we enforce the boundary conditions as

$$\sum_{i=1}^{N} \alpha_i \mathcal{L}_B\phi(\|x - y_i\|_2) = 0, \quad j = N_I + 1, \ldots, N \tag{88}$$

or

Please cite this article in press as: Neves AMA et al. Static, free vibration and buckling analysis of isotropic and sandwich functionally graded plates using a quasi-3D higher-order shear deformation theory and a meshless technique. Composites: Part B (2012), doi:10.1016/j.compositesb.2012.01.089

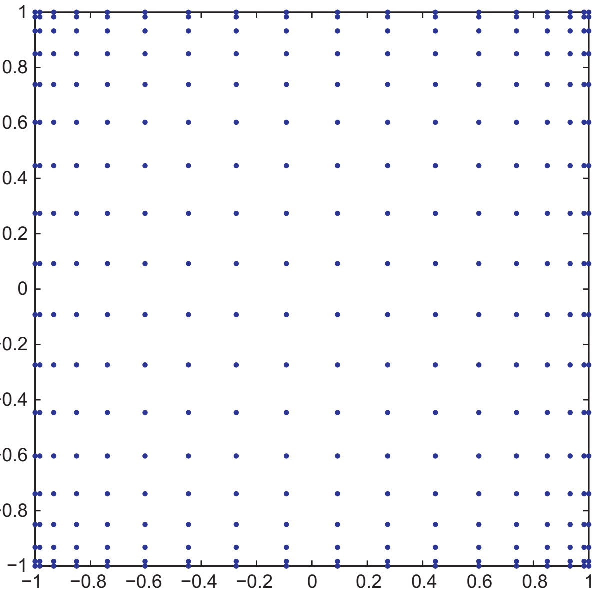

Fig. 6. Chebyshev grid with $N = 17$.

$$\mathbf{B}\boldsymbol{\alpha} = 0 \tag{89}$$

Eqs. (86) and (89) can now be solved as a generalized eigenvalue problem

$$\begin{bmatrix} \mathcal{L}^I \\ \mathbf{B} \end{bmatrix} \boldsymbol{\alpha} = \lambda \begin{bmatrix} \mathbf{A}^I \\ \mathbf{0} \end{bmatrix} \boldsymbol{\alpha} \tag{90}$$

where

$$\mathbf{A}^I = \phi[(\|x_{N_I} - y_j\|_2)]_{N_I \times N}$$

5.6. Discretization of the governing equations and boundary conditions

The radial basis collocation method follows a simple implementation procedure. Taking Eq. (83), we compute

$$\boldsymbol{\alpha} = \begin{bmatrix} L^I \\ \mathbf{B} \end{bmatrix}^{-1} \begin{bmatrix} \mathbf{F} \\ \mathbf{G} \end{bmatrix} \tag{91}$$

This $\boldsymbol{\alpha}$ vector is then used to obtain solution $\tilde{\mathbf{u}}$, by using (72). If derivatives of $\tilde{\mathbf{u}}$ are needed, such derivatives are computed as

$$\frac{\partial \tilde{\mathbf{u}}}{\partial x} = \sum_{j=1}^{N} \alpha_j \frac{\partial \phi_j}{\partial x}; \qquad \frac{\partial^2 \tilde{\mathbf{u}}}{\partial x^2} = \sum_{j=1}^{N} \alpha_j \frac{\partial^2 \phi_j}{\partial x^2}, \text{etc} \tag{92}$$

In the present collocation approach, we need to impose essential and natural boundary conditions. Consider, for example, the condition $w_0 = 0$, on a simply supported or clamped edge. We enforce the conditions by interpolating as

$$w_0 = 0 \rightarrow \sum_{j=1}^{N} \alpha_j^{W_0} \phi_j = 0 \tag{93}$$

Other boundary conditions are interpolated in a similar way.

Table 1
w convergence study for the bending analysis of plate A using higher-order plate theory, $p = 1$, and $a/h = 10$.

Grid	13^2	17^2	21^2
w	0.5868	0.5868	0.5868

Table 2
σ_{xx} convergence study for the bending analysis of plate A using higher-order plate theory, $p = 1$, and $a/h = 10$.

Grid	13^2	17^2	21^2
σ_{xx}	1.4911	1.4917	1.4917

5.7. Free vibrations problems

For free vibration problems we set the external force to zero, and assume harmonic solution in terms of displacements u_0, u_1, u_3, v_0, v_1, v_3, w_0, w_1, w_2 as

$$\begin{aligned} &u_0 = U_0(w,y)e^{i\omega t}; \quad u_1 = U_1(w,y)e^{i\omega t}; \quad u_3 = U_3(w,y)e^{i\omega t}; \\ &v_0 = V_0(w,y)e^{i\omega t}; \quad v_1 = V_1(w,y)e^{i\omega t}; \quad v_3 = V_3(w,y)e^{i\omega t}; \\ &w_0 = W_0(w,y)e^{i\omega t}; \quad w_1 = W_1(w,y)e^{i\omega t}; \quad w_2 = W_2(w,y)e^{i\omega t} \end{aligned} \tag{94}$$

where ω is the frequency of natural vibration. Substituting the harmonic expansion into Eq. (90) in terms of the amplitudes U_0, U_1, U_3, V_0, V_1, V_3, W_0, W_1, W_2, we may obtain the natural frequencies and vibration modes for the plate problem, by solving the eigenproblem

$$[\mathcal{L} - \omega^2 \mathcal{G}]\mathbf{X} = \mathbf{0} \tag{95}$$

where $\mathcal{L}$ collects all stiffness terms and $\mathcal{G}$ collects all terms related to the inertial terms. In (95) $\mathbf{X}$ are the modes of vibration associated with the natural frequencies defined as ω.

5.8. Buckling problems

The eigenproblem associated to the governing equations is defined as

$$[\mathcal{L} - \lambda \mathcal{G}]\mathbf{X} = \mathbf{0} \tag{96}$$

where $\mathcal{L}$ collects all stiffness terms and $\mathcal{G}$ collects all terms related to the in-plane forces. In (96) $\mathbf{X}$ are the buckling modes associated with the buckling loads defined as λ.

6. Numerical examples

In the next examples the higher-order plate theory presented before and collocation with RBFs are used for the analysis of simply supported functionally graded square plates. It should be noted that for the $\epsilon_{zz} = 0$ case, we consider $w = w_0$ instead of (6).

All examples use the Wendland RBF function [98] defined as

$$\phi(r) = (1 - cr)^8 + (32(cr)^3 + 25(cr)^2 + 8cr + 1) \tag{97}$$

The shape parameter (c) is obtained by an optimization procedure as detailed in Ferreira and Fasshauer [99]. The interpolation points are Chebyshev $\mathbb{R}^2$ points. For a given number of nodes per side (N) they are generated by MATLAB code as:

```
x = cos(pi*(0:N)/N)';   y = x;
```

A 17^2 points Chebyshev grid is illustrated in Fig. 6.

91 mathematical layers were considered in order to model the continuous variation of properties across the thickness direction. A significant number of mathematical layers is needed to ensure correct computation of material properties at each thickness position. The Young's modulus of each layer, $E^k(z)$, are computed considering a simple law-of-mixtures (33) or the Mori–Tanaka procedure (36). Poisson's ratio is considered constant for both materials $\nu_m = \nu_c = \nu = 0.3$.

Please cite this article in press as: Neves AMA et al. Static, free vibration and buckling analysis of isotropic and sandwich functionally graded plates using a quasi-3D higher-order shear deformation theory and a meshless technique. Composites: Part B (2012), doi:10.1016/j.compositesb.2012.01.089

Table 3
A-type plate in bending. Effect of transverse normal strain ϵ_{zz} on σ_{xx} and deflection under present higher-order theory and using 17^2 points.

p		ϵ_{zz}	$\bar{\sigma}_{xx}(h/3)$			$\bar{u}_z(0)$		
	a/h		4	10	100	4	10	100
0	Present	0	0.5151	1.3124	13.161	0.3786	0.2961	0.2803
	Present	≠0	0.5278	1.3176	13.161	0.3665	0.2942	0.2803
0.5	Present	0	0.5736	1.4629	14.672	0.5699	0.4579	0.4365
	Present	≠0	0.5860	1.4680	14.673	0.5493	0.4548	0.4365
1	Ref. [59]	≠0	0.6221	1.5064	14.969	0.7171	0.5875	0.5625
	CLPT	0	0.8060	2.0150	20.150	0.5623	0.5623	0.5623
	FSDT (k = 5/6)	0	0.8060	2.0150	20.150	0.7291	0.5889	0.5625
	GSDT [19]	0	1.4894			0.5889		
	Ref. [53] N = 4	0	0.7856	2.0068	20.149	0.7289	0.5890	0.5625
	Ref. [53] N = 4	≠0	0.6221	1.5064	14.969	0.7171	0.5875	0.5625
	Ref. [68]	≠0	0.5925	1.4945	14.969	0.6997	0.5845	0.5624
	Present	0	0.5806	1.4874	14.944	0.7308	0.5913	0.5648
	Present	≠0	0.5911	1.4917	14.945	0.7020	0.5868	0.5647
4	Ref. [59]	≠0	0.4877	1.1971	11.923	1.1585	0.8821	0.8286
	CLPT	0	0.6420	1.6049	16.049	0.8281	0.8281	0.8281
	FSDT (k = 5/6)	0	0.6420	1.6049	16.049	1.1125	0.8736	0.828
	GSDT [19]	0	1.1783			0.8651		
	Ref. [53] N = 4	0	0.5986	1.5874	16.047	1.1673	0.8828	0.8286
	Ref. [53] N = 4	≠0	0.4877	1.1971	11.923	1.1585	0.8821	0.8286
	Ref. [68]	≠0	0.4404	1.1783	11.932	1.1178	0.8750	0.8286
	Present	0	0.4338	1.1592	11.737	1.1552	0.8770	0.8241
	Present	≠0	0.4330	1.1588	11.737	1.1108	0.8700	0.8240
10	Ref. [59]	≠0	0.3695	0.8965	8.9077	1.3745	1.0072	0.9361
	CLPT	0	0.4796	1.1990	11.990	0.9354	0.9354	0.9354
	FSDT (k = 5/6)	0	0.4796	1.1990	11.990	1.3178	0.9966	0.9360
	GSDT [19]	0	0.8775			1.0089		
	Ref. [53] N = 4	0	0.4345	1.1807	11.989	1.3925	1.0090	0.9361
	Ref. [53] N = 4	≠0	0.1478	0.8965	8.9077	1.3745	1.0072	0.9361
	Ref. [68]	≠0	0.3227	1.1783	11.932	1.3490	0.8750	0.8286
	Present	0	0.3112	0.8468	8.6011	1.3760	0.9952	0.9228
	Present	≠0	0.3097	0.8462	8.6010	1.3334	0.9888	0.9227

6.1. Plates in bending

In the following static examples, we consider that the plate is subjected to a bi-sinusoidal transverse mechanical load of amplitude load $p_z = \bar{p}_z sin(\frac{\pi x}{a}) sin(\frac{\pi y}{a})$ applied at the top of the plate with $\bar{p}_z = 1$. It should be noted that the load is applied at the top surface ($z = h/2$).

6.1.1. Isotropic FGM square plate

In this example, an isotropic FGM square plate of type *A* is considered. The plate is graded from aluminum E_m = 70 GPa at the bottom to alumina E_c = 380 GPa at the top. The law-of-mixtures was used for computing the Young's modulus at each layer.

The transverse displacement, the normal stresses and the in-plane and transverse shear stresses are presented in normalized form as

$$\bar{u}_z = \frac{10h^3 E_c}{a^4 \bar{p}_z} u_z, \quad \bar{\sigma}_{xx} = \frac{h}{a\bar{p}_z}\sigma_{xx}, \quad \bar{\sigma}_{xz} = \frac{h}{a\bar{p}_z}\sigma_{xz}, \quad \bar{\sigma}_{zz} = \frac{\sigma_{zz}}{\bar{p}_z} \tag{98}$$

An initial convergence study was performed for $\sigma_{xx}(\frac{h}{3})$ and transverse displacement $w(0)$ at the center of the plate, considering $p = 1$, $a/h = 10$, and Chebyshev grids of 13^2, 17^2, and 21^2 points. Results are presented in Tables 1 and 2. As seen in these tables, it is sufficient to use 17^2 grid.

In Table 3 we present results for σ_{xx} and transverse displacement for various exponents p of the power-law (1) considering a 17^2 points grid. The considered side-to-thickness ratios (a/h) are 4, 10 and 100, which means thickness h equals 0.25, 0.1 and 0.01, respectively. Results are compared with the Classical Plate Theory (CLPT), the first-order shear deformation theory (FSDT) with a correction factor k = 5/6, and those from Zenkour's generalized shear deformation theory [19], considering ϵ_{zz} = 0, and those from Carrera et al. [59,53], and Neves et al. [68], accounting for ϵ_{zz}.

The results from present higher-order plate theory considering $\epsilon_{zz} \neq 0$ are in good agreement with those from Refs. [59,53,68] who also considers $\epsilon_{zz} \neq 0$. The present theory allows to conclude that the values of σ_{xx} and transverse displacement considering ϵ_{zz} = 0 are higher than those considering $\epsilon_{zz} \neq 0$. These differences decrease as the thickness of the plate decreases which is not surprising as thicker plates can stretch more in the thickness direction.

In Figs. 7 and 8 we present the evolution of the displacement and stresses across the thickness direction according to present shear deformation theory for various values of the exponent p, and side to thickness ratio a/h = 4, using a 19^2 grid.

It can be concluded that the present higher-order ($\epsilon_{zz} \neq 0$) theory with radial basis function collocation provides excellent solution for FGM plates.

6.1.2. Sandwich with FGM core

In this example we analyze the bending of a square sandwich *B*-type plate with thickness h. The bottom skin is aluminum (E_m = 70 GPa) with thickness $h_b = 0.1h$ and the top skin is alumina (E_c = 380 GPa) with thickness $h_t = 0.1h$. The core is in FGM with volume fraction of the ceramic according to (2). The functional relationship for Young's modulus $E^k(z)$ in the thickness direction z is obtained by the rule of mixtures as in (33).

The transverse displacement and the normal stresses are presented in normalized form as

$$\bar{u}_z = \frac{10h^3 E_c}{a^4 \bar{p}_z} u_z\left(\frac{a}{2}, \frac{b}{2}\right), \quad \bar{\sigma}_{xx} = \frac{h}{a\bar{p}_z}\sigma_{xx}\left(\frac{a}{2}, \frac{b}{2}\right)$$
$$\bar{\sigma}_{yy} = \frac{h}{a\bar{p}_z}\sigma_{yy}\left(\frac{a}{2}, \frac{b}{2}\right), \quad \bar{\sigma}_{zz} = \frac{\sigma_{zz}}{\bar{p}_z}\left(\frac{a}{2}, \frac{b}{2}\right) \tag{99}$$

Please cite this article in press as: Neves AMA et al. Static, free vibration and buckling analysis of isotropic and sandwich functionally graded plates using a quasi-3D higher-order shear deformation theory and a meshless technique. Composites: Part B (2012), doi:10.1016/j.compositesb.2012.01.089

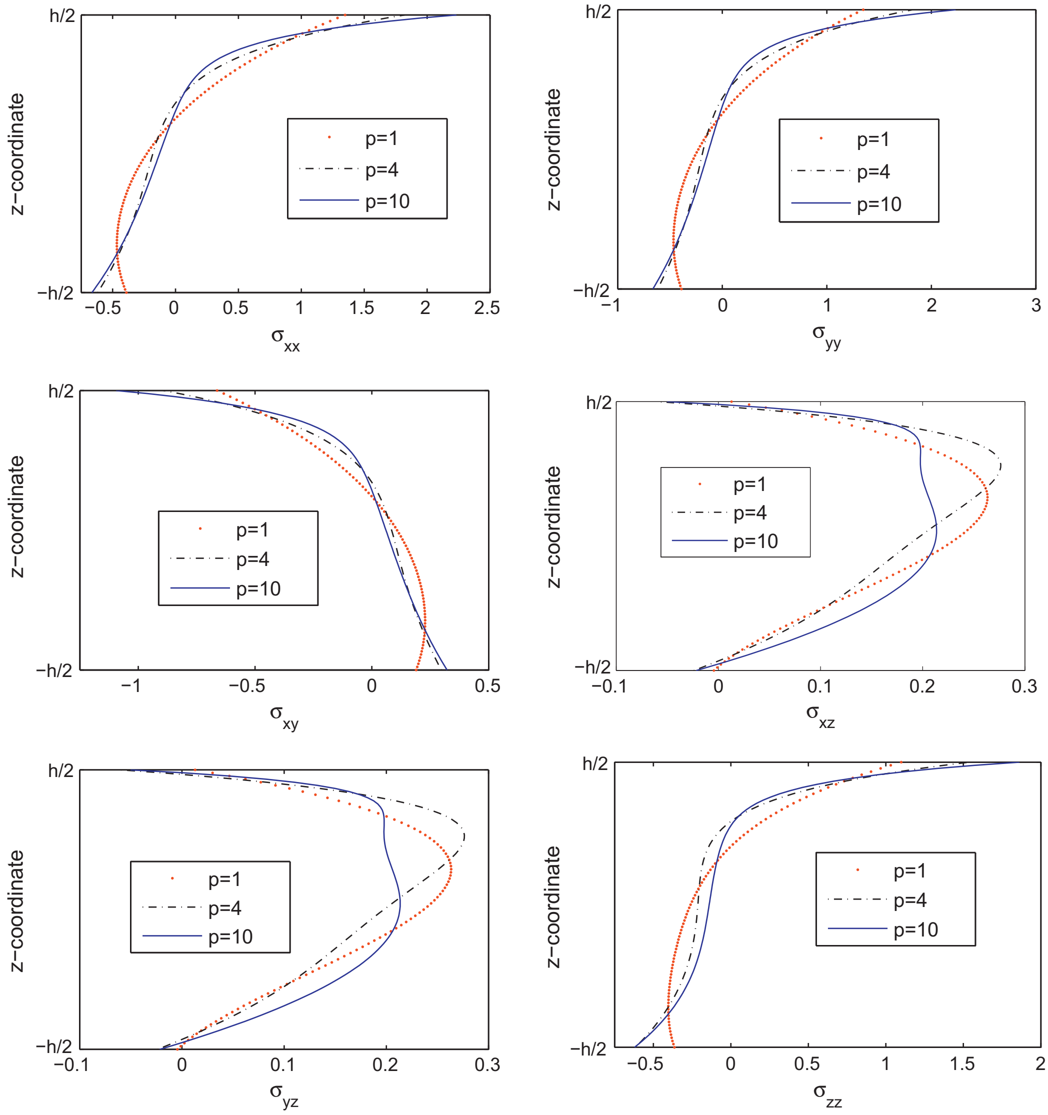

Fig. 7. *A*-type square plate subjected to sinusoidal load at the top, with $a/h = 4$. Dimensionless stresses ($\bar{\sigma}$) through the thickness direction according to present higher-order theory for different values of *p*.

The transverse shear stresses are normalized according to

$$\bar{\sigma}_{xy} = \frac{h}{a\bar{p}_z}\sigma_{xy}(0,0), \quad \bar{\sigma}_{xz} = \frac{h}{a\bar{p}_z}\sigma_{xz}\left(0,\frac{b}{2}\right), \quad \bar{\sigma}_{yz} = \frac{h}{a\bar{p}_z}\sigma_{yz}\left(\frac{a}{2},0\right) \qquad (100)$$

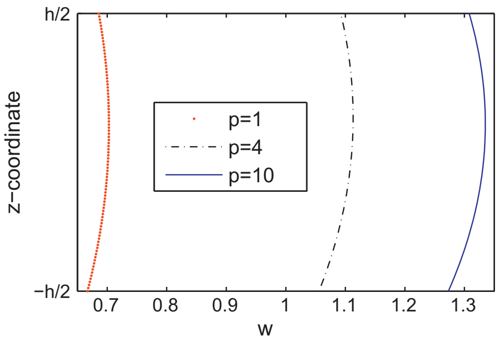

Fig. 8. *A*-type square plate subjected to sinusoidal load at the top, with $a/h = 4$. Dimensionless displacement ($\bar{w}$) through the thickness direction according to present higher-order theory for different values of *p*.

An initial convergence study was performed for $\sigma_{xz}(\frac{h}{6})$ and transverse displacement $w(0)$ considering $p = 4$, $a/h = 100$, and Chebyshev grids of 13^2, 17^2, 19^2, and 21^2 points. Results are presented in Tables 4 and 5. We consider that a 19^2 grid should be used inthe following computation.

In Table 6 we present the values of σ_{xz} and out-of-plane displacement for various values of exponent *p* of the material

Table 4
w convergence study for the bending analysis of *B*-type plate using higher-order plate theory, $p = 4$, and $a/h = 100$.

Grid	13^2	17^2	19^2	21^2
w	0.7749	0.7782	0.7784	0.7785

Table 5
σ_{xz} convergence study for the bending analysis of *B*-type plate using higher-order plate theory, $p = 4$, and $a/h = 100$.

Grid	13^2	17^2	19^2	21^2
σ_{xz}	0.2696	0.2749	0.2753	0.2753

Please cite this article in press as: Neves AMA et al. Static, free vibration and buckling analysis of isotropic and sandwich functionally graded plates using a quasi-3D higher-order shear deformation theory and a meshless technique. Composites: Part B (2012), doi:10.1016/j.compositesb.2012.01.089

Table 6
Square *B*-type plate in bending. Effect of transverse normal strain ϵ_{zz} on σ_{xz} and w according to present higher-order plate theory, using 19^2 points.

p		ϵ_{zz}	$\bar{\sigma}_{xz}(h/6)$			$\bar{u}_z(0)$		
	a/h		4	10	100	4	10	100
0	Present	0	0.2193	0.2202	0.2202	0.4612	0.3736	0.3568
	Present	≠0	0.2208	0.2227	0.2228	0.4447	0.3711	0.3568
0.5	Present	0	0.2511	0.2522	0.2522	0.6422	0.5277	0.5058
	Present	≠0	0.2546	0.2581	0.2585	0.6168	0.5238	0.5058
1	Ref. [58]	≠0	0.2613	0.2605	0.2603	0.7628	0.6324	0.6072
	CLPT	0	0.0000	0.0000	0.0000	0.6070	0.6070	0.6070
	FSDT (k = 5/6)	0	0.2458	0.2458	0.2458	0.7738	0.6337	0.6073
	Ref. [53] N = 4	0	0.2596	0.2593	0.2593	0.7735	0.6337	0.6072
	Ref. [53] N = 4	≠0	0.2604	0.2594	0.2593	0.7628	0.6324	0.6072
	Ref. [68]	0	0.2703	0.2718	0.2720	0.7744	0.6356	0.6092
	Ref. [68]	≠0	0.2742	0.2788	0.2793	0.7416	0.6305	0.6092
	Present	0	0.2706	0.2720	0.2721	0.7746	0.6357	0.6092
	Present	≠0	0.2745	0.2789	0.2795	0.7417	0.6305	0.6092
4	Ref. [58]	≠0	0.2429	0.2431	0.2432	1.0934	0.8321	0.7797
	CLPT	0	0.0000	0.0000	0.0000	0.7792	0.7792	0.7792
	FSDT (k = 5/6)	0	0.1877	0.1877	0.1877	1.0285	0.8191	0.7796
	Ref. [53] N = 4	0	0.2400	0.2398	0.2398	1.0977	0.8308	0.7797
	Ref. [53] N = 4	≠0	0.2400	0.2398	0.2398	1.0930	0.8307	0.7797
	Ref. [68]	0	0.2699	0.2726	0.2728	1.0847	0.8276	0.7785
	Ref. [68]	≠0	0.2723	0.2778	0.2785	1.0391	0.8202	0.7784
	Present	0	0.2671	0.2695	0.2696	1.0826	0.8272	0.7785
	Present	≠0	0.2696	0.2747	0.2753	1.0371	0.8199	0.7784
10	Ref. [58]	≠0	0.2150	0.2174	0.2179	1.2232	0.8753	0.8077
	CLPT	0	0.0000	0.0000	0.0000	0.8070	0.8070	0.8070
	FSDT (k = 5/6)	0	0.1234	0.1234	0.1234	1.1109	0.8556	0.8075
	Ref. [53] N = 4	0	0.1935	0.1944	0.1946	1.2240	0.8743	0.8077
	Ref. [53] N = 4	≠0	0.1932	0.1944	0.1946	1.2172	0.8740	0.8077
	Ref. [68]	0	0.1998	0.2021	0.2022	1.2212	0.8718	0.8050
	Ref. [68]	≠0	0.2016	0.2059	0.2064	1.1780	0.8650	0.8050
	Present	0	0.1996	0.2018	0.2019	1.2183	0.8712	0.8050
	Present	≠0	0.1995	0.2034	0.2039	1.1752	0.8645	0.8050

power-law (p = 0, 0.5, 1, 4, 10) and various thickness to side ratios (a/h = 4, 10, 100) according to the present higher-order theory considering zero and non-zero ϵ_{zz} strain using 19^2 points. Results are tabulated and compared with available references.

In Figs. 9 and 10 we present the evolution of the displacement and stresses across the thickness direction according to present shear deformation theory for various values of the exponent p of a plate with side to thickness ratio a/h = 100, using a 19^2 grid.

It can be concluded that the present approach is in very good agreement with similar theories in the literature.

6.2. Free vibration of plates

In this example we study the free vibration of a simply supported isotropic FGM square plate ($a = b = 1$) of type *A*. The plate is graded from aluminum (bottom) to zirconia (top). E_m = 70 GPa, ρ_m = 2702 kg/m^3, E_c = 200 GPa, and ρ_c = 5700 kg/m^3 are the corresponding properties of the metal and zirconia, respectively.

We consider the Mori–Tanaka homogeneization scheme (36), as in Vel and Batra [28] (here considered to be the exact solution), and as in Qian et al. [17] and Neves et al. [68].

The frequency w has been non-dimensionalized as follows:

$$\bar{w} = wh\sqrt{\rho_m/E_m} \tag{101}$$

In Table 7 we present the results obtained with the theories considered and different values of p for a side to thickness ratio a/h = 5.

The first 10 natural frequencies obtained with present higher-order shear deformation theory are listed in Table 8 (a/h = 20) and Table 9 (a/h = 10) for p = 1.

In Fig. 11 the first 4 frequencies of a simply supported isotropic functionally graded (Al/ZrO2) square plate, with p = 1, a 21^2 grid, using present higher-order shear deformation theory and a side to thickness ratio a/h = 20 are presented.

Excellent correlation is obtained with exact theories when $\epsilon_{zz} \neq 0$ is considered. Convergence solutions are obtained for all cases.

6.3. Buckling loads of plates

In the next examples the higher-order plate theory and collocation with RBFs are used for the buckling analysis of simply supported functionally graded sandwich square plates ($a = b$) of type *C* with side-to-thickness ratio a/h = 10. The uni-and bi-axial critical buckling loads are analised.

The material properties are $E_m = 70E_0$ (aluminum) for the metal and $E_c = 380E_0$ (alumina) for the ceramic being E_0 = 1GPa. The law-of-mixtures (33) was used for the computation of Young's modulus for each layer. The non-dimensional parameter used is

$$\bar{P} = \frac{Pa^2}{100h^3E_0}.$$

An initial convergence study with the higher-order theory was conducted for each buckling load type considerind grids of 13^2, 17^2, and 21^2 points. The uni-axial case is presented in Table 10 for the 2-2-1 sandwich with p = 5 and the bi-axial case is presented in Table 11 for the 1-2-1 sandwich with p = 1. Further results are obtained by considering a grid of 17^2 points, which seems acceptable by the convergence study.

The critical buckling loads obtained from the present approach with $\epsilon_{zz} \neq 0$ and $\epsilon_{zz} = 0$ are tabulated in Tables 12 and 13 for various power-law exponents p and thickness ratios. Both tables include results obtained from classical plate theory (CLPT), first-order shear

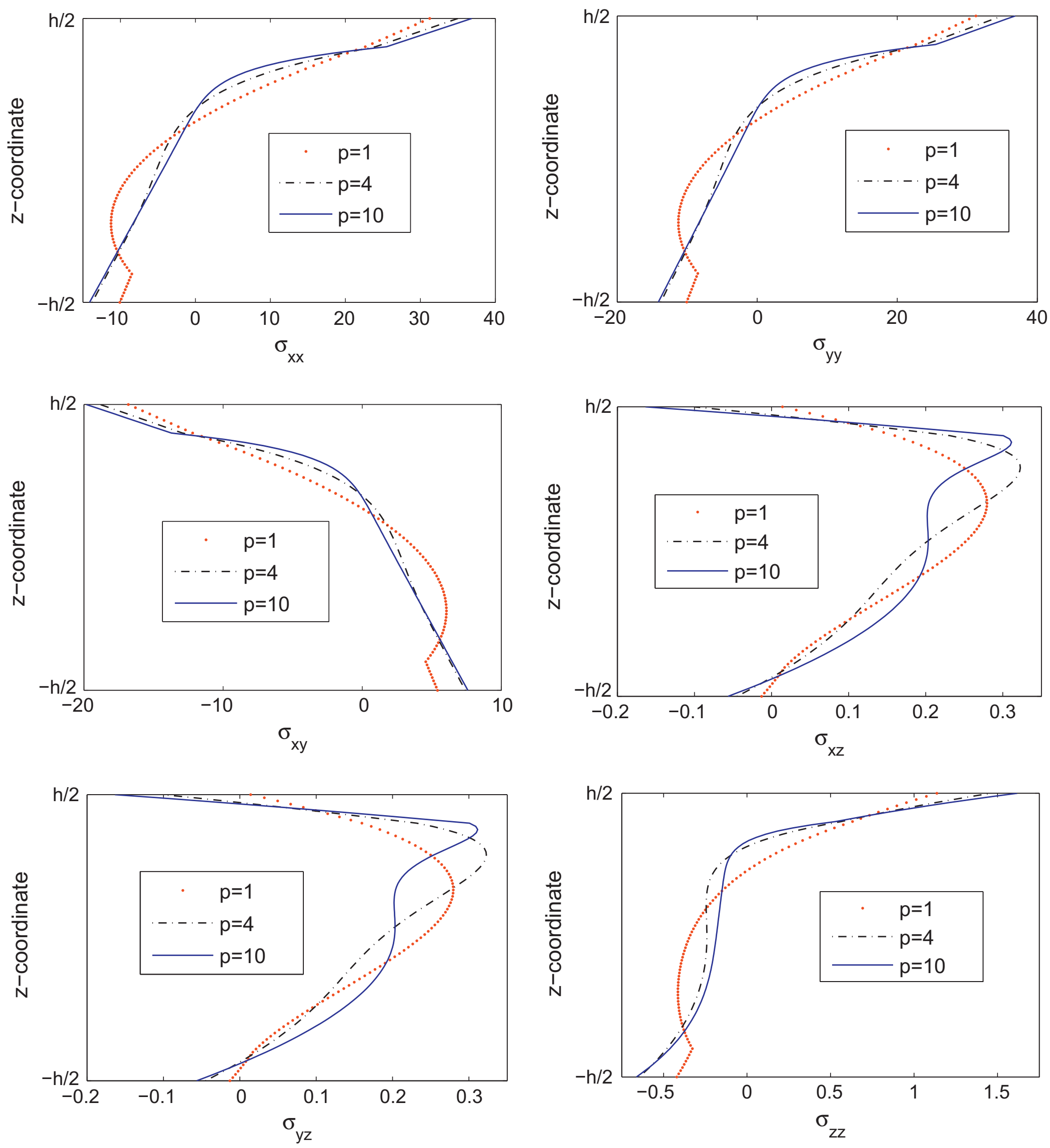

Fig. 9. Square *B*-type plate subjected to sinusoidal load at the top, with $a/h = 100$. Dimensionless stresses ($\bar{\sigma}$) through the thickness direction according to present higher-order theory for different values of p.

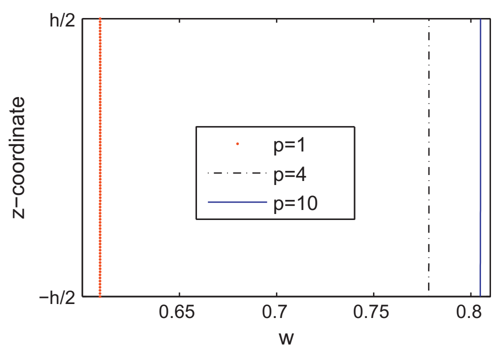

Fig. 10. Square *B*-type plate subjected to sinusoidal load at the top, with $a/h = 100$. Dimensionless displacement ($\bar{w}$) through the thickness direction according to present higher-order theory for different values of p.

deformation plate theory (FSDPT, $K = 5/6$ as shear correction factor), Reddy's higher-order shear deformation plate theory (TSDPT) [10], and Zenkour's sinusoidal shear deformation plate theory (SSDPT) [29]. Table 12 refers to the uni-axial buckling load and Table 13 refers to the bi-axial buckling load.

A good agreement between the present solution and references considered, specially [10,29] is obtained. This allow us to conclude that the present higher-order plate theory is good for the modeling of simply supported sandwich FGM plates and that collocation with RBFs is a good formulation. Present results with $\epsilon_{zz} = 0$ approximates better Refs. [10,29] than $\epsilon_{zz} \neq 0$ as the authors use the $\epsilon_{zz} = 0$ approach. This study also lead us to conclude that the thickness stretching effect has a strong influence on the buckling analysis of sandwich FGM plates as $\epsilon_{zz} = 0$ gives higher fundamental buckling loads than $\epsilon_{zz} \neq 0$.

The isotropic fully ceramic plate (first line on Tables 12 and 13) has the higher fundamental buckling loads. As the core thickness to the total thickness of the plate ratio ($(h_2 - h_1)/h$) increases the buckling loads increase as well. Considering each column of both tables we may conclude that the critical buckling loads decrease as the power-law exponent p increases. By comparing Tables 12 and 13 we also conclude that the bi-axial buckling load of simply supported sandwich square plate with FGM skins is half the uni-axial one for the same plate.

Please cite this article in press as: Neves AMA et al. Static, free vibration and buckling analysis of isotropic and sandwich functionally graded plates using a quasi-3D higher-order shear deformation theory and a meshless technique. Composites: Part B (2012), doi:10.1016/j.compositesb.2012.01.089

Table 7
Fundamental frequency of a SSSS *A*-type square plate (Al/ZrO$_2$) with $a/h = 5$, using a 21^2 grid and present higher-order theory.

Source	$p = 0$	$p = 0.5$	$p = 1$	$p = 2$	$p = 3$	$p = 5$	$p = 10$
Exact [28]			0.2192	0.2197	0.2211	0.2225	
Ref. [17]			0.2152	0.2153	0.2172	0.2194	
Ref. [68] ($\epsilon_{zz} = 0$)			0.2184	0.2189	0.2202	0.2215	
Ref. [68] ($\epsilon_{zz} \neq 0$)			0.2193	0.2198	0.2212	0.2225	
Present ($\epsilon_{zz} = 0$)	0.2459	0.2219	0.2184	0.2191	0.2206	0.2220	0.2219
Present ($\epsilon_{zz} \neq 0$)	0.2469	0.2228	0.2193	0.2200	0.2215	0.2230	0.2229

Table 8
First 10 frequencies of a SSSS *A*-type square plate (Al/ZrO$_2$) with $p = 1$ with $a/h = 20$ and using the higher-order theory.

Source	1	2	3	4	5	6	7	8	9	10
Ref. [17]	0.0149	0.0377	0.0377	0.0593	0.0747	0.0747	0.0769	0.0912	0.0913	0.1029
Ref. [68]	0.0153	0.0377	0.0377	0.0596	0.0739	0.0739	0.0950	0.0950	0.1029	0.1029
$\epsilon_z = 0$ 13^2	0.0153	0.0377	0.0377	0.0596	0.0740	0.0740	0.0951	0.0951	0.1030	0.1030
$\epsilon_z \neq 0$ 13^2	0.0153	0.0377	0.0377	0.0596	0.0741	0.0741	0.0953	0.0953	0.1030	0.1030
$\epsilon_z = 0$ 17^2	0.0153	0.0377	0.0377	0.0595	0.0738	0.0738	0.0949	0.0949	0.1030	0.1030
$\epsilon_z \neq 0$ 17^2	0.0153	0.0377	0.0377	0.0596	0.0739	0.0739	0.0950	0.0950	0.1030	0.1030
$\epsilon_z = 0$ 21^2	0.0153	0.0377	0.0377	0.0595	0.0738	0.0738	0.0948	0.0948	0.1030	0.1030
$\epsilon_z \neq 0$ 21^2	0.0153	0.0377	0.0377	0.0596	0.0739	0.0739	0.0950	0.0950	0.1030	0.1030

Table 9
First 10 frequencies of a SSSS *A*-type square plate (Al/ZrO$_2$) with $p = 1$ and $a/h = 10$ and using present higher-order theory.

Source	1	2	3	4	5	6	7	8	9	10
Ref. [17]	0.0584	0.1410	0.1410	0.2058	0.2058	0.2164	0.2646	0.2677	0.2913	0.3264
Ref. [68]	0.0596	0.1426	0.1426	0.2058	0.2058	0.2193	0.2676	0.2676	0.2910	0.3363
$\epsilon_z = 0$ 13^2	0.0595	0.1422	0.1422	0.2059	0.2059	0.2185	0.2664	0.2664	0.2912	0.3347
$\epsilon_z \neq 0$ 13^2	0.0596	0.1426	0.1426	0.2059	0.2059	0.2194	0.2678	0.2678	0.2912	0.3367
$\epsilon_z = 0$ 17^2	0.0595	0.1422	0.1422	0.2059	0.2059	0.2184	0.2663	0.2663	0.2912	0.3344
$\epsilon_z \neq 0$ 17^2	0.0596	0.1426	0.1426	0.2059	0.2059	0.2193	0.2676	0.2676	0.2912	0.3364
$\epsilon_z = 0$ 21^2	0.0595	0.1422	0.1422	0.2059	0.2059	0.2184	0.2663	0.2663	0.2912	0.3344
$\epsilon_z \neq 0$ 21^2	0.0596	0.1426	0.1426	0.2059	0.2059	0.2193	0.2676	0.2676	0.2912	0.3364

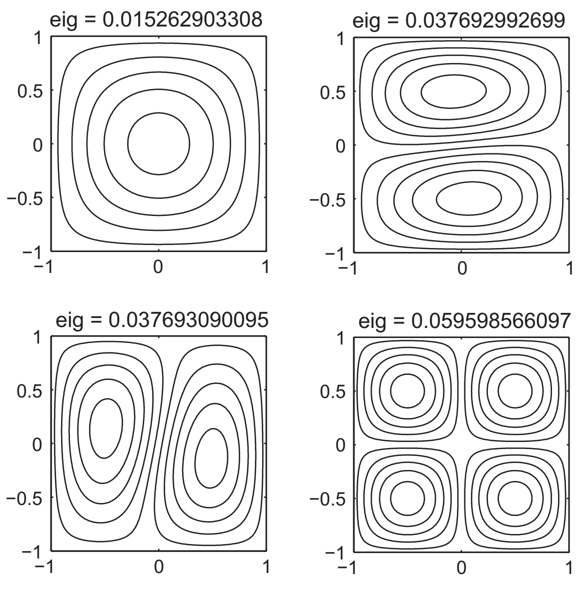

Fig. 11. First 4 frequencies of a SSSS square plate of type *A* (Al/ZrO2), with $p = 1$, a 21^2 grid, present higher-order shear deformation theory and $a/h = 20$.

In Fig. 12 the first four buckling modes of a simply supported 2-1-2 sandwich square plate with FGM skins, $p = 0.5$, subjected to a uni-axial in-plane compressive load, using the higher-order plate theory and 17^2 grid is presented. Fig. 13 presents the first four buckling modes of a simply supported 2-1-1 sandwich square plate with FGM skins, $p = 10$, subjected to a bi-axial in-plane compressive load.

Table 10
Convergence study for the uni-axial buckling load of a simply supported 2-2-1 sandwich square plate with FGM skins and $p = 5$ case using the higher-order theory.

Grid	13^2	17^2	21^2
$\overline{P}$	4.05112	4.05070	4.05065

Table 11
Convergence study for the bi-axial buckling load of a simply supported 1-2-1 sandwich square plate with FGM skins and $p = 1$ case using the higher-order theory.

Grid	13^2	17^2	21^2
$\overline{P}$	3.66028	3.65998	3.65994

7. Conclusions

A Unified formulation coupled with collocation with radial basis functions was proposed. A thickness-stretching higher-order shear deformation theory was successfully implemented for the static, free vibration, and linearized buckling analysis of functionally graded plates.

The present formulation was compared with analytical, meshless or finite element methods and proved very accurate in both static, vibration and buckling problems. The effect of $\epsilon_{zz} \neq 0$ showed significance in thicker plates. Even for a thinner functionally graded plate, the σ_{zz} should always be considered in the formulation.

For the first time, the complete governing equations and boundary conditions of the higher-order plate theory are presented to

Table 12
Uni-axial buckling load of simply supported plate of *C*-type using the higher-order theory and a grid with 17^2 points.

p	Theory	$\bar{P}$					
		1-0-1	2-1-2	2-1-1	1-1-1	2-2-1	1-2-1
0	CLPT	13.73791	13.73791	13.73791	13.73791	13.73791	13.73791
	FSDPT	13.00449	13.00449	13.00449	13.00449	13.00449	13.00449
	TSDPT [10]	13.00495	13.00495	13.00495	13.00495	13.00495	13.00495
	SSDPT [29]	13.00606	13.00606	13.00606	13.00606	13.00606	13.00606
	present $\epsilon_{zz} \neq 0$	12.95287	12.95287	12.95287	12.95287	12.95287	12.95287
	present $\epsilon_{zz} = 0$	13.00508	13.00508	13.00508	13.00508	13.00508	13.00508
0.5	CLPT	7.65398	8.25597	8.56223	8.78063	9.18254	9.61525
	FSDPT	7.33732	7.91320	8.20015	8.41034	8.78673	9.19517
	TSDPT [10]	7.36437	7.94084	8.22470	8.43645	8.80997	9.21681
	SSDPT [29]	7.36568	7.94195	8.22538	8.43712	8.81037	9.21670
	present $\epsilon_{zz} \neq 0$	7.16207	7.71627	7.98956	8.19278	8.55172	8.94190
	present $\epsilon_{zz} = 0$	7.18728	7.74326	8.01701	8.22133	8.58129	8.97310
1	CLPT	5.33248	6.02733	6.40391	6.68150	7.19663	7.78406
	FSDPT	5.14236	5.81379	6.17020	6.43892	6.92571	7.48365
	TSDPT [10]	5.16713	5.84006	6.19394	6.46474	6.94944	7.50656
	SSDPT [29]	5.16846	5.84119	6.19461	6.46539	6.94980	7.50629
	present $\epsilon_{zz} \neq 0$	5.06137	5.71135	6.05467	6.31500	6.78405	7.31995
	present $\epsilon_{zz} = 0$	5.07848	5.73022	6.07358	6.33556	6.80547	7.34367
5	CLPT	2.73080	3.10704	3.48418	3.65732	4.21238	4.85717
	FSDPT	2.63842	3.02252	3.38538	3.55958	4.09285	4.71475
	TSDPT [10]	2.65821	3.04257	3.40351	3.57956	4.11209	4.73469
	SSDPT [29]	2.66006	3.04406	3.40449	3.58063	4.11288	4.73488
	present $\epsilon_{zz} \neq 0$	2.63652	3.00791	3.36255	3.53005	4.05070	4.64701
	present $\epsilon_{zz} = 0$	2.64681	3.01865	3.37196	3.54148	4.06163	4.66059
10	CLPT	2.56985	2.80340	3.16427	3.25924	3.79238	4.38221
	FSDPT	2.46904	2.72626	3.07428	3.17521	3.68890	4.26040
	TSDPT [10]	2.48727	2.74632	3.09190	3.19471	3.70752	4.27991
	SSDPT [29]	2.48928	2.74844	3.13443	3.19456	3.14574	4.38175
	present $\epsilon_{zz} \neq 0$	2.47216	2.72046	3.06067	3.15761	3.66166	4.20550
	present $\epsilon_{zz} = 0$	2.48219	2.73080	3.06943	3.16837	3.67153	4.21792

Table 13
Bi-axial buckling load of simply supported plate of *C*-type using the higher-order theory and a grid with 17^2 points.

p	Theory	$\bar{P}$					
		1-0-1	2-1-2	2-1-1	1-1-1	2-2-1	1-2-1
0	CLPT	6.86896	6.86896	6.86896	6.86896	6.86896	6.86896
	FSDPT	6.50224	6.50224	6.50224	6.50224	6.50224	6.50224
	TSDPT [10]	6.50248	6.50248	6.50248	6.50248	6.50248	6.50248
	SSDPT [29]	6.50303	6.50303	6.50303	6.50303	6.50303	6.50303
	present $\epsilon_{zz} \neq 0$	6.47643	6.47643	6.47643	6.47643	6.47643	6.47643
	present $\epsilon_{zz} = 0$	6.50254	6.50254	6.50254	6.50254	6.50254	6.50254
0.5	CLPT	3.82699	4.12798	4.28112	4.39032	4.59127	4.80762
	FSDPT	3.66866	3.95660	4.10007	4.20517	4.39336	4.59758
	TSDPT [10]	3.68219	3.97042	4.11235	4.21823	4.40499	4.60841
	SSDPT [29]	3.68284	3.97097	4.11269	4.21856	4.40519	4.60835
	present $\epsilon_{zz} \neq 0$	3.58104	3.85813	3.99478	4.09639	4.27586	4.47095
	present $\epsilon_{zz} = 0$	3.59364	3.87163	4.00851	4.11067	4.29064	4.48655
1	CLPT	2.66624	3.01366	3.20195	3.34075	3.59831	3.89203
	FSDPT	2.57118	2.90690	3.08510	3.21946	3.46286	3.74182
	TSDPT [10]	2.58357	2.92003	3.09697	3.23237	3.47472	3.75328
	SSDPT [29]	2.58423	2.92060	3.09731	3.23270	3.47490	3.75314
	present $\epsilon_{zz} \neq 0$	2.53069	2.85568	3.02733	3.15750	3.39202	3.65998
	present $\epsilon_{zz} = 0$	2.53924	2.86511	3.03679	3.16778	3.40274	3.67183
5	CLPT	1.36540	1.55352	1.74209	1.82866	2.10619	2.42859
	FSDPT	1.31921	1.51126	1.69269	1.77979	2.04642	2.35737
	TSDPT [10]	1.32910	1.52129	1.70176	1.78978	2.05605	2.36734
	SSDPT [29]	1.33003	1.52203	1.70224	1.79032	2.05644	2.36744
	present $\epsilon_{zz} \neq 0$	1.31826	1.50395	1.68128	1.76502	2.02535	2.32351
	present $\epsilon_{zz} = 0$	1.32340	1.50933	1.68598	1.77074	2.03081	2.33029
10	CLPT	1.28493	1.40170	1.58214	1.62962	1.89619	2.19111
	FSDPT	1.23452	1.36313	1.53714	1.58760	1.84445	2.13020
	TSDPT [10]	1.24363	1.37316	1.54595	1.59736	1.85376	2.13995
	SSDPT [29]	1.24475	1.37422	1.56721	1.59728	1.57287	2.19087
	present $\epsilon_{zz} \neq 0$	1.23608	1.36023	1.53034	1.57880	1.83083	2.10275
	present $\epsilon_{zz} = 0$	1.24109	1.36540	1.53472	1.58419	1.83576	2.10896

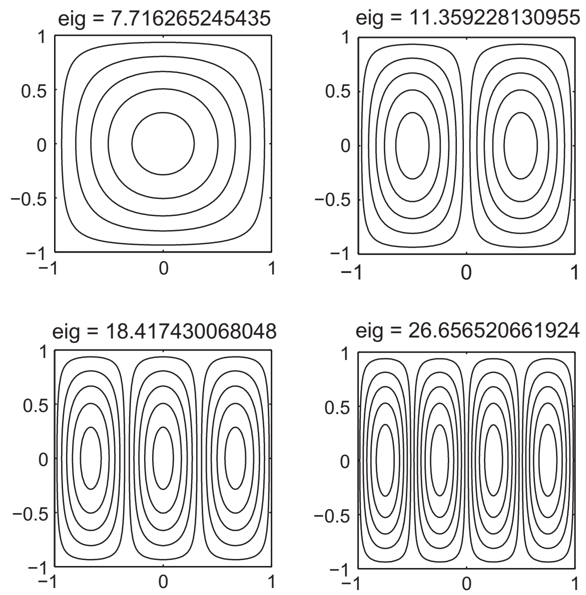

Fig. 12. First four buckling modes. Uni-axial buckling load of a simply supported 2-1-2 plate *C*-type, $p = 0.5$, a 17^2 points grid, and using the higher-order theory.

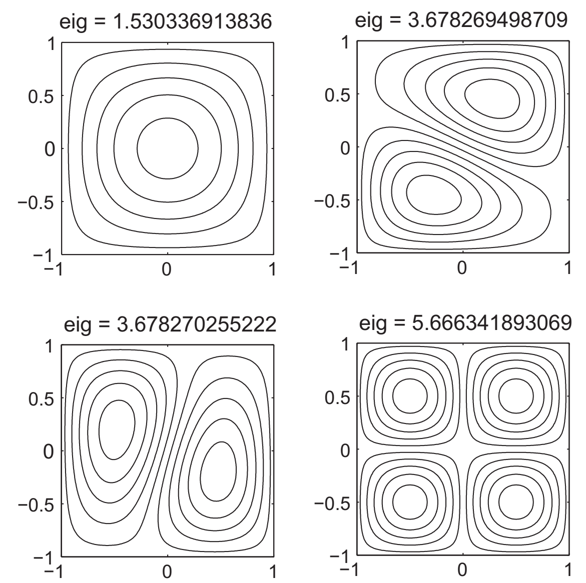

Fig. 13. First four buckling modes. Bi-axial buckling load of a simply supported 2-1-1 plate *C*-type, $p = 10$, a 17^2 points grid, and using the higher-order theory.

help readers to implement it successfully with the present or other strong-form techniques.

Acknowledgment

The FCT support given to the first author under Grant SFRH/BD/45554/2008 is acknowledged.

References

[1] Bever MB, Duwez PE. Gradients in composite materials. Mater Sci Eng 1972;10(0):1–8.
[2] Miyamoto Y, Kaysser WA, Rabin BH, Kawasaki A, Ford RG. Functionally graded materials: design, processing and applications. Kluwer Academic Publishers; 1999.
[3] Ferrante FJ, Graham-Brady LL. Stochastic simulation of non-gaussian/non-stationary properties in a functionally graded plate. Comput Methods Appl Mech Eng 2005;194(12–16):1675–92.
[4] M Yin H, Z Sun L, H Paulino G. Micromechanics-based elastic model for functionally graded materials with particle interactions. Acta Mater 2004;52(12):3535–43.
[5] Zhong Zheng, Shang Ertao. Closed-form solutions of three-dimensional functionally graded plates. Mech Adv Mater Struct 2008;15(5):355–63.
[6] Nguyen TK, Sab K, Bonnet G. Shear correction factors for functionally graded plates. Mech Adv Mater Struct 2007;14(8):567–75.
[7] Birman Victor, Byrd Larry W. Modeling and analysis of functionally graded materials and structures. Appl Mech Rev 2007;60(5):195–216.
[8] Koizumi M. Fgm activities in Japan. Compos Part B: Eng 1997;28(1–2):1–4. Use of composites multi-phased and functionally graded materials.
[9] Reddy JN, Chin CD. Thermomechanical analysis of functionally graded cylinders and plates. J Therm Stress 1998;21(6):593–626.
[10] Reddy JN. Analysis of functionally graded plates. Int J Numer Methods Eng 2000;47:663–84.
[11] Vel SS, Batra RC. Three-dimensional analysis of transient thermal stresses in functionally-graded plates. Int J Solids Struct 2003;40(25):7181–96.
[12] Vel SS, Batra RC. Exact solution for thermoelastic deformations of functionally graded thick rectangular plates. AIAA J 2002;40:1421–33.
[13] Cheng ZQ, Batra RC. Three-dimensional thermoelastic deformations of a functionally graded-elliptic plate. Composites: Part B 2000;31:97–106.
[14] Javaheri R, Eslami MR. Thermal buckling of functionally graded plates based on higher order theory. J Therm Stress 2002;25(7):603–25.
[15] Kashtalyan M. Three-dimensional elasticity solution for bending of functionally graded rectangular plates. Eur J Mech – A/Solids 2004;23(5):853–64.
[16] Kashtalyan M, Menshykova M. Three-dimensional elasticity solution for sandwich panels with a functionally graded core. Compos Struct 2009;87(1):36–43.
[17] Qian LF, Batra RC, Chen LM. Static and dynamic deformations of thick functionally graded elastic plate by using higher-order shear and normal deformable plate theory and meshless local Petrov–Galerkin method. Composites: Part B 2004;35:685–97.
[18] Zenkour AM. A comprehensive analysis of functionally graded sandwich plates: Part 1 – deflection and stresses. Int J Solids Struct 2005;42(18–19):5224–42.
[19] Zenkour AM. Generalized shear deformation theory for bending analysis of functionally graded plates. Appl Math Modell 2006;30:67–84.
[20] Ramirez Fernando, Heyliger Paul R, Pan Ernian. Static analysis of functionally graded elastic anisotropic plates using a discrete layer approach. Compos Part B: Eng 2006;37(1):10–20.
[21] Ferreira AJM, Batra RC, Roque CMC, Qian LF, Martins PALS. Static analysis of functionally graded plates using third-order shear deformation theory and a meshless method. Compos Struct 2005;69(4):449–57.
[22] Ferreira AJM, Roque CMC, Jorge RMN, Fasshauer GE, Batra RC. Analysis of functionally graded plates by a robust meshless method. Mech Adv Mater Struct 2007;14(8):577–87.
[23] Chi Shyang-Ho, Chung Yen-Ling. Mechanical behavior of functionally graded material plates under transverse load – part i: analysis. Int J Solids Struct 2006;43(13):3657–74.
[24] Chi Shyang-Ho, Chung Yen-Ling. Mechanical behavior of functionally graded material plates under transverse load – part ii: numerical results. Int J Solids Struct 2006;43(13):3675–91.
[25] Cheng ZQ, Batra RC. Deflection relationships between the homogeneous kirchhoff plate theory and different functionally graded plate theories. Arch Mech 2000;52:143–58.
[26] Batra RC, Jin J. Natural frequencies of a functionally graded anisotropic rectangular plate. J Sound Vib 2005;282(1–2):509–16.
[27] Ferreira AJM, Batra RC, Roque CMC, Qian LF, Jorge RMN. Natural frequencies of functionally graded plates by a meshless method. Compos Struct 2006;75(1–4):593–600.
[28] Vel SS, Batra RC. Three-dimensional exact solution for the vibration of functionally graded rectangular plates. J Sound Vib 2004;272:703–30.
[29] Zenkour AM. A comprehensive analysis of functionally graded sandwich plates: part 2 – buckling and free vibration. Int J Solids Struct 2005;42(18–19):5243–58.
[30] Roque CMC, Ferreira AJM, Jorge RMN. A radial basis function approach for the free vibration analysis of functionally graded plates using a refined theory. J Sound Vib 2007;300(3–5):1048–70.
[31] Cheng ZQ, Batra RC. Exact correspondence between eigenvalues of membranes and functionally graded simply supported polygonal plates. J Sound Vib 2000;229:879–95.
[32] Najafizadeh MM, Eslami MR. Buckling analysis of circular plates of functionally graded materials under uniform radial compression. Int J Mech Sci 2002;44(12):2479–93.
[33] Birman V. Buckling of functionally graded hybrid composite plates. In: Proceedings of the 10th conference on engineering mechanics; 1995. p. 1199–202.
[34] Javaheri R, Eslami MR. Buckling of functionally graded plates under in-plane compressive loading. ZAMM – J Appl Math Mech/Zeitschrift f++r Angewandte Mathematik und Mechanik 2002;82(4):277–83.
[35] Kant T, Owen DRJ, Zienkiewicz OC. A refined higher-order c° plate element. Comput Struct 1982;15(2):177–83.

Please cite this article in press as: Neves AMA et al. Static, free vibration and buckling analysis of isotropic and sandwich functionally graded plates using a quasi-3D higher-order shear deformation theory and a meshless technique. Composites: Part B (2012), doi:10.1016/j.compositesb.2012.01.089

[36] Pandya BN, Kant T. Higher-order shear deformable theories for flexure of sandwich plates–finite element evaluations. Int J Solids Struct 1988;24(12):1267–86.
[37] Pandya BN, Kant T. Finite element analysis of laminated composite plates using a higher-order displacement model. Compos Sci Technol 1988;32(2):137–55.
[38] Kant T, Swaminathan K. Analytical solutions for the static analysis of laminated composite and sandwich plates based on a higher order refined theory. Compos Struct 2002;56(4):329–44.
[39] Kant T, Swaminathan K. Analytical solutions for free vibration of laminated composite and sandwich plates based on a higher-order refined theory. Compos Struct 2001;53(1):73–85.
[40] Garg Ajay Kumar, Khare Rakesh Kumar, Kant Tarun. Higher-order closed-form solutions for free vibration of laminated composite and sandwich shells. J Sandwich Struct Mater 2006;8(3):205–35.
[41] Batra RC, Vidoli S. Higher-order piezoelectric plate theory derived from a three-dimensional variational principle. AIAA J 2002;40:91–104.
[42] Batra RC, Vidoli S, Vestroni F. Plane wave solutions and modal analysis in higher order shear and normal deformable plate theories. J Sound Vib 2002;257(1):63–88.
[43] Qian LF, Batra RC, Chen LM. Analysis of cylindrical bending thermoelastic deformations of functionally graded plates by a meshless local petrovâĂŞgalerkin method. Comput Mech 2004;33:263–73. doi:10.1007/s00466-003-0527-z.
[44] Qian LF, Batra RC. Transient thermoelastic deformations of a thick functionally graded plate. J Therm Stress 2004;27(8):705–40.
[45] Qian LF, Batra RC. Three-dimensional transient heat conduction in a functionally graded thick plate with a higher-order plate theory and a meshless local Petrov–Galerkin method. Comput Mech 2005;35:214–26. doi:10.1007/s00466-004-0617-6.
[46] Qian LF, Batra RC, Chen LM. Free and forced vibrations of thick rectangular plates using higher-order shear and normal deformable plate theory and meshless Petrov–Galerkin (mlpg) method. Comput Model Eng Sci 2003;4:519–34.
[47] Qian LF, Batra RC, Chen LM. Elastostatic deformations of a thick plate by using a higher-order shear and normal deformable plate theory and two meshless local Petrov–Galerkin (mlpg) methods. Comput Model Eng Sci 2003;4:161–75.
[48] Qian LF, Batra RC. Design of bidirectional functionally graded plate for optimal natural frequencies. J Sound Vib 2005;280(1–2):415–24.
[49] Batra RC, Qian LF, Chen LM. Natural frequencies of thick square plates made of orthotropic, trigonal, monoclinic, hexagonal and triclinic materials. J Sound Vib 2004;270(4–5):1074–86.
[50] Batra RC, Aimmanee S. Vibrations of thick isotropic plates with higher order shear and normal deformable plate theories. Comput Struct 2005;83(12–13):934–55.
[51] Gilhooley DF, Batra RC, Xiao JR, McCarthy MA, Gillespie Jr JW. Analysis of thick functionally graded plates by using higher-order shear and normal deformable plate theory and mlpg method with radial basis functions. Compos Struct 2007;80(4):539–52.
[52] Xiao JR, Gilhooley DF, Batra RC, Gillespie Jr JW, McCarthy MA. Analysis of thick composite laminates using a higher-order shear and normal deformable plate theory (hosndpt) and a meshless method. Compos Part B: Eng 2008;39(2):414–27.
[53] Carrera E, Brischetto S, Cinefra M, Soave M. Effects of thickness stretching in functionally graded plates and shells. Compos Part B: Eng 2011;42:123–33.
[54] Carrera E. Evaluation of layer-wise mixed theories for laminated plate analysis. AIAA J 1998(36):830–9.
[55] Carrera E. Developments, ideas, and evaluations based upon reissner's mixed variational theorem in the modelling of multilayered plates and shells. Appl Mech Rev 2001;54:301–29.
[56] Carrera Erasmo. Theories and finite elements for multilayered plates and shells: a unified compact formulation with numerical assessment and benchmarking. Arch Comput Methods Eng 2003;10:215–96.
[57] Brischetto S, Carrera E. Advanced mixed theories for bending analysis of functionally graded plates. Comput Struct 2010;88(23–24):1474–83.
[58] Brischetto S. Classical and mixed advanced models for sandwich plates embedding functionally graded cores. J Mech Mater Struct 2009;4:13–33.
[59] Carrera E, Brischetto S, Robaldo A. Variable kinematic model for the analysis of functionally graded material plates. AIAA J 2008;46:194–203.
[60] Demasi L. ∞^3 hierarchy plate theories for thick and thin composite plates: the generalized unified formulation. Compos Struct 2008;84:256–70.
[61] Luciano, Demasi. Mixed plate theories based on the generalized unified formulation. Part i: governing equations. Compos Struct 2009;87(1):1–11.
[62] Luciano, Demasi. Mixed plate theories based on the generalized unified formulation. Part ii: layerwise theories. Compos Struct 2009;87(1):12–22.
[63] Luciano, Demasi. Mixed plate theories based on the generalized unified formulation. Part iii: advanced mixed high order shear deformation theories. Compos Struct 2009;87(3):183–94.
[64] Luciano, Demasi. Mixed plate theories based on the generalized unified formulation. Part iv: zig-zag theories. Compos Struct 2009;87(3):195–205.
[65] Luciano, Demasi. Mixed plate theories based on the generalized unified formulation. Part v: results. Compos Struct 2009;88(1):1–16.
[66] Luciano, Demasi. Partially zig-zag advanced higher order shear deformation theories based on the generalized unified formulation. Compos Struct 2012;94(2):363–75.
[67] Neves AMA, Ferreira AJM, Carrera E, Roque CMC, Cinefra M, Jorge RMN, et al. Bending of fgm plates by a sinusoidal plate formulation and collocation with radial basis functions. Mech Res Commun 2011;38(5):368–71.
[68] Neves AMA, Ferreira AJM, Carrera E, Roque CMC, Cinefra M, Jorge RMN, et al. A quasi-3d sinusoidal shear deformation theory for the static and free vibration analysis of functionally graded plates. Compos Part B: Eng 2012;43:711–25.
[69] Neves AMA, Ferreira AJM, Carrera E, Cinefra M, Roque CMC, Jorge RMN, et al. A quasi-3d hyperbolic shear deformation theory for the static and free vibration analysis of functionally graded plates. Compos Struct, in press.
[70] Williams Todd O. Efficiency and accuracy considerations in a unified plate theory with delamination. Compos Struct 2001;52(1):27–40.
[71] Williams Todd O, Addessio Frank L. A general theory for laminated plates with delaminations. Int J Solids Struct 1997;34(16):2003–24.
[72] Pindera Marek-Jerzy, Williams Todd O, Arnold Steven M. Thermoplstic response of metal–matrix composites with homogenized and functionally graded interfaces. Compos Eng 1994;4(1):129–45. Use of composites in functionally graded materials.
[73] Williams Todd O. A generalized, multilength scale framework for thermo-diffusional-mechanically coupled, nonlinear, laminated plate theories with delaminations. Int J Solids Struct 2005;42(5–6):1465–90.
[74] Williams Todd O. A generalized multilength scale nonlinear composite plate theory with delamination. Int J Solids Struct 1999;36(20):3015–50.
[75] Mourad Hashem M, Williams Todd O, Addessio Francis L. Finite element analysis of inelastic laminated plates using a global-local formulation with delamination. Comput Methods Appl Mech Eng 2008;198(3–4):542–54.
[76] Ferreira AJM. A formulation of the multiquadric radial basis function method for the analysis of laminated composite plates. Compos Struct 2003;59:385–92.
[77] Ferreira AJM. Thick composite beam analysis using a global meshless approximation based on radial basis functions. Mech Adv Mater Struct 2003;10:271–84.
[78] Ferreira AJM, Roque CMC, Martins PALS. Analysis of composite plates using higher-order shear deformation theory and a finite point formulation based on the multiquadric radial basis function method. Composites: Part B 2003;34:627–36.
[79] Ferreira AJM, Roque CMC, Jorge RMN, Kansa EJ. Static deformations and vibration analysis of composite and sandwich plates using a layerwise theory and multiquadrics discretizations. Eng Anal Bound Elem 2005;29(12):1104–14.
[80] Ferreira AJM, Roque CMC, Jorge RMN. Analysis of composite plates by trigonometric shear deformation theory and multiquadrics. Comput Struct 2005;83(27):2225–37.
[81] Ferreira AJM, Batra RC, Roque CMC, Qian LF, Jorge RMN. Natural frequencies of functionally graded plates by a meshless method. Compos Struct 2006;75(1–4):593–600.
[82] Ferreira AJM, Roque CMC, Jorge RMN. Free vibration analysis of symmetric laminated composite plates by fsdt and radial basis functions. Comput Methods Appl Mech Eng 2005;194(39–41):4265–78.
[83] Ferreira AJM, Roque CMC, Martins PALS. Radial basis functions and higher-order shear deformation theories in the analysis of laminated composite beams and plates. Compos Struct 2004;66(1–4):287–93.
[84] Ferreira AJM, Roque CMC, Carrera E, Cinefra M, Polit O. Radial basis functions collocation and a unified formulation for bending, vibration and buckling analysis of laminated plates, according to a variation of murakamiâĂŹs zig-zag theory. Eur J Mech – A/Solids 2011;30(4):559–70.
[85] Rodrigues JD, Roque CMC, Ferreira AJM, Carrera E, Cinefra M. Radial basis functions-finite differences collocation and a unified formulation for bending, vibration and buckling analysis of laminated plates, according to murakami's zig-zag theory. Compos Struct 2011;93(7):1613–20.
[86] Ferreira AJM, Roque CMC, Carrera E, Cinefra M. Analysis of thick isotropic and cross-ply laminated plates by radial basis functions and a unified formulation. J Sound Vib 2011;330(4):771–87.
[87] Ferreira AJM, Roque CMC, Carrera E, Cinefra M, Polit O. Two higher order zig-zag theories for the accurate analysis of bending, vibration and buckling response of laminated plates by radial basis functions collocation and a unified formulation. J Compos Mater 2011.
[88] Carrera E. C^0 Reissner–Mindlin multilayered plate elements including zig-zag and interlaminar stress continuity. Int J Numer Methods Eng 1996;39:1797–820.
[89] Mori T, Tanaka K. Average stress in matrix and average elastic energy of materials with misfitting inclusions. Acta Metall 1973;21(5):571–4.
[90] Benveniste Y. A new approach to the application of Mori–Tanaka's theory in composite materials. Mech Mater 1987;6(2):147–57.
[91] Hardy RL. Multiquadric equations of topography and other irregular surfaces. Geophys Res 1971;176:1905–15.
[92] Kansa EJ. Multiquadrics – a scattered data approximation scheme with applications to computational fluid dynamics. Part i: surface approximations and partial derivative estimates. Comput Math Appl 1990;19(8/9):127–45.
[93] Kansa EJ. Multiquadrics – a scattered data approximation scheme with applications to computational fluid dynamics. Part ii: solutions to parabolic, hyperbolic and elliptic partial differential equations. Comput Math Appl 1990;19(8/9):147–61.
[94] Larsson E, Fornberg B. A numerical study of some radial basis function based solution methods for elliptic pdes. Comput Math Appl 2003;46(5–6):891–902.
[95] Franke C, Schaback R. Solving partial differential equations by collocation using radial basis functions. Appl Math Comput 1998;93(1):73–82.

Please cite this article in press as: Neves AMA et al. Static, free vibration and buckling analysis of isotropic and sandwich functionally graded plates using a quasi-3D higher-order shear deformation theory and a meshless technique. Composites: Part B (2012), doi:10.1016/j.compositesb.2012.01.089

[96] Fasshauer GE. Newton iteration with multiquadrics for the solution of nonlinear pdes. Comput Math Appl 2002(43):423–38.
[97] Fasshauer Gregory. Solving differential equations with radial basis functions: multilevel methods and smoothing. Adv Comput Math 1999;11:139–59. doi:10.1023/A:1018919824891.
[98] Wendland H. Error estimates for interpolation by compactly supported radial basis functions of minimal degree. J Approx Theory 1998;93:258–96.
[99] Ferreira AJM, Fasshauer GE. Computation of natural frequencies of shear deformable beams and plates by a rbf-pseudospectral method. Comput Methods Appl Mech Eng 2006;196:134–46.

2.5 Buckling analysis of sandwich plates with functionally graded skins using a new quasi-3D hyperbolic sine shear deformation theory and collocation with radial basis functions

A. M. A. Neves, A. J. M. Ferreira, E. Carrera, M. Cinefra, R. M. N. Jorge, C. M. M. Soares, Buckling analysis of sandwich plates with functionally graded skins using a new quasi-3D hyperbolic sine shear deformation theory and collocation with radial basis functions, Zeitschrift für Angewandte Mathematik und Mechanik, 2012, in press.

Early View publication on wileyonlinelibrary.com
(issue and page numbers not yet assigned;
citable using Digital Object Identifier – DOI)

ZAMM · Z. Angew. Math. Mech., 1 – 18 (2012) / **DOI** 10.1002/zamm.201100186

Buckling analysis of sandwich plates with functionally graded skins using a new quasi-3D hyperbolic sine shear deformation theory and collocation with radial basis functions

A. M. A. Neves[1,*], A. J. M. Ferreira[2], E. Carrera[3], M. Cinefra[3], R. M. N. Jorge[2], and C. M. M. Soares[4]

[1] Departamento de Engenharia Mecânica, Faculdade de Engenharia, Universidade do Porto, Rua Dr. Roberto Frias, 4200-465 Porto, Portugal
[2] Departamento de Engenharia Mecânica, Faculdade de Engenharia, Universidade do Porto, Rua Dr. Roberto Frias, 4200-465 Porto, Portugal
[3] Departament of Aeronautics and Aerospace Engineering, Politecnico di Torino, Corso Duca degli Abruzzi, 24, 10129 Torino, Italy
[4] Instituto Superior Técnico, Av. Rovisco Pais, Lisboa, Portugal

Received 20 December 2011, revised 16 March 2012, accepted 12 April 2012
Published online 25 May 2012

Key words Buckling sandwich plates, functionally graded materials, meshless methods.

A hyperbolic sine shear deformation theory is used for the linear buckling analysis of functionally graded plates. The theory accounts for through-the-thickness deformations.

The buckling governing equations and boundary conditions are derived using Carrera's Unified Formulation and further interpolated by collocation with radial basis functions. The collocation method is truly meshless, allowing a fast and simple discretization of equations in the domain and on the boundary.

A numerical investigation has been conducted considering and neglecting the thickness stretching effects on the buckling of sandwich plates with functionally graded skins. Numerical results demonstrate the high accuracy of the present approach.

1 Introduction

The concept of functionally graded materials (FGM) was first proposed by materials scientists in Japan in 1984 [1]. It was introduced to satisfy the demand of ultra-high-temperature environment and to eliminate the stress singularities [2]. Due to the continuous change in material properties of an FGM, the interfaces between two materials disappear but the characteristics of two or more different materials of the composite are preserved. Interested readers on FGM application fields can refer to [1] or [3]. A review of the main developments in FGM can be found in Birman and Byrd [4].

In a conventional FGM plate a continuous variation of material properties over the thickness direction is obtained by mixing two different materials [3]. The material properties of the FGM plate are assumed to change continuously throughout the thickness of the plate, according to the volume fraction of the constituent materials. To describe the volume fractions an exponential function can be used as in [5], or the sigmoid function as proposed in [6]. In the present work a power-law function is used as in [7–10].

Many studies have been performed to analyse the behaviour of FGM plates. The static analysis of FGM plates has been performed by Kashtalyan [11], Kashtalyan and Menshykova [12], Qian et al. [13], Zenkour [9, 10], Ramirez et al. [14], Ferreira et al. [15, 16], and Chi and Chung [17, 18]. Vibrations problems of FGM plates can be found in Batra and Jin [19], Ferreira et al. [20], Vel and Batra [21], Zenkour [22], and Cheng and Batra [23]. Other works could be mentioned on static and free vibration analysis of FGM plates. There is also literature on the thermo-mechanical response of FGM plates: Reddy and Chin [24], Reddy [25], Vel and Batra [26, 27], Cheng and Batra [28], Javaheri and Eslami [29]. However, the analysis of mechanical buckling of FGM structures is less commom in the literature. It can be found in Najafizadeh and Eslami [8], Zenkour [22], Cheng and Batra [23], Birman [30], Javaheri and Eslami [31].

* Corresponding author E-mail: ananeves@fe.up.pt

Analysis of shear deformation plates with hyperbolic functions is not typical in the literature, in particular for FGM plates. In fact, the analysis of FGM plates is tipically performed using the clasical plate theory (CLPT) [17, 18], the first-order shear deformation theory (FSDT) [10,19,20,32] or higher-order shear deformation theories (HSDT) [13,15,20,25,32]. In [33–35] various hyperbolic functions were considered for the analysis of laminated plates. A hyperbolic function is used for FGM plates in [36], using a specialized function.

In all previous investigations with hyperbolic functions, these latter are used for the in-plane expansions only and the transverse displacement is considered as constant resulting in shear deformation theories that neglect the thickness stretching $\epsilon_{zz} = 0$. Carrera et al. [37] recently investigated the effect of thickness stretching in FGM plates, using finite element approximations. Most of refered studies on FGM plates was performed using the Finite Element Method. The use of alternative methods for the analysis of plates, such as the meshless methods based on collocation with radial basis functions (RBFs) is atractive due to the absence of a mesh and the ease of collocation methods. In recent years, radial basis functions showed excellent accuracy in the interpolation of data and functions. Kansa [38] introduced the concept of solving partial differential equations by an unsymmetric RBF collocation method based upon the multiquadric interpolation functions. The authors have applied successfully the RBF collocation technique to the static and dynamic analysis of composite structures [39–48].

The use of hyperbolic shear deformation theory accounting for $\epsilon_{zz} \neq 0$ for the buckling analysis of plates has not been considered before. This paper adresses the thickness stretching effect on the buckling analysis of FGM plate by a meshless technique based on collocation with radial basis functions. Carrera's Unified Formulation (further denoted as CUF) [49,50] is employed to obtain the algebraic governing equations and boundary conditions of the present shear deformation theory. Such equations are then interpolated by radial basis functions to obtain an algebraic system of equations. The used theory is a quasi-3D hyperbolic shear deformation theory, with different expansion for the in-plane displacements (u, v) and the out-of-plane displacement (w). In-plane displacements are considered to be of hyperbolic sine type across the thickness coordinate and the out-of-plane displacement is defined as quadratic in the thickness direction

$$u = u_0 + zu_1 + \sinh\left(\frac{\pi z}{h}\right) u_Z; \quad v = v_0 + zv_1 + \sinh\left(\frac{\pi z}{h}\right) v_Z; \quad w = w_0 + zw_1 + z^2 w_Z. \tag{1}$$

For the $\epsilon_{zz} = 0$ case the transverse displacement is defined as $w = w_0$. It turns out that the present formulation can be seen as a generalization of the original CUF, by introducing different displacement fields for in-plane and out-of-plane displacements.

2 Problem formulation

Consider a rectangular sandwich plate of plan-form dimensions a and b and uniform thickness h. The co-ordinate system is taken such that the x-y plane coincides with the midplane of the plate ($z \in [-h/2, h/2]$).

The sandwich core is a ceramic material and skins are composed of a functionally graded material across the thickness direction. The bottom skin varies from a metal-rich surface ($z = h_0 = -h/2$) to a ceramic-rich surface while the top skin face varies from a ceramic-rich surface to a metal-rich surface ($z = h_3 = h/2$) as illustrated in Fig. 1. The volume fraction of the ceramic phase is obtained from a simple rule of mixtures as:

$$\begin{aligned} V_c &= \left(\frac{z - h_0}{h_1 - h_0}\right)^p, \quad z \in [h_0, h_1], \\ V_c &= 1, \quad z \in [h_1, h_2], \end{aligned} \tag{2}$$

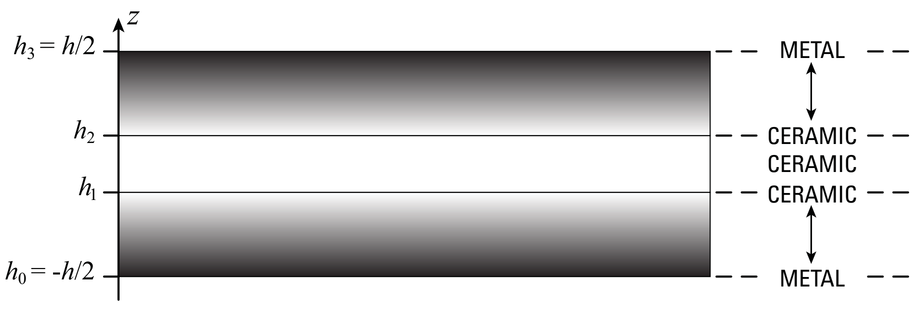

Fig. 1 Sandwich with isotropic core and FGM skins.

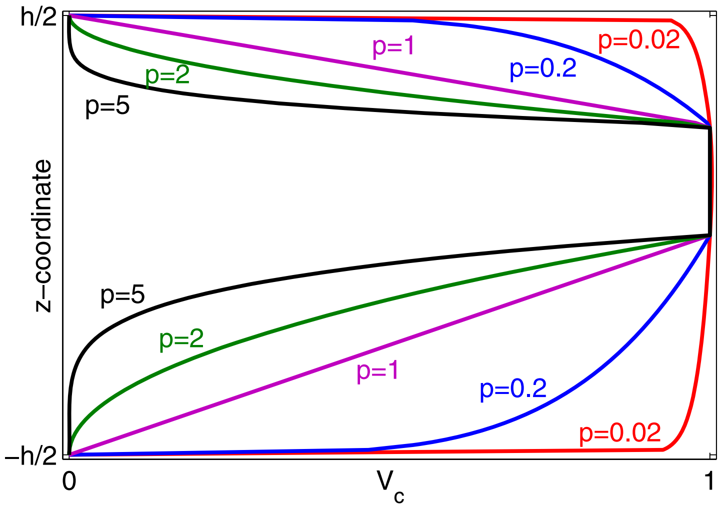

Fig. 2 (online colour at: www.zamm-journal.org) Illustration of a 2-1-1 sandwich with FGM skins for several volume fractions.

$$V_c = \left(\frac{z - h_3}{h_2 - h_3}\right)^p, \quad z \in [h_2, h_3],$$

where p is a scalar parameter that allows the user to define the gradation of material properties across the thickness direction of the skins. With this formulation the interfaces between core and skins disappear. Note that the core of the present sandwich and any isotropic material can be obtained as a particular case of the power-law function by setting $p = 0$. The volume fraction for the metal phase is given as $V_m = 1 - V_c$. The sandwich may be symmetric or non-symmetric about the mid-plane as we may vary the thickness of each face. Figure 2 shows a non-symmetric sandwich with volume fraction defined by the power-law (2) for various exponents p, in which top skin thickness is the same as the core thickness and the bottom skin thickness is twice the core thickness. Such thickness relation is denoted as 2-1-1. A bottom-core-top notation is used. 1-1-1 means that skins and core have the same thickness.

The sandwich plate is subjected to compressive in-plane forces acting on the mid-plane of the plate. $\bar{N}_{xx}$ and $\bar{N}_{yy}$ denote the in-plane loads perpendicular to the edges $x = 0$ and $y = 0$ respectively, and $\bar{N}_{xy}$ denotes the distributed shear force parallel to the edges $x = 0$ and $y = 0$ respectively (see Fig. 3).

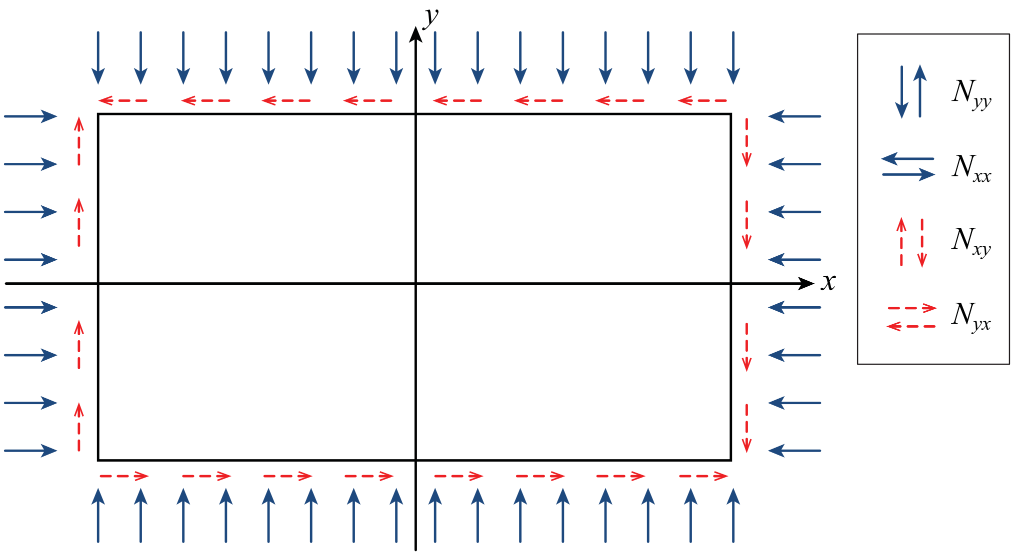

Fig. 3 (online colour at: www.zamm-journal.org) Rectangular plate subjected to in-plane forces.

3 A quasi-3D hyperbolic sine plate shear deformation theory

In the following we derive the boundary conditions and the linearized equations of the hyperbolic sine plate shear deformation theory leading to the eigenproblem for the study of buckling plates. The inertial terms are also accounted to help readers to implement the hyperbolic sine theory successfully with any strong-form technique for free vibration or static problems of plates as well.

3.1 Displacement field

The present theory is based on the following displacement field:

$$u(x,y,z,t) = u_0(x,y,t) + zu_1(x,y,t) + \sinh\left(\frac{\pi z}{h}\right) u_Z(x,y,t), \tag{3}$$

$$v(x,y,z,t) = v_0(x,y,t) + zv_1(x,y,t) + \sinh\left(\frac{\pi z}{h}\right) v_Z(x,y,t), \tag{4}$$

$$w(x,y,z,t) = w_0(x,y,t) + zw_1(x,y,t) + z^2 w_2(x,y,t), \tag{5}$$

where u, v, and w are the displacements in the $x-$, $y-$, and $z-$ directions, respectively. $u_0, u_1, u_Z, v_0, v_1, v_Z, w_0, w_1$, and w_2 are the unknowns to be determined. A constant term is assumed for the transverse displacement component instead of (5) ($w = w_0$) to investigate the effect of the thickness stretching on the buckling loads.

3.2 Strains

The strains can be related to the displacement field as:

$$\begin{Bmatrix} \epsilon_{xx} \\ \epsilon_{yy} \\ \gamma_{xy} \end{Bmatrix} = \begin{Bmatrix} \frac{\partial u}{\partial x} + \frac{1}{2}\left(\frac{\partial w_0}{\partial x}\right)^2 \\ \frac{\partial v}{\partial y} + \frac{1}{2}\left(\frac{\partial w_0}{\partial y}\right)^2 \\ \frac{\partial u}{\partial y} + \frac{\partial v}{\partial x} + \frac{\partial w_0}{\partial x}\frac{\partial w_0}{\partial y} \end{Bmatrix}, \quad \begin{Bmatrix} \gamma_{xz} \\ \gamma_{yz} \\ \epsilon_{zz} \end{Bmatrix} = \begin{Bmatrix} \frac{\partial u}{\partial z} + \frac{\partial w}{\partial x} \\ \frac{\partial v}{\partial z} + \frac{\partial w}{\partial y} \\ \frac{\partial w}{\partial z} \end{Bmatrix}, \tag{6}$$

By substitution of the displacement field in (6), the strains are obtained:

$$\begin{Bmatrix} \epsilon_{xx} \\ \epsilon_{yy} \\ \gamma_{xy} \end{Bmatrix} = \begin{Bmatrix} \epsilon_{xx}^{(0)} \\ \epsilon_{yy}^{(0)} \\ \gamma_{xy}^{(0)} \end{Bmatrix} + \begin{Bmatrix} \epsilon_{xx}^{(nl)} \\ \epsilon_{yy}^{(nl)} \\ \gamma_{xy}^{(nl)} \end{Bmatrix} + z \begin{Bmatrix} \epsilon_{xx}^{(1)} \\ \epsilon_{yy}^{(1)} \\ \gamma_{xy}^{(1)} \end{Bmatrix} + \sinh\left(\frac{\pi z}{h}\right) \begin{Bmatrix} \epsilon_{xx}^{(Z)} \\ \epsilon_{yy}^{(Z)} \\ \gamma_{xy}^{(Z)} \end{Bmatrix}, \tag{7}$$

$$\begin{Bmatrix} \gamma_{xz} \\ \gamma_{yz} \\ \epsilon_{zz} \end{Bmatrix} = \begin{Bmatrix} \gamma_{xz}^{(0)} \\ \gamma_{yz}^{(0)} \\ \epsilon_{zz}^{(0)} \end{Bmatrix} + z \begin{Bmatrix} \gamma_{xz}^{(1)} \\ \gamma_{yz}^{(1)} \\ \epsilon_{zz}^{(1)} \end{Bmatrix} + z^2 \begin{Bmatrix} \gamma_{xz}^{(2)} \\ \gamma_{yz}^{(2)} \\ \epsilon_{zz}^{(2)} \end{Bmatrix} + \frac{\pi}{h}\cosh\left(\frac{\pi z}{h}\right) \begin{Bmatrix} \gamma_{xz}^{(Z)} \\ \gamma_{yz}^{(Z)} \\ \epsilon_{zz}^{(Z)} \end{Bmatrix} \tag{8}$$

being the strain components obtained as

$$\begin{Bmatrix} \epsilon_{xx}^{(0)} \\ \epsilon_{yy}^{(0)} \\ \gamma_{xy}^{(0)} \end{Bmatrix} = \begin{Bmatrix} \frac{\partial u_0}{\partial x} \\ \frac{\partial v_0}{\partial y} \\ \frac{\partial u_0}{\partial y} + \frac{\partial v_0}{\partial x} \end{Bmatrix}; \quad \begin{Bmatrix} \epsilon_{xx}^{(nl)} \\ \epsilon_{yy}^{(nl)} \\ \gamma_{xy}^{(nl)} \end{Bmatrix} = \begin{Bmatrix} \frac{1}{2}\left(\frac{\partial w_0}{\partial x}\right)^2 \\ \frac{1}{2}\left(\frac{\partial w_0}{\partial y}\right)^2 \\ \frac{\partial w_0}{\partial x}\frac{\partial w_0}{\partial y} \end{Bmatrix}, \tag{9}$$

$$\begin{Bmatrix} \epsilon_{xx}^{(1)} \\ \epsilon_{yy}^{(1)} \\ \gamma_{xy}^{(1)} \end{Bmatrix} = \begin{Bmatrix} \frac{\partial u_1}{\partial x} \\ \frac{\partial v_1}{\partial y} \\ \frac{\partial u_1}{\partial y} + \frac{\partial v_1}{\partial x} \end{Bmatrix}; \quad \begin{Bmatrix} \epsilon_{xx}^{(Z)} \\ \epsilon_{yy}^{(Z)} \\ \gamma_{xy}^{(Z)} \end{Bmatrix} = \begin{Bmatrix} \frac{\partial u_Z}{\partial x} \\ \frac{\partial v_Z}{\partial y} \\ \frac{\partial u_Z}{\partial y} + \frac{\partial v_Z}{\partial x} \end{Bmatrix}, \tag{10}$$

$$\begin{Bmatrix} \gamma_{xz}^{(0)} \\ \gamma_{yz}^{(0)} \\ \epsilon_{zz}^{(0)} \end{Bmatrix} = \begin{Bmatrix} u_1 + \frac{\partial w_0}{\partial x} \\ v_1 + \frac{\partial w_0}{\partial y} \\ w_1 \end{Bmatrix}; \quad \begin{Bmatrix} \gamma_{xz}^{(1)} \\ \gamma_{yz}^{(1)} \\ \epsilon_{zz}^{(1)} \end{Bmatrix} = \begin{Bmatrix} \frac{\partial w_1}{\partial x} \\ \frac{\partial w_1}{\partial y} \\ 2w_2 \end{Bmatrix}, \tag{11}$$

$$\begin{Bmatrix} \gamma_{xz}^{(2)} \\ \gamma_{yz}^{(2)} \\ \epsilon_{zz}^{(2)} \end{Bmatrix} = \begin{Bmatrix} \frac{\partial w_2}{\partial x} \\ \frac{\partial w_2}{\partial y} \\ 0 \end{Bmatrix}; \quad \begin{Bmatrix} \gamma_{xz}^{(Z)} \\ \gamma_{yz}^{(Z)} \\ \epsilon_{zz}^{(Z)} \end{Bmatrix} = \begin{Bmatrix} u_Z \\ v_Z \\ 0 \end{Bmatrix}, \tag{12}$$

where $\epsilon_{\alpha\beta}^{(nl)}$ are the non-linear terms that will originate the linearized buckling equations.

3.3 Elastic stress-strain relations

In the case of isotropic functionally graded materials, the 3D constitutive equations can be written as:

$$\begin{Bmatrix} \sigma_{xx} \\ \sigma_{yy} \\ \tau_{xy} \end{Bmatrix} = \begin{bmatrix} C_{11} & C_{12} & 0 \\ C_{12} & C_{11} & 0 \\ 0 & 0 & C_{44} \end{bmatrix} \begin{Bmatrix} \epsilon_{xx} \\ \epsilon_{yy} \\ \gamma_{xy} \end{Bmatrix} + \begin{bmatrix} 0 & 0 & C_{12} \\ 0 & 0 & C_{12} \\ 0 & 0 & 0 \end{bmatrix} \begin{Bmatrix} \gamma_{xz} \\ \gamma_{yz} \\ \epsilon_{zz} \end{Bmatrix},$$
$$\begin{Bmatrix} \tau_{xz} \\ \tau_{yz} \\ \sigma_{zz} \end{Bmatrix} = \begin{bmatrix} 0 & 0 & 0 \\ 0 & 0 & 0 \\ C_{12} & C_{12} & 0 \end{bmatrix} \begin{Bmatrix} \epsilon_{xx} \\ \epsilon_{yy} \\ \gamma_{xy} \end{Bmatrix} + \begin{bmatrix} C_{44} & 0 & 0 \\ 0 & C_{44} & 0 \\ 0 & 0 & C_{33} \end{bmatrix} \begin{Bmatrix} \gamma_{xz} \\ \gamma_{yz} \\ \epsilon_{zz} \end{Bmatrix}. \tag{13}$$

The computation of the elastic constants C_{ij} depends on which assumption of ϵ_{zz} we consider. If $\epsilon_{zz} = 0$, then C_{ij} are the plane-stress reduced elastic constants:

$$C_{11} = \frac{E}{1-\nu^2}; \quad C_{12} = \nu\frac{E}{1-\nu^2}; \quad C_{44} = G; \quad C_{33} = 0, \tag{14}$$

where E is the modulus of elasticity, ν is the Poisson's ratio, and G is the shear modulus $G = \frac{E}{2(1+\nu)}$.

It is interesting to note that the present theory does not require the use of shear-correction factors, as would be the case of the first-order shear deformation theory (FSDT).

If $\epsilon_{zz} \neq 0$ (thickness stretching), then the elastic coefficients C_{ij} are those of the three-dimensional stress state, given by

$$C_{11} = \frac{E(1-\nu^2)}{1-3\nu^2-2\nu^3}, \quad C_{12} = \frac{E(\nu+\nu^2)}{1-3\nu^2-2\nu^3}, \tag{15}$$

$$C_{44} = G, \quad C_{33} = \frac{E(1-\nu^2)}{1-3\nu^2-2\nu^3}. \tag{16}$$

3.4 Governing equations and boundary conditions

The governing equations of present theory are derived from the dynamic version of the Principle of Virtual Displacements (also known as Hamilton's Principle). It states that:

$$\delta U + \delta V = \delta K, \tag{17}$$

where δU is the virtual strain energy, δV is the virtual work done by applied forces, and δK is the virtual kinetic energy.

The internal virtual work is

$$\begin{aligned} \delta U = \int_{\Omega_0} \Bigg\{ \int_{-h/2}^{h/2} \Bigg[& \sigma_{xx}\left(\delta\epsilon_{xx}^{(0)} + z\delta\epsilon_{xx}^{(1)} + \sinh\left(\frac{\pi z}{h}\right)\delta\epsilon_{xx}^{(Z)}\right) + \sigma_{yy}\left(\delta\epsilon_{yy}^{(0)} + z\delta\epsilon_{yy}^{(1)} + \sinh\left(\frac{\pi z}{h}\right)\delta\epsilon_{yy}^{(Z)}\right) \\ & + \sigma_{xy}\left(\delta\gamma_{xy}^{(0)} + z\delta\gamma_{xy}^{(1)} + \sinh\left(\frac{\pi z}{h}\right)\delta\gamma_{xy}^{(Z)}\right) \\ & + \sigma_{xz}\left(\delta\gamma_{xz}^{(0)} + z\delta\gamma_{xz}^{(1)} + z^2\delta\gamma_{xz}^{(2)} + \frac{\pi}{h}\cosh\left(\frac{\pi z}{h}\right)\delta\gamma_{xz}^{(Z)}\right) \\ & + \sigma_{yz}\left(\delta\gamma_{yz}^{(0)} + z\delta\gamma_{yz}^{(1)} + z^2\delta\gamma_{yz}^{(2)} + \frac{\pi}{h}\cosh\left(\frac{\pi z}{h}\right)\delta\gamma_{yz}^{(Z)}\right) + \sigma_{zz}\left(\delta\epsilon_{zz}^{(0)} + z\delta\epsilon_{zz}^{(1)}\right)\Bigg] dz \Bigg\} dx\, dy, \end{aligned} \tag{18}$$

$$\begin{aligned} \delta U = \int_{\Omega_0} \big(& N_{xx}\delta\epsilon_{xx}^{(0)} + M_{xx}\delta\epsilon_{xx}^{(1)} + R_{xx}^Z\delta\epsilon_{xx}^{(Z)} + N_{yy}\delta\epsilon_{yy}^{(0)} + M_{yy}\delta\epsilon_{yy}^{(1)} + R_{yy}^Z\delta\epsilon_{yy}^{(Z)} \\ & + N_{xy}\delta\gamma_{xy}^{(0)} + M_{xy}\delta\gamma_{xy}^{(1)} + R_{xy}^Z\delta\gamma_{xy}^{(Z)} \\ & + Q_{xz}\delta\gamma_{xz}^{(0)} + M_{xz}\delta\gamma_{xz}^{(1)} + R_{xz}^2\delta\gamma_{xz}^{(2)} + R_{xz}^Z\delta\gamma_{xz}^{(Z)} \\ & + Q_{yz}\delta\gamma_{yz}^{(0)} + M_{yz}\delta\gamma_{yz}^{(1)} + R_{yz}^2\delta\gamma_{yz}^{(2)} + R_{yz}^Z\delta\gamma_{yz}^{(Z)} + Q_{zz}\delta\epsilon_{zz}^{(0)} + M_{zz}\delta\epsilon_{zz}^{(1)}\big) dx\, dy, \end{aligned} \tag{19}$$

where Ω_0 is the integration domain on plane (x, y) and

$$\left\{\begin{array}{c} N_{xx} \\ N_{yy} \\ N_{xy} \end{array}\right\} = \int_{-h/2}^{h/2} \left\{\begin{array}{c} \sigma_{xx} \\ \sigma_{yy} \\ \sigma_{xy} \end{array}\right\} dz, \quad \left\{\begin{array}{c} Q_{xz} \\ Q_{yz} \\ Q_{zz} \end{array}\right\} = \int_{-h/2}^{h/2} \left\{\begin{array}{c} \sigma_{xz} \\ \sigma_{yz} \\ \sigma_{zz} \end{array}\right\} dz, \tag{20}$$

$$\left\{\begin{array}{c} M_{xx} \\ M_{yy} \\ M_{xy} \end{array}\right\} = \int_{-h/2}^{h/2} z \left\{\begin{array}{c} \sigma_{xx} \\ \sigma_{yy} \\ \sigma_{xy} \end{array}\right\} dz, \quad \left\{\begin{array}{c} M_{xz} \\ M_{yz} \\ M_{zz} \end{array}\right\} = \int_{-h/2}^{h/2} z \left\{\begin{array}{c} \sigma_{xz} \\ \sigma_{yz} \\ \sigma_{zz} \end{array}\right\} dz, \tag{21}$$

$$\left\{\begin{array}{c} R^Z_{xx} \\ R^Z_{yy} \\ R^Z_{xy} \end{array}\right\} = \int_{-h/2}^{h/2} \sinh\left(\frac{\pi z}{h}\right) \left\{\begin{array}{c} \sigma_{xx} \\ \sigma_{yy} \\ \sigma_{xy} \end{array}\right\} dz, \quad \left\{\begin{array}{c} R^Z_{xz} \\ R^Z_{yz} \end{array}\right\} = \int_{-h/2}^{h/2} \frac{\pi}{h} \cosh\left(\frac{\pi z}{h}\right) \left\{\begin{array}{c} \sigma_{xz} \\ \sigma_{yz} \end{array}\right\} dz, \tag{22}$$

$$\left\{\begin{array}{c} R^2_{xz} \\ R^2_{yz} \end{array}\right\} = \int_{-h/2}^{h/2} z^2 \left\{\begin{array}{c} \sigma_{xz} \\ \sigma_{yz} \end{array}\right\} dz. \tag{23}$$

The external virtual work due to external loads applied to the plate is given as:

$$\begin{aligned} \delta V &= -\int_{\Omega_0} \left(p_x \delta u + p_y \delta v + p_z \delta w\right) dx\ dy \\ &= -\int_{\Omega_0} \Big(p_x \left(\delta u_0 + z\delta u_1 + \sinh\left(\frac{\pi z}{h}\right) \delta u_Z\right) + p_y \left(\delta v_0 + z\delta v_1 + \sinh\left(\frac{\pi z}{h}\right) \delta v_Z\right) \\ &\quad + p_z \left(\delta w_0 + z\delta w_1 + z^2 \delta w_2\right) \Big) dx\ dy. \end{aligned} \tag{24}$$

The external virtual work due to in-plane forces and shear forces applied to the plate is given as:

$$\delta V = -\int_{\Omega_0} \left[\bar{N}_{xx} \frac{\partial w_0}{\partial x} \frac{\delta \partial w_0}{\partial x} + \bar{N}_{xy} \frac{\partial w_0}{\partial y} \frac{\delta \partial w_0}{\partial x} + \bar{N}_{yx} \frac{\partial w_0}{\partial x} \frac{\delta \partial w_0}{\partial y} + \bar{N}_{yy} \frac{\partial w_0}{\partial y} \frac{\delta \partial w_0}{\partial y}\right] dx\ dy \tag{25}$$

being $\bar{N}_{xx}$ and $\bar{N}_{yy}$ the in-plane loads perpendicular to the edges $x = 0$ and $y = 0$, respectively, and $\bar{N}_{xy}$ and $\bar{N}_{yx}$ the distributed shear forces parallel to the edges $x = 0$ and $y = 0$, respectively.

The virtual kinetic energy is given as:

$$\begin{aligned} \delta K &= \int_{\Omega_0} \left\{ \int_{-h/2}^{h/2} \rho \left(\dot{u}\delta\dot{u} + \dot{v}\delta\dot{v} + \dot{w}\delta\dot{w}\right) dz \right\} dx\ dy \\ &= \int_{\Omega_0} \big[I_0 \left(\dot{u}_0\delta\dot{u}_0 + \dot{v}_0\delta\dot{v}_0 + \dot{w}_0\delta\dot{w}_0\right) \\ &\quad + I_1 \left(\dot{u}_0\delta\dot{u}_1 + \dot{u}_1\delta\dot{u}_0 + \dot{v}_0\delta\dot{v}_1 + \dot{v}_1\delta\dot{v}_0 + \dot{w}_0\delta\dot{w}_1 + \dot{w}_1\delta\dot{w}_0\right) \\ &\quad + I_2 \left(\dot{u}_1\delta\dot{u}_1 + \dot{v}_1\delta\dot{v}_1 + \dot{w}_0\delta\dot{w}_2 + \dot{w}_1\delta\dot{w}_1 + \dot{w}_2\delta\dot{w}_0\right) \\ &\quad + I_3 \left(\dot{w}_1\delta\dot{w}_2 + \dot{w}_2\delta\dot{w}_1\right) + I_4 \dot{w}_2\delta\dot{w}_2 \\ &\quad + I_5 \left(\dot{u}_0\delta\dot{u}_Z + \dot{u}_Z\delta\dot{u}_0 + \dot{v}_0\delta\dot{v}_Z + \dot{v}_Z\delta\dot{v}_0\right) \\ &\quad + I_6 \left(\dot{u}_Z\delta\dot{u}_Z + \dot{v}_Z\delta\dot{v}_Z\right) \\ &\quad + I_7 \left(\dot{u}_1\delta\dot{u}_Z + \dot{u}_Z\delta\dot{u}_1 + \dot{v}_Z\delta\dot{v}_1 + \dot{v}_1\delta\dot{v}_Z\right) \big] dx\ dy, \end{aligned} \tag{26}$$

where the dots denote the derivative with respect to time t and the inertia terms are defined as

$$I_i = \int_{-h/2}^{h/2} \rho z^i dz \quad i = 0, 1, 2, 3, 4\,, \tag{27}$$

$$I_5 = \int_{-h/2}^{h/2} \rho \sinh\left(\frac{\pi z}{h}\right) dz; \quad I_6 = \int_{-h/2}^{h/2} \rho \sinh^2\left(\frac{\pi z}{h}\right) dz; \quad I_7 = \int_{-h/2}^{h/2} \rho z \sinh\left(\frac{\pi z}{h}\right) dz. \tag{28}$$

Substituting δU, δV, and δK in the virtual work statement (17), integrating by parts with respect to x, y, and t and collecting the coefficients of δu_0, δu_1, δu_Z, δv_0, δv_1, δv_Z, δw_0, δw_1, δw_2, the following governing equations are obtained:

$$\begin{aligned}
&\delta u_0 : -\frac{\partial N_{xx}}{\partial x} - \frac{\partial N_{xy}}{\partial y} = I_0 \ddot{u}_0 + I_1 \ddot{u}_1 + I_5 \ddot{u}_Z + p_x,\\
&\delta v_0 : -\frac{\partial N_{xy}}{\partial x} - \frac{\partial N_{yy}}{\partial y} = I_0 \ddot{v}_0 + I_1 \ddot{v}_1 + I_5 \ddot{v}_Z + p_y,\\
&\delta w_0 : -\frac{\partial Q_{xz}}{\partial x} - \frac{\partial Q_{yz}}{\partial y} + \bar{N}_{xx}\frac{\partial^2 w_0}{\partial x^2} + \bar{N}_{xy}\frac{\partial^2 w_0}{\partial y \partial x} + \bar{N}_{yx}\frac{\partial^2 w_0}{\partial x \partial y}\\
&\qquad + \bar{N}_{yy}\frac{\partial^2 w_0}{\partial y^2} = I_0 \ddot{w}_0 + I_1 \ddot{w}_1 + I_2 \ddot{w}_2 + p_z,\\
&\delta u_1 : -\frac{\partial M_{xx}}{\partial x} - \frac{\partial M_{xy}}{\partial y} + Q_{xz} = I_1 \ddot{u}_0 + I_2 \ddot{u}_1 + I_7 \ddot{u}_Z + z p_x,\\
&\delta v_1 : -\frac{\partial M_{xy}}{\partial x} - \frac{\partial M_{yy}}{\partial y} + Q_{yz} = I_1 \ddot{v}_0 + I_2 \ddot{v}_1 + I_7 \ddot{v}_Z + z p_y,\\
&\delta w_1 : -\frac{\partial M_{xz}}{\partial x} - \frac{\partial M_{yz}}{\partial y} + Q_{zz} = I_1 \ddot{w}_0 + I_2 \ddot{w}_1 + I_3 \ddot{w}_2 + z p_z,\\
&\delta u_Z : -\frac{\partial R^Z_{xx}}{\partial x} - \frac{\partial R^Z_{xy}}{\partial y} + R^Z_{xz} = I_5 \ddot{u}_0 + I_7 \ddot{u}_1 + I_6 \ddot{u}_Z + \sinh\left(\frac{\pi z}{h}\right) p_x,\\
&\delta v_Z : -\frac{\partial R^Z_{xy}}{\partial x} - \frac{\partial R^Z_{yy}}{\partial y} + R^Z_{yz} = I_5 \ddot{v}_0 + I_7 \ddot{v}_1 + I_6 \ddot{v}_Z + \sinh\left(\frac{\pi z}{h}\right) p_y,\\
&\delta w_2 : -\frac{\partial R^2_{xz}}{\partial x} - \frac{\partial R^2_{yz}}{\partial y} + 2M_{zz} = I_2 \ddot{w}_0 + I_3 \ddot{w}_1 + I_4 \ddot{w}_2 + z^2 p_z.
\end{aligned} \tag{29}$$

The mechanical boundary conditions are:

$$\begin{aligned}
&\delta u_0 : n_x N_{xx} + n_y N_{xy} = n_x \bar{N}_{xx} + n_y \bar{N}_{xy},\\
&\delta v_0 : n_x N_{xy} + n_y N_{yy} = n_x \bar{N}_{xy} + n_y \bar{N}_{yy},\\
&\delta w_0 : n_x Q_{xz} + n_y Q_{yz} = n_x \bar{Q}_{xz} + n_y \bar{Q}_{yz},\\
&\delta u_1 : n_x M_{xx} + n_y M_{xy} = n_x \bar{M}_{xx} + n_y \bar{M}_{xy},\\
&\delta v_1 : n_x M_{xy} + n_y M_{yy} = n_x \bar{M}_{xy} + n_y \bar{M}_{yy}\\
&\delta w_1 : n_x M_{xz} + n_y M_{yz} = n_x \bar{M}_{xz} + n_y \bar{M}_{yz},\\
&\delta u_Z : n_x R^Z_{xx} + n_y R^Z_{xy} = n_x \bar{R}^Z_{xx} + n_y \bar{R}^Z_{xy},\\
&\delta v_Z : n_x R^Z_{xy} + n_y R^Z_{yy} = n_x \bar{R}^Z_{xy} + n_y \bar{R}^Z_{yy},\\
&\delta w_2 : n_x R^2_{xz} + n_y R^2_{yz} = n_x \bar{R}^2_{xz} + n_y \bar{R}^2_{yz},
\end{aligned} \tag{30}$$

where (n_x, n_y) denotes the unit normal-to-boundary vector.

4 Governing equations and boundary conditions in the framework of Unified Formulation

The governing equations and the boundary conditions are automatically obtained by the Carrera's Unified Formulation (CUF). Readers should consult [49, 50] for details.

In the CUF formulation we consider N_L virtual (mathematical) layers of constant thickness, each containing a homogenized modulus of elasticity, E^k, and a homogenized Poisson's ratio, ν^k. The volume fraction of the ceramic phase is defined for each layer k according to (2) and the elastic properties E^k and ν^k are computed considering the law-of-mixtures:

$$E^k(z) = E_m V_m + E_c V_c; \qquad \nu^k(z) = \nu_m V_m + \nu_c V_c. \tag{31}$$

4.1 Strains

Stresses and strains are separated into in-plane and normal components, denoted respectively by the subscripts p and n. The mechanical strains in the kth layer can be related to the displacement field $\mathbf{u}^k = \{u_x^k, u_y^k, u_z^k\}$ via the geometrical relations:

$$\begin{aligned} \epsilon_{pG}^k &= [\epsilon_{xx}, \epsilon_{yy}, \gamma_{xy}]^{kT} = \mathbf{D}_p^{k(nl)} \mathbf{u}^k \ , \\ \epsilon_{nG}^k &= [\gamma_{xz}, \gamma_{yz}, \epsilon_{zz}]^{kT} = (\mathbf{D}_{np}^k + \mathbf{D}_{nz}^k)\, \mathbf{u}^k \ , \end{aligned} \tag{32}$$

wherein the differential operator arrays are defined as follows:

$$\mathbf{D}_p^{k(nl)} = \begin{bmatrix} \partial_x & 0 & \partial_x^2/2 \\ 0 & \partial_y & \partial_y^2/2 \\ \partial_y & \partial_x & \partial_x \partial_y \end{bmatrix}, \quad \mathbf{D}_{np}^k = \begin{bmatrix} 0 & 0 & \partial_x \\ 0 & 0 & \partial_y \\ 0 & 0 & 0 \end{bmatrix}, \quad \mathbf{D}_{nz}^k = \begin{bmatrix} \partial_z & 0 & 0 \\ 0 & \partial_z & 0 \\ 0 & 0 & \partial_z \end{bmatrix}. \tag{33}$$

Although one needs to account for the nonliner contributions for the buckling analysis, we can use the linear version of CUF as the non-linear terms will only influence the equation refering to δw_0. In fact, the compressive in-plane forces and distributed shear forces only actuate on the mid-plane ($z = 0$) and the nonlinear terms are reduced to $\frac{1}{2}\left(\frac{\partial w_0}{\partial x}\right)^2$, $\frac{1}{2}\left(\frac{\partial w_0}{\partial y}\right)^2$, and $\frac{\partial w_0}{\partial x}\frac{\partial w_0}{\partial y}$. So we use

$$\mathbf{D}_p^k = \begin{bmatrix} \partial_x & 0 & 0 \\ 0 & \partial_y & 0 \\ \partial_y & \partial_x & 0 \end{bmatrix} \tag{34}$$

instead of $\mathbf{D}_p^{k(nl)}$ and just add the terms in referred equation.

4.2 Elastic stress-strain relations

The 3D constitutive equations in each layer k are given as:

$$\begin{aligned} \sigma_{pC}^k &= \mathbf{C}_{pp}^k\, \epsilon_{pG}^k + \mathbf{C}_{pn}^k\, \epsilon_{nG}^k, \\ \sigma_{nC}^k &= \mathbf{C}_{np}^k\, \epsilon_{pG}^k + \mathbf{C}_{nn}^k\, \epsilon_{nG}^k \end{aligned} \tag{35}$$

with

$$\begin{aligned} \mathbf{C}_{pp}^k &= \begin{bmatrix} C_{11} & C_{12} & 0 \\ C_{12} & C_{11} & 0 \\ 0 & 0 & C_{44} \end{bmatrix}, \qquad \mathbf{C}_{pn}^k = \begin{bmatrix} 0 & 0 & C_{12} \\ 0 & 0 & C_{12} \\ 0 & 0 & 0 \end{bmatrix}, \\ \mathbf{C}_{np}^k &= \begin{bmatrix} 0 & 0 & 0 \\ 0 & 0 & 0 \\ C_{12} & C_{12} & 0 \end{bmatrix}, \qquad \mathbf{C}_{nn}^k = \begin{bmatrix} C_{44} & 0 & 0 \\ 0 & C_{44} & 0 \\ 0 & 0 & C_{33} \end{bmatrix}. \end{aligned} \tag{36}$$

These are the reduced matrices for isotropic or functionally graded materials only.

The computation of the elastic constants C_{ij}^k depends on which assumption of ϵ_{zz} we consider. If $\epsilon_{zz} = 0$, then C_{ij}^k are the plane-stress reduced elastic constants:

$$C_{11}^k = \frac{E^k}{1-(\nu^k)^2}, \quad C_{12}^k = \nu^k \frac{E^k}{1-(\nu^k)^2}, \quad C_{44}^k = G^k, \quad C_{33}^k = 0, \tag{37}$$

where E^k is the modulus of elasticity, ν^k is the Poisson's ratio, and G^k is the shear modulus $G^k = \frac{E^k}{2(1+\nu^k)}$ for each layer.

If $\epsilon_{zz} \neq 0$ (thickness stretching), then C_{ij}^k are the three-dimensional elastic constants, given by

$$C_{11}^k = C_{33}^k = \frac{E^k(1-(\nu^k)^2)}{1-3(\nu^k)^2-2(\nu^k)^3}, \quad C_{12}^k = \frac{E^k(\nu^k+(\nu^k)^2)}{1-3(\nu^k)^2-2(\nu^k)^3}, \quad C_{44}^k = G^k. \tag{38}$$

Substituting in the equilibrium equations (28) and performing the products, one obtains the following governing equations of the buckling problem:

$$\begin{aligned}
&\delta u_0 : -\partial_x N_{xx} - \partial_y N_{xy} = 0, \\
&\delta v_0 : -\partial_x N_{xy} - \partial_y N_{yy} = 0, \\
&\delta w_0 : -\partial_x Q_{xz} - \partial_y Q_{yz} + \bar{N}_{xx}\frac{\partial^2 w_0}{\partial x^2} + 2\bar{N}_{xy}\frac{\partial^2 w_0}{\partial x \partial y} + \bar{N}_{yy}\frac{\partial^2 w_0}{\partial y^2} = 0, \\
&\delta u_1 : -\partial_x M_{xx} - \partial_y M_{xy} + Q_{xz} = 0, \\
&\delta v_1 : -\partial_x M_{xy} - \partial_y M_{yy} + Q_{yz} = 0, \\
&\delta w_1 : -\partial_x M_{xz} - \partial_y M_{yz} + Q_{zz} = 0, \\
&\delta u_Z : -\partial_x R_{xx}^Z - \partial_y R_{xy}^Z + R_{xz}^Z = 0, \\
&\delta v_Z : -\partial_x R_{xy}^Z - \partial_y R_{yy}^Z + R_{yz}^Z = 0, \\
&\delta w_2 : -\partial_x R_{xz}^2 - \partial_y R_{yz}^2 + 2M_{zz}^2 = 0,
\end{aligned} \tag{39}$$

and the mechanical boundary conditions are as in (30).

4.3 Governing equations in terms of displacements

In order to discretize the governing equations by radial basis functions, we present in the following the explicit terms of the equations of motion and the boundary conditions in terms of the generalized displacements.

$$\begin{aligned}
\delta u_0 :& -\left(G_{11}\frac{\partial^2 u_Z}{\partial x^2} + G_{66}\frac{\partial^2 u_Z}{\partial y^2}\right) - (G_{12}+G_{66})\frac{\partial^2 v_Z}{\partial x \partial y} - \left(A_{11}\frac{\partial^2 u_0}{\partial x^2} + A_{66}\frac{\partial^2 u_0}{\partial y^2}\right) \\
&- (A_{12}+A_{66})\frac{\partial^2 v_0}{\partial x \partial y} - \left(B_{11}\frac{\partial^2 u_1}{\partial x^2} + B_{66}\frac{\partial^2 u_1}{\partial y^2}\right) - (B_{12}+B_{66})\frac{\partial^2 v_1}{\partial x \partial y} \\
&- A_{13}\frac{\partial w_1}{\partial x} - 2B_{13}\frac{\partial w_2}{\partial x} = 0,
\end{aligned} \tag{40}$$

$$\begin{aligned}
\delta u_1 :& \left(-D_{11}\frac{\partial^2 u_1}{\partial x^2} + A_{55}u_1 - D_{66}\frac{\partial^2 u_1}{\partial y^2}\right) + \left(H_{55}u_Z + N_{11}\frac{\partial^2 u_Z}{\partial x^2} + N_{66}\frac{\partial^2 u_Z}{\partial y^2}\right) \\
&+ (N_{12}+N_{66})\frac{\partial^2 v_Z}{\partial x \partial y} - \left(B_{11}\frac{\partial^2 u_0}{\partial x^2} + B_{66}\frac{\partial^2 u_0}{\partial y^2}\right) - (B_{12}+B_{66})\frac{\partial^2 v_0}{\partial x \partial y} \\
&- (D_{12}+D_{66})\frac{\partial^2 v_1}{\partial x \partial y} + (B_{55}-B_{13})\frac{\partial w_1}{\partial x} + (D_{55}-2D_{13})\frac{\partial w_2}{\partial x} + A_{55}\frac{\partial w_0}{\partial x} = 0,
\end{aligned} \tag{41}$$

$$\begin{aligned}
&\delta u_Z : -\left(G_{11}\frac{\partial^2 u_0}{\partial x^2} + G_{66}\frac{\partial^2 u_0}{\partial y^2}\right) + (O_{55} - G_{55} - G_{13})\frac{\partial w_1}{\partial x} \\
&+\left(H_{55}u_1 + N_{11}\frac{\partial^2 u_1}{\partial x^2} + N_{66}\frac{\partial^2 u_1}{\partial y^2}\right) - (G_{12} + G_{66})\frac{\partial^2 v_0}{\partial x \partial y} \\
&+\left(-J_{11}\frac{\partial^2 u_Z}{\partial x^2} + R_{55}u_Z - J_{66}\frac{\partial^2 u_Z}{\partial y^2}\right) + (P_{55} + 2N_{55} + 2N_{13})\frac{\partial w_2}{\partial x} \\
&+ (N_{12} + N_{66})\frac{\partial^2 v_1}{\partial x \partial y} - (J_{12} + J_{66})\frac{\partial^2 v_Z}{\partial x \partial y} + H_{55}\frac{\partial w_0}{\partial x} = 0,
\end{aligned} \tag{42}$$

$$\begin{aligned}
&\delta v_0 : -(G_{12} + G_{66})\frac{\partial^2 u_Z}{\partial x \partial y} - \left(G_{22}\frac{\partial^2 v_Z}{\partial y^2} + G_{66}\frac{\partial^2 v_Z}{\partial x^2}\right) - (A_{12} + A_{66})\frac{\partial^2 u_0}{\partial x \partial y} \\
&-\left(A_{22}\frac{\partial^2 v_0}{\partial y^2} + A_{66}\frac{\partial^2 v_0}{\partial x^2}\right) - (B_{12} + B_{66})\frac{\partial^2 u_1}{\partial x \partial y} - \left(B_{22}\frac{\partial^2 v_1}{\partial y^2} + B_{66}\frac{\partial^2 v_1}{\partial x^2}\right) \\
&- A_{23}\frac{\partial w_1}{\partial y} - 2B_{23}\frac{\partial w_2}{\partial y} = 0,
\end{aligned} \tag{43}$$

$$\begin{aligned}
&\delta v_1 : \left(-D_{22}\frac{\partial^2 v_1}{\partial y^2} + A_{44}v_1 - D_{66}\frac{\partial^2 v_1}{\partial x^2}\right) \\
&+\left(H_{44}v_Z + N_{22}\frac{\partial^2 v_Z}{\partial y^2} + N_{66}\frac{\partial^2 v_Z}{\partial x^2}\right) + (N_{12} + N_{66})\frac{\partial^2 u_Z}{\partial x \partial y} \\
&- (B_{12} + B_{66})\frac{\partial^2 u_0}{\partial x \partial y} - (D_{12} + D_{66})\frac{\partial^2 u_1}{\partial x \partial y} - \left(B_{22}\frac{\partial^2 v_0}{\partial y^2} + B_{66}\frac{\partial^2 v_0}{\partial x^2}\right) \\
&+ (B_{44} - B_{23})\frac{\partial w_1}{\partial y} + (D_{44} - 2D_{23})\frac{\partial w_2}{\partial y} + A_{44}\frac{\partial w_0}{\partial y} = 0,
\end{aligned} \tag{44}$$

$$\begin{aligned}
&\delta v_Z : -(G_{12} + G_{66})\frac{\partial^2 u_0}{\partial x \partial y} + (O_{44} - G_{44} - G_{23})\frac{\partial w_1}{\partial y} \\
&+\left(H_{44}v_1 + N_{22}\frac{\partial^2 v_1}{\partial y^2} + N_{66}\frac{\partial^2 v_1}{\partial x^2}\right) - \left(G_{22}\frac{\partial^2 v_0}{\partial y^2} + G_{66}\frac{\partial^2 v_0}{\partial x^2}\right) \\
&+\left(-J_{22}\frac{\partial^2 v_Z}{\partial y^2} + R_{44}v_Z - J_{66}\frac{\partial^2 v_Z}{\partial x^2}\right) + (P_{44} + 2N_{44} + 2N_{23})\frac{\partial w_2}{\partial y} \\
&+ (N_{12} + N_{66})\frac{\partial^2 u_1}{\partial x \partial y} - (J_{12} + J_{66})\frac{\partial^2 u_Z}{\partial x \partial y} + H_{44}\frac{\partial w_0}{\partial y} = 0,
\end{aligned} \tag{45}$$

$$\begin{aligned}
&\delta w_0 : -\left(A_{55}\frac{\partial^2 w_0}{\partial x^2} + A_{44}\frac{\partial^2 w_0}{\partial y^2}\right) - \left(B_{55}\frac{\partial^2 w_1}{\partial x^2} + B_{44}\frac{\partial^2 w_1}{\partial y^2}\right) \\
&-\left(D_{55}\frac{\partial^2 w_2}{\partial x^2} + D_{44}\frac{\partial^2 w_2}{\partial y^2}\right) - H_{55}\frac{\partial u_Z}{\partial x} - H_{44}\frac{\partial v_Z}{\partial y} - A_{55}\frac{\partial u_1}{\partial x} - A_{44}\frac{\partial v_1}{\partial y} \\
&+ \bar{N}_{xx}\frac{\partial^2 w_0}{\partial x^2} + 2\bar{N}_{xy}\frac{\partial^2 w_0}{\partial x \partial y} + \bar{N}_{yy}\frac{\partial^2 w_0}{\partial y^2} = 0,
\end{aligned} \tag{46}$$

$$\begin{aligned}
&\delta w_1 : \left(-E_{55}\frac{\partial^2 w_2}{\partial x^2} + 2B_{33}w_2 - E_{44}\frac{\partial^2 w_2}{\partial y^2}\right) + (-O_{55} + G_{55} + G_{13})\frac{\partial u_Z}{\partial x} \\
&+ (-O_{44} + G_{44} + G_{23})\frac{\partial v_Z}{\partial y} + \left(-D_{55}\frac{\partial^2 w_1}{\partial x^2} + A_{33}w_1 - D_{44}\frac{\partial^2 w_1}{\partial y^2}\right) + (B_{13} - B_{55})\frac{\partial u_1}{\partial x} \\
&+ (B_{23} - B_{44})\frac{\partial v_1}{\partial y} - \left(B_{55}\frac{\partial^2 w_0}{\partial x^2} + B_{44}\frac{\partial^2 w_0}{\partial y^2}\right) + A_{13}\frac{\partial u_0}{\partial x} + A_{23}\frac{\partial v_0}{\partial y} = 0,
\end{aligned} \tag{47}$$

$$\delta w_2 : \left(-E_{55}\frac{\partial^2 w_1}{\partial x^2} + 2B_{33}w_1 - E_{44}\frac{\partial^2 w_1}{\partial y^2}\right) + \left(-F_{55}\frac{\partial^2 w_2}{\partial x^2} + 4D_{33}w_2 - F_{44}\frac{\partial^2 w_2}{\partial y^2}\right)$$
$$- (P_{55} + 2N_{55} + 2N_{13})\frac{\partial u_Z}{\partial x} - (P_{44} + 2N_{44} + 2N_{23})\frac{\partial v_Z}{\partial y} + (2D_{13} - D_{55})\frac{\partial u_1}{\partial x}$$
$$+ (2D_{23} - D_{44})\frac{\partial v_1}{\partial y} - \left(D_{55}\frac{\partial^2 w_0}{\partial x^2} + D_{44}\frac{\partial^2 w_0}{\partial y^2}\right) + 2B_{13}\frac{\partial u_0}{\partial x} + 2B_{23}\frac{\partial v_0}{\partial y} = 0. \tag{48}$$

Being N_l the number of mathematical layers across the thickness direction, the stiffness components can be computed as follows.

$$A_{ij} = \sum_{k=1}^{N_l} C_{ij}^{(k)} (z_{k+1} - z_k) \qquad B_{ij} = \frac{1}{2}\sum_{k=1}^{N_l} C_{ij}^{(k)} \left(z_{k+1}^2 - z_k^2\right),$$
$$D_{ij} = \frac{1}{3}\sum_{k=1}^{N_l} C_{ij}^{(k)} \left(z_{k+1}^3 - z_k^3\right) \qquad E_{ij} = \frac{1}{4}\sum_{k=1}^{N_l} C_{ij}^{(k)} \left(z_{k+1}^4 - z_k^4\right),$$
$$F_{ij} = \frac{1}{5}\sum_{k=1}^{N_l} C_{ij}^{(k)} \left(z_{k+1}^5 - z_k^5\right),$$
$$G_{ij} = \sum_{k=1}^{N_l} C_{ij}^{(k)} \frac{h_k}{\pi}\left[\cosh\left(\frac{\pi z_{k+1}}{h_k}\right) - \cosh\left(\frac{\pi z_k}{h_k}\right)\right],$$
$$H_{ij} = \sum_{k=1}^{N_l} C_{ij}^{(k)} \left[\sinh\left(\frac{\pi z_{k+1}}{h_k}\right) - \sinh\left(\frac{\pi z_k}{h_k}\right)\right],$$
$$J_{ij} = \sum_{k=1}^{N_l} C_{ij}^{(k)} \left[\frac{h_k}{4\pi}\left[\sinh\left(\frac{2\pi z_{k+1}}{h_k}\right) - \sinh\left(\frac{2\pi z_k}{h_k}\right)\right] - \frac{1}{2}(z_{k+1} - z_k)\right],$$
$$N_{ij} = \sum_{k=1}^{N_l} C_{ij}^{(k)} \left[\left(\frac{h_k}{\pi}\right)^2\left(\sinh\left(\frac{\pi z_{k+1}}{h_k}\right) - \sinh\left(\frac{\pi z_k}{h_k}\right)\right)\right.$$
$$\left. - \frac{h_k}{\pi}\left(z_{k+1}\cosh\left(\frac{\pi z_{k+1}}{h_k}\right) - z_k\cosh\left(\frac{\pi z_k}{h_k}\right)\right)\right], \tag{49}$$
$$O_{ij} = \sum_{k=1}^{N_l} C_{ij}^{(k)} \left[z_{k+1}\sinh\left(\frac{\pi z_{k+1}}{h_k}\right) - z_k\sinh\left(\frac{\pi z_k}{h_k}\right)\right],$$
$$P_{ij} = \sum_{k=1}^{N_l} C_{ij}^{(k)} \left[z_{k+1}^2\sinh\left(\frac{\pi z_{k+1}}{h_k}\right) - z_k^2\sinh\left(\frac{\pi z_k}{h_k}\right)\right],$$
$$R_{ij} = \sum_{k=1}^{N_l} C_{ij}^{(k)} \left[\frac{\pi}{4h_k}\left[\sinh\left(\frac{2\pi z_{k+1}}{h_k}\right) - \sinh\left(\frac{2\pi z_k}{h_k}\right)\right] + \frac{1}{2}\left(\frac{\pi}{h_k}\right)^2 (z_{k+1} - z_k)\right],$$

where h_k is the thickness of each layer and z_k, z_{k+1} are the lower and upper z coordinate for each layer k.

4.4 Natural boundary conditions

This meshless method based on collocation with radial basis functions needs the imposition of essential (e.g. $w = 0$) and mechanical (e.g. $M_{xx} = 0$) boundary conditions. Assuming a rectangular plate (for the sake of simplicity) Eqs. (39) are expressed as follows.

Given the number of degrees of freedom, at each boundary point at edges $x = \min$ or $x = \max$ we impose:

$$M_{xxu0} = 2B_{13}w_2 + A_{13}w_1 + A_{11}\frac{\partial u_0}{\partial x} + A_{12}\frac{\partial v_0}{\partial y} + B_{11}\frac{\partial u_1}{\partial x} + B_{12}\frac{\partial v_1}{\partial y} + G_{11}\frac{\partial u_Z}{\partial x} + G_{12}\frac{\partial v_Z}{\partial y}, \quad (50)$$

$$M_{xxu1} = -N_{11}\frac{\partial u_Z}{\partial x} + 2D_{13}w_2 + B_{13}w_1 - N_{12}\frac{\partial v_Z}{\partial y} + B_{11}\frac{\partial u_0}{\partial x} + D_{11}\frac{\partial u_1}{\partial x} + B_{12}\frac{\partial v_0}{\partial y} + D_{12}\frac{\partial v_1}{\partial y}, \quad (51)$$

$$M_{xxuZ} = -2N_{13}w_2 - N_{11}\frac{\partial u_1}{\partial x} - N_{12}\frac{\partial v_1}{\partial y} + J_{11}\frac{\partial u_Z}{\partial x} + J_{12}\frac{\partial v_Z}{\partial y} + G_{13}w_1 + G_{11}\frac{\partial u_0}{\partial x} + G_{12}\frac{\partial v_0}{\partial y}, \quad (52)$$

$$M_{xxv0} = A_{66}\frac{\partial u_0}{\partial y} + A_{66}\frac{\partial v_0}{\partial x} + B_{66}\frac{\partial u_1}{\partial y} + B_{66}\frac{\partial v_1}{\partial x} + G_{66}\frac{\partial u_Z}{\partial y} + G_{66}\frac{\partial v_Z}{\partial x}, \quad (53)$$

$$M_{xxv1} = -N_{66}\frac{\partial u_Z}{\partial y} - N_{66}\frac{\partial v_Z}{\partial x} + B_{66}\frac{\partial u_0}{\partial y} + D_{66}\frac{\partial u_1}{\partial y} + B_{66}\frac{\partial v_0}{\partial x} + D_{66}\frac{\partial v_1}{\partial x}, \quad (54)$$

$$M_{xxvZ} = -N_{66}\frac{\partial u_1}{\partial y} - N_{66}\frac{\partial v_1}{\partial x} + J_{66}\frac{\partial u_Z}{\partial y} + J_{66}\frac{\partial v_Z}{\partial x} + G_{66}\frac{\partial u_0}{\partial y} + G_{66}\frac{\partial v_0}{\partial x}, \quad (55)$$

$$M_{xxw0} = H_{55}u_Z + A_{55}u_1 + A_{55}\frac{\partial w_0}{\partial x} + B_{55}\frac{\partial w_1}{\partial x} + D_{55}\frac{\partial w_2}{\partial x}, \quad (56)$$

$$M_{xxw1} = B_{55}u_1 + (O_{55} - G_{55})\,u_Z + B_{55}\frac{\partial w_0}{\partial x} + D_{55}\frac{\partial w_1}{\partial x} + E_{55}\frac{\partial w_2}{\partial x}, \quad (57)$$

$$M_{xxw2} = D_{55}u_1 + (P_{55} + 2N_{55})\,u_Z + D_{55}\frac{\partial w_0}{\partial x} + E_{55}\frac{\partial w_1}{\partial x} + F_{55}\frac{\partial w_2}{\partial x}. \quad (58)$$

Similarly, given the number of degrees of freedom, at each boundary point at edges $y = \min$ or $y = \max$ we impose:

$$M_{yyu0} = A_{66}\frac{\partial u_0}{\partial y} + A_{66}\frac{\partial v_0}{\partial x} + B_{66}\frac{\partial u_1}{\partial y} + B_{66}\frac{\partial v_1}{\partial x} + G_{66}\frac{\partial u_Z}{\partial y} + G_{66}\frac{\partial v_Z}{\partial x}, \quad (59)$$

$$M_{yyu1} = -N_{66}\frac{\partial u_Z}{\partial y} - N_{66}\frac{\partial v_Z}{\partial x} + B_{66}\frac{\partial u_0}{\partial y} + D_{66}\frac{\partial u_1}{\partial y} + B_{66}\frac{\partial v_0}{\partial x} + D_{66}\frac{\partial v_1}{\partial x}, \quad (60)$$

$$M_{yyuZ} = -N_{66}\frac{\partial u_1}{\partial y} - N_{66}\frac{\partial v_1}{\partial x} + J_{66}\frac{\partial u_Z}{\partial y} + J_{66}\frac{\partial v_Z}{\partial x} + G_{66}\frac{\partial u_0}{\partial y} + G_{66}\frac{\partial v_0}{\partial x}, \quad (61)$$

$$M_{yyv0} = A_{12}\frac{\partial u_0}{\partial x} + A_{22}\frac{\partial v_0}{\partial y} + B_{12}\frac{\partial u_1}{\partial x} + B_{22}\frac{\partial v_1}{\partial y} + G_{12}\frac{\partial u_Z}{\partial x} + G_{22}\frac{\partial v_Z}{\partial y}, \quad (62)$$

$$M_{yyv1} = -N_{12}\frac{\partial u_Z}{\partial x} - N_{22}\frac{\partial v_Z}{\partial y} + B_{12}\frac{\partial u_0}{\partial x} + D_{12}\frac{\partial u_1}{\partial x} + B_{22}\frac{\partial v_0}{\partial y} + D_{22}\frac{\partial v_1}{\partial y}, \quad (63)$$

$$M_{yyvZ} = -N_{12}\frac{\partial u_1}{\partial x} - N_{22}\frac{\partial v_1}{\partial y} + J_{12}\frac{\partial u_Z}{\partial x} + J_{22}\frac{\partial v_Z}{\partial y} + G_{12}\frac{\partial u_0}{\partial x} + G_{22}\frac{\partial v_0}{\partial y}, \quad (64)$$

$$M_{yyw0} = H_{44}v_Z + A_{44}v_1 + A_{44}\frac{\partial w_0}{\partial y} + B_{44}\frac{\partial w_1}{\partial y} + D_{44}\frac{\partial w_2}{\partial y}, \quad (65)$$

$$M_{yyw1} = B_{44}v_1 + (O_{44} - G_{44})\,v_Z + B_{44}\frac{\partial w_0}{\partial y} + D_{44}\frac{\partial w_1}{\partial y} + E_{44}\frac{\partial w_2}{\partial y}, \quad (66)$$

$$M_{yyw2} = D_{44}v_1 + (P_{44} + 2N_{44})\,v_Z + D_{44}\frac{\partial w_0}{\partial y} + E_{44}\frac{\partial w_1}{\partial y} + F_{44}\frac{\partial w_2}{\partial y}, \quad (67)$$

with A_{ij}, B_{ij}, D_{ij}, E_{ij}, F_{ij}, G_{ij}, H_{ij}, J_{ij}, N_{ij}, O_{ij}, P_{ij}, R_{ij} already given in (49).

5 The radial basis function method for buckling problems

The equations of motion and the boundary conditions are discretized by collocation with radial basis functions. Readers should consult [38–48, 51, 52] for details.

6 Numerical examples

In the next examples the hyperbolic sine plate theory and collocation with RBFs are used for the buckling analysis of simply supported functionally graded sandwich square plates. The uni- and bi-axial critical buckling loads are analised. The plates have side lengths $a = b$, thickness h, and the side-to-thickness ratio is $a/h = 10$.

The core material of the present sandwich plate is fully ceramic. The bottom skin varies from a metal-rich surface to a ceramic-rich surface while the top skin face varies from a ceramic-rich surface to a metal-rich surface. The material properties are $E_m = 70E_0$ (aluminum) and $E_c = 380E_0$ (alumina) being $E_0 = 1$GPa. Poisson's ratio is $\nu_m = \nu_c = \nu = 0.3$ for both aluminum and alumina. The non-dimensional parameter used is

$$\bar{P} = \frac{Pa^2}{100h^3E_0}.$$

The chosen RBF is the Wendland with an optimized shape parameter. Readers should consult [16] for details on the optimization method. All numerical examples consider a Chebyshev grid. A 17^2 points Chebyshev grid is illustrated in Fig. 4. For a given number of nodes per side (N), it is generated by MATLAB code:

```
x = cos(pi*(0:N)/N)';
y=x;
```

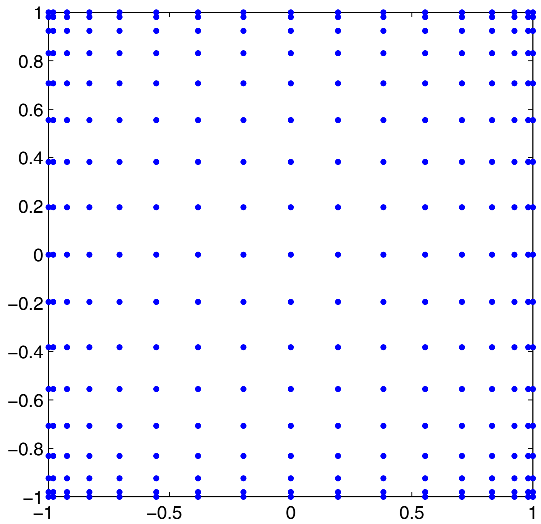

Fig. 4 (online colour at: www.zamm-journal.org) Chebyshev grid with N=17.

91 mathematical layers were considered in order to model the continuous variation of properties across the thickness direction. A significant number of mathematical layers is needed to ensure correct material properties at each thickness position.

An initial convergence study with the hyperbolic sine theory was conducted for each buckling load type considerind grids of 13^2, 17^2, and 21^2 points. The uni-axial case is presented in Table 1 for the 2-1-2 sandwich with $p = 0.5$ and the bi-axial case is presented in Table 2 for the 2-2-1 sandwich with $p = 10$. Further results are obtained by considering a grid of 17^2 points.

Table 1 Convergence study for the uni-axial buckling load of a simply supported 2-1-2 sandwich square plate with FGM skins and $p = 0.5$ case using the hyperbolic sine theory.

grid	13^2	17^2	21^2
$\bar{P}$	7.71678	7.71617	7.71610

Table 2 Convergence study for the bi-axial buckling load of a simply supported 2-2-1 sandwich square plate with FGM skins and $p = 10$ case using the hyperbolic sine theory.

grid	13^2	17^2	21^2
$\bar{P}$	1.83092	1.83083	1.83081

The critical buckling loads obtained from the present approach with $\epsilon_{zz} \neq 0$ and $\epsilon_{zz} = 0$ are tabulated and compared with those from Zenkour [22] in Tables 3 and 4 for various power-law exponents p and thickness ratios. Both tables include results obtained from classical plate theory (CLPT), first-order shear deformation plate theory (FSDT, $K = 5/6$ as shear correction factor), Reddy's third-order shear deformation plate theory (TSDPT) [25], and Zenkour's sinusoidal shear deformation plate theory (SSDPT) [22]. Table 3 refers to the uni-axial buckling load and Table 4 refers to the bi-axial buckling load.

Table 3 Uni-axial buckling load of simply supported sandwich square plates with FGM skins using the hyperbolic sine theory and a grid with 17^2 points.

p	Theory	$\bar{P}$					
		1-0-1	2-1-2	2-1-1	1-1-1	2-2-1	1-2-1
0	CLPT	13.73791	13.73791	13.73791	13.73791	13.73791	13.73791
	FSDT	13.00449	13.00449	13.00449	13.00449	13.00449	13.00449
	TSDPT [25]	13.00495	13.00495	13.00495	13.00495	13.00495	13.00495
	SSDPT [22]	13.00606	13.00606	13.00606	13.00606	13.00606	13.00606
	present $\epsilon_{zz} \neq 0$	12.95304	12.95304	12.95304	12.95304	12.95304	12.95304
	present $\epsilon_{zz} = 0$	13.00532	13.00532	13.00532	13.00532	13.00532	13.00532
0.5	CLPT	7.65398	8.25597	8.56223	8.78063	9.18254	9.61525
	FSDT	7.33732	7.91320	8.20015	8.41034	8.78673	9.19517
	TSDPT [25]	7.36437	7.94084	8.22470	8.43645	8.80997	9.21681
	SSDPT [22]	7.36568	7.94195	8.22538	8.43712	8.81037	9.21670
	present $\epsilon_{zz} \neq 0$	7.16191	7.71617	7.98959	8.19283	8.55184	8.94221
	present $\epsilon_{zz} = 0$	7.18707	7.74315	8.01707	8.22141	8.58146	8.97351
1	CLPT	5.33248	6.02733	6.40391	6.68150	7.19663	7.78406
	FSDT	5.14236	5.81379	6.17020	6.43892	6.92571	7.48365
	TSDPT [25]	5.16713	5.84006	6.19394	6.46474	6.94944	7.50656
	SSDPT [22]	5.16846	5.84119	6.19461	6.46539	6.94980	7.50629
	present $\epsilon_{zz} \neq 0$	5.06123	5.71125	6.05467	6.31501	6.78413	7.32025
	present $\epsilon_{zz} = 0$	5.07825	5.73007	6.07357	6.33558	6.80559	7.34408
5	CLPT	2.73080	3.10704	3.48418	3.65732	4.21238	4.85717
	FSDT	2.63842	3.02252	3.38538	3.55958	4.09285	4.71475
	TSDPT [25]	2.65821	3.04257	3.40351	3.57956	4.11209	4.73469
	SSDPT [22]	2.66006	3.04406	3.40449	3.58063	4.11288	4.73488
	present $\epsilon_{zz} \neq 0$	2.63658	3.00819	3.36256	3.53014	4.05069	4.64707
	present $\epsilon_{zz} = 0$	2.64662	3.01870	3.37187	3.54145	4.06157	4.66071
10	CLPT	2.56985	2.80340	3.16427	3.25924	3.79238	4.38221
	FSDT	2.46904	2.72626	3.07428	3.17521	3.68890	4.26040
	TSDPT [25]	2.48727	2.74632	3.09190	3.19471	3.70752	4.27991
	SSDPT [22]	2.48928	2.74844	3.13443	3.19456	3.14574	4.38175
	present $\epsilon_{zz} \neq 0$	2.47199	2.72089	3.06071	3.15785	3.66166	4.20550
	present $\epsilon_{zz} = 0$	2.48179	2.73094	3.06936	3.16842	3.67146	4.21795

There is a good agreement between the present solution and references considered, specially [25] and [22]. This allow us to conclude that the present hyperbolic plate theory is good for the modeling of simply supported sandwich FGM plates and that the collocation with RBFs is a good approach. Present results with $\epsilon_{zz} = 0$ approximate better the results of references [25] and [22] than $\epsilon_{zz} \neq 0$ as the authors use the $\epsilon_{zz} = 0$ approach. This study also leads us to conclude that the

Table 4 Bi-axial buckling load of simply supported sandwich square plates with FGM skins using the hyperbolic sine theory and a grid with 17^2 points.

p	Theory	$\bar{P}$					
		1-0-1	2-1-2	2-1-1	1-1-1	2-2-1	1-2-1
0	CLPT	6.86896	6.86896	6.86896	6.86896	6.86896	6.86896
	FSDT	6.50224	6.50224	6.50224	6.50224	6.50224	6.50224
	TSDPT [25]	6.50248	6.50248	6.50248	6.50248	6.50248	6.50248
	SSDPT [22]	6.50303	6.50303	6.50303	6.50303	6.50303	6.50303
	present $\epsilon_{zz} \neq 0$	6.47652	6.47652	6.47652	6.47652	6.47652	6.47652
	present $\epsilon_{zz} = 0$	6.50266	6.50266	6.50266	6.50266	6.50266	6.50266
0.5	CLPT	3.82699	4.12798	4.28112	4.39032	4.59127	4.80762
	FSDT	3.66866	3.95660	4.10007	4.20517	4.39336	4.59758
	TSDPT [25]	3.68219	3.97042	4.11235	4.21823	4.40499	4.60841
	SSDPT [22]	3.68284	3.97097	4.11269	4.21856	4.40519	4.60835
	present $\epsilon_{zz} \neq 0$	3.58096	3.85809	3.99480	4.09641	4.27592	4.47110
	present $\epsilon_{zz} = 0$	3.59354	3.87157	4.00853	4.11071	4.29073	4.48676
1	CLPT	2.66624	3.01366	3.20195	3.34075	3.59831	3.89203
	FSDT	2.57118	2.90690	3.08510	3.21946	3.46286	3.74182
	TSDPT [25]	2.58357	2.92003	3.09697	3.23237	3.47472	3.75328
	SSDPT [22]	2.58423	2.92060	3.09731	3.23270	3.47490	3.75314
	present $\epsilon_{zz} \neq 0$	2.53062	2.85563	3.02733	3.15750	3.39207	3.66013
	present $\epsilon_{zz} = 0$	2.53913	2.86503	3.03679	3.16779	3.40280	3.67204
5	CLPT	1.36540	1.55352	1.74209	1.82866	2.10619	2.42859
	FSDT	1.31921	1.51126	1.69269	1.77979	2.04642	2.35737
	TSDPT [25]	1.32910	1.52129	1.70176	1.78978	2.05605	2.36734
	SSDPT [22]	1.33003	1.52203	1.70224	1.79032	2.05644	2.36744
	present $\epsilon_{zz} \neq 0$	1.31829	1.50409	1.68128	1.76507	2.02534	2.32354
	present $\epsilon_{zz} = 0$	1.32331	1.50935	1.68594	1.77072	2.03078	2.33036
10	CLPT	1.28493	1.40170	1.58214	1.62962	1.89619	2.19111
	FSDT	1.23452	1.36313	1.53714	1.58760	1.84445	2.13020
	TSDPT [25]	1.24363	1.37316	1.54595	1.59736	1.85376	2.13995
	SSDPT [22]	1.24475	1.37422	1.56721	1.59728	1.57287	2.19087
	present $\epsilon_{zz} \neq 0$	1.23599	1.36044	1.53036	1.57893	1.83083	2.10275
	present $\epsilon_{zz} = 0$	1.24090	1.36547	1.53468	1.58421	1.83573	2.10897

thickness stretching effect has some influence on the buckling analysis of sandwich FGM plates as $\epsilon_{zz} = 0$ gives higher fundamental buckling loads than $\epsilon_{zz} \neq 0$. The last model is globally less stiff due to transverse stretching and for that reason smaller critical loads are obtained.

The isotropic fully ceramic plate (first line on Tables 3 and 4) has the highest fundamental buckling loads. This may be explained by the bending stiffness which is the highest for this ceramic case. Considering each column of both tables we may conclude that the critical buckling loads decrease as the power-law exponent p increases. As the core to plate total thickness ratio $((h_2 - h_1)/h)$ increases the buckling loads increase as well, as can be seen in Tables 3 and 4). From the comparison of Tables 3 and 4 we conclude that the bi-axial buckling load of any simply supported sandwich square plate with FGM skins is half the uni-axial one for the same plate.

In Fig. 5 the first four buckling modes of a simply supported 2-1-1 sandwich square plate with FGM skins, $p = 5$, subjected to a uni-axial in-plane compressive load, using the hyperbolic sine theory and a grid with 17^2 points is presented. Figure 6 presents the first four buckling modes of a simply supported 1-1-1 sandwich square plate with FGM skins, $p = 1$, subjected to a bi-axial in-plane compressive load.

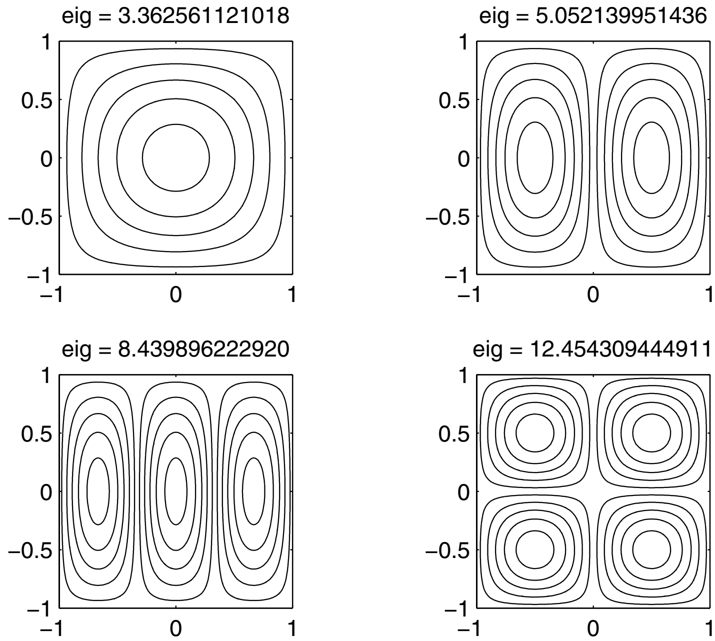

Fig. 5 First four buckling modes. Uni-axial buckling load of a simply supported 2-1-1 sandwich square plate with FGM skins, $p = 5$, a 17^2 points grid, and using the hyperbolic sine theory.

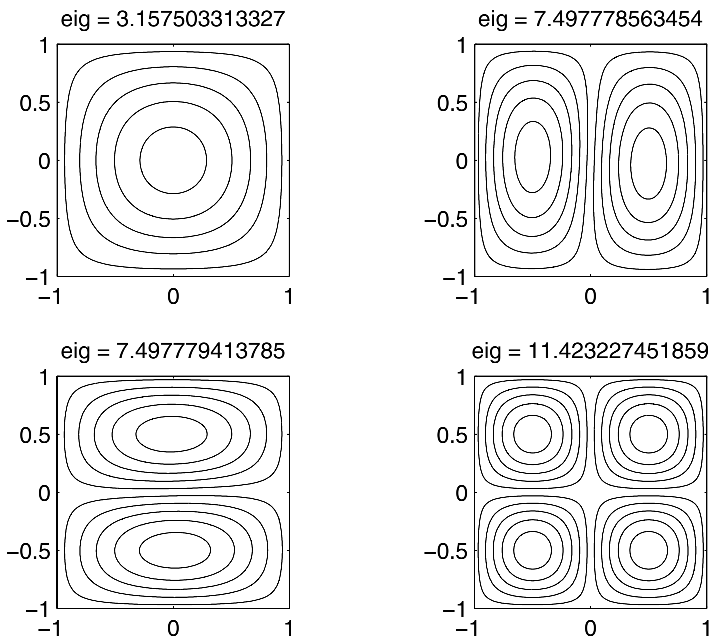

Fig. 6 First four buckling modes. Bi-axial buckling load of a simply supported 1-1-1 sandwich square plate with FGM skins, $p = 1$, a 17^2 points grid, and using the hyperbolic sine theory.

7 Conclusions

A novel application of a unified formulation by a meshless discretization is proposed. A thickness-stretching hyperbolic sine shear deformation theory was implemented for the buckling analysis of functionally graded sandwich plates.

The present formulation was compared with analytical, meshless or finite element methods and showed very accurate results. The effect of $\epsilon_{zz} \neq 0$ showed to be significant in such sandwich problems.

For the first time, the complete governing equations and boundary conditions of the hyperbolic sine theory are presented to help readers to implement it successfully with this or other strong-form techniques.

Acknowledgements The first author acknowledges support from FCT grant SFRH/BD/45554/2008. The support from FCT-Project LAETA-Composites-Mechanical Design and FCT-PTDC/EME/120830/2010 is also acknowledged.

References

[1] M. Koizumi, FGM activities in Japan. Use of composites multi-phased and functionally graded materials, Compos. B, Eng. **28**(1–2), 1–4 (1997).
[2] M. Niino and S. Maeda, Recent development status of functionally gradient materials, ISIJ International **30**(9), 699–703 (1990).
[3] Y. Miyamoto, W. Kaysser, B. Rabin, A. Kawasaki, and R. Ford, Functionally Graded Materials: Design, Processing and Applications (Kluwer Academic Publishers, Dordrecht, 1999).
[4] V. Birman and L. W. Byrd, Modeling and analysis of functionally graded materials and structures, Appl. Mech. Rev. **60**(5), 195–216 (2007).
[5] Z. H. Jin and R. C. Batra, Stress intensity relaxation at the tip of an edge crack in a functionally graded material subjected to a thermal shock, J. Thermal Stresses **19**, 317–339 (1996).
[6] Y. Chung and S. Chi, The residual stress of functionally graded materials, J. Chin. Inst. Civil Hydr. Eng. **13**, 1–9 (2001).
[7] G. N. Praveen and J. N. Reddy, Nonlinear transient thermoelastic analysis of functionally graded ceramic-metal plates, Int. J. Solids Struct. **35**(33), 4457–4476 (1998).
[8] M. M. Najafizadeh and M. R. Eslami, Buckling analysis of circular plates of functionally graded materials under uniform radial compression, Int. J. Mech. Sci. **44**(12), 2479–2493 (2002).
[9] A. Zenkour, A comprehensive analysis of functionally graded sandwich plates: Part 1 – deflection and stresses, Int. J. Solids Struct. **42**(18–19), 5224–5242 (2005).
[10] A. M. Zenkour, Generalized shear deformation theory for bending analysis of functionally graded plates, Appl. Math. Modell. **30** (2006).
[11] M. Kashtalyan, Three-dimensional elasticity solution for bending of functionally graded rectangular plates, Eur. J. Mech. A, Solids **23**(5), 853–864 (2004).
[12] M. Kashtalyan and M. Menshykova, Three-dimensional elasticity solution for sandwich panels with a functionally graded core, Compos. Struct. **87**(1), 36–43 (2009).
[13] L. F. Qian, R. C. Batra, and L. M. Chen, Static and dynamic deformations of thick functionally graded elastic plate by using higher-order shear and normal deformable plate theory and meshless local petrov-galerkin method, Compos. B **35**, 685–697 (2004).
[14] F. Ramirez, P. R. Heyliger, and E. Pan, Static analysis of functionally graded elastic anisotropic plates using a discrete layer approach, Compos. B, Eng. **37**(1), 10–20 (2006).
[15] A. J. M. Ferreira, R. C. Batra, C. M. C. Roque, L. F. Qian, and P. A. L. S. Martins, Static analysis of functionally graded plates using third-order shear deformation theory and a meshless method, Compos. Struct. **69**(4), 449–457 (2005).
[16] A. J. M. Ferreira, C. M. C. Roque, R. M. N. Jorge, G. E. Fasshauer, and R. C. Batra, Analysis of functionally graded plates by a robust meshless method, Mech. Adv. Mater. Struct. **14**(8), 577–587 (2007).
[17] S. H. Chi and Y. L. Chung, Mechanical behavior of functionally graded material plates under transverse load – Part I: Analysis, Int. J. Solids Struct. **43**(13), 3657–3674 (2006).
[18] S. H. Chi and Y. L. Chung, Mechanical behavior of functionally graded material plates under transverse load – Part II: Numerical results, Int. J. Solids Struct. **43**(13), 3675–3691 (2006).
[19] R. Batra and J. Jin, Natural frequencies of a functionally graded anisotropic rectangular plate, J. Sound Vib. **282**(1–2), 509–516 (2005).
[20] A. J. M. Ferreira, R. C. Batra, C. M. C. Roque, L. F. Qian, and R. M. N. Jorge, Natural frequencies of functionally graded plates by a meshless method, Compos. Struct. **75**(1–4), 593–600 (2006).
[21] S. S. Vel and R. C. Batra, Three-dimensional exact solution for the vibration of functionally graded rectangular plates, J. Sound Vib. **272**, 703–730 (2004).
[22] A. Zenkour, A comprehensive analysis of functionally graded sandwich plates: Part 2 – buckling and free vibration, Int. J. Solids Struct. **42**(18–19), 5243–5258 (2005).
[23] Z. Q. Cheng and R. C. Batra, Exact correspondence between eigenvalues of membranes and functionally graded simply supported polygonal plates, J. Sound Vib. **229**, 879–895 (2000).
[24] J. N. Reddy and C. D. Chin, Thermomechanical analysis of functionally graded cylinders and plates, J. Thermal Stresses **21**(6), 593–626 (1998).
[25] J. N. Reddy, Analysis of functionally graded plates, Int. J. Numer. Methods Eng. **47**, 663–684 (2000).

[26] S. S. Vel and R. C. Batra, Three-dimensional analysis of transient thermal stresses in functionally-graded plates, Int. J. Solids Struct. **40**, 7181–7196 (2003).

[27] S. S. Vel and R. C. Batra, Exact solution for thermoelastic deformations of functionally graded thick rectangular plates, AIAA J. **40**, 1421–1433 (2002).

[28] Z. Q. Cheng and R. C. Batra, Three-dimensional thermoelastic deformations of a functionally graded-elliptic plate, Compos. B **31**, 97–106 (2000).

[29] R. Javaheri and M. R. Eslami, Thermal buckling of functionally graded plates based on higher order theory, J. Thermal Stresses **25**(7), 603–625 (2002).

[30] V. Birman, Buckling of Functionally Graded Hybrid Composite Plates, in: Proceedings of the 10th Conference on Engineering Mechanics (Boulder, Colorado, 1995), pp. 1199–1202.

[31] R. Javaheri and M. R. Eslami, Buckling of functionally graded plates under in-plane compressive loading, Z. Angew. Math. Mech. **82**(4), 277–283 (2002).

[32] Z. Q. Cheng and R. C. Batra, Deflection relationships between the homogeneous Kirchhoff plate theory and different functionally graded plate theories, Arch. Mech. **52**, 143–158 (2000).

[33] K. Soldatos, A transverse shear deformation theory for homogeneous monoclinic plates, Acta Mech. **94**, 195–220 (1992), 10.1007/BF01176650.

[34] S. Akavci, Two new hyperbolic shear displacement models for orthotropic laminated composite plates, Mech. Compos. Mater. **46**, 215–226 (2010), 10.1007/s11029-010-9140-3.

[35] S. Akavci and A. Tanrikulu, Buckling and free vibration analyses of laminated composite plates by using two new hyperbolic shear-deformation theories, Mech. Compos. Mater. **44**, 145–154 (2008), 10.1007/s11029-008-9004-2.

[36] N. E. Meiche, A. Tounsi, N. Ziane, I. Mechab, and E. A. Adda.Bedia, A new hyperbolic shear deformation theory for buckling and vibration of functionally graded sandwich plate, Int. J. Mech. Sci. **53**(4), 237–247 (2011).

[37] E. Carrera, S. Brischetto, M. Cinefra, and M. Soave, Effects of thickness stretching in functionally graded plates and shells, Compos. B, Eng. **42**, 123–133 (2011).

[38] E. J. Kansa, Multiquadrics – a scattered data approximation scheme with applications to computational fluid dynamics. I: Surface approximations and partial derivative estimates, Comput. Math. Appl. **19**(8/9), 127–145 (1990).

[39] A. J. M. Ferreira, A formulation of the multiquadric radial basis function method for the analysis of laminated composite plates, Compos. Struct. **59**, 385–392 (2003).

[40] A. J. M. Ferreira, Thick composite beam analysis using a global meshless approximation based on radial basis functions, Mech. Adv. Mater. Struct. **10**, 271–284 (2003).

[41] A. J. M. Ferreira, C. M. C. Roque, and P. A. L. S. Martins, Analysis of composite plates using higher-order shear deformation theory and a finite point formulation based on the multiquadric radial basis function method, Compos. B **34**, 627–636 (2003).

[42] A. Ferreira, C. Roque, R. Jorge, and E. Kansa, Static deformations and vibration analysis of composite and sandwich plates using a layerwise theory and multiquadrics discretizations, Eng. Anal. Bound. Elem. **29**(12), 1104–1114 (2005).

[43] A. Ferreira, C. Roque, and R. Jorge, Analysis of composite plates by trigonometric shear deformation theory and multiquadrics, Comput. Struct. **83**(27), 2225–2237 (2005).

[44] A. Ferreira, R. Batra, C. Roque, L. Qian, and R. Jorge, Natural frequencies of functionally graded plates by a meshless method, Thirteenth International Conference on Composite Structures – ICCS/13 Compos. Struct. **75**(1–4), 593–600 (2006).

[45] A. Ferreira, C. Roque, and R. Jorge, Free vibration analysis of symmetric laminated composite plates by fsdt and radial basis functions, Comput. Methods Appl. Mech. Eng. **194**(39–41), 4265–4278 (2005).

[46] A. J. M. Ferreira, C. M. C. Roque, and P. A. L. S. Martins, Radial basis functions and higher-order shear deformation theories in the analysis of laminated composite beams and plates, Twelfth International Conference on Composite Structures, Compos. Struct. **66**(1–4), 287–293 (2004).

[47] A. Neves, A. Ferreira, E. Carrera, C. Roque, M. Cinefra, R. Jorge, and C. Soares, Bending of FGM plates by a sinusoidal plate formulation and collocation with radial basis functions, Mech. Res. Commun. **38**(5), 368–371 (2011).

[48] A. Neves, A. Ferreira, E. Carrera, C. Roque, M. Cinefra, R. Jorge, and C. Soares, A quasi-3d sinusoidal shear deformation theory for the static and free vibration analysis of functionally graded plates, Compos. B, Eng. **43**(2), 711–725 (2012).

[49] E. Carrera, C^0 Reissner-Mindlin multilayered plate elements including zig-zag and interlaminar stress continuity, Int. J. Numer. Methods Eng. **39**, 1797–1820 (1996).

[50] E. Carrera, Developments, ideas, and evaluations based upon Reissner's mixed variational theorem in the modelling of multilayered plates and shells, Appl. Mech. Rev. **54**, 301–329 (2001).

[51] E. J. Kansa, Multiquadrics – a scattered data approximation scheme with applications to computational fluid dynamics. II: Solutions to parabolic, hyperbolic and elliptic partial differential equations, Comput. Math. Appl. **19**(8/9), 147–161 (1990).

[52] A. J. M. Ferreira and G. E. Fasshauer, Computation of natural frequencies of shear deformable beams and plates by a rbf-pseudospectral method, Comput. Methods Appl. Mech. Eng. **196**, 134–146 (2006).

2.6 Static analysis of functionally graded sandwich plates according to a hyperbolic theory considering Zig-Zag and warping effects

A. M. A. Neves, A. J. M. Ferreira, E. Carrera, M. Cinefra, R. M. N. Jorge, C. M. M. Soares, Static analysis of functionally graded sandwich plates according to a hyperbolic theory considering Zig-Zag and warping effects, Advances in Engineering Software, Volume 52, 2012, pages 30-43.

Advances in Engineering Software 52 (2012) 30–43

Contents lists available at SciVerse ScienceDirect

Advances in Engineering Software

journal homepage: www.elsevier.com/locate/advengsoft

Static analysis of functionally graded sandwich plates according to a hyperbolic theory considering Zig-Zag and warping effects

A.M.A. Neves [a], A.J.M. Ferreira [a,*], E. Carrera [b], M. Cinefra [b], R.M.N. Jorge [a], C.M.M. Soares [c]

[a] Departamento de Engenharia Mecânica, Faculdade de Engenharia, Universidade do Porto, Rua Dr. Roberto Frias, 4200-465 Porto, Portugal
[b] Departament of Aeronautics and Aerospace Engineering, Politecnico di Torino, Corso Duca degli Abruzzi, 24, 10129 Torino, Italy
[c] Instituto Superior Técnico, Av. Rovisco Pais, Lisboa, Portugal

ARTICLE INFO

Article history:
Received 27 December 2011
Received in revised form 18 April 2012
Accepted 23 May 2012

Keywords:
Sandwich plates
Plates
Functionally graded materials
Meshless methods
Higher-order theories
Composites

ABSTRACT

In this paper, a variation of Murakami's Zig-Zag theory is proposed for the analysis of functionally graded plates. The new theory includes a hyperbolic sine term for the in-plane displacements expansion and accounts for through-the-thickness deformation, by considering a quadratic evolution of the transverse displacement with the thickness coordinate.

The governing equations and the boundary conditions are obtained by a generalization of Carrera's Unified Formulation, and further interpolated by collocation with radial basis functions.

Numerical examples on the static analysis of functionally graded sandwich plates demonstrate the accuracy of the present approach. The thickness stretching effect on such problems is studied.

1. Introduction

The strong difference of mechanical properties between faces and core in sandwich structures (or layered composites) introduces a discontinuity of the deformed core-faces planes at the interfaces. This is known as Zig-Zag (ZZ) effect. Such discontinuities make difficult the use of classical theories such as Kirchhoff [1] or Reissner–Mindlin [2,3] type theories (see the books by Zenkert [4], and Vinson [5] to trace accurate responses of sandwich structures). Two possibilities can be used to capture the ZZ effect (see the overviews by Burton and Noor [6], Noor et al. [7], Altenbach [8], Librescu and Hause [9], Vinson [10], and Demasi [11]): the so-called layer-wise models, and a Zig-Zag function (ZZF) in the framework of mixed multilayered plate theories. An historical review on ZZ theories has been provided by Carrera [12].

The first alternative can be computational expensive for laminates with large number of layers as the degrees-of-freedom increase as the number of layers increases. Considering the second alternative, Murakami [13] proposed a ZZF that is able to reproduce the slope discontinuity. Equivalent single layer models with only displacement unknowns can be developed on the basis of ZZF. A review of early developments on the application of ZZF has been provided in the review article by Carrera [14]. The advantages of analyze multilayered anisotropic plate and shells using the ZZF as well as the Finite Element implementation have been discussed by Carrera [15]. Further studies on the use of Murakami's Zig-Zag function (MZZF) have been documented in [15–17].

The use of alternative methods to the Finite Element Methods for the analysis of plates, such as the meshless methods based on radial basis functions (RBFs) is attractive due to the absence of a mesh and the ease of collocation methods. The use of radial basis function for the analysis of structures and materials has been previously studied by numerous authors [18–34].

Carrera's Unified Formulation (CUF) was proposed in [14,35,36] for laminated plates and shells and extended to functionally graded (FG) plates in [37–39]. The present formulation is a generalization of the original CUF in the sense that considers different displacement fields for in-plane and out-of-plane displacements.

In this paper the application of ZZF to bending analysis of thin and thick FG sandwich plates is studied. A new displacement theory is used, considering a quadratic variation of the transverse displacements (allowing for through-the-thickness deformations), and introducing a hyperbolic sine term in the in-plane displacement expansion. This can be seen as a variation of the original Murakami's ZZ displacement field. CUF is combined with RBFs for the static analysis: the principle of virtual displacements is used under CUF to obtain the governing equations and boundary equations and these are interpolated by collocation with RBFs.

The paper is organized as follows. The problem we are dealing with is introduced in Section 2. Then, the state-of-the-art review on the use of Zig-Zag functions and the displacement field of the

* Corresponding author.
E-mail address: ferreira@fe.up.pt (A.J.M. Ferreira).

0965-9978/$ - see front matter © 2012 Elsevier Ltd. All rights reserved.
http://dx.doi.org/10.1016/j.advengsoft.2012.05.005

Nomenclature

CUF	Carrera's Unified Formulation	PVD	Principle of virtual displacements
FG	Functionally graded	RBF	Radial basis function
FGM	Functionally graded material	SSSS	Simply-supported
FSDT	First-order shear deformation theory	ZZ	Zig-Zag
MZZF	Murakami's Zig-Zag function	ZZF	Zig-Zag function
PDE	Partial differential equations		

present shear deformation theory is presented in Section 3. For the sake of completeness CUF and the radial basis functions collocation technique for the static analysis of FG plates are briefly reviewed in Sections 4 and 5, respectively. Numerical examples on the static analysis of simply supported functionally graded sandwich square plates are presented and discussed in Section 6. These include the computation of the displacements and stresses of sandwich plates with FGM in the core or in the skins, considering several material power-law exponents, side-to-thickness ratios and skin-core-skin ratios as well. Final conclusions are presented in Section 7.

2. Problem formulation

Consider a rectangular plate of plan-form dimensions a and b and uniform thickness h. The co-ordinate system is taken such that the x-y plane ($z = 0$) coincides with the midplane of the plate ($z \in [-h/2, h/2]$). The plate is subjected to a transverse mechanical load applied at the top of the plate.

Two different types of functionally graded sandwich plates are studied: sandwich plates with FG core and sandwich plates with FG skins.

In the sandwich plate with FG core the bottom skin is fully metal (isotropic) and the top skin is fully ceramic (isotropic as well). The core layer is graded from metal to ceramic so that there are no interfaces between core and skins, as illustrated in Fig. 1. The volume fraction of the ceramic phase in the core is obtained by adapting the typical polynomial material law as:

$$V_c = \left(0.5 + \frac{z_c}{h_c}\right)^p \tag{1}$$

where $z_c \in [h_1, h_2]$, $h_c = h_2 - h_1$ is the thickness of the core, and $p > 0$ is the power-law exponent that defines the gradation of material properties across the thickness direction as shown in Fig. 3 (left).

In sandwich plates with FG skins the core is fully ceramic (isotropic) and skins are composed of a functionally graded material across the thickness direction. The bottom skin varies from a metal-rich surface ($z = -h/2$) to a ceramic-rich surface while the top skin face varies from a ceramic-rich surface to a metal-rich surface ($z = h/2$), as illustrated in Fig. 2. There are no interfaces between core and skins. The volume fraction of the ceramic phase in the skins is obtained as:

$$\begin{aligned} V_c &= \left(\tfrac{z-h_0}{h_1-h_0}\right)^p, \quad z \in [-h/2, h_1] \\ V_c &= \left(\tfrac{z-h_3}{h_2-h_3}\right)^p, \quad z \in [h_2, h/2] \end{aligned} \tag{2}$$

where $p \geqslant 0$ is a scalar parameter that allows the user to define gradation of material properties across the thickness direction of the skins. The $p = 0$ case corresponds to the (isotropic) fully ceramic plate.

The sandwich plate with FG skins may be symmetric or nonsymmetric about the mid-plane as we may vary the thickness of each face. Fig. 3 (right) shows a non-symmetric sandwich with volume fraction defined by the power-law (2) for various exponents p, in which top skin thickness is the same as the core thickness and the bottom skin thickness is twice the core thickness. Such thickness relation is denoted as 2-1-1. A bottom-core-top notation is

Fig. 1. Sandwich plate with FG core and isotropic skins.

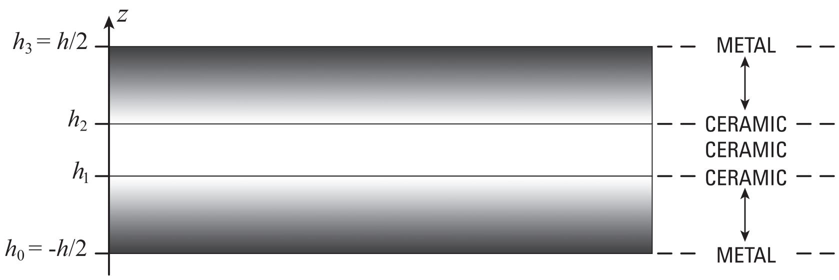

Fig. 2. Sandwich plate with isotropic core and FG skins.

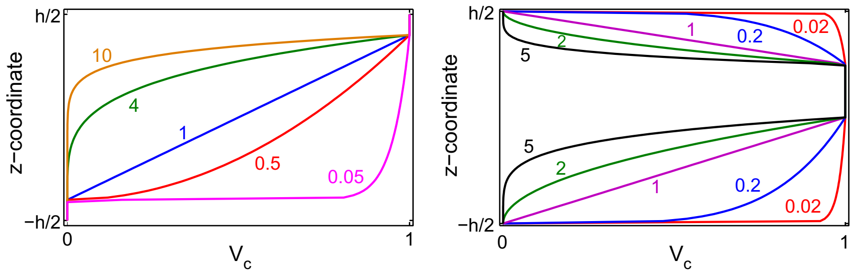

Fig. 3. Effect of the power-law exponent in a sandwich plate with FG core (left) and in a 2-1-1 sandwich plate with FG skins (right).

being used. 1-1-1 means that skins and core have the same thickness.

In both sandwich plates the volume fraction for the metal phase is given as $V_m = 1 - V_c$.

3. A new hyperbolic sine ZZF theory

3.1. The Zig-Zag function

The Murakami's Zig-Zag function $Z(z)$ dependes on the adimensioned layer coordinate, ζ_k, according to the following formula:

$$Z(z) = (-1)^k \zeta_z \tag{3}$$

ζ_k is defined as $\zeta_k = \frac{2z_k}{h_k}$ where z_k is the layer thickness coordinate and h_k is the thickness of the kth layer.

$Z(z)$ has the following properties:

(1) It is a piece-wise linear function of layer coordinates z_k.
(2) $Z(z)$ has unit amplitude for the whole layers.
(3) The slope $Z\prime(z) = \frac{dZ}{dz}$ assumes opposite sign between two-adjacent layers. Its amplitude is layer thickness independent.

3.2. Overview on Murakami's Zig-Zag theories

In 1986, a refinement of FSDT by inclusion of ZZ effects and transverse normal strains was introduced in Murakami's original ZZF [13], defined by the following displacement field:

$$\begin{cases} u = u_0 + zu_1 + (-1)^k \frac{2}{h_k}\left(z - \frac{1}{2}(z_k + z_{k+1})\right)u_Z \\ v = v_0 + zv_1 + (-1)^k \frac{2}{h_k}\left(z - \frac{1}{2}(z_k + z_{k+1})\right)v_Z \\ w = w_0 + zw_1 + (-1)^k \frac{2}{h_k}\left(z - \frac{1}{2}(z_k + z_{k+1})\right)w_Z \end{cases} \tag{4}$$

where u and v are the in-plane displacements and w is the transverse displacement. The involved unknowns are u_0, u_1, u_Z, v_0, v_1, v_Z, w_0, w_1, and w_Z: u_0, v_0 and w_0 are translations of a point at the mid-plane; u_1, v_1 and w_1 are rotations as in the typical FSDT; and the additional degrees of freedom u_Z, v_Z and w_Z have a meaning of displacement. z_k, z_{k+1} are the bottom and top z-coordinates at each layer.

More recently, another possible FSDT theory has been investigated by Carrera [15] and Demasi [16], ignoring the through-the-thickness deformations:

$$\begin{cases} u = u_0 + zu_1 + (-1)^k \frac{2}{h_k}\left(z - \frac{1}{2}(z_k + z_{k+1})\right)u_Z \\ v = v_0 + zv_1 + (-1)^k \frac{2}{h_k}\left(z - \frac{1}{2}(z_k + z_{k+1})\right)v_Z \\ w = w_0 \end{cases} \tag{5}$$

with u_0, u_1, u_Z, v_0, v_1, v_Z, w_0, z_k, and z_{k+1} as before.

Ferreira et al. [40] and Rodrigues et al. [41] used a ZZF theory involving the following expansion of displacements

$$\begin{cases} u = u_0 + zu_1 + (-1)^k \frac{2}{h_k}\left(z - \frac{1}{2}(z_k + z_{k+1})\right)u_Z \\ v = v_0 + zv_1 + (-1)^k \frac{2}{h_k}\left(z - \frac{1}{2}(z_k + z_{k+1})\right)v_Z \\ w = w_0 + zw_1 + z^2 w_2 \end{cases} \tag{6}$$

This represents a variation of the Murakami's original theory, allowing for a quadratic evolution of the transverse displacement across the thickness direction. Furthermore, Ferreira et al. [42] used two higher order ZZF theories allowing for a quadratic evolution of the transverse displacement across the thickness direction as well and involving the following displacement fields:

$$\begin{cases} u = u_0 + zu_1 + z^3 u_3 + (-1)^k \frac{2}{h_k}\left(z - \frac{1}{2}(z_k + z_{k+1})\right)u_Z \\ v = v_0 + zv_1 + z^3 v_3 + (-1)^k \frac{2}{h_k}\left(z - \frac{1}{2}(z_k + z_{k+1})\right)v_Z \\ w = w_0 + zw_1 + z^2 w_2 \end{cases} \tag{7}$$

$$\begin{cases} u = u_0 + zu_1 + sin\left(\frac{\pi z}{h}\right)u_3 + (-1)^k \frac{2}{h_k}\left(z - \frac{1}{2}(z_k + z_{k+1})\right)u_Z \\ v = v_0 + zv_1 + sin\left(\frac{\pi z}{h}\right)v_3 + (-1)^k \frac{2}{h_k}\left(z - \frac{1}{2}(z_k + z_{k+1})\right)v_Z \\ w = w_0 + zw_1 + z^2 w_2 \end{cases} \tag{8}$$

In Eqs. (7) and (8), w_2 denote higher-order translations and u_3 and v_3 denote rotations. u_0, v_0, w_0, u_1, v_1, w_1, u_z, and v_z, are as in (4)–(6).

3.3. The hyperbolic sine ZZF shear deformation theory

All previous cited work using ZZ functions deals with laminated plates or shells. In the present work a new hyperbolic sine ZZF theory is introduced for the analysis of functionally graded sandwich plates. The choice of the new displacement field is based on previous work by the authors and the role of the Zig-Zag effect on sandwich structures. The authors have sucessfuly used a hyperbolic sine quasi-3D shear deformation theory accounting for thickness stretching without the Zig-Zag effect in the study of functionally graded plates [43]. The present theory adds the terms to consider the Zig-Zag effect. The present theory is based on the following displacement field:

$$\begin{cases} u = u_0 + zu_1 + sinh\left(\frac{\pi z}{h}\right)u_3 + (-1)^k \frac{2}{h_k}\left(z - \frac{1}{2}(z_k + z_{k+1})\right)u_Z \\ v = v_0 + zv_1 + sinh\left(\frac{\pi z}{h}\right)v_3 + (-1)^k \frac{2}{h_k}\left(z - \frac{1}{2}(z_k + z_{k+1})\right)v_Z \\ w = w_0 + zw_1 + z^2 w_2 \end{cases} \tag{9}$$

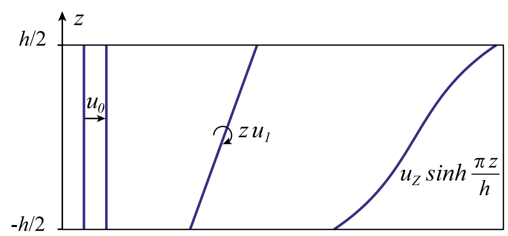

Fig. 4. Scheme of the expansions involved in the displacement field.

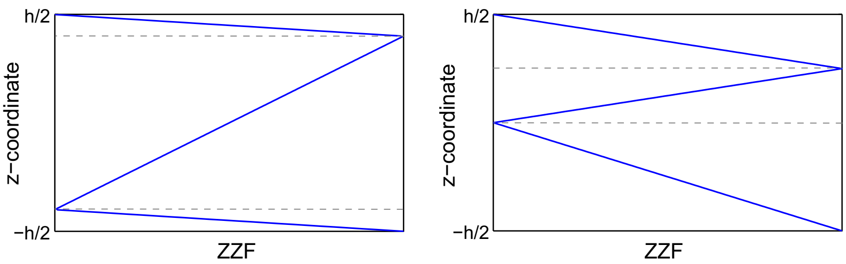

Fig. 5. Zig-Zag effect for the 1-8-1 (left) and the 2-1-1 sandwichs (right).

The involved unknowns have the same meaning as in equations (7) and (8). The expansion of the degrees of freedom u_0, u_1, u_3, v_0, v_1, v_3, w_0, w_1, and w_2 are functions of the thickness coordinate only. These are layer-independent, unlike those of u_Z and v_Z, as illustrated in Figs. 4 and 5. Fig. 4 shows the meaning of the unknows in the in-plane displacements expansion in present theory: u_0, v_0 (translations), u_1, v_1 (rotations), u_3 and v_3 (rotations). In Fig. 5 one can visualize that this ZZF correspondence to a rotation per layer.

4. The Unified Formulation for the static analysis of FG sandwich plates

In this section it is shown how to obtain the fundamental nuclei under CUF, which allows the derivation of the governing equations and boundary conditions for FG plates.

4.1. Functionally graded materials

A conventional FG plate considers a continuous variation of material properties over the thickness direction by mixing two different materials [44]. The material properties of the FG plate are assumed to change continuously throughout the thickness of the plate, according to the volume fraction of the constituent materials. Although one can use CUF for one-layer, isotropic plate, we consider a multi-layered plate. In fact, the sandwiches in study present three physical layers, $kp = 1, 2, 3$, each containing a different displacement field. Nevertheless, we are dealing with functionally graded materials and becomes mandatory to model the continuos variation of properties across the thickness direction. A considerable number of layers is needed to ensure correct computation of material properties at each thickness position, and for that reason we consider $N_l = 91$ virtual (mathematical) layers of constant thickness. In the following, kp refers to physical layers and $k = 1, \ldots, 91$ refers to virtual layers.

The CUF procedure applied to FG materials starts by evaluating the volume fraction of the two constituents for each layer. Then, a homogenization technique is employed to find the values of the modulus of elasticity, E^k, and Poisson's ratio, ν^k, of each layer.

To describe the volume fractions an exponential function can be used as in [45], or the sigmoid function as proposed in [46]. In the present work a power-law function is used as most researchers do [47–50]. In the typical FG plate the power-law function defines the volume fraction of the ceramic phase as:

$$V_c = \left(0.5 + \frac{z}{h}\right)^p \tag{10}$$

where $z \in [-h/2, h/2]$, h is the thickness of the plate, and p is a scalar parameter that allows the user to define gradation of material properties across the thickness direction. In both sandwich plates, the volume fraction of the ceramic phase of the FG layers are obtained by adapting the typical power-law. Furthermore, we need to compute the volume fraction for each layer. In the sandwich plate with FG core case, (1) becomes:

$$\begin{cases} V_c^k = 0, & \text{in the bottom skin} \\ V_c^k = \left(0.5 + \frac{\tilde{z}_c}{h_c}\right)^p, & \text{in the core} \\ V_c^k = 1, & \text{in the top skin} \end{cases} \tag{11}$$

where $\tilde{z}_c$ is the thickness coordinate of a point of each (virtual) core layer, and h_c and p are as in (1).

Considering (2), for the sandwich plate with FG skins case one has:

$$\begin{cases} V_c^k = \left(\frac{\tilde{z}-h_0}{h_1-h_0}\right)^p, & \text{in the bottom skin} \\ V_c^k = 1, & \text{in the core} \\ V_c^k = \left(\frac{\tilde{z}-h_3}{h_2-h_3}\right)^p, & \text{in the top skin} \end{cases} \tag{12}$$

where $\tilde{z}$ is the thickness coordinate of a point of each (virtual) skin layer.

At this step, a homogenization procedure is used. The one considered in present work is the law-of-mixtures, the same used by the referenced authors, which states that:

$$E^k(z) = E_m V_m + E_c V_c; \quad \nu^k(z) = \nu_m V_m + \nu_c V_c \tag{13}$$

Other homogeneization procedures could be used, for example the Mori–Tanaka one [51,52].

4.2. Modeling of the displacement components

According to the Unified Formulation by Carrera, the three displacement components u_x, $u_y(=v)$ and $u_z(=w)$ and their relative variations are modeled as:

$$\begin{aligned} (u_x, u_y, u_z) &= F_\tau\ (u_{x\tau}, u_{y\tau}, u_{z\tau}) \\ (\delta u_x, \delta u_y, \delta u_z) &= F_s\ (\delta u_{xs}, \delta u_{ys}, \delta u_{zs}) \end{aligned} \tag{14}$$

Resorting to the displacement field in Eq. (9), we choose vectors $F_\tau = \left[1 \quad z \quad \sinh\left(\frac{\pi z}{h}\right) \quad (-1)^{kp} \frac{2}{h_{kp}}\left(z - \frac{1}{2}(z_{kp} + z_{kp+1})\right)\right]$ for in-plane displacements and $F_\tau = [1 \quad z \quad z^2]$ for displacement w. In this case, thickness-stretching is considered. For the thickness effect study, in the case that thickness-stretching is not allowed, the vector for transverse displacement is replaced with $F_\tau = 1$, meaning that we are considering the expansion $w = w_0$ in the displacement field.

4.3. Strains

Strains are separated into in-plane and normal components, denoted respectively by the subscripts p and n. The mechanical strains in the kth layer can be related to the displacement field $\mathbf{u}^k = \left\{u_x^k, u_y^k, u_z^k\right\}$ via the geometrical relations (G):

$$\begin{aligned} \boldsymbol{\epsilon}_{pG}^k &= [\epsilon_{xx}, \epsilon_{yy}, \gamma_{xy}]^{kT} = \mathbf{D}_p^k \mathbf{u}^k, \\ \boldsymbol{\epsilon}_{nG}^k &= [\gamma_{xz}, \gamma_{yz}, \epsilon_{zz}]^{kT} = (\mathbf{D}_{np}^k + \mathbf{D}_{nz}^k)\ \mathbf{u}^k, \end{aligned} \tag{15}$$

wherein the differential operator arrays are defined as follows:

$$\mathbf{D}_p^k = \begin{bmatrix} \partial_x & 0 & 0 \\ 0 & \partial_y & 0 \\ \partial_y & \partial_x & 0 \end{bmatrix}, \quad \mathbf{D}_{np}^k = \begin{bmatrix} 0 & 0 & \partial_x \\ 0 & 0 & \partial_y \\ 0 & 0 & 0 \end{bmatrix}, \quad \mathbf{D}_{nz}^k = \begin{bmatrix} \partial_z & 0 & 0 \\ 0 & \partial_z & 0 \\ 0 & 0 & \partial_z \end{bmatrix}, \tag{16}$$

If $\epsilon_{zz} = 0$ is considered, thickness-stretching is not allowed. In this case, $\boldsymbol{\epsilon}_{pG}^k$ and the differential operator array $\mathbf{D}_p^k$ remain as before, but the other strains are reduced to

$$\boldsymbol{\epsilon}_{nG}^k = [\gamma_{xz}, \gamma_{yz}]^{kT} = \left(\mathbf{D}_{np}^k + \mathbf{D}_{nz}^k\right) \mathbf{u}^k, \tag{17}$$

wherein the differential operator arrays are defined as:

$$\mathbf{D}_{np}^k = \begin{bmatrix} 0 & 0 & \partial_x \\ 0 & 0 & \partial_y \end{bmatrix}, \quad \mathbf{D}_{nz}^k = \begin{bmatrix} \partial_z & 0 & 0 \\ 0 & \partial_z & 0 \end{bmatrix}, \tag{18}$$

4.4. Elastic stress–strain relations

To define the constitutive equations (C), stresses are separated into in-plane and normal components as well.

The 3D constitutive equations are given as:

$$\begin{aligned} \boldsymbol{\sigma}_{pC}^k &= [\sigma_{xx}, \sigma_{yy}, \sigma_{xy}]^{kT} = \mathbf{C}_{pp}^k\ \boldsymbol{\epsilon}_{pG}^k + \mathbf{C}_{pn}^k\ \boldsymbol{\epsilon}_{nG}^k \\ \boldsymbol{\sigma}_{nC}^k &= [\sigma_{xz}, \sigma_{yz}, \sigma_{zz}]^{kT} = \mathbf{C}_{np}^k\ \boldsymbol{\epsilon}_{pG}^k + \mathbf{C}_{nn}^k\ \boldsymbol{\epsilon}_{nG}^k \end{aligned} \tag{19}$$

with

$$\begin{aligned} \mathbf{C}_{pp}^k &= \begin{bmatrix} C_{11}^k & C_{12}^k & 0 \\ C_{12}^k & C_{22}^k & 0 \\ 0 & 0 & C_{66}^k \end{bmatrix} \qquad \mathbf{C}_{pn}^k = \begin{bmatrix} 0 & 0 & C_{13}^k \\ 0 & 0 & C_{23}^k \\ 0 & 0 & 0 \end{bmatrix} \\ \mathbf{C}_{np}^k &= \begin{bmatrix} 0 & 0 & 0 \\ 0 & 0 & 0 \\ C_{13}^k & C_{23}^k & 0 \end{bmatrix} \qquad \mathbf{C}_{nn}^k = \begin{bmatrix} C_{55}^k & 0 & 0 \\ 0 & C_{44}^k & 0 \\ 0 & 0 & C_{33}^k \end{bmatrix} \end{aligned} \tag{20}$$

and the C_{ij}^k are the three-dimensional elastic constants

$$\begin{aligned} C_{11}^k &= C_{22}^k = C_{33}^k = \tfrac{E^k(1-(\nu^k)^2)}{1-3(\nu^k)^2-2(\nu^k)^3}, \\ C_{12}^k &= C_{13}^k = C_{23}^k = \tfrac{E^k(\nu^k+(\nu^k)^2)}{1-3(\nu^k)^2-2(\nu^k)^3}, \\ C_{44}^k &= C_{55}^k = C_{66}^k = G^k \end{aligned} \tag{21}$$

where the modulus of elasticity and Poisson's ratio were defined in (13), and G is the shear modulus $G^k = \frac{E^k}{2(1+\nu^k)}$.

For the $\epsilon_{zz} = 0$ case, the plane-stress case is used:

$$\begin{aligned} \boldsymbol{\sigma}_{pC}^k &= [\sigma_{xx}, \sigma_{yy}, \sigma_{xy}]^{kT} = \mathbf{C}_{pp}^k\ \boldsymbol{\epsilon}_{pG}^k \\ \boldsymbol{\sigma}_{nC}^k &= [\sigma_{xz}, \sigma_{yz}]^{kT} = \mathbf{C}_{nn}^k\ \boldsymbol{\epsilon}_{nG}^k \end{aligned} \tag{22}$$

with $\mathbf{C}_{pp}^k$ and $\boldsymbol{\epsilon}_{pG}^k$ as before, $\boldsymbol{\epsilon}_{nG}^k = [\gamma_{xz}, \gamma_{yz}]^{kT}$ and

$$\mathbf{C}_{nn}^k = \begin{bmatrix} C_{55}^k & 0 \\ 0 & C_{44}^k \end{bmatrix} \tag{23}$$

and C_{ij}^k are the plane-stress reduced elastic constants:

$$C_{11}^k = C_{22}^k = \frac{E^k}{1-(\nu^k)^2}, \quad C_{12}^k = \nu^k \frac{E^k}{1-(\nu^k)^2}, \tag{24}$$

$$C_{44}^k = C_{55}^k = C_{66}^k = G^k \tag{25}$$

4.5. Principle of virtual displacements

In the framework of the Unified Formulation, the Principle of Virtual Displacements (PVD) for the pure-mechanical case is written as:

$$\sum_{k=1}^{N_l} \int_{\Omega_k} \int_{A_k} \left\{ \delta \boldsymbol{\epsilon}_{pG}^{k\ T} \boldsymbol{\sigma}_{pC}^k + \delta \boldsymbol{\epsilon}_{nG}^{k\ T} \boldsymbol{\sigma}_{nC}^k \right\} d\Omega_k dz = \sum_{k=1}^{N_l} \delta L_e^k \tag{26}$$

where Ω_k and A_k are the integration domains in plane (x,y) and z direction, respectively. As stated before, G means geometrical relations and C constitutive equations, and k indicates the virtual layer. T is the transpose operator and δL_e^k is the external work for the kth layer.

Substituting the geometrical relations (G), the constitutive equations (C), and the modeled displacement field (F_τ and F_s), all for the kth layer, (26) becomes:

$$\begin{aligned} &\int_{\Omega_k} \int_{A_k} \Big[\left(\mathbf{D}_p^k F_s \delta \mathbf{u}_s^k\right)^T \left(\mathbf{C}_{pp}^k \mathbf{D}_p^k F_\tau \mathbf{u}_\tau^k + \mathbf{C}_{pn}^k (\mathbf{D}_{n\Omega}^k + \mathbf{D}_{nz}^k) F_\tau \mathbf{u}_\tau^k\right) \\ &\quad + \left(\left(\mathbf{D}_{n\Omega}^k + \mathbf{D}_{nz}^k\right) F_s \delta \mathbf{u}_s^k\right)^T \left(\mathbf{C}_{np}^k \mathbf{D}_p^k F_\tau \mathbf{u}_\tau^k + \mathbf{C}_{nn}^k (\mathbf{D}_{n\Omega}^k + \mathbf{D}_{nz}^k) F_\tau \mathbf{u}_\tau^k\right) \Big] d\Omega_k dz \\ &= \delta L_e^k \end{aligned} \tag{27}$$

Applying now the formula of integration by parts, (27) becomes:

$$\begin{aligned} \int_{\Omega_k} ((\mathbf{D}_\Omega) \delta \mathbf{a}^k)^T \mathbf{a}^k d\Omega_k = &- \int_{\Omega_k} \delta \mathbf{a}^{k^T} \left(\left(\mathbf{D}_\Omega^T\right) \mathbf{a}^k \right) d\Omega_k \\ &+ \int_{\Gamma_k} \delta \mathbf{a}^{k^T} ((\mathbf{I}_\Omega) \mathbf{a}^k) d\Gamma_k \end{aligned} \tag{28}$$

where $\mathbf{I}_\Omega$ matrix is obtained applying the *Gradient theorem*:

$$\int_\Omega \frac{\partial \psi}{\partial x_i} d\upsilon = \oint_\Gamma n_i \psi ds \tag{29}$$

being n_i the components of the normal $\hat{n}$ to the boundary along the direction i. After integration by parts, the governing equations and boundary conditions for the plate in the mechanical case are obtained:

$$\begin{aligned} &\int_{\Omega_k} \int_{A_k} (\delta \mathbf{u}_s^k)^T \Big[\Big(\left(-\mathbf{D}_p^k\right)^T \left(\mathbf{C}_{pp}^k (\mathbf{D}_p^k) + \mathbf{C}_{pn}^k (\mathbf{D}_{n\Omega}^k) + \mathbf{D}_{nz}^k \right) \\ &\quad + \left(-\mathbf{D}_{n\Omega}^k + \mathbf{D}_{nz}^k\right)^T \left(\mathbf{C}_{np}^k (\mathbf{D}_p^k) + \mathbf{C}_{nn}^k (\mathbf{D}_{n\Omega}^k + \mathbf{D}_{nz}^k) \right) \Big) \mathbf{F}_\tau \mathbf{F}_s \mathbf{u}_\tau^k \Big] dxdydz \\ &\quad + \int_{\Omega_k} \int_{A_k} (\delta \mathbf{u}_s^k)^T \Big[\Big(\mathbf{I}_p^{kT} \left(\mathbf{C}_{pp}^k (\mathbf{D}_p^k) \ + \mathbf{C}_{pn}^k (\mathbf{D}_{n\Omega}^k + \mathbf{D}_{nz}^k) \right) + \mathbf{I}_{np}^{kT} \Big(\mathbf{C}_{np}^k \left(\mathbf{D}_p^k\right) \\ &\quad + \mathbf{C}_{nn}^k \left(\mathbf{D}_{n\Omega}^k + \mathbf{D}_{nz}^k\right) \Big) \Big) \mathbf{F}_\tau \mathbf{F}_s \mathbf{u}_\tau^k \Big] dxdydz = \int_{\Omega_k} \delta \mathbf{u}_s^{kT} F_s \mathbf{p}_u^k d\Omega_k. \end{aligned} \tag{30}$$

where $\mathbf{I}_p^k$ and $\mathbf{I}_{np}^k$ depend on the boundary geometry:

$$\mathbf{I}_p^k = \begin{bmatrix} n_x & 0 & 0 \\ 0 & n_y & 0 \\ n_y & n_x & 0 \end{bmatrix}, \quad \mathbf{I}_{np}^k = \begin{bmatrix} 0 & 0 & n_x \\ 0 & 0 & n_y \\ 0 & 0 & 0 \end{bmatrix}. \tag{31}$$

The normal to the boundary of domain Ω is:

$$\hat{\mathbf{n}} = \begin{bmatrix} n_x \\ n_y \end{bmatrix} = \begin{bmatrix} cos(\varphi_x) \\ cos(\varphi_y) \end{bmatrix} \tag{32}$$

where φ_x and φ_y are the angles between the normal $\hat{n}$ and the direction x and y respectively.

4.6. Governing equations and boundary conditions

The governing equations for a multi-layered plate subjected to mechanical loadings are:

$$\delta \mathbf{u}_s^{k^T} : \mathbf{K}_{uu}^{k\tau s}\ \mathbf{u}_\tau^k = \mathbf{P}_{u\tau}^k \tag{33}$$

where the fundamental nucleus $\mathbf{K}_{uu}^{k\tau s}$ is obtained as:

$$\mathbf{K}_{uu}^{k\tau s} = \left[\left(-\mathbf{D}_p^k\right)^T\left(\mathbf{C}_{pp}^k\left(\mathbf{D}_p^k\right) + \mathbf{C}_{pn}^k(\mathbf{D}_{n\Omega}^k) + \mathbf{D}_{nz}^k\right) + \left(-\mathbf{D}_{n\Omega}^k + \mathbf{D}_{nz}^k\right)^T\left(\mathbf{C}_{np}^k(\mathbf{D}_p^k) + \mathbf{C}_{nn}^k(\mathbf{D}_{n\Omega}^k + \mathbf{D}_{nz}^k)\right)\right]\mathbf{F}_\tau\mathbf{F}_s \tag{34}$$

and the corresponding Neumann-type boundary conditions on Γ_k are:

$$\mathbf{\Pi}_d^{k\tau s}\ \mathbf{u}_\tau^k = \mathbf{\Pi}_d^{k\tau s}\ \bar{\mathbf{u}}_\tau^k, \tag{35}$$

where:

$$\mathbf{\Pi}_d^{k\tau s} = \left[\mathbf{I}_p^{kT}\left(\mathbf{C}_{pp}^k\left(\mathbf{D}_p^k\right) + \mathbf{C}_{pn}^k(\mathbf{D}_{n\Omega}^k + \mathbf{D}_{nz}^k)\right) + \mathbf{I}_{np}^{kT}\left(\mathbf{C}_{np}^k(\mathbf{D}_p^k) + \mathbf{C}_{nn}^k(\mathbf{D}_{n\Omega}^k + \mathbf{D}_{nz}^k)\right)\right]\mathbf{F}_\tau\mathbf{F}_s \tag{36}$$

and $\mathbf{P}_{u\tau}^k$ are variationally consistent loads with applied pressure.

For FG materials, the fundamental nuclei in explicit form becomes:

$$\begin{aligned}
K_{uu_{11}}^{k\tau s} &= \left(-\partial_x^\tau\partial_x^s C_{11} + \partial_z^\tau\partial_z^s C_{55} - \partial_y^\tau\partial_y^s C_{66}\right)F_\tau F_s\\
K_{uu_{12}}^{k\tau s} &= \left(-\partial_x^\tau\partial_y^s C_{12} - \partial_y^\tau\partial_x^s C_{66}\right)F_\tau F_s\\
K_{uu_{13}}^{k\tau s} &= (-\partial_x^\tau\partial_z^s C_{13} + \partial_z^\tau\partial_x^s C_{55})F_\tau F_s\\
K_{uu_{21}}^{k\tau s} &= \left(-\partial_y^\tau\partial_x^s C_{12} - \partial_x^\tau\partial_y^s C_{66}\right)F_\tau F_s\\
K_{uu_{22}}^{k\tau s} &= \left(-\partial_y^\tau\partial_y^s C_{22} + \partial_z^\tau\partial_z^s C_{44} - \partial_x^\tau\partial_x^s C_{66}\right)F_\tau F_s\\
K_{uu_{23}}^{k\tau s} &= \left(-\partial_y^\tau\partial_z^s C_{23} + \partial_z^\tau\partial_y^s C_{44}\right)F_\tau F_s\\
K_{uu_{31}}^{k\tau s} &= (\partial_z^\tau\partial_x^s C_{13} - \partial_x^\tau\partial_z^s C_{55})F_\tau F_s\\
K_{uu_{32}}^{k\tau s} &= \left(\partial_z^\tau\partial_y^s C_{23} - \partial_y^\tau\partial_z^s C_{44}\right)F_\tau F_s\\
K_{uu_{33}}^{k\tau s} &= \left(\partial_z^\tau\partial_z^s C_{33} - \partial_y^\tau\partial_y^s C_{44} - \partial_x^\tau\partial_x^s C_{55}\right)F_\tau F_s
\end{aligned} \tag{37}$$

$$\begin{aligned}
\Pi_{11}^{k\tau s} &= \left(n_x\partial_x^s C_{11} + n_y\partial_y^s C_{66}\right)F_\tau F_s\\
\Pi_{12}^{k\tau s} &= \left(n_x\partial_y^s C_{12} + n_y\partial_x^s C_{66}\right)F_\tau F_s\\
\Pi_{13}^{k\tau s} &= (n_x\partial_z^s C_{13})F_\tau F_s\\
\Pi_{21}^{k\tau s} &= \left(n_y\partial_x^s C_{12} + n_x\partial_y^s C_{66}\right)F_\tau F_s\\
\Pi_{22}^{k\tau s} &= \left(n_y\partial_y^s C_{22} + n_x\partial_x^s C_{66}\right)F_\tau F_s\\
\Pi_{23}^{k\tau s} &= (n_y\partial_z^s C_{23})F_\tau F_s\\
\Pi_{31}^{k\tau s} &= (n_x\partial_z^s C_{55})F_\tau F_s\\
\Pi_{32}^{k\tau s} &= (n_y\partial_z^s C_{44})F_\tau F_s\\
\Pi_{33}^{k\tau s} &= \left(n_y\partial_y^s C_{44} + n_x\partial_x^s C_{55}\right)F_\tau F_s
\end{aligned} \tag{38}$$

5. The radial basis function method applied to static problems

Recently, radial basis functions (RBFs) have enjoyed considerable success and research as a technique for interpolating data and functions. A radial basis function, $\phi(\|x - x_j\|)$ is a spline that depends on the Euclidian distance between distinct data centers $x_j,\ j = 1, 2, \ldots, N \in \mathbb{R}^n$, also called nodal or collocation points. Although most work to date on RBFs relates to scattered data approximation and in general to interpolation theory, there has recently been an increased interest in their use for solving partial differential equations (PDEs). This approach, which approximates the whole solution of the PDE directly using RBFs, is truly a mesh-free technique. Kansa [53] introduced the concept of solving PDEs by an unsymmetric RBF collocation method based upon the MQ interpolation functions, in which the shape parameter may vary across the problem domain.

The radial basis function (ϕ) approximation of a function ($\mathbf{u}$) is given by

$$\tilde{\mathbf{u}}(\mathbf{x}) = \sum_{i=1}^{N}\alpha_i\phi(\|x - y_i\|_2), \mathbf{x} \in \mathbb{R}^n \tag{39}$$

where y_i, $i = 1, \ldots, N$ is a finite set of distinct points (centers) in $\mathbb{R}^n$.

The most common RBFs are

$$\begin{aligned}
&\text{Cubic}: \quad \phi(r) = r^3\\
&\text{Thin plate splines}: \quad \phi(r) = r^2\log(r)\\
&\text{Wendland functions}: \quad \phi(r) = (1 - r)_+^m p(r)\\
&\text{Gaussian}: \quad \phi(r) = e^{-(cr)^2}\\
&\text{Multiquadrics}: \quad \phi(r) = \sqrt{c^2 + r^2}\\
&\text{Inverse Multiquadrics}: \quad \phi(r) = (c^2 + r^2)^{-1/2}
\end{aligned}$$

where the Euclidian distance r is real and non-negative and c is a positive shape parameter. In the present work, we consider the compact-support Wendland function defined as

$$\phi(r) = (1 - c\ r)_+^8(32(c\ r)^3 + 25(c\ r)^2 + 8c\ r + 1) \tag{40}$$

The shape parameter (c) is obtained by an optimization procedure, as detailed in Ferreira and Fasshauer [54].

Considering N distinct interpolations, and knowing $u(x_j)$, $j = 1, 2, \ldots, N$, we find α_i by the solution of a $N \times N$ linear system

$$\mathbf{A\alpha} = \mathbf{u} \tag{41}$$

where $\mathbf{A} = [\phi(\|x - y_i\|_2)]_{N\times N}$, $\boldsymbol{\alpha} = [\alpha_1, \alpha_2, \ldots, \alpha_N]^T$ and $\mathbf{u} = [u(x_1), u(x_2), \ldots, u(x_N)]^T$.

Consider a linear elliptic partial differential operator $\mathcal{L}$ acting in a bounded region Ω in $\mathbb{R}^n$ and another operator $\mathcal{L}_B$ acting on a boundary $\partial\Omega$. In the static problems we seek the computation of displacements ($\mathbf{u}$) from the global system of equations

$$\mathcal{L}\mathbf{u} = \mathbf{f} \text{ in } \Omega \tag{42}$$

$$\mathcal{L}_B\mathbf{u} = \mathbf{g} \text{ on } \partial\Omega \tag{43}$$

The right-hand side of (42) and (43) represent the external forces applied on the plate and the boundary conditions applied along the perimeter of the plate, respectively. The PDE problem defined in (42) and (43) will be replaced by a finite problem, defined by an algebraic system of equations, after the radial basis expansions.

The solution of a static problem by radial basis functions considers N_I nodes in the domain and N_B nodes on the boundary, with a total number of nodes $N = N_I + N_B$. In the present work, a $\Re^2$ Chebyshev grid is employed (see Fig. 6) and a square plate is com-

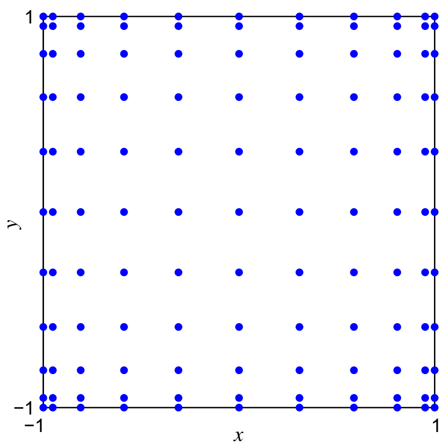

Fig. 6. A sketch of a $\Re^2$ Chebyshev grid with 11^2 points.

puted with side length $a = 2$. For a given number of nodes per side $(N + 1)$ they are generated by MATLAB code as:

$\mathtt{x = cos(pi*(0:N)/N)'; y = x;}$

One advantage of such mesh is the concentration of points near the boundary.

We denote the sampling points by $x_i \in \Omega$, $i = 1, \ldots, N_I$ and $x_i \in \partial\Omega$, $i = N_I + 1, \ldots, N$. At the points in the domain we solve the following system of equations

$$\sum_{i=1}^{N} \alpha_i \mathcal{L}\phi(\|x - y_i\|_2) = \mathbf{f}(x_j), \quad j = 1, 2, \ldots, N_I \tag{44}$$

or

$$\mathcal{L}^I \boldsymbol{\alpha} = \mathbf{F} \tag{45}$$

where

$$\mathcal{L}^I = [\mathcal{L}\phi(\|x - y_i\|_2)]_{N_I \times N} \tag{46}$$

At the points on the boundary, we impose boundary conditions as

$$\sum_{i=1}^{N} \alpha_i \mathcal{L}_B \phi(\|x - y_i\|_2) = \mathbf{g}(x_j), \quad j = N_I + 1, \ldots, N \tag{47}$$

or

$$\mathbf{B}\boldsymbol{\alpha} = \mathbf{G} \tag{48}$$

where

$$\mathbf{B} = \mathcal{L}_B \phi[(\|x_{N_I+1} - y_j\|_2)]_{N_B \times N}$$

Therefore, we can write a finite-dimensional static problem as

$$\begin{bmatrix} \mathcal{L}^I \\ \mathbf{B} \end{bmatrix} \boldsymbol{\alpha} = \begin{bmatrix} \mathbf{F} \\ \mathbf{G} \end{bmatrix} \tag{49}$$

By inverting the system (49), we obtain the vector $\boldsymbol{\alpha}$. We then obtain the solution $\mathbf{u}$ using the interpolation Eq. (39).

The radial basis collocation method follows a simple implementation procedure. Taking Eq. (49), we compute

$$\boldsymbol{\alpha} = \begin{bmatrix} L^I \\ \mathbf{B} \end{bmatrix}^{-1} \begin{bmatrix} \mathbf{F} \\ \mathbf{G} \end{bmatrix} \tag{50}$$

This $\boldsymbol{\alpha}$ vector is then used to obtain solution $\tilde{\mathbf{u}}$, by using (39). If derivatives of $\tilde{\mathbf{u}}$ are needed, such derivatives are computed as

$$\frac{\partial \tilde{\mathbf{u}}}{\partial x} = \sum_{j=1}^{N} \alpha_j \frac{\partial \phi_j}{\partial x} \tag{51}$$

$$\frac{\partial^2 \tilde{\mathbf{u}}}{\partial x^2} = \sum_{j=1}^{N} \alpha_j \frac{\partial^2 \phi_j}{\partial x^2}, \quad \text{etc} \tag{52}$$

In the present collocation approach, we need to impose essential and natural boundary conditions. Consider, for example, the condition $w = 0$, on a simply supported or clamped edge. We enforce the conditions by interpolating as

$$w = 0 \rightarrow \sum_{j=1}^{N} \alpha_j^W \phi_j = 0 \tag{53}$$

Other boundary conditions are interpolated in a similar way.

6. Numerical examples

In this section the shear deformation plate theory is combined with radial basis functions collocation for the static analysis of functionally graded sandwich plates. Displacements and stresses of simply supported (SSSS) square $(a = b = 2)$ sandwich plates with FGM in the core or in the skins, both symmetric and unsymmetric, are analyzed. Various side-to-thickness ratios, power-law exponents, and skin-core-skin thickness ratios are considered. The plate is subjected to a bi-sinusoidal transverse mechanical load, $p = p_z \cos\left(\frac{\pi x}{a}\right) \cos\left(\frac{\pi y}{a}\right)$ (see Fig. 6), applied at the top of the plate.

As stated before, all numerical examples are performed employing a Chebyshev grid and the Wendland function as defined in (40) with an optimized shape parameter. The plate is a sandwich, physicaly divided into 3 layers, but we consider 91 virtual layers. The power-law function is used to describe the volume fraction of the metal and ceramic phases (see (1) and (2)) and the material homogeneization technique adopted is the law of mixtures (13), the same used in the references.

The following material properties are used:

$$\text{zirconia Young's modulus}: E_c = 151\ \text{GPa} \tag{54}$$

$$\text{aluminum Young's modulus}: E_m = 70\ \text{GPa} \tag{55}$$

$$\text{alumina Young's modulus}: E_c = 380\ \text{GPa} \tag{56}$$

with Poisson's ratio constant $\nu = 0.3$. Only Young's modulus needs a homogeneization technique.

An initial study was performed for each type of sandwich to show the convergence of the present approach and select the number of Chebyshev points to use in the computation of the static problems problems.

6.1. Sandwich with FG core

The static analysis of sandwich plates with FG core is now performed. In the following examples the materials are aluminum (55) and alumina (56). The thickness of each skin layer is $h_s = 0.1h$ and the core layer thickness is $h_c = 0.8h$, i.e., we are dealing with a 1-8-1 sandwich.

The non-dimensional parameters used are:

$$\begin{aligned}
\bar{w} &= \frac{10E_c h^3}{a^4 p_z} w, \quad \text{evaluated at the center of the plate} \\
\bar{\sigma}_{xx} &= \frac{h}{a p_z} \sigma_{xx}, \quad \text{evaluated at the center of the plate} \\
\bar{\sigma}_{xy} &= \frac{h}{a p_z} \sigma_{xy}, \quad \text{evaluated at the corner of the plate} \\
\bar{\sigma}_{xz} &= \frac{h}{a p_z} \sigma_{xz}, \quad \text{evaluated at the midpoint of the side} \\
\sigma_{zz} &= \sigma_{zz}, \quad \text{evaluated at center of the plate}
\end{aligned} \tag{57}$$

Two convergence studies were performed, varying the exponent power-law p and the side-to-thickness ratio a/h. Table 1 refers to $p = 1$ and $a/h = 4$ and Table 2 refers to $p = 10$ and $a/h = 100$. A 15^2 grid was chosen for the following static problems.

Table 3 and Figs. 7 and 8 refer to the out-of-plane displacement. In Table 3 we tabulate the values of the deflection obtained with

Table 1
Convergence study for a sandwich with FG core with $p = 1$ and $a/h = 4$.

Grid	9^2	11^2	13^2	15^2	17^2	19^2
$\bar{w}(0)$	0.7411	0.7417	0.7417	0.7417	0.7417	0.7417
$\bar{\sigma}_{xx}(\frac{h}{3})$	0.6224	0.6236	0.6235	0.6236	0.6236	0.6236
$\bar{\sigma}_{xy}(\frac{h}{3})$	0.3263	0.3164	0.3164	0.3165	0.3164	0.3164
$\bar{\sigma}_{xz}(0)$	0.2329	0.2333	0.2332	0.2332	0.2332	0.2332
$\bar{\sigma}_{xz}(\frac{h}{6})$	0.2745	0.2748	0.2747	0.2747	0.2747	0.2747
$\bar{\sigma}_{xz}(\frac{h}{3})$	0.2195	0.2193	0.2192	0.2192	0.2192	0.2192
$\sigma_{zz}(0)$	0.3316	0.3311	0.3312	0.3312	0.3312	0.3312

Table 2
Convergence study for a sandwich with FG core with $p = 10$ and $a/h = 100$.

Grid	9^2	11^2	13^2	15^2	17^2	19^2
$\bar{w}(0)$	0.6794	0.8035	0.8009	0.8045	0.8048	0.8050
$\bar{\sigma}_{xx}(\frac{h}{3})$	7.5645	9.1864	9.3955	9.4300	9.4187	9.4272
$\bar{\sigma}_{xy}(\frac{h}{3})$	3.4217	4.9099	5.0405	5.0641	5.0641	5.0735
$\bar{\sigma}_{xz}(0)$	0.2002	0.2188	0.2017	0.2056	0.2047	0.2052
$\bar{\sigma}_{xz}(\frac{h}{6})$	0.1970	0.2216	0.2025	0.2065	0.2055	0.2060
$\bar{\sigma}_{xz}(\frac{h}{3})$	0.2137	0.3072	0.2612	0.2685	0.2657	0.2659
$\sigma_{zz}(0)$	0.2003	0.1858	0.1850	0.1834	0.1850	0.1839

Table 3
$\bar{w}(0)$ of a sandwich plate with FG core, for several exponents p and ratios a/h.

	ϵ_{zz}	$p = 1$	$p = 4$	$p = 5$	$p = 10$
$a/h = 4$					
Ref. LD4 [38]	0	0.7629		1.1327	1.2232
Ref. LM4 [38]	≠0	0.7629		1.1329	1.2244
Ref. [55] $N = 4$	0	0.7735	1.0977		1.2240
Ref. [55] $N = 4$	≠0	0.7628	1.0930		1.2172
Ref. [?]	0	0.7744	1.0847		1.2212
Ref. [?]	≠0	0.7416	1.0391		1.1780
Present	0	0.7746	1.0833	1.1236	1.2183
Present	≠0	0.7417	1.0378	1.0783	1.1753
$a/h = 10$					
Ref. [55] $N = 4$	0	0.6337	0.8308		0.8743
Ref. [55] $N = 4$	≠0	0.6324	0.8307		0.8740
Ref. [?]	0	0.6356	0.8276		0.8718
Ref. [?]	≠0	0.6305	0.8202		0.8650
Present	0	0.6357	0.8273	0.8415	0.8712
Present	≠0	0.6305	0.8200	0.8342	0.8645
$a/h = 100$					
Ref. LD4 [38]	0	0.6073		0.7892	0.8077
Ref. LM4 [38]	≠0	0.6073		0.7892	0.8077
Ref. [55] $N = 4$	0	0.6072	0.7797		0.8077
Ref. [55] $N = 4$	≠0	0.6072	0.7797		0.8077
Ref. [?]	0	0.6092	0.7785		0.8050
Ref. [?]	≠0	0.6092	0.7784		0.8050
Present	0	0.6087	0.7779	0.7870	0.8045
Present	≠0	0.6086	0.7778	0.7870	0.8045

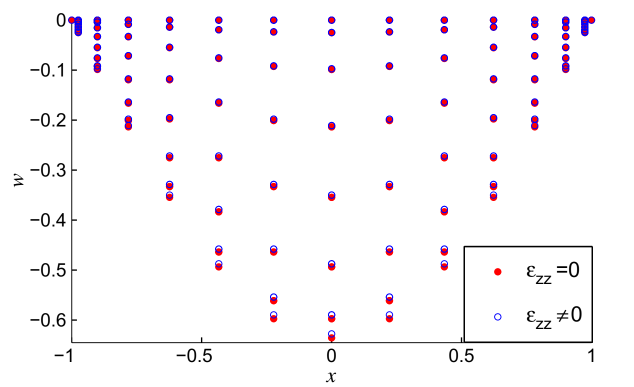

Fig. 7. Deformed of the SSSS sandwich square plate with FG core ($p = 1$, $a/h = 10$), subjected to sinusoidal load at the top, according to the hyperbolic sine ZZ theory, considering and disregarding thickness-stretching.

present approach for various power-law exponents p and side-to-thickness ratios a/h, and compare with available references. In Fig. 7, the thickness-stretching effect on the deformed of the simply supported sandwich square plate with FG core, with $p = 1$ and $a/h = 10$, is visualized. Figure is the plot of the top ($z = h/2$) of the plate. Fig. 8 presents the out-of-plane displacement through

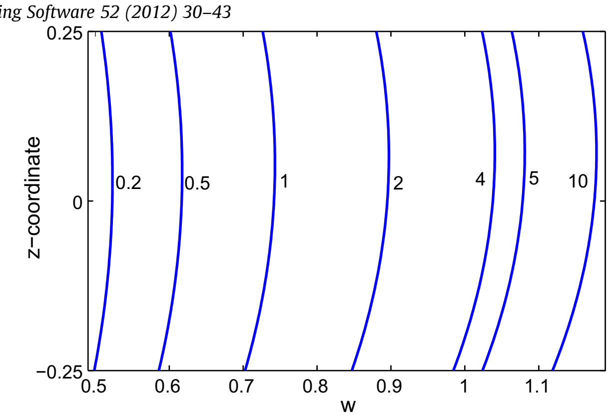

Fig. 8. Out-of-plane displacement through the thickness direction of a SSSS sandwich square plate with FG core, $a/h = 4$, subjected to sinusoidal load at the top, according to the hyperbolic sine ZZ theory, for several values of p.

the thickness direction, for a sandwich with FG core with side-to-thickness ratio $a/h = 4$, varying the exponent power-law value p.

Table 3 and Fig. 8 lead us to the conclusion that the deflection of a SSSS sandwich plate with FG core increases as the power-law exponent of the material p increases. The results depend on consider or neglect warping in the thickness direction. The warping effect is more significative in thicker plates.

Tables 4–8 and Figs. 9–14, refer to stresses. In tables we tabulate and compare with available references the results obtained

Table 4
$\bar{\sigma}_{xx}(h/3)$ of a sandwich plate with FG core, for several exponents p and ratios a/h.

	ϵ_{zz}	$p = 1$	$p = 4$	$p = 5$	$p = 10$
$a/h = 4$					
Ref. LD4 [38]	0	0.6530		0.4693	0.3627
Ref. LM4 [38]	≠0	0.6531		0.4672	0.3611
Present	0	0.6130	0.4643	0.4304	0.3247
Present	≠0	0.6236	0.4605	0.4243	0.3156
$a/h = 10$					
Present	0	1.5700	1.2514	1.1777	0.9214
Present	≠0	1.5743	1.2498	1.1751	0.9176
$a/h = 100$					
Ref. LD4 [38]	0	15.784		12.065	9.5501
Ref. LM4 [38]	≠0	15.784		12.065	9.5500
Present	0	15.7826	12.6971	11.9800	9.4300
Present	≠0	15.7841	12.6975	11.9805	9.4300

Table 5
$\bar{\sigma}_{xy}(h/3)$ of a sandwich plate with FG core, for several exponents p and ratios a/h.

	ϵ_{zz}	$p = 1$	$p = 4$	$p = 5$	$p = 10$
$a/h = 4$					
Ref. LD4 [38]	0	0.3007		0.1999	0.1412
Ref. LM4 [38]	≠0	0.3007		0.1996	0.1403
Ref. [?]	0	0.3303		0.2317	0.1745
Ref. [?]	≠0	0.3167		0.2248	0.1687
Present	0	0.3301	0.2500	0.2318	0.1749
Present	≠0	0.3165	0.2425	0.2249	0.1692
$a/h = 10$					
Present	0	0.8453	0.6738	0.6341	0.4962
Present	≠0	0.8400	0.6709	0.6315	0.4939
$a/h = 100$					
Ref. LD4 [38]	0	8.4968		6.4942	5.1402
Ref. LM4 [38]	≠0	8.4968		6.4942	5.1401
Ref. [?]	0	8.4888		6.4454	5.0745
Ref. [?]	≠0	8.4911		6.4441	5.0754
Present	0	8.4644	6.8194	6.4400	5.0672
Present	≠0	8.4689	6.8102	6.4392	5.0628

Table 6
$\bar{\sigma}_{xz}(0)$ of a sandwich plate with FG core, for several exponents p and ratios a/h.

	ϵ_{zz}	$p=1$	$p=4$	$p=5$	$p=10$
$a/h=4$					
Ref. LD4 [38]	0	0.2345		0.1998	0.2113
Ref. LM4 [38]	≠0	0.2345		0.2026	0.2124
Present	0	0.2334	0.1880	0.1863	0.2017
Present	≠0	0.2332	0.1873	0.1857	0.2015
$a/h=10$					
Present	0	0.2353	0.1905	0.1889	0.2044
Present	≠0	0.2353	0.1900	0.1887	0.2050
$a/h=100$					
Ref. LD4 [38]	0	0.2375		0.2046	0.2149
Ref. LM4 [38]	≠0	0.2375		0.2055	0.2122
Present	0	0.2367	0.1911	0.1895	0.2050
Present	≠0	0.2368	0.1907	0.1894	0.2056

Table 7
$\bar{\sigma}_{zz}(0)=\frac{h}{ap_z}\sigma_{zz}(\frac{a}{2},\frac{a}{2},0)$ of a sandwich plate with FG core, for several exponents p and ratios a/h.

	ϵ_{zz}	$p=1$	$p=4$	$p=5$	$p=10$
$a/h=4$					
Ref. LD4 [38]	0	0.0922		0.0911	0.1064
Ref. LM4 [38]	≠0	0.0922		0.0924	0.1067
Ref. [?]	≠0	0.0827		0.0522	0.0443
Present	≠0	0.0828	0.0580	0.0524	0.0445
$a/h=10$					
Present	≠0	0.0338	0.0239	0.0216	0.0183
$a/h=100$					
Ref. LD4 [38]	0	0.0038		0.0037	0.0043
Ref. LM4 [38]	≠0	0.0038		0.0037	0.0042
Ref. [?]	≠0	0.0034		0.0022	0.0018
Present	≠0	0.0034	0.0024	0.0022	0.0018

Table 8
$\bar{\sigma}_{xz}(h/6)$ of a sandwich plate with FG core, for several exponents p and ratios a/h.

	ϵ_{zz}	$p=1$	$p=4$	$p=5$	$p=10$
$a/h=4$					
Ref. [55] $N=4$	0	0.2604	0.2400		0.1932
Ref. [55] $N=4$	≠0	0.2596	0.2400		0.1935
Ref. [?]	0	0.2703	0.2699		0.1998
Ref. [?]	≠0	0.2742	0.2723		0.2016
Present	0	0.2709	0.2706	0.2537	0.1995
Present	≠0	0.2747	0.2732	0.2560	0.2013
$a/h=10$					
Ref. [55] $N=4$	0	0.2594	0.2398		0.1944
Ref. [55] $N=4$	≠0	0.2593	0.2398		0.1944
Ref. [?]	0	0.2718	0.2726		0.2021
Ref. [?]	≠0	0.2788	0.2778		0.2059
Present	0	0.2724	0.2735	0.2566	0.2017
Present	≠0	0.2793	0.2789	0.2615	0.2055
$a/h=100$					
Ref. [55] $N=4$	0	0.2593	0.2398		0.1946
Ref. [55] $N=4$	≠0	0.2593	0.2398		0.1946
Ref. [?]	0	0.2720	0.2728		0.2022
Ref. [?]	≠0	0.2793	0.2785		0.2064
Present	0	0.2743	0.2747	0.2576	0.2230
Present	≠0	0.2816	0.2805	0.2630	0.2065

with present approach for various exponents of the power-law p and side-to-thickness ratios a/h. In figures we present stresses through the thickness direction of a SSSS sandwich square plate with FG core, $a/h=100$ according to the hyperbolic sine ZZ theory, for several values of p.

In all tables, results obtained with present hyperbolic sine ZZ theory and RBF collocation are in good agreement with references.

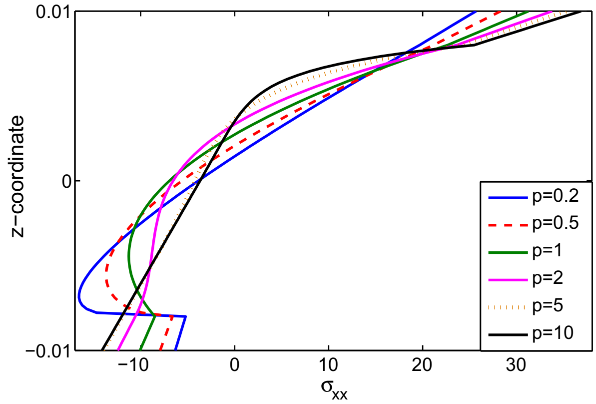

Fig. 9. $\bar{\sigma}_{xx}$ through the thickness direction of a SSSS sandwich square plate with FG core, $a/h=100$, subjected to sinusoidal load at the top, according to the hyperbolic sine ZZ theory, for several values of p.

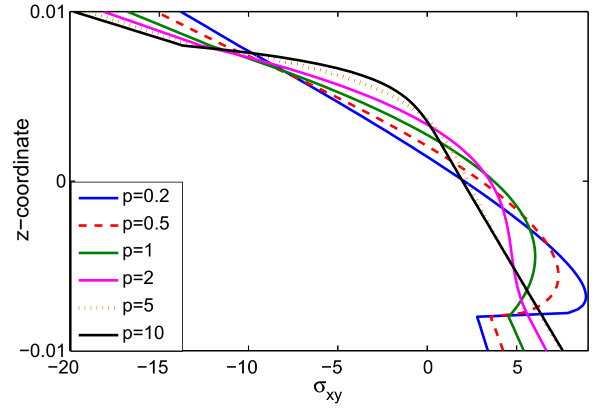

Fig. 10. $\bar{\sigma}_{xy}$ through the thickness direction of a SSSS sandwich square plate with FG core, $a/h=100$, subjected to sinusoidal load at the top, according to the hyperbolic sine ZZ theory, for several values of p.

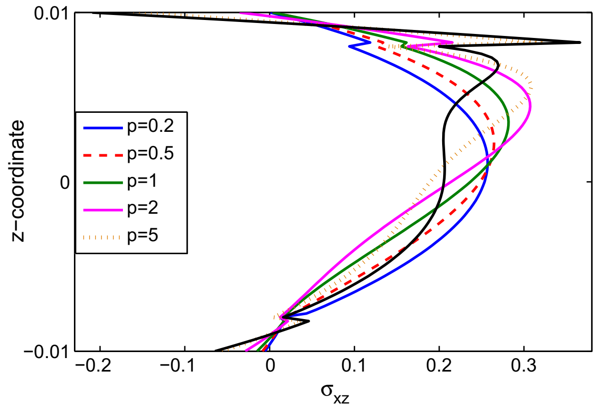

Fig. 11. $\bar{\sigma}_{xz}$ through the thickness direction of a SSSS sandwich square plate with FG core, $a/h=100$, subjected to sinusoidal load at the top, according to the hyperbolic sine ZZ theory, for several values of p.

6.2. Sandwich with FG skins

We now focus on sandwich plates with isotropic core and FG skins. All examples consider a sandwich plate made of aluminum (55) and zirconia (54) and with side-to-thickness ratio $a/h=10$. Ta-

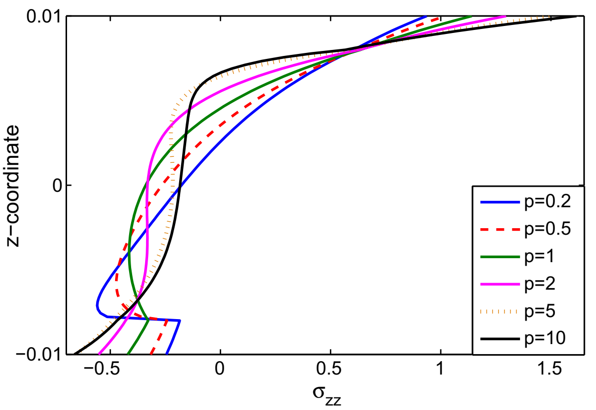

Fig. 12. $\bar{\sigma}_{zz}$ through the thickness direction of a SSSS sandwich square plate with FG core, $a/h = 100$, subjected to sinusoidal load at the top, according to the hyperbolic sine ZZ theory, for several values of p.

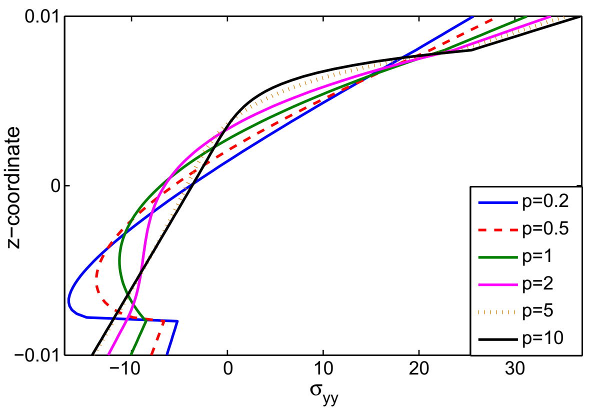

Fig. 13. $\bar{\sigma}_{yy}$ through the thickness direction of a SSSS sandwich square plate with FG core, $a/h = 100$, subjected to sinusoidal load at the top, according to the hyperbolic sine ZZ theory, for several values of p.

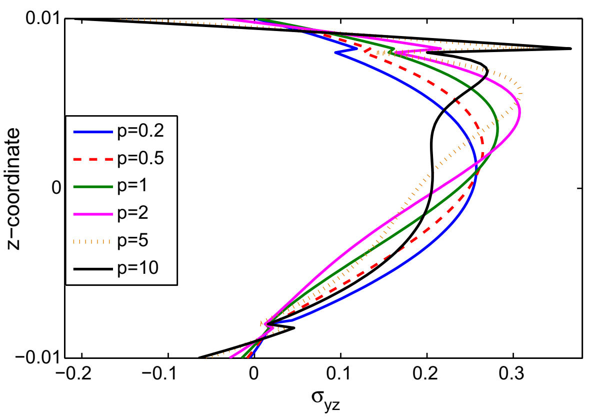

Fig. 14. $\bar{\sigma}_{yz}$ through the thickness direction of a SSSS sandwich square plate with FG core, $a/h = 100$, subjected to sinusoidal load at the top, according to the hyperbolic sine ZZ theory, for several values of p.

Table 9
Convergence study for a 2-1-2 sandwich with FG skins and $p = 1$.

Grid	11^2	13^2	15^2	17^2	19^2
$\bar{w}(0)$	0.3069	0.3069	0.3070	0.3070	0.3070
$\bar{\sigma}_{xx}$	1.4835	1.4801	1.4813	1.4810	1.4811
$\bar{\sigma}_{xz}$	0.2749	0.2744	0.2745	0.2745	0.2745

bles are organized so that the material power-law exponent increases from up to down ($p = 0$, 0.2, 0.5, 1, 2, 5, 10) and the core thickness to the total thickness of the plate ratio increases from left to right $\left(\frac{h_c}{h} = \frac{1}{5}, \frac{1}{4}, \frac{1}{3}, \frac{2}{5}, \frac{1}{2}\right)$.

The non-dimensional displacements and stresses are given as

$$\begin{aligned}
\bar{w} &= \frac{10hE_0}{a^2p_z}w, \quad \text{evaluated at the center of the plate}\\
\bar{u} &= \frac{10hE_0^2}{a^2p_z}u, \quad \text{evaluated at the center of the plate}\\
\bar{\sigma}_{xx} &= \frac{10h^2}{a^2p_z}\sigma_{xx}, \quad \text{evaluated at the center of theplate}\\
\bar{\sigma}_{xz} &= \frac{h}{ap_z}\sigma_{xz}, \quad \text{evaluated at the midpoint of the side}
\end{aligned} \tag{58}$$

Table 10
Convergence study for a 2-2-1 sandwich with FG skins and $p = 5$.

Grid	11^2	13^2	15^2	17^2	19^2
$\bar{w}(0)$	0.3489	0.3490	0.3490	0.3490	0.3490
$\bar{\sigma}_{xx}$	1.5917	1.5880	1.5893	1.5889	1.5891
$\bar{\sigma}_{xz}$	0.2673	0.2667	0.2669	0.2668	0.2668

Table 11
$\bar{w}(0)$ of a sandwich plate with FG skins, for several exponents p and skin-core-skin ratios.

Source	2-1-2	2-1-1	1-1-1	2-2-1	1-2-1
$p = 0$					
SSDPT	0.19605		0.19605	0.19605	0.19605
TSDPT	0.19606		0.19606	0.19606	0.19606
FSDPT	0.19607		0.19607	0.19607	0.19607
CLPT	0.18560		0.18560	0.18560	0.18560
Present $\epsilon_{zz} = 0$	0.1961	0.1961	0.1961	0.1961	0.1961
Present $\epsilon_{zz} \neq 0$	0.1949	0.1949	0.1949	0.1949	0.1949
$p = 0.2$					
Present $\epsilon_{zz} = 0$	0.2312	0.2290	0.2276	0.2249	0.2223
Present $\epsilon_{zz} \neq 0$	0.2297	0.2275	0.2261	0.2235	0.2209
$p = 0.5$					
Present $\epsilon_{zz} = 0$	0.2667	0.2614	0.2583	0.2519	0.2460
Present $\epsilon_{zz} \neq 0$	0.2650	0.2597	0.2566	0.2503	0.2444
$p = 1$					
SSDPT	0.30624		0.29194	0.28082	0.27093
TSDPT	0.30632		0.29199	0.28085	0.27094
FSDPT	0.30750		0.29301	0.28168	0.27167
CLPT	0.29417		0.28026	0.26920	0.25958
Present $\epsilon_{zz} = 0$	0.3090	0.2995	0.2949	0.2838	0.2740
Present $\epsilon_{zz} \neq 0$	0.3070	0.2975	0.2929	0.2820	0.2722
$p = 2$					
SSDPT	0.35218		0.33280	0.31611	0.30260
TSDPT	0.35231		0.33289	0.31617	0.30263
FSDPT	0.35408		0.33441	0.31738	0.30370
CLPT	0.33942		0.32067	0.30405	0.29095
Present $\epsilon_{zz} = 0$	0.3542	0.3399	0.3351	0.3186	0.3053
Present $\epsilon_{zz} \neq 0$	0.3519	0.3376	0.3329	0.3164	0.3032
$p = 5$					
SSDPT	0.39160		0.37128	0.34950	0.33474
TSDPT	0.39183		0.37145	0.34960	0.33480
FSDPT	0.39418		0.37356	0.35123	0.33631
CLPT	0.37789		0.35865	0.33693	0.32283
Present $\epsilon_{zz} = 0$	0.3930	0.3746	0.3729	0.3514	0.3370
Present $\epsilon_{zz} \neq 0$	0.3905	0.3722	0.3705	0.3490	0.3347
$p = 10$					
SSDPT	0.40376		0.38490	0.34916	0.34119
TSDPT	0.40407		0.38551	0.36215	0.34824
FSDPT	0.40657		0.38787	0.36395	0.34996
CLPT	0.38941		0.37236	0.34915	0.33612
Present $\epsilon_{zz} = 0$	0.4051	0.3861	0.3868	0.3637	0.3503
Present $\epsilon_{zz} \neq 0$	0.4026	0.3835	0.3843	0.3612	0.3480

Two convergence studies were performed, varying the exponent power-law p and the symmetry of the sandwich. Table 9 refers to the symmetric 2-1-2 plate with $p = 1$ and Table 10 refers to the non-symmetric 2-2-1 plate with $p = 5$. A 15^2 grid was chosen for the following static problems.

Results refering to the displacements of a sandwich plate with FG skins are presented in Table 11 and Figs. 15–17. In Table 11, the transverse displacement are tabulated and compared with available references, for several values of p and skin-core-skin thickness ratios. In Fig. 15, the influence of the thickness-stretching on the deformed of the symmetric 1-2-1 simply supported sandwich square plate with FG skins, with $p = 10$, subjected to sinusoidal load at the top, is visualized. Fig. 15 is the plot of the bottom $(z = -h/2)$ of the plate. In Figs. 16 and 17 the influence of the

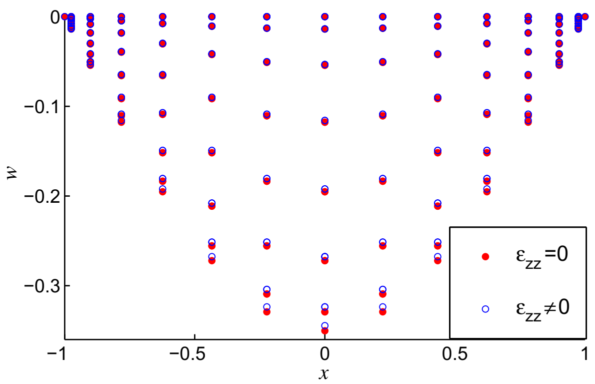

Fig. 15. Deformed of the SSSS 1-2-1 sandwich square plate with FG skins, $p = 10$, subjected to sinusoidal load at the top, according to the hyperbolic sine ZZ theory, considering and disregarding thickness-stretching.

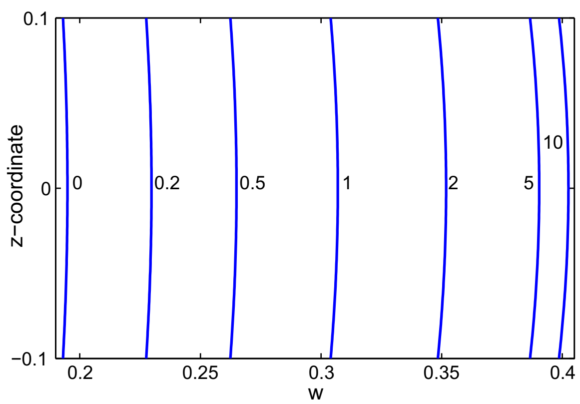

Fig. 16. Out-of-plane displacement through the thickness of the SSSS 2-1-2 sandwich square plate with FG skins, subjected to sinusoidal load at the top, according to the hyperbolic sine ZZ theory, for various values of p.

Table 12

$\bar{\sigma}_{xx}(h/2)$ of a sandwich plate with FG skins, for several exponents p and skin-core-skin ratios.

Source	2-1-2	2-1-1	1-1-1	2-2-1	1-2-1
$p = 0$					
SSDPT	2.05452		2.05452	2.05452	2.05452
TSDPT	2.04985		2.04985	2.04985	2.04985
FSDPT	1.97576		1.97576	1.97576	1.97576
Present $\epsilon_{zz} = 0$	1.9947	1.9945	1.9947	1.9946	1.9946
Present $\epsilon_{zz} \neq 0$	2.0066	2.0064	2.0066	2.0065	2.0064
$p = 0.2$					
Present $\epsilon_{zz} = 0$	1.0962	1.0705	1.0795	1.0526	1.0533
Present $\epsilon_{zz} \neq 0$	1.1024	1.0767	1.0857	1.0587	1.0595
$p = 0.5$					
Present $\epsilon_{zz} = 0$	1.2690	1.2088	1.2285	1.1679	1.1694
Present $\epsilon_{zz} \neq 0$	1.2757	1.2153	1.2351	1.1743	1.1759
$p = 1$					
SSDPT	1.49859		1.42892	1.32342	1.32590
TSDPT	1.49587		1.42617	1.32062	1.32309
FSDPT	1.45167		1.38303	1.27749	1.28096
Present $\epsilon_{zz} = 0$	1.4742	1.3700	1.4067	1.3026	1.3064
Present $\epsilon_{zz} \neq 0$	1.4813	1.3768	1.4137	1.3092	1.3133
$p = 2$					
SSDPT	1.72412		1.63025	1.47387	1.48283
TSDPT	1.72144		1.62748	1.47095	1.47988
FSDPT	1.67496		1.58242	1.42528	1.43580
Present $\epsilon_{zz} = 0$	1.6920	1.5386	1.6017	1.4476	1.4588
Present $\epsilon_{zz} \neq 0$	1.6994	1.5456	1.6088	1.4543	1.4659
$p = 5$					
SSDPT	1.91547		1.81838	1.61477	1.64106
TSDPT	1.91302		1.81580	1.61181	1.63814
FSDPT	1.86479		1.76988	1.56401	1.59309
Present $\epsilon_{zz} = 0$	1.8761	1.6836	1.7833	1.5826	1.6123
Present $\epsilon_{zz} \neq 0$	1.8838	1.6909	1.7906	1.5893	1.6195
$p = 10$					
SSDPT	1.97313		1.88147	1.61979	1.64851
TSDPT	1.97126		1.88376	1.66660	1.70417
FSDPT	1.92165		1.83754	1.61645	1.65844
Present $\epsilon_{zz} = 0$	1.9316	1.7328	1.8485	1.6327	1.6761
Present $\epsilon_{zz} \neq 0$	1.9397	1.7405	1.8559	1.6395	1.6832

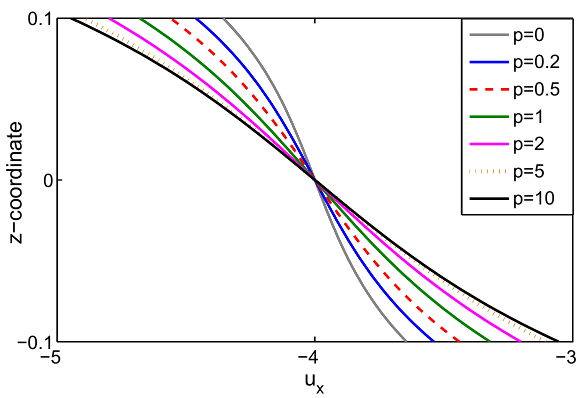

Fig. 17. In-plane displacement through the thickness of the SSSS 2-1-2 sandwich square plate with FG skins, subjected to sinusoidal load at the top, according to the hyperbolic sine ZZ theory, for various values of p.

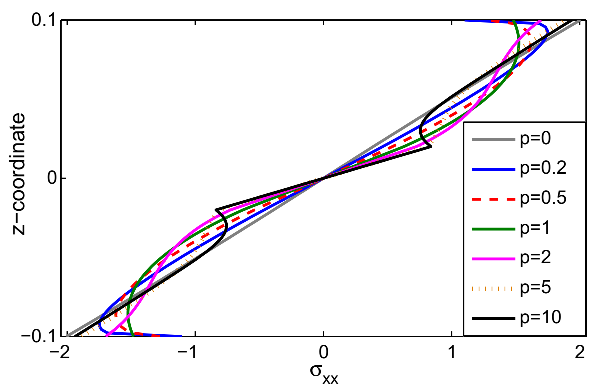

Fig. 18. $\bar{\sigma}_{xx}$ through the thickness of the SSSS 2-1-2 sandwich square plate with FG skins, subjected to sinusoidal load at the top, according to the hyperbolic sine ZZ theory, for various values of p.

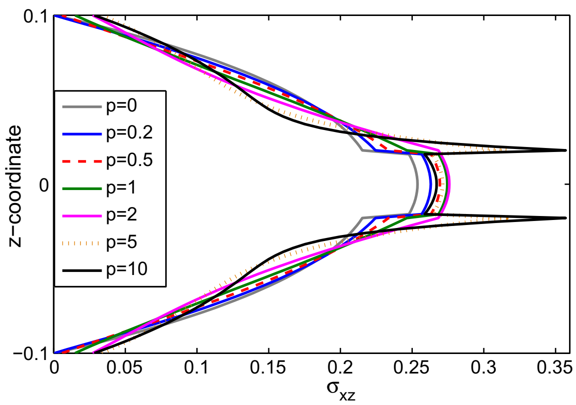

Fig. 19. $\bar{\sigma}_{xz}$ through the thickness of the SSSS 2-1-2 sandwich square plate with FG skins, subjected to sinusoidal load at the top, according to the hyperbolic sine ZZ theory, for various values of *p*.

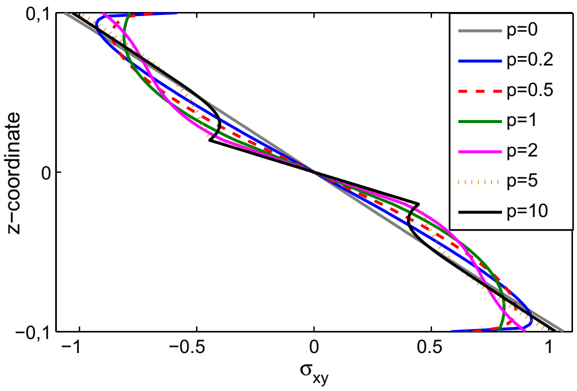

Fig. 20. $\bar{\sigma}_{xy}$ through the thickness of the SSSS 2-1-2 sandwich square plate with FG skins, subjected to sinusoidal load at the top, according to the hyperbolic sine ZZ theory, for various values of *p*.

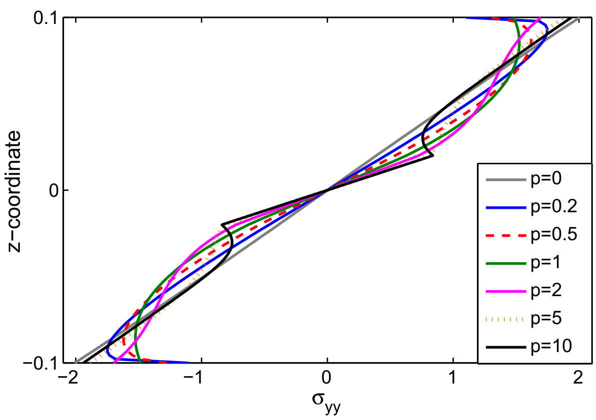

Fig. 21. $\bar{\sigma}_{yy}$ through the thickness of the SSSS 2-1-2 sandwich square plate with FG skins, subjected to sinusoidal load at the top, according to the hyperbolic sine ZZ theory, for various values of *p*.

power-law exponent p in the displacements u_x and w, respectively, can be visualized. The figures refer to the simply supported 2-1-2 sandwich square plate with FG skins, subjected to sinusoidal load at the top, and presents the displacements through the thickness, according to the hyperbolic sine ZZ theory, for various values of p.

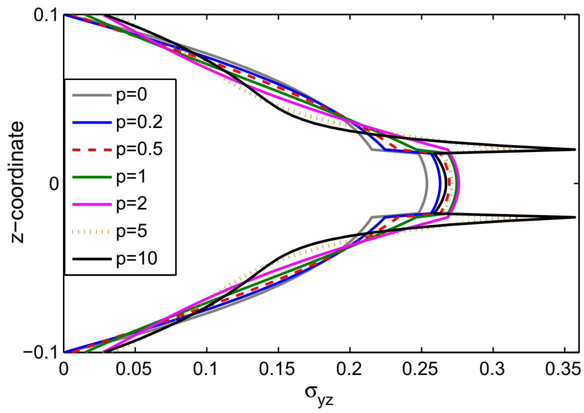

Fig. 22. $\bar{\sigma}_{yz}$ through the thickness of the SSSS 2-1-2 sandwich square plate with FG skins, subjected to sinusoidal load at the top, according to the hyperbolic sine ZZ theory, for various values of *p*.

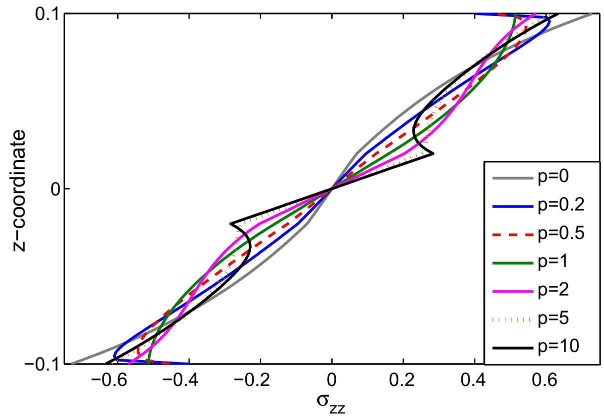

Fig. 23. $\bar{\sigma}_{zz}$ through the thickness of the SSSS 2-1-2 sandwich square plate with FG skins, subjected to sinusoidal load at the top, according to the hyperbolic sine ZZ theory, for various values of *p*.

The deflection of a simply supported sandwich plate with FG skins increases as the power-law of the material increases. This is seen in Table 11 for all studied plates and in Fig. 16 for a particular one. As the core thickness to the plate thickness ratio increases, the transverse displacement decreases. The results depend on the ϵ_{zz} approach.

Table 12 and Fig. 18 present results refering to $\bar{\sigma}_{xx}$. The values obtained with present hyperbolic sine ZZ theory and RBF collocation are tabulated in Table 12 and compared with available references, for various p and skin-core-skin thickness ratios. Fig. 18 shows the stress through the thickness for the simply supported 2-1-2 sandwich square plate with FG skins, subjected to sinusoidal load at the top, for various values of p (see Figs. 19–23).

In all tables, a good agreement between the present solution and references considered is obtained. (See Table 13).

7. Conclusions

In this paper we presented a study using the radial basis function collocation method to analyze static deformations of thin and thick functionally graded sandwich plates using a variation of Murakami's Zig-Zag function, considering a hyperbolic sine term for the in-plane displacement expansion and allowing for through-the-thickness deformations. This has not been done before and serves to fill the gap of knowledge in this area.

Table 13
$\bar{\sigma}_{xz}(0)$ of a sandwich plate with FG skins, for several exponents p and skin-core-skin ratios.

Source	2-1-2	2-1-1	1-1-1	2-2-1	1-2-1
$p = 0$					
SSDPT	0.24618		0.24618	0.24618	0.24618
TSDPT	0.23857		0.23857	0.23857	0.23857
FSDPT	0.19099		0.19099	0.19099	0.19099
Present $\epsilon_{zz} = 0$	0.2538	0.2284	0.2459	0.2407	0.2358
Present $\epsilon_{zz} \neq 0$	0.2538	0.2291	0.2461	0.2411	0.2363
$p = 0.2$					
Present $\epsilon_{zz} = 0$	0.2629	0.2388	0.2539	0.2483	0.2419
Present $\epsilon_{zz} \neq 0$	0.2630	0.2396	0.2541	0.2488	0.2424
$p = 0.5$					
Present $\epsilon_{zz} = 0$	0.2693	0.2489	0.2593	0.2537	0.2455
Present $\epsilon_{zz} \neq 0$	0.2694	0.2498	0.2595	0.2542	0.2461
$p = 1$					
SSDPT	0.27774		0.26809	0.26680	0.26004
TSDPT	0.27104		0.26117	0.25951	0.25258
FSDPT	0.24316		0.23257	0.22762	0.22057
Present $\epsilon_{zz} = 0$	0.2744	0.2630	0.2640	0.2590	0.2489
Present $\epsilon_{zz} \neq 0$	0.2745	0.2640	0.2643	0.2594	0.2496
$p = 2$					
SSDPT	0.29422		0.27807	0.27627	0.26543
TSDPT	0.28838		0.27188	0.26939	0.25834
FSDPT	0.26752		0.25077	0.24316	0.23257
Present $\epsilon_{zz} = 0$	0.2758	0.2866	0.2664	0.2632	0.2515
Present $\epsilon_{zz} \neq 0$	0.2760	0.2877	0.2668	0.2636	0.2523
$p = 5$					
SSDPT	0.31930		0.29150	0.28895	0.27153
TSDPT	0.31454		0.28643	0.28265	0.26512
FSDPT	0.29731		0.27206	0.26099	0.24596
Present $\epsilon_{zz} = 0$	0.2710	0.3367	0.2651	0.2666	0.2538
Present $\epsilon_{zz} \neq 0$	0.2712	0.3377	0.2655	0.2669	0.2546
$p = 10$					
SSDPT	0.33644		0.29529	0.29671	0.27676
TSDPT	0.33242		0.29566	0.29080	0.26895
FSDPT	0.31316		0.28299	0.26998	0.25257
Present $\epsilon_{zz} = 0$	0.2669	0.3795	0.2635	0.2690	0.2559
Present $\epsilon_{zz} \neq 0$	0.2671	0.3806	0.2639	0.2692	0.2568

Using the Unified Formulation, the plate formulation was easily discretized by radial basis functions collocation. The hardworking of deriving the equations of motion and boundary conditions is eliminated with the present approach. The combination of Carrera's Unified Formulation and collocation with RBFs proved to be a simple yet powerful alternative to other finite element or meshless methods in the static deformation of thin and thick functionally graded sandwich plates.

Numerical examples were performed on simply supported sandwich plates, made of functionally graded materials in the core or in the skins, for various material power-law exponents and side-to-thickness and skin-core-skin thickness ratios. Obtained results were presented in figures and tables and compared with references and these demonstrate the accuracy of present approach.

Allow or not extensibility in the thickness direction has influence on the obtained results, more significatively in thicker plates. The σ_{zz} should be considered in the formulation, even for thinner functionally graded samdwich plates.

Acknowledgements

The first author is grateful for the grant SFRH/BD/45554/2008 assured by FCT. The authors thank the financial support of FCT, through POCTI and POCI (2010)/FEDER. In particular the support to LAETA via project Composites in Mechanical Design and the support to PTDC/EME-PME/120830/2012 is gratefully acknowledged.

References

[1] Kirchhoff G. Uber das gleichgewicht und die bewegung einer elastischen scheibe. J Angew Math 1850;40:51–88.
[2] Reissner E. The effect of transverse shear deformations on the bending of elastic plates. J Appl Mech 1945;12:A69–77.
[3] Mindlin RD. Influence of rotary inertia and shear in flexural motions of isotropic elastic plates. J Appl Mech 1951;18:31–8.
[4] Zenkert D. An introduction to sandwich structures. Oxford: Chamelon Press; 1995.
[5] Vinson JR. The behavior of sandwich structures of isotropic and composite materials. Technomic Publishing Co.; 1999.
[6] Burton S, Noor AK. Assessment of computational model for sandwich panels and shells. Comput Methods Appl Mech Eng 1995;124:125–51.
[7] Noor AK, Burton S, Bert CW. Computational model for sandwich panels and shells. Appl Mech Rev 1996;49:155–99.
[8] Altenbach H. Theories for laminated and sandwich plates. Mech Compos Mater 1998;34:243–52. http://dx.doi.org/10.1007/BF02256043.
[9] Librescu Liviu, Hause Terry. Recent developments in the modeling and behavior of advanced sandwich constructions: a survey. Compos Struct 2000;48(1–3):1–17.
[10] Vinson Jack R. Sandwich structures. Appl Mech Rev 2001;54(3):201–14.
[11] Demasi L. 2D, quasi 3d and 3d exact solutions for bending of thick and thin sandwich plates. J Sandwich Struct Mater 2008;10:271–310.
[12] Carrera E. Historical review of zig-zag theories for multilayered plates and shells. Appl Mech Rev 2003;56:287–308.
[13] Murakami H. Laminated composite plate theory with improved in-plane responses. J Appl Mech 1986;53:661–6.
[14] Carrera E. Developments, ideas, and evaluations based upon reissner's mixed variational theorem in the modelling of multilayered plates and shells. Appl Mech Rev 2001;54:301–29.
[15] Carrera E. The use of murakami's zig-zag function in the modeling of layered plates and shells. Compos Struct 2004;82:541–54.
[16] Demasi L. ∞^3 hierarchy plate theories for thick and thin composite plates: the generalized unified formulation. Compos Struct 2008;84:256–70.
[17] Brischetto S, Carrera E, Demasi L. Improved bending analysis of sandwich plate by using zig-zag function. Compos Struct 2009;89:408–15.
[18] Hon YC, Lu MW, Xue WM, Zhu YM. Multiquadric method for the numerical solution of byphasic mixture model. Appl Math Comput 1997;88:153–75.
[19] Hon YC, Cheung KF, Mao XZ, Kansa EJ. A multiquadric solution for the shallow water equation. ASCE J Hydraul Eng 1999;125(5):524–33.
[20] Wang JG, Liu GR, Lin P. Numerical analysis of biot's consolidation process by radial point interpolation method. Int J Solids Struct 2002;39(6):1557–73.
[21] Liu GR, Gu YT. A local radial point interpolation method (lrpim) for free vibration analyses of 2-d solids. J Sound Vib 2001;246(1):29–46.
[22] Liu GR, Wang JG. A point interpolation meshless method based on radial basis functions. Int J Numer Methods Eng 2002;54:1623–48.
[23] Wang JG, Liu GR. On the optimal shape parameters of radial basis functions used for 2-d meshless methods. Comput Methods Appl Mech Eng 2002;191:2611–30.
[24] Chen XL, Liu GR, Lim SP. An element free galerkin method for the free vibration analysis of composite laminates of complicated shape. Compos Struct 2003;59:279–89.
[25] Dai KY, Liu GR, Lim SP, Chen XL. An element free galerkin method for static and free vibration analysis of shear-deformable laminated composite plates. J Sound Vib 2004;269:633–52.
[26] Liu GR, Chen XL. Buckling of symmetrically laminated composite plates using the element-free galerkin method. Int J Struct Stability Dynam 2002;2:281–94.
[27] Liew KM, Chen XL, Reddy JN. Mesh-free radial basis function method for buckling analysis of non-uniformity loaded arbitrarily shaped shear deformable plates. Comput Methods Appl Mech Eng 2004;193:205–25.
[28] Q Huang Y, Li QS. Bending and buckling analysis of antisymmetric laminates using the moving least square differential quadrature method. Comput Methods Appl Mech Eng 2004;193:3471–92.
[29] Liu L, Liu GR, Tan VCB. Element free method for static and free vibration analysis of spatial thin shell structures. Comput Methods Appl Mech Eng 2002;191:5923–42.
[30] Xiang S, Wang KM, Ai YT, Sha YD, Shi H. Analysis of isotropic, sandwich and laminated plates by a meshless method and various shear deformation theories. Compos Struct 2009;91(1):31–7.
[31] Xiang S, Shi H, Wang KM, Ai YT, Sha YD. Thin plate spline radial basis functions for vibration analysis of clamped laminated composite plates. Eur J Mech A/ Solids 2010;29:844–50.
[32] Ferreira AJM. A formulation of the multiquadric radial basis function method for the analysis of laminated composite plates. Compos Struct 2003;59:385–92.
[33] Ferreira AJM. Thick composite beam analysis using a global meshless approximation based on radial basis functions. Mech Adv Mater Struct 2003;10:271–84.
[34] Ferreira AJM, Roque CMC, Martins PALS. Analysis of composite plates using higher-order shear deformation theory and a finite point formulation based on the multiquadric radial basis function method. Composites: Part B 2003;34:627–36.
[35] Carrera E. Evaluation of layer-wise mixed theories for laminated plate analysis. AIAA J 1998(36):830–9.

[36] Carrera Erasmo. Theories and finite elements for multilayered plates and shells: a unified compact formulation with numerical assessment and benchmarking. Arch Comput Methods Eng 2003;10:215–96.
[37] Brischetto S, Carrera E. Advanced mixed theories for bending analysis of functionally graded plates. Comput Struct 2010;88(23–24):1474–83.
[38] Brischetto S. Classical and mixed advanced models for sandwich plates embedding functionally graded cores. J Mech Mater Struct 2009;4:13–33.
[39] Carrera E, Brischetto S, Robaldo A. Variable kinematic model for the analysis of functionally graded material plates. AIAA J 2008;46:194–203.
[40] Ferreira AJM, Roque CMC, Carrera E, Cinefra M, Polit O. Radial basis functions collocation and a unified formulation for bending, vibration and buckling analysis of laminated plates, according to a variation of murakami's zig-zag theory. Eur J Mech – A/Solids 2011;30(4):559–70.
[41] Rodrigues JD, Roque CMC, Ferreira AJM, Carrera E, Cinefra M. Radial basis functions-finite differences collocation and a unified formulation for bending, vibration and buckling analysis of laminated plates, according to murakami's zig-zag theory. Compos Struct 2011;93(7):1613–20.
[42] Ferreira AJM, Roque CMC, Carrera E, Cinefra M, Polit O. Two higher order zig-zag theories for the accurate analysis of bending, vibration and buckling response of laminated plates by radial basis functions collocation and a unified formulation. J Compos Mater 2011;45(24):2523–36.
[43] Neves AMA, Ferreira AJM, Carrera E, Cinefra M, Roque CMC, Jorge RMN, et al. A quasi-3D hyperbolic shear deformation theory for the static and free vibration analysis of functionally graded plates. Compos Struct 2012;94(5):1814–25.
[44] Miyamoto Y, Kaysser WA, Rabin BH, Kawasaki A, Ford RG. Functionally graded materials: design, processing and applications. Kluwer Academic Publishers; 1999.
[45] Jin ZH, Batra RC. Stress intensity relaxation at the tip of an edge crack in a functionally graded material subjected to a thermal shock. J Therm Stress 1996;19:317–39.
[46] Chung YL, Chi SH. The residual stress of functionally graded materials. J Chinese Inst Civil Hydraul Eng 2001;13:1–9.
[47] Praveen GN, Reddy JN. Nonlinear transient thermoelastic analysis of functionally graded ceramic-metal plates. Int J Solids Struct 1998;35(33):4457–76.
[48] Najafizadeh MM, Eslami MR. Buckling analysis of circular plates of functionally graded materials under uniform radial compression. Int J Mech Sci 2002;44(12):2479–93.
[49] Zenkour AM. A comprehensive analysis of functionally graded sandwich plates: part 1 – deflection and stresses. Int J Solids Struct 2005;42(18–19):5224–42.
[50] Zenkour AM. Generalized shear deformation theory for bending analysis of functionally graded plates. Appl Math Modell 2006;30:67–84.
[51] Mori T, Tanaka K. Average stress in matrix and average elastic energy of materials with misfitting inclusions. Acta Metall 1973;21(5):571–4.
[52] Benveniste Y. A new approach to the application of mori-tanaka's theory in composite materials. Mech Mater 1987;6(2):147–57.
[53] Kansa EJ. Multiquadrics – a scattered data approximation scheme with applications to computational fluid dynamics. I: surface approximations and partial derivative estimates. Comput Math Appl 1990;19(8/9):127–45.
[54] Ferreira AJM, Fasshauer GE. Computation of natural frequencies of shear deformable beams and plates by a rbf-pseudospectral method. Comput Methods Appl Mech Eng 2006;196:134–46.
[55] Carrera E, Brischetto S, Cinefra M, Soave M. Effects of thickness stretching in functionally graded plates and shells. Compos Part B: Eng 2011;42:23–133.

2.7 Influence of Zig-Zag and warping effects on buckling of functionally graded sandwich plates according to sinusoidal shear deformation theories

A. M. A. Neves, A. J. M. Ferreira, E. Carrera, M. Cinefra, R. M. N. Jorge, C. M. M. Soares, Influence of Zig-Zag and warping effects on buckling of functionally graded sandwich plates according to sinusoidal shear deformation theories, submetido para publicação em International Journal of Solids and Structures, 2012.

Influence of Zig-Zag and warping effects on buckling of functionally graded sandwich plates according to sinusoidal shear deformation theories

A. M. A. Neves [a], A. J. M. Ferreira [b], E. Carrera [c], M. Cinefra [c], R. M. N. Jorge [a], C. M. M. Soares [d]

[a] *Departamento de Engenharia Mecânica, Faculdade de Engenharia, Universidade do Porto, Rua Dr. Roberto Frias, 4200-465 Porto, Portugal*

[b] *(Corresponding author: ferreira@fe.up.pt)*
Departamento de Engenharia Mecânica, Faculdade de Engenharia, Universidade do Porto, Rua Dr. Roberto Frias, 4200-465 Porto, Portugal

[c] *Departament of Aeronautics and Aerospace Engineering, Politecnico di Torino, Corso Duca degli Abruzzi, 24, 10129 Torino, Italy*

[d] *Instituto Superior Técnico, Av. Rovisco Pais, Lisboa, Portugal*

Abstract

In this paper various sinusoidal shear deformation theories are used for the buckling analysis of functionally graded sandwich plates. The theories may account for through-the-thickness deformations and the Zig-Zag effect.

The governing equations and boundary conditions are derived using the Principle of Virtual Work under a generalization of Carrera's Unified Formulation and further interpolated by collocation with radial basis functions.

A numerical investigation has been conducted on the buckling analysis of sandwich plates with functionally graded skins. The influence of the thickness stretching and the Zig-Zag effects on these problems is investigated. Numerical results demonstrate the accuracy of the present approach.

Keywords: Buckling; plates; Functionally graded materials; meshless methods

1 Introduction

The buckling phenomenon consists of a sudden change of equilibrium geometry at a certain critical load. It is one of the characteristic failure modes of slender structures such as laminated composite plates.

Functionally graded (FG) materials were first proposed by Bever and Duwez [Bever and Duwez, 1972] in 1972. The modelling of FG materials is important to understand the behavior of FG structures.

When compared to isotropic and laminated plates, the literature on FG plates is relatively scarce [Miyamoto et al., 1999,Ferrante and Graham-Brady, 2005] [Yin et al., 2004,Zhong and Shang, 2008,Nguyen et al., 2007,Birman and Byrd, 2007] [Koizumi, 1997]. The thermo-mechanical response of FG plates was considered by Reddy and Chin [Reddy and Chin, 1998], Reddy [Reddy, 2000], Vel and Batra [Vel and Batra, 2003,Vel and Batra, 2002], Cheng and Batra [Cheng and Batra, 2000c], Javaheri and Eslami [R. and R., 2002]. Studies on the mechanical behaviour of FG plates include the static analysis of FG plates performed by Kashtalyan [Kashtalyan, 2004], Kashtalyan and Menshykova [Kashtalyan and Menshykova, 2009], Qian et al. [Qian et al., 2004], Zenkour [Zenkour, 2005a,Zenkour, 2006], Ramirez et al. [Ramirez et al., 2006], Ferreira et al. [Ferreira et al., 2005d,Ferreira et al., 2007], Chi and Chung [Chi and Chung, 2006a,Chi and Chung, 2006b], and Cheng and Batra [Cheng and Batra, 2000a]. Vibrations problems of FG plates can be found in Batra and Jin [Batra and Jin, 2005], Ferreira et al. [Ferreira et al., 2006b], Vel and Batra [Vel and Batra, 2004], Zenkour [Zenkour, 2005b], Roque et al. [Roque et al., 2007], and Cheng and Batra [Cheng and Batra, 2000b]. Mechanical buckling of FG plates can be found in Najafizadeh and Eslami [Najafizadeh and Eslami, 200 Zenkour [Zenkour, 2005b], Cheng and Batra [Cheng and Batra, 2000b], Birman [Birman, 1995], Javaheri and Eslami [Javaheri and Eslami, 2002].

Most of the shear deformation theories neglect the thickness stretching ϵ_{zz}, being the transverse displacement considered to be independent of thickness coordinates. The effect of thickness stretching in FG plates has been recently investigated by Carrera et al. [Carrera et al., 2011]. The zig-zag effect is produced by the large difference of mechanical properties of sandwich skins and core. For sandwich plates, the classical plate theories of Kirchhoff [Kirchhoff, 1850] or Reissner-Mindlin [Reissner, 1945,Mindlin, 1951] present some difficulties. Two possibilities can be used to capture the ZZ effect (see the overviews by Burton and Noor [Burton and Noor, 1995], Noor et al. [Noor et al., 1996], Altenbach [Altenbach, 1998], Librescu and Hause [Librescu and Hause, 2000], Vinson [Vinson, 2001], and Demasi [Demasi, 2008a]): the so-called layer-wise models, and a zig-zag function (ZZF) in the framework of mixed multilayered plate theories. An historical review on ZZ theories has been provided by Carrera [Carrera, 2003].

In order to avoid the computationally expensive layerwise theories, Murakami [Murakami, 1986] proposed a ZZF that is able to reproduce the slope discontinuity. A review of early developments on the application of ZZF has been provided in the review article by Carrera [Carrera, 2001]. The advantages of analysing multilayered anisotropic plate and shells using the ZZF as well as the Finite Element implementation have been discussed by Carrera [Carrera, 2004], and by others [Carrera, 2004,Demasi, 2008b,Brischetto et al., 2009].

This paper focus on the buckling analysis of functionally graded sandwich plates. It adresses the influence of the warping effects in the thickness direction as well as the Zig-Zag (ZZ) effects on these problems. Four sinusoidal theories are used. The governing equations and boundary conditions are derived under a generalized version of Carrera's Unified Formulation (CUF) [Carrera, 1996,Carrera, 2001] based on the principle of virtual displacements and further interpolated by collocation with radial basis functions (RBF). This meshless technique can be seen as an efficient alternative to the finite elements method [Ferreira, 2003a,Ferreira, 2003b,Ferreira et al., 2003,Ferreira et al., 2005c] [Ferreira et al., 2005a,Ferreira et al., 2006a,Ferreira et al., 2005b,Ferreira et al., 2004] [Neves et al., 2011a,Neves et al., 2011b].

2 Problem formulation

A rectangular sandwich plate of plan-form dimensions a and b and uniform thickness h is considered. The co-ordinate system is taken such that the x-y plane ($z = 0$) coincides with the midplane of the plate.

The sandwich core is fully ceramic (isotropic) and skins are composed of a functionally graded material across the thickness direction. The bottom skin varies from a metal-rich surface ($z = -h/2$) to a ceramic-rich surface while the top skin face varies from a ceramic-rich surface to a metal-rich surface

($z = h/2$) as illustrated in figure 1. There are no interfaces between core and skins. The volume fraction of the ceramic phase is obtained from a simple rule of mixtures as:

$$\begin{cases} V_c = \left(\frac{z-h_0}{h_1-h_0}\right)^p & \text{in the bottom skin} \\ V_c = 1 \quad \text{in the core} \\ V_c = \left(\frac{z-h_3}{h_2-h_3}\right)^p & \text{in the top skin} \end{cases} \tag{1}$$

where $z \in [-h/2, h/2]$, h_0, h_1, h_2, and h_3 are the z-coordinates of the interfaces of the layers as visualized in figure 1, and $p \geq 0$ is a scalar parameter that allows the user to define gradation of material properties across the thickness direction of the skins. The $p = 0$ case corresponds to the (isotropic) fully ceramic plate. The volume fraction for the metal phase is given as $V_m = 1 - V_c$.

The sandwiches may be symmetric or non-symmetric about the mid-plane as we may vary the thickness of each face. Figure 2 shows a non-symmetric sandwich with volume fraction defined by the power-law (1) for various exponents p, in which top skin thickness is the same as the core thickness and the bottom skin thickness is twice the core thickness. Such thickness relation is denoted as 2-1-1. A bottom-core-top notation is being used. 1-1-1 means that skins and core have the same thickness.

The sandwich plate is subjected to compressive in-plane forces acting on the mid-plane of the plate. $\bar{N}_{xx}$ and $\bar{N}_{yy}$ denote the in-plane loads perpendicular to the edges $x = 0$ and $y = 0$ respectively, and $\bar{N}_{xy}$ denote the distributed shear force parallel to the edges $x = 0$ and $y = 0$ respectively (see fig. 3).

3 Overview of existing zig-zag theories

The Murakami's zig-zag function $Z(z)$ dependes on the adimensioned layer coordinate, ζ_k, according to the following formula:

$$Z(z) = (-1)^k \zeta_z \tag{2}$$

ζ_k is defined as $\zeta_k = \frac{2z_k}{h_k}$ where z_k is the layer coordinate in the thickness direction and h_k is the thickness of the kth layer.

$Z(z)$ has the following properties:

(1) It is a piece-wise linear function of layer coordinates z_k,
(2) $Z(z)$ has unit amplitude for the whole layers,
(3) the slope $Z'(z) = \frac{dZ}{dz}$ assumes opposite sign between two-adjacent layers. Its amplitude is layer thickness independent.

In 1986, a refinement of FSDT by inclusion of ZZ effects and transverse normal strains was introduced in Murakami's original ZZF [Murakami, 1986], defined by the following displacement field:

$$\begin{cases} u = u_0 + zu_1 + (-1)^k \frac{2}{h_k} \left(z - \frac{1}{2} \left(z_k + z_{k+1} \right) \right) u_Z \\ v = v_0 + zv_1 + (-1)^k \frac{2}{h_k} \left(z - \frac{1}{2} \left(z_k + z_{k+1} \right) \right) v_Z \\ w = w_0 + zw_1 + (-1)^k \frac{2}{h_k} \left(z - \frac{1}{2} \left(z_k + z_{k+1} \right) \right) w_Z \end{cases} \tag{3}$$

where u and v are the in-plane displacements and w is the transverse displacement. The involved unknows are u_0, u_1, u_Z, v_0, v_1, v_Z, w_0, w_1, and w_Z: u_0, v_0 and w_0 are translations of a point at the midplane; u_1, v_1 and w_1 are rotations as in the typical FSDT; and the additional degrees of freedom u_Z, v_Z and w_Z have a meaning of displacement. z_k, z_{k+1} are the bottom and top z-coordinates at each layer.

More recently, another possible FSDT theory has been investigated by Carrera [Carrera, 2004] and Demasi [Demasi, 2008b], ignoring the through-the-thickness deformations:

$$\begin{cases} u = u_0 + zu_1 + (-1)^k \frac{2}{h_k} \left(z - \frac{1}{2} \left(z_k + z_{k+1} \right) \right) u_Z \\ v = v_0 + zv_1 + (-1)^k \frac{2}{h_k} \left(z - \frac{1}{2} \left(z_k + z_{k+1} \right) \right) v_Z \\ w = w_0 \end{cases} \tag{4}$$

with u_0, u_1, u_Z, v_0, v_1, v_Z, w_0, z_k, and z_{k+1} as before.

Ferreira et al. [Ferreira et al., 2011a] and Rodrigues et al. [Rodrigues et al., 2011] used a ZZF theory involving the following expansion of displacements

$$\begin{cases} u = u_0 + zu_1 + (-1)^k \frac{2}{h_k} \left(z - \frac{1}{2} \left(z_k + z_{k+1} \right) \right) u_Z \\ v = v_0 + zv_1 + (-1)^k \frac{2}{h_k} \left(z - \frac{1}{2} \left(z_k + z_{k+1} \right) \right) v_Z \\ w = w_0 + zw_1 + z^2 w_2 \end{cases} \tag{5}$$

This represents a variation of the Murakami's original theory, allowing for a quadratic evolution of the transverse displacement across the thickness direction. Furthermore, Ferreira et al. [Ferreira et al., 2011b] used two higher order ZZF theories allowing for a quadratic evolution of the transverse displacement across the thickness direction as well and involving the following displacement fields:

$$\begin{cases} u = u_0 + zu_1 + z^3 u_3 + (-1)^k \frac{2}{h_k} \left(z - \frac{1}{2}\left(z_k + z_{k+1}\right)\right) u_Z \\ v = v_0 + zv_1 + z^3 v_3 + (-1)^k \frac{2}{h_k} \left(z - \frac{1}{2}\left(z_k + z_{k+1}\right)\right) v_Z \\ w = w_0 + zw_1 + z^2 w_2 \end{cases} \tag{6}$$

The use of a sinusoidal shear deformation theory for composite laminated plates and shells was first presented by Touratier [Touratier, 1992a,Touratier, 1991] [Touratier, 1992b] in the early 1990's. Later Vidal and Polit [Vidal and Polit, 2008] used a sinusoidal shear deformation theory for composite laminated beams. The use of sinusoidal plate theories for functionally graded plates was first presented by Zenkour [Zenkour, 2006], where a $\epsilon_{zz} = 0$ approach was used. Recently Neves et al. [Neves et al., 2011a,Neves et al., 2011b] successfully used a sinusoidal plate theory for the bending and stress analysis of functionally graded plates.

$$\begin{cases} u = u_0 + zu_1 + sin\left(\frac{\pi z}{h}\right) u_3 + (-1)^k \frac{2}{h_k} \left(z - \frac{1}{2}\left(z_k + z_{k+1}\right)\right) u_Z \\ v = v_0 + zv_1 + sin\left(\frac{\pi z}{h}\right) v_3 + (-1)^k \frac{2}{h_k} \left(z - \frac{1}{2}\left(z_k + z_{k+1}\right)\right) v_Z \\ w = w_0 + zw_1 + z^2 w_2 \end{cases} \tag{7}$$

All previous cited work using ZZ functions deals with laminated plates or shells. Refering to functionally graded sandwiches, the authors have sucessfuly used two hyperbolic-sine shear deformation theories for the static study of functionally graded sandwich plates [Neves et al., 2012]. They both account for the Zig-Zag effect, but only one allows for warping in the thickness direction:

$$\begin{cases} u = u_0 + zu_1 + sinh\left(\frac{\pi z}{h}\right) u_3 + (-1)^k \frac{2}{h_k} \left(z - \frac{1}{2}\left(z_k + z_{k+1}\right)\right) u_Z \\ v = v_0 + zv_1 + sinh\left(\frac{\pi z}{h}\right) v_3 + (-1)^k \frac{2}{h_k} \left(z - \frac{1}{2}\left(z_k + z_{k+1}\right)\right) v_Z \\ w = w_0 \end{cases} \tag{8}$$

$$
\begin{cases}
u = u_0 + zu_1 + sinh\left(\frac{\pi z}{h}\right) u_3 + (-1)^k \frac{2}{h_k}\left(z - \frac{1}{2}\left(z_k + z_{k+1}\right)\right) u_Z \\
v = v_0 + zv_1 + sinh\left(\frac{\pi z}{h}\right) v_3 + (-1)^k \frac{2}{h_k}\left(z - \frac{1}{2}\left(z_k + z_{k+1}\right)\right) v_Z \\
w = w_0 + zw_1 + z^2 w_2
\end{cases}
\tag{9}
$$

4 The present sinus shear deformation theories

In this paper we compare four sinusoidal shear deformation theories. In-plane displacements (u, v) are considered to be of sinusoidal type across the thickness coordinate and may include or not the terms to account for the zig-zag effect. The transverse displacement (w) may be defined as constant if warping is not allowed, or as parabolic in the thickness direction if warping is allowed.

For the easy reading of the paper, nomenclature is now introduced. All theories are named *sinus*, as they all consider a sinusoidal expansion across the thickness coordinate for the in-plane displacements. In addition the name will include the ZZ letters if the zig-zag effect is considered, and will include the 0 number if $\epsilon_{zz} = 0$, i. e., thickness-stretching is not allowed (see table 1).

The displacement fields of each theory are as follows:

Displacement field of sinus theory:

$$
\begin{cases}
u = u_0 + zu_1 + \sin\left(\frac{\pi z}{h}\right) u_s \\
v = v_0 + zv_1 + \sin\left(\frac{\pi z}{h}\right) v_s \\
w = w_0 + zw_1 + z^2 w_2
\end{cases}
\tag{10}
$$

Displacement field of sinus0 theory:

$$
\begin{cases}
u = u_0 + zu_1 + \sin\left(\frac{\pi z}{h}\right) u_s \\
v = v_0 + zv_1 + \sin\left(\frac{\pi z}{h}\right) v_s \\
w = w_0
\end{cases}
\tag{11}
$$

Displacement field of sinusZZ theory:

$$\begin{cases} u = u_0 + zu_1 + \sin\left(\frac{\pi z}{h}\right) u_s + (-1)^k \frac{2}{h_k}\left(z - \frac{1}{2}\left(z_k + z_{k+1}\right)\right) u_Z \\ v = v_0 + zv_1 + \sin\left(\frac{\pi z}{h}\right) v_s + (-1)^k \frac{2}{h_k}\left(z - \frac{1}{2}\left(z_k + z_{k+1}\right)\right) v_Z \\ w = w_0 + zw_1 + z^2 w_2 \end{cases} \tag{12}$$

Displacement field of sinusZZ0 theory:

$$\begin{cases} u = u_0 + zu_1 + \sin\left(\frac{\pi z}{h}\right) u_s + (-1)^k \frac{2}{h_k}\left(z - \frac{1}{2}\left(z_k + z_{k+1}\right)\right) u_Z \\ v = v_0 + zv_1 + \sin\left(\frac{\pi z}{h}\right) v_s + (-1)^k \frac{2}{h_k}\left(z - \frac{1}{2}\left(z_k + z_{k+1}\right)\right) v_Z \\ w = w_0 \end{cases} \tag{13}$$

The expansion of the degrees of freedom u_0, u_1, u_s, v_0, v_1, v_s, w_0, w_1, and w_2 are functions of the thickness coordinate only. These are layer-independent, unlike those of u_Z and v_Z, as illustrated in figures 4 and 5.

5 The Unified Formulation for the buckling analysis of FG sandwich plates

In this section it is shown how to obtain the fundamental nuclei under CUF, which allows the derivation of the governing equations and boundary conditions for FG plates.

5.1 Functionally graded materials

A conventional FG plate considers a continuous variation of material properties over the thickness direction by mixing two different materials [Miyamoto et al., 1999]. The material properties of the FG plate are assumed to change continuously throughout the thickness of the plate, according to the volume fraction of the constituent materials. Although one can use CUF for one-layer, isotropic plate, we consider a multi-layered plate. In fact, the sandwiches in study present 3 physical layers, $kp = 1, 2, 3$, and depending on the considered theory may have different displacement fields. Nevertheless, we are dealing with functionally graded materials and becomes mandatory to model the continuos variation of properties across the thickness direction. A considerable number of layers is needed to ensure correct computation of material properties at each thickness position, and for that reason we consider $N_l = 91$ virtual (mathematical) layers of constant thickness. In the following, kp refers to physical layers and $k = 1, ..., 91$ refers to virtual layers.

The CUF procedure applied to FG materials starts by evaluating the volume fraction of the two constituents for each layer. To describe the volume fractions an exponential function can be used as in [Jin and Batra, 1996], or the sigmoid function as proposed in [Chung and Chi, 2001]. In the present work a power-law function is used as most researchers do [Praveen and Reddy, 1998] [Najafizadeh and Eslami, 2002,Zenkour, 2005a,Zenkour, 2006]. In the typical FG plate the power-law function defines the volume fraction of the ceramic phase as:

$$V_c = \left(0.5 + \frac{z}{h}\right)^p \tag{14}$$

where $z \in [-h/2, h/2]$, h is the thickness of the plate, and p is a scalar parameter that allows the user to define gradation of material properties across the thickness direction. In the present sandwich plate, the volume fraction of the ceramic phase of the FG skins are obtained by adapting the typical power-law. Furthermore, we need to compute the volume fraction for each layer. Considering (1), one has:

$$\begin{cases} V_c^k = \left(\frac{\tilde{z}-h_0}{h_1-h_0}\right)^p, \quad z \in [h_0, h_1] \\ V_c^k = 1, \quad z \in [h_1, h_2] \\ V_c^k = \left(\frac{\tilde{z}-h_3}{h_2-h_3}\right)^p, \quad z \in [h_2, h_3] \end{cases} \tag{15}$$

where $\tilde{z}$ is the thickness coordinate of a point of each (virtual) skin layer, and h_0, h_1, h_2, h_3, and $p \geq 0$ are as in (1).

Having the volume fraction of each constituent, a homogenization procedure is employed to find the values of the modulus of elasticity, E^k, and Poisson's ratio, ν^k, of each layer. A possible homogenization technique is the Mori-Tanaka one [Mori and Tanaka, 1973,Y. and Benveniste, 1987], and other possibility is the law-of-mixtures. In the present work we use the last one so that we can compare our results with referenced authors. The law-of-mixtures states that:

$$E^k(z) = E_m V_m + E_c V_c; \qquad \nu^k(z) = \nu_m V_m + \nu_c V_c \tag{16}$$

According to the Unified Formulation by Carrera, the three displacement components u_x, $u_y(=v)$ and $u_z(=w)$ and their relative variations are modeled as:

$$(u_x, u_y, u_z) = F_\tau \,(u_{x\tau}, u_{y\tau}, u_{z\tau}) \qquad (\delta u_x, \delta u_y, \delta u_z) = F_s \,(\delta u_{xs}, \delta u_{ys}, \delta u_{zs}) \tag{17}$$

The vectors are chosen by resorting to the displacement field. In the present formulation the thickness functions of each theory are as follows

sinus theory:

$$\begin{cases} F_{sux} = F_{suy} = F_{\tau ux} = F_{\tau uy} = \left[1 \quad z \quad \sin\left(\frac{\pi z}{h}\right)\right] \\ F_{suz} = F_{\tau uz} = [1 \quad z \quad z^2] \end{cases} \tag{18}$$

sinus0 theory:

$$\begin{cases} F_{sux} = F_{suy} = F_{\tau ux} = F_{\tau uy} = \left[1 \quad z \quad \sin\left(\frac{\pi z}{h}\right)\right] \\ F_{suz} = F_{\tau uz} = [1] \end{cases} \tag{19}$$

sinusZZ theory:

$$\begin{cases} F_{sux} = F_{suy} = F_{\tau ux} = F_{\tau uy} = \left[1 \quad z \quad \sin\left(\frac{\pi z}{h}\right) \quad (-1)^{kp}\frac{2}{h_{kp}}\left(z - \frac{1}{2}\left(z_{kp} + z_{kp+1}\right)\right)\right] \\ F_{suz} = F_{\tau uz} = [1 \quad z \quad z^2] \end{cases} \tag{20}$$

sinusZZ0 theory:

$$\begin{cases} F_{sux} = F_{suy} = F_{\tau ux} = F_{\tau uy} = \left[1 \quad z \quad \sin\left(\frac{\pi z}{h}\right) \quad (-1)^{kp}\frac{2}{h_{kp}}\left(z - \frac{1}{2}\left(z_{kp} + z_{kp+1}\right)\right)\right] \\ F_{suz} = F_{\tau uz} = [1] \end{cases} \tag{21}$$

The present formulation can be seen as a generalization of the original Carrera's Unified Formulation in the sense that different expansions for the in-plane and the out-of-plane displacement are considered.

Stresses and strains are separated into in-plane and normal components, denoted respectively by the subscripts p and n.

The geometrical relations (G) between the mechanical strains in the kth layer and the displacement field $\mathbf{u}^k = \{u_x^k, u_y^k, u_z^k\}$ depend on the option of considering or not the warping in thickness direction.

For the *sinus* and *sinusZZ* theories, G can be stated as follows:

$$\begin{aligned}\epsilon_{pG}^k &= [\epsilon_{xx}, \epsilon_{yy}, \gamma_{xy}]^{kT} = \mathbf{D}_p^{k(nl)}\mathbf{u}^k\ ,\\ \epsilon_{nG}^k &= [\gamma_{xz}, \gamma_{yz}, \epsilon_{zz}]^{kT} = (\mathbf{D}_{np}^k + \mathbf{D}_{nz}^k)\ \mathbf{u}^k\ ,\end{aligned} \tag{22}$$

wherein the differential operator arrays are defined as follows:

$$\mathbf{D}_p^{k(nl)} = \begin{bmatrix} \partial_x & 0 & \partial_x^2/2 \\ 0 & \partial_y & \partial_y^2/2 \\ \partial_y & \partial_x & \partial_x\partial_y \end{bmatrix}\ ,\quad \mathbf{D}_{np}^k = \begin{bmatrix} 0 & 0 & \partial_x \\ 0 & 0 & \partial_y \\ 0 & 0 & 0 \end{bmatrix}\ ,\quad \mathbf{D}_{nz}^k = \begin{bmatrix} \partial_z & 0 & 0 \\ 0 & \partial_z & 0 \\ 0 & 0 & \partial_z \end{bmatrix}\ , \tag{23}$$

Although one needs to account for the nonliner contributions for the buckling analysis, we can use the linear version of CUF as the non-linear terms will only influence the equation refering to δw_0. In fact, the compressive in-plane forces and distributed shear forces only actuate on the mid-plane ($z = 0$) and the nonlinear terms are reduced to $\frac{1}{2}\left(\frac{\partial w_0}{\partial x}\right)^2$, $\frac{1}{2}\left(\frac{\partial w_0}{\partial y}\right)^2$, and $\frac{\partial w_0}{\partial x}\frac{\partial w_0}{\partial y}$.

For the *sinus* and *sinusZZ* theories ($\epsilon_{zz} \neq 0$, i.e., warping is allowed), we use

$$\mathbf{D}_p^k = \begin{bmatrix} \partial_x & 0 & 0 \\ 0 & \partial_y & 0 \\ \partial_y & \partial_x & 0 \end{bmatrix} \tag{24}$$

instead of $\mathbf{D}_p^{k(nl)}$ and just add the terms in referred equation.

For the *sinus0* and *sinusZZ0* theories ($\epsilon_{zz} = 0$, i.e., warping is not allowed), ϵ_{pG}^k and the differential operator array $\mathbf{D}_p^k$ remain as before, but the other strains are reduced to

$$\epsilon_{nG}^k = [\gamma_{xz}, \gamma_{yz}]^{kT} = (\mathbf{D}_{np}^k + \mathbf{D}_{nz}^k)\ \mathbf{u}^k\ , \tag{25}$$

wherein the differential operator arrays are defined as:

$$\mathbf{D}_{np}^k = \begin{bmatrix} 0 & 0 & \partial_x \\ 0 & 0 & \partial_y \end{bmatrix}\ , \quad \mathbf{D}_{nz}^k = \begin{bmatrix} \partial_z & 0 & 0 \\ 0 & \partial_z & 0 \end{bmatrix}\ , \tag{26}$$

5.4 Elastic stress-strain relations

To define the constitutive equations (C), stresses are separated into in-plane and normal components as well. The elastic stress-strain relations depend on which assumption of ϵ_{zz} we consider.

For the *sinus* and *sinusZZ* theories, the 3D constitutive equations are used:

$$\begin{aligned} \sigma_{pC}^k &= [\sigma_{xx}, \sigma_{yy}, \sigma_{xy}]^{kT} = \mathbf{C}_{pp}^k\ \epsilon_{pG}^k + \mathbf{C}_{pn}^k\ \epsilon_{nG}^k \\ \sigma_{nC}^k &= [\sigma_{xz}, \sigma_{yz}, \sigma_{zz}]^{kT} = \mathbf{C}_{np}^k\ \epsilon_{pG}^k + \mathbf{C}_{nn}^k\ \epsilon_{nG}^k \end{aligned} \tag{27}$$

with

$$\begin{aligned} \mathbf{C}_{pp}^k &= \begin{bmatrix} C_{11}^k & C_{12}^k & 0 \\ C_{12}^k & C_{11}^k & 0 \\ 0 & 0 & C_{44}^k \end{bmatrix} \qquad \mathbf{C}_{pn}^k = \begin{bmatrix} 0 & 0 & C_{12}^k \\ 0 & 0 & C_{12}^k \\ 0 & 0 & 0 \end{bmatrix} \\ \mathbf{C}_{np}^k &= \begin{bmatrix} 0 & 0 & 0 \\ 0 & 0 & 0 \\ C_{12}^k & C_{12}^k & 0 \end{bmatrix} \qquad \mathbf{C}_{nn}^k = \begin{bmatrix} C_{44}^k & 0 & 0 \\ 0 & C_{44}^k & 0 \\ 0 & 0 & C_{11}^k \end{bmatrix} \end{aligned} \tag{28}$$

and the C_{ij}^k are the three-dimensional elastic constants

$$C_{11}^k = \frac{E^k(1-(\nu^k)^2)}{1-3(\nu^k)^2-2(\nu^k)^3}; \quad C_{12}^k = \frac{E^k(\nu^k+(\nu^k)^2)}{1-3(\nu^k)^2-2(\nu^k)^3}; \quad C_{44}^k = \frac{E^k}{2(1+\nu^k)} \tag{29}$$

where the modulus of elasticity and Poisson's ratio were defined in (16).

For the $sinus0$ and $sinusZZ0$ theories, as we have $\epsilon_{zz} = 0$, the plane-stress case is used:

$$\begin{aligned}
\sigma_{pC}^k &= [\sigma_{xx}, \sigma_{yy}, \sigma_{xy}]^{kT} = \mathbf{C}_{pp}^k \; \epsilon_{pG}^k \\
\sigma_{nC}^k &= [\sigma_{xz}, \sigma_{yz}]^{kT} = \mathbf{C}_{nn}^k \; \epsilon_{nG}^k
\end{aligned} \tag{30}$$

with $\mathbf{C}_{pp}^k$ and ϵ_{pG}^k as before, $\epsilon_{nG}^k = [\gamma_{xz}, \gamma_{yz}]^{kT}$ and

$$\mathbf{C}_{nn}^k = \begin{bmatrix} C_{44}^k & 0 \\ 0 & C_{44}^k \end{bmatrix} \tag{31}$$

and C_{ij}^k are the plane-stress reduced elastic constants:

$$C_{11}^k = \frac{E^k}{1-(\nu^k)^2}; \quad C_{12}^k = \nu^k \frac{E^k}{1-(\nu^k)^2}; \quad C_{44}^k = \frac{E^k}{2(1+\nu^k)} \tag{32}$$

5.5 *Principle of virtual displacements*

In the framework of the Unified Formulation, the Principle of Virtual Displacements (PVD) for the pure-mechanical case is written as:

$$\sum_{k=1}^{N_l} \int_{\Omega_k} \int_{A_k} \left\{ \delta {\epsilon_{pG}^k}^T \sigma_{pC}^k + \delta {\epsilon_{nG}^k}^T \sigma_{nC}^k \right\} d\Omega_k dz = \sum_{k=1}^{N_l} \delta L_e^k \tag{33}$$

where Ω_k and A_k are the integration domains in plane (x,y) and z direction, respectively. As stated before, G means geometrical relations and C constitutive equations, and k indicates the virtual layer. T is the transpose operator and δL_e^k is the external work for the kth layer.

Substituting the geometrical relations (G), the constitutive equations (C), and the modeled displacement field (F_τ and F_s), all for the kth layer, (33) becomes:

$$\begin{aligned}
\int_{\Omega_k} \int_{A_k} \Big[& (\mathbf{D}_p^k \; F_s \delta \mathbf{u}_s^k)^T (\mathbf{C}_{pp}^k \mathbf{D}_p^k \; F_\tau \mathbf{u}_\tau^k + \mathbf{C}_{pn}^k (\mathbf{D}_{n\Omega}^k + \mathbf{D}_{nz}^k) F_\tau \mathbf{u}_\tau^k) \\
& + ((\mathbf{D}_{n\Omega}^k + \mathbf{D}_{nz}^k) F_s \delta \mathbf{u}_s^k)^T (\mathbf{C}_{np}^k \mathbf{D}_p^k \; F_\tau \mathbf{u}_\tau^k + \mathbf{C}_{nn}^k (\mathbf{D}_{n\Omega}^k + \mathbf{D}_{nz}^k) F_\tau \mathbf{u}_\tau^k) \Big] d\Omega_k dz = \delta L_e^k
\end{aligned} \tag{34}$$

Applying now the formula of integration by parts, (34) becomes:

$$\int_{\Omega_k} \Big((\mathbf{D}_\Omega)\delta\mathbf{a}^k\Big)^T \mathbf{a}^k d\Omega_k = -\int_{\Omega_k} \delta\mathbf{a}^{k^T} \Big((\mathbf{D}_\Omega^T)\mathbf{a}^k\Big) d\Omega_k + \int_{\Gamma_k} \delta\mathbf{a}^{k^T} \Big((\mathbf{I}_\Omega)\mathbf{a}^k\Big) d\Gamma_k \tag{35}$$

where $\mathbf{I}_\Omega$ matrix is obtained applying the *Gradient theorem*:

$$\int_\Omega \frac{\partial\psi}{\partial x_i} d\upsilon = \oint_\Gamma n_i \psi ds \tag{36}$$

being n_i the components of the normal $\widehat{n}$ to the boundary along the direction i. After integration by parts, the governing equations and boundary conditions for the plate in the mechanical case are obtained:

$$\begin{aligned}
&\int_{\Omega_k}\int_{A_k} (\ \delta\mathbf{u}_s^k)^T \Big[\Big(\Big(-\mathbf{D}_p^k\Big)^T \Big(\mathbf{C}_{pp}^k(\mathbf{D}_p^k)\ +\mathbf{C}_{pn}^k(\mathbf{D}_{n\Omega}^k+\mathbf{D}_{nz}^k\Big)\\
&+\Big(-\mathbf{D}_{n\Omega}^k+\mathbf{D}_{nz}^k\Big)^T\Big(\mathbf{C}_{np}^k(\mathbf{D}_p^k)+\mathbf{C}_{nn}^k(\mathbf{D}_{n\Omega}^k+\mathbf{D}_{nz}^k)\Big)\Big)\mathbf{F}_\tau\mathbf{F}_s\mathbf{u}_\tau^k\Big] dxdydz\\
&+\int_{\Omega_k}\int_{A_k} (\ \delta\mathbf{u}_s^k)^T \Big[\Big(\mathbf{I}_p^{kT}\Big(\mathbf{C}_{pp}^k(\mathbf{D}_p^k)\ +\mathbf{C}_{pn}^k(\mathbf{D}_{n\Omega}^k+\mathbf{D}_{nz}^k)\Big)\\
&+\mathbf{I}_{np}^{kT}\Big(\mathbf{C}_{np}^k(\mathbf{D}_p^k)\ +\mathbf{C}_{nn}^k(\mathbf{D}_{n\Omega}^k+\mathbf{D}_{nz}^k)\Big)\Big)\mathbf{F}_\tau\mathbf{F}_s\mathbf{u}_\tau^k\Big] dxdydz = \int_{\Omega_k} \delta\mathbf{u}_s^{kT} F_s \mathbf{p}_u^k d\Omega_k\ .
\end{aligned} \tag{37}$$

where $\mathbf{I}_p^k$ and $\mathbf{I}_{np}^k$ depend on the boundary geometry:

$$\mathbf{I}_p^k = \begin{bmatrix} n_x & 0 & 0 \\ 0 & n_y & 0 \\ n_y & n_x & 0 \end{bmatrix}, \quad \mathbf{I}_{np}^k = \begin{bmatrix} 0 & 0 & n_x \\ 0 & 0 & n_y \\ 0 & 0 & 0 \end{bmatrix}. \tag{38}$$

The normal to the boundary of domain Ω is:

$$\widehat{\mathbf{n}} = \begin{bmatrix} n_x \\ n_y \end{bmatrix} = \begin{bmatrix} cos(\varphi_x) \\ cos(\varphi_y) \end{bmatrix} \tag{39}$$

where φ_x and φ_y are the angles between the normal $\widehat{n}$ and the direction x and y respectively.

The governing equations for a multi-layered plate subjected to mechanical loadings are:

$$\delta \mathbf{u}_s^{k^T} : \qquad \mathbf{K}_{uu}^{k\tau s}\, \mathbf{u}_\tau^k = \mathbf{P}_{u\tau}^k \tag{40}$$

where the fundamental nucleus $\mathbf{K}_{uu}^{k\tau s}$ is obtained as:

$$\begin{aligned}\mathbf{K}_{uu}^{k\tau s} =& \Big[\Big(-\mathbf{D}_p^k\Big)^T\Big(\mathbf{C}_{pp}^k(\mathbf{D}_p^k) + \mathbf{C}_{pn}^k(\mathbf{D}_{n\Omega}^k + \mathbf{D}_{nz}^k\Big) \\ &+ \Big(-\mathbf{D}_{n\Omega}^k + \mathbf{D}_{nz}^k\Big)^T\Big(\mathbf{C}_{np}^k(\mathbf{D}_p^k) + \mathbf{C}_{nn}^k(\mathbf{D}_{n\Omega}^k + \mathbf{D}_{nz}^k)\Big)\Big]\mathbf{F}_\tau \mathbf{F}_s\end{aligned} \tag{41}$$

and the corresponding Neumann-type boundary conditions on Γ_k are:

$$\mathbf{\Pi}_d^{k\tau s}\, \mathbf{u}_\tau^k = \mathbf{\Pi}_d^{k\tau s}\, \bar{\mathbf{u}}_\tau^k , \tag{42}$$

where:

$$\begin{aligned}\mathbf{\Pi}_d^{k\tau s} =& \Big[\mathbf{I}_p^{kT}\Big(\mathbf{C}_{pp}^k(\mathbf{D}_p^k) + \mathbf{C}_{pn}^k(\mathbf{D}_{n\Omega}^k + \mathbf{D}_{nz}^k)\Big) + \\ &\mathbf{I}_{np}^{kT}\Big(\mathbf{C}_{np}^k(\mathbf{D}_p^k) + \mathbf{C}_{nn}^k(\mathbf{D}_{n\Omega}^k + \mathbf{D}_{nz}^k)\Big)\Big]\mathbf{F}_\tau \mathbf{F}_s\end{aligned} \tag{43}$$

and $\mathbf{P}_{u\tau}^k$ are variationally consistent loads with applied pressure.

For FG materials, the fundamental nuclei in explicit form becomes:

$$\begin{aligned}
K_{uu_{11}}^{k\tau s} =& (-\partial_x^\tau \partial_x^s C_{11} + \partial_z^\tau \partial_z^s C_{55} - \partial_y^\tau \partial_y^s C_{66}) F_\tau F_s \\
K_{uu_{12}}^{k\tau s} =& (-\partial_x^\tau \partial_y^s C_{12} - \partial_y^\tau \partial_x^s C_{66}) F_\tau F_s \\
K_{uu_{13}}^{k\tau s} =& (-\partial_x^\tau \partial_z^s C_{13} + \partial_z^\tau \partial_x^s C_{55}) F_\tau F_s \\
K_{uu_{21}}^{k\tau s} =& (-\partial_y^\tau \partial_x^s C_{12} - \partial_x^\tau \partial_y^s C_{66}) F_\tau F_s \\
K_{uu_{22}}^{k\tau s} =& (-\partial_y^\tau \partial_y^s C_{22} + \partial_z^\tau \partial_z^s C_{44} - \partial_x^\tau \partial_x^s C_{66}) F_\tau F_s \\
K_{uu_{23}}^{k\tau s} =& (-\partial_y^\tau \partial_z^s C_{23} + \partial_z^\tau \partial_y^s C_{44}) F_\tau F_s \\
K_{uu_{31}}^{k\tau s} =& (\partial_z^\tau \partial_x^s C_{13} - \partial_x^\tau \partial_z^s C_{55}) F_\tau F_s \\
K_{uu_{32}}^{k\tau s} =& (\partial_z^\tau \partial_y^s C_{23} - \partial_y^\tau \partial_z^s C_{44}) F_\tau F_s \\
K_{uu_{33}}^{k\tau s} =& (\partial_z^\tau \partial_z^s C_{33} - \partial_y^\tau \partial_y^s C_{44} - \partial_x^\tau \partial_x^s C_{55}) F_\tau F_s
\end{aligned} \tag{44}$$

$$
\begin{aligned}
\Pi_{11}^{k\tau s} =& (n_x \partial_x^s C_{11} + n_y \partial_y^s C_{66}) F_\tau F_s \\
\Pi_{12}^{k\tau s} =& (n_x \partial_y^s C_{12} + n_y \partial_x^s C_{66}) F_\tau F_s \\
\Pi_{13}^{k\tau s} =& (n_x \partial_z^s C_{13}) F_\tau F_s \\
\Pi_{21}^{k\tau s} =& (n_y \partial_x^s C_{12} + n_x \partial_y^s C_{66}) F_\tau F_s \\
\Pi_{22}^{k\tau s} =& (n_y \partial_y^s C_{22} + n_x \partial_x^s C_{66}) F_\tau F_s \\
\Pi_{23}^{k\tau s} =& (n_y \partial_z^s C_{23}) F_\tau F_s \\
\Pi_{31}^{k\tau s} =& (n_x \partial_z^s C_{55}) F_\tau F_s \\
\Pi_{32}^{k\tau s} =& (n_y \partial_z^s C_{44}) F_\tau F_s \\
\Pi_{33}^{k\tau s} =& (n_y \partial_y^s C_{44} + n_x \partial_x^s C_{55}) F_\tau F_s
\end{aligned}
\tag{45}
$$

5.7 Equations of motion and boundary conditions in terms of displacements

In order to discretize the linearized buckling equations by radial basis functions, we need the explicit terms of that equations and the corresponding boundary conditions as well in terms of the generalized displacements. The explicit governing equations and corresponding boundary conditions in terms of generalized displacements for the static and free vibration analysis of functionally graded plates of the *sinus* theory can be found in [Neves et al., 2011b]. Those equations are the same for the buckling problem, by setting to zero the terms with the inertias (I_i) as well as the external forces (p_z), and adding the non-linear terms to the δw_0 equation. For the sake of completeness we present here the equation of the buckling problem of *sinus* theory that corresponds to the w_0 variable.

$$
\begin{aligned}
\delta w_0 : \; & A_{13} \frac{\partial u_1}{\partial x} + 2B_{13} \frac{\partial u_Z}{\partial x} + A_{23} \frac{\partial v_1}{\partial y} + 2B_{23} \frac{\partial v_Z}{\partial y} - A_{55} \frac{\partial^2 w_0}{\partial x^2} - A_{44} \frac{\partial^2 w_0}{\partial y^2} \\
& - B_{55} \frac{\partial^2 w_1}{\partial x^2} - B_{44} \frac{\partial^2 w_1}{\partial y^2} - D_{55} \frac{\partial^2 w_Z}{\partial x^2} - D_{44} \frac{\partial^2 w_Z}{\partial y^2} \\
& + \bar{N}_{xx} \frac{\partial^2 w_0}{\partial x^2} + 2\bar{N}_{xy} \frac{\partial^2 w_0}{\partial x \partial y} + \bar{N}_{yy} \frac{\partial^2 w_0}{\partial y^2} = 0
\end{aligned}
\tag{46}
$$

The stiffness components of this equation can be computed as follows:

$$A_{ij} = \sum_{k=1}^{N_l} c_{ij}^k \left(z_{k+1} - z_k\right); \quad B_{ij} = \frac{1}{2}\sum_{k=1}^{N_l} c_{ij}^k \left(z_{k+1}^2 - z_k^2\right); \quad D_{ij} = \frac{1}{3}\sum_{k=1}^{N_l} c_{ij}^k \left(z_{k+1}^3 - z_k^3\right) \tag{47}$$

where N_l is the number of mathematical layers across the thickness direction, h_k is the thickness of each layer, and z_k, z_{k+1} are the lower and upper z coordinate for each layer k. $\bar{N}_{xx}$, $\bar{N}_{xy}$, and $\bar{N}_{yy}$ denote the in-plane applied loads.

6 The radial basis function method applied to buckling problems

Recently, radial basis functions (RBFs) have enjoyed considerable success and research as a technique for interpolating data and functions. A radial basis function, $\phi(\|x - x_j\|)$ is a spline that depends on the Euclidian distance between distinct data centers $x_j, j = 1, 2, ..., N \in \mathbb{R}^n$, also called nodal or collocation points. Although most work to date on RBFs relates to scattered data approximation and in general to interpolation theory, there has recently been an increased interest in their use for solving partial differential equations (PDEs). This approach, which approximates the whole solution of the PDE directly using RBFs, is truly a mesh-free technique. Kansa [Kansa, 1990] introduced the concept of solving PDEs by an unsymmetric RBF collocation method based upon the MQ interpolation functions, in which the shape parameter may vary across the problem domain.

The radial basis function (ϕ) approximation of a function ($\mathbf{u}$) is given by

$$\tilde{\mathbf{u}}(\mathbf{x}) = \sum_{i=1}^{N} \alpha_i \phi\left(\|x - y_i\|_2\right), \mathbf{x} \in \mathbb{R}^n \tag{48}$$

where $y_i, i = 1, .., N$ is a finite set of distinct points (centers) in $\mathbb{R}^n$.

Derivatives of $\tilde{\mathbf{u}}$ are computed as

$$\frac{\partial \tilde{\mathbf{u}}}{\partial x} = \sum_{j=1}^{N} \alpha_j \frac{\partial \phi_j}{\partial x} \tag{49}$$

$$\frac{\partial^2 \tilde{\mathbf{u}}}{\partial x^2} = \sum_{j=1}^{N} \alpha_j \frac{\partial^2 \phi_j}{\partial x^2}, \text{etc} \tag{50}$$

In the present collocation approach, one needs to impose essential and natural boundary conditions. Consider, for example, the condition $w = 0$, on a simply supported or clamped edge. The conditions are enforced by interpolating as

$$w = 0 \to \sum_{j=1}^{N} \alpha_j^W \phi_j = 0 \tag{51}$$

Other boundary conditions are interpolated in a similar way.

The most common RBFs are

$$\begin{aligned}
\text{Cubic:} \quad & \phi(r) = r^3 \\
\text{Thin plate splines:} \quad & \phi(r) = r^2 \log(r) \\
\text{Wendland functions:} \quad & \phi(r) = (1-r)_+^m p(r) \\
\text{Gaussian:} \quad & \phi(r) = e^{-(cr)^2} \\
\text{Multiquadrics:} \quad & \phi(r) = \sqrt{c^2 + r^2} \\
\text{Inverse Multiquadrics:} \quad & \phi(r) = (c^2 + r^2)^{-1/2}
\end{aligned}$$

where the Euclidian distance r is real and non-negative and c is a positive shape parameter. In the present work, we consider the compact-support Wendland function [Wendland, 1998] defined as

$$\phi(r) = (1 - c\, r)_+^8 \left(32(c\, r)^3 + 25(c\, r)^2 + 8c\, r + 1\right) \tag{52}$$

The shape parameter (c) is obtained by an optimization procedure, as detailed in Ferreira and Fasshauer [Ferreira and Fasshauer, 2006].

Considering N distinct interpolations, and knowing $u(x_j), j = 1, 2, ..., N$, one finds α_i by the solution of a $N \times N$ linear system

$$\mathbf{A}\boldsymbol{\alpha} = \mathbf{u} \tag{53}$$

where $\mathbf{A} = [\phi(\|x - y_i\|_2)]_{N\times N}$, $\boldsymbol{\alpha} = [\alpha_1, \alpha_2, ..., \alpha_N]^T$ and $\mathbf{u} = [u(x_1), u(x_2), ..., u(x_N)]^T$.

Consider a linear elliptic partial differential operator $\mathcal{L}$ acting in a bounded region Ω in $\mathbb{R}^n$ and another operator $\mathcal{L}_B$ acting on a boundary $\partial\Omega$. The eigenproblem looks for eigenvalues (λ) and eigenvectors ($\mathbf{u}$) that satisfy

$$\mathcal{L}\mathbf{u} + \lambda\mathbf{u} = 0 \text{ in } \Omega \tag{54}$$

$$\mathcal{L}_B\mathbf{u} = 0 \text{ on } \partial\Omega \tag{55}$$

The eigenproblem defined in (54) and (55) will be replaced by a finite-dimensional eigenvalue problem, after the radial basis approximations.

The solution of the eigenproblem by radial basis functions considers N_I nodes in the interior of the domain and N_B nodes on the boundary, with a total number of nodes $N = N_I + N_B$. In the present work, a $\Re^2$ Chebyshev grid is employed (see figure 6) and a square plate is computed with side length $a = 2$. For a given number of nodes per side $(N+1)$ they are generated by MATLAB code as:

```
x = cos(pi*(0:N)/N)'; y=x;
```

One advantage of such mesh is the concentration of points near the boundary.

The interpolation points are denoted by $x_i \in \Omega, i = 1, ..., N_I$ and $x_i \in \partial\Omega, i = N_I{+}1, ..., N$. At the points in the domain, the following eigenproblem is defined

$$\sum_{i=1}^{N} \alpha_i \mathcal{L}\phi\left(\|x - y_i\|_2\right) = \lambda\tilde{\mathbf{u}}(x_j), j = 1, 2, ..., N_I \tag{56}$$

or

$$\mathcal{L}^I\boldsymbol{\alpha} = \lambda\tilde{\mathbf{u}}^I \tag{57}$$

where

$$\mathcal{L}^I = \left[\mathcal{L}\phi\left(\|x - y_i\|_2\right)\right]_{N_I \times N} \tag{58}$$

At the points on the boundary, the imposed boundary conditions are

$$\sum_{i=1}^{N} \alpha_i \mathcal{L}_B\phi\left(\|x - y_i\|_2\right) = 0, j = N_I + 1, ..., N \tag{59}$$

or

$$\mathbf{B}\boldsymbol{\alpha} = 0 \tag{60}$$

where $\mathbf{B} = \mathcal{L}_B\phi\left[\left(\|x_{N_I+1} - y_j\|_2\right)\right]_{N_B \times N}$.

Therefore, one can write a finite-dimensional eigenvalue problem and solve equations (57) and (60) as a generalized eigenvalue problem

$$\begin{bmatrix} \mathcal{L}^I \\ \\ \mathbf{B} \end{bmatrix} \boldsymbol{\alpha} = \lambda \begin{bmatrix} \mathbf{A}^I \\ \\ \mathbf{0} \end{bmatrix} \boldsymbol{\alpha} \tag{61}$$

where

$$\mathbf{A}^I = \phi\left[(\|x_{N_I} - y_j\|_2)\right]_{N_I \times N}$$

The eigenproblem associated to the linearized buckling equations is defined as

$$[\mathcal{L} - \lambda\mathcal{G}]\,\mathbf{X} = \mathbf{0} \tag{62}$$

where $\mathcal{L}$ collects all stiffness terms and $\mathcal{G}$ collects all terms related to the in-plane forces. In (62) $\mathbf{X}$ are the buckling modes associated with the buckling loads defined as λ.

7 Numerical results

In this section the sinusoidal shear deformation plate theories are combined with radial basis functions collocation for the buckling analysis of functionally graded sandwich plates. The plate is subjected to compressive in-plane forces acting on the mid-plane of the plate. The buckling loads of simply supported (SSSS) square ($a = b = 2$, see figure 6) sandwich plates with FG materials in the skins are analysed, for both symmetric and unsymmetric plates. The plates have side lengths $a = b$, thickness h, being the span-to-thickness ratio a/h taken to be 10.

As stated before, all numerical examples are performed employing a Chebyshev grid and the Wendland function as defined in (52) with an optimized shape parameter. The bottom skin varies from a metal-rich surface to a ceramic-rich surface while the top skin face varies from a ceramic-rich surface to a metal-rich surface. The core material of the present sandwich plate is fully ceramic. Recall that the plate is a sandwich, physicaly divided into 3 layers, although 91 virtual layers are considered for the evaluation of stiffness components. The power-law function is used to describe the volume fraction of the metal and ceramic phases (see (1)) and the material homogeneization technique adopted is the law of mixtures (16), the same used in the references. The material properties are $E_m = 70E_0$ (aluminum) and $E_c = 380E_0$ (alumina) being $E_0 = 1\text{GPa}$. Poisson's ratio is $\nu_m = \nu_c = \nu = 0.3$ for both aluminum and alumina. The homogeneization technique is applied to the Young's modulus only. Various power-law exponents, and skin-core-skin thickness ratios are considered in the following.

Both the uni- and bi-axial critical buckling load are studied. An initial study was performed for each type of buckling load to show the convergence of the present approach and select the number of Chebyshev points to use in the computation of the buckling problems. The non-dimensional parameter used is

$$\bar{P} = \frac{Pa^2}{100h^3E_0}.$$

7.1 Uni-axial buckling load

The uni-axial case convergence study is presented in table 2 for the 1-1-1 sandwich with $p = 1$. Based on this study a grid of 17^2 points was used for the forward uni-axial buckling study.

The first four buckling modes of a simply supported 2-2-1 sandwich square plate with FG skins, $p = 10$, subjected to a uni-axial in-plane compressive load, using present sinusoidal theories are presented in figures 7 to 10.

The critical buckling loads obtained from the present approach with $sinus$, $sinus0$, $sinusZZ$, and $sinusZZ0$ theories are tabulated and compared with available references in table 3 for various power-law exponents p and skin-core-skin thickness ratios. The table includes results obtained from classical plate theory (CLPT), first-order shear deformation plate theory (FSDPT, $K = 5/6$ as shear correction factor), Reddy's third-order shear deformation plate theory (TSDPT) [Reddy, 2000], and Zenkour's sinusoidal shear deformation plate theory (SSDPT) [Zenkour, 2005b]. The table is organized so that the material power-law exponent increases from up to down ($p = 0$, 0.5, 1, 5, 10) and the core thickness to the total thickness of the plate ratio increases from left to right $\left(\frac{h_c}{h} = 0, \frac{1}{5}, \frac{1}{4}, \frac{1}{3}, \frac{2}{5}, \frac{1}{2}\right)$. In the particular case of the 1-0-1 sandwich, the sandwich degenerates in a FG two layers plate (see figure 11 on the left) and the ZZF is as in figure 11 on the right.

7.2 Bi-axial buckling load

The bi-axial case convergence study is presented in table 4 for the 2-1-1 sandwich with $p = 5$. A grid of 17^2 points was used for the forward bi-axial buckling study.

In figures 12 to 15 the first four buckling modes of a simply supported 2-1-2 sandwich square plate with FG skins, $p = 0.5$, subjected to a bi-axial in-plane compressive load, using present sinusoidal theories are presented.

The critical buckling loads obtained from the present approach with $sinus$, $sinus0$, $sinusZZ$, and $sinusZZ0$ theories are tabulated in table 5 for various power-law exponents p and skin-core-skin thickness ratios. As for the uni-axial case, results are compared with those from classical plate theory (CLPT), first-order shear deformation plate theory (FSDPT, $K = 5/6$ as shear correction factor), Reddy's third-order shear deformation plate theory (TSDPT) [Reddy, 2000], and Zenkour's sinusoidal shear deformation plate theory (SSDPT) [Zenkour, 2005b]. The table is organized so that the material power-law exponent increases from up to down and the core thickness to the total thickness of the plate ratio increases from left to right. As in the uni-axial load case, the 1-0-1 case becomes as in figure 11.

7.3 Discussion of results

Results obtained with the present formulation are in good agreement with considered references (except for the classical plate theory, which is not adequate for this type of plates). This allow us to conclude that the sinusoidal plate theories combined with collocation with radial basis functions are good for the modeling of SSSS sandwich plates with FG skins.

The isotropic fully ceramic plate (first line on tables 3 and 5) has the higher fundamental buckling loads. As the core thickness to the total thickness of the plate ratio increases the buckling loads increase as well. We may also conclude that the critical buckling loads decrease as the power-law exponent p increases. From the comparison of tables 3 and 5 we deduce that the bi-axial buckling load of any simply supported sandwich square plate with FG skins is half the uni-axial one for the same plate.

The zig-zag effects have influence on the buckling loads of SSSS sandwich plates with functionally graded skins. By comparing *sinus* and $sinusZZ$ theories we see that the first one (without ZZ effect) gives higher buckling loads than the other (with ZZ effects). Same happens to $sinus0$ and $sinusZZ0$ theories. The influence of the ZZ effect is also seen in the first column of tables 3 and 5: for the isotropic fully ceramic plate, different values are obtained.

Another thing to note is that the $sinus0$ and $sinusZZ0$ theories are in better agreement with [Reddy, 2000] and [Zenkour, 2005b] than *sinus* and $sinusZZ$ theories. This can be explained by the $\epsilon_{zz} = 0$ option that the four theories $sinus0$, $sinusZZ0$, [Reddy, 2000] and [Zenkour, 2005b] share. The influence of the warping effects is stronger than the ZZ effects.

8 Conclusions

For the first time, a study on the influence of Zig-Zag and warping effects on buckling problems of functionally graded sandwich plates by radial basis function collocation was performed. For that purpose, four sinusoidal theories were compared. The computation procedure becomes fast and straightforward in MATLAB as a consequence of combining a generalized version of Carrera's Unified Formulation and collocation with radial basis functions. The collocation code depends only on the choice of two vectors and the buckling loads for any type of C_z^0 shear deformation theory are obtained just by changing F_τ and F_s. The present formulation was compared with available references and proved very accurate in buckling problems.

Although buckling loads of sandwich plates with functionally graded skins depend on both warping and zig-zag effects, the influence of the warping effects is stronger.

Acknowledgements

The first author is grateful for the support from FCT grant SFRH/BD/45554/2008. The authors acknowledge the financial support from FCT under colaboration project within LAETA, Mechanical Design - Composites, 2012.

References

[Altenbach, 1998] Altenbach, H. (1998). Theories for laminated and sandwich plates. *Mechanics of Composite Materials*, 34:243–252. 10.1007/BF02256043.

[Batra and Jin, 2005] Batra, R. and Jin, J. (2005). Natural frequencies of a functionally graded anisotropic rectangular plate. *Journal of Sound and Vibration*, 282(1-2):509 – 516.

[Bever and Duwez, 1972] Bever, M. and Duwez, P. (1972). Gradients in composite materials. *Materials Science and Engineering*, 10(0):1 – 8.

[Birman, 1995] Birman, V. (1995). Buckling of functionally graded hybrid composite plates. *Proceedings of the 10th Conference on Engineering Mechanics*, pages 1199–1202.

[Birman and Byrd, 2007] Birman, V. and Byrd, L. W. (2007). Modeling and analysis of functionally graded materials and structures. *Applied Mechanics Reviews*, 60(5):195–216.

[Brischetto et al., 2009] Brischetto, S., Carrera, E., and Demasi, L. (2009). Improved bending analysis of sandwich plate by using zig-zag function. *Compos. Struct.*, 89:408–415.

[Burton and Noor, 1995] Burton, S. and Noor, A. K. (1995). Assessment of computational model for sandwich panels and shells. *Comput. Meth. Appl. Mech. Eng.*, 124:125–151.

[Carrera, 1996] Carrera, E. (1996). C^0 reissner-mindlin multilayered plate elements including zig-zag and interlaminar stress continuity. *International Journal of Numerical Methods in Engineering*, 39:1797–1820.

[Carrera, 2001] Carrera, E. (2001). Developments, ideas, and evaluations based upon reissner's mixed variational theorem in the modelling of multilayered plates and shells. *Applied Mechanics Reviews*, 54:301–329.

[Carrera, 2003] Carrera, E. (2003). Historical review of zig-zag theories for multilayered plates and shells. *Applied Mechanics Reviews*, (56):287–308.

[Carrera, 2004] Carrera, E. (2004). The use of murakami's zig-zag function in the modeling of layered plates and shells. *Compos. Struct.*, 82:541–554.

[Carrera et al., 2011] Carrera, E., Brischetto, S., Cinefra, M., and Soave, M. (2011). Effects of thickness stretching in functionally graded plates and shells. *Composites Part B: Engineering*, 42:123–133.

[Cheng and Batra, 2000a] Cheng, Z. Q. and Batra, R. C. (2000a). Deflection relationships between the homogeneous kirchhoff plate theory and different functionally graded plate theories. *Archive of Mechanics*, 52:143–158.

[Cheng and Batra, 2000b] Cheng, Z. Q. and Batra, R. C. (2000b). Exact correspondence between eigenvalues of membranes and functionally graded simply supported polygonal plates. *Journal of Sound and Vibration*, 229:879–895.

[Cheng and Batra, 2000c] Cheng, Z. Q. and Batra, R. C. (2000c). Three-dimensional thermoelastic deformations of a functionally graded-elliptic plate. *Composites: Part B*, 31:97–106.

[Chi and Chung, 2006a] Chi, S.-H. and Chung, Y.-L. (2006a). Mechanical behavior of functionally graded material plates under transverse load–part i: Analysis. *International Journal of Solids and Structures*, 43(13):3657 – 3674.

[Chi and Chung, 2006b] Chi, S.-H. and Chung, Y.-L. (2006b). Mechanical behavior of functionally graded material plates under transverse load–part ii: Numerical results. *International Journal of Solids and Structures*, 43(13):3675 – 3691.

[Chung and Chi, 2001] Chung, Y. and Chi, S. (2001). The residual stress of functionally graded materials. *Journal of the Chinese Institute of Civil and Hydraulic Engineering*, 13:1–9.

[Demasi, 2008a] Demasi, L. (2008a). 2d, quasi 3d and 3d exact solutions for bending of thick and thin sandwich plates. *J. Sandwich Struct. Mater.*, 10:271–310.

[Demasi, 2008b] Demasi, L. (2008b). ∞^3 hierarchy plate theories for thick and thin composite plates: the generalized unified formulation. *Compos. Struct.*, 84:256–270.

[Ferrante and Graham-Brady, 2005] Ferrante, F. and Graham-Brady, L. (2005). Stochastic simulation of non-gaussian/non-stationary properties in a functionally graded plate. *Computer Methods in Applied Mechanics and Engineering*, 194(12-16):1675 – 1692.

[Ferreira et al., 2006a] Ferreira, A., Batra, R., Roque, C., Qian, L., and Jorge, R. (2006a). Natural frequencies of functionally graded plates by a meshless method. *Composite Structures*, 75(1-4):593 – 600. Thirteenth International Conference on Composite Structures - ICCS/13.

[Ferreira et al., 2011a] Ferreira, A., Roque, C., Carrera, E., Cinefra, M., and Polit, O. (2011a). Radial basis functions collocation and a unified formulation for bending, vibration and buckling analysis of laminated plates, according to a variation of murakami's zig-zag theory. *European Journal of Mechanics - A/Solids*, 30(4):559 – 570.

[Ferreira et al., 2011b] Ferreira, A., Roque, C., Carrera, E., Cinefra, M., and Polit, O. (2011b). Two higher order zig-zag theories for the accurate analysis of bending, vibration and buckling response of laminated plates by radial basis functions collocation and a unified formulation. *Journal of Composite Materials*, 45(24):2523–2536.

[Ferreira et al., 2005a] Ferreira, A., Roque, C., and Jorge, R. (2005a). Analysis of composite plates by trigonometric shear deformation theory and multiquadrics. *Computers & Structures*, 83(27):2225 – 2237.

[Ferreira et al., 2005b] Ferreira, A., Roque, C., and Jorge, R. (2005b). Free vibration analysis of symmetric laminated composite plates by fsdt and radial basis functions. *Computer Methods in Applied Mechanics and Engineering*, 194(39-41):4265 – 4278.

[Ferreira et al., 2005c] Ferreira, A., Roque, C., Jorge, R., and Kansa, E. (2005c). Static deformations and vibration analysis of composite and sandwich plates using a layerwise theory and multiquadrics discretizations. *Engineering Analysis with Boundary Elements*, 29(12):1104 – 1114.

[Ferreira, 2003a] Ferreira, A. J. M. (2003a). A formulation of the multiquadric radial basis function method for the analysis of laminated composite plates. *Composite Structures*, 59:385–392.

[Ferreira, 2003b] Ferreira, A. J. M. (2003b). Thick composite beam analysis using a global meshless approximation based on radial basis functions. *Mechanics of Advanced Materials and Structures*, 10:271–284.

[Ferreira et al., 2006b] Ferreira, A. J. M., Batra, R. C., Roque, C. M. C., Qian, L. F., and Jorge, R. M. N. (2006b). Natural frequencies of functionally graded plates by a meshless method. *Composite Structures*, 75(1-4):593–600.

[Ferreira et al., 2005d] Ferreira, A. J. M., Batra, R. C., Roque, C. M. C., Qian, L. F., and Martins, P. A. L. S. (2005d). Static analysis of functionally graded plates using third-order shear deformation theory and a meshless method. *Composite Structures*, 69(4):449–457.

[Ferreira and Fasshauer, 2006] Ferreira, A. J. M. and Fasshauer, G. E. (2006). Computation of natural frequencies of shear deformable beams and plates by a rbf-pseudospectral method. *Computer Methods in Applied Mechanics and Engineering*, 196:134–146.

[Ferreira et al., 2007] Ferreira, A. J. M., Roque, C. M. C., Jorge, R. M. N., Fasshauer, G. E., and Batra, R. C. (2007). Analysis of functionally graded plates by a robust meshless method. *Mechanics of Advanced Materials and Structures*, 14(8):577–587.

[Ferreira et al., 2003] Ferreira, A. J. M., Roque, C. M. C., and Martins, P. A. L. S. (2003). Analysis of composite plates using higher-order shear deformation theory and a finite point formulation based on the multiquadric radial basis function method. *Composites: Part B*, 34:627–636.

[Ferreira et al., 2004] Ferreira, A. J. M., Roque, C. M. C., and Martins, P. A. L. S. (2004). Radial basis functions and higher-order shear deformation theories in the analysis of laminated composite beams and plates. *Composite Structures*, 66(1-4):287 – 293. Twelfth International Conference on Composite Structures.

[Javaheri and Eslami, 2002] Javaheri, R. and Eslami, M. (2002). Buckling of functionally graded plates under in-plane compressive loading. *ZAMM - Journal of Applied Mathematics and Mechanics / Zeitschrift fÃijr Angewandte Mathematik und Mechanik*, 82(4):277–283.

[Jin and Batra, 1996] Jin, Z. H. and Batra, R. C. (1996). Stress intensity relaxation at the tip of an edge crack in a functionally graded material subjected to a thermal shock. *Journal of Thermal Stresses*, 19:317–339.

[Kansa, 1990] Kansa, E. J. (1990). Multiquadrics- a scattered data approximation scheme with applications to computational fluid dynamics. i: Surface approximations and partial derivative estimates. *Computers and Mathematics with Applications*, 19(8/9):127–145.

[Kashtalyan, 2004] Kashtalyan, M. (2004). Three-dimensional elasticity solution for bending of functionally graded rectangular plates. *European Journal of Mechanics - A/Solids*, 23(5):853 – 864.

[Kashtalyan and Menshykova, 2009] Kashtalyan, M. and Menshykova, M. (2009). Three-dimensional elasticity solution for sandwich panels with a functionally graded core. *Composite Structures*, 87(1):36 – 43.

[Kirchhoff, 1850] Kirchhoff, G. (1850). Uber das gleichgewicht und die bewegung einer elastischen scheibe. *J. Angew. Math.*, 40:51–88.

[Koizumi, 1997] Koizumi, M. (1997). Fgm activities in japan. *Composites Part B: Engineering*, 28(1-2):1 – 4. Use of Composites Multi-Phased and Functionally Graded Materials.

[Librescu and Hause, 2000] Librescu, L. and Hause, T. (2000). Recent developments in the modeling and behavior of advanced sandwich constructions: a survey. *Composite Structures*, 48(1-3):1 – 17.

[Mindlin, 1951] Mindlin, R. D. (1951). Influence of rotary inertia and shear in flexural motions of isotropic elastic plates. *Journal of Applied mechanics*, 18:31–38.

[Miyamoto et al., 1999] Miyamoto, Y., Kaysser, W., Rabin, B., Kawasaki, A., and Ford, R. (1999). *Functionally Graded Materials: Design, Processing and Applications*. Kluwer Academic Publishers.

[Mori and Tanaka, 1973] Mori, T. and Tanaka, K. (1973). Average stress in matrix and average elastic energy of materials with misfitting inclusions. *Acta Metallurgica*, 21(5):571 – 574.

[Murakami, 1986] Murakami, H. (1986). Laminated composite plate theory with improved in-plane responses. *Journal of Applied Mechanics*, 53:661–666.

[Najafizadeh and Eslami, 2002] Najafizadeh, M. M. and Eslami, M. R. (2002). Buckling analysis of circular plates of functionally graded materials under uniform radial compression. *International Journal of Mechanical Sciences*, 44(12):2479 – 2493.

[Neves et al., 2011a] Neves, A., Ferreira, A., Carrera, E., Roque, C., Cinefra, M., Jorge, R., and Soares, C. (2011a). Bending of fgm plates by a sinusoidal plate formulation and collocation with radial basis functions. *Mechanics Research Communications*, 38(5):368 – 371.

[Neves et al., 2011b] Neves, A., Ferreira, A., Carrera, E., Roque, C., Cinefra, M., Jorge, R., and Soares, C. (2011b). A quasi-3d sinusoidal shear deformation theory for the static and free vibration analysis of functionally graded plates. *Composites Part B: Engineering*, (0):–.

[Neves et al., 2012] Neves, A. M. A., Ferreira, A. J. M., Carrera, E., Cinefra, M., Jorge, R. M. N., and Soares, C. M. M. (2012). Static analysis of functionally graded sandwich plates according to a hyperbolic theory considering zig-zag and warping effects. *Advances in Engineering Software*, submitted.

[Nguyen et al., 2007] Nguyen, T. K., Sab, K., and Bonnet, G. (2007). Shear correction factors for functionally graded plates. *Mechanics of Advanced Materials and Structures*, 14(8):567–575.

[Noor et al., 1996] Noor, A. K., Burton, S., and Bert, C. W. (1996). Computational model for sandwich panels and shells. *Appl. Mech. Rev.*, 49:155–199.

[Praveen and Reddy, 1998] Praveen, G. N. and Reddy, J. N. (1998). Nonlinear transient thermoelastic analysis of functionally graded ceramic-metal plates. *International Journal of Solids and Structures*, 35(33):4457 – 4476.

[Qian et al., 2004] Qian, L. F., Batra, R. C., and Chen, L. M. (2004). Static and dynamic deformations of thick functionally graded elastic plate by using higher-order shear and normal deformable plate theory and meshless local petrov-galerkin method. *Composites: Part B*, 35:685–697.

[R. and R., 2002] R., J. and R., E. M. (2002). Thermal buckling of functionally graded plates based on higher order theory. *Journal of Thermal Stresses*, 25(7):603–625.

[Ramirez et al., 2006] Ramirez, F., Heyliger, P. R., and Pan, E. (2006). Static analysis of functionally graded elastic anisotropic plates using a discrete layer approach. *Composites Part B: Engineering*, 37(1):10 – 20.

[Reddy, 2000] Reddy, J. N. (2000). Analysis of functionally graded plates. *International Journal for Numerical Methods in Engineering*, 47:663–684.

[Reddy and Chin, 1998] Reddy, J. N. and Chin, C. D. (1998). Thermomechanical analysis of functionally graded cylinders and plates. *Journal of Thermal Stresses*, 21(6):593–626.

[Reissner, 1945] Reissner, E. (1945). The effect of transverse shear deformations on the bending of elastic plates. *Journal of Applied mechanics*, 12:A69–A77.

[Rodrigues et al., 2011] Rodrigues, J., Roque, C., Ferreira, A., Carrera, E., and Cinefra, M. (2011). Radial basis functions-finite differences collocation and a unified formulation for bending, vibration and buckling analysis of laminated plates, according to murakami's zig-zag theory. *Composite Structures*, 93(7):1613 – 1620.

[Roque et al., 2007] Roque, C., Ferreira, A., and Jorge, R. (2007). A radial basis function approach for the free vibration analysis of functionally graded plates using a refined theory. *Journal of Sound and Vibration*, 300(3-5):1048 – 1070.

[Touratier, 1991] Touratier, M. (1991). An efficient standard plate theory. *International Journal of Engineering Science*, 29:901–916.

[Touratier, 1992a] Touratier, M. (1992a). A generalization of shear deformation theories for axisymmetric multilayered shells. *International Journal of Solids and Structures*, 29:1379–1399.

[Touratier, 1992b] Touratier, M. (1992b). A refined theory of laminated shallow shells. *International Journal of Solids and Structures*, 29(11):1401–1415.

[Vel and Batra, 2002] Vel, S. S. and Batra, R. C. (2002). Exact solution for thermoelastic deformations of functionally graded thick rectangular plates. *AIAA Journal*, 40:1421–1433.

[Vel and Batra, 2003] Vel, S. S. and Batra, R. C. (2003). Three-dimensional analysis of transient thermal stresses in functionally-graded plates. *International Journal of Solids and Structures*, in press.

[Vel and Batra, 2004] Vel, S. S. and Batra, R. C. (2004). Three-dimensional exact solution for the vibration of functionally graded rectangular plates. *Journal of Sound and Vibration*, 272:703–730.

[Vidal and Polit, 2008] Vidal, P. and Polit, O. (2008). A family of sinus finite elements for the analysis of rectangular laminated beams. *Composite Structures*, 84:56–72.

[Vinson, 2001] Vinson, J. R. (2001). Sandwich structures. *Applied Mechanics Reviews*, 54(3):201–214.

[Wendland, 1998] Wendland, H. (1998). Error estimates for interpolation by compactly supported radial basis functions of minimal degree. *J. Approx. Theory*, 93:258–296.

[Y. and Benveniste, 1987] Y. and Benveniste (1987). A new approach to the application of mori-tanaka's theory in composite materials. *Mechanics of Materials*, 6(2):147 – 157.

[Yin et al., 2004] Yin, H., Sun, L., and Paulino, G. (2004). Micromechanics-based elastic model for functionally graded materials with particle interactions. *Acta Materialia*, 52(12):3535 – 3543.

[Zenkour, 2005a] Zenkour, A. (2005a). A comprehensive analysis of functionally graded sandwich plates: Part 1–deflection and stresses. *International Journal of Solids and Structures*, 42(18-19):5224 – 5242.

[Zenkour, 2005b] Zenkour, A. (2005b). A comprehensive analysis of functionally graded sandwich plates: Part 2–buckling and free vibration. *International Journal of Solids and Structures*, 42(18-19):5243 – 5258.

[Zenkour, 2006] Zenkour, A. M. (2006). Generalized shear deformation theory for bending analysis of functionally graded plates. *Appl Math Modell*, 30:67–84.

[Zhong and Shang, 2008] Zhong, Z. and Shang, E. (2008). Closed-form solutions of three-dimensional functionally graded plates. *Mechanics of Advanced Materials and Structures*, 15(5):355–363.

List of Figures

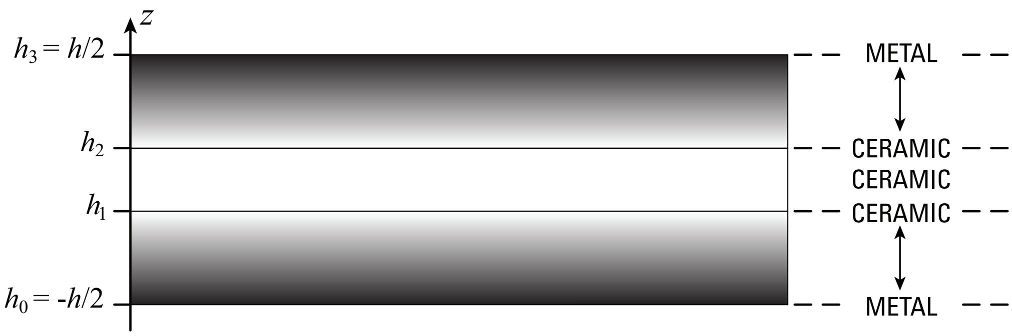

Fig. 1. Sandwich with isotropic core and FG skins.

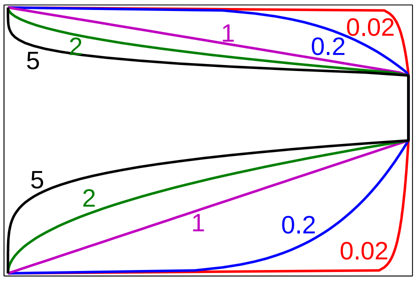

Fig. 2. A 2-1-1 sandwich with FG skins for various power-law exponents in (1).

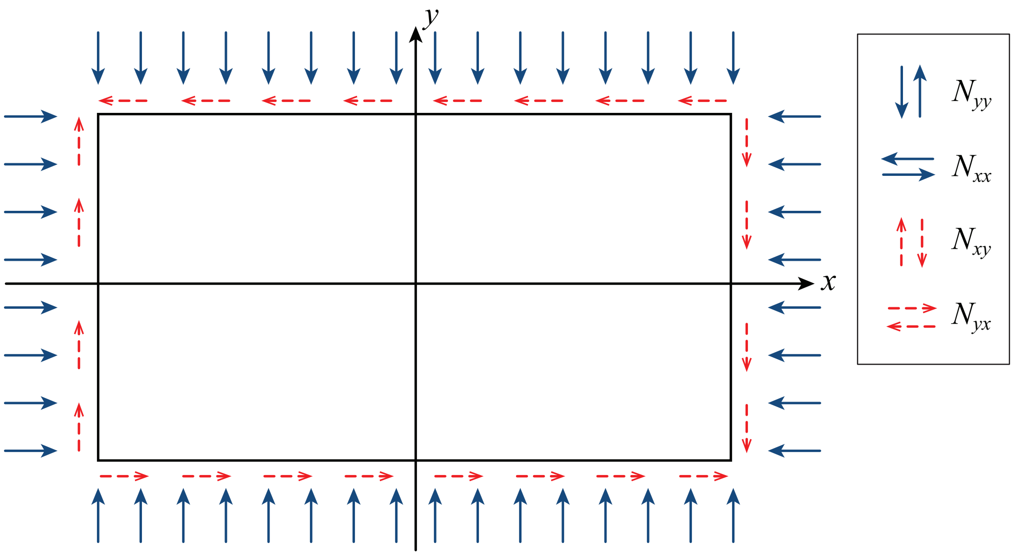

Fig. 3. Rectangular plate subjected to in-plane forces.

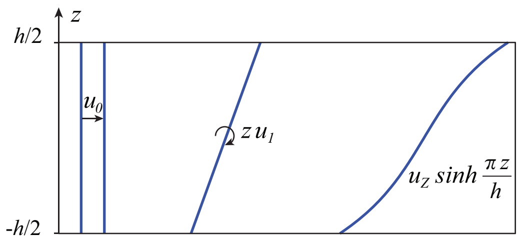

Fig. 4. Scheme of the expansions involved in the displacement field.

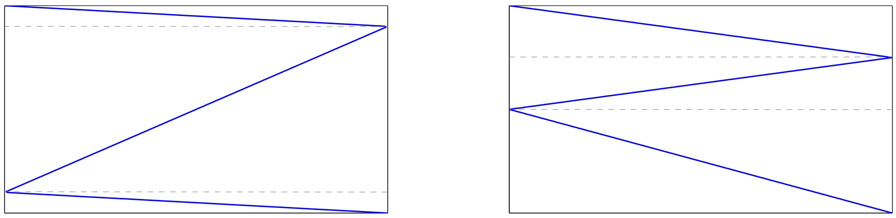

Fig. 5. Zig-Zag effect for the 1-8-1 (left) and the 2-1-1 sandwichs (right).

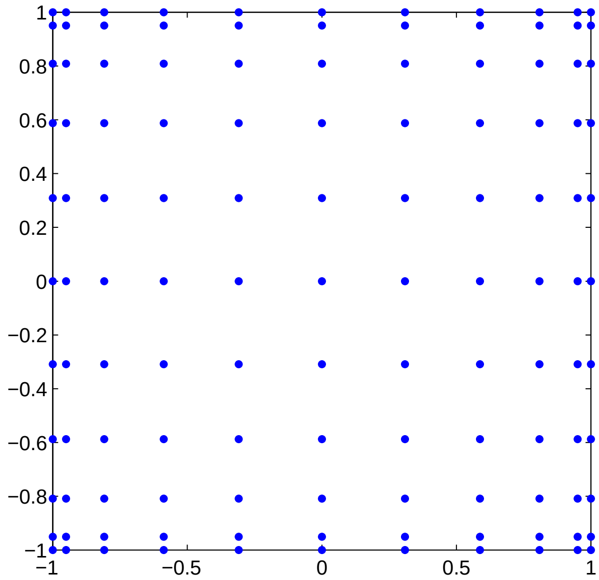

Fig. 6. A sketch of a $\Re^2$ Chebyshev grid with 11^2 points

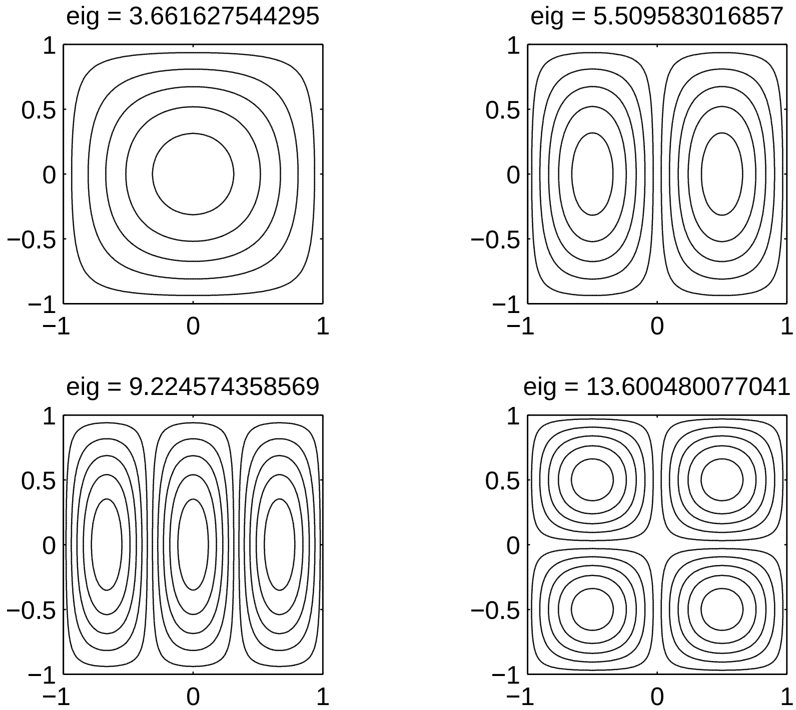

Fig. 7. First four buckling modes. Uni-axial buckling load of a simply supported 2-2-1 sandwich square plate with FG skins, $p = 10$, and using the sinus theory.

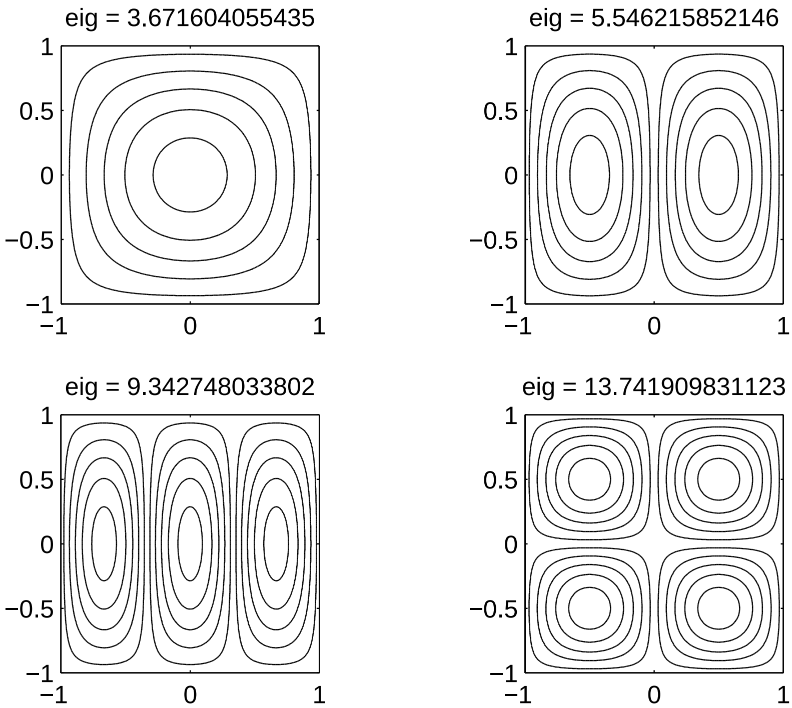

Fig. 8. First four buckling modes. Uni-axial buckling load of a simply supported 2-2-1 sandwich square plate with FG skins, $p = 10$, and using the sinus0 theory.

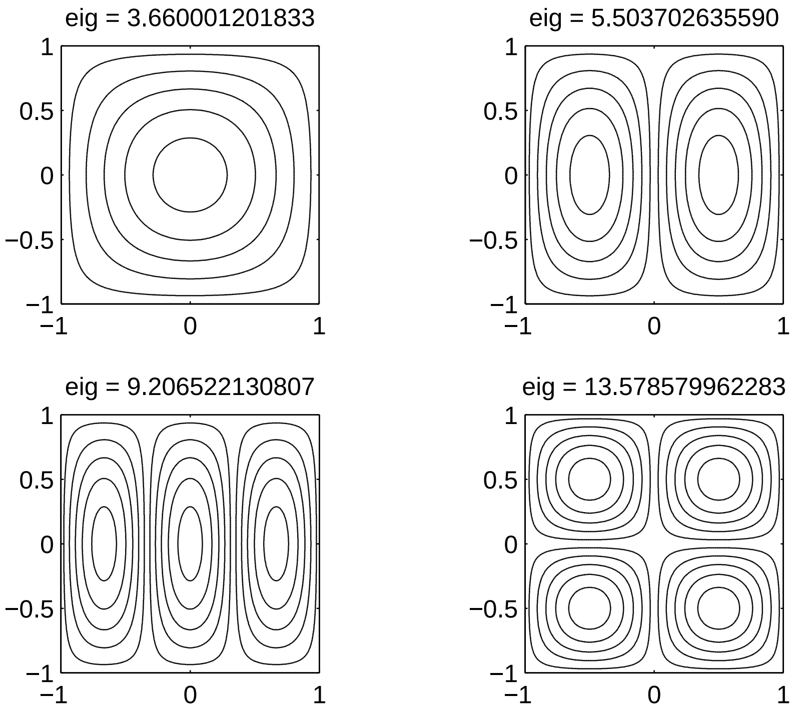

Fig. 9. First four buckling modes. Uni-axial buckling load of a simply supported 2-2-1 sandwich square plate with FG skins, $p = 10$, and using the sinusZZ theory.

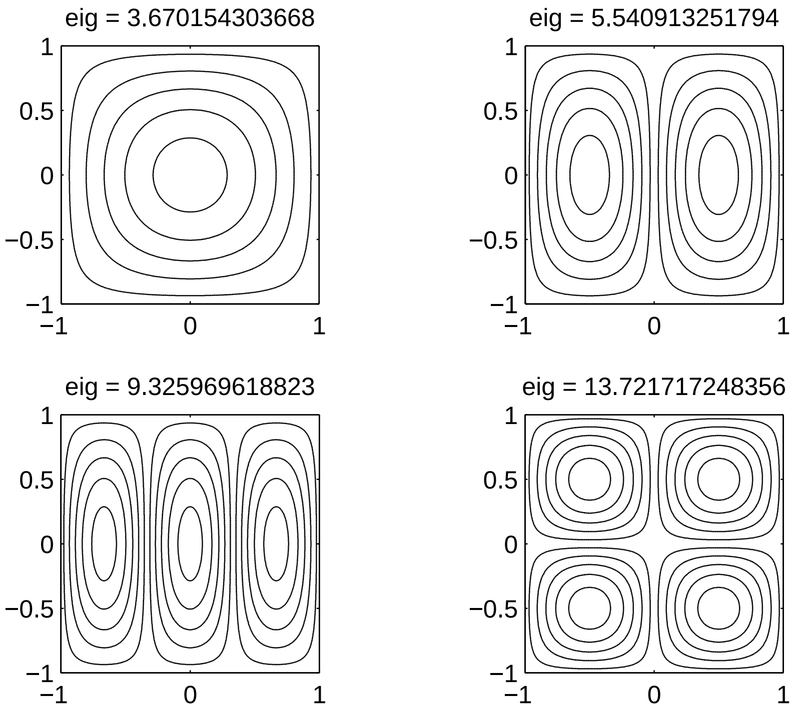

Fig. 10. First four buckling modes. Uni-axial buckling load of a simply supported 2-2-1 sandwich square plate with FG skins, $p = 10$, and using the sinusZZ0 theory.

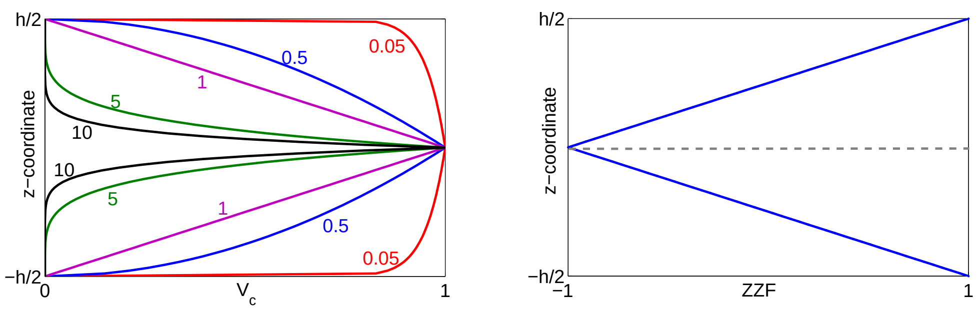

Fig. 11. The 1-0-1 sandwich with FG skins: influence of the exponent power-law (left) and the ZZF (right).

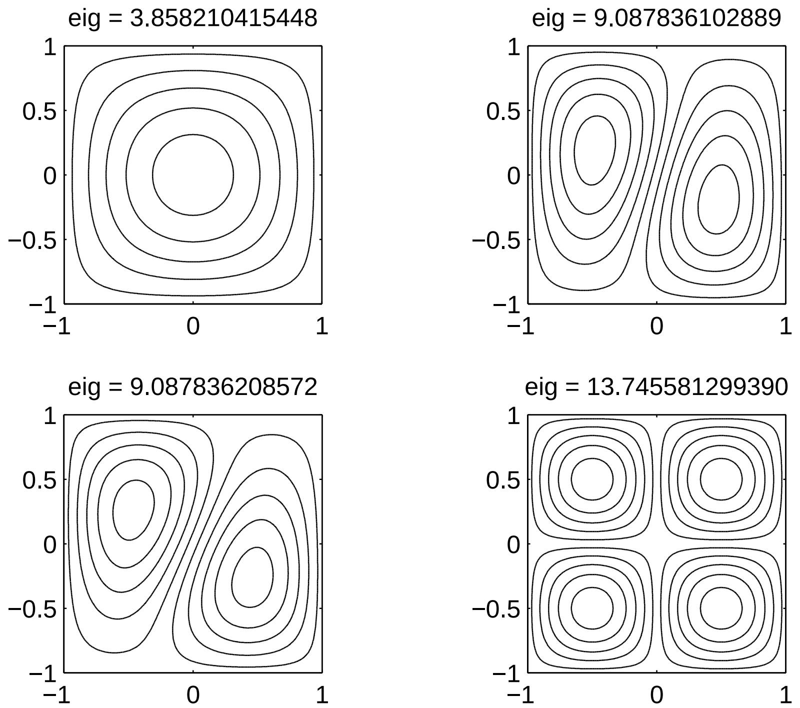

Fig. 12. First four buckling modes. Bi-axial buckling load of a simply supported 2-1-2 sandwich square plate with FG skins, $p = 0.5$, and using the sinus theory.

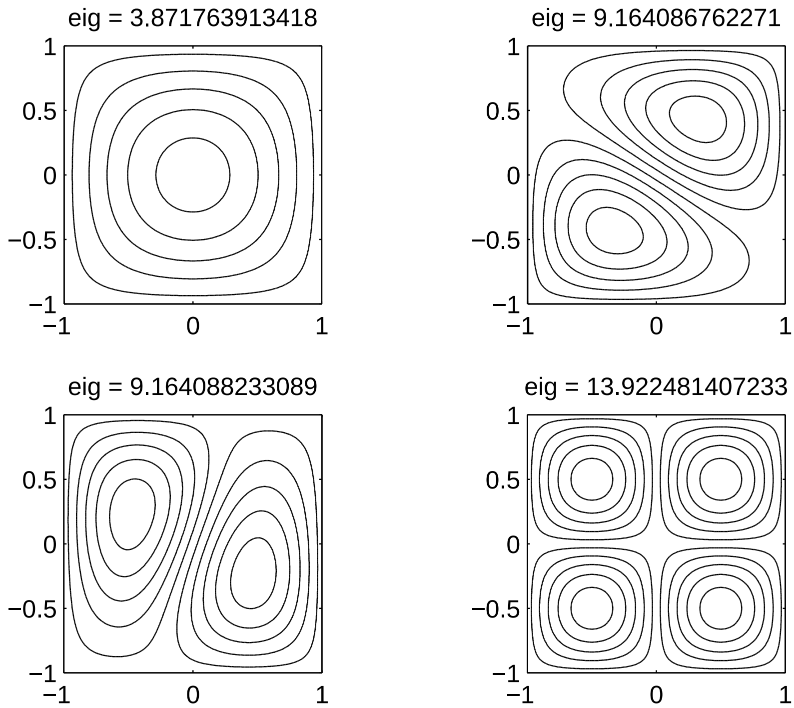

Fig. 13. First four buckling modes. Bi-axial buckling load of a simply supported 2-1-2 sandwich square plate with FG skins, $p = 0.5$, and using the sinus0 theory.

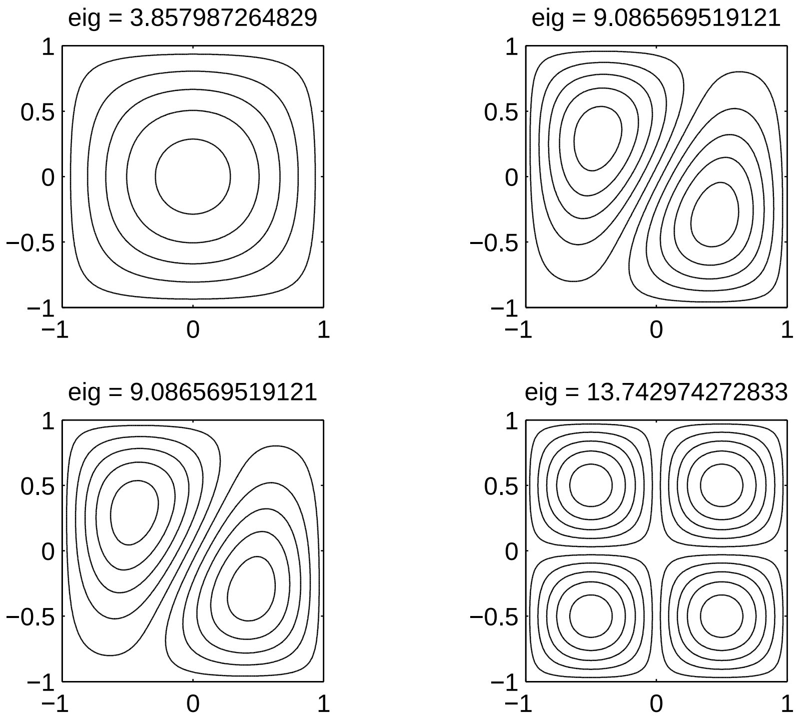

Fig. 14. First four buckling modes. Bi-axial buckling load of a simply supported 2-1-2 sandwich square plate with FG skins, $p = 0.5$, and using the sinusZZ theory.

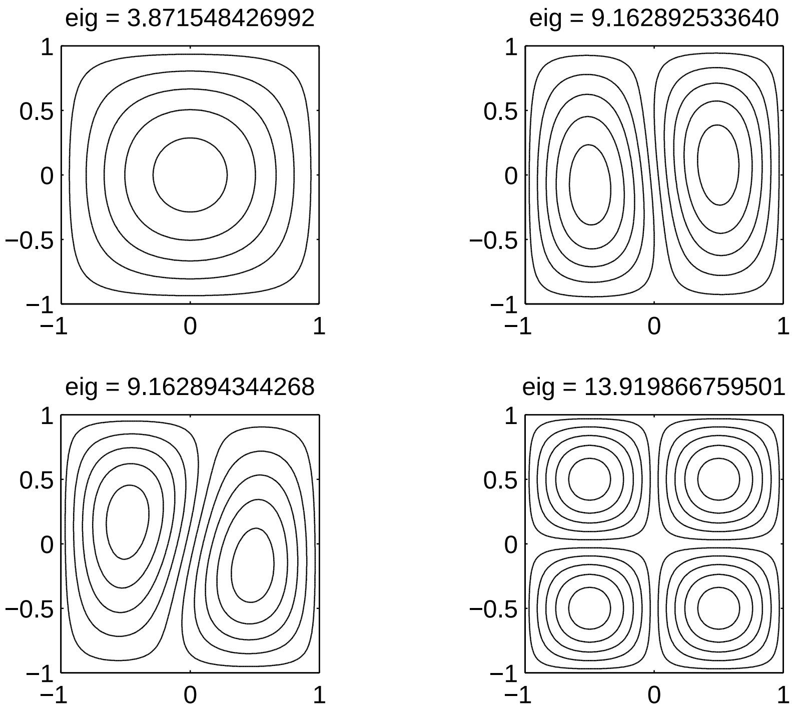

Fig. 15. First four buckling modes. Bi-axial buckling load of a simply supported 2-1-2 sandwich square plate with FG skins, $p = 0.5$, and using the sinusZZ0 theory.

List of Tables

theory	considers Zig-Zag effect	allows tichness-stretching
sinus	no	yes
sinus0	no	no
sinusZZ	yes	yes
sinusZZ0	yes	no

Table 1
The present sinus theories.

grid	13^2	17^2	21^2
$\bar{P}$ sinus	6.31557	6.31502	6.31495
$\bar{P}$ sinusZZ	6.31474	6.31414	6.31406

Table 2
Convergence study for the uni-axial buckling load of a simply supported 1-1-1 sandwich square plate with FG skins and $p = 1$ case using the sinus and sinusZZ theory.

p	Theory	1-0-1	2-1-2	2-1-1	1-1-1	2-2-1	1-2-1
0	CLPT	13.73791	13.73791	13.73791	13.73791	13.73791	13.73791
	FSDPT	13.00449	13.00449	13.00449	13.00449	13.00449	13.00449
	TSDPT [Reddy, 2000]	13.00495	13.00495	13.00495	13.00495	13.00495	13.00495
	SSDPT [Zenkour, 2005b]	13.00606	13.00606	13.00606	13.00606	13.00606	13.00606
	sinus	12.95311	12.95311	12.95311	12.95311	12.95311	12.95311
	sinus0	13.00543	13.00543	13.00543	13.00543	13.00543	13.00543
	sinusZZ	12.95300	12.95196	12.95281	12.95203	12.95190	12.95310
	sinusZZ0	13.00532	13.00437	13.00515	13.00447	13.00427	13.00545
0.5	CLPT	7.65398	8.25597	8.56223	8.78063	9.18254	9.61525
	FSDPT	7.33732	7.91320	8.20015	8.41034	8.78673	9.19517
	TSDPT [Reddy, 2000]	7.36437	7.94084	8.22470	8.43645	8.80997	9.21681
	SSDPT [Zenkour, 2005b]	7.36568	7.94195	8.22538	8.43712	8.81037	9.21670
	sinus	7.16230	7.71642	7.98960	8.19279	8.55168	8.94166
	sinus0	7.18761	7.74350	8.01710	8.22139	8.58128	8.97284
	sinusZZ	7.16223	7.71597	7.98960	8.19183	8.55081	8.94150
	sinusZZ0	7.18755	7.74310	8.01710	8.22052	8.58039	8.97271
1	CLPT	5.33248	6.02733	6.40391	6.68150	7.19663	7.78406
	FSDPT	5.14236	5.81379	6.17020	6.43892	6.92571	7.48365
	TSDPT [Reddy, 2000]	5.16713	5.84006	6.19394	6.46474	6.94944	7.50656
	SSDPT [Zenkour, 2005b]	5.16846	5.84119	6.19461	6.46539	6.94980	7.50629
	sinus	5.06151	5.71145	6.05468	6.31499	6.78398	7.31966
	sinus0	5.07874	5.73041	6.07363	6.33558	6.80542	7.34331
	sinusZZ	5.06147	5.71123	6.05471	6.31414	6.78338	7.31949
	sinusZZ0	5.07869	5.73022	6.07366	6.33480	6.80476	7.34317
5	CLPT	2.73080	3.10704	3.48418	3.65732	4.21238	4.85717
	FSDPT	2.63842	3.02252	3.38538	3.55958	4.09285	4.71475
	TSDPT [Reddy, 2000]	2.65821	3.04257	3.40351	3.57956	4.11209	4.73469
	SSDPT [Zenkour, 2005b]	2.66006	3.04406	3.40449	3.58063	4.11288	4.73488
	sinus	2.63640	3.00755	3.36252	3.52992	4.05069	4.64692
	sinus0	2.64695	3.01855	3.37203	3.54149	4.06168	4.66043
	sinusZZ	2.63631	3.00698	3.35966	3.52994	4.05056	4.64688
	sinusZZ0	2.64687	3.01793	3.36937	3.54152	4.06160	4.66038
10	CLPT	2.56985	2.80340	3.16427	3.25924	3.79238	4.38221
	FSDPT	2.46904	2.72626	3.07428	3.17521	3.68890	4.26040
	TSDPT [Reddy, 2000]	2.48727	2.74632	3.09190	3.19471	3.70752	4.27991
	SSDPT [Zenkour, 2005b]	2.48928	2.74844	3.13443	3.19456	3.14574	4.38175
	sinus	2.47230	2.71991	3.06061	3.15730	3.66163	4.20546
	sinus0	2.48259	2.73058	3.06950	3.16827	3.67158	4.21787
	sinusZZ	2.47213	2.71679	3.05227	3.15658	3.66000	4.20449
	sinusZZ0	2.48242	2.72733	3.06150	3.16749	3.67015	4.21685

Table 3
Uni-axial buckling $\bar{P}$ load of simply supported sandwich square plates with FG skins using the sinusoidal theory.

grid	13^2	17^2	21^2
$\bar{P}$ sinus	1.68144	1.68127	1.68125
$\bar{P}$ sinusZZ	1.68002	1.67983	1.67981

Table 4
Convergence study for the bi-axial buckling load of a simply supported 2-1-1 sandwich square plate with FG skins and $p = 5$ case using the sinus and sinusZZ theory.

p	Theory	1-0-1	2-1-2	2-1-1	1-1-1	2-2-1	1-2-1
0	CLPT	6.86896	6.86896	6.86896	6.86896	6.86896	6.86896
	FSDPT	6.50224	6.50224	6.50224	6.50224	6.50224	6.50224
	TSDPT [Reddy, 2000]	6.50248	6.50248	6.50248	6.50248	6.50248	6.50248
	SSDPT [Zenkour, 2005b]	6.50303	6.50303	6.50303	6.50303	6.50303	6.50303
	sinus	6.47656	6.47656	6.47656	6.47656	6.47656	6.47656
	sinus0	6.50272	6.50272	6.50272	6.50272	6.50272	6.50272
	sinusZZ	6.47650	6.47598	6.47641	6.47601	6.47595	6.47655
	sinusZZ0	6.50266	6.50219	6.50258	6.50224	6.50214	6.50272
0.5	CLPT	3.82699	4.12798	4.28112	4.39032	4.59127	4.80762
	FSDPT	3.66866	3.95660	4.10007	4.20517	4.39336	4.59758
	TSDPT [Reddy, 2000]	3.68219	3.97042	4.11235	4.21823	4.40499	4.60841
	SSDPT [Zenkour, 2005b]	3.68284	3.97097	4.11269	4.21856	4.40519	4.60835
	sinus	3.58115	3.85821	3.99480	4.09640	4.27584	4.47083
	sinus0	3.59380	3.87175	4.00855	4.11069	4.29064	4.48642
	sinusZZ	3.58112	3.85799	3.99480	4.09592	4.27541	4.47075
	sinusZZ0	3.59377	3.87155	4.00855	4.11026	4.29020	4.48636
1	CLPT	2.66624	3.01366	3.20195	3.34075	3.59831	3.89203
	FSDPT	2.57118	2.90690	3.08510	3.21946	3.46286	3.74182
	TSDPT [Reddy, 2000]	2.58357	2.92003	3.09697	3.23237	3.47472	3.75328
	SSDPT [Zenkour, 2005b]	2.58423	2.92060	3.09731	3.23270	3.47490	3.75314
	sinus	2.53076	2.85573	3.02734	3.15750	3.39199	3.65983
	sinus0	2.53937	2.86520	3.03681	3.16779	3.40271	3.67165
	sinusZZ	2.53073	2.85562	3.02735	3.15707	3.39169	3.65975
	sinusZZ0	2.53935	2.86511	3.03683	3.16740	3.40238	3.67158
5	CLPT	1.36540	1.55352	1.74209	1.82866	2.10619	2.42859
	FSDPT	1.31921	1.51126	1.69269	1.77979	2.04642	2.35737
	TSDPT [Reddy, 2000]	1.32910	1.52129	1.70176	1.78978	2.05605	2.36734
	SSDPT [Zenkour, 2005b]	1.33003	1.52203	1.70224	1.79032	2.05644	2.36744
	sinus	1.31820	1.50377	1.68126	1.76496	2.02535	2.32346
	sinus0	1.32348	1.50927	1.68601	1.77075	2.03084	2.33022
	sinusZZ	1.31816	1.50349	1.67983	1.76497	2.02528	2.32344
	sinusZZ0	1.32344	1.50897	1.68469	1.77076	2.03080	2.33019
10	CLPT	1.28493	1.40170	1.58214	1.62962	1.89619	2.19111
	FSDPT	1.23452	1.36313	1.53714	1.58760	1.84445	2.13020
	TSDPT [Reddy, 2000]	1.24363	1.37316	1.54595	1.59736	1.85376	2.13995
	SSDPT [Zenkour, 2005b]	1.24475	1.37422	1.56721	1.59728	1.57287	2.19087
	sinus	1.23615	1.35996	1.53030	1.57865	1.83081	2.10273
	sinus0	1.24130	1.36529	1.53475	1.58414	1.83579	2.10893
	sinusZZ	1.23606	1.35840	1.52613	1.57829	1.83000	2.10224
	sinusZZ0	1.24121	1.36367	1.53075	1.58374	1.83508	2.10843

Table 5
Bi-axial buckling load $\bar{P}$ of simply supported sandwich square plates with FG skins using the sinusoidal theory.

2.8 Free vibration analysis of functionally graded shells by a higher-order shear deformation theory and radial basis functions collocation, accounting for through-the-thickness deformations

A. M. A. Neves, A. J. M. Ferreira, E. Carrera, M. Cinefra, C. M. C. Roque, R. M. N. Jorge, C. M. M. Soares, Free vibration analysis of functionally graded shells by a higher-order shear deformation theory and radial basis functions collocation, accounting for through-the-thickness deformations, European Journal of Mechanics -A/Solids, Volume 37, 2013, Pages 24-34.

European Journal of Mechanics A/Solids 37 (2013) 24–34

Contents lists available at SciVerse ScienceDirect

European Journal of Mechanics A/Solids

journal homepage: www.elsevier.com/locate/ejmsol

Free vibration analysis of functionally graded shells by a higher-order shear deformation theory and radial basis functions collocation, accounting for through-the-thickness deformations

A.M.A. Neves [a], A.J.M. Ferreira [a,*], E. Carrera [b], M. Cinefra [b], C.M.C. Roque [c], R.M.N. Jorge [a], C.M.M. Soares [d]

[a] Departamento de Engenharia Mecânica, Faculdade de Engenharia, Universidade do Porto, Rua Dr. Roberto Frias, 4200-465 Porto, Portugal
[b] Department of Aeronautics and Aerospace Engineering, Politecnico di Torino, Corso Duca degli Abruzzi 24, 10129 Torino, Italy
[c] INEGI, Faculdade de Engenharia, Universidade do Porto, Rua Dr. Roberto Frias, 4200-465 Porto, Portugal
[d] Instituto Superior Técnico, Av. Rovisco Pais, Lisboa, Portugal

ARTICLE INFO

Article history:
Received 15 November 2011
Accepted 6 May 2012
Available online 17 May 2012

Keywords:
Functionally graded materials
Shells
Free vibration

ABSTRACT

This paper deals with free vibration problems of functionally graded shells. The analysis is performed by radial basis functions collocation, according to a higher-order shear deformation theory that accounts for through-the-thickness deformation.

The equations of motion and the boundary conditions are obtained by Carrera's Unified Formulation resting upon the principle of virtual work, and further interpolated by collocation with radial basis functions.

Numerical results include spherical as well as cylindrical shell panels with all edges clamped or simply supported and demonstrate the accuracy of the present approach.

1. Introduction

Functionally graded materials (FGM) are a class of composite materials that were first proposed by Bever and Duwez in 1972. In a typical FGM shell the material properties continuously vary over the thickness direction by mixing two different materials (Miyamoto et al., 1999). The computational modeling of FGM is an important tool to the understanding of the structures behavior, and has been the target of intense research (Miyamoto et al., 1999; Ferrante and Graham-Brady, 2005; Yin et al., 2004; Zhong and Shang, 2008; Nguyen et al., 2007; Birman and Byrd, 2007; Koizumi, 1997). The continuous development of new structural materials leads to ever increasingly complex structural designs that require careful analysis. Although analytical techniques are very important, the use of numerical methods to solve shell mathematical models of complex structures has become essential.

The most common numerical procedure for the analysis of the shells is the finite element method (Carrera, 2003; Chapelle and Bathe, 2003; Flügge, 1960; Scordelis and Lo, 1964; Reddy, 1982). This paper considers collocation with radial basis functions as a meshless technique. A radial basis function, $\phi(\|x-x_j\|)$ depends on the Euclidian distance between distinct collocation points $x_{j,j} = 1,2,\ldots,N \in \mathbb{R}^n$. The unsymmetrical Kansa method (Kansa, 1990) is employed in this work, for its good accuracy and easy implementation. The use of radial basis function for the analysis of structures and materials has been previously studied (Hon et al., 1997, 1999; Wang et al., 2002; Liu and Gu, 2001; Liu and Wang, 2002; Wang and Liu, 2002; Chen et al., 2003; Dai et al., 2004; Liu and Chen, 2002; Liew et al., 2004; Huang and Li, 2004; Liu et al., 2002; Xiang et al., 2009, 2010; Ferreira et al., 2006). Advantages of this technique are absence of mesh, ease of discretization of governing equations and boundary conditions and ease of coding as well. The authors have applied the RBF collocation to the analysis of composite beams and plates (Ferreira, 2003a, 2003b; Ferreira et al., 2003). The combination of CUF and meshless methods has been performed in Ferreira et al. (2011a, 2011b, 2011c) and Rodrigues et al. (2011) for laminated plates, in Ferreira et al. (2011d, 2011e) for laminated shells, and in Neves et al. (2011, 2012) for FGM plates.

In this paper it is investigated for the first time how the Unified Formulation by Carrera (Carrera, 2001; Carrera, 2004; Carrera and Brischetto, 2008; Soave et al., 2010; Kröplin et al., 2006; Carrera, 2003) can be combined with radial basis functions collocation to the free vibration analysis of thin and thick FG shells, using a higher-order shear deformation theory (HSDT), allowing for through-the-thickness deformations. The effect of $\epsilon_{zz} \neq 0$ in these

* Corresponding author.
E-mail address: ferreira@fe.up.pt (A.J.M. Ferreira).

0997-7538/$ – see front matter © 2012 Elsevier Masson SAS. All rights reserved.
doi:10.1016/j.euromechsol.2012.05.005

problems is also investigated. The quality of the present method in predicting free vibrations of thin and thick FG shells is demonstrated through numerical examples.

2. The Unified Formulation applied to shell HSDT

The Unified Formulation (UF) proposed by Carrera has been applied in several finite element analysis of beams, plates, and shells, either using the Principle of Virtual Displacements, or by using the Reissner's Mixed Variational theorem. The stiffness matrix components, the external force terms or the inertia terms can be obtained directly with this UF, irrespective of the shear deformation theory being considered. We present in the following the details of the formulation.

2.1. Shell geometry

Shells are bi-dimensional structures in which one dimension (in general the thickness in z direction) is negligible with respect to the other two in-plane dimensions. The CUF formulation applied to FGM shells considers virtual (mathematical) layers of constant thickness. The geometry and the reference system are indicated in Fig. 1.

2.2. A higher-order shear deformation theory

The present higher-order shear deformation theory involves the following expansion of displacements

$$u(\alpha,\beta,z,t) = u_0(\alpha,\beta,t) + zu_1(\alpha,\beta,t) + z^3u_3(\alpha,\beta,t) \tag{1}$$

$$v(\alpha,\beta,z,t) = v_0(\alpha,\beta,t) + zv_1(\alpha,\beta,t) + z^3v_3(\alpha,\beta,t) \tag{2}$$

$$w(\alpha,\beta,z,t) = w_0(\alpha,\beta,t) + zw_1(\alpha,\beta,t) + z^2w_2(\alpha,\beta,t) \tag{3}$$

where u, v, and w are the displacements in the α-, β-, and z-directions, respectively. $u_0, u_1, u_3, v_0, v_1, v_3, w_0, w_1$, and w_2 are functions to be determined. u_0, v_0 and w_0 are translations of a point at the middle-surface of the shell, and u_1, v_1, u_3, v_3 denote rotations. The consideration of higher-order terms in w allows the study of the thickness-stretching effects.

2.3. Governing equations and boundary conditions

The functionally graded shell is divided into a number (NL) of uniform thickness layers. The square of an infinitesimal linear segment in the kth layer, the associated infinitesimal area and volume are given by:

$$\begin{aligned} ds_k^2 &= H_\alpha^{k^2} d\alpha^2 + H_\beta^{k^2} d\beta^2 + H_z^{k^2} dz^2, \\ d\Omega_k &= H_\alpha^k H_\beta^k d\alpha\, d\beta, \\ dV_k &= H_\alpha^k H_\beta^k H_z^k d\alpha\, d\beta\, dz, \end{aligned} \tag{4}$$

where the metric coefficients are:

$$H_\alpha^k = A^k\left(1 + z/R_\alpha^k\right),\ \ H_\beta^k = B^k\left(1 + z/R_\beta^k\right),\ \ H_z^k = 1. \tag{5}$$

k denotes the k-layer of the multilayered shell; R_α^k and R_β^k are the principal radii of curvature along the coordinates α and β respectively. A^k and B^k are the coefficients of the first fundamental form of Ω_k (Γ_k is the Ω_k boundary). In this work, the attention has been restricted to shells with constant radii of curvature (cylindrical, spherical, toroidal geometries) for which $A^k = B^k = 1$.

The Principle of Virtual Displacements (PVD) for the pure-mechanical case can be expressed as:

$$\sum_{k=1}^{NL} \int_{\Omega_k} \int_{A_k} \left\{ \delta\epsilon_{pG}^{k\ T} \sigma_{pC}^k + \delta\epsilon_{nG}^{k\ T} \sigma_{nC}^k \right\} d\Omega_k dz = \sum_{k=1}^{NL} \delta L_e^k \tag{6}$$

where Ω_k and A_k are the integration domains in plane (α, β) and z direction, respectively. Here, k indicates the layer and T the transpose of a vector. G means geometrical relations and C constitutive equations and δL_e^k is the external work for the kth layer.

Stresses and strains are separated into in-plane and normal components, denoted respectively by the subscripts p and n. The mechanical strains in the kth layer can be related to the displacement field $\boldsymbol{u}^k = \left\{u_\alpha^k, u_\beta^k, u_z^k\right\}$ via the geometrical relations:

$$\begin{aligned} \epsilon_{pG}^k &= \left[\epsilon_{\alpha\alpha}^k, \epsilon_{\beta\beta}^k, \epsilon_{\alpha\beta}^k\right]^T = \left(\boldsymbol{D}_p^k + \boldsymbol{A}_p^k\right)\boldsymbol{u}^k, \epsilon_{nG}^k = \left[\epsilon_{\alpha z}^k, \epsilon_{\beta z}^k, \epsilon_{zz}^k\right]^T \\ &= \left(\boldsymbol{D}_{n\Omega}^k + \boldsymbol{D}_{nz}^k - \boldsymbol{A}_n^k\right)\boldsymbol{u}^{kT} \end{aligned} \tag{7}$$

The explicit form of the introduced arrays follows:

$$\boldsymbol{D}_p^k = \begin{bmatrix} \frac{\partial_\alpha}{H_\alpha^k} & 0 & 0 \\ 0 & \frac{\partial_\beta}{H_\beta^k} & 0 \\ \frac{\partial_\beta}{H_\beta^k} & \frac{\partial_\alpha}{H_\alpha^k} & 0 \end{bmatrix}, \boldsymbol{D}_{n\Omega}^k = \begin{bmatrix} 0 & 0 & \frac{\partial_\alpha}{H_\alpha^k} \\ 0 & 0 & \frac{\partial_\beta}{H_\beta^k} \\ 0 & 0 & 0 \end{bmatrix}, \boldsymbol{D}_{nz}^k = \begin{bmatrix} \partial_z & 0 & 0 \\ 0 & \partial_z & 0 \\ 0 & 0 & \partial_z \end{bmatrix}, \tag{8}$$

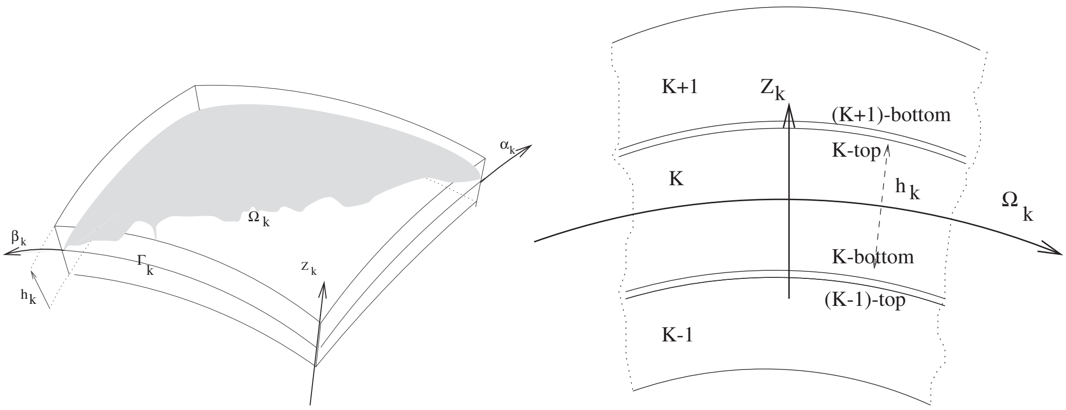

Fig. 1. Geometry and notations for a multilayered shell (doubly curved).

$$\boldsymbol{A}_p^k = \begin{bmatrix} 0 & 0 & \frac{1}{H_\alpha^k R_\alpha^k} \\ 0 & 0 & \frac{1}{H_\beta^k R_\beta^k} \\ 0 & 0 & 0 \end{bmatrix}, \quad \boldsymbol{A}_n^k = \begin{bmatrix} \frac{1}{H_\alpha^k R_\alpha^k} & 0 & 0 \\ 0 & \frac{1}{H_\beta^k R_\beta^k} & 0 \\ 0 & 0 & 0 \end{bmatrix}. \tag{9}$$

The 3D constitutive equations are given as:

$$\begin{aligned} \sigma_{pC}^k &= \boldsymbol{C}_{pp}^k \epsilon_{pG}^k + \boldsymbol{C}_{pn}^k \epsilon_{nG}^k \\ \sigma_{nC}^k &= \boldsymbol{C}_{np}^k \epsilon_{pG}^k + \boldsymbol{C}_{nn}^k \epsilon_{nG}^k \end{aligned} \tag{10}$$

In the case of functionally graded materials, the matrices $\boldsymbol{C}_{pp}^k$, $\boldsymbol{C}_{pn}^k$, $\boldsymbol{C}_{np}^k$, and $\boldsymbol{C}_{nn}^k$ are reduced to:

$$\begin{aligned} \boldsymbol{C}_{pp}^k &= \begin{bmatrix} C_{11}^k & C_{12}^k & 0 \\ C_{12}^k & C_{11}^k & 0 \\ 0 & 0 & C_{44}^k \end{bmatrix} \quad \boldsymbol{C}_{pn}^k = \begin{bmatrix} 0 & 0 & C_{12}^k \\ 0 & 0 & C_{12}^k \\ 0 & 0 & 0 \end{bmatrix} \\ \boldsymbol{C}_{np}^k &= \begin{bmatrix} 0 & 0 & 0 \\ 0 & 0 & 0 \\ C_{12}^k & C_{12}^k & 0 \end{bmatrix} \quad \boldsymbol{C}_{nn}^k = \begin{bmatrix} C_{44}^k & 0 & 0 \\ 0 & C_{44}^k & 0 \\ 0 & 0 & C_{33}^k \end{bmatrix} \end{aligned} \tag{11}$$

The computation of elastic constants C_{ij}^k for each layer, considers the following steps:

(1) computation of volume fraction of the ceramic and metal phases
(2) computation of elastic properties E^k and ν^k
(3) computation of elastic constants C_{ij}

In the present work, the volume fraction of the ceramic phase is defined according to the power-law:

$$V_c^k = \left(0.5 + \frac{z}{h}\right)^p \tag{12}$$

being $z \in [-h/2, h/2]$, h the thickness of the shell, and the exponent p a scalar parameter that defines gradation of material properties across the thickness direction. The volume fraction of the metal phase is given as $V_m^k = 1 - V_c^k$.

The Young's modulus, E^k, and Poisson's ratio, ν^k, are computed by the law-of-mixtures:

$$E^k(z) = E_m V_m^k + E_c V_c^k; \quad \nu^k(z) = \nu_m V_m^k + \nu_c V_c^k; \tag{13}$$

Then, the computation of the elastic constants C_{ij}^k is performed, depending on the assumption of ϵ_{zz}. If $\epsilon_{zz} = 0$, then C_{ij}^k are the plane-stress reduced elastic constants:

$$C_{11}^k = \frac{E^k}{1-(\nu^k)^2}; \; C_{12}^k = \nu^k \frac{E^k}{1-(\nu^k)^2}; \; C_{44}^k = \frac{E^k}{2(1+\nu^k)}; \; C_{33} = 0 \tag{14}$$

where E^k is the modulus of elasticity, ν^k is the Poisson's ratio found in previous step.

If $\epsilon_{zz} \neq 0$ (thickness-stretching), then C_{ij}^k are the three-dimensional elastic constants, given by

$$C_{11}^k = \frac{E^k\left(1-(\nu^k)^2\right)}{1-3(\nu^k)^2-2(\nu^k)^3}, \quad C_{12}^k = \frac{E^k\left(\nu^k+(\nu^k)^2\right)}{1-3(\nu^k)^2-2(\nu^k)^3} \tag{15}$$

$$C_{44}^k = \frac{E^k}{2(1+\nu^k)}, \quad C_{33}^k = \frac{E^k\left(1-(\nu^k)^2\right)}{1-3(\nu^k)^2-2(\nu^k)^3} \tag{16}$$

The three displacement components u_α, u_β and u_z (given in (1)–(3)) and their relative variations can be modeled by CUF as:

$$\begin{aligned} \left(u_\alpha, u_\beta, u_z\right) &= F_\tau\left(u_{\alpha\tau}, u_{\beta\tau}, u_{z\tau}\right) \quad \left(\delta u_\alpha, \delta u_\beta, \delta u_z\right) \\ &= F_s\left(\delta u_{\alpha s}, \delta u_{\beta s}, \delta u_{zs}\right) \end{aligned} \tag{17}$$

where F_τ are functions of the thickness coordinate z and τ is a sum index. In the present formulation the thickness functions are

$$F_{su\alpha} = F_{su\beta} = F_{\tau u\alpha} = F_{\tau u\beta} = \begin{bmatrix} 1 & z & z^3 \end{bmatrix} \tag{18}$$

for in-plane displacements u, v and

$$F_{sw} = F_{\tau w} = \begin{bmatrix} 1 & z & z^2 \end{bmatrix} \tag{19}$$

for transverse displacement w. All the terms of the equations of motion are then obtained by integrating through the thickness direction.

Substituting the geometrical relations, the constitutive equations and the unified formulation into the variational statement PVD, for the kth layer, one obtains:

$$\begin{aligned} &\sum_{k=1}^{NL} \Bigg\{ \int_{\Omega_k} \int_{A_k} \Big\{ \left((\boldsymbol{D}_p + \boldsymbol{A}_p)\delta \boldsymbol{u}^k\right)^T \Big(\boldsymbol{C}_{pp}^k (\boldsymbol{D}_p + \boldsymbol{A}_p)\boldsymbol{u}^k \\ &\quad + \boldsymbol{C}_{pn}^k (\boldsymbol{D}_{n\Omega} + \boldsymbol{D}_{nz} - \boldsymbol{A}_n)\boldsymbol{u}^k\Big) + \left((\boldsymbol{D}_{n\Omega} + \boldsymbol{D}_{nz} - \boldsymbol{A}_n)\delta \boldsymbol{u}^k\right)^T \\ &\quad \times \Big(\boldsymbol{C}_{np}^k (\boldsymbol{D}_p + \boldsymbol{A}_p)\boldsymbol{u}^k + \boldsymbol{C}_{nn}^k (\boldsymbol{D}_{n\Omega} + \boldsymbol{D}_{nz} - \boldsymbol{A}_n)\boldsymbol{u}^k\Big) \Big\} d\Omega_k dz_k \Bigg\} \\ &= \sum_{k=1}^{NL} \delta L_e^k \end{aligned} \tag{20}$$

At this point, the formula of integration by parts is applied:

$$\begin{aligned} \int_{\Omega_k} \left((\mathbf{D}_\Omega)\delta \mathbf{a}^k\right)^T \mathbf{a}^k d\Omega_k &= -\int_{\Omega_k} \delta \mathbf{a}^{k^T} \left(\left(\mathbf{D}_\Omega^T\right)\mathbf{a}^k\right) d\Omega_k \\ &\quad + \int_{\Gamma_k} \delta \mathbf{a}^{k^T} \left((\mathbf{I}_\Omega)\mathbf{a}^k\right) d\Gamma_k \end{aligned} \tag{21}$$

where $\mathbf{I}_\Omega$ matrix is obtained applying the *Divergence theorem*:

$$\int_\Omega \frac{\partial \psi}{\partial x_i} dv = \oint_\Gamma n_i \psi ds \tag{22}$$

being n_i the components of the normal $\hat{n}$ to the boundary along the direction i. After integration by parts and the substitution of CUF, the governing equations and boundary conditions for the shell in the mechanical case are obtained:

$$\sum_{k=1}^{NL}\Bigg\{\int_{\Omega_k}\int_{A_k}\Big\{\delta\boldsymbol{u}_s^{kT}\Big[(-\boldsymbol{D}_p+\boldsymbol{A}_p)^T F_s\Big(\boldsymbol{C}_{pp}^k(\boldsymbol{D}_p+\boldsymbol{A}_p)F_\tau\boldsymbol{u}_\tau^k+\boldsymbol{C}_{pn}^k(\boldsymbol{D}_{n\Omega}+\boldsymbol{D}_{nz}-\boldsymbol{A}_n)F_\tau\boldsymbol{u}_\tau^k\Big)\Big]+\delta\boldsymbol{u}_s^{kT}\Big[(-\boldsymbol{D}_{n\Omega}+\boldsymbol{D}_{nz}-\boldsymbol{A}_n)^T F_s\Big(\boldsymbol{C}_{np}^k(\boldsymbol{D}_p+\boldsymbol{A}_p)F_\tau\boldsymbol{u}_\tau^k$$

$$+\boldsymbol{C}_{nn}^k(\boldsymbol{D}_{n\Omega}+\boldsymbol{D}_{nz}-\boldsymbol{A}_n)F_\tau\boldsymbol{u}_\tau^k\Big)\Big]\Big\}d\Omega_k dz_k\Bigg\}+\sum_{k=1}^{NL}\Bigg\{\int_{\Gamma_k}\int_{A_k}\Big\{\delta\boldsymbol{u}_s^{kT}\Big[\boldsymbol{I}_p^T F_s\Big(\boldsymbol{C}_{pp}^k(\boldsymbol{D}_p+\boldsymbol{A}_p)F_\tau\boldsymbol{u}_\tau^k+\boldsymbol{C}_{pn}^k(\boldsymbol{D}_{n\Omega}+\boldsymbol{D}_{nz}-\boldsymbol{A}_n)F_\tau\boldsymbol{u}_\tau^k\Big)\Big]$$

$$+\delta\boldsymbol{u}_s^{kT}\Big[\boldsymbol{I}_{np}^T F_s\Big(\boldsymbol{C}_{np}^k(\boldsymbol{D}_p-\boldsymbol{A}_p)F_\tau\boldsymbol{u}_\tau^k+\boldsymbol{C}_{nn}^k(\boldsymbol{D}_{n\Omega}+\boldsymbol{D}_{nz}-\boldsymbol{A}_n)F_\tau\boldsymbol{u}_\tau^k\Big)\Big]\Big\}d\Gamma_k dz_k\Bigg\}=\sum_{k=1}^{NL}\Bigg\{\int_{\Omega_k}\delta\boldsymbol{u}_s^{kT}F_s\boldsymbol{p}_u^k\Bigg\}. \tag{23}$$

where $\boldsymbol{I}_p^k$ and $\boldsymbol{I}_{np}^k$ depend on the boundary geometry:

$$\boldsymbol{I}_p=\begin{bmatrix}\frac{n_\alpha}{H_\alpha} & 0 & 0\\ 0 & \frac{n_\beta}{H_\beta} & 0\\ \frac{n_\beta}{H_\beta} & \frac{n_\alpha}{H_\alpha} & 0\end{bmatrix};\boldsymbol{I}_{np}=\begin{bmatrix}0 & 0 & \frac{n_\alpha}{H_\alpha}\\ 0 & 0 & \frac{n_\beta}{H_\beta}\\ 0 & 0 & 0\end{bmatrix};. \tag{24}$$

The normal to the boundary of domain Ω is:

$$\hat{\boldsymbol{n}}=\begin{bmatrix}n_\alpha\\ n_\beta\end{bmatrix}=\begin{bmatrix}cos(\varphi_\alpha)\\ cos(\varphi_\beta)\end{bmatrix} \tag{25}$$

where φ_α and φ_β are the angles between the normal $\hat{\boldsymbol{n}}$ and the direction α and β respectively.

The governing equations for a multi-layered shell subjected to mechanical loadings are:

$$\delta\boldsymbol{u}_s^{kT}:\ \ \mathbf{K}_{uu}^{k\tau s}\boldsymbol{u}_\tau^k=\mathbf{P}_{u\tau}^k \tag{26}$$

where the fundamental nucleus $\mathbf{K}_{uu}^{k\tau s}$ is obtained as:

$$\mathbf{K}_{uu}^{k\tau s}=\int_{A_k}\Big[[-\boldsymbol{D}_p+\boldsymbol{A}_p]^T\boldsymbol{C}_{pp}^k[\boldsymbol{D}_p+\boldsymbol{A}_p]+[-\boldsymbol{D}_p+\boldsymbol{A}_p]^T\boldsymbol{C}_{pn}^k[\boldsymbol{D}_{n\Omega}+\boldsymbol{D}_{nz}-\boldsymbol{A}_n]+[-\boldsymbol{D}_{n\Omega}+\boldsymbol{D}_{nz}-\boldsymbol{A}_n]^T\boldsymbol{C}_{np}^k[\boldsymbol{D}_p+\boldsymbol{A}_p]+[-\boldsymbol{D}_{n\Omega}+\boldsymbol{D}_{nz}-\boldsymbol{A}_n]^T\boldsymbol{C}_{nn}^k[\boldsymbol{D}_{n\Omega}+\boldsymbol{D}_{nz}-\boldsymbol{A}_n]\Big]F_\tau F_s H_\alpha^k H_\beta^k dz. \tag{27}$$

and the corresponding Neumann-type boundary conditions on Γ_k are:

$$\mathbf{\Pi}_d^{k\tau s}\,\boldsymbol{u}_\tau^k=\mathbf{\Pi}_d^{k\tau s}\,\overline{\boldsymbol{u}}_\tau^k, \tag{28}$$

where:

$$\mathbf{\Pi}_d^{k\tau s}=\int_{A_k}\Big[\boldsymbol{I}_p^T\boldsymbol{C}_{pp}^k[\boldsymbol{D}_p+\boldsymbol{A}_p^\tau]+\boldsymbol{I}_p^T\boldsymbol{C}_{pn}^k[\boldsymbol{D}_{n\Omega}+\boldsymbol{D}_{nz}-\boldsymbol{A}_n^\tau]+\boldsymbol{I}_{np}^T\boldsymbol{C}_{np}^k[\boldsymbol{D}_p+\boldsymbol{A}_p^\tau]+\boldsymbol{I}_{np}^T\boldsymbol{C}_{nn}^k[\boldsymbol{D}_{n\Omega}+\boldsymbol{D}_{nz}-\boldsymbol{A}_n^\tau]\Big]F_\tau F_s H_\alpha^k H_\beta^k dz. \tag{29}$$

and $\mathbf{P}_{u\tau}^k$ are variationally consistent loads with applied pressure.

2.4. Fundamental nuclei

The fundamental nucleo $\mathbf{K}_{uu}^{k\tau s}$ is reported for functionally graded doubly curved shells (radii of curvature in both α and β directions (see Fig. 1)):

$$\begin{aligned}
\left(\mathbf{K}_{uu}^{\tau sk}\right)_{11}&=-C_{11}^k J_{\beta/\alpha}^{k\tau s}\partial_\alpha^s\partial_\alpha^\tau-C_{44}^k J_{\alpha/\beta}^{k\tau s}\partial_\beta^s\partial_\beta^\tau+C_{44}^k\left(J_{\alpha\beta}^{k\tau_z s_z}-\frac{1}{R_{\alpha_k}}J_\beta^{k\tau_z s}-\frac{1}{R_{\alpha_k}}J_\beta^{k\tau s_z}+\frac{1}{R_{\alpha_k}^2}J_{\beta/\alpha}^{k\tau s}\right)\\
\left(\mathbf{K}_{uu}^{\tau sk}\right)_{12}&=-C_{12}^k J^{k\tau s}\partial_\alpha^\tau\partial_\beta^s-C_{44}^k J^{k\tau s}\partial_\alpha^s\partial_\beta^\tau\\
\left(\mathbf{K}_{uu}^{\tau sk}\right)_{13}&=-C_{11}^k\frac{1}{R_{\alpha_k}}J_{\beta/\alpha}^{k\tau s}\partial_\alpha^\tau-C_{12}^k\frac{1}{R_{\beta_k}}J^{k\tau s}\partial_\alpha^\tau-C_{12}^k J_\beta^{k\tau s_z}\partial_\alpha^\tau+C_{44}^k\left(J_\beta^{k\tau_z s}\partial_\alpha^s-\frac{1}{R_{\alpha_k}}J_{\beta/\alpha}^{k\tau s}\partial_\alpha^s\right)\\
\left(\mathbf{K}_{uu}^{\tau sk}\right)_{21}&=-C_{12}^k J^{k\tau s}\partial_\alpha^s\partial_\beta^\tau-C_{44}^k J^{k\tau s}\partial_\alpha^\tau\partial_\beta^s\\
\left(\mathbf{K}_{uu}^{\tau sk}\right)_{22}&=-C_{22}^k J_{\alpha/\beta}^{k\tau s}\partial_\beta^s\partial_\beta^\tau-C_{26}^k J^{k\tau s}\partial_\alpha^s\partial_\beta^\tau-C_{26}^k J^{k\tau s}\partial_\alpha^\tau\partial_\beta^s-C_{44}^k J_{\beta/\alpha}^{k\tau s}\partial_\alpha^s\partial_\alpha^\tau+C_{44}^k\left(J_{\alpha\beta}^{k\tau_z s_z}-\frac{1}{R_{\beta_k}}J_\alpha^{k\tau_z s}-\frac{1}{R_{\beta_k}}J_\alpha^{k\tau s_z}+\frac{1}{R_{\beta_k}^2}J_{\alpha/\beta}^{k\tau s}\right)\\
\left(\mathbf{K}_{uu}^{\tau sk}\right)_{23}&=-C_{12}^k\frac{1}{R_{\alpha_k}}J^{k\tau s}\partial_\beta^\tau-C_{22}^k\frac{1}{R_{\beta_k}}J_{\alpha/\beta}^{k\tau s}\partial_\beta^\tau-C_{12}^k J_\alpha^{k\tau s_z}\partial_\beta^\tau+C_{44}^k\left(J_\alpha^{k\tau_z s}\partial_\beta^s-\frac{1}{R_{\beta_k}}J_{\alpha/\beta}^{k\tau s}\partial_\beta^s\right)\\
\left(\mathbf{K}_{uu}^{\tau sk}\right)_{31}&=C_{11}^k\frac{1}{R_{\alpha_k}}J_{\beta/\alpha}^{k\tau s}\partial_\alpha^s+C_{12}^k\frac{1}{R_{\beta_k}}J^{k\tau s}\partial_\alpha^s+C_{12}^k J_\beta^{k\tau_z s}\partial_\alpha^s-C_{44}^k\left(J_\beta^{k\tau s_z}\partial_\alpha^\tau-\frac{1}{R_{\alpha_k}}J_{\beta/\alpha}^{k\tau s}\partial_\alpha^\tau\right)\\
\left(\mathbf{K}_{uu}^{\tau sk}\right)_{32}&=C_{12}^k\frac{1}{R_{\alpha_k}}J^{k\tau s}\partial_\beta^s+C_{22}^k\frac{1}{R_{\beta_k}}J_{\alpha/\beta}^{k\tau s}\partial_\beta^s+C_{12}^k J_\alpha^{k\tau_z s}\partial_\beta^s-C_{44}^k\left(J_\alpha^{k\tau s_z}\partial_\beta^\tau-\frac{1}{R_{\beta_k}}J_{\alpha/\beta}^{k\tau s}\partial_\beta^\tau\right)\\
\left(\mathbf{K}_{uu}^{\tau sk}\right)_{33}&=C_{11}^k\frac{1}{R_{\alpha_k}^2}J_{\beta/\alpha}^{k\tau s}+C_{22}^k\frac{1}{R_{\beta_k}^2}J_{\alpha/\beta}^{k\tau s}+C_{33}^k J_{\alpha\beta}^{k\tau_z s_z}+2C_{12}^k\frac{1}{R_{\alpha_k}}\frac{1}{R_{\beta_k}}J^{k\tau s}+C_{12}^k\frac{1}{R_{\alpha_k}}\left(J_\beta^{k\tau_z s}+J_\beta^{k\tau s_z}\right)\\
&\quad+C_{12}^k\frac{1}{R_{\beta_k}}\left(J_\alpha^{k\tau_z s}+J_\alpha^{k\tau s_z}\right)-C_{44}^k J_{\alpha/\beta}^{k\tau s}\partial_\beta^s\partial_\beta^\tau-C_{44}^k J_{\beta/\alpha}^{k\tau s}\partial_\alpha^s\partial_\alpha^\tau
\end{aligned} \tag{30}$$

where

$$\begin{aligned}
\left(J^{k\tau s}, J_\alpha^{k\tau s}, J_\beta^{k\tau s}, J_{\frac{\alpha}{\beta}}^{k\tau s}, J_{\frac{\beta}{\alpha}}^{k\tau s}, J_{\alpha\beta}^{k\tau s}\right) &= \int_{A_k} F_\tau F_s \left(1, H_\alpha, H_\beta, \frac{H_\alpha}{H_\beta}, \frac{H_\beta}{H_\alpha}, H_\alpha H_\beta\right) dz \\
\left(J^{k\tau_z s}, J_\alpha^{k\tau_z s}, J_\beta^{k\tau_z s}, J_{\frac{\alpha}{\beta}}^{k\tau_z s}, J_{\frac{\beta}{\alpha}}^{k\tau_z s}, J_{\alpha\beta}^{k\tau_z s}\right) &= \int_{A_k} \frac{\partial F_\tau}{\partial z} F_s \left(1, H_\alpha, H_\beta, \frac{H_\alpha}{H_\beta}, \frac{H_\beta}{H_\alpha}, H_\alpha H_\beta\right) dz \\
\left(J^{k\tau s_z}, J_\alpha^{k\tau s_z}, J_\beta^{k\tau s_z}, J_{\frac{\alpha}{\beta}}^{k\tau s_z}, J_{\frac{\beta}{\alpha}}^{k\tau s_z}, J_{\alpha\beta}^{k\tau s_z}\right) &= \int_{A_k} F_\tau \frac{\partial F_s}{\partial z} \left(1, H_\alpha, H_\beta, \frac{H_\alpha}{H_\beta}, \frac{H_\beta}{H_\alpha}, H_\alpha H_\beta\right) dz \\
\left(J^{k\tau_z s_z}, J_\alpha^{k\tau_z s_z}, J_\beta^{k\tau_z s_z}, J_{\frac{\alpha}{\beta}}^{k\tau_z s_z}, J_{\frac{\beta}{\alpha}}^{k\tau_z s_z}, J_{\alpha\beta}^{k\tau_z s_z}\right) &= \int_{A_k} \frac{\partial F_\tau}{\partial z} \frac{\partial F_s}{\partial z} \left(1, H_\alpha, H_\beta, \frac{H_\alpha}{H_\beta}, \frac{H_\beta}{H_\alpha}, H_\alpha H_\beta\right) dz
\end{aligned} \tag{31}$$

The application of boundary conditions makes use of the fundamental nucleo $\mathbf{\Pi}_d$ in the form:

$$\begin{aligned}
\left(\mathbf{\Pi}_{uu}^{\tau sk}\right)_{11} &= n_\alpha C_{11}^k J_{\beta/\alpha}^{k\tau s} \partial_\alpha^s + n_\beta C_{44}^k J_{\alpha/\beta}^{k\tau s} \partial_\beta^s \\
\left(\mathbf{\Pi}_{uu}^{\tau sk}\right)_{12} &= n_\alpha C_{12}^k J^{k\tau s} \partial_\beta^s + n_\beta C_{44}^k J^{k\tau s} \partial_\alpha^s \\
\left(\mathbf{\Pi}_{uu}^{\tau sk}\right)_{13} &= n_\alpha \frac{1}{R_{\alpha k}} C_{11}^k J_{\beta/\alpha}^{k\tau s} + n_\alpha \frac{1}{R_{\beta k}} C_{12}^k J^{k\tau s} + n_\alpha C_{12}^k J_\beta^{k\tau s_z} \\
\left(\mathbf{\Pi}_{uu}^{\tau sk}\right)_{21} &= n_\beta C_{12}^k J^{k\tau s} \partial_\alpha^s + n_\alpha C_{44}^k J^{k\tau s} \partial_\beta^s \\
\left(\mathbf{\Pi}_{uu}^{\tau sk}\right)_{22} &= n_\alpha C_{44}^k J_{\beta/\alpha}^{k\tau s} \partial_\alpha^s + n_\beta C_{22}^k J_{\alpha/\beta}^{k\tau s} \partial_\beta^s + n_\beta C_{26}^k J^{k\tau s} \partial_\alpha^s + n_\alpha C_{26}^k J^{k\tau s} \partial_\beta^s \\
\left(\mathbf{\Pi}_{uu}^{\tau sk}\right)_{23} &= n_\beta \frac{1}{R_{\alpha k}} C_{12}^k J^{k\tau s} + n_\beta \frac{1}{R_{\beta k}} C_{22}^k J_{\alpha/\beta}^{k\tau s} + n_\beta C_{12}^k J_\alpha^{k\tau s_z} \\
\left(\mathbf{\Pi}_{uu}^{\tau sk}\right)_{31} &= -n_\alpha \frac{1}{R_{\alpha k}} C_{44}^k J_{\beta/\alpha}^{k\tau s} + n_\alpha C_{44}^k J_\beta^{k\tau s_z} \\
\left(\mathbf{\Pi}_{uu}^{\tau sk}\right)_{32} &= -n_\beta \frac{1}{R_{\beta k}} C_{44}^k J_{\alpha/\beta}^{k\tau s} + n_\beta C_{44}^k J_\alpha^{k\tau s_z} \\
\left(\mathbf{\Pi}_{uu}^{\tau sk}\right)_{33} &= n_\alpha C_{44}^k J_{\beta/\alpha}^{k\tau s} \partial_\alpha^s + n_\beta C_{44}^k J_{\alpha/\beta}^{k\tau s} \partial_\beta^s
\end{aligned} \tag{32}$$

Note that all the equations written for the shell degenerate to those for the plate when $1/R_{\alpha k} = 1/R_{\beta k} = 0$. In practice, the radii of curvature are set to 10^9 for analysis of plates with the present formulation.

2.5. Dynamic governing equations

The PVD for the dynamic case is expressed as:

$$\begin{aligned}
&\sum_{k=1}^{NL} \int_{\Omega_k} \int_{A_k} \left\{\delta\epsilon_{pG}^{k\ T} \sigma_{pC}^k + \delta\epsilon_{nG}^k T \sigma_{nC}^k\right\} d\Omega_k dz \\
&= \sum_{k=1}^{NL} \int_{\Omega_k} \int_{A_k} \rho^k \delta\mathbf{u}^{kT} \ddot{\mathbf{u}}^k d\Omega_k dz + \sum_{k=1}^{NL} \delta L_e^k
\end{aligned} \tag{33}$$

where ρ^k is the mass density of the kth layer and double dots denote acceleration.

By substituting the geometrical relations and the constitutive equations, one obtains the following governing equations:

$$\delta\mathbf{u}_s^{k^T}: \quad \mathbf{K}_{uu}^{k\tau s} \mathbf{u}_\tau^k = \mathbf{M}^{k\tau s} \ddot{\mathbf{u}}_\tau^k + \mathbf{P}_{u\tau}^k \tag{34}$$

In the case of free vibrations one has:

$$\delta\mathbf{u}_s^{k^T}: \quad \mathbf{K}_{uu}^{k\tau s} \mathbf{u}_\tau^k = \mathbf{M}^{k\tau s} \ddot{\mathbf{u}}_\tau^k \tag{35}$$

where $\mathbf{M}^{k\tau s}$ is the fundamental nucleus for the inertial term, given by

$$\begin{aligned}
\mathbf{M}_{ij}^{k\tau s} &= \rho^k J_{\alpha\beta}^{k\tau s}, \quad i = j \\
\mathbf{M}_{ij}^{k\tau s} &= 0, \quad i \neq j
\end{aligned} \tag{36}$$

The meaning of the integral $J_{\alpha\beta}^{k\tau s}$ has been illustrated in Equation (31). The geometrical and mechanical boundary conditions are the same of the static case.

3. The radial basis function method for free vibration problems

Consider a linear elliptic partial differential operator $\mathcal{L}$ acting in a bounded region Ω in $\mathbb{R}^n$ and another operator $\mathcal{L}_B$ acting on a boundary $\partial\Omega$. The eigenproblem looks for eigenvalues (λ) and eigenvectors ($\mathbf{u}$) that satisfy

$$\mathcal{L}\mathbf{u} + \lambda\mathbf{u} = 0 \text{ in } \Omega \tag{37}$$

$$\mathcal{L}_B\mathbf{u} = 0 \text{ on } \partial\Omega \tag{38}$$

The eigenproblem defined in (37) and (38) will be replaced by a finite-dimensional eigenvalue problem, after the radial basis approximations.

The radial basis function (ϕ) approximation of a function ($\mathbf{u}$) is given by

$$\tilde{\mathbf{u}}(\mathbf{x}) = \sum_{i=1}^{N} \alpha_i \phi(\|x - y_i\|_2), \mathbf{x} \in \mathbb{R}^n \tag{39}$$

where $y_i, i = 1, .., N$ is a finite set of distinct points (centers) in $\mathbb{R}^n$.

Derivatives of $\tilde{\mathbf{u}}$ are computed as

$$\frac{\partial \tilde{\mathbf{u}}}{\partial x} = \sum_{j=1}^{N} \alpha_j \frac{\partial \phi_j}{\partial x} \tag{40}$$

$$\frac{\partial^2 \tilde{\mathbf{u}}}{\partial x^2} = \sum_{j=1}^{N} \alpha_j \frac{\partial^2 \phi_j}{\partial x^2}, \text{etc} \tag{41}$$

In the present collocation approach, one needs to impose essential and natural boundary conditions. Consider, for example, the condition $w = 0$, on a simply supported or clamped edge. The conditions are enforced by interpolating as

$$w = 0 \rightarrow \sum_{j=1}^{N} \alpha_j^W \phi_j = 0 \tag{42}$$

Other boundary conditions are interpolated in a similar way.
Examples of some common RBFs are

Cubic: $\phi(r) = r^3$
Thin plate splines: $\phi(r) = r^2 \log(r)$
Wendland functions: $\phi(r) = (1-r)_+^m p(r)$
Gaussian: $\phi(r) = e^{-(cr)^2}$
Multiquadrics: $\phi(r) = \sqrt{c^2 + r^2}$
Inverse Multiquadrics: $\phi(r) = (c^2 + r^2)^{-1/2}$

where the Euclidian distance r is real and non-negative and c is a positive shape parameter. Considering N distinct interpolations, and knowing $u(x_j), j = 1, 2, \ldots, N$, one finds α_i by the solution of a $N \times N$ linear system

$$\mathbf{A}\alpha = \mathbf{u} \tag{43}$$

where $\mathbf{A} = [\phi(\|x - y_i\|_2)]_{N \times N}$, $\alpha = [\alpha_1, \alpha_2, \ldots, \alpha_N]^T$ and $\mathbf{u} = [u(x_1), u(x_2), \ldots, u(x_N)]^T$.

The solution of the eigenproblem by radial basis functions considers N_I nodes in the interior of the domain and N_B nodes on the boundary, with a total number of nodes $N = N_I + N_B$. The interpolation points are denoted by $x_i \in \Omega$, $i = 1, \ldots, N_I$ and $x_i \in \partial\Omega$, $i = N_I + 1, \ldots, N$. At the points in the domain, the following eigenproblem is defined

$$\sum_{i=1}^{N} \alpha_i \mathcal{L}\phi(\|x - y_i\|_2) = \lambda \tilde{\mathbf{u}}(x_j), \ j = 1, 2, \ldots, N_I \tag{44}$$

or

$$\mathcal{L}^I \alpha = \lambda \tilde{\mathbf{u}}^I \tag{45}$$

where

$$\mathcal{L}^I = [\mathcal{L}\phi(\|x - y_i\|_2)]_{N_I \times N} \tag{46}$$

At the points on the boundary, the imposed boundary conditions are

$$\sum_{i=1}^{N} \alpha_i \mathcal{L}_B \phi(\|x - y_i\|_2) = 0, \ j = N_I + 1, \ldots, N \tag{47}$$

or

$$\mathbf{B}\alpha = 0 \tag{48}$$

where $\mathbf{B} = \mathcal{L}_B \phi[\|x_{N_I+1} - y_j\|_2]_{N_B \times N}$.

Therefore, one can write a finite-dimensional eigenvalue problem and solve Equations (45) and (48) as a generalized eigenvalue problem

$$\begin{bmatrix} \mathcal{L}^I \\ \mathbf{B} \end{bmatrix} \alpha = \lambda \begin{bmatrix} \mathbf{A}^I \\ 0 \end{bmatrix} \alpha \tag{49}$$

where

$$\mathbf{A}^I = \phi\left[\left(\left\| x_{N_I} - y_j \right\|_2\right)\right]_{N_I \times N}$$

For free vibration problems an harmonic solution is assumed for the displacements $u_0, u_1, v_0, v_1, \ldots$

$$\begin{aligned} u_0 &= U_0(x,y)e^{i\omega t};\ u_1 = U_1(x,y)e^{i\omega t};\ u_3 = U_3(x,y)e^{i\omega t} \\ v_0 &= V_0(x,y)e^{i\omega t};\ v_1 = V_1(x,y)e^{i\omega t};\ v_3 = V_3(x,y)e^{i\omega t} \\ w_0 &= W_0(x,y)e^{i\omega t};\ w_1 = W_1(x,y)e^{i\omega t};\ w_2 = W_2(x,y)e^{i\omega t} \end{aligned} \tag{50}$$

where ω is the frequency of natural vibration. Substituting the harmonic expansion into Equation (49) in terms of the amplitudes U_0, U_1, U_3, V_0, V_1, V_3, W_0, W_1, W_2, one can obtain the natural frequencies and vibration modes for the plate or shell problem, by solving the eigenproblem

$$\left[\mathcal{L} - \omega^2 \mathcal{G}\right]\mathbf{X} = 0 \tag{51}$$

where $\mathcal{L}$ collects all stiffness terms and $\mathcal{G}$ collects all terms related to the inertial terms. In (51) $\mathbf{X}$ are the modes of vibration associated with the natural frequencies defined as ω.

4. Numerical results

In this section the higher-order shear deformation theory is combined with radial basis functions collocation for the free vibration analysis of functionally graded shell panels. Examples include spherical ($R_x = R_y = R$) as well as cylindrical ($R_x = R$ and $R_y = \infty$) shell panels with all edges clamped (CCCC) or simply supported (SSSS). Particular cases of these are also considered: isotropic materials (fully ceramic, $p = 0$, and fully metal, $p = \infty$) and plates ($R_x = R_y = \infty$). To study the effect of $\epsilon_{zz} \neq 0$ in these problems, the case $\epsilon_{zz} = 0$ is implemented by considering $w = w_0$ instead (3).

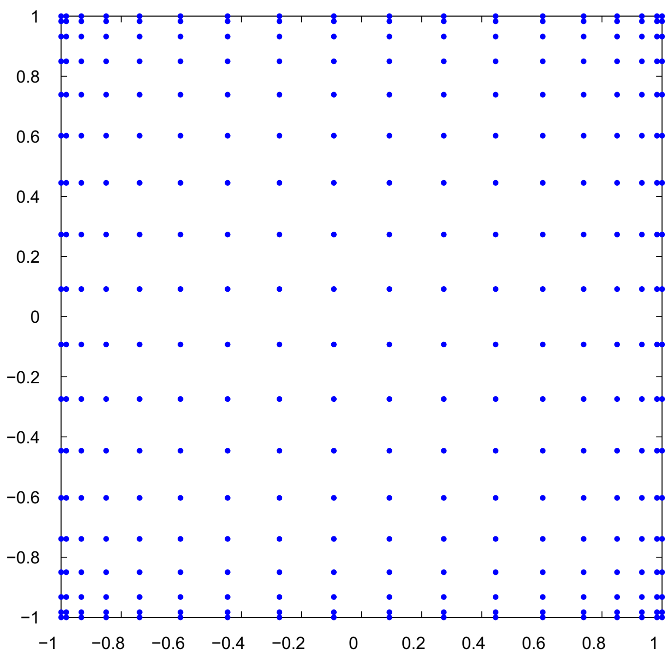

Fig. 2. A sketch of a Chebyshev grid for 17^2 points.

Table 1
Initial study. Square CCCC FG cylindrical panel, Si_3N_4 and SUS304, $a/h = 10$, $a/R = 0.1$, $p = 0.2$.

Grid	13^2	17^2	19^2	21^2
1st	60.3483	60.3431	60.3499	60.3479
2nd	115.2450	115.2134	115.2315	115.2044
3rd	115.3917	115.3665	115.3755	115.3347
4th	162.1741	162.0337	162.0727	162.0860

Results are compared with those from Pradyumna and Bandyopadhyay (2008), who used finite elements formulation and a HSDT disregarding through-the-thickness deformations.

The following material properties are used:

$$\text{silicon nitride } (Si_3N_4): \quad E_c = 322.2715\text{ GPa},\ \nu_c = 0.24,\ \rho_c = 2370\text{ Kg/m}^3 \tag{52}$$

$$\text{stainless steel (SUS304)}: \quad E_m = 207.7877\text{ GPa},\ \nu_m = 0.31776,\ \rho_m = 8166\text{ Kg/m}^3 \tag{53}$$

$$\text{aluminum}: \quad E_m = 70\text{ GPa},\ \nu_m = 0.3,\ \rho_m = 2707\text{ Kg/m}^3 \tag{54}$$

$$\text{alumina}: \quad E_c = 380\text{ GPa},\ \nu_c = 0.3,\ \rho_c = 3000\text{ Kg/m}^3 \tag{55}$$

The non-dimensional frequency is given as

$$\overline{w} = wa^2\sqrt{\frac{\rho_m h}{D}} \text{ where } D = \frac{E_m h^3}{12(1-\nu_m^2)}. \tag{56}$$

In all numerical examples a Chebyshev grid is employed (see Fig. 2) and the Wendland function defined as

$$\phi(r) = (1-cr)_+^8\left(32(cr)^3+25(cr)^2+8cr+1\right) \tag{57}$$

Here, the shape parameter (c) is obtained by an optimization procedure, as detailed in Ferreira and Fasshauer (2006).

An initial study was performed to show the convergence of the present approach and select the number of points to use in the computation of the vibration problems. Results are presented in Table 1 and refer to the first four vibration modes of a clamped functionally graded cylindrical shell panel composed of silicon nitride (52) and stainless steel (53), with side-to-thickness ratio $a/h = 10$, side-to-radius ratio $a/R = 0.1$, power law exponent $p = 0.2$, and $a = b = 2$. A 17^2 grid was chosen for the following vibration problems.

4.1. Clamped functionally graded cylindrical shell panel

The free vibration of clamped FG cylindrical shell panels is analyzed.

In Table 2 the first 4 vibration modes of a square clamped FG cylindrical shell panel with constituents silicon nitride (52) and stainless steel (53), side-to-thickness ratio $a/h = 10$, side-to-radius ratio $a/R = 0.1$, and several power law exponents p are presented. Results are compared with Pradyumna and Bandyopadhyay (2008) and those from Yang and Shen (2003), with the differential quadrature approximation and Galerkin technique, both neglecting through-the-thickness deformations.

In Fig. 3 the first 4 modes of a CCCC square FG cylindrical shell panel, with constituents silicon nitride and stainless steel, ratios $a/h = 10$ and $R/a = 10$, and power law exponent $p = 0.2$ are presented.

The fundamental frequency of square clamped FG cylindrical shell panels composed of aluminum (54) and alumina (55), with side-to-radius ratio $a/R = 0.1$, various side-to-thickness ratios a/h and power law exponents p are presented in Table 3.

The results of the present approach in Tables 2 and 3 compare well with references. The combination of present HSDT and the meshless technique based on collocation with radial basis function shows very good accuracy in the free vibration analysis of FG shells.

In Table 4 the fundamental frequency of square clamped FG cylindrical shell panels composed of aluminum (54) and alumina (55), with side-to-thickness ratios $a/h = 10$, are presented considering various side-to-radius ratio a/R, and power law exponents p.

4.2. Simply supported functionally graded cylindrical shell panel

The free vibration of simply supported FG cylindrical shell panels is now analyzed.

Table 5 presents the fundamental frequency of a square simply supported FG cylindrical shell panel with constituents aluminum (54) and alumina (55), length-to-thickness ratio $a/h = 10$, and several length-to-radius ratio a/R and several power law exponents p as well.

In Fig. 4 the relationships between fundamental frequency and the radius-to-length ratio R/a is visualized for various power law exponents p. It refers to the square simply supported FG cylindrical shell panel composed from aluminum (54) and alumina

Table 2
First 4 modes of a CCCC square FG cylindrical shell panel, Si_3N_4 and SUS304, $a/h = 10$, $a/R = 0.1$, for several p.

Mode	Source	$p = 0$ (Si_3N_4)	$p = 0.2$	$p = 2$	$p = 10$	$p = \infty$ (SUS304)
1	Ref. (Pradyumna and Bandyopadhyay, 2008)	72.9613	60.0269	39.1457	33.3666	32.0274
	Ref. (Yang and Shen, 2003)	74.518	57.479	40.750	35.852	32.761
	Present $\epsilon_{zz} = 0$	74.2634	60.0061	40.5259	35.1663	32.6108
	Present $\epsilon_{zz} \neq 0$	74.5821	60.3431	40.8262	35.4229	32.8593
2	Ref. (Pradyumna and Bandyopadhyay, 2008)	138.5552	113.8806	74.2915	63.2869	60.5546
	Ref. (Yang and Shen, 2003)	144.663	111.717	78.817	69.075	63.314
	Present $\epsilon_{zz} = 0$	141.6779	114.3788	76.9725	66.6482	61.9329
	Present $\epsilon_{zz} \neq 0$	142.4281	115.2134	77.6639	67.1883	62.4886
3	Ref. (Pradyumna and Bandyopadhyay, 2008)	138.5552	114.0266	74.3868	63.3668	60.6302
	Ref. (Yang and Shen, 2003)	145.740	112.531	79.407	69.609	63.806
	Present $\epsilon_{zz} = 0$	141.8485	114.5495	77.0818	66.7332	62.0082
	Present $\epsilon_{zz} \neq 0$	142.6024	115.3665	77.7541	67.2689	62.5668
4	Ref. (Pradyumna and Bandyopadhyay, 2008)	195.5366	160.6235	104.7687	89.1970	85.1788
	Ref. (Yang and Shen, 2003)	206.992	159.855	112.457	98.386	90.370
	Present $\epsilon_{zz} = 0$	199.1566	160.7355	107.9484	93.3350	86.8160
	Present $\epsilon_{zz} \neq 0$	200.3158	162.0337	108.9677	94.0923	87.6341

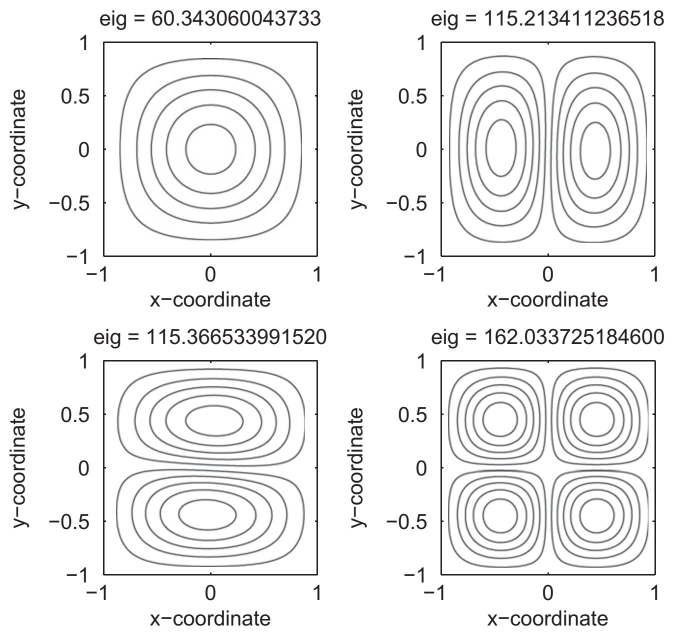

Fig. 3. First 4 modes of a CCCC square FG cylindrical shell panel, Si_3N_4 and SUS304, $a/h = 10$, $a/R = 0.1$, $p = 0.2$.

(55), with side-to-thickness ratio $a/h = 10$. The graphic on the left was obtained from tabulated values on Table 5 and the right one is more detailed for values of p smaller or equal than 5 ($p = 0.5$, 1, 2, 3, 4, 5).

4.3. Clamped functionally graded spherical shell panel

We now study the free vibration of clamped FG spherical shell panels.

The fundamental frequency of a square clamped FG spherical shell panel with constituents aluminum (54) and alumina (55), and side-to-thickness ratio $a/h = 10$, considering various side-to-radius ratios a/R, and several power law exponents p are presented in Table 6.

4.4. Simply supported functionally graded spherical shell panel

This example considers the free vibration of simply supported FG spherical shell panels.

The fundamental frequency of a square simply supported FG spherical shell panel composed of aluminum (54) and alumina (55), with side-to-thickness ratio $a/h = 10$, are presented in Table 7 considering various side-to-radius ratios a/R as well power law exponents p.

4.5. Discussion

All results presented in Tables 2–7 are in excellent agreement with references considered. Exceptions are $p = 10$ and $R/a = 5$, 10, 50 for the SSSS panels where the maximum difference is 26%, and $p = 2$, 10 and $R/a = 5$, 10, 50 for the CCCC panels where the maximum difference is 33%. The authors did not find any explanation for these exceptions. In all other cases the maximum difference is 7%. The relative errors here presented were evaluated as (present value − reference value/reference value) × 100.

A detailed analysis of previous tables lead us to the following conclusions:

- **Boundary conditions:** Clamped FG shell panels present higher frequency values than simply supported ones.
- **Geometry:** Lower radii of curvature values present higher frequency values, i.e., the fundamental frequency decreases as the ratio R/a increases.
- **Material properties:** The fundamental frequency of FG shell panels decreases as the exponent p in power-law increases.

Another conclusion from all tables, as easily seen in Fig. 4, is that the fundamental frequency decreases as the radius of curvature increases. The fall-off is faster for smaller values of R (R/a) and then shows fast convergence.

In all studied cases the $\epsilon_{zz} = 0$ approach gives lower values than the $\epsilon_{zz} \neq 0$ one suggesting a small impact on the fundamental frequency over the range of parameters used in the study. The effect of the ϵ_{zz} approach shows higher significance in thicker shells (see Table 2) and seems independent of the radius of curvature (see Tables 4–7).

5. Concluding remarks

For the first time, Carrera's Unified Formulation was combined with the radial basis functions collocation technique for the free vibration analysis of functionally graded shells. A higher-order shear deformation theory that allows extensibility in the thickness direction was implemented and the effect of $\epsilon_{zz} \neq 0$ was studied.

Numerical results were compared with other sources and the present approach demonstrated to be successful in the free vibration analysis of functionally graded shells and easy to implement.

This paper deals only with shells with constant curvature radius. In the future further studies on structures with arbitrary geometry are to be done.

Table 3
Fundamental frequencies of CCCC square FG cylindrical shell panels composed of aluminum and alumina, $R/a = 0.1$, for various a/h and p.

p	Source	$a/h = 5$	$a/h = 10$	$a/h = 15$	$a/h = 20$	$a/h = 50$	$a/h = 100$
0	FSDT	56.5548	70.8035	75.7838	77.5654	85.4346	103.4855
	Ref. (Pradyumna and Bandyopadhyay, 2008)	58.2858	71.7395	75.0439	77.0246	84.8800	102.9227
	Present $\epsilon_{zz} = 0$	59.0433	72.3272	76.4904	78.4918	85.6073	102.3351
	Present $\epsilon_{zz} \neq 0$	59.7741	72.8141	76.8148	78.7342	85.7713	102.7871
0.5	FSDT	47.2468	57.7597	62.2838	63.8393	70.3199	87.1049
	Ref. (Pradyumna and Bandyopadhyay, 2008)	48.7185	58.5305	61.5835	63.1381	69.8604	86.5452
	Present $\epsilon_{zz} = 0$	49.3050	59.5188	62.6780	64.2371	70.4237	85.4780
	Present $\epsilon_{zz} \neq 0$	49.9508	59.9353	62.9544	64.4438	70.5664	85.9029
1	FSDT	42.0305	51.0884	55.4209	56.7991	62.8458	77.7762
	Ref. (Pradyumna and Bandyopadhyay, 2008)	43.4243	52.0173	54.7015	56.0880	62.2152	77.0774
	Present $\epsilon_{zz} = 0$	43.9548	52.8776	55.6437	57.0255	62.7088	76.6386
	Present $\epsilon_{zz} \neq 0$	44.5754	53.2759	55.9081	57.2226	62.8414	77.0381

Table 4
Fundamental frequencies of CCCC square FG cylindrical shell panels composed of aluminum and alumina, $a/h = 10$, for various R/a and p.

p	Source	$R/a = 0.5$	$R/a = 1$	$R/a = 5$	$R/a = 10$	$R/a = 50$	Plate
0	Ref. (Pradyumna and Bandyopadhyay, 2008)	129.9808	94.4973	71.8861	71.0394	70.7660	70.7546
	Present $\epsilon_{zz} = 0$	133.6037	95.5849	73.1640	72.3304	72.0614	72.0502
	Present $\epsilon_{zz} \neq 0$	134.5056	96.0131	73.6436	72.8141	72.5465	72.5353
0.2	Ref. (Pradyumna and Bandyopadhyay, 2008)	119.6109	87.3930	68.1152	67.3320	67.0801	67.0698
	Present $\epsilon_{zz} = 0$	121.8612	87.8148	66.6620	65.8808	65.6371	65.6299
	Present $\epsilon_{zz} \neq 0$	122.7375	88.1659	67.1004	66.3235	66.0814	66.0743
0.5	Ref. (Pradyumna and Bandyopadhyay, 2008)	108.1546	79.5689	63.1896	62.4687	62.2380	62.2291
	Present $\epsilon_{zz} = 0$	110.2017	80.0146	60.2477	59.5215	59.3022	59.2985
	Present $\epsilon_{zz} \neq 0$	111.0739	80.3049	60.6568	59.9353	59.7178	59.7142
1	Ref. (Pradyumna and Bandyopadhyay, 2008)	96.0666	71.2453	56.5546	55.8911	55.6799	55.6722
	Present $\epsilon_{zz} = 0$	97.9069	71.6716	53.5430	52.8800	52.6864	52.6856
	Present $\epsilon_{zz} \neq 0$	98.7955	71.9167	53.9340	53.2759	53.0841	53.0835
2	Ref. (Pradyumna and Bandyopadhyay, 2008)	84.4431	62.9748	36.2487	35.6633	35.4745	35.4669
	Present $\epsilon_{zz} = 0$	86.3088	63.4398	47.5205	46.9447	46.7820	46.7835
	Present $\epsilon_{zz} \neq 0$	87.2271	63.6675	47.9060	47.3343	47.1726	47.1741
10	Ref. (Pradyumna and Bandyopadhyay, 2008)	69.8224	51.3803	33.6611	33.1474	32.9812	32.9743
	Present $\epsilon_{zz} = 0$	71.7634	52.0900	40.8099	40.4145	40.3028	40.3037
	Present $\epsilon_{zz} \neq 0$	72.3922	52.2780	41.0985	40.7046	40.5923	40.5929
∞	Ref. (Pradyumna and Bandyopadhyay, 2008)	61.0568	44.2962	32.4802	32.0976	31.9741	31.9689
	Present $\epsilon_{zz} = 0$	60.3660	43.1880	33.0576	32.6810	32.5594	32.5543
	Present $\epsilon_{zz} \neq 0$	60.7735	43.3815	33.2743	32.8995	32.7786	32.7735

Table 5
Fundamental frequencies of SSSS square FG cylindrical shell panels composed of aluminum and alumina, $a/h = 10$, for various R/a and p.

p	Source	$R/a = 0.5$	$R/a = 1$	$R/a = 5$	$R/a = 10$	$R/a = 50$	Plate
0	Ref. (Pradyumna and Bandyopadhyay, 2008)	68.8645	51.5216	42.2543	41.9080	41.7963	41.7917
	Present $\epsilon_{zz} = 0$	70.1594	52.1938	42.6701	42.3153	42.2008	42.1961
	Present $\epsilon_{zz} \neq 0$	69.9872	52.1101	42.7172	42.3684	42.2560	42.2513
0.2	Ref. (Pradyumna and Bandyopadhyay, 2008)	64.4001	47.5968	40.1621	39.8472	39.7465	39.7426
	Present $\epsilon_{zz} = 0$	65.3889	47.9338	38.7168	38.3840	38.2842	38.2827
	Present $\epsilon_{zz} \neq 0$	65.2100	47.8590	38.7646	38.4368	38.3384	38.3368
0.5	Ref. (Pradyumna and Bandyopadhyay, 2008)	59.4396	43.3019	37.2870	36.9995	36.9088	36.9057
	Present $\epsilon_{zz} = 0$	60.4255	43.6883	34.8768	34.5672	34.4809	34.4820
	Present $\epsilon_{zz} \neq 0$	60.2422	43.6239	34.9273	34.6219	34.5365	34.5376
1	Ref. (Pradyumna and Bandyopadhyay, 2008)	53.9296	38.7715	33.2268	32.9585	32.8750	32.8726
	Present $\epsilon_{zz} = 0$	54.8909	39.1753	30.9306	30.6485	30.5759	30.5792
	Present $\epsilon_{zz} \neq 0$	54.7074	39.1246	30.9865	30.7077	30.6355	30.6386
2	Ref. (Pradyumna and Bandyopadhyay, 2008)	47.8259	34.3338	27.4449	27.1789	27.0961	27.0937
	Present $\epsilon_{zz} = 0$	48.7807	34.7654	27.5362	27.2979	27.2423	27.2472
	Present $\epsilon_{zz} \neq 0$	48.6005	34.7289	27.5977	27.3616	27.3055	27.3102
10	Ref. (Pradyumna and Bandyopadhyay, 2008)	37.2593	28.2757	19.3892	19.1562	19.0809	19.0778
	Present $\epsilon_{zz} = 0$	38.2792	28.8072	24.2472	24.1063	24.0762	24.0802
	Present $\epsilon_{zz} \neq 0$	38.1172	28.7611	24.2839	24.1444	24.1125	24.1171
∞	Ref. (Pradyumna and Bandyopadhyay, 2008)	31.9866	24.1988	19.0917	18.9352	18.8848	18.8827
	Present $\epsilon_{zz} = 0$	31.7000	23.5827	19.2796	19.1193	19.0675	19.0654
	Present $\epsilon_{zz} \neq 0$	31.6222	23.5448	19.3008	19.1433	19.0924	19.0903

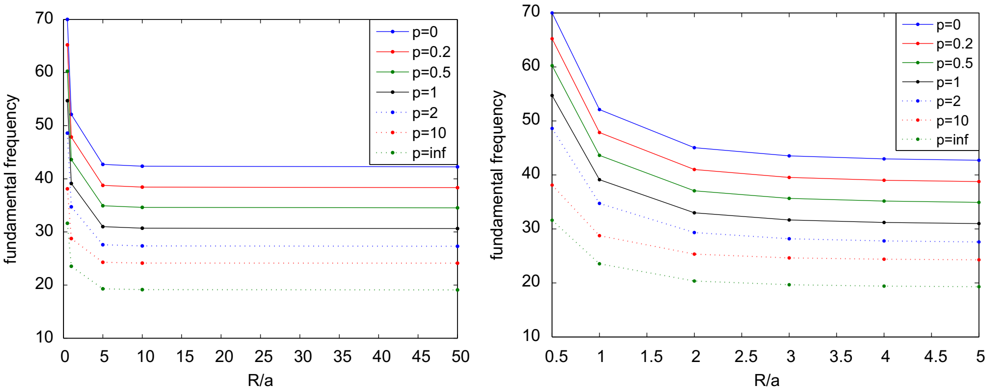

Fig. 4. Fundamental frequency as a function of the radius-to-length ratio for several p.

Table 6
Fundamental frequencies of CCCC square FG spherical shell panels composed of aluminum and alumina, $a/h = 10$, for various R/a and p.

p	Source	$R/a = 0.5$	$R/a = 1$	$R/a = 5$	$R/a = 10$	$R/a = 50$	Plate
0	Ref. (Pradyumna and Bandyopadhyay, 2008)	173.9595	120.9210	73.5550	71.4659	70.7832	70.7546
	Present $\epsilon_{zz} = 0$	176.8125	122.0934	74.8207	72.7536	72.0784	72.0502
	Present $\epsilon_{zz} \neq 0$	176.8356	122.3533	75.2810	73.2322	72.5633	72.5353
0.2	Ref. (Pradyumna and Bandyopadhyay, 2008)	161.3704	112.2017	69.6597	67.7257	67.0956	67.0698
	Present $\epsilon_{zz} = 0$	163.0852	112.7143	68.2142	66.2686	65.6498	65.6299
	Present $\epsilon_{zz} \neq 0$	163.0460	112.8132	68.6329	66.7063	66.0938	66.0743
0.5	Ref. (Pradyumna and Bandyopadhyay, 2008)	147.4598	102.5983	64.6114	62.8299	62.2519	62.2291
	Present $\epsilon_{zz} = 0$	149.0931	103.1804	61.6902	59.8745	59.3112	59.2985
	Present $\epsilon_{zz} \neq 0$	149.0095	103.1490	62.0789	60.2831	59.7265	59.7142
1	Ref. (Pradyumna and Bandyopadhyay, 2008)	132.3396	92.2147	57.8619	56.2222	55.6923	55.6722
	Present $\epsilon_{zz} = 0$	133.8751	92.8282	54.8597	53.1956	52.6921	52.6856
	Present $\epsilon_{zz} \neq 0$	133.7710	92.6962	55.2302	53.5864	53.0895	53.0835
2	Ref. (Pradyumna and Bandyopadhyay, 2008)	116.4386	81.3963	37.3914	35.9568	35.4861	35.4669
	Present $\epsilon_{zz} = 0$	118.0167	82.0948	48.6656	47.2135	46.7849	46.7835
	Present $\epsilon_{zz} \neq 0$	117.9317	81.9179	49.0328	47.5990	47.1754	47.1741
10	Ref. (Pradyumna and Bandyopadhyay, 2008)	92.1387	64.8773	34.6658	33.4057	32.9916	32.9743
	Present $\epsilon_{zz} = 0$	93.9111	65.8103	41.6016	40.5998	40.3049	40.3037
	Present $\epsilon_{zz} \neq 0$	93.8398	65.7018	41.8796	40.8883	40.5946	40.5929
∞	Ref. (Pradyumna and Bandyopadhyay, 2008)	80.7722	56.2999	33.2343	32.2904	31.9819	31.9689
	Present $\epsilon_{zz} = 0$	79.8889	55.1653	33.8061	32.8722	32.5671	32.5543
	Present $\epsilon_{zz} \neq 0$	79.8994	55.2827	34.0141	33.0884	32.7862	32.7735

Table 7
Fundamental frequencies of SSSS square FG spherical shell panels composed of aluminum and alumina, $a/h = 10$, for various R/a and p.

p	Source	$R/a = 0.5$	$R/a = 1$	$R/a = 5$	$R/a = 10$	$R/a = 50$	Plate
0	Ref. (Pradyumna and Bandyopadhyay, 2008)	124.1581	78.2306	44.0073	42.3579	41.8145	41.7917
	Present $\epsilon_{zz} = 0$	126.2994	79.2626	44.4455	42.7709	42.2192	42.1961
	Present $\epsilon_{zz} \neq 0$	126.0882	79.0008	44.4697	42.8180	42.2741	42.2513
0.2	Ref. (Pradyumna and Bandyopadhyay, 2008)	115.7499	72.6343	41.7782	40.2608	39.7629	39.7426
	Present $\epsilon_{zz} = 0$	117.3053	73.2663	40.3936	38.8074	38.2988	38.2827
	Present $\epsilon_{zz} \neq 0$	117.0197	73.0034	40.4211	38.8551	38.3528	38.3368
0.5	Ref. (Pradyumna and Bandyopadhyay, 2008)	106.5014	66.5025	38.7731	37.3785	36.9234	36.9057
	Present $\epsilon_{zz} = 0$	108.0044	67.1623	36.4453	34.9574	34.4922	34.4820
	Present $\epsilon_{zz} \neq 0$	107.6572	66.9033	36.4782	35.0080	34.5478	34.5376
1	Ref. (Pradyumna and Bandyopadhyay, 2008)	96.2587	59.8521	34.6004	33.3080	32.8881	32.8726
	Present $\epsilon_{zz} = 0$	97.6938	60.5121	32.3691	31.0012	30.5840	30.5792
	Present $\epsilon_{zz} \neq 0$	97.2968	60.2636	32.4101	31.0572	30.6437	30.6386
2	Ref. (Pradyumna and Bandyopadhyay, 2008)	84.8206	52.7875	28.7459	27.5110	27.1085	27.0937
	Present $\epsilon_{zz} = 0$	86.2288	53.4659	28.7833	27.5984	27.2474	27.2472
	Present $\epsilon_{zz} \neq 0$	85.8028	53.2311	28.8329	27.6602	27.3109	27.3102
10	Ref. (Pradyumna and Bandyopadhyay, 2008)	65.2296	41.6702	20.4691	19.4357	19.0922	19.0778
	Present $\epsilon_{zz} = 0$	66.7088	42.4365	25.0772	24.3034	24.0791	24.0802
	Present $\epsilon_{zz} \neq 0$	66.3594	42.2155	25.1038	24.3401	24.1168	24.1171
∞	Ref. (Pradyumna and Bandyopadhyay, 2008)	57.2005	36.2904	19.8838	19.1385	18.8930	18.8827
	Present $\epsilon_{zz} = 0$	57.0657	35.8131	20.0818	19.3251	19.0759	19.0654
	Present $\epsilon_{zz} \neq 0$	56.9702	35.6948	20.0927	19.3464	19.1006	19.0903

Acknowledgment

The first author is grateful for the grant SFRH/BD/45554/2008 assured by FCT.

References

Bever, M.B., Duwez, P.E., 1972. Gradients in composite materials. Materials Science and Engineering 10 (0), 1–8.
Birman, Victor, Byrd, Larry W., 2007. Modeling and analysis of functionally graded materials and structures. Applied Mechanics Reviews 60 (5), 195–216.
Carrera, E., 2001. Developments, ideas, and evaluations based upon reissner's mixed variational theorem in the modelling of multilayered plates and shells. Applied Mechanics Reviews 54, 301–329.
Carrera, E., 2003. Theories and finite elements for multilayered plates and shells: a unified compact formulation with numerical assessment and benchmarking. Archives of Computational Methods in Engineering 10, 215–296.
Carrera, E., 2004. On the use of murakami's zig-zag function in the modeling of layered plates and shells. Computers & Structures 82, 541–554.
Carrera, E., Brischetto, S., 2008. Analysis of thickness locking in classical, refined and mixed theories for layered shells. Composite Structures 85, 83–90.
Chapelle, D., Bathe, K.-J., 2003. The Finite Element Analysis of Shells.-Fundamentals. Springer, Berlin.
Chen, X.L., Liu, G.R., Lim, S.P., 2003. An element free galerkin method for the free vibration analysis of composite laminates of complicated shape. Composite Structures 59, 279–289.
Dai, K.Y., Liu, G.R., Lim, S.P., Chen, X.L., 2004. An element free galerkin method for static and free vibration analysis of shear-deformable laminated composite plates. Journal of Sound and Vibration 269, 633–652.
Ferrante, F.J., Graham-Brady, L.L., 2005. Stochastic simulation of non-gaussian/non-stationary properties in a functionally graded plate. Computer Methods in Applied Mechanics and Engineering 194 (12–16), 1675–1692.
Ferreira, A.J.M., 2003a. A formulation of the multiquadric radial basis function method for the analysis of laminated composite plates. Composite Structures 59, 385–392.
Ferreira, A.J.M., 2003b. Thick composite beam analysis using a global meshless approximation based on radial basis functions. Mechanics of Advanced Materials and Structures 10, 271–284.
Ferreira, A.J.M., Fasshauer, G.E., 2006. Computation of natural frequencies of shear deformable beams and plates by a rbf-pseudospectral method. Computer Methods in Applied Mechanics and Engineering 196, 134–146.
Ferreira, A.J.M., Roque, C.M.C., Martins, P.A.L.S., 2003. Analysis of composite plates using higher-order shear deformation theory and a finite point formulation based on the multiquadric radial basis function method. Composites: Part B 34, 627–636.
Ferreira, A.J.A., Roque, C.M.C., Jorge, R.M.N., 2006. Analysis of composite and sandwich plate by trigonometric layer-wise deformation theory and radial basis function. Journal of Sandwich Structures and Materials 8, 497–515.

Ferreira, A.J.M., Roque, C.M.C., Carrera, E., Cinefra, M., Polit, O., 2011a. Radial basis functions collocation and a unified formulation for bending, vibration and buckling analysis of laminated plates, according to a variation of murakamiâ's zig-zag theory. European Journal of Mechanics – A/Solids 30 (4), 559–570.
Ferreira, A.J.M., Roque, C.M.C., Carrera, E., Cinefra, M., 2011b. Analysis of thick isotropic and cross-ply laminated plates by radial basis functions and a unified formulation. Journal of Sound and Vibration 330 (4), 771–787.
Ferreira, AJ.M., Roque, CM.C., Carrera, E., Cinefra, M., Polit, O., 2011c. Two higher order zig-zag theories for the accurate analysis of bending, vibration and buckling response of laminated plates by radial basis functions collocation and a unified formulation. Journal of Composite Materials.
Ferreira, A., Carrera, E., Cinefra, M., Roque, C., 2011d. Analysis of laminated doubly-curved shells by a layerwise theory and radial basis functions collocation, accounting for through-the-thickness deformations. Computational Mechanics 48 (13–25). doi:10.1007/s00466-011-0579-4.
Ferreira, A.J.M., Carrera, E., Cinefra, M., Roque, C.M.C., Polit, O., 2011e. Analysis of laminated shells by a sinusoidal shear deformation theory and radial basis functions collocation, accounting for through-the-thickness deformations. Composites Part B: Engineering 42 (5), 1276–1284.
Flügge, W., 1960. Stresses in Shells, second ed. Springer, Berlin.
Hon, Y.C., Lu, M.W., Xue, W.M., Zhu, Y.M., 1997. Multiquadric method for the numerical solution of byphasic mixture model. Applied Mathematics and Computation 88, 153–175.
Hon, Y.C., Cheung, K.F., Mao, X.Z., Kansa, E.J., 1999. A multiquadric solution for the shallow water equation. ASCE Journal of Hydraulic Engineering 125 (5), 524–533.
Huang, Y.Q., Li, Q.S., 2004. Bending and buckling analysis of antisymmetric laminates using the moving least square differential quadrature method. Computer Methods in Applied Mechanics and Engineering 193, 3471–3492.
Kansa, E.J., 1990. Multiquadrics- a scattered data approximation scheme with applications to computational fluid dynamics. I: surface approximations and partial derivative estimates. Computers and Mathematics with Applications 19 (8/9), 127–145.
Koizumi, M., 1997. Fgm activities in japan. Composites Part B: Engineering 28 (1–2), 1–4. Use of Composites Multi-Phased and Functionally Graded Materials.
Kröplin, B., D'Ottavio, M., Ballhause, D., Carrera, E., 2006. Closed-form solutions for the free-vibration problem of multilayered piezoelectric shells. Computers and Structures 84, 1506–1518.
Liew, K.M., Chen, X.L., Reddy, J.N., 2004. Mesh-free radial basis function method for buckling analysis of non-uniformity loaded arbitrarily shaped shear deformable plates. Computer Methods in Applied Mechanics and Engineering 193, 205–225.
Liu, G.R., Chen, X.L., 2002. Buckling of symmetrically laminated composite plates using the element-free galerkin method. International Journal of Structural Stability and Dynamics 2, 281–294.
Liu, G.R., Gu, Y.T., 2001. A local radial point interpolation method (lrpim) for free vibration analyses of 2-d solids. Journal of Sound and Vibration 246 (1), 29–46.
Liu, G.R., Wang, J.G., 2002. A point interpolation meshless method based on radial basis functions. International Journal for Numerical Methods in Engineering 54, 1623–1648.
Liu, L., Liu, G.R., Tan, V.C.B., 2002. Element free method for static and free vibration analysis of spatial thin shell structures. Computer Methods in Applied Mechanics and Engineering 191, 5923–5942.
Miyamoto, Y., Kaysser, W.A., Rabin, B.H., Kawasaki, A., Ford, R.G., 1999. Functionally Graded Materials: Design, Processing and Applications. Kluwer Academic Publishers.
Neves, A.M.A., Ferreira, A.J.M., Carrera, E., Roque, C.M.C., Cinefra, M., Jorge, R.M.N., Soares, C.M.M., 2011. Bending of fgm plates by a sinusoidal plate formulation and collocation with radial basis functions. Mechanics Research Communications 38 (5), 368–371.
Neves, A.M.A., Ferreira, A.J.M., Carrera, E., Roque, C.M.C., Cinefra, M., Jorge, R.M.N., Soares, C.M.M., 2012. A quasi-3D sinusoidal shear deformation theory for the static and free vibration analysis of functionally graded plates. Composites Part B: Engineering 43 (2), 711–725.
Nguyen, T.K., Sab, K., Bonnet, G., 2007. Shear correction factors for functionally graded plates. Mechanics of Advanced Materials and Structures 14 (8), 567–575.
Pradyumna, S., Bandyopadhyay, J.N., 2008. Free vibration analysis of functionally graded curved panels using a higher-order finite element formulation. Journal of Sound and Vibration 318 (1–2), 176–192.
Reddy, J.N., 1982. Bending of laminated anisotropic shells by a shear deformable finite element. Fibre Science and Technology 17, 9–24.
Rodrigues, J.D., Roque, C.M.C., Ferreira, A.J.M., Carrera, E., Cinefra, M., 2011. Radial basis functions-finite differences collocation and a unified formulation for bending, vibration and buckling analysis of laminated plates, according to murakami's zig-zag theory. Composite Structures 93 (7), 1613–1620.
Scordelis, A., Lo, K.S., 1964. Computer analysis in cylindrical shells. Journal of American Concrete Institute 61, 561–593.
Soave, M., Cinefra, M., Belouettar, S., Carrera, E., 2010. Variable kinematic models applied to free-vibration analysis of functionally graded material shells. European Journal of Mechanics A/Solids 29, 1078–1087.
Wang, J.G., Liu, G.R., 2002. On the optimal shape parameters of radial basis functions used for 2-d meshless methods. Computer Methods in Applied Mechanics and Engineering 191, 2611–2630.
Wang, J.G., Liu, G.R., Lin, P., 2002. Numerical analysis of biot's consolidation process by radial point interpolation method. International Journal of Solids and Structures 39 (6), 1557–1573.
Xiang, S., Wang, K.M., Ai, Y.T., Sha, Y.D., Shi, H., 2009. Analysis of isotropic, sandwich and laminated plates by a meshless method and various shear deformation theories. Composite Structures 91 (1), 31–37.
Xiang, S., Shi, H., Wang, K.M., Ai, Y.T., Sha, Y.D., 2010. Thin plate spline radial basis functions for vibration analysis of clamped laminated composite plates. European Journal of Mechanics A/Solids 29, 844–850.
Yang, J., Shen, Hui-Shen, 2003. Free vibration and parametric resonance of shear deformable functionally graded cylindrical panels. Journal of Sound and Vibration 261 (5), 871–893.
Yin, H.M., Sun, L.Z., Paulino, G.H., 2004. Micromechanics-based elastic model for functionally graded materials with particle interactions. Acta Materialia 52 (12), 3535–3543.
Zhong, Zheng, Shang, Ertao, 2008. Closed-form solutions of three-dimensional functionally graded plates. Mechanics of Advanced Materials and Structures 15 (5), 355–363.

2.9 Buckling behaviour of cross-ply laminated plates by a higher-order shear deformation theory

A. M. A. Neves, A. J. M. Ferreira, E. Carrera, M. Cinefra, C. M. C. Roque, R. M. N. Jorge, C. M. M. Soares, Buckling behaviour of cross-ply laminated plates by a higher-order shear deformation theory, Science and Engineering of Composite Materials, Volume 19, Issue 2, 2012, Pages 119-125.

Buckling behaviour of cross-ply laminated plates by a higher-order shear deformation theory

A. M. A. Neves [a], A. J. M. Ferreira [b], E. Carrera [c], M. Cinefra [c], C. M. C. Roque [d], R. M. N. Jorge [a], C. M. M. Soares [e]

[a] *Departamento de Engenharia Mecânica, Faculdade de Engenharia, Universidade do Porto, Rua Dr. Roberto Frias, 4200-465 Porto, Portugal*

[b] *(Corresponding author: ferreira@fe.up.pt)*
Departamento de Engenharia Mecânica, Faculdade de Engenharia, Universidade do Porto, Rua Dr. Roberto Frias, 4200-465 Porto, Portugal

[c] *Departament of Aeronautics and Aerospace Engineering, Politecnico di Torino, Corso Duca degli Abruzzi, 24, 10129 Torino, Italy*

[d] *INEGI, Faculdade de Engenharia, Universidade do Porto, Rua Dr. Roberto Frias, 4200-465 Porto, Portugal*

[e] *Instituto Superior Técnico, Av. Rovisco Pais, Lisboa, Portugal*

Abstract

In this paper the Carrera's Unified Formulation (CUF) is combined with a radial basis function collocation technique. A higher-order theory that considers deformations in the thickness direction was developed under CUF to predict the buckling behaviour of laminated plates. The obtained governing equations and boundary conditions are then interpolated by collocation with radial basis functions.

The accuracy and efficiency of the combination of the two techniques for buckling problems of laminated plates are demonstrated through numerical experiments.

1 Introduction

The buckling phenomenon consists of a sudden change of equilibrium geometry at a certain critical load. It is one of the characteristic failure modes of slender structures such as plates. Laminated plates are widely used in the aerospace industry. The buckling analysis of laminated plates by numerical methods is fundamental for adequate design.

Some relevant work on the buckling of thick plates includes those of Putcha and Reddy [1], Baba [2], Reddy and Phan [3], Liew et al. [4,5], Tumino et al. [6], Wang et al. [7], Ni et al. [8], and Kitipornchai et al. [9]. A comprehensive state-of-the-art review was presented by Leissa [10,11]. Recent reviews on buckling of laminated structures can be found in [12,13].

The present higher-order plate theory considers a third-order expansion across the thickness coordinate, z, for the in-plane displacements and a quadratic expansion in the thickness direction for the transverse displacement, w, allowing for through-the-thickness deformations. The linearized buckling equations and boundary conditions are obtained using the Principle of Virtual Displacements under Carrera's Unified Formulation (CUF) [14]. This formulation proposed by Carrera has been successfully applied in the analysis of composite laminated and functionally graded beams, plates and shells in [15–18], using either the Principle of Virtual Displacements or the Reissner mixed variational theorem, and layer-wise as well as equivalent single-layer descriptions, mostly with finite element methods.

The analysis of plates by finite elements methods is now fully established. In recent years, radial basis functions (RBFs) showed excellent accuracy in the interpolation of data and functions. Kansa [19] introduced the concept of solving partial differential equations by an unsymmetric RBF collocation method based upon the multiquadric interpolation functions. The authors have recently applied the RBF collocation to the static deformations and free vibrations of composite beams and plates [20–27].

The authors have successfully combined CUF and meshless methods in [28–31] for laminated plates and in [32,33] for functionally graded plates. In this paper, CUF is adopted to provide the linearized buckling equations and boundary conditions of the higher-order theory for laminated plates. The governing equations and the boundary conditions are then collocated with radial basis functions. The objective of this paper is to study the buckling behaviour of multilayered plates by a combination of CUF and the radial basis functions collocation technique, as a first endeavour.

Examples are presented in section 4 and include both uni- and bi-axial compressive loadings and several boundary conditions of symmetric cross-ply plates.

2 Formulation

2.1 Geometry and forces

Consider a rectangular plate of plan-form dimensions a and b and uniform thickness h. The co-ordinate system is taken such that the x-y plane coincides

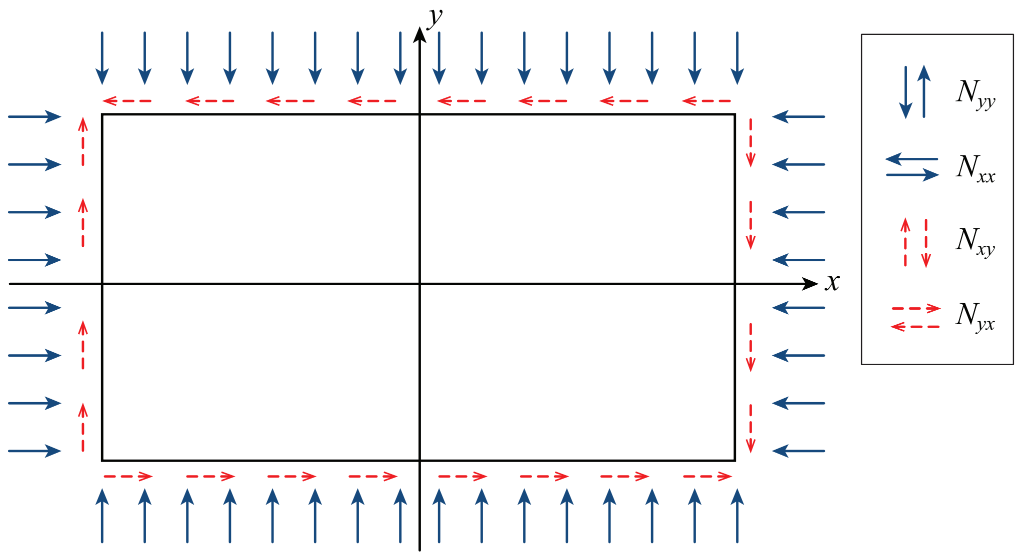

Fig. 1. Rectangular plate subjected to compressive in-plane forces and distributed shear forces.

with the midplane of the plate ($z \in [-h/2, h/2]$). The plate is composed of a number of layers (NL) of orthotropic material.

The plate may be subjected to compressive in-plane forces acting on the mid-plane of the plate $z = 0$ and distributed shear force (see fig. 1). $\bar{N}_{xx}$ and $\bar{N}_{yy}$ denote the in-plane loads perpendicular to the edges $x = 0$ and $y = 0$ respectively, and $\bar{N}_{xy}$ denote the distributed shear force parallel to the edges $x = 0$ and $y = 0$ respectively.

2.2 Constitutive equations

For each lamina, the generic constitutive equations are expressed by Hooke's Law, in material axes:

$$\boldsymbol{\sigma}_m = \boldsymbol{H}_m \boldsymbol{\epsilon}_m \tag{1}$$

being $\boldsymbol{\sigma}_m$ and $\boldsymbol{\epsilon}_m$ the stresses vector and strains vector, respectively, written in material reference coordinates as:

$$\boldsymbol{\sigma}_m^T = [\sigma_{11} \; \sigma_{22} \; \sigma_{12} \; \sigma_{13} \; \sigma_{23} \; \sigma_{33}] \tag{2}$$

$$\boldsymbol{\epsilon}_m^T = [\epsilon_{11} \; \epsilon_{22} \; \gamma_{12} \; \gamma_{13} \; \gamma_{23} \; \epsilon_{33}] \tag{3}$$

being $\boldsymbol{H}_m$ the stiffness matrix

$$\boldsymbol{H}_m = \begin{pmatrix} C_{11} & C_{12} & 0 & 0 & 0 & C_{13} \\ C_{12} & C_{22} & 0 & 0 & 0 & C_{23} \\ 0 & 0 & C_{66} & 0 & 0 & 0 \\ 0 & 0 & 0 & C_{55} & 0 & 0 \\ 0 & 0 & 0 & 0 & C_{44} & 0 \\ C_{13} & C_{23} & 0 & 0 & 0 & C_{33} \end{pmatrix} \tag{4}$$

The computation of the elastic constants C_{ij} depends on the assumption on the strain ϵ_{zz}.

Thickness-stretching effects can be considered by allowing $\epsilon_{zz} \neq 0$. In this case, C_{ij} are the 3D elastic constants given by

$$\begin{aligned} & C_{11} = E_1 \frac{(1-\nu_{23}\nu_{32})}{\Delta}, \quad C_{12} = E_1 \frac{(\nu_{21}+\nu_{31}\nu_{23})}{\Delta} = E_2 \frac{(\nu_{12}+\nu_{32}\nu_{13})}{\Delta} \\ & C_{22} = E_2 \frac{(1-\nu_{13}\nu_{31})}{\Delta}, \quad C_{13} = E_1 \frac{(\nu_{31}+\nu_{21}\nu_{32})}{\Delta} = E_3 \frac{(\nu_{13}+\nu_{12}\nu_{23})}{\Delta} \\ & C_{33} = E_3 \frac{(1-\nu_{12}\nu_{21})}{\Delta}, \quad C_{23} = E_2 \frac{(\nu_{32}+\nu_{12}\nu_{31})}{\Delta} = E_3 \frac{(\nu_{23}+\nu_{21}\nu_{13})}{\Delta} \\ & C_{44} = G_{23}, \quad C_{55} = G_{13}, \quad C_{66} = G_{12} \\ & \Delta = 1 - \nu_{12}\nu_{21} - \nu_{23}\nu_{32} - \nu_{13}\nu_{31} - 2\nu_{12}\nu_{32}\nu_{13} \end{aligned} \tag{5}$$

Here, E_1, E_2, and E_3 are the Young's moduli in directions 1, 2, and 3, respectively, ν_{ij} $(i,j = 1,2,3)$ are the Poisson's ratios, defined as the ratio of transverse strain in the jth direction to the axial strain in the ith direction, when stressed in the i-direction, and G_{23}, G_{13}, and G_{13} are the shear moduli in the 2-3, 1-3, 1-2 planes, respectively.

On the other hand, if $\epsilon_{zz} = 0$ is considered, thickness stretching is not allowed. Consequently, C_{ij} are the plane-stress reduced elastic constants in the material axes:

$$\begin{aligned} & C_{11} = \frac{E_1}{\Delta}; \quad C_{12} = \nu_{21}\frac{E_1}{\Delta} = \nu_{12}\frac{E_2}{\Delta}; \quad C_{22} = \frac{E_2}{\Delta}; \quad \Delta = 1 - \nu_{12}\nu_{21} \\ & C_{66} = G_{12}; \quad C_{44} = G_{23}; \quad C_{55} = G_{13}; \quad C_{33} = C_{13} = C_{23} = 0 \end{aligned} \tag{6}$$

The material coordinate system (x_1, y_1, z_1) is obtained from the plate coordinate system (x, y, z) by rotating the xy-plane by an angle θ, see figure 2. Note that $z = z_1$. For each layer, a rotation matrix is considered depending on the

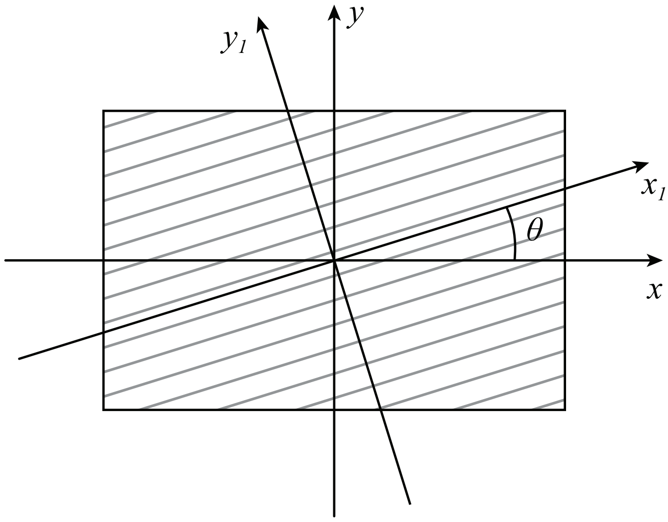

Fig. 2. A layer with plate and material coordinate systems.

angle θ between the 1-coordinate and the x-coordinate.

$$\boldsymbol{T}^k = \begin{pmatrix} \cos^2\theta & \sin^2\theta & -\sin 2\theta & 0 & 0 & 0 \\ \sin^2\theta & \cos^2\theta & \sin 2\theta & 0 & 0 & 0 \\ \frac{1}{2}\sin 2\theta & -\frac{1}{2}\sin 2\theta & \cos 2\theta & 0 & 0 & 0 \\ 0 & 0 & 0 & \cos\theta & \sin\theta & 0 \\ 0 & 0 & 0 & -\sin\theta & \cos\theta & 0 \\ 0 & 0 & 0 & 0 & 0 & 1 \end{pmatrix} \tag{7}$$

Stresses and deformations can be then obtained by

$$\boldsymbol{\sigma} = \boldsymbol{T}\boldsymbol{\sigma}_m \quad \text{and} \quad \boldsymbol{\epsilon} = \boldsymbol{T}^T\boldsymbol{\epsilon}_m \tag{8}$$

being $\boldsymbol{\sigma}$ and $\boldsymbol{\epsilon}$ the stresses vector and strains vector, respectively, written in plate reference coordinates

$$\boldsymbol{\sigma}^T = [\sigma_{xx}\ \sigma_{yy}\ \sigma_{xy}\ \sigma_{xz}\ \sigma_{yz}\ \sigma_{zz}] \tag{9}$$

$$\boldsymbol{\epsilon}^T = [\epsilon_{xx}\ \epsilon_{yy}\ \gamma_{xy}\ \gamma_{xz}\ \gamma_{yz}\ \epsilon_{zz}] \tag{10}$$

Considering equations (1) and (8), the constitutive law in plate coordinates can be obtaines as

$$\boldsymbol{\sigma} = \boldsymbol{T}\boldsymbol{H}_m\boldsymbol{T}^T\boldsymbol{\epsilon} \tag{11}$$

Defining $\boldsymbol{H} = \boldsymbol{T}\boldsymbol{H}_m\boldsymbol{T}^T$ for each layer, the elastic stress-strains relation becomes $\boldsymbol{\sigma}^k = \boldsymbol{H}^k\boldsymbol{\epsilon}^k$.

2.3 Displacement field

In the present work, the buckling behaviour of the laminated plate is modelled by an higher-order plate theory based on the following displacement field:

$$
\begin{aligned}
u(x,y,z,t) &= u_0(x,y,t) + zu_1(x,y,t) + z^3u_3(x,y,t)\\
v(x,y,z,t) &= v_0(x,y,t) + zv_1(x,y,t) + z^3v_3(x,y,t)\\
w(x,y,z,t) &= w_0(x,y,t) + zw_1(x,y,t) + z^2w_2(x,y,t)
\end{aligned}
\tag{12}
$$

where u, v, and w are the displacements in the $x-$, $y-$, and $z-$ directions, respectively. u_0, u_1, u_3, v_0, v_1, v_3, w_0, w_1, and w_2 are the generalized displacements to be determined.

According to CUF, the displacement vector $\boldsymbol{u}^k$ of a single layer is defined as:

$$
\boldsymbol{u}^k(x,y,z) = [u_x^k \quad u_y^k \quad u_z^k]^T \tag{13}
$$

where the superscript T denotes the transpose operator.

2.4 Strains

For the buckling analysis we need to account for the nonlinear contributions. Strains $\boldsymbol{\epsilon}$ are related to the displacement primary unknowns $\boldsymbol{u}$ according to

$$
\boldsymbol{\epsilon}^k = \boldsymbol{D}^{(nl)}\boldsymbol{u}^k \qquad \text{where} \quad \boldsymbol{D}^{(nl)} = \begin{pmatrix} \partial_x & 0 & \partial_x^2/2 \\ 0 & \partial_y & \partial_y^2/2 \\ \partial_y & \partial_x & \partial_x\partial_y \\ \partial_z & 0 & \partial_x \\ 0 & \partial_z & \partial_y \\ 0 & 0 & \partial_z \end{pmatrix} \tag{14}
$$

Noting that the compressive in-plane forces and distributed shear forces only actuate on the mid-plane, then $z = 0$, and the nonlinear terms are reduced to $\frac{1}{2}\left(\frac{\partial w_0}{\partial x}\right)^2$, $\frac{1}{2}\left(\frac{\partial w_0}{\partial y}\right)^2$, and $\frac{\partial w_0}{\partial x}\frac{\partial w_0}{\partial y}$. As these terms will only influence the equation refering to $\delta \boldsymbol{w}_0$, we use the linear version of CUF and just add the terms in referred equation. The linear strain-displacement relation can be written as

$$\boldsymbol{\epsilon}^k = \boldsymbol{D}\boldsymbol{u}^k \qquad \text{with} \quad \boldsymbol{D} = \begin{pmatrix} \partial_x & 0 & 0 \\ 0 & \partial_y & 0 \\ \partial_y & \partial_x & 0 \\ \partial_z & 0 & \partial_x \\ 0 & \partial_z & \partial_y \\ 0 & 0 & \partial_z \end{pmatrix} \tag{15}$$

2.5 Governing equations

Some results are here repeated for the sake of completeness. Details on the meshless version of CUF such as how to obtain the fundamental nuclei, governing equations and boundary conditions in terms of resultants, and governing equations and boundary conditions in terms of resultants can be found in [33,34].

The three displacement components u_x, u_y and u_z, given in (12) or (13), and their relative variations can be modelled as:

$$(u_x, u_y, u_z) = F_\tau \ (u_{x\tau}, u_{y\tau}, u_{z\tau}) \qquad (\delta u_x, \delta u_y, \delta u_z) = F_s \ (\delta u_{xs}, \delta u_{ys}, \delta u_{zs}) \tag{16}$$

In the present HSDT the thickness functions for inplane displacements u, v are

$$F_{sux} = F_{suy} = F_{\tau ux} = F_{\tau uy} = \begin{bmatrix} 1 & z & z^3 \end{bmatrix} \tag{17}$$

and for transverse displacement w are

$$F_{suz} = F_{\tau uz} = \begin{bmatrix} 1 & z & z^2 \end{bmatrix}. \tag{18}$$

According to CUF, the Principle of Virtual Displacements (PVD) can be stated as:

$$\sum_{k=1}^{NL} \int_{\Omega_k} \int_{A_k} \left\{ \delta {\epsilon^k}^T \sigma^k \right\} d\Omega_k dz = 0 \tag{19}$$

where Ω_k and A_k are the integration domains in plane (x,y) and z direction, respectively, k indicates the layer and T the transpose of a vector. Substituting the constitutive equations and applying the formula of integration by parts, the governing equations and boundary conditions for the multi-layered plate are obtained:

$$\delta \mathbf{u}_s^{kT} \ : \qquad \mathbf{K}_{uu}^{k\tau s}\,\mathbf{u}_\tau^k \ = 0 \tag{20}$$

except for δw_0, that will include more terms due to the nonlinear contributions.

The fundamental nuclei $\mathbf{K}_{uu}^{k\tau s}$ in explicit form is obtained as:

$$\begin{aligned}
K_{uu_{11}}^{k\tau s} =&(-\partial_x^\tau \partial_x^s C_{11} - \partial_x^\tau \partial_y^s C_{16} + \partial_z^\tau \partial_z^s C_{55} - \partial_y^\tau \partial_x^s C_{16} - \partial_y^\tau \partial_y^s C_{66}) F_\tau F_s \\
K_{uu_{12}}^{k\tau s} =&(-\partial_x^\tau \partial_y^s C_{12} - \partial_x^\tau \partial_x^s C_{16} + \partial_z^\tau \partial_z^s C_{45} - \partial_y^\tau \partial_y^s C_{26} - \partial_y^\tau \partial_x^s C_{66}) F_\tau F_s \\
K_{uu_{13}}^{k\tau s} =&(-\partial_x^\tau \partial_z^s C_{13} - \partial_y^\tau \partial_z^s C_{36} + \partial_z^\tau \partial_y^s C_{45} + \partial_z^\tau \partial_x^s C_{55}) F_\tau F_s \\
K_{uu_{21}}^{k\tau s} =&(-\partial_y^\tau \partial_x^s C_{12} - \partial_y^\tau \partial_y^s C_{26} + \partial_z^\tau \partial_z^s C_{45} - \partial_x^\tau \partial_x^s C_{16} - \partial_x^\tau \partial_y^s C_{66}) F_\tau F_s \\
K_{uu_{22}}^{k\tau s} =&(-\partial_y^\tau \partial_y^s C_{22} - \partial_y^\tau \partial_x^s C_{26} + \partial_z^\tau \partial_z^s C_{44} - \partial_x^\tau \partial_y^s C_{26} - \partial_x^\tau \partial_x^s C_{66}) F_\tau F_s \\
K_{uu_{23}}^{k\tau s} =&(-\partial_y^\tau \partial_z^s C_{23} - \partial_x^\tau \partial_z^s C_{36} + \partial_z^\tau \partial_y^s C_{44} + \partial_z^\tau \partial_x^s C_{45}) F_\tau F_s \\
K_{uu_{31}}^{k\tau s} =&(\partial_z^\tau \partial_x^s C_{13} + \partial_z^\tau \partial_y^s C_{36} - \partial_y^\tau \partial_z^s C_{45} - \partial_x^\tau \partial_z^s C_{55}) F_\tau F_s \\
K_{uu_{32}}^{k\tau s} =&(\partial_z^\tau \partial_y^s C_{23} + \partial_z^\tau \partial_x^s C_{36} - \partial_y^\tau \partial_z^s C_{44} - \partial_x^\tau \partial_z^s C_{45}) F_\tau F_s \\
K_{uu_{33}}^{k\tau s} =&(\partial_z^\tau \partial_z^s C_{33} - \partial_y^\tau \partial_y^s C_{44} - \partial_y^\tau \partial_x^s C_{45} - \partial_x^\tau \partial_y^s C_{45} - \partial_x^\tau \partial_x^s C_{55}) F_\tau F_s
\end{aligned} \tag{21}$$

and the corresponding Neumann-type boundary conditions on Γ_k are:

$$\begin{aligned}
\Pi_{11}^{k\tau s} =&(n_x \partial_x^s C_{11} + n_x \partial_y^s C_{16} + n_y \partial_x^s C_{16} + n_y \partial_y^s C_{66}) F_\tau F_s \\
\Pi_{12}^{k\tau s} =&(n_x \partial_y^s C_{12} + n_x \partial_x^s C_{16} + n_y \partial_y^s C_{26} + n_y \partial_x^s C_{66}) F_\tau F_s \\
\Pi_{13}^{k\tau s} =&(n_x \partial_z^s C_{13} + n_y \partial_z^s C_{36}) F_\tau F_s \\
\Pi_{21}^{k\tau s} =&(n_y \partial_x^s C_{12} + n_y \partial_y^s C_{26} + n_x \partial_x^s C_{16} + n_x \partial_y^s C_{66}) F_\tau F_s \\
\Pi_{22}^{k\tau s} =&(n_y \partial_y^s C_{22} + n_y \partial_x^s C_{26} + n_x \partial_y^s C_{26} + n_x \partial_x^s C_{66}) F_\tau F_s \\
\Pi_{23}^{k\tau s} =&(n_y \partial_z^s C_{23} + n_x \partial_z^s C_{36}) F_\tau F_s \\
\Pi_{31}^{k\tau s} =&(n_y \partial_z^s C_{45} + n_x \partial_z^s C_{55}) F_\tau F_s \\
\Pi_{32}^{k\tau s} =&(n_y \partial_z^s C_{44} + n_x \partial_z^s C_{45}) F_\tau F_s \\
\Pi_{33}^{k\tau s} =&(n_y \partial_y^s C_{44} + n_y \partial_x^s C_{45} + n_x \partial_y^s C_{45} + n_x \partial_x^s C_{55}) F_\tau F_s
\end{aligned} \tag{22}$$

where (n_x, n_y) denotes the unit normal-to-boundary vector.

The linearized buckling equations in terms of resultants are:

$$
\begin{aligned}
\delta u_0 &: \sum_{k=1}^{NL} \left(-\frac{\partial N_{xx}^k}{\partial x} - \frac{\partial N_{xy}^k}{\partial y} \right) = 0 \\
\delta v_0 &: \sum_{k=1}^{NL} \left(-\frac{\partial N_{xy}^k}{\partial x} - \frac{\partial N_{yy}^k}{\partial y} \right) = 0 \\
\delta w_0 &: \sum_{k=1}^{NL} \left(-\frac{\partial Q_{xz}^k}{\partial x} - \frac{\partial Q_{yz}^k}{\partial y} \right) + \bar{N}_{xx} \frac{\partial^2 w_0}{\partial x^2} + 2\bar{N}_{xy} \frac{\partial^2 w_0}{\partial x \partial y} + \bar{N}_{yy} \frac{\partial^2 w_0}{\partial y^2} = 0 \\
\delta u_1 &: \sum_{k=1}^{NL} \left(-\frac{\partial M_{xx}^k}{\partial x} - \frac{\partial M_{xy}^k}{\partial y} + Q_{xz}^k \right) = 0 \\
\delta v_1 &: \sum_{k=1}^{NL} \left(-\frac{\partial M_{xy}^k}{\partial x} - \frac{\partial M_{yy}^k}{\partial y} + Q_{yz}^k \right) = 0 \\
\delta w_1 &: \sum_{k=1}^{NL} \left(-\frac{\partial M_{xz}^k}{\partial x} - \frac{\partial M_{yz}^k}{\partial y} + Q_{zz}^k \right) = 0 \\
\delta u_3 &: \sum_{k=1}^{NL} \left(-\frac{\partial R_{xx}^k}{\partial x} - \frac{\partial R_{xy}^k}{\partial y} + 3R_{xz}^k \right) = 0 \\
\delta v_3 &: \sum_{k=1}^{NL} \left(-\frac{\partial R_{xy}^k}{\partial x} - \frac{\partial R_{yy}^k}{\partial y} + 3R_{yz}^k \right) = 0 \\
\delta w_2 &: \sum_{k=1}^{NL} \left(-\frac{\partial R_{xz}^k}{\partial x} - \frac{\partial R_{yz}^k}{\partial y} + 2M_{zz}^k \right) = 0
\end{aligned}
\tag{23}
$$

where the resultants are given by

$$
\begin{Bmatrix} N_{xx}^k \\ N_{yy}^k \\ N_{xy}^k \end{Bmatrix} = (z_{k+1} - z_k) \begin{Bmatrix} \sigma_{xx}^k \\ \sigma_{yy}^k \\ \sigma_{xy}^k \end{Bmatrix} dz, \qquad \begin{Bmatrix} Q_{xz}^k \\ Q_{yz}^k \\ Q_{zz}^k \end{Bmatrix} = (z_{k+1} - z_k) \begin{Bmatrix} \sigma_{xz}^k \\ \sigma_{yz}^k \\ \sigma_{zz}^k \end{Bmatrix} dz \tag{24}
$$

$$
\begin{Bmatrix} M_{xx}^k \\ M_{yy}^k \\ M_{xy}^k \end{Bmatrix} = \frac{z_{k+1}^2 - z_k^2}{2} \begin{Bmatrix} \sigma_{xx}^k \\ \sigma_{yy}^k \\ \sigma_{xy}^k \end{Bmatrix} dz, \qquad \begin{Bmatrix} M_{xz}^k \\ M_{yz}^k \\ M_{zz}^k \end{Bmatrix} = \frac{z_{k+1}^2 - z_k^2}{2} \begin{Bmatrix} \sigma_{xz}^k \\ \sigma_{yz}^k \\ \sigma_{zz}^k \end{Bmatrix} dz \tag{25}
$$

$$
\begin{Bmatrix} R_{xx}^k \\ R_{yy}^k \\ R_{xy}^k \end{Bmatrix} = \frac{z_{k+1}^4 - z_k^4}{4} \begin{Bmatrix} \sigma_{xx}^k \\ \sigma_{yy}^k \\ \sigma_{xy}^k \end{Bmatrix} dz, \qquad \begin{Bmatrix} R_{xz}^k \\ R_{yz}^k \end{Bmatrix} = \frac{z_{k+1}^3 - z_k^3}{3} \begin{Bmatrix} \sigma_{xz}^k \\ \sigma_{yz}^k \end{Bmatrix} dz. \tag{26}
$$

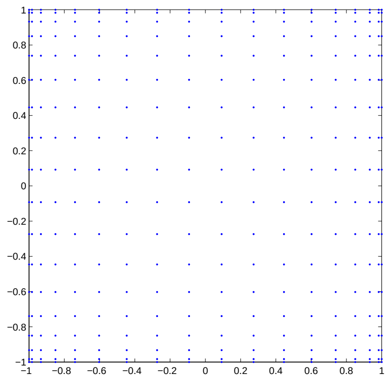

Fig. 3. Chebyshev grid with N=17

Here, z_k and z_{k+1} are the lower and upper z coordinate of the kth layer, respectively.

The linearized governing equations and boundary conditions in terms of displacements of the present HSDT for functionally graded plates were derived by the authors and presented in detail in [34]. Note that the case of functionally graded materials is a particular case of the present HSDT and more terms are necessary in equations for laminated composites.

3 The radial basis function method

The equations of motion previously obtained are interpolated by means of collocation with radial basis functions. The unsymmetrical method by Kansa [19] is adopted on a Chebyshev grid. For a given number of nodes per side (N), it is generated by MATLAB code:

```
x = cos(pi*(0:N)/N)';
y=x;
```

A 17^2 points ($N = 17$) Chebyshev grid is illustrated in figure 3. The radial basis function used is the Wendland function [35] defined as

$$\phi(r) = (1 - cr)_+^8 \left(32(cr)^3 + 25(cr)^2 + 8cr + 1\right) \tag{27}$$

where the Euclidian distance r is real and non-negative and c is a positive shape parameter. In the present work the shape parameter (c) is obtained by an optimization procedure, as detailed in Ferreira and Fasshauer [36].

Details on the application of this meshless method to buckling problems can be found in previous works by the authors [28,31,37,38].

	present	Ref. [39]	Ref. [5]	Ref. [3]	Ref. [37] 19^2 points	Ref. [38] 21^2 points
13^2	23.3706	23.453	23.463	23.849	23.2444	23.4261
17^2	23.3697					
21^2	23.3696					

Table 1
Uni-axial buckling load of four-layer [0/90/90/0] SSSS laminated plate according to the higher-order theory. $\bar{N} = \bar{N}_{xx}a^2/(E_2h^3), \bar{N}_{xy} = 0, \bar{N}_{yy} = 0$

4 Numerical examples

In the next examples we use the present higher-order plate theory for the buckling analysis of square laminated plates. Three-layer [0/90/0] and four-layer [0/90/90/0] square cross-ply laminates with various boundary conditions are chosen to compute the uni- and bi-axial buckling loads. The plates have side lengths $a = b$, thickness h, and the span-to-thickness ratio a/h is taken to be 10. All layers are assumed to be of the same thickness and material properties:

$$E_1/E_2 = 40; G_{12}/E_2 = G_{13}/E_2 = 0.6; G_{23}/E_2 = 0.5; \nu_{12} = 0.25$$

Figure 4 and table 1 refer to the uni-axial buckling load of four-layer [0/90/90/0] laminated plate with all edges simply supported. The first four buckling modes are presented in figure 4 and table 1 lists the critical uni-axial buckling load for 13^2, 17^2, and 21^2 points grid. We compare results with exact solutions by Khdeir and Librescu [39], differential quadrature results by Liew and Huang [5] based on the FSDT, analytical results by Reddy and Phan [3] based on an HSDT, Ferreira et al. [37] based on the same HSDT as in [3] but using a meshless technique, and Ferreira et al. [38] based on the FSDT and using a meshless technique.

Figures 5, 6, and 7, and table 2 refer to the bi-axial buckling load of three-layer [0/90/0] laminated plate simply supported along the edges parallel to the x-axis. The other two edges may be simply supported (S) or clamped (C). Each figure illustrates the first 4 buckling modes of a plate with a different boundary condition. For these figures a 17^2 points grid was used and $\bar{N} = \bar{N}_{xx}a^2/(E_2h^3), \bar{N}_{xy} = 0, \bar{N}_y y = \bar{N}_x x$. In table 2 results are compared with exact solutions by Khdeir and Librescu [39], differential quadrature results by Liew and Huang [5] based on the FSDT, and Ferreira et al. [38] based on the FSDT and using a meshless technique and 21^2 points.

The present approach is in very good agreement with the reference solutions.

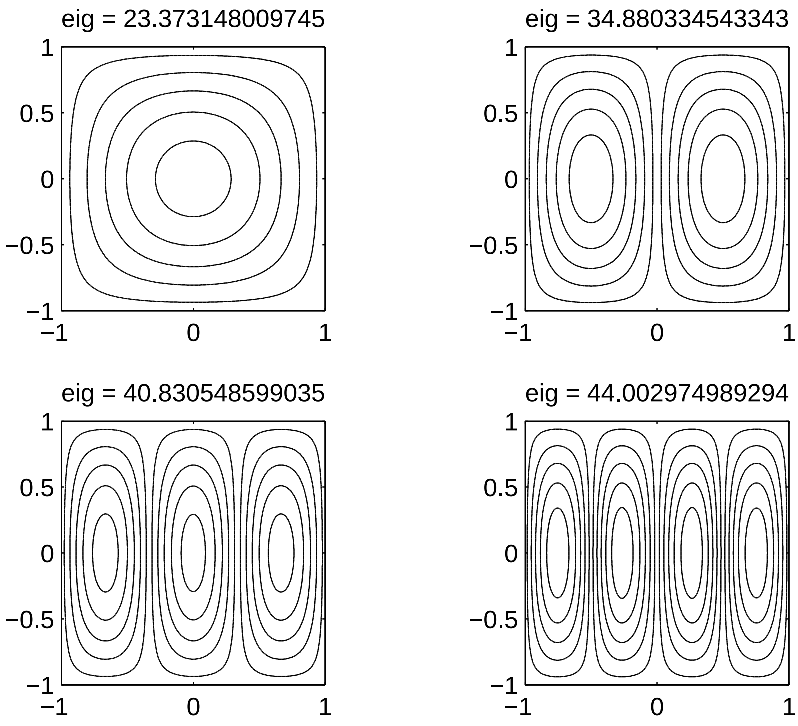

Fig. 4. First 4 buckling modes for a uni-axial buckling load of four-layer [0/90/90/0] SSSS laminated plate, using a 11^2 points grid and higher-order theory. $\bar{N} = \bar{N}_{xx}a^2/(E_2h^3), \bar{N}_{xy} = 0, \bar{N}_{yy} = 0$

.

Method	SSSS	SSSC	SCSC
Ref. [39]	10.202	11.602	13.290
Ref. [5]	10.178	11.575	13.260
Ref. [38]	10.1969	11.5972	13.2919
present 13^2	10.1498	11.5888	13.3592
present 17^2	10.1487	11.5877	13.3582
present 21^2	10.1486	11.5876	13.3581

Table 2
Bi-axial buckling load of three-layer [0/90/0] laminated plate according to the higher-order theory. $\bar{N} = \bar{N}_{xx}a^2/(E_2h^3), \bar{N}_{xy} = 0, \bar{N}_{yy} = \bar{N}_{xx}$

The present HSDT computed by combining CUF and the radial basis functions collocation technique is very accurate for the buckling analysis of cross-ply plates.

In figures 4 to 7 the mode shapes are correct. Note that in figures 5 to 7 the first mode does not correspond to the critical mode. However, we decided to

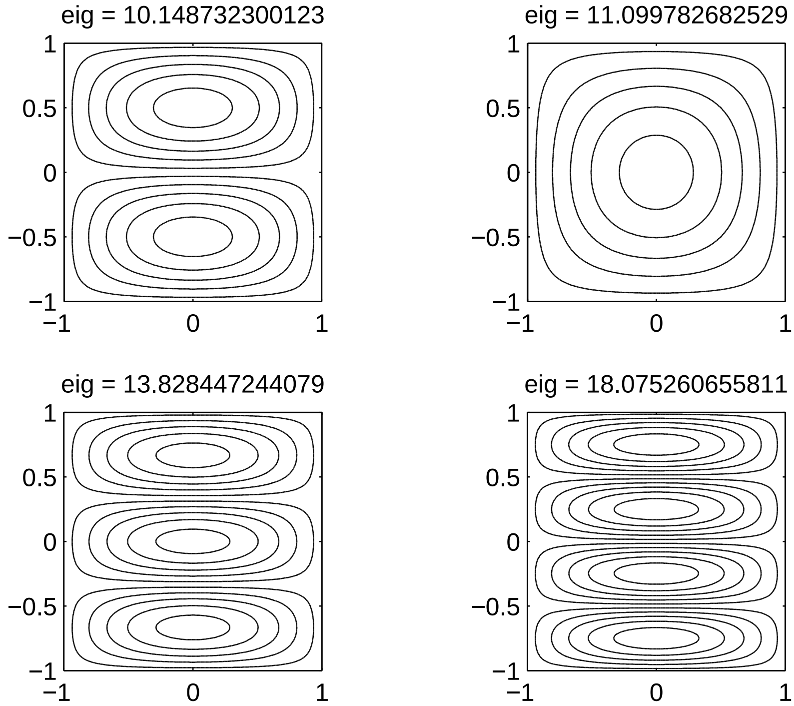

Fig. 5. First 4 buckling modes for a bi-axial buckling load of three-layer [0/90/0] SSSS laminated plate, using a 17^2 points grid and the higher-order theory. $\bar{N} = \bar{N}_{xx}a^2/(E_2h^3), \bar{N}_{xy} = 0, \bar{N}_{yy} = \bar{N}_{xx}$

.

keep the same organization of modes as in comparative sources.

5 Conclusions

A novel application of a Unified formulation by a meshless discretization was proposed. A thickness-stretching higher-order shear deformation theory was implemented for the buckling analysis of composite laminated plates.

The present formulation was compared with analytical, meshless or finite element methods and proved very accurate in buckling problems.

Acknowledgements

The first author acknowledges support from FCT grant SFRH/BD/45554/2008.

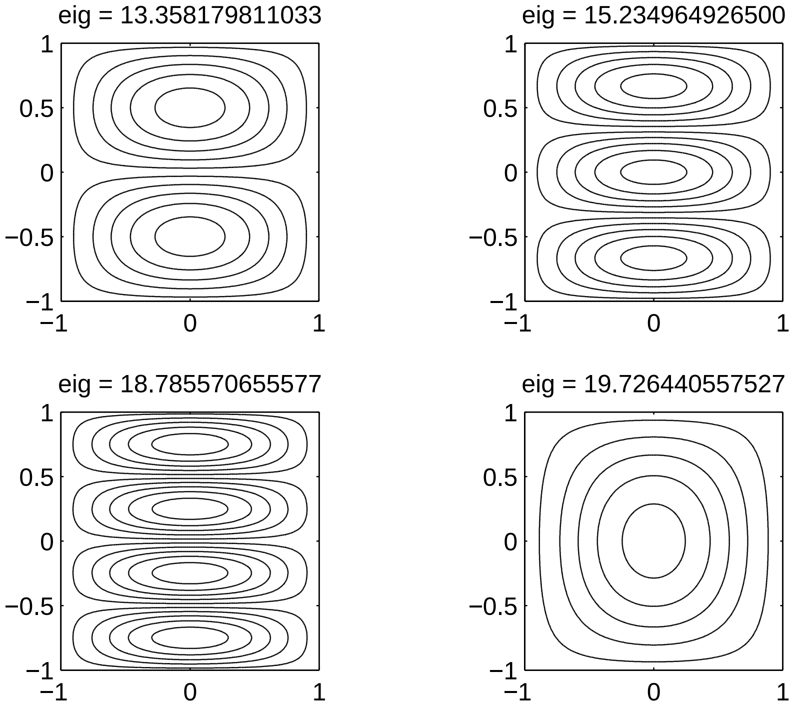

Fig. 6. First 4 buckling modes for a bi-axial buckling load of three-layer [0/90/0] SCSC laminated plate, using a 17^2 points grid and the higher-order theory. $\bar{N} = \bar{N}_{xx}a^2/(E_2h^3), \bar{N}_{xy} = 0, \bar{N}_{yy} = \bar{N}_{xx}$

.

References

[1] N. S. Putcha and J. N. Reddy. Stability and natural vibration analysis of laminated plates by using a mixed element based on a refined plate theory. *J. Sound and Vibration*, 104(2):285–300, 1986.

[2] B.O.Baba. Buckling response of rectangular laminated composite plates with cutouts. *Science and Engineering of Composite Materials*, 14:17–24, 2007.

[3] J. N. Reddy and N. D. Phan. Stability and vibration of isotropic, orthotropic and laminated plates according to a higher-order shear deformation theory. *J. Sound and Vibration*, 98(2):157–170, 1985.

[4] K. M. Liew, J. Wang, T. Y. Ng, and M. J. Tan. Free vibration and buckling analyses of shear-deformable plates based on fsdt meshfree method. *Journal of Sound and Vibration*, 276:997–1017, 2004.

[5] K. M. Liew and Y. Q. Huang. Bending and buckling of thick symmetric rectangular laminates using the moving least-squeares differential quadrature method. *Int J Mech Sci*, 45:95–114, 2003.

[6] D. Tumino, F. Cappello, and D. Rocco. 3d buckling analysis of multidelaminated

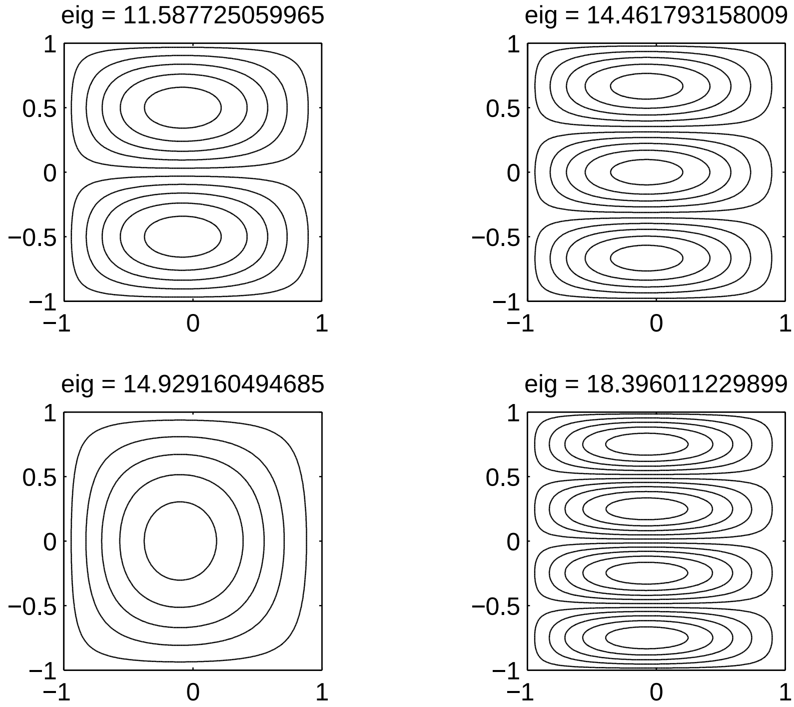

Fig. 7. First 4 buckling modes for a bi-axial buckling load of three-layer [0/90/0] SSSC laminated plate, using a 17^2 points grid and the higher-order theory. $\bar{N} = \bar{N}_{xx}a^2/(E_2h^3), \bar{N}_{xy} = 0, \bar{N}_{yy} = \bar{N}_{xx}$

.

composite specimens. *Science and Engineering of Composite Materials*, 14:181–188, 2007.

[7] C.M. Wang, K.M. Liew, Y. Xiang, and S. Kitipornchai. Buckling of rectangular mindlin plates with internal line supports. *International Journal of Solids and Structures*, 30(1):1 – 17, 1993.

[8] Q.-Q. Ni, J. Xie, and M. Iwamoto. Shear buckling analysis of angle-ply laminates with higher- order shear deformation and pb-2 ritz functions. *Science and Engineering of Composite Materials*, 11:123–136, 2004.

[9] S. Kitipornchai, Y. Xiang, C. M. Wang, and K. M. Liew. Buckling of thick skew plates. *International Journal for Numerical Methods in Engineering*, 36(8):1299–1310, 1993.

[10] Arthur W. Leissa. Buckling of laminated composite plates and shell panels. *Flight Dynamics Laboratory Report No. AFWAL-TR-85-3069*, 1985.

[11] Arthur W. Leissa. A review of laminated composite plate buckling. *Applied Mechanics Reviews*, 40(5):575–591, 1987.

[12] M. D'Ottavio and E. Carrera. Variable-kinematics approach for linearized buckling analysis of laminated plates and shells. *American Institute of Aeronautics and Astronautics Journal*, 48(9):1987–1996, 2010.

[13] P. Nali, E. Carrera, and S. Lecca. Assessments of refined theories for buckling analysis of laminated plates. *Composite Structures*, 93(2):456 – 464, 2011.

[14] Erasmo Carrera. Theories and finite elements for multilayered plates and shells: A unified compact formulation with numerical assessment and benchmarking. *Archives of Computational Methods in Engineering*, 10:215–296.

[15] E. Carrera, F. Miglioretti, and M. Petrolo. Accuracy of refined finite elements for laminated plate analysis. *Composite Structures*, 93(5):1311 – 1327, 2011.

[16] M. Cinefra, E. Carrera, L. Della Croce, and C. Chinosi. Refined shell elements for the analysis of functionally graded structures. *Composite Structures*, In Press, Accepted Manuscript:–, 2011.

[17] M. Cinefra and M. Soave. Accurate vibration analysis of multilayered plates made of functionally graded materials. *Mechanics of Advanced Materials and Structures*, 18(1):3–13, 2011.

[18] E. Carrera, M. Petrolo, and P. Nali. Unified formulation applied to free vibrations finite element analysis of beams with arbitrary section. *Shock and Vibration*, 18(3):485–502, 2011.

[19] E. J. Kansa. Multiquadrics- a scattered data approximation scheme with applications to computational fluid dynamics. i: Surface approximations and partial derivative estimates. *Computers and Mathematics with Applications*, 19(8/9):127–145, 1990.

[20] A. J. M. Ferreira. A formulation of the multiquadric radial basis function method for the analysis of laminated composite plates. *Composite Structures*, 59:385–392, 2003.

[21] A. J. M. Ferreira. Thick composite beam analysis using a global meshless approximation based on radial basis functions. *Mechanics of Advanced Materials and Structures*, 10:271–284, 2003.

[22] A. J. M. Ferreira, C. M. C. Roque, and P. A. L. S. Martins. Analysis of composite plates using higher-order shear deformation theory and a finite point formulation based on the multiquadric radial basis function method. *Composites: Part B*, 34:627–636, 2003.

[23] A.J.M. Ferreira, C.M.C. Roque, R.M.N. Jorge, and E.J. Kansa. Static deformations and vibration analysis of composite and sandwich plates using a layerwise theory and multiquadrics discretizations. *Engineering Analysis with Boundary Elements*, 29(12):1104 – 1114, 2005.

[24] A.J.M. Ferreira, C.M.C. Roque, and R.M.N. Jorge. Analysis of composite plates by trigonometric shear deformation theory and multiquadrics. *Computers & Structures*, 83(27):2225 – 2237, 2005.

[25] A.J.M. Ferreira, R.C. Batra, C.M.C. Roque, L.F. Qian, and R.M.N. Jorge. Natural frequencies of functionally graded plates by a meshless method. *Composite Structures*, 75(1-4):593 – 600, 2006.

[26] A.J.M. Ferreira, C.M.C. Roque, and R.M.N. Jorge. Free vibration analysis of symmetric laminated composite plates by fsdt and radial basis functions. *Computer Methods in Applied Mechanics and Engineering*, 194(39-41):4265 – 4278, 2005.

[27] A. J. M. Ferreira, C. M. C. Roque, and P. A. L. S. Martins. Radial basis functions and higher-order shear deformation theories in the analysis of laminated composite beams and plates. *Composite Structures*, 66(1-4):287 – 293, 2004.

[28] A.J.M. Ferreira, C.M.C. Roque, E. Carrera, M. Cinefra, and O. Polit. Radial basis functions collocation and a unified formulation for bending, vibration and buckling analysis of laminated plates, according to a variation of murakamiâĂŹs zig-zag theory. *European Journal of Mechanics - A/Solids*, 30(4):559 – 570, 2011.

[29] J.D. Rodrigues, C.M.C. Roque, A.J.M. Ferreira, E. Carrera, and M. Cinefra. Radial basis functions-finite differences collocation and a unified formulation for bending, vibration and buckling analysis of laminated plates, according to murakami's zig-zag theory. *Composite Structures*, 93(7):1613 – 1620, 2011.

[30] A.J.M. Ferreira, C.M.C. Roque, E. Carrera, and M. Cinefra. Analysis of thick isotropic and cross-ply laminated plates by radial basis functions and a unified formulation. *Journal of Sound and Vibration*, 330(4):771 – 787, 2011.

[31] A. J.M. Ferreira, C. M.C. Roque, E. Carrera, M. Cinefra, and O. Polit. Two higher order zig-zag theories for the accurate analysis of bending, vibration and buckling response of laminated plates by radial basis functions collocation and a unified formulation. *Journal of Composite Materials*, 2011.

[32] A.M.A. Neves, A.J.M. Ferreira, E. Carrera, C.M.C. Roque, M. Cinefra, R.M.N. Jorge, and C.M.M. Soares. Bending of fgm plates by a sinusoidal plate formulation and collocation with radial basis functions. *Mechanics Research Communications*, 38(5):368 – 371, 2011.

[33] A.M.A. Neves, A.J.M. Ferreira, E. Carrera, C.M.C. Roque, M. Cinefra, R. M.N. Jorge, and C.M.M. Soares. A quasi-3d sinusoidal shear deformation theory for the static and free vibration analysis of functionally graded plates. *Composites Part B*, In Press, Accepted Manuscript:–, 2011.

[34] A.M.A. Neves, A.J.M. Ferreira, E. Carrera, M. Cinefra, C.M.C. Roque, R. M.N. Jorge, and C.M.M. Soares. Static, free vibration and buckling analysis of isotropic and sandwich functionally graded plates using a quasi-3d higher-order shear deformation theory and a meshless technique. *Composites Part B: Engineering*, submitted:–, 2011.

[35] H. Wendland. Error estimates for interpolation by compactly supported radial basis functions of minimal degree. *J. Approx. Theory*, 93:258–296, 1998.

[36] A. J. M. Ferreira and G. E. Fasshauer. Computation of natural frequencies of shear deformable beams and plates by a rbf-pseudospectral method. *Computer Methods in Applied Mechanics and Engineering*, 196:134–146, 2006.

[37] A.J.M. Ferreira, C.M.C. Roque, A.M.A. Neves, R.M.N. Jorge, C.M.M. Soares, and J.N. Reddy. Buckling analysis of isotropic and laminated plates by radial basis functions according to a higher-order shear deformation theory. *Thin-Walled Structures*, 49(7):804 – 811, 2011.

[38] A.J.M. Ferreira, C.M.C. Roque, A.M.A. Neves, R.M.N. Jorge, C.M.M. Soares, and K.M. Liew. Buckling and vibration analysis of isotropic and laminated plates by radial basis functions. *Composites Part B: Engineering*, 42(3):592 – 606, 2011.

[39] A. A. Khdeir and L. Librescu. Analysis of symmetric cross-ply elastic plates using a higher-order theory. part ii: buckling and free vibration. *Compos Struct*, 9:259–277, 1988.

3

Papers on the radial basis function collocation technique

3.1 On the RBF-Direct method

3.1.1 Adaptive methods for analysis of composite plates with radial basis functions

Ana M. A. Neves, T. A. Driscoll, A. R. H. Heryudono, A. J. M. Ferreira, C. M. M. Soares, R. M. N. Jorge, C. M. C. Roque, Adaptive methods for analysis of composite plates with radial basis functions, Mechanics of Advanced Materials and Structures, Volume 18, 2011, pages 420-430.

Mechanics of Advanced Materials and Structures, 18:420–430, 2011

ISSN: 1537-6494 print / 1537-6532 online
DOI: 10.1080/15376494.2010.528155

Adaptive Methods for Analysis of Composite Plates with Radial Basis Functions

A. M. A. Neves,[1] T. A. Driscoll,[2] A. R. H. Heryudono,[2] A. J. M. Ferreira,[1] C. M. M. Soares,[3] and R. M. N. Jorge[1]

[1]*Departamento de Engenharia Mecânica e Gestão Industrial, Faculdade de Engenharia da Universidade do Porto, Rua Dr. Roberto Frias, Porto, Portugal*
[2]*Department of Mathematical Sciences, University of Delaware, Newark, Delaware, USA*
[3]*IDMEC—Instituto de Engenharia Mecânica—Instituto Superior Técnico, Av. Rovisco Pais, 1096 Lisboa Codex, Portugal*

Driscoll and Heryudono [1] developed an adaptive method for radial basis functions method. This article addresses the adaptive analysis of composite plates in bending with radial basis multiquadric functions using Driscoll and Heryudono's technique. In this article, various laminates, thickness to side length ratios, and boundary conditions are considered. The method allows for a more natural and automatic selection of the problem grid, where the user must only define the error tolerance. The results obtained show an interesting and promising approach to the static analysis of composite laminates.

Keywords radial basis functions, adaptive methods, composite, plates, residual, subsampling, multiquadric

1. INTRODUCTION

Radial basis function (RBF) methods are a good alternative method for the numerical solution of partial differential equations (PDEs) [2–6]. Compared to low-order methods, such as finite differences, finite volumes, and finite elements, RBF-based methods offer numerous advantages, such as mesh-free discretization and simple implementation. The imposition of the essential and natural boundary conditions is straightforward.

Also, depending on how the RBFs are chosen, high-order or spectral convergence can be achieved [7].

For the application of fixed-grid RBF methods to laminated composite beams and plates, readers should consult [8–10].

Adaptive methods may be preferred over fixed grid methods in problems that exhibit high degrees of localizations such as steep gradients or corners. The goal is to obtain a numerical solution such that the error is below a prescribed accuracy with the smallest number of degrees of freedom. Since RBF methods are completely meshfree, requiring only interpolation nodes and a set of points called centers defining the basis functions, implementing adaptivity in terms of refining and coarsening nodes is straightforward. Driscoll and Heryudono [1] developed an adaptive algorithm for RBFs where results obtained on interpolation, boundary-value, and time-dependent problems are encouraging.

In the present work, we apply the residual subsampling technique developed by Driscoll and Heryudono to the static analysis of isotropic and symmetric laminated composite plates.

We considered the First Order-Shear Deformation Theory (FSDT) [11].

The method starts with nonoverlapping boxes, each containing an active center. Once an interpolant has been computed for the active center set, the residual of the resulting approximation is sampled on a finer node set in each box. Nodes from the finer set are added to or removed from the set of centers based on the size of the residual of the PDE at those points. The interpolant is then recomputed using the new active center set for a new approximation.

We organize the article as follows. In Section 2 we review the governing differential equations for the bending of laminated plates using the FSDT. The RBF implementation is shortly reviewed in Section 3. In Section 4 we explain in detail the application of the residual subsampling technique to plates. Numerical results for isotropic and composite square plates are presented in subsections 5.1 and 5.2, respectively, and discussed in subsections 5.3. Finally some conclusions are presented in Section 6.

2. ANALYSIS OF SYMMETRIC LAMINATED PLATES

Several laminate theories, such as the classical laminate theory, the first-order shear deformation theory, and the higher-order shear deformation theory, have been proposed in the literature (see [11] for a review).

Received 21 August 2008; accepted 25 January 2010.
Address correspondence to António Ferreira, Departamento de Engenharia Mecânica e Gestão Industrial, Faculdade de Engenharia da Universidade do Portó, Rua Dr. Robertó Frias, Portó, 4200-465, Portugal. E-mail: ferreira@fe.up.pt

In the present study, the First-Order Shear Deformation Theory (FSDT) was used. This theory is based on the assumed displacement field

$$\begin{aligned} u &= u_0 + z\theta_x \\ v &= v_0 + z\theta_y \\ w &= w_0 \end{aligned} \tag{1}$$

where u and v are the in-plane displacements at any point (x, y, z) and (u_0, v_0, w_0) are the displacement components along the (x, y, z) coordinate directions, respectively, of a point on the midplane, usually considered at $z = 0$.

The transverse displacement $w(x, y)$ and the rotations $\theta_x(x, y)$ and $\theta_y(x, y)$ about the y- and x- axes are independently interpolated due to uncoupling between inplane displacements and bending displacements for symmetrically laminated plates. The equations of motion for the bending of laminated plates [11,12] are obtained as:

$$\begin{aligned} &D_{11}\frac{\partial^2\theta_x}{\partial x^2} + D_{16}\frac{\partial^2\theta_y}{\partial x^2} + (D_{12}+D_{66})\frac{\partial^2\theta_y}{\partial x\partial y} + 2D_{16}\frac{\partial^2\theta_x}{\partial x\partial y} \\ &\quad + D_{66}\frac{\partial^2\theta_x}{\partial y^2} + D_{26}\frac{\partial^2\theta_y}{\partial y^2} + -kA_{45}\left(\theta_y + \frac{\partial w}{\partial y}\right) \\ &\quad - kA_{55}\left(\theta_x + \frac{\partial w}{\partial x}\right) = 0 \end{aligned} \tag{2}$$

$$\begin{aligned} &D_{16}\frac{\partial^2\theta_x}{\partial x^2} + D_{66}\frac{\partial^2\theta_y}{\partial x^2} + (D_{12}+D_{66})\frac{\partial^2\theta_x}{\partial x\partial y} + 2D_{26}\frac{\partial^2\theta_y}{\partial x\partial y} \\ &\quad + D_{26}\frac{\partial^2\theta_x}{\partial y^2} + D_{22}\frac{\partial^2\theta_y}{\partial y^2} + -kA_{44}\left(\theta_y + \frac{\partial w}{\partial y}\right) \\ &\quad - kA_{45}\left(\theta_x + \frac{\partial w}{\partial x}\right) = 0 \end{aligned} \tag{3}$$

$$\begin{aligned} &\frac{\partial}{\partial x}\left[kA_{45}\left(\theta_y + \frac{\partial w}{\partial y}\right) + kA_{55}\left(\theta_x + \frac{\partial w}{\partial x}\right)\right] \\ &\quad + \frac{\partial}{\partial y}\left[kA_{44}\left(\theta_y + \frac{\partial w}{\partial y}\right) + kA_{45}\left(\theta_x + \frac{\partial w}{\partial x}\right)\right] = q, \end{aligned} \tag{4}$$

where q is the applied load, D_{ij} and A_{ij} are the bending and shear stiffness components, and k is the shear correction factor. Here h denotes the total thickness of the composite plate.

The bending moments M_x, M_y, and M_{xy} and the shear forces Q_x and Q_y are expressed as functions of the displacement gradients and the material stiffness components as

$$M_x = D_{11}\frac{\partial\theta_x}{\partial x} + D_{12}\frac{\partial\theta_y}{\partial y} + D_{16}\left(\frac{\partial\theta_x}{\partial y} + \frac{\partial\theta_y}{\partial x}\right) \tag{5}$$

$$M_y = D_{12}\frac{\partial\theta_x}{\partial x} + D_{22}\frac{\partial\theta_y}{\partial y} + D_{26}\left(\frac{\partial\theta_x}{\partial y} + \frac{\partial\theta_y}{\partial x}\right) \tag{6}$$

$$M_{xy} = D_{16}\frac{\partial\theta_x}{\partial x} + D_{26}\frac{\partial\theta_y}{\partial y} + D_{66}\left(\frac{\partial\theta_x}{\partial y} + \frac{\partial\theta_y}{\partial x}\right) \tag{7}$$

$$Q_x = kA_{55}\left(\theta_x + \frac{\partial w}{\partial x}\right) + kA_{45}\left(\theta_y + \frac{\partial w}{\partial y}\right) \tag{8}$$

$$Q_y = kA_{45}\left(\theta_x + \frac{\partial w}{\partial x}\right) + kA_{55}\left(\theta_y + \frac{\partial w}{\partial y}\right). \tag{9}$$

The boundary conditions for an arbitrary edge with simply supported, clamped, or free-edge conditions are defined as follows:

1. Simply supported:
   - SS1: $w = 0; M_n = 0; M_{ns} = 0.$
   - SS2: $w = 0; M_n = 0; \theta_s = 0.$
2. Clamped: $w = 0; \theta_n = 0; \theta_s = 0.$
3. Free: $Q_n = 0; M_n = 0; M_{ns} = 0.$

In previous equations, the subscripts n and s refer to the normal and tangential directions of the edge, respectively; M_n, $M_{ns,}$ and Q_n represent the normal bending moment, twisting moment and shear force on the plate edge; θ_n and θ_s represent the rotations about the tangential and normal coordinates at the plate edge. The stress resultants on an edge whose normal is represented by $\mathbf{n} = (n_x, n_y)$ can be expressed as

$$M_n = n_x^2 M_x + 2n_x n_y M_{xy} + n_y^2 M_y \tag{10}$$

$$M_{ns} = \left(n_x^2 - n_y^2\right)M_{xy} - n_x n_y (M_y - M_x) \tag{11}$$

$$Q_n = n_x Q_x + n_y Q_y \tag{12}$$

$$\theta_n = n_x\theta_x + n_y\theta_y \tag{13}$$

$$\theta_s = n_x\theta_y - n_y\theta_x, \tag{14}$$

where n_x and n_y are the direction cosines of a unit normal vector at a point at the laminated plate boundary [11,12].

Note that we can analyze Mindlin isotropic plates by considering $D_{11} = D_{22} = D = \frac{Eh^3}{12(1-\nu^2)}$, $D_{12} = \nu D_{11}$, $D_{66} = \frac{Gh^3}{12}$, $A_{55} = A_{44} = kGh$ and $D_{16} = D_{26} = A_{45} = 0$, where E is the modulus of elasticity and ν is Poisson's ratio of the isotropic material.

For further details about the FSDT, readers should consult [11].

3. THE COLLOCATION TECHNIQUE

The meshless radial basis functions method was first used by Hardy [13, 14] in the interpolation of geographical data. Later, Kansa used it for the solution of PDE [2, 3]. Nowadays this technique is well known for solving systems of PDEs with excellent accuracy [2–6].

Both Hardy and Kansa used the multiquadric radial basis function

$$g(r, c) = \sqrt{(r^2 + c^2)}; \tag{15}$$

but many other radial basis functions can be used as interpolation functions [15], such as the

$$g(r,c) = 1/\sqrt{(r^2+c^2)}; \qquad \text{inverse multiquadric}$$
$$g(r,c) = e^{-cr^2};\ c>0 \qquad \text{gaussian}$$
$$g(r) = r^2\log r; \qquad \text{thin plate spline}$$

Radial basis functions depend on a distance r between points in a grid and may depend on a shape parameter c. Typically, r represents the Euclidean distance, but it is not necessary to be this one.

More details about the RBF meshfree method can be found in [15].

In this article, we use the multiquadric radial basis function. It depends on the Euclidean distance r and on a shape parameter c that influences the function surface shape.

3.1. Collocation with Radial Basis Functions

Consider the generic boundary value problem with a domain Ω and boundary $\partial\Omega$, and linear differential operators L and B:

$$Lu(x) = f(x),\ x\in\Omega\subset\mathbb{R}^n; \qquad Bu|_{\partial\Omega} = q. \tag{16}$$

The function $\mathbf{u(x)}$ is approximated considering N interpolation points:

$$\mathbf{u} \simeq \bar{\mathbf{u}} = \sum_{j=1}^{N}\alpha_j g_j, \tag{17}$$

where α_j are parameters to be determined. We consider a global collocation method where the linear operators L and B acting at the domain $\Omega\backslash\partial\Omega$ and at the boundary $\partial\Omega$ define a set of global equations in the form

$$\begin{pmatrix}\mathbf{L}_{ii} & \mathbf{L}_{ib}\\ \mathbf{B}_{bi} & \mathbf{B}_{bb}\end{pmatrix}\begin{pmatrix}\alpha_i\\ \alpha_b\end{pmatrix} = \begin{pmatrix}f_i\\ q_b\end{pmatrix} \quad \text{or} \quad [\mathcal{L}][\alpha] = [\lambda], \tag{18}$$

where i and b denote the domain (interior) and boundary nodes, respectively; f_i and q_b are external conditions at the domain and at the boundary. The collocation technique produces an unsymmetric (full) coefficient matrix.

The function g represents a radial basis function. In our formulation we consider the multiquadric function in the form

$$g(r,\epsilon) = \sqrt{1+(\epsilon r)^2}. \tag{19}$$

It depends on the Euclidean distance r and on a shape parameter ϵ that works as a fine tuning for better performance. This formulation is equivalent to the one in (15) if we set $\epsilon = 1/c$.

We are using different shape function ϵ for all nodes, so that:

$$g_i(r,\epsilon) = (1+(\|x-x_j\|\epsilon_i)^2)^{\frac{1}{2}}. \tag{20}$$

Applying the collocation method with N centers (boundary and interior included) and g_j defined in (20), the governing differential equations (2) to (4) are interpolated for each node as

$$\begin{aligned}
&\sum_{j=1}^{N}\alpha_j^{\theta_x}D_{11}\frac{\partial^2 g_j}{\partial x^2}+\sum_{j=1}^{N}\alpha_j^{\theta_y}D_{16}\frac{\partial^2 g_j}{\partial x^2}+\sum_{j=1}^{N}\alpha_j^{\theta_y}(D_{12}+D_{16})\frac{\partial^2 g_j}{\partial x\partial y}\\
&\quad+2\sum_{j=1}^{N}\alpha_j^{\theta_x}D_{16}\frac{\partial^2 g_j}{\partial x\partial y}+\sum_{j=1}^{N}\alpha_j^{\theta_x}D_{66}\frac{\partial^2 g_j}{\partial y^2}+\sum_{j=1}^{N}\alpha_j^{\theta_y}D_{26}\frac{\partial^2 g_j}{\partial y^2}\\
&\quad-k\sum_{j=1}^{N}\alpha_j^{\theta_y}A_{45}g_j-k\sum_{j=1}^{N}\alpha_j^{w}A_{45}\frac{\partial g_j}{\partial y}-k\sum_{j=1}^{N}\alpha_j^{\theta_x}A_{55}g_j\\
&\quad-k\sum_{j=1}^{N}\alpha_j^{w}A_{55}\frac{\partial g_j}{\partial x}=0
\end{aligned}\tag{21}$$

$$\begin{aligned}
&\sum_{j=1}^{N}\alpha_j^{\theta_x}D_{16}\frac{\partial^2 g_j}{\partial x^2}+\sum_{j=1}^{N}\alpha_j^{\theta_y}D_{66}\frac{\partial^2 g_j}{\partial x^2}+\sum_{j=1}^{N}\alpha_j^{\theta_x}(D_{12}+D_{66})\frac{\partial^2 g_j}{\partial x\partial y}\\
&\quad+2\sum_{j=1}^{N}\alpha_j^{\theta_y}D_{26}\frac{\partial^2 g_j}{\partial x\partial y}+\sum_{j=1}^{N}\alpha_j^{\theta_x}D_{26}\frac{\partial^2 g_j}{\partial y^2}+\sum_{j=1}^{N}\alpha_j^{\theta_y}D_{22}\frac{\partial^2 g_j}{\partial y^2}\\
&\quad-k\sum_{j=1}^{N}\alpha_j^{\theta_y}A_{44}g_j-k\sum_{j=1}^{N}\alpha_j^{w}A_{44}\frac{\partial g_j}{\partial y}-k\sum_{j=1}^{N}\alpha_j^{\theta_x}A_{45}g_j\\
&\quad-k\sum_{j=1}^{N}\alpha_j^{w}A_{45}\frac{\partial g_j}{\partial x}=0
\end{aligned}\tag{22}$$

$$\begin{aligned}
&k\sum_{j=1}^{N}\alpha_j^{\theta_y}A_{45}\frac{\partial g_j}{\partial x}+k\sum_{j=1}^{N}\alpha_j^{w}A_{45}\frac{\partial^2 g_j}{\partial x\partial y}+k\sum_{j=1}^{N}\alpha_j^{\theta_x}A_{55}\frac{\partial g_j}{\partial x}\\
&\quad+k\sum_{j=1}^{N}\alpha_j^{w}A_{55}\frac{\partial^2 g_j}{\partial x^2}+k\sum_{j=1}^{N}\alpha_j^{\theta_y}A_{44}\frac{\partial g_j}{\partial y}+k\sum_{j=1}^{N}\alpha_j^{w}A_{44}\frac{\partial^2 g_j}{\partial y^2}\\
&\quad+k\sum_{j=1}^{N}\alpha_j^{\theta_x}A_{45}\frac{\partial g_j}{\partial y}+k\sum_{j=1}^{N}\alpha_j^{w}A_{45}\frac{\partial^2 g_j}{\partial x\partial y}=q.
\end{aligned}\tag{23}$$

The vector of $3N$ unknowns α_j is composed by the α_i parameters for w_0, θ_x, and θ_y, denoted as α_j^w, $\alpha_j^{\theta_x}$, and $\alpha_j^{\theta_y}$, respectively.

Both simply supported and clamped nodes include the boundary condition $w_i = 0$, interpolated as

$$\sum_{j=1}^{N}\alpha_j^{w}g_i = 0. \tag{24}$$

Depending on the boundary condition, different equations have to be added to this one, by modifying the corresponding ith row:

1. For a clamped edge, we also impose $\theta_x = 0$ and $\theta_y = 0$ at all boundary nodes i by the following interpolation

$$\sum_{j=1}^{N} \alpha_j^{\theta_x} g_i = 0 \tag{25}$$

$$\sum_{j=1}^{N} \alpha_j^{\theta_y} g_i = 0. \tag{26}$$

2. Simply supported edge
   (a) For each node i of a simply supported edge $x = a$, we must add $M_x = 0$ and $\theta_y = 0$,

$$D_{11} \sum_{j=1}^{N} \alpha_j^{\theta_x} \frac{\partial g_i}{\partial x} + D_{12} \sum_{j=1}^{N} \alpha_j^{\theta_y} \frac{\partial g_i}{\partial y} + D_{16} \left(\sum_{j=1}^{N} \alpha_j^{\theta_x} \frac{\partial g_i}{\partial y} + \sum_{j=1}^{N} \alpha_j^{\theta_y} \frac{\partial g_i}{\partial x} \right) = 0 \tag{27}$$

$$\sum_{j=1}^{N} \alpha_j^{\theta_y} g_i = 0 \tag{28}$$

   (b) Similarly, for each node i of a simply supported edge $y = a$, we will impose $M_y = 0$ and $\theta_x = 0$,

$$D_{12} \sum_{j=1}^{N} \alpha_j^{\theta_x} \frac{\partial g_i}{\partial x} + D_{22} \sum_{j=1}^{N} \alpha_j^{\theta_y} \frac{\partial g_i}{\partial y} + D_{26} \left(\sum_{j=1}^{N} \alpha_j^{\theta_x} \frac{\partial g_i}{\partial y} + \sum_{j=1}^{N} \alpha_j^{\theta_y} \frac{\partial g_i}{\partial x} \right) = 0 \tag{29}$$

$$\sum_{j=1}^{N} \alpha_j^{\theta_x} g_i = 0. \tag{30}$$

4. THE RESIDUAL SUBSAMPLING TECHNIQUE APPLIED TO PLATES

The application of the residual subsampling technique [1] to plates can be summarized as follows.

The user prescribes first both the lower and the higher residual thresholds and the number of initial non-overlapping boxes in the domain Ω. When applied to 2D, the boxes are quadrilaterals and each box contains one RBF center and four residual points, in which the residual is evaluated. The residual points do not contribute to the RBF solution, only the RBF centers do.

Figure 1 represents four initial boxes with its centers and residual points.

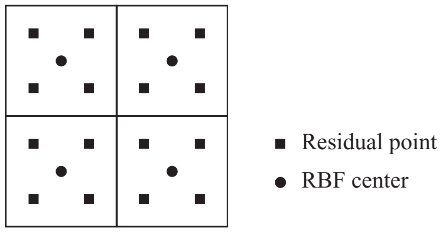

FIG. 1. Initial set of boxes, RBF centers, and residual points.

With the current set of RBF centers, we evaluate the PDE solution, as

$$L\alpha = f, \tag{31}$$

where L, f correspond to Eqs. (16)–(18).

Parameters α are then used to obtain the solution

$$A\alpha = u, \tag{32}$$

where A is the RBF interpolation matrix and u the current solution at the RBF centers (displacements w and rotations θ_x, θ_y).

At each residual point the residual is obtained by

$$Lu - f = r. \tag{33}$$

If, in each box, any residual value is larger than the higher prescribed residual tolerance, we then proceed to the next iteration with a refined set of boxes. At any box it is possible to have up to 4 new boxes. The case where we have 3 new ones is illustrated in Figure 2.

For every new box the value of the shape parameter ϵ_i (see Eq. (19)) is set double of that of its parents. Furthermore, whenever a box generates a new box the value of ϵ of the existing box is also doubled. We are somehow trying to keep the shape of the basis function constant on all scales as defined by local node spacing, since we double the shape parameter when centers become twice together.

In those boxes, wherein all residual points, the residual r is lower than the lower prescribed tolerance, RBF centers are

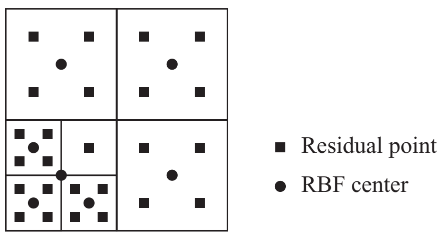

FIG. 2. Refined set of boxes, RBF centers, and residual points.

removed. In Figure 3 is illustrated the case of the four residual points associated to the RBF center located at the left and bottom having all residual smaller than the lower threshold imposed at the beginning.

If in each box all residuals meet the expected tolerance, we then remove that RBF center and proceed with a coarser grid.

For the new RBF center grid we iterate again by

- setting up a new shape parameter for each box;
- evaluating the solution $L\alpha = f$ and $A\alpha = u$; and
- controling residuals at the new residual points in each box $Lu - f = r$ and proceed as before.

5. NUMERICAL EXPERIMENTS FOR PLATES IN BENDING

We consider both isotropic and composite square plates in bending with length a and thickness h. The thickness to length ratios considered are $a/h = 10$ and $a/h = 100$.

The boundary conditions are either all edges simply-supported (SSSS) or all edges clamped (CCCC).

We consider a fixed boundary with 49 equally spaced points per side.

In the domain, we start with $N = 4$ (corresponding to $4^2 = 16$ boxes) or $N = 5$ (corresponding to $5^2 = 25$ boxes), being these quite coarse grids.

In Figure 4 the initial centers and residual points considered are presented for $N = 4$ and $N = 5$. When the chosen N is even, we introduce the plate central point as a center, without considering any checkbox or residual ckeckpoint. This was done to make possible the comparison with the exact solution as we always compare results by this adaptive method with analytical solutions obtained by series solutions. Errors are expressed in %.

The initial shape parameter is $\epsilon = 2/N$ for each center box, corresponding to $\epsilon = 2/4$ or $\epsilon = 2/5$. The chosen higher residual tolerance is $5{*}10^{-4}$ and the lower one is $5{*}10^{-7}$.

When applying the RBF collocation technique, the same set of points is usually used for centers and interpolation (collocation). In the present study that was done at the step of the algorithm where we obtain α by solving Eq. (31). However, at the step of the algorithm where the residual is evaluated by Eq. (33), the boxes centers were the collocation points and the residual points were the boxes centers and so matrix L in (33) has dimension $3N * 3M$, being N the total number of centers (center boxes and boundary points) and M the number of residual points.

The process stops when there are no more points to be added.

TABLE 1
Isotropic square plate SSSS, $a/h = 10$, 16 initial boxes.

Centers	Error (%)	Adds
209	1.077958e + 000	64
273	4.654796e − 001	63
336	7.690783e − 001	9
345	7.477775e − 001	2
347	7.407987e − 001	2
349	7.634622e − 001	0

TABLE 2
Isotropic square plate SSSS, $a/h = 10$, 25 initial boxes.

Centers	Eerror (%)	Adds
217	3.545147e + 000	100
317	7.549590e − 001	5
322	7.601606e − 001	0

5.1. Isotropic Plates

In this subsection, we consider an isotropic plate with modulus of elasticity $E = 10,920$ and Poisson's coefficient $\nu = 0.25$. The non-dimensional transverse displacement is given by

$$\overline{w} = 10^2 \frac{E_2 h^3}{a^4} w \tag{34}$$

for every solution.

In the following tables, we present the number of centers, the relative error in percentage, and the number of centers to be added at each iteration for the different isotropic plates analyzed. In all performed tests, there are no points to be removed.

In Tables 1 and 2 we present the evolution of the method for the isotropic square plate in bending, with thickness to length ratio $a/h = 10$, and simply-supported (SSSS) boundary condition. In Table 1 we show results with 16 initial boxes and in Table 2 we show results with 25 initial boxes. The analytical solution obtained by Lévy series solutions for this case is 4.7543.

In Figure 3 the centers and the boxes at the third iteration are presented for the isotropic square plate in bending, with thickness to length ratio $a/h = 10$, simply-supported, and starting with 16 boxes. In Figure 6 we present the final centers and the deformed shape for the same case.

The final RBF centers and deformed shape of the isotropic square plate in bending, with thickness to length ratio $a/h = 10$, simply supported, starting with 25 boxes are shown in Figure 7.

In Table 3 is possible to see the evolution of the iterative method when applied to the isotropic simply supported

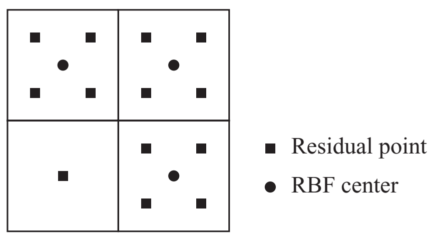

FIG. 3. Coarse set of RBF centers.

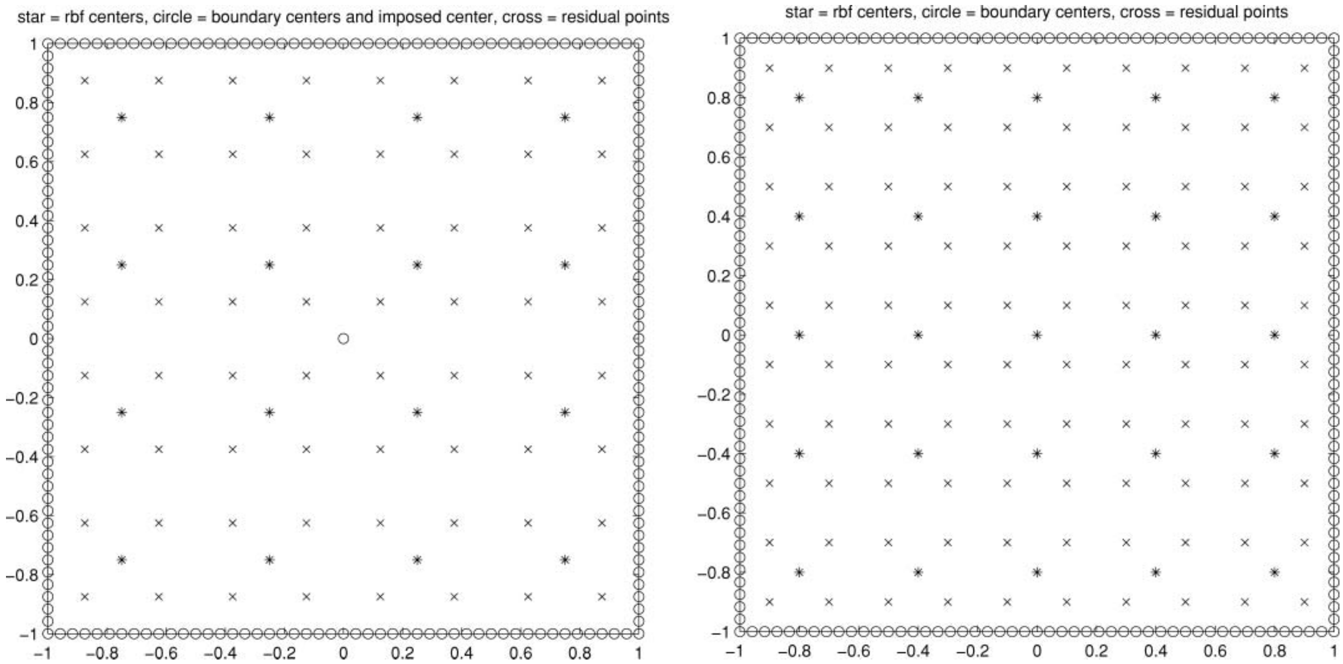

FIG. 4. Initial boxes for $N = 4$ (on the left) and $N = 5$ (on the right).

square plate, with thickness to length ratio $a/h = 100$, in bending, starting with 16 boxes. Results for the same plate but using 25 initial boxes are shown in Table 4. The analytical solution obtained by Lévy series solutions for this case is 4.5720.

The final set of RBF centers of the isotropic simply supported square plate in bending, with thickness to length ratio $a/h = 100$ are shown in Figure 8. On the left the case of 16 initial boxes is illustrated, and on the right the case of 25 initial boxes is illustrated.

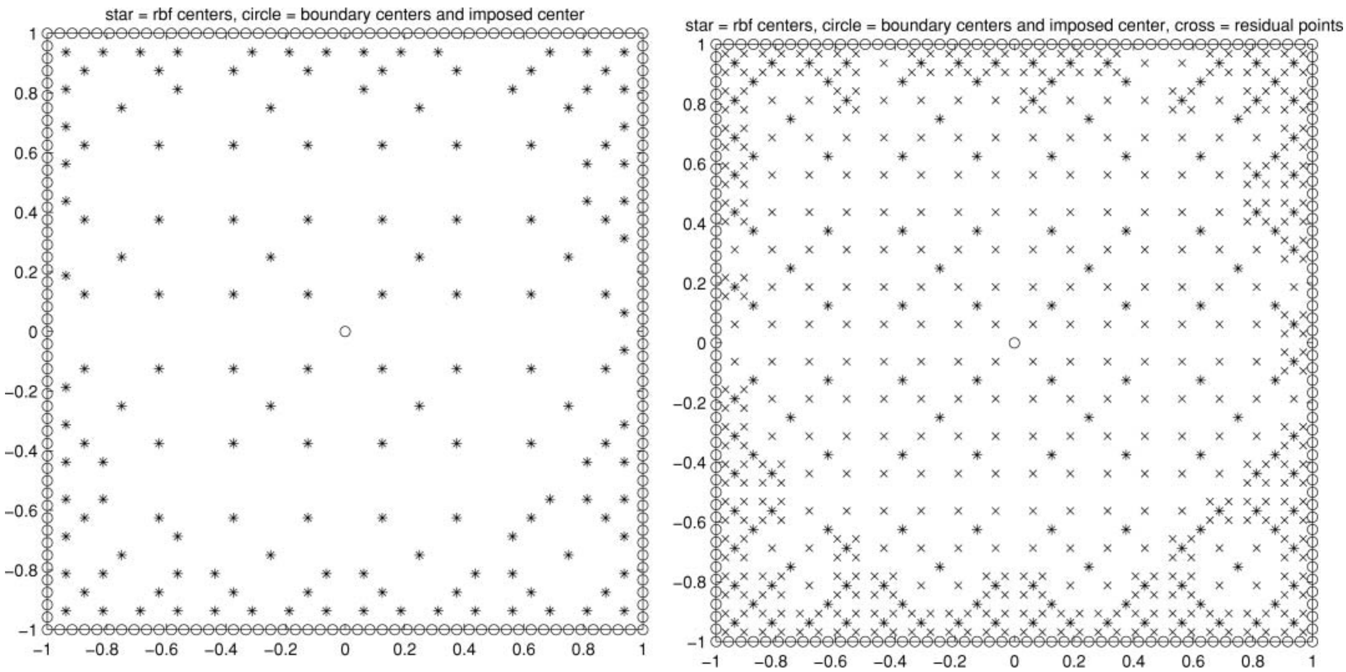

FIG. 5. Distribution of centers (left) and boxes (right) at third iteration, isotropic square plate, SSSS, $a/h = 10$, 16 initial boxes.

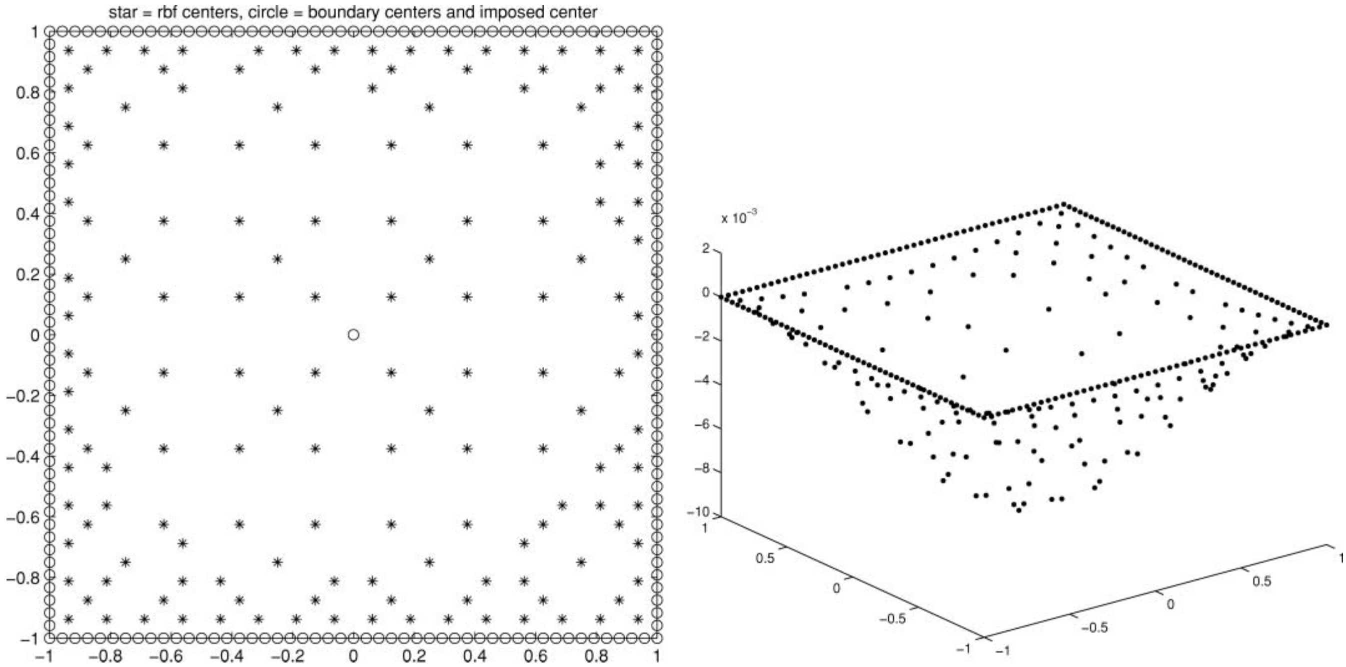

FIG. 6. Final centers and deformed shape of isotropic square plate, SSSS, $a/h = 10$, 16 initial boxes.

TABLE 3
Isotropic square plate SSSS, $a/h = 100$, 16 initial boxes.

Centers	Error (%)	Adds
209	9.999748e + 001	64
273	3.417590e + 000	168
441	5.100564e − 001	175
616	1.198528e − 002	25
641	5.794928e − 002	0

TABLE 4
Isotropic square plate SSSS, $a/h = 100$, 25 initial boxes.

Centers	Error (%)	Adds
217	1.728831e + 001	100
317	1.162787e + 000	141
458	7.501994e − 002	16
474	2.619898e − 002	19
493	5.042478e − 002	6
499	1.589558e − 002	2
501	5.990400e − 002	5
506	3.266486e − 002	2
508	3.155965e − 002	8
516	2.367293e − 002	1
517	1.635045e − 002	1
518	2.050627e − 002	0

5.2. Composite Plates

The examples considered here are limited to symmetric cross-ply laminates with layers of equal thickness and with identical material properties. The composite plates laminates are [0/90/0] (having 3 layers, each one with thickness $h/3$), and [0/90/90/0] (denoted as $[0/90]_s$ and having 4 layers, each one with thickness $h/4$).

The material properties are

$$E_1 = 25E_2;\ G_{23} = 0.2E_2;\ G_{12} = G_{13} = 0.5E_2;$$
$$\nu_{12} = 0.25;\ \nu_{21} = \nu_{12}\frac{E_2}{E_1}$$

As in the isotropic case, the tables below illustrate the evolution of the entire process of the iterative technique applied to the bending analysis of plates with respect to the number of RBF centers, the percentual relative error, and the number of centers to be added at each iteration. Once again, there are no points to be removed in all studied cases.

We use the same non-dimensional factor as in Eq. (34).

Tables 5 (16 initial boxes) and 6 (25 initial boxes) refer to the case of the composite [0/90/0] square plate in bending, with thickness to length ratio $a/h = 10$, and simply-supported (SSSS) boundary condition. The error is obtained by comparing with Mindlin solution [16], $\bar{w} = 1.0211$.

The set of RBF centers at the end of the iterative process of the [0/90/0] simply-supported square plate in bending, with thickness to length ratio $a/h = 10$ are presented in Figure 7.

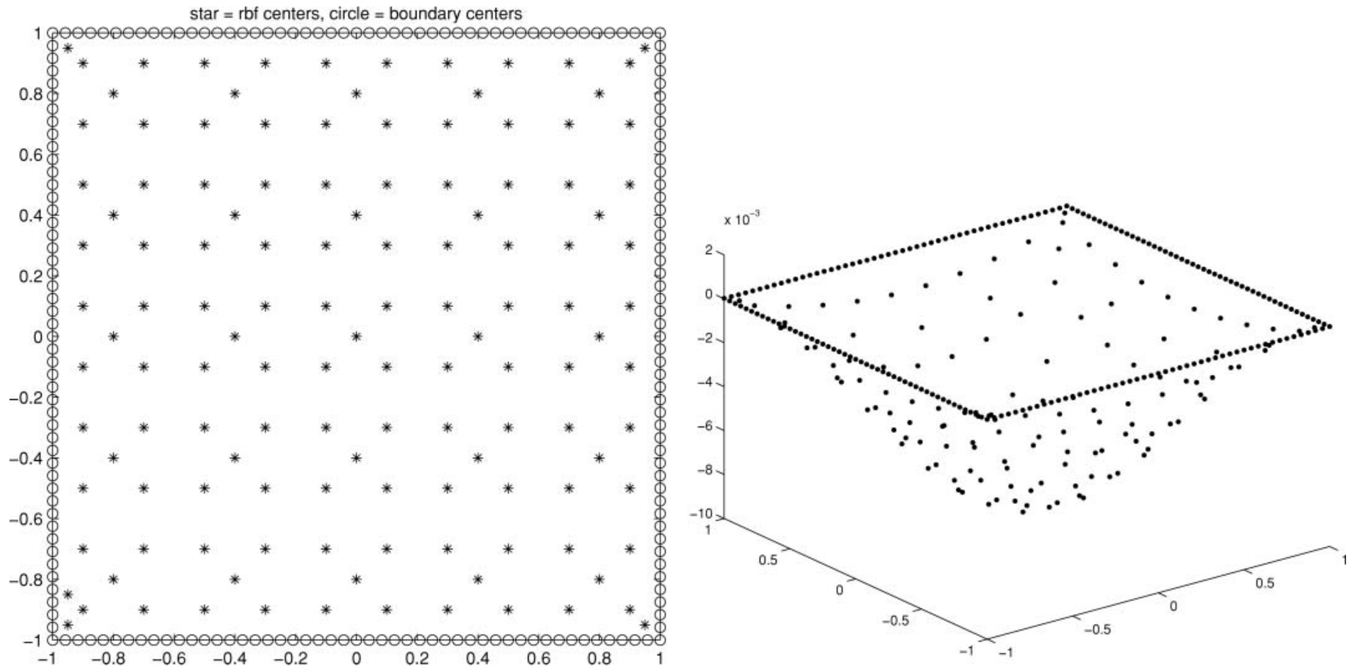

FIG. 7. Final centers and deformed shape of isotropic square plate, SSSS, $a/h = 10$, 25 initial boxes.

TABLE 5
[0/90/0] square plate SSSS, $a/h = 10$, 16 initial boxes.

Centers	Error (%)	Adds
209	1.654938e + 000	64
273	5.681379e − 002	33
306	2.037581e − 001	70
376	3.746343e − 001	78
454	1.127763e − 001	23
477	1.680405e − 001	4
481	3.267953e − 001	3
484	9.192459e − 002	4
488	5.203128e − 002	2
490	1.329159e − 001	0

TABLE 6
[0/90/0] square plate SSSS, $a/h = 10$, 25 initial boxes.

Centers	Error (%)	Adds
217	2.534830e+000	98
315	1.683086e − 001	31
346	1.696108e − 001	21
367	1.790651e − 001	1
368	1.612302e − 001	0

On the left we show the case of 16 initial boxes and on the right the case of 25 initial boxes.

Table 7 illustrates the iterative process results for laminated [0/90/0] simply supported square plate in bending, with $a/h = 100$ and 16 initial boxes. Table 8 presents results for the same problem, but with 25 initial boxes. Error is obtained by comparing the solution with the Mindlin solution [16], $\bar{w} = 0.6701$.

Table 9 illustrates the iterative process results for laminated [0/90/0] clamped square plate in bending, with $a/h = 10$ and 16 initial boxes. Table 10 presents results for the same problem, but with 25 initial boxes. Error is obtained by comparing the solution with the Mindlin solution [16], $\bar{w} = 0.4829$.

Table 11 illustrates the iterative process results for laminated $[0/90]_s$ simply supported square plate in bending, with $a/h = 10$ and 16 initial boxes. Table 12 presents results for the same

TABLE 7
[0/90/0] square plate SSSS, $a/h = 100$, 16 initial boxes.

Centers	Error (%)	Adds
209	3.619099e + 000	64
273	7.461579e − 001	170
443	1.243793e + 000	125
568	1.816361e − 001	50
618	5.638896e − 002	15
633	1.571762e − 001	4
637	1.110252e − 001	0

TABLE 8
[0/90/0] square plate SSSS, $a/h = 100$, 25 initial boxes.

Centers	Error (%)	Adds
217	9.756506e + 000	100
317	2.809135e − 001	71
388	1.355320e − 001	27
415	2.087332e − 001	20
435	2.012888e − 001	19
454	1.142907e − 001	11
465	1.947379e − 001	28
493	2.773958e − 001	16
509	1.792259e − 001	5
514	2.683916e − 001	6
520	2.199761e − 001	0

problem, but with 25 initial boxes. Error is obtained by comparing the solution with the Navier solution [11], $\bar{w} = 1.0250$.

Table 13 illustrates the iterative process results for laminated $[0/90]_s$ simply supported square plate in bending, with $a/h = 100$ and 16 initial boxes. Table 14 presents results for the same problem, but with 25 initial boxes. Error is obtained by comparing the solution with the Navier solution [11], $\bar{w} = 0.6833$.

5.3. Discussion of Results

On the numerical examples presented, the number of iterations varies from 3 to 13. In every case the error is inferior to 1% after a few iterations. This is a very satisfactory result.

TABLE 9
[0/90/0] square plate CCCC, $a/h = 10$, 16 initial boxes.

Centers	Error (%)	Adds
209	1.882287e + 000	60
269	4.101527e − 001	60
329	3.416589e − 002	41
370	2.623125e − 001	86
456	4.951293e − 001	28
484	6.473929e − 002	8
492	1.792660e − 002	24
516	1.677414e − 002	11
527	2.957150e − 002	2
529	4.054957e − 003	2
531	1.841740e − 002	2
533	1.273115e − 002	4
537	8.016174e − 003	0

TABLE 10
[0/90/0] square plate CCCC, $a/h = 10$, 25 initial boxes.

Centers	Error (%)	Adds
217	1.810916e − 001	100
317	7.859572e − 003	31
348	2.139349e − 002	28
376	6.628577e − 003	2
378	2.498585e − 002	10
388	1.358878e − 002	0

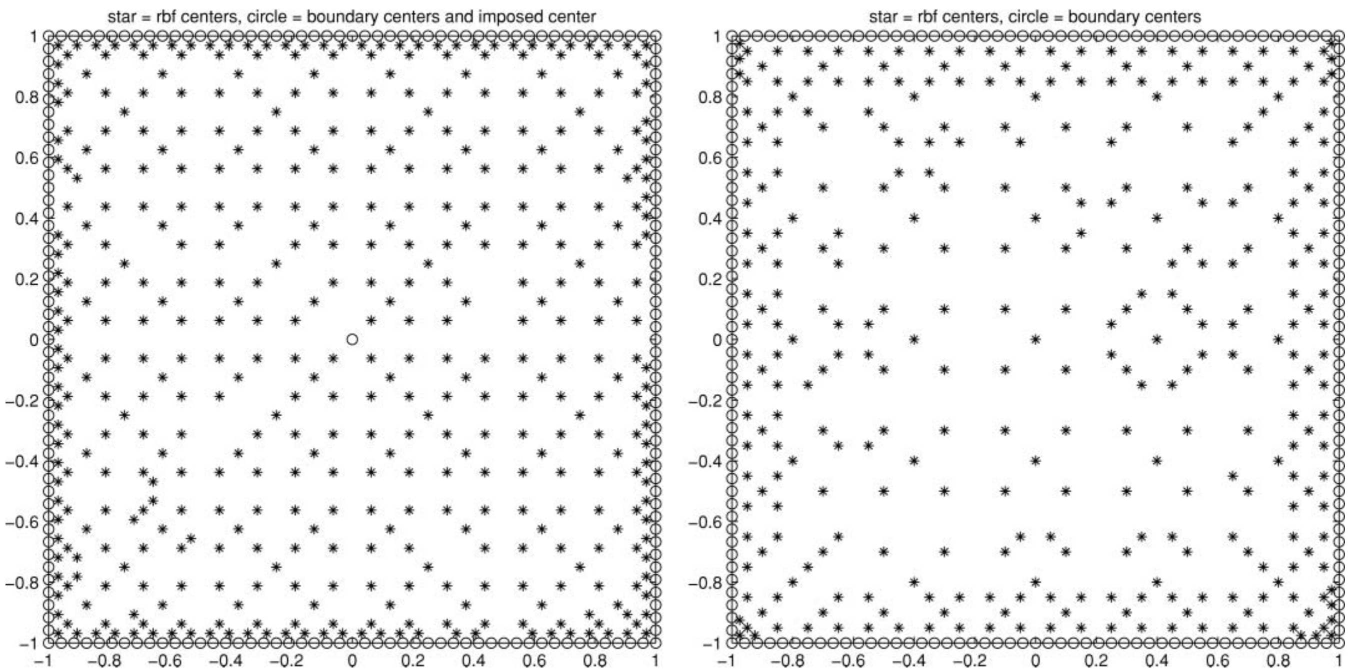

FIG. 8. Final centers of the isotropic square plate, SSSS, $a/h = 100$, 16 (left) and 25 (right) initial boxes.

TABLE 11
$[0/90]_s$ square plate SSSS, $a/h = 10$, 16 initial boxes.

Centers	Error (%)	Adds
401	1.556392e + 000	64
465	2.962116e − 001	68
533	1.578955e − 001	75
608	4.448880e − 001	48
656	2.274114e − 001	18
674	9.422296e − 002	8
682	1.123366e − 001	7
689	1.659383e − 001	10
699	2.400472e − 001	3
702	2.035321e − 001	3
705	2.367390e − 001	6
711	2.533541e − 001	0

TABLE 12
$[0/90]_s$ square plate SSSS, $a/h = 10$, 25 initial boxes.

Centers	Error (%)	Adds
409	2.607549e + 000	97
506	2.909581e − 001	37
543	2.425400e − 001	15
558	2.032778e − 001	11
569	2.095007e − 001	0

TABLE 13
$[0/90]_s$ square plate SSSS, $a/h = 100$, 16 initial boxes.

Centers	Error (%)	Adds
401	1.158316e + 001	64
465	6.423911e − 001	155
620	2.633451e + 000	131
751	1.097797e − 001	74
825	2.712160e − 001	1
826	2.015782e − 001	3
829	2.789185e − 001	0

TABLE 14
$[0/90]_s$ square plate SSSS, $a/h = 100$, 25 initial boxes.

Centers	Error (%)	Adds
409	9.781134e + 000	100
509	6.547123e − 001	86
595	2.146976e − 001	9
604	4.799680e − 001	30
634	3.497355e − 001	15
649	3.209971e − 001	16
665	3.653390e − 001	7
672	3.684787e − 001	0

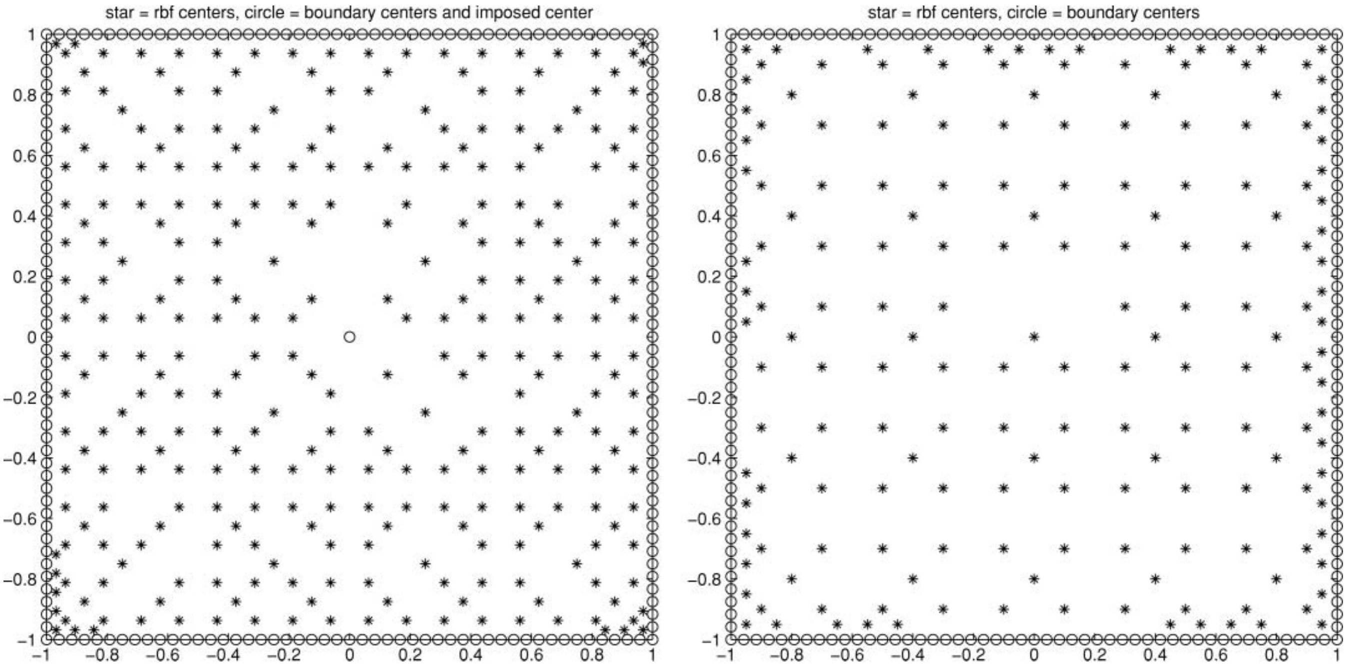

FIG. 9. Final centers of the [0/90/0] square plate, SSSS, $a/h = 10$, 16 (left) and 25 (right) initial boxes.

Taking in to consideration the number of initial boxes, two remarks are to be made. At the end of the iterative process, we always obtain more points if we start with 16 boxes, but it doesn't seem to have any influence in the number of iterations.

Thin plates generate more points than thick plates. The clamped case needs more points than the simply supported case.

At the end of each iteration process, the cloud of points is more dense near the boundary than in the central zone of the plate.

The process used to find α from equation $L\alpha = f$ is determinant for the performance of the process. The GMRES method is less sensitive to the shape parameter ϵ than the backslash Matlab operator \ and it has influence on the number of centers to add and remove and, consequently, in the number of final RBF centers. The backslash Matlab operator generates more points and the deformed plate frequently degenerates. Using the GMRES Matlab command, the deformed is more stable from the beginning till the end of the iterative process, but it is much more time consuming. This can be explained with the computational cost and the storage requirements that, according to [17], increases linearly with the number of iterations.

6. CONCLUSION

This article addresses the adaptive static analysis of isotropic and composite plates with radial basis multiquadric functions.

The residual subsampling technique proposed by Driscoll and Heryudono [1] was used for the domain with a fixed boundary grid.

Numerical tests were then performed on the bending analysis of isotropic and symmetric cross-ply laminated square plates. A first-order shear deformation theory was used. When applying the Driscoll and Heryudono residual subsampling technique to bending analysis, the residual has to be improved to take in to consideration the degrees of freedom, three in this case.

In this technique, the user must prescribe the residual tolerance, the initial number of nodes, and the initial shape parameter. This parameter is then modified for each nodal box in order to control the conditioning of the coefficient matrix.

We calculate the error of the present method with respect to the exact solutions. The results obtained show that the adaptive method converges to a very good solution after a few iterations even by starting with a very coarse grid.

Further studies, including optimization of the shape parameter in each iteration, are sought. The combination of optimization techniques with adaptive methods may reduce the number of nodes in each iteration. The present method may generate quite a large number of nodes, depending on the thickness of the plate, and the way we select the shape parameters.

REFERENCES

1. T.A. Driscoll, and A.R.H. Heryudono, Adaptive Residual Subsampling Methods for Radial Basis Function Interpolation and Collocation Problems, Comput. & Math. Appl., vol. 53, no. 6, pp. 927–939, 2007.
2. E.J. Kansa, Multiquadrics. A Scattered Data Approximation Scheme with Applications to Computational Fluid-dynamics. I. Surface Approximations and Partial Derivative Estimates, Comput. & Math. Appl., vol. 19, no. (8–9), pp. 127–145, 1990.
3. E.J. Kansa, Multiquadrics. A Scattered Data Approximation Scheme with Applications to Computational Fluid-dynamics. II. Solutions to Parabolic, Hyperbolic and Elliptic Partial Differential Equations, Comput. & Math. Appl., vol. 19, no. (8–9), pp. 147–161, 1990.
4. E. Larsson, and B. Fornberg, A Numerical Study of Some Radial Basis Function Based Solution Methods for Elliptic PDEs, Comput. & Math. Appl., vol. 46, no. (5–6), pp. 891–902, 2003.
5. G.E. Fasshauer, Solving Partial Differential Equations by Collocation with Radial Basis Functions, Surface Fitting and Multiresolution Methods, vol. 2. Proceedings of the 3rd International Conference on Curves and Surfaces, vol. 2, pp. 131–138, 1997.
6. S.A. Sarra, Adaptive Radial Basis Function Methods for Time Dependent Partial Differential Equations, Appl. Numer. Math., vol. 54, no. 11, pp. 79–94, 2005.
7. A.H.-D. Cheng, M.A. Golberg, E.J. Kansa, and G. Zammito, Exponential Convergence and H-c Multiquadric Collocation Method for Partial Differential Equations, Numer Methods Partial Differential Eq. 19: 571594, 2003.
8. A.J.M. Ferreira, C.M.C. Roque, and P.A.L.S. Martins, Analysis of Composite Plates Using Higher-Order Shear Deformation Theory and a Finite Point Formulation Based on the Multiquadric Radial Basis Function Method, Composites Part B: Engineering, vol. 34, pp. 627–636, 2003.
9. A.J.M. Ferreira, Polyharmonic (Thin-Plate) Splines in the Analysis of Composite Plates, Int. J. Mech. Sci., vol. 46, no. 10, pp. 1549–1569, 2004.
10. A.J.M. Ferreira, C.M.C. Roque, and P.A.L.S. Martins, Radial Basis Functions and Higher-Order Theories in the Analysis of Laminated Composite Beams and Plates, Composite Struct., Vol. 66, pp. 287–293, 2004.
11. J.N. Reddy, Mechanics of Laminated Composite Plates. CRC Press, New York, 1997.
12. K.M. Liew, Y.Q. Huang, and J.N. Reddy, Vibration Analysis of Symmetrically Laminated Plates Based on FSDT Using the Moving Least Squares Differential Quadrature Method, Comp. Meth. Appl. Mech. Eng., vol. 192, pp. 2203–2222, 2003.
13. R.L. Hardy, Multiquadrics Equations of Topography and Other Irregular Surfaces, J. Geophys. Res., vol. 176, no. (8–9), pp. 1905–1915, 1971.
14. R.L. Hardy, Theory and Apllications of the Multiquadric-Biharmonic Method: 20 years of Discovery, Comput. Math. Appl., vol. 19, no. (8–9), pp. 163–208, 1990.
15. G.L. Liu, Mesh Free Methods: Moving Beyond the Finite Element Method. Boca Raton, FL: CRC Press, 2003.
16. B.N. Pandya, and T. Kant, Flexural Analysis of Laminated Composites Using Refined Higher-Order C^0 Plate Bending Elements, Comput. Methods Appl. Mech. Eng., vol. 66, pp. 173–198, 1988.
17. B. Bradie, A Friendly Introduction to Numerical Analysis. Pearson Prentice Hall, Upper Saddle River, NJ, 2006.

3.1.2 Vibration and buckling of composite structures using oscillatory radial basis functions

Ana M. A. Neves, A. J. M. Ferreira, C. M. C. Roque, R. M. N. Jorge, C. M. M. Soares,
submetido para publicação em Applied Mathematics and Mechanics, 2011.

Vibration and buckling of composite structures using oscillatory radial basis functions

A. M. A. Neves [a], A. J. M. Ferreira [a], C. M. C. Roque [b], R. M. N. Jorge [a], C. M. M. Soares [c]

[a] *Departamento de Engenharia Mecânica, Faculdade de Engenharia da Universidade do Porto, Rua Dr. Roberto Frias, 4200-465 Porto, Portugal*

[b] *INEGI, Faculdade de Engenharia da Universidade do Porto, Rua Dr. Roberto Frias, 4200-465 Porto, Portugal*

[c] *Departamento de Engenharia Mecânica, Instituto Superior Técnico, Av. Rovisco Pais, Lisboa, Portugal*

1 Introduction

This paper addresses for the first time the analysis of laminated composite plates by oscillatory radial basis functions. These functions are very rarely used in the solution of PDEs, and this paper aims to prove that such functions can be very accurate in the vibration and buckling analysis of laminated composite plates.

A radial basis function, $\phi(\|x - x_j\|)$ is a spline that depends on the Euclidian distance between distinct data centers $x_j, j = 1, 2, ..., N \in \mathbb{R}^n$, also called nodal or collocation points.

The use of oscillatory radial basis functions has not been seen in the literature. This paper investigates the accuracy of such functions in the analysis of laminated composite plates.

It is well known that the classical laminated plate theory(CLPT) based on the Kirchhoff theory yields acceptable results only for thin laminates [1]. First-order [2,3] and higher-order [4,5] shear deformation theories have been developed to include transverse shear deformation effects. Here we use a refined version of Kant's theories (see Kant [4]) with the following displacement field for isotropic or symmetric cross-ply laminated plates:

$$u = zu_1 + z^3 u_3; \quad v = zv_1 + z^3 v_3; \quad w = w_0 + z^2 w_2 \tag{1}$$

This theory accounts for transverse normal stress and through-the-thickness deformation.

Some relevant works on vibration and buckling of thick plates include those of Wang et al. [6], Khdeir and Librescu [7], Bhimaraddi [8], Kitipornchai et al. [9], Liew et al. [10–12], and Reddy et al. [13,14]. An historical review on laminated plates and shells has been presented by Carrera [15]. The use of alternative methods to the finite element methods such as the meshless methods based on radial basis functions is atractive due to the absence of a mesh and the ease of collocation methods. The use of radial basis function for the analysis of structures and materials has been previously studied by numerous authors [16–27]. More recently the authors have applied RBFs to the static deformations of composite beams and plates [28–30].

Although much work has been done with analytical or meshless methods, there is no research on vibration and buckling analysis of laminated plates by oscillating radial basis functions.

2 Radial basis functions

The radial basis function (ϕ) approximation of a function ($\mathbf{u}$) is given by

$$\tilde{\mathbf{u}}(\mathbf{x}) = \sum_{i=1}^{N} \alpha_i \phi\left(\|x - y_i\|_2\right), \mathbf{x} \in \mathbb{R}^n \tag{2}$$

where $y_i, i = 1, .., N$ is a finite set of distinct points (centers) in $\mathbb{R}^n$. The coefficients α_i are chosen so that $\tilde{\mathbf{u}}$ satisfies some boundary conditions. The most common RBFs are

$$\begin{array}{ll}
\phi(r) = r^3 & \text{,cubic} \\
\phi(r) = r^2 \log(r) & \text{,thin plate splines} \\
\phi(r) = (1 - r)_+^m p(r) & \text{,Wendland functions} \\
\phi(r) = e^{-(cr)^2} & \text{,Gaussian} \\
\phi(r) = \sqrt{c^2 + r^2} & \text{,Multiquadrics} \\
\phi(r) = (c^2 + r^2)^{-1/2} & \text{,Inverse Multiquadrics}
\end{array}$$

where the Euclidian distance r is real and non-negative, $p(r)$ is a polinomial, and c is a shape parameter, a positive constant.

In this paper we use an oscillating function, a linear Gaussian-Laguerre, defined as

$$\phi(r) = 1/\pi \; e^{-(cr)^2} \left(2 - (cr)^2\right) \quad (3)$$

This function is strictly positive definite in $\mathbb{R}^2$ and infinitely smooth. The Laguerre-Gaussians functions family tends to a Gaussian function $\phi(r) = e^{-(cr)^2}$. We will compare the Gaussian with oscillating function in the paper.

In figure 1 we illustrate the shape of the oscillating functions.

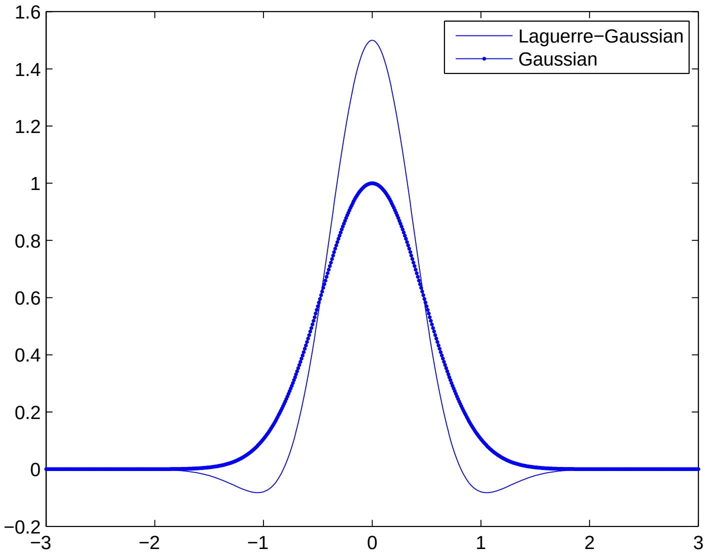

Fig. 1. Oscillating and Gaussian functions

2.1 Solution of the interpolation problem

Hardy [31] introduced multiquadrics in the analysis of scattered geographical data. In the 1990's Kansa [32] used multiquadrics for the solution of partial differential equations.

Considering N distinct interpolations, and given $u(x_j), j = 1, 2, ..., N$, we find α_i by the solution of a $N \times N$ linear system

$$\mathbf{A}\underline{\alpha} = \mathbf{u} \quad (4)$$

where $\mathbf{A} = [\phi(\|x - y_i\|_2)]_{N\times N}$, $\underline{\alpha} = [\alpha_1, \alpha_2, ..., \alpha_N]^T$ and $\mathbf{u} = [u(x_1), u(x_2), ..., u(x_N)]^T$.

The RBF interpolation matrix A is positive definite for some RBFs [33], but in general provides ill-conditioned systems.

2.2 Solution of the static problem

The solution of a static problem by radial basis functions considers N_I nodes in the domain and N_B nodes on the boundary, with total number of nodes $N = N_I + N_B$.

We denote the sampling points by $x_i \in \Omega, i = 1, ..., N_I$ and $x_i \in \partial\Omega, i = N_I + 1, ..., N$. At the points in the domain we solve the following system of equations

$$\sum_{i=1}^{N} \alpha_i \mathcal{L}\phi\left(\|x - y_i\|_2\right) = \mathbf{f}(x_j), j = 1, 2, ..., N_I \tag{5}$$

or

$$\mathcal{L}^I \underline{\alpha} = \mathbf{F} \tag{6}$$

where

$$\mathcal{L}^I = \left[\mathcal{L}\phi\left(\|x - y_i\|_2\right)\right]_{N_I \times N} \tag{7}$$

For the boundary conditions we have

$$\sum_{i=1}^{N} \alpha_i \mathcal{L}_B\phi\left(\|x - y_i\|_2\right) = \mathbf{g}(x_j), j = N_I + 1, ..., N \tag{8}$$

or

$$\mathbf{B}\underline{\alpha} = \mathbf{G} \tag{9}$$

Therefore we can write a finite-dimensional static problem as

$$\begin{bmatrix} \mathcal{L}^I \\ \mathbf{B} \end{bmatrix} \underline{\alpha} = \begin{bmatrix} \mathbf{F} \\ \mathbf{G} \end{bmatrix} \tag{10}$$

where

$$\mathcal{L}^I = L\phi\left[\left(\|x_{N_I} - y_j\|_2\right)\right]_{N_I \times N}, \mathbf{B} = L_B\phi\left[\left(\|x_{N_I+1} - y_j\|_2\right)\right]_{N_B \times N}$$

By inverting the system (10), we obtain the vector of parameters $\underline{\alpha}$. We then proceed to the solution by the interpolation equation (2).

2.3 Solution of the eigenproblem

We consider N_I nodes in the interior of the domain and N_B nodes on the boundary, with $N = N_I + N_B$.

We denote interpolation points by $x_i \in \Omega, i = 1, ..., N_I$ and $x_i \in \partial\Omega, i = N_I + 1, ..., N$. For the points in the domain, the following problem is defined

$$\sum_{i=1}^{N} \alpha_i \mathcal{L}\phi\left(\|x - y_i\|_2\right) = \lambda \tilde{\mathbf{u}}(x_j), j = 1, 2, ..., N_I \tag{11}$$

or

$$\mathcal{L}^I \underline{\alpha} = \lambda \tilde{\mathbf{u}}^I \tag{12}$$

where

$$\mathcal{L}^I = \left[\mathcal{L}\phi\left(\|x - y_i\|_2\right)\right]_{N_I \times N} \tag{13}$$

For the boundary conditions we have

$$\sum_{i=1}^{N} \alpha_i \mathcal{L}_B\phi\left(\|x - y_i\|_2\right) = 0, j = N_I + 1, ..., N \tag{14}$$

or

$$\mathbf{B}\underline{\alpha} = 0 \tag{15}$$

Therefore we can write a finite-dimensional problem as a generalized eigenvalue problem

$$\begin{bmatrix} \mathcal{L}^I \\ \mathbf{B} \end{bmatrix} \underline{\alpha} = \lambda \begin{bmatrix} \mathbf{A}^I \\ \mathbf{0} \end{bmatrix} \underline{\alpha} \tag{16}$$

where

$$\mathbf{A}^I = \phi\left[\left(\|x_{N_I} - y_j\|_2\right)\right]_{N_I \times N}, \mathbf{B} = \mathcal{L}_B\phi\left[\left(\|x_{N_I+1} - y_j\|_2\right)\right]_{N_B \times N}$$

We seek the generalized eigenvalues and eigenvectors of these matrices.

3 Numerical examples

3.1 Free vibrations

The example considered is a simply supported square plate of the cross-ply lamination $[0°/90°/90°/0°]$. The thickness and length of the plate are denoted by h and a, respectively. The thickness-to-span ratio $h/a = 0.2$ is employed in the computation. The example considers a Chebyshev grid. All layers of the laminate are assumed to be of the same thickness, density and made of the same linearly elastic composite material. The following material parameters of a layer are used:

$$\frac{E_1}{E_2} = 10, 20, 30 \text{ or } 40; G_{12} = G_{13} = 0.6E_2; G_3 = 0.5E_2; \nu_{12} = 0.25$$

The subscripts 1 and 2 denote the directions normal and transverse to the fiber direction in a lamina, which may be oriented at an angle to the plate axes. The ply angle of each layer is measured from the global x-axis to the fiber direction. In all examples we use a shear correction factor $k = \pi^2/12$, as proposed in [34].

Table 1 lists the fundamental frequency of the simply supported laminate made of various modulus ratios of E_1/E_2. It is found that the results are in very close agreement with the values of [35,36] and the meshfree results of Liew [34] based on the FSDT. The relative errors between the analytical and present solutions are shown in brackets. For all E_1/E_2 ratios errors are below 0.5%. Results for all E_1/E_2 ratios converge quite well. In figures 2 the first eight modes are illustrated, for $E_1/E_2 = 10$, using 13×13 nodes, showing a very smooth shape.

3.2 Buckling

The following typical dimensionless composite material properties are used in the buckling analysis:

$$E_1/E_2 = 10, 20, 30, 40; G_{12}/E_2 = G_{13}/E_2 = 0.6; G_{23}/E_2 = 0.5; \nu_{12} = 0.25$$

The critical buckling loads are xomputed for simply-supported square bidirectional composite plates, with $a/h = 10$, under adimensional uni-axial buckling load $(\bar{N}_{xx}a^2/(E_2h^3))$. All layers are assumed to be of the same thickness and material properties. Table 2 lists the uni-axial buckling loads of the four-layer simply supported laminated plate discretized with a regular grid. Exact solutions by Khdeir and Librescu [7] and differential quadrature results by Liew et al. [11] based on the FSDT are also presented for comparison. It is found that the critical buckling load is obtained with a few grid points. The present results are in excellent correlation with those of Khdeir and Librescu [7], and those of Liew et al. [11]. Both linear Laguerre-Gaussian and Gaussian functions present excellent convergence properties.

4 Conclusions

In this paper we used the radial basis function collocation method to analyse buckling loads and free vibrations of isotropic and laminated plates. Here we used oscillating functions, and a higher-order shear deformation theory by Kant, accounting for through-the-thickness deformation.

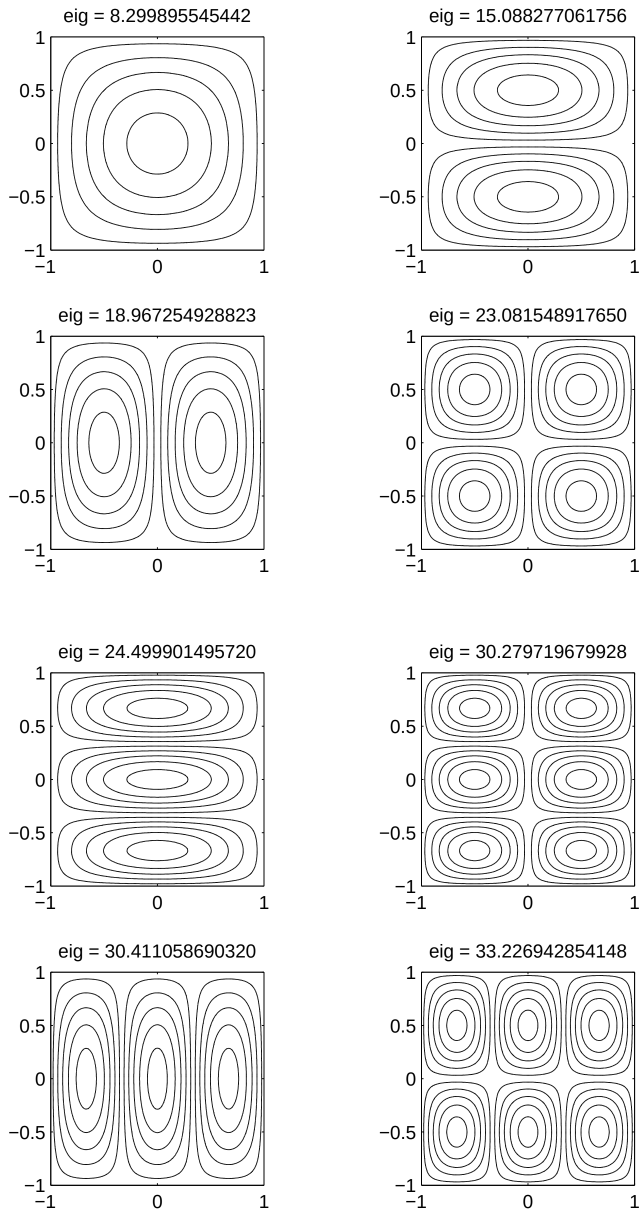

Fig. 2. First eight vibration modes of the simply-supported cross-ply laminated square plate $[0°/90°/90°/0°]$, $E_1/E_2 = 10$, 13×13 nodes

The oscillating radial basis functions, here used for the first time in the vibration and buckling analysis of composite plates, prove to be excellent alternative to non-oscillating functions, such as the Gaussians, and present excellent convergence and accurate results.

Acknowledgements

The financial support of the National Foundation for Science and Technology (FCT) to LAETA is gratefully acknowledged. The first author is supported by FCT through grant SFRH/BD/45554/2008.

References

[1] E. Reissner and Y. Stavsky. Bending and stretching of certain types of aelotropic elastic plates. *J. Appl. Mech.*, 28:402–408, 1961.

[2] R. D. Mindlin. Influence of rotary inertia and shear in flexural motions of isotropic elastic plates. *J. Appl. Mech.*, 18:31–38, 1951.

[3] E. Reissner. The effect of transverse shear deformations on the bending of elastic plates. *J. Appl. Mech.*, 12:A69–A77, 1945.

[4] T. Kant. Numerical analysis of thick plates. *Computer Methods in Applied Mechanics and Engineering*, 31:1–18, 1982.

[5] J. N. Reddy. A simple higher-order theory for laminated composite plates. *Journal of Applied Mechanics*, 51:745–752, 1984.

[6] C. M. Wang, K. M. Liew, Y. Xiang, and S. Kipornchai. Buckling of rectangular mindlin plates with internal line supports. *Int J Solid Struct*, 30(1):1–17, 1993.

[7] A. A. Khdeir and L. Librescu. Analysis of symmetric cross-ply elastic plates using a higher-order theory. part ii: buckling and free vibration. *Compos Struct*, 9:259–277, 1988.

[8] A. Bhimaraddi. Free vibration analysis of doubly curved shallow shells on rectangular planform using three-dimensional elasticity theory. *Int J Solids Struct*, 27(7):897–913, 1991.

[9] S. Kitipornchai, Y. Xiang, C.M. Wang, and K.M. Liew. Buckling of thick skew plates. *Int J Num Meth Eng*, 36:1299–1310, 1993.

[10] K. M. Liew, J. Wang, T. Y. Ng, and M. J. Tan. Free vibration and buckling analyses of shear-deformable plates based on fsdt meshfree method. *Journal of Sound and Vibration*, 276:997–1017, 2004.

[11] K. M. Liew and Y. Q. Huang. Bending and buckling of thick symmetric rectangular laminates using the moving least-squeares differential quadrature method. *Int J Mech Sci*, 45:95–114, 2003.

[12] K. M. Liew, Y. Q. Huang, and J. N. Reddy. Vibration analysis of symmetrically laminated plates based on fsdt using the moving least squares differential quadrature method. *Comp. Meth. Appl. Mech. Eng.*, 192(19):2203–2222, 2003.

[13] N. S. Putcha and J. N. Reddy. Stability and natural vibration analysis of laminated plates by using a mixed element based on a refined plate theory. *J. Sound and Vibration*, 104(2):285–300, 1986.

[14] J. N. Reddy and N. D. Phan. Stability and vibration of isotropic, orthotropic and laminated plates according to a higher-order shear deformation theory. *J. Sound and Vibration*, 98(2):157–170, 1985.

[15] E. Carrera. Historical review of zig-zag theories for multilayered plates and shells. *Appl. Mech. Rev.*, (56):287–308, 2003.

[16] Y. C. Hon, M. W. Lu, W. M. Xue, and Y. M. Zhu. Multiquadric method for the numerical solution of byphasic mixture model. *Appl. Math Comput.*, 88:153–175, 1997.

[17] Y. C. Hon, K. F. Cheung, X. Z. Mao, and E. J. Kansa. A multiquadric solution for the shallow water equation. *ASCE J. Hydraulic Engineering*, 125(5):524–533, 1999.

[18] J. G. Wang, G. R. Liu, and P. Lin. Numerical analysis of biot's consolidation process by radial point interpolation method. *Int. J. Solids and Structures*, 39(6):1557–1573, 2002.

[19] G. R. Liu and Y. T. Gu. A local radial point interpolation method (lrpim) for free vibration analyses of 2-d solids. *Journal of Sound and Vibration*, 246(1):29–46, 2001.

[20] G. R. Liu and J. G. Wang. A point interpolation meshless method based on radial basis functions. *Int. J. Num. Meth. Eng.*, 54:1623–1648, 2002.

[21] J. G. Wang and G. R. Liu. On the optimal shape parameters of radial basis functions used for 2-d meshless methods. *Comp. Meth. in Appl. Mech. and Eng.*, 191:2611–2630, 2002.

[22] X. L. Chen, G. R. Liu, and S. P. Lim. An element free galerkin method for the free vibration analysis of composite laminates of complicated shape. *Composite Structures*, 59:279–289, 2003.

[23] K. Y. Dai, G. R. Liu, S. P. Lim, and X. L. Chen. An element free galerkin method for static and free vibration analysis of shear-deformable laminated composite plates. *Journal of Sound and Vibration*, 269:633–652, 2004.

[24] G. R. Liu and X. L. Chen. Buckling of symmetrically laminated composite plates using the element-free galerkin method. *International Journal of Structural Stability and Dynamics*, 2:281–294, 2002.

[25] K. M. Liew, X. L. Chen, and J. N. Reddy. Mesh-free radial basis function method for buckling analysis of non-uniformity loaded arbitrarily shaped shear deformable plates. *Computer Methods in Applied Mechanics and Engineering*, 193:205–225, 2004.

[26] Y. Q Huang and Q. S. Li. Bending and buckling analysis of antisymmetric laminates using the moving least square differential quadrature method. *Computer Methods in Applied Mechanics and Engineering*, 193:3471–3492, 2004.

[27] L. Liu, G. R. Liu, and V. C. B. Tan. Element free method for static and free vibration analysis of spatial thin shell structures. *Computer Methods in Applied Mechanics and Engineering*, 191:5923–5942, 2002.

[28] A. J. M. Ferreira. A formulation of the multiquadric radial basis function method for the analysis of laminated composite plates. *Composite Structures*, 59:385–392, 2003.

[29] A. J. M. Ferreira. Thick composite beam analysis using a global meshless approximation based on radial basis functions. *Mechanics of Advanced Materials and Structures*, 10:271–284, 2003.

[30] A. J. M. Ferreira, C. M. C. Roque, and P. A. L. S. Martins. Analysis of composite plates using higher-order shear deformation theory and a finite point formulation based on the multiquadric radial basis function method. *Composites: Part B*, 34:627–636, 2003.

[31] R. L. Hardy. Multiquadric equations of topography and other irregular surfaces. *Geophysical Research*, 176:1905–1915, 1971.

[32] E. J. Kansa. Multiquadrics- a scattered data approximation scheme with applications to computational fluid dynamics. i: Surface approximations and partial derivative estimates. *Comput. Math. Appl.*, 19(8/9):127–145, 1990.

[33] M. D. Buhmann. Radial basis functions. *Acta numerica*, 9:1–38, 2000.

[34] K. M. Liew, Y. Q. Huang, and J. N. Reddy. Vibration analysis of symmetrically laminated plates based on fsdt using the moving least squares differential quadrature method. *Comp. Meth. Appl. Mech. Eng.*, 192:2203–2222, 2003.

[35] J. N. Reddy. *Mechanics of Laminated Composite Plates: Theory and Analysis*. CRC Press, Boca Raton,, 1997.

[36] A. A. Khdeir and L. Librescu. Analysis of symmetric cross-ply elastic plates using a higher-order theory,part ii: buckling and free vibration. *Composite Structures*, 9:259–277, 1988.

Method	Grid	E_1/E_2			
		10	20	30	40
Liew [34]		8.2924	9.5613	10.320	10.849
Exact (Reddy, Khdeir)[35,36]		8.2982	9.5671	10.326	10.854
Present Oscillatory	9×9	8.3000	9.5413	10.2688	10.7654
	13×13	8.2999	9.5411	10.2686	10.7652
	17×17	8.2999	9.5411	10.2686	10.7652
	21×21	8.2999	9.5411	10.2686	10.7652
	Error in % w.r.t. [35,36]	(0.09)	(0.21)	(0.49)	(0.77)
Present Gaussians	9×9	8.2999	9.5411	10.2686	10.7652
	13×13	8.2999	9.5411	10.2686	10.7652
	17×17	8.2999	9.5411	10.2686	10.7652
	21×21	8.2999	9.5411	10.2686	10.7652

Table 1
The normalized fundamental frequency of the simply-supported cross-ply laminated square plate $[0°/90°/90°/0°]$ ($\bar{w} = (wa^2/h)\sqrt{\rho/E_2}, h/a = 0.2$)

Grid	Approach	Liew et al. [11]	Khdeir and Librescu [7]
		23.463	23.453
	Present, Oscillatory		
9×9	23.2928		
13×13	23.2915		
17×17	23.2916 (0.69)		
	Present, Gaussian		
9×9	23.2916		
13×13	23.2916		
17×17	23.2916 (0.69)		

Table 2
Uni-axial buckling load of four-layer $[0°/90°/90°/0°]$ simply supported laminated plate ($\bar{N} = \bar{N}_{xx}a^2/(E_2h^3), \bar{N}_{xy} = 0, \bar{N}_{yy} = 0$)

3.1.3 Analysis of plates on Pasternak foundations by radial basis functions

A. J. M. Ferreira, C. M. C. Roque, Ana M. A. Neves, R. M. N. Jorge, C. M. M. Soares, Analysis of plates on Pasternak foundations by radial basis functions, Computational Mechanics, Volume 46, Number 6, 2010, pages 791 - 803.

Comput Mech (2010) 46:791–803
DOI 10.1007/s00466-010-0518-9

ORIGINAL PAPER

Analysis of plates on Pasternak foundations by radial basis functions

A. J. M. Ferreira · C. M. C. Roque · A. M. A. Neves · R. M. N. Jorge · C. M. M. Soares

Received: 19 February 2010 / Accepted: 22 June 2010 / Published online: 22 July 2010

Abstract This paper addresses the static and free vibration analysis of rectangular plates resting on Pasternak foundations. The Pasternak foundation is described by a two-parameter model. The numerical approach is based on collocation with radial basis functions. The model allows the analysis of arbitrary boundary conditions and irregular geometries. It is shown that the present method, based on a first-order shear deformation theory produces highly accurate displacements and stresses, as well as natural frequencies and modes.

Keywords Plates on Pasternak foundations · Plates on elastic foundations · Plates on Winkler foundations · Free vibrations · Radial basis functions · Collocation

1 Introduction

Many engineering problems can be modeled as isotropic rectangular plates, such as bases of machines, pavement of roads or footing of buildings. One way to describe the behaviour of such plates is the Pasternak (two-parameter) model [1]. The Winkler model [2] can be considered a special case of the Pasternak model.

The analysis of Pasternak plates was conducted previously by several authors, using various approaches. Leissa [3] considered a thin-plate theory, Lam et al. [4] derived the exact solutions of bending, buckling and vibration of a Levy-plate, Xiang et al. [5] derived an analytical vibration solution, Omurtag et al. [6] used the finite element method, Matsunaga [7] developed a special higher-order plate theory, Shen et al. [8] used the the Rayleigh-Ritz method, and Ayvaz et al. [9] used the modified Vlasov model to study the earthquake response of rectangular thin plates on elastic foundation.

In the recent years, some attempts have been made for the vibration analysis of rectangular thick plates on Pasternak foundations. Liew and Teo [10], and Liew et al. [11], Han and Liew [12] used the differential quadrature method to analyse the vibration characteristics of rectangular plates on elastic foundations. Also, Zhou et al. [13] used the Chebyshev polynomials as admissible functions to study the three-dimensional vibration of rectangular plates on elastic foundations by the Ritz method.

Meshless methods are not widely used for the analysis of Mindlin plates on elastic foundations. Civalek [14] used the singular convolution method for the bending analysis of Mindlin plates on elastic foundations. Also, a boundary element method was used by Chucheepsakul and Chinnaboon [15] to analyse plates by a two-parameter model.

Recently, radial basis functions (RBFs) have enjoyed considerable success and research as a technique for interpolating data and functions. A RBFs, $\phi(\|x - x_j\|)$ is a spline that depends on the Euclidian distance from distinct data centers x_j, $j = 1, 2, \ldots, N \in \mathbb{R}^n$, also called nodal or collocation points.

Although most work to date on RBFs relates to scattered data approximation and in general to interpolation theory, there has recently been an increased interest in their use for solving partial differential equations (PDEs). This approach, which approximates the whole solution of the PDE directly

A. J. M. Ferreira (✉) · C. M. C. Roque · A. M. A. Neves · R. M. N. Jorge
Departamento de Engenharia Mecânica, Faculdade de Engenharia da, Universidade do Porto, Rua Dr. Roberto Frias, 4200-465 Porto, Portugal
e-mail: ferreira@fe.up.pt

C. M. M. Soares
Departamento de Engenharia Mecânica, Instituto Superior Técnico, Av. Rovisco Pais, Lisboa, Portugal

using RBFs, is very attractive due to the fact that this is truly a mesh-free technique.

Kansa [16] introduced the concept of solving PDEs using RBFs. Kansa's method is an unsymmetric RBF collocation method based upon the MQ interpolation functions, in which the shape parameter is considered to be variable across the problem domain. The distribution of the shape parameter is obtained by an optimization approach, in which the value of the shape parameter is assumed to be proportional to the curvature of the unknown solution of the original PDE. In this way, it is possible to reduce the condition number of the matrix at the expense of implementing an additional iterative algorithm. In the present work, we implemented the unsymmetric collocation method in its simpler form, without any optimization of the interpolation functions and the collocation points.

The analysis of plates by finite element methods is now fully established. The use of alternative methods such as the meshless methods based on RBFs is atractive due to the absence of a mesh and the ease of collocation methods. The use of RBF for the analysis of structures and materials has been previously studied by numerous authors [17–28]. More recently the authors have applied RBFs to the static deformations of composite beams and plates [29–31].

In this paper it is investigated for the first time the use of RBFs to plates on elastic foundations by the Pasternak model, using a first-order shear deformation theory. The quality of the present method in predicting static deformations, and free vibrations of plates on Winkler and Pasternak foundations is compared and discussed with other methods in some numerical examples.

2 The RBF method

2.1 The static problem

RBF approximations are grid-free numerical schemes that can exploit accurate representations of the boundary, are easy to implement and can be spectrally accurate [32,33].

In this section the formulation of a global unsymmetrical collocation RBF-based method to compute eigenvalues of elliptic operators is presented.

Consider a linear elliptic partial differential operator L and a bounded region Ω in $\mathbb{R}^n$ with some boundary $\partial\Omega$.

The static problems aims the computation of displacements (primary variables) $(\mathbf{u})$ from the global system of equations

$$L\mathbf{u} = \mathbf{f} \text{ in } \Omega \tag{1}$$

$$L_B\mathbf{u} = \mathbf{g} \text{ on } \partial\Omega \tag{2}$$

where L and L_B are linear operators in the domain and on the boundary, respectively. The right-hand side of (1) and (2) represent the external forces applied on the plate and the boundary conditions applied along the perimeter of the plate, respectively. The PDE problem defined in (1) and (2) will be replaced by a finite problem, defined by an algebraic system of equations, after the radial basis expansions.

2.2 The eigenproblem

The eigenproblem looks for eigenvalues (λ) and eigenvectors $(\mathbf{u})$ that satisfy

$$L\mathbf{u} - \lambda\mathbf{u} = 0 \text{ in } \Omega \tag{3}$$

$$L_B\mathbf{u} = 0 \text{ on } \partial\Omega \tag{4}$$

As in the static problem, the eigenproblem defined in (3) and (4) is replaced by a finite-dimensional eigenvalue problem, based on RBF approximations.

2.3 Radial basis functions

The RBF (ϕ) approximation of a function $(\mathbf{u})$ is given by

$$\widetilde{\mathbf{u}}(\mathbf{x}) = \sum_{i=1}^{N} \alpha_i \phi\left(\|x - y_i\|_2\right), \mathbf{x} \in \mathbb{R}^n \tag{5}$$

where $y_i, i = 1, \ldots, N$ is a finite set of distinct points (centers) in $\mathbb{R}^n$. The coefficients α_i are chosen so that $\widetilde{\mathbf{u}}$ satisfies some boundary conditions. The most common RBFs are

$$\phi(r) = r^3, \quad \text{cubic}$$
$$\phi(r) = r^2 \log(r), \quad \text{thin plate splines}$$
$$\phi(r) = (1 - r)_+^m p(r), \quad \text{Wendland functions}$$
$$\phi(r) = e^{-(cr)^2}, \quad \text{Gaussian}$$
$$\phi(r) = \sqrt{c^2 + r^2}, \quad \text{multiquadrics}$$
$$\phi(r) = (c^2 + r^2)^{-1/2}, \quad \text{inverse multiquadrics}$$

where the Euclidian distance r is real and non-negative and c is a shape parameter, a positive constant. In the Wendland functions, $p(r)$ is a polynomial function, which can be defined in various ways. In this paper, the Wendland function was chosen as

$$\phi(r) = (1 - cr)_+^8 \left(32(cr)^3 + 25(cr)^2 + 8cr + 1\right). \tag{6}$$

2.4 Solution of the interpolation problem

Hardy [34] introduced multiquadrics in the analysis of scattered geographical data. In the 1990s Kansa [16] used multiquadrics for the solution of PDEs.

Considering N distinct interpolations, and knowing $u(x_j)$, $j = 1, 2, \ldots, N$, we find α_i by the solution of a $N \times N$ linear system

$$\mathbf{A}\underline{\alpha} = \mathbf{u} \tag{7}$$

where $\mathbf{A} = [\phi(\|x - y_i\|_2)]_{N\times N}$, $\underline{\alpha} = [\alpha_1, \alpha_2, \ldots, \alpha_N]^T$ and $\mathbf{u} = [u(x_1), u(x_2), \ldots, u(x_N)]^T$. The RBF interpolation matrix A is positive definite for some RBFs [35], but in general provides ill-conditioned systems.

2.5 Solution of the static problem

The solution of a static problem by RBFs considers N_I nodes in the domain and N_B nodes on the boundary, with total number of nodes $N = N_I + N_B$.

We denote the sampling points by $x_i \in \Omega, i = 1, \ldots, N_I$ and $x_i \in \partial\Omega, i = N_I + 1, \ldots, N$. At the domain points we solve the following system of equations

$$\sum_{i=1}^{N} \alpha_i L\phi\left(\|x - y_i\|_2\right) = \mathbf{f}(x_j), \quad j = 1, 2, \ldots, N_I \tag{8}$$

or

$$L^I \underline{\alpha} = \mathbf{F} \tag{9}$$

where

$$L^I = \left[L\phi\left(\|x - y_i\|_2\right)\right]_{N_I\times N}. \tag{10}$$

For the boundary conditions we have

$$\sum_{i=1}^{N} \alpha_i L_B\phi\left(\|x - y_i\|_2\right) = \mathbf{g}(x_j), \quad j = N_I + 1, \ldots, N \tag{11}$$

or

$$\mathbf{B}\underline{\alpha} = \mathbf{G}. \tag{12}$$

Therefore we can write a finite-dimensional static problem as

$$\begin{bmatrix} L^I \\ \mathbf{B} \end{bmatrix} \underline{\alpha} = \begin{bmatrix} \mathbf{F}^I \\ \mathbf{G}^I \end{bmatrix} \tag{13}$$

where

$$\mathbf{A}^I = \phi\left[\left(\left\|x_{N_I} - y_j\right\|_2\right)\right]_{N_I\times N},$$
$$\mathbf{B}^I = L_B\phi\left[\left(\|x_{N_I+1} - y_j\|_2\right)\right]_{N_B\times N}.$$

By inverting the system (13), we obtain the vector of $\underline{\alpha}$. We then proceed to the solution by the interpolation equation (5).

2.6 Solution of the eigenproblem

We consider N_I nodes in the interior of the domain and N_B nodes on the boundary, with $N = N_I + N_B$.

We denote interpolation points by $x_i \in \Omega, i = 1, \ldots, N_I$ and $x_i \in \partial\Omega, i = N_I + 1, \ldots, N$. For the interior points we have that

$$\sum_{i=1}^{N} \alpha_i L\phi\left(\|x - y_i\|_2\right) = \lambda\tilde{\mathbf{u}}(x_j), \quad j = 1, 2, \ldots, N_I \tag{14}$$

or

$$L^I \underline{\alpha} = \lambda\tilde{\mathbf{u}}^I \tag{15}$$

where

$$L^I = \left[L\phi\left(\|x - y_i\|_2\right)\right]_{N_I\times N} \tag{16}$$

For the boundary conditions we have

$$\sum_{i=1}^{N} \alpha_i L_B\phi\left(\|x - y_i\|_2\right) = 0, \quad j = N_I + 1, \ldots, N \tag{17}$$

or

$$\mathbf{B}\underline{\alpha} = 0. \tag{18}$$

Therefore we can write a finite-dimensional problem as a generalized eigenvalue problem

$$\begin{bmatrix} L^I \\ \mathbf{B} \end{bmatrix} \underline{\alpha} = \lambda \begin{bmatrix} \mathbf{A}^I \\ \mathbf{0} \end{bmatrix} \underline{\alpha} \tag{19}$$

where

$$\mathbf{A}^I = \phi\left[\left(\left\|x_{N_I} - y_j\right\|_2\right)\right]_{N_I\times N},$$
$$\mathbf{B}^I = L_B\phi\left[\left(\left\|x_{N_I+1} - y_j\right\|_2\right)\right]_{N_B\times N}$$

We seek the generalized eigenvalues and eigenvectors of these matrices.

In this paper we follow a second algorithm (see [36] for details) that can be formulated as follows. We can write

$$\underline{\alpha} = \underline{\mathbf{A}}^{-1} \begin{bmatrix} \underline{\mathbf{u}}^I \\ \mathbf{0}_{N_B\times 1} \end{bmatrix} \tag{20}$$

where $\mathbf{0}_{p\times q}$ is a $p \times q$ zero matrix, and

$$\underline{\mathbf{A}} = \begin{bmatrix} \mathbf{A}^I \\ \mathbf{B} \end{bmatrix} \tag{21}$$

We can write a standard eigenvalue problem as

$$L_\phi \underline{\mathbf{u}}^I = \lambda\underline{\mathbf{u}}^I \tag{22}$$

where L_ϕ is a $N_I \times N_I$ matrix given by

$$L_\phi = L^I \underline{\mathbf{A}}^{-1} \begin{bmatrix} I_{N_I\times N_I} \\ \mathbf{0}_{N_B\times N_I} \end{bmatrix} \tag{23}$$

The RBF approximation of the eigenpairs of (3)–(4) is now obtained by computing the eigenvalues and eigenvectors of the matrix L_ϕ. The eigenproblem (22) has dimension $N_I \times N_I$ whereas eigenproblem (19) has dimension $N \times N$. However in (22) we need to invert matrix $\underline{\mathbf{A}}$, which represents an extra computing cost when compared to (19).

3 Static and free vibration analysis of plates on Pasternak foundations

3.1 Equations of motion and boundary conditions

Based on the FSDT (first-order shear deformation theory), the transverse displacement $w(x, y, t)$ and the rotations $\theta_x(x, y, t)$ and $\theta_y(x, y, t)$ about the $y-$ and $x-$axes as functions of time, t, are independently interpolated due to uncoupling between inplane displacements and bending displacements for plates on Pasternak foundations. The equations of motion for the free vibration of plates on Pasternak foundations [10–12] are:

$$D_{11}\frac{\partial^2\theta_x}{\partial x^2} + D_{16}\frac{\partial^2\theta_y}{\partial x^2} + (D_{12}+D_{66})\frac{\partial^2\theta_y}{\partial x\partial y} +2D_{16}\frac{\partial^2\theta_x}{\partial x\partial y} + D_{66}\frac{\partial^2\theta_x}{\partial y^2} + D_{26}\frac{\partial^2\theta_y}{\partial y^2} -kA_{45}\left(\theta_y+\frac{\partial w}{\partial y}\right) - kA_{55}\left(\theta_x+\frac{\partial w}{\partial x}\right) = I_2\frac{\partial^2\theta_x}{\partial t^2} \tag{24}$$

$$D_{16}\frac{\partial^2\theta_x}{\partial x^2} + D_{66}\frac{\partial^2\theta_y}{\partial x^2} + (D_{12}+D_{66})\frac{\partial^2\theta_x}{\partial x\partial y} +2D_{26}\frac{\partial^2\theta_y}{\partial x\partial y} + D_{26}\frac{\partial^2\theta_x}{\partial y^2} + D_{22}\frac{\partial^2\theta_y}{\partial y^2} -kA_{44}\left(\theta_y+\frac{\partial w}{\partial y}\right) - kA_{45}\left(\theta_x+\frac{\partial w}{\partial x}\right) = I_2\frac{\partial^2\theta_y}{\partial t^2} \tag{25}$$

$$\frac{\partial}{\partial x}\left[kA_{45}\left(\theta_y+\frac{\partial w}{\partial y}\right)+kA_{55}\left(\theta_x+\frac{\partial w}{\partial x}\right)\right] +\frac{\partial}{\partial y}\left[kA_{44}\left(\theta_y+\frac{\partial w}{\partial y}\right)+kA_{45}\left(\theta_x+\frac{\partial w}{\partial x}\right)\right] -k_f w + G_f\left(\frac{\partial^2 w}{\partial x^2}+\frac{\partial^2 w}{\partial y^2}\right) + q = I_0\frac{\partial^2 w}{\partial t^2} \tag{26}$$

where q is the external applied load, D_{ij} and A_{ij} are the bending and shear stiffness components, and I_i are the mass inertias defined as [37]

$$I_0 = \int_{-\frac{h}{2}}^{\frac{h}{2}} \rho dz, \quad I_2 = \int_{-\frac{h}{2}}^{\frac{h}{2}} \rho z^2 dz. \tag{27}$$

Here ρ and h denote the density and the total thickness of the plate, respectively. Also, k_f is the Winkler foundation stiffness while G_f is the shear stiffness of the elastic foundation. The Winkler foundation can be considered as a special case of the Pasternak foundation where a shear interaction between the spring elements is assumed. The shear correction factor, k, is here taken as $5/6$, by assuming a rectangular cross-section of the plate.

The bending moments and shear forces are expressed as functions of the displacement gradients and the material constitutive equations by

$$M_x = D_{11}\frac{\partial\theta_x}{\partial x} + D_{12}\frac{\partial\theta_y}{\partial y} + D_{16}\left(\frac{\partial\theta_x}{\partial y}+\frac{\partial\theta_y}{\partial x}\right) \tag{28}$$

$$M_y = D_{12}\frac{\partial\theta_x}{\partial x} + D_{22}\frac{\partial\theta_y}{\partial y} + D_{26}\left(\frac{\partial\theta_x}{\partial y}+\frac{\partial\theta_y}{\partial x}\right) \tag{29}$$

$$M_{xy} = D_{16}\frac{\partial\theta_x}{\partial x} + D_{26}\frac{\partial\theta_y}{\partial y} + D_{66}\left(\frac{\partial\theta_x}{\partial y}+\frac{\partial\theta_y}{\partial x}\right) \tag{30}$$

$$Q_x = kA_{55}\left(\theta_x+\frac{\partial w}{\partial x}\right) + kA_{45}\left(\theta_y+\frac{\partial w}{\partial y}\right) \tag{31}$$

$$Q_y = kA_{45}\left(\theta_x+\frac{\partial w}{\partial x}\right) + kA_{55}\left(\theta_y+\frac{\partial w}{\partial y}\right) \tag{32}$$

For free vibration problems we set $q = 0$, and assume harmonic solution in terms of displacements w, θ_x, θ_y in the form

$$w(x, y, t) = W(w, y)e^{i\omega t} \tag{33}$$

$$\theta_x(x, y, t) = \Psi_x(w, y)e^{i\omega t} \tag{34}$$

$$\theta_y(x, y, t) = \Psi_y(w, y)e^{i\omega t} \tag{35}$$

where ω is the frequency of natural vibration. Substituting the harmonic expansion into equations of motion we obtain the following equations in terms of the amplitudes W, Ψ_x, Ψ_y

$$D_{11}\frac{\partial^2\Psi_x}{\partial x^2} + D_{16}\frac{\partial^2\Psi_y}{\partial x^2} + (D_{12}+D_{66})\frac{\partial^2\Psi_y}{\partial x\partial y} +2D_{16}\frac{\partial^2\Psi_x}{\partial x\partial y} + D_{66}\frac{\partial^2\Psi_x}{\partial y^2} + D_{26}\frac{\partial^2\Psi_y}{\partial y^2} -kA_{45}\left(\Psi_y+\frac{\partial W}{\partial y}\right) - kA_{55}\left(\Psi_x+\frac{\partial W}{\partial x}\right) = -I_2\omega^2\Psi_x \tag{36}$$

$$D_{16}\frac{\partial^2\Psi_x}{\partial x^2} + D_{66}\frac{\partial^2\Psi_y}{\partial x^2} + (D_{12}+D_{66})\frac{\partial^2\Psi_x}{\partial x\partial y} +2D_{26}\frac{\partial^2\Psi_y}{\partial x\partial y} + D_{26}\frac{\partial^2\Psi_x}{\partial y^2} + D_{22}\frac{\partial^2\Psi_y}{\partial y^2} -kA_{44}\left(\Psi_y+\frac{\partial W}{\partial y}\right) - kA_{45}\left(\Psi_x+\frac{\partial W}{\partial x}\right) = -I_2\omega^2\Psi_y \tag{37}$$

$$\frac{\partial}{\partial x}\left[kA_{45}\left(\Psi_y+\frac{\partial W}{\partial y}\right)+kA_{55}\left(\Psi_x+\frac{\partial W}{\partial x}\right)\right] +\frac{\partial}{\partial y}\left[kA_{44}\left(\Psi_y+\frac{\partial W}{\partial y}\right)+kA_{45}\left(\Psi_x+\frac{\partial W}{\partial x}\right)\right] -k_f W + G_f\left(\frac{\partial^2 W}{\partial x^2}+\frac{\partial^2 W}{\partial y^2}\right) = -I_0\omega^2 W. \tag{38}$$

The boundary conditions for an arbitrary edge with simply supported, clamped and free edge conditions are as follows:

(a) Simply supported

- SS1, $w = 0$; $M_n = 0$; $M_{ns} = 0$
- SS2, $w = 0$; $M_n = 0$; $\theta_s = 0$

(b) Clamped, $w = 0$; $\theta_n = 0$; $\theta_s = 0$
(c) Free, $Q_n = 0$; $M_n = 0$; $M_{ns} = 0$

In previous equations, the subscripts n and s refer to the normal and tangential directions of the edge, respectively; M_n, M_{ns} and Q_n represent the normal bending moment, twisting moment and shear force on the plate edge; θ_n and θ_s represent the rotations about the tangential and normal coordinates at the plate edge.

The stress resultants on an edge whose normal is represented by $\mathbf{n} = (n_x, n_y)$ can be expressed as

$$M_n = n_x^2 M_x + 2n_x n_y M_{xy} + n_y^2 M_y \tag{39}$$

$$M_{ns} = \left(n_x^2 - n_y^2\right) M_{xy} - n_x n_y (My - Mx) \tag{40}$$

$$Q_n = n_x Q_x + n_y Q_y \tag{41}$$

$$\theta_n = n_x \theta_x + n_y \theta_y \tag{42}$$

$$\theta_s = n_x \theta_y - n_y \theta_x \tag{43}$$

where n_x and n_y are the direction cosines of a unit normal vector at a point at the laminated plate boundary [37,38].

4 Discretization of the equations of motion and boundary conditions

The radial basis collocation method follows a simple implementation procedure. Taking Eq. (13), we compute

$$\alpha = \begin{bmatrix} L^I \\ \mathbf{B} \end{bmatrix}^{-1} \begin{bmatrix} \mathbf{F}^I \\ \mathbf{G}^I \end{bmatrix} \tag{44}$$

This α vector is then used to obtain solution $\tilde{\mathbf{u}}$, by using (7). If derivatives of $\tilde{\mathbf{u}}$ are needed, such derivatives are computed as

$$\frac{\partial \tilde{\mathbf{u}}}{\partial x} = \sum_{j=1}^{N} \alpha_j \frac{\partial \phi_j}{\partial x} \tag{45}$$

$$\frac{\partial^2 \tilde{\mathbf{u}}}{\partial x^2} = \sum_{j=1}^{N} \alpha_j \frac{\partial^2 \phi_j}{\partial x^2}, \text{ etc.} \tag{46}$$

The equations of motion and the boundary conditions can now be discretized according to the RBF collocation, as

$$\begin{aligned}
&D_{11} \sum_{j=1}^{N} \alpha_j^{\Psi_x} \frac{\partial^2 \phi_j}{\partial x^2} + D_{16} \sum_{j=1}^{N} \alpha_j^{\Psi_y} \frac{\partial^2 \phi_j}{\partial x^2} \\
&\quad + (D_{12} + D_{66}) \sum_{j=1}^{N} \alpha_j^{\Psi_y} \frac{\partial^2 \phi_j}{\partial x \partial y} \\
&\quad + 2D_{16} \sum_{j=1}^{N} \alpha_j^{\Psi_x} \frac{\partial^2 \phi_j}{\partial x \partial y} + D_{66} \sum_{j=1}^{N} \alpha_j^{\Psi_x} \frac{\partial^2 \phi_j}{\partial y^2} \\
&\quad + D_{26} \sum_{j=1}^{N} \alpha_j^{\Psi_y} \frac{\partial^2 \phi_j}{\partial y^2} \\
&\quad - kA_{45} \left(\sum_{j=1}^{N} \alpha_j^{\Psi_y} \phi_j + \sum_{j=1}^{N} \alpha_j^{W} \frac{\partial \phi_j}{\partial y} \right) \\
&\quad - kA_{55} \left(\sum_{j=1}^{N} \alpha_j^{\Psi_x} \phi_j + \sum_{j=1}^{N} \alpha_j^{W} \frac{\partial \phi_j}{\partial x} \right) \\
&= -I_2 \omega^2 \sum_{j=1}^{N} \alpha_j^{\Psi_x} \phi_j
\end{aligned} \tag{47}$$

$$\begin{aligned}
&D_{16} \sum_{j=1}^{N} \alpha_j^{\Psi_x} \frac{\partial^2 \phi_j}{\partial x^2} + D_{66} \sum_{j=1}^{N} \alpha_j^{\Psi_y} \frac{\partial^2 \phi_j}{\partial x^2} \\
&\quad + (D_{12} + D_{66}) \sum_{j=1}^{N} \alpha_j^{\Psi_x} \frac{\partial^2 \phi_j}{\partial x \partial y} \\
&\quad + 2D_{26} \sum_{j=1}^{N} \alpha_j^{\Psi_y} \frac{\partial^2 \phi_j}{\partial x \partial y} + D_{26} \sum_{j=1}^{N} \alpha_j^{\Psi_x} \frac{\partial^2 \phi_j}{\partial y^2} \\
&\quad + D_{22} \sum_{j=1}^{N} \alpha_j^{\Psi_y} \frac{\partial^2 \phi_j}{\partial y^2} \\
&\quad - kA_{44} \left(\sum_{j=1}^{N} \alpha_j^{\Psi_y} \phi_j + \sum_{j=1}^{N} \alpha_j^{W} \frac{\partial \phi_j}{\partial y} \right) \\
&\quad - kA_{45} \left(\sum_{j=1}^{N} \alpha_j^{\Psi_x} \phi_j + \sum_{j=1}^{N} \alpha_j^{W} \frac{\partial \phi_j}{\partial x} \right) \\
&= -I_2 \omega^2 \sum_{j=1}^{N} \alpha_j^{\Psi_y} \phi_j
\end{aligned} \tag{48}$$

$$\begin{aligned}
&\frac{\partial}{\partial x} \left[kA_{45} \left(\sum_{j=1}^{N} \alpha_j^{\Psi_y} \phi_j + \sum_{j=1}^{N} \alpha_j^{W} \frac{\partial \phi_j}{\partial y} \right) \right. \\
&\quad \left. + kA_{55} \left(\sum_{j=1}^{N} \alpha_j^{\Psi_x} \phi_j + \sum_{j=1}^{N} \alpha_j^{W} \frac{\partial \phi_j}{\partial x} \right) \right] \\
&\quad + \frac{\partial}{\partial y} \left[kA_{44} \left(\sum_{j=1}^{N} \alpha_j^{\Psi_y} \phi_j + \sum_{j=1}^{N} \alpha_j^{W} \frac{\partial \phi_j}{\partial y} \right) \right.
\end{aligned}$$

Table 1 Convergence study for deflections, moments and shear forces of uniformly loaded square CCCC plates on Winkler foundations ($K = 1$; $\nu = 0.3$)

h/a	Grid (points)	w ($\times 10^{-3} qa^4/D$) $x = y = 0$	M_{xx} ($\times 10^{-2} qa^2/D$) $x = y = 0$	M_{yy} ($\times 10^{-2} qa^2/D$) $x = y = 0$	M_{xy} ($\times 10^{-2} qa^2/D$) $x = y = -1$	Q_x ($\times qa$) $x = 0; y = -1$	Q_y ($\times qa$) $x = -1, y = 0$
0.01	13 × 13	1.783	2.390	3.300	0.062	0.133	−0.648
	17 × 17	1.924	2.441	3.292	0.190	0.206	−0.507
	21 × 21	1.819	1.978	2.592	0.156	0.832	−0.225
	25 × 25	1.965	2.500	3.548	0.101	0.284	−0.512
	29 × 29	1.918	2.414	3.333	0.102	0.233	−0.513
	33 × 33	1.918	2.437	3.319	0.101	0.246	−0.515
0.05	13 × 13	1.990	2.454	3.276	0.463	0.239	−0.515
	17 × 17	1.989	2.471	3.319	0.465	0.244	−0.509
	21 × 21	1.989	2.473	3.321	0.468	0.245	−0.509
	25 × 25	1.989	2.472	3.322	0.466	0.245	−0.509
0.1	13 × 13	2.204	2.561	3.282	0.849	0.246	−0.502
	17 × 17	2.205	2.573	3.317	0.849	0.248	−0.500
	21 × 21	2.206	2.575	3.321	0.851	0.248	−0.500
	25 × 25	2.206	2.575	3.321	0.850	0.248	−0.500
0.2	13 × 13	3.014	2.910	3.283	1.432	0.256	−0.476
	17 × 17	3.015	2.914	3.296	1.432	0.256	−0.475
	21 × 21	3.015	2.914	3.298	1.433	0.256	−0.474
	25 × 25	3.015	2.915	3.298	1.433	0.256	−0.474

Table 2 Convergence study for deflections, moments and shear forces of uniformly loaded square CCCC plates on Winkler foundations ($K = 3$; $\nu = 0.3$)

h/a	Grid (points)	w ($\times 10^{-3} qa^4/D$) $x = y = 0$	M_{xx} ($\times 10^{-2} qa^2/D$) $x = y = 0$	M_{yy} ($\times 10^{-2} qa^2/D$) $x = y = 0$	M_{xy} ($\times 10^{-2} qa^2/D$) $x = y = -1$	Q_x ($\times qa$) $x = 0; y = -1$	Q_y ($\times qa$) $x = -1, y = 0$
0.01	13 × 13	1.629	2.161	2.991	0.059	0.125	−0.607
	17 × 17	1.750	2.187	2.962	0.179	0.194	−0.474
	21 × 21	1.656	1.759	2.313	0.148	0.785	−0.208
	25 × 25	1.785	2.239	3.197	0.095	0.267	−0.477
	29 × 29	1.745	2.163	3.001	0.097	0.219	−0.479
	33 × 33	1.744	2.184	2.988	0.095	0.231	−0.481
0.05	13 × 13	1.803	2.189	2.936	0.434	0.224	−0.480
	17 × 17	1.803	2.206	2.976	0.436	0.229	−0.474
	21 × 21	1.802	2.208	2.978	0.439	0.229	−0.474
	25 × 25	1.803	2.207	2.979	0.437	0.230	−0.474
0.1	13 × 13	1.975	2.258	2.905	0.786	0.229	−0.464
	17 × 17	1.976	2.270	2.937	0.787	0.230	−0.462
	21 × 21	1.976	2.272	2.941	0.788	0.231	−0.462
	25 × 25	1.976	2.272	2.941	0.787	0.231	−0.462
0.2	13 × 13	2.589	2.459	2.777	1.276	0.232	−0.426
	17 × 17	2.590	2.462	2.789	1.277	0.232	−0.425
	21 × 21	2.590	2.463	2.790	1.278	0.231	−0.425
	25 × 25	2.590	2.463	2.790	1.278	0.232	−0.425

Table 3 Convergence study for deflections, moments and shear forces of uniformly loaded square CCCC plates on Winkler foundations ($K = 5$; $\nu = 0.3$)

h/a	Grid (points)	w ($\times 10^{-3} qa^4/D$) $x = y = 0$	M_{xx} ($\times 10^{-2} qa^2/D$) $x = y = 0$	M_{yy} ($\times 10^{-2} qa^2/D$) $x = y = 0$	M_{xy} ($\times 10^{-2} qa^2/D$) $x = y = -1$	Q_x ($\times qa$) $x = 0; y = -1$	Q_y ($\times qa$) $x = -1, y = 0$
0.01	13 × 13	1.016	1.258	1.772	0.045	0.091	−0.443
	17 × 17	1.071	1.211	1.688	0.137	0.144	−0.343
	21 × 21	1.018	0.910	1.227	0.114	0.600	−0.140
	25 × 25	1.090	1.238	1.848	0.073	0.199	−0.342
	29 × 29	1.069	1.195	1.718	0.074	0.164	−0.346
	33 × 33	1.069	1.212	1.709	0.073	0.173	−0.347
0.05	13 × 13	1.088	1.188	1.643	0.324	0.167	−0.343
	17 × 17	1.088	1.203	1.672	0.325	0.170	−0.340
	21 × 21	1.088	1.205	1.673	0.327	0.170	−0.339
	25 × 25	1.088	1.204	1.674	0.326	0.171	−0.340
0.1	13 × 13	1.140	1.170	1.545	0.555	0.166	−0.324
	17 × 17	1.141	1.180	1.567	0.556	0.167	−0.322
	21 × 21	1.141	1.181	1.569	0.557	0.167	−0.322
	25 × 25	1.141	1.181	1.569	0.556	0.167	−0.322
0.2	13 × 13	1.289	1.095	1.245	0.787	0.155	−0.271
	17 × 17	1.289	1.097	1.251	0.788	0.155	−0.270
	21 × 21	1.289	1.098	1.252	0.789	0.154	−0.269
	25 × 25	1.289	1.098	1.252	0.788	0.154	−0.269

Table 4 Convergence study for deflections, moments and shear forces of uniformly loaded square SSSS plates on Winkler foundations ($K = 1$; $\nu = 0.3$)

h/a	Grid (points)	w ($\times 10^{-3} qa^4/D$) $x = y = 0$	M_{xx} ($\times 10^{-2} qa^2/D$) $x = y = 0$	M_{yy} ($\times 10^{-2} qa^2/D$) $x = y = 0$	M_{xy} ($\times 10^{-2} qa^2/D$) $x = y = -1$	Q_x ($\times qa$) $x = 0; y = -1$	Q_y ($\times qa$) $x = -1, y = 0$
0.01	13 × 13	3.957	4.664	4.664	2.832	0.378	−0.378
	17 × 17	4.046	4.753	4.754	3.224	0.336	−0.335
	21 × 21	4.063	4.780	4.780	3.242	0.337	−0.335
	25 × 25	4.049	4.770	4.770	3.237	0.333	−0.331
	29 × 29	4.054	4.775	4.775	3.240	0.336	−0.336
	33 × 33	4.054	4.775	4.775	3.241	0.337	−0.337
0.05	13 × 13	4.100	4.751	4.751	3.237	0.338	−0.338
	17 × 17	4.103	4.773	4.773	3.241	0.337	−0.337
	21 × 21	4.104	4.775	4.775	3.240	0.337	−0.337
	25 × 25	4.104	4.775	4.775	3.241	0.337	−0.337
0.1	13 × 13	4.258	4.760	4.760	3.241	0.338	−0.338
	17 × 17	4.261	4.773	4.773	3.241	0.337	−0.337
	21 × 21	4.261	4.774	4.774	3.240	0.337	−0.337
	25 × 25	4.261	4.774	4.774	3.240	0.337	−0.337
0.2	13 × 13	4.887	4.768	4.768	3.241	0.338	−0.338
	17 × 17	4.888	4.771	4.771	3.240	0.337	−0.337
	21 × 21	4.888	4.772	4.772	3.238	0.337	−0.337
	25 × 25	4.888	4.772	4.772	3.239	0.337	−0.337

Table 5 Convergence study for deflections, moments and shear forces of uniformly loaded square SSSS plates on Winkler foundations ($K = 3$; $\nu = 0.3$)

h/a	Grid (points)	w ($\times 10^{-3} qa^4/D$) $x = y = 0$	M_{xx} ($\times 10^{-2} qa^2/D$) $x = y = 0$	M_{yy} ($\times 10^{-2} qa^2/D$) $x = y = 0$	M_{xy} ($\times 10^{-2} qa^2/D$) $x = y = -1$	Q_x ($\times qa$) $x = 0$; $y = -1$	Q_y ($\times qa$) $x = -1$, $y = 0$
0.01	13 × 13	3.270	3.785	3.785	2.354	0.335	−0.335
	17 × 17	3.343	3.855	3.856	2.736	0.292	−0.291
	21 × 21	3.356	3.878	3.878	2.751	0.293	−0.291
	25 × 25	3.345	3.871	3.872	2.748	0.289	−0.287
	29 × 29	3.349	3.875	3.875	2.751	0.292	−0.292
	33 × 33	3.349	3.875	3.875	2.751	0.293	−0.293
0.05	13 × 13	3.378	3.843	3.843	2.743	0.294	−0.294
	17 × 17	3.381	3.863	3.863	2.746	0.292	−0.292
	21 × 21	3.381	3.865	3.865	2.745	0.292	−0.292
	25 × 25	3.381	3.865	3.865	2.745	0.292	−0.292
0.1	13 × 13	3.481	3.821	3.821	2.729	0.292	−0.292
	17 × 17	3.483	3.833	3.833	2.729	0.291	−0.291
	21 × 21	3.483	3.834	3.834	2.727	0.291	−0.291
	25 × 25	3.483	3.834	3.834	2.728	0.291	−0.291
0.2	13 × 13	3.871	3.713	3.713	2.662	0.286	−0.286
	17 × 17	3.873	3.715	3.715	2.661	0.285	−0.285
	21 × 21	3.873	3.716	3.716	2.659	0.285	−0.285
	25 × 25	3.873	3.716	3.716	2.660	0.285	−0.285

Table 6 Convergence study for deflections, moments and shear forces of uniformly loaded square SSSS plates on Winkler foundations ($K = 5$; $\nu = 0.3$)

h/a	Grid (points)	w ($\times 10^{-3} qa^4/D$) $x = y = 0$	M_{xx} ($\times 10^{-2} qa^2/D$) $x = y = 0$	M_{yy} ($\times 10^{-2} qa^2/D$) $x = y = 0$	M_{xy} ($\times 10^{-2} qa^2/D$) $x = y = -1$	Q_x ($\times qa$) $x = 0$; $y = -1$	Q_y ($\times qa$) $x = -1$, $y = 0$
0.01	13 × 13	1.471	1.502	1.502	1.098	0.221	−0.221
	17 × 17	1.503	1.525	1.526	1.450	0.175	−0.175
	21 × 21	1.509	1.539	1.539	1.460	0.177	−0.174
	25 × 25	1.504	1.539	1.540	1.461	0.173	−0.171
	29 × 29	1.506	1.540	1.540	1.461	0.176	−0.176
	33 × 33	1.506	1.540	1.540	1.462	0.176	−0.176
0.05	13 × 13	1.508	1.507	1.507	1.451	0.177	−0.177
	17 × 17	1.509	1.524	1.524	1.453	0.176	−0.176
	21 × 21	1.509	1.525	1.525	1.451	0.176	−0.176
	25 × 25	1.509	1.526	1.526	1.452	0.176	−0.176
0.1	13 × 13	1.518	1.471	1.471	1.423	0.174	−0.174
	17 × 17	1.519	1.480	1.480	1.422	0.173	−0.173
	21 × 21	1.519	1.482	1.482	1.420	0.173	−0.173
	25 × 25	1.519	1.482	1.482	1.421	0.173	−0.173
0.2	13 × 13	1.550	1.326	1.326	1.313	0.163	−0.163
	17 × 17	1.551	1.327	1.327	1.312	0.162	−0.162
	21 × 21	1.551	1.328	1.328	1.310	0.162	−0.162
	25 × 25	1.551	1.328	1.328	1.311	0.162	−0.162

Table 7 Deflections, moments and shear forces of uniformly loaded square SS plates on Winkler foundations ($\nu = 0.3$)

K	h/a	Method	w $(\times 10^{-3}qa^4/D)$ $x=y=0$	M_{xx} $(\times 10^{-2}qa^2/D)$ $x=y=0$	M_{yy} $(\times 10^{-2}qa^2/D)$ $x=y=0$	M_{xy} $(\times 10^{-2}qa^2/D)$ $x=y=-1$	Q_x $(\times qa)$ $x=0;\ y=-1$	Q_y (xqa) $x=-1, y=0$
1	0.01	Present (21 × 21 points)	4.050	4.776	4.784	3.234	0.334	−0.341
		Kobayashi and Sonoda [39]	4.054	4.775	4.775	3.241	0.337	−0.337
	0.05	Present (21 × 21 points)	4.104	4.775	4.775	3.241	0.337	−0.337
		Kobayashi and Sonoda [39]	4.104	4.775	4.775	3.241	0.337	−0.337
	0.1	Present (21 × 21 points)	4.261	4.774	4.774	3.240	0.337	−0.337
		Kobayashi and Sonoda [39]	4.261	4.774	4.774	3.240	0.337	−0.337
	0.2	Present (21 × 21 points)	4.888	4.772	4.772	3.239	0.337	−0.337
		Kobayashi and Sonoda [39]	4.888	4.772	4.772	3.239	0.337	−0.337
3	0.01	Present (21 × 21 points)	3.345	3.877	3.885	2.745	0.290	−0.297
		Kobayashi and Sonoda [39]	3.349	3.875	3.875	2.751	0.293	−0.293
	0.05	Present (21 × 21 points)	3.381	3.865	3.865	2.745	0.292	−0.292
		Kobayashi and Sonoda [39]	3.381	3.865	3.865	2.746	0.292	−0.292
	0.1	Present (21 × 21 points)	3.483	3.834	3.834	2.728	0.291	−0.291
		Kobayashi and Sonoda [39]	3.483	3.834	3.834	2.728	0.291	−0.291
	0.2	Present (21 × 21 points)	3.873	3.716	3.716	2.660	0.285	−0.285
		Kobayashi and Sonoda [39]	3.873	3.716	3.716	2.660	0.284	−0.284
5	0.01	Present (21 × 21 points)	1.505	1.545	1.552	1.458	0.174	−0.181
		Kobayashi and Sonoda [39]	1.506	1.540	1.540	1.462	0.176	−0.176
	0.05	Present (21 × 21 points)	1.509	1.526	1.526	1.452	0.176	−0.176
		Kobayashi and Sonoda [39]	1.509	1.526	1.526	1.452	0.175	−0.175
	0.1	Present (21 × 21 points)	1.519	1.482	1.482	1.421	0.173	−0.173
		Kobayashi and Sonoda [39]	1.519	1.482	1.482	1.421	0.172	−0.172
	0.2	Present (21 × 21 points)	1.551	1.328	1.328	1.311	0.162	−0.162
		Kobayashi and Sonoda [39]	1.551	1.328	1.328	1.311	0.162	−0.162

$$+\,kA_{45}\left(\sum_{j=1}^{N}\alpha_j^{\Psi_x}\phi_j+\sum_{j=1}^{N}\alpha_j^{W}\frac{\partial\phi_j}{\partial x}\right)\Bigg]$$
$$-k_f\sum_{j=1}^{N}\alpha_j^{W}\phi_j+G_f\left(\sum_{j=1}^{N}\alpha_j^{W}\frac{\partial^2\phi_j}{\partial x^2}+\sum_{j=1}^{N}\alpha_j^{W}\frac{\partial^2\phi_j}{\partial y^2}\right)$$
$$=-I_0\omega^2\sum_{j=1}^{N}\alpha_j^{W}\phi_j \tag{49}$$

where N represents the total number of points of the discretization. Vectors $\alpha_j^W, \alpha^{\Psi_x}, \alpha^{\Psi_y}$ correspond to the vector of unknowns related to translations W, and rotations Ψ_x, Ψ_y, respectively.

Boundary conditions can be discretized as follows. For a simply supported plate, along the perimeter we enforce the SS2 conditions as

$$w=0\rightarrow\sum_{j=1}^{N}\alpha_j^{W}\phi_j=0 \tag{50}$$

$$M_n=0\rightarrow n_x^2\left(D_{11}\sum_{j=1}^{N}\alpha_j^{\Psi_x}\frac{\partial\phi_j}{\partial x}+D_{12}\sum_{j=1}^{N}\alpha_j^{\Psi_y}\frac{\partial\phi_j}{\partial x}\right.$$
$$\left.+\,D_{16}\sum_{j=1}^{N}\left(\alpha_j^{\Psi_y}\frac{\partial\phi_j}{\partial x}+\alpha_j^{\Psi_x}\frac{\partial\phi_j}{\partial y}\right)\right)$$
$$+2n_xn_y\left(D_{16}\sum_{j=1}^{N}\alpha_j^{\Psi_x}\frac{\partial\phi_j}{\partial x}+D_{26}\sum_{j=1}^{N}\alpha_j^{\Psi_y}\frac{\partial\phi_j}{\partial x}\right.$$
$$\left.+D_{66}\sum_{j=1}^{N}\left(\alpha_j^{\Psi_y}\frac{\partial\phi_j}{\partial x}+\alpha_j^{\Psi_x}\frac{\partial\phi_j}{\partial y}\right)\right)$$
$$+n_y^2\left(D_{12}\sum_{j=1}^{N}\alpha_j^{\Psi_x}\frac{\partial\phi_j}{\partial x}+D_{22}\sum_{j=1}^{N}\alpha_j^{\Psi_y}\frac{\partial\phi_j}{\partial x}\right.$$
$$\left.+D_{26}\sum_{j=1}^{N}\left(\alpha_j^{\Psi_y}\frac{\partial\phi_j}{\partial x}+\alpha_j^{\Psi_x}\frac{\partial\phi_j}{\partial y}\right)\right)=0 \tag{51}$$

$$\theta_s=0\rightarrow n_x\sum_{j=1}^{N}\alpha_j^{\Psi_y}\phi_j+n_y\sum_{j=1}^{N}\alpha_j^{\Psi_x}\phi_j=0. \tag{52}$$

The eigenproblem is then defined as a generalized eigenproblem (19) or standard eigenproblem (22) and solved by MATLAB in our case.

Table 8 Deflections, moments and shear forces of uniformly loaded square CC plates on Winkler foundations ($\nu = 0.3$)

K	h/a	Method	w ($\times 10^{-3} qa^4/D$) $x = y = 0$	M_{xx} ($\times 10^{-2} qa^2/D$) $x = y = 0$	M_{yy} ($\times 10^{-2} qa^2/D$) $x = y = 0$	M_{xy} ($\times 10^{-2} qa^2/D$) $x = y = -1$	Q_x ($\times qa$) $x = 0; y = -1$	Q_y ($\times qa$) $x = -1, y = 0$
1	0.01	Present (21×21 points)	1.868	2.629	2.876	0.094	0.408	−0.190
		Kobayashi and Sonoda [39]	1.918	2.437	3.320	0.101	0.244	−0.515
	0.05	Present (21×21 points)	1.989	2.471	3.322	0.467	0.244	−0.509
		Kobayashi and Sonoda [39]	1.989	2.472	3.321	0.466	0.245	−0.509
	0.1	Present (21×21 points)	2.206	2.575	3.321	0.850	0.248	−0.500
		Kobayashi and Sonoda [39]	2.206	2.575	3.321	0.850	0.245	−0.500
	0.2	Present (21×21 points)	3.015	2.915	3.298	1.433	0.256	−0.474
		Kobayashi and Sonoda [39]	3.015	2.915	3.298	1.433	0.256	−0.474
3	0.01	Present (21×21 points)	1.701	2.371	2.578	0.089	0.384	−0.174
		Kobayashi and Sonoda [39]	1.744	2.184	2.989	0.095	0.229	−0.480
	0.05	Present (21×21 points)	1.803	2.206	2.978	0.438	0.229	−0.474
		Kobayashi and Sonoda [39]	1.802	2.207	2.978	0.437	0.230	−0.474
	0.1	Present (21×21 points)	1.976	2.272	2.941	0.787	0.231	−0.462
		Kobayashi and Sonoda [39]	1.976	2.272	2.941	0.787	0.231	−0.462
	0.2	Present (21×21 points)	2.590	2.463	2.790	1.277	0.232	−0.425
		Kobayashi and Sonoda [39]	2.590	2.463	2.790	1.278	0.231	−0.425
5	0.01	Present (21×21 points)	1.047	1.369	1.423	0.067	0.291	−0.112
		Kobayashi and Sonoda [39]	1.069	1.212	1.709	0.073	0.172	−0.347
	0.05	Present (21×21 points)	1.088	1.204	1.673	0.326	0.170	−0.340
		Kobayashi and Sonoda [39]	1.088	1.204	1.673	0.326	0.171	−0.340
	0.1	Present (21×21 points)	1.141	1.181	1.569	0.556	0.167	−0.322
		Kobayashi and Sonoda [39]	1.141	1.181	1.569	0.556	0.167	−0.322
	0.2	Present (21×21 points)	1.289	1.098	1.252	0.788	0.154	−0.269
		Kobayashi and Sonoda [39]	1.289	1.098	1.252	0.788	0.154	−0.269

Table 9 Convergence of frequency parameters $\Delta_{1,1}$ for the flexural modes of thin and moderately thick square plates on Winkler foundation ($K_2 = 0$)

Boundary condition	t/b	K_1	13×13 points	17×17 points	21×21 points
SSSS ($\nu = 0.3$)	0.01	10^2	2.2444	2.2416	2.2414
		5×10^2	3.0238	3.0217	3.0215
	0.1	2×10^2	2.3990	2.3989	2.3989
		10^3	3.7008	3.7213	3.7213
CCCC ($\nu = 0.15$)	0.015	1390.2	5.3073	5.2440	5.2442
		2780.4	6.5141	6.4626	6.4627

5 Numerical examples

In all following examples a Chebyshev grid was used (in MATLAB : $x = cos(pi * (0 : N)/N)'$; $y = x$). The Wendland function used was

$$\phi(r) = (1 - cr)_+^8 \left(32(cr)^3 + 25(cr)^2 + 8cr + 1\right). \quad (53)$$

where the shape parameter is taken as 0.1.

5.1 Static results

Numerical results are presented for the uniformly loaded square plate ($a/b = 1$) for the various values of thickness-to-span ratio h/a and dimensionless foundation modulus $K = \left(k_f a^4/D\right)^{1/4}$. Here, $D = \frac{Eh^3}{12(1-\nu^2)}$ is the flexural rigidity. The Poisson's ratio of 0.3 is taken for all cases. In Tables 1, 2, 3 we present a convergence study for fully-clamped (CCCC) plates, using various thickness-to-side ratios, for $K = 1, 3,$ and $K = 5$. In Tables 4, 5, 6, we perform a similar convergence study for simply-supported (SSSS) plates. For both clamped and simply-supported plates the convergence is excellent. For thinner plates ($h/a = 0.01$) we need more

Table 10 Comparison of frequency parameters Δ for the flexural modes of thin and moderately thick square plates on Winkler foundation ($K_2 = 0$)

Boundary condition	t/b	K_1	Methods	$\Delta_{1,1}$	$\Delta_{1,2}$,$\Delta_{2,1}$	$\Delta_{2,2}$
SSSS ($\nu = 0.3$)	0.01	10^2	Zhou et al. [13]	2.2413	5.0973	8.0527
			Classical [3]	2.2420	5.1016	8.0639
			Mindlin [5]	2.2413	5.0971	8.0523
			Present (21 × 21 points)	2.2414	5.0967	8.0542
		5×10^2	Zhou et al. [13]	3.0214	5.4850	8.3035
			Classical [3]	3.0221	5.4894	8.3146
			Mindlin [5]	3.0215	5.4850	8.3032
			Present (21 × 21 points)	3.0216	5.4846	8.3051
	0.1	2×10^2	Zhou et al. [13]	2.3951	4.8262	7.2338
			Mindlin [5]	2.3989	4.8194	7.2093
			Present (21 × 21 points)	2.3989	4.8194	7.2093
		10^3	Zhou et al. [13]	3.7008	5.5661	7.7335
			Mindlin [5]	3.7212	5.5844	7.7353
			Present (21 × 21 points)	3.7213	5.5844	7.7353
CCCC ($\nu = 0.15$)	0.015	1390.2	Zhou et al. [13]	5.2446	8.3156	11.541
			Classical [3]	5.2510	8.3427	11.602
			Finite element [6]	5.2588	8.4322	11.674
			Present (21 × 21 points)	5.2438	8.3129	11.546
		2780.4	Zhou et al. [13]	6.4629	9.1324	12.142
			Classical [3]	6.4686	9.1582	12.202
			Finite element [6]	6.4601	9.2482	12.263
			Present (21 × 21 points)	6.4625	9.1302	12.147

Table 11 Comparison of frequency parameters Δ for the flexural modes of thin and moderately thick square plates on Pasternak foundation

Boundary condition	t/b	K_1	K_2	Methods	$\Delta_{1,1}$	$\Delta_{1,2}$,$\Delta_{2,1}$	$\Delta_{2,2}$
SSSS ($\nu = 0.3$)	0.01	10^2	10	Zhou et al. [13]	2.6551	5.5717	8.5406
				Mindlin [5]	2.6551	5.5718	8.5405
				Present (21 × 21 points)	2.6559	5.5718	8.5384
		5×10^2	10	Zhou et al. [13]	3.3398	5.9285	8.7775
				Mindlin [5]	3.3400	5.9287	8.7775
				Present (21 × 21 points)	3.3406	5.9285	8.7754
	0.1	2×10^2	10	Zhou et al. [13]	2.7756	5.2954	7.7279
				Mindlin [5]	2.7842	5.3043	7.7287
				Present (21 × 21 points)	2.7902	5.3452	7.8255
		10^3	10	Zhou et al. [13]	3.9566	5.9757	8.1954
				Mindlin [5]	3.9805	6.0078	8.2214
				Present (21 × 21 points)	3.9844	6.0430	8.3112
CCCC ($\nu = 0.15$)	0.015	1390.2	166.83	Zhou et al. [13]	8.1675	12.823	16.833
				Finite element [6]	8.1375	12.898	16.932
				Present (21 × 21 points)	8.1669	12.821	16.842

points than for thicker plates, to obtain an acceptable convergence of the transverse displacements.

The present method is compared with a Levy-type method by Kobayashi and Sonoda [39], Tables 7 and 8. Due to the Levy approach, edges $y = constant$ are simply-supported. The boundary conditions denoted by SS represent simply-supported bords along the perimeter, while CC indicates that the edges $y = constant$ are simply-supported and the opposite edges are clamped. From the convergence results in Tables 1, 2, 3, 4, 5, 6, it seems quite reasonable to use a 21 × 21 grid for all SSSS and CCCC cases. The results here presented show an excellent correlation with results by Kobayashi and Sonoda [39]. In most cases, results are identical, being the larger differences obtained for CCCC plates, and $h/a = 0.01$.

5.2 Free vibration results

Numerical results are presented for square plates ($a/b = 1$). The non-dimensional parameters are given as

$$\Delta = \frac{\omega b^2}{\pi^2}\sqrt{\rho t/D}, \quad K_1 = \frac{k_f a^4}{D}, \quad K_2 = \frac{G_f a^2}{D} \tag{54}$$

In Table 9 we present a convergence study of the frequency parameters $\Delta_{1,1}$ for the flexural modes of thin and moderately thick square plates on Winkler foundation ($K_2 = 0$). A 21 × 21 points grid was chosen to compare the present method with 3D results by Zhou et al. [13] who used a Ritz method to solve the three-dimensional problem of plates on Winkler foundations, Table 10. Natural frequencies are in excellent agreement with the Mindlin [5] results for thicker plates, and in good agreement with the results by Zhou et al. [13] and the classical results of Leissa [3] for thinner plates.

In Table 11 we present the frequency parameters Δ for the flexural modes of thin and moderately thick square plates on Pasternak foundation. We present results for SSSS and CCCC boundary conditions, and several values of K_1, K_2. We compare our results with those of Zhou et al. [13], using a 3D Ritz approach, and those of Xiang et al. [5] , who used a Mindlin approach. Our results are in excellent agreement with those of [5] and [13] in both SSSS and CCCC boundary conditions, and in both thin and thick plates.

In Figs. 1 and 2, we illustrate the eigenmodes for a CCCC plate, with $t/b = 0.015$, $K_1 = 2780.4$, using a 21 × 21 grid. The modes are quite stable.

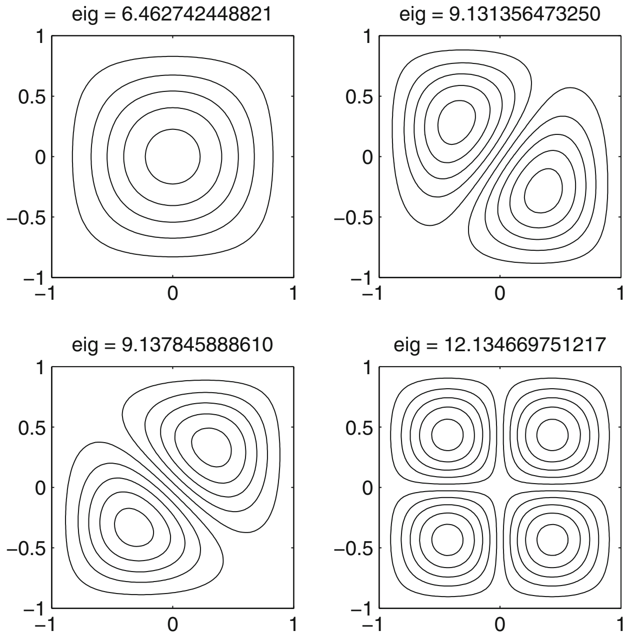

Fig. 1 First four vibrational modes: CCCC, $t/b = 0.015$, $K_1 = 2780.4$, grid 21 × 21

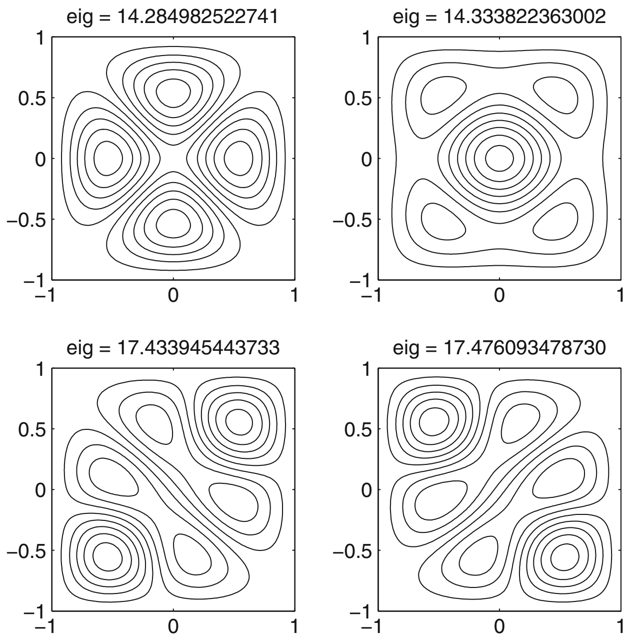

Fig. 2 Fifth to eighth vibrational modes: CCCC, $t/b = 0.015$, $K_1 = 2780.4$, grid 21 × 21

6 Conclusions

In this paper we used, for the first time, the RBF collocation method to analyse static deformations and free vibrations of plates on Pasternak foundations. The first-order shear deformation theory set of equations of motion define a static problem and an eigenproblem which can be solved by various algorithms.

The present results were compared with existing analytical solutions, and finite element schemes and are in very good agreement.

The present method is a simple yet powerful alternative to other finite element or meshless methods in the static deformation and free vibration analysis of plates on Pasternak foundations.

Acknowledgments The support of Ministério da Ciência Tecnologia e do Ensino Superior and Fundo Social Europeu (MCTES and FSE) under programs POPH-QREN are gratefully acknowledged.

References

1. Pasternak PL (1954) On a new method of analysis of an elastic foundation by means of two foundation constants. Gosudarstvennoe Izdatelstvo Literaturi po Stroitelstvu i Arkhitekture, Moscow, USSR, pp 1–56 (in Russian)
2. Winkler E (1867) Die Lehre von der Elasticitaet und Festigkeit. Prag, Dominicus
3. Leissa AW (1973) The free vibration of plates. J Sound Vib 31:257–293
4. Lam KY, Wang CM, He XQ (2000) Canonical exact solutions for levy-plates on two-parameter foundation using green's functions. Eng Struct 22:364–378
5. Xiang Y, Wang CM, Kitipornchai S (1994) Exact vibration solution for initially stressed Mindlin plates on pasternak foundation. Int J Mech Sci 36:311–316
6. Omurtag MH, Ozutok A, Akoz AY (1997) Free vibration analysis of kirchhoff plates resting on elastic foundation by mixed finite element formulation based on gateaux differential. Int J Numer Methods Eng 40:295–317
7. Matsunaga H (2000) Vibration and stability of thick plates on elastic foundations. J Eng Mech ASCE 126:27–34
8. Shen HS, Yang J, Zhang L (2001) Free and forced vibration of Reissner–Mindlin plates with free edges resting on elastic foundations. J Sound Vib 244:299–320
9. Ayvaz Y, Daloglu A, Dogangun A (1998) Application of a modified Vlasov model to earthquake analysis of plates resting on elastic foundations. J Sound Vib 212:499–509
10. Liew KM, Teo TM (2002) Differential cubature method for analysis of shear deformable rectangular plates on pasternak foundations. Int J Mech Sci 44:1179–1194
11. Liew KM, Han JB, Xiao ZM, Du H (1996) Differential quadrature method for Mindlin plates on winkler foundations. Int J Mech Sci 38:405–421
12. Han JB, Liew KM (1997) Numerical differential quadrature method for Reissner–Mindlin plates on two-parameter foundations. Int J Mech Sci 39:977–989
13. Zhou D, Cheung YK, Lo SH, Au FTK (2004) Three-dimensional vibration analysis of rectangular thick plates on pasternak foundation. Int J Numer Methods Eng 59:1313–1334
14. Civalek O, Acar MH (2007) Discrete singular convolution method for the analysis of Mindlin plates on elastic foundations. Int J Pres Vessel Pip 84:527–535
15. Chucheepsakul S, Chinnaboom B (2002) An alternative domain-boundary element technique for analyzing plates on two-parameter elastic foundations. Eng Anal Bound Elem 26:547–555
16. Kansa EJ (1990) Multiquadrics—a scattered data approximation scheme with applications to computational fluid dynamics. i: Surface approximations and partial derivative estimates. Comput Math Appl 19(8/9):127–145
17. Hon YC, Lu MW, Xue WM, Zhu YM (1997) Multiquadric method for the numerical solution of byphasic mixture model. Appl Math Comput 88:153–175
18. Hon YC, Cheung KF, Mao XZ, Kansa EJ (1999) A multiquadric solution for the shallow water equation. J Hydr Eng ASCE 125(5):524–533
19. Wang JG, Liu GR, Lin P (2002) Numerical analysis of biot's consolidation process by radial point interpolation method. Int J Solids Struct 39(6):1557–1573
20. Liu GR, Gu YT (2001) A local radial point interpolation method (LRPIM) for free vibration analyses of 2-d solids. J Sound Vib 246(1):29–46
21. Liu GR, Wang JG (2002) A point interpolation meshless method based on radial basis functions. Int J Numer Methods Eng 54:1623–1648
22. Wang JG, Liu GR (2002) On the optimal shape parameters of radial basis functions used for 2-d meshless methods. Comput Meth Appl Mech Eng 191:2611–2630
23. Chen XL, Liu GR, Lim SP (2003) An element free Galerkin method for the free vibration analysis of composite laminates of complicated shape. Compos Struct 59:279–289
24. Dai KY, Liu GR, Lim SP, Chen XL (2004) An element free Galerkin method for static and free vibration analysis of shear-deformable laminated composite plates. J Sound Vib 269:633–652
25. Liu GR, Chen XL (2002) Buckling of symmetrically laminated composite plates using the element-free Galerkin method. Int J Struct Stabil Dyn 2:281–294
26. Liew KM, Chen XL, Reddy JN (2004) Mesh-free radial basis function method for buckling analysis of non-uniformity loaded arbitrarily shaped shear deformable plates. Comput Meth Appl Mech Eng 193:205–225
27. Huang YQ, Li QS (2004) Bending and buckling analysis of antisymmetric laminates using the moving least square differential quadrature method. Comput Meth Appl Mech Eng 193:3471–3492
28. Liu L, Liu GR, Tan VCB (2002) Element free method for static and free vibration analysis of spatial thin shell structures. Comput Meth Appl Mech Eng 191:5923–5942
29. Ferreira AJM (2003) A formulation of the multiquadric radial basis function method for the analysis of laminated composite plates. Compos Struct 59:385–392
30. Ferreira AJM (2003) Thick composite beam analysis using a global meshless approximation based on radial basis functions. Mech Adv Mater Struct 10:271–284
31. Ferreira AJM, Roque CMC, Martins PALS (2003) Analysis of composite plates using higher-order shear deformation theory and a finite point formulation based on the multiquadric radial basis function method. Compos Part B Eng 34:627–636
32. Madich WR, Nelson SA (1990) Multivariate interpolation and conditionally positive definite functions. ii. Math Comp 54(189):211–230
33. Yoon J (2001) Spectral approximation orders of radial basis function interpolation on the sobolev space. SIAM J Math Anal 33(4):946–958
34. Hardy RL (1971) Multiquadric equations of topography and other irregular surfaces. J Geophys Res 176:1905–1915
35. Buhmann MD (2000) Radial basis functions. Acta Numer 9:1–38
36. Platte RB, Driscoll TA (2004) Computing eigenmodes of elliptic operators using radial basis functions. Comput Math Appl 48:561–576
37. Reddy JN (1997) Mechanics of laminated composite plates: theory and analysis. CRC Press, Boca Raton
38. Liew KM, Huang YQ, Reddy JN (2003) Vibration analysis of symmetrically laminated plates based on fsdt using the moving least squares differential quadrature method. Comput Meth Appl Mech Eng 192:2203–2222
39. Kobayashi H, Sonoda K (1989) Rectangular Mindlin plates on elastic foundation. Int J Mech Sci 31(9):679–692

3.1.4 Buckling and vibration analysis of isotropic and laminated plates by radial basis functions

A. J. M. Ferreira, C. M. C. Roque, Ana M. A. Neves, R. M. N. Jorge, C. M. M. Soares, K. M. Liew, Buckling and vibration analysis of isotropic and laminated plates by radial basis functions, Composites: Part B, Volume 42, Issue 3, 2011, pages 592-606.

Composites: Part B 42 (2011) 592–606

Contents lists available at ScienceDirect

Composites: Part B

journal homepage: www.elsevier.com/locate/compositesb

Buckling and vibration analysis of isotropic and laminated plates by radial basis functions

A.J.M. Ferreira [a,*], C.M.C. Roque [b], A.M.A. Neves [a], R.M.N. Jorge [a], C.M.M. Soares [c], K.M. Liew [d]

[a] Departamento de Engenharia Mecânica, Faculdade de Engenharia da Universidade do Porto, Rua Dr. Roberto Frias, 4200-465 Porto, Portugal
[b] INEGI, Faculdade de Engenharia da Universidade do Porto, Rua Dr. Roberto Frias, 4200-465 Porto, Portugal
[c] Departamento de Engenharia Mecânica, Instituto Superior Técnico, Av. Rovisco Pais, Lisboa, Portugal
[d] City University of Hong Kong, Tat Chee Avenue, Kowloon, Hong Kong

ARTICLE INFO

Article history:
Received 5 July 2010
Received in revised form 30 July 2010
Accepted 3 August 2010
Available online 10 August 2010

Keywords:
A. Plates
C. Computational modelling
C. Laminate mechanics

ABSTRACT

This paper addresses the buckling and vibration analysis of isotropic and laminated plates by a first-order shear deformation theory. The numerical approach is based on collocation with radial basis functions. The model allows the analysis of arbitrary boundary conditions and irregular geometries. It is shown that the present method, based on a first-order shear deformation theory produces highly accurate natural frequencies and modes of vibration, as well as critical loads and modes.

1. Introduction

Composite laminated plates are widely used in various applications due to their high strength-to-weight ratio and flexibility in design. It is well known that the classical laminated plate theory (CLPT) based on the Kirchhoff hypothesis yields acceptable results only for thin laminates [1]. The structures designed based on the CLPT analysis may be unsafe because the CLPT underestimates the transverse deformation and overpredicts the buckling load of the laminated plate. Therefore, first-order [2,3] and higher-order [4,5] shear deformation theories have been developed to include transverse shear deformation effects.

Recently, radial basis functions (RBFs) have enjoyed considerable success and research as a technique for interpolating data and functions. A radial basis function, $\phi(\|x - x_j\|)$ is a spline that depends on the Euclidian distance between distinct data centers $x_j, j = 1, 2, \ldots, N \in \mathbb{R}^n$, also called nodal or collocation points.

Although most work to date on RBFs relates to scattered data approximation and in general to interpolation theory, there has recently been an increased interest in their use for solving partial differential equations (PDEs). This approach, which approximates the whole solution of the PDE directly using RBFs, is very attractive due to the fact that this is truly a mesh-free technique. Kansa [6] introduced the concept of solving PDEs using RBFs. Kansa's method is an unsymmetric RBF collocation method based upon the multiquadrics (MQ) interpolation functions, in which the shape parameter is considered to be variable across the problem domain. The distribution of the shape parameter is obtained by an optimization approach, in which the value of the shape parameter is assumed to be proportional to the curvature of the unknown solution of the original partial differential equation. In this way, it is possible to reduce the condition number of the matrix at the expense of implementing an additional iterative algorithm. In the present work, we have implemented the unsymmetric collocation method in its simpler form, without any optimization of the interpolation functions and the collocation points.

The analysis of plates by finite element methods is now fully established. The use of alternative methods such as the meshless methods based on radial basis functions is attractive due to the absence of a mesh and the ease of collocation methods. The use of radial basis function for the analysis of structures and materials has been previously studied by numerous authors [7–18]. More recently the authors have applied RBFs to the static deformations of composite beams and plates [19–21].

Some relevant works on vibration and buckling of thick plates include those of Wang et al. [22], Khdeir and Librescu [23], Bhimaraddi [24], Kitipornchai et al. [25], Liew et al. [26–28], and Reddy et al. [29,30]. An historical review on laminated plates and shells has been presented by Carrera [31]. Although much work has been done with analytical or meshless methods, there is no research on buckling analysis of laminated plates by radial basis functions. This paper tries to fill that gap in this research field.

* Corresponding author.
E-mail address: ferreira@fe.up.pt (A.J.M. Ferreira).

1359-8368/$ - see front matter © 2010 Elsevier Ltd. All rights reserved.
doi:10.1016/j.compositesb.2010.08.001

The objective of this paper is then to determine both the elastic buckling loads of the Mindlin plates that are subjected to partial in-plane edge loads and the natural frequencies and modes of vibration by collocation with radial basis functions.

2. The radial basis function method

2.1. The static problem

Radial basis functions (RBF) approximations are grid-free numerical schemes that can exploit accurate representations of the boundary, are easy to implement and can be spectrally accurate [32,33].

In this section the formulation of a global unsymmetrical collocation RBF-based method to compute eigenvalues of elliptic operators is presented.

Consider a linear elliptic partial differential operator $\mathscr{L}$ and a bounded region Ω in $\mathbb{R}^n$ with some boundary $\partial\Omega$.

The static problems aims the computation of displacements (primary variables) ($\mathbf{u}$) from the global system of equations

$$\mathscr{L}\mathbf{u} = \mathbf{f} \quad \text{in} \quad \Omega; \quad \mathscr{L}_B\mathbf{u} = \mathbf{g} \quad \text{on} \quad \partial\Omega \tag{1}$$

where $\mathscr{L}$, $\mathscr{L}_B$ are linear operators in the domain and on the boundary, respectively. The right-hand side of (1) represents the external forces applied on the plate and the boundary conditions applied along the perimeter of the plate, respectively. The PDE problem defined in (1) is replaced by a finite problem, defined by an algebraic system of equations, from the radial basis expansions.

2.2. The eigenproblem

The eigenproblem looks for eigenvalues (λ) and eigenvectors ($\mathbf{u}$) that satisfy

$$\mathscr{L}\mathbf{u} + \lambda\mathbf{u} = 0 \quad \text{in} \quad \Omega; \quad \mathscr{L}_B\mathbf{u} = 0 \quad \text{on} \quad \partial\Omega \tag{2}$$

As in the static problem, the eigenproblem defined in (2) is replaced by a finite-dimensional eigenvalue problem, based on RBF approximations.

2.3. Radial basis functions

The radial basis function (ϕ) approximation of a function (u) is defined as

$$\widetilde{\mathbf{u}}(\mathbf{x}) = \sum_{i=1}^{N} \alpha_i \phi(\|x - y_i\|_2), \mathbf{x} \in \mathbb{R}^n \tag{3}$$

where y_i, $i = 1,\ldots,N$ is a finite set of distinct points (centers) in $\mathbb{R}^n$. The coefficients α_i are chosen so that $\widetilde{\mathbf{u}}$ satisfies some variationally-consistent boundary conditions. The most common RBFs are

$$\begin{aligned}
&\phi(r) = r^3, \quad \text{cubic}\\
&\phi(r) = r^2\log(r), \quad \text{thin plate splines}\\
&\phi(r) = (1-r)_+^m p(r), \quad \text{Wendland functions}\\
&\phi(r) = e^{-(cr)^2}, \quad \text{Gaussian}\\
&\phi(r) = \sqrt{c^2 + r^2}, \quad \text{Multiquadrics}\\
&\phi(r) = (c^2 + r^2)^{-1/2}, \text{Inverse Multiquadrics}
\end{aligned}$$

2.4. Solution of the interpolation problem

Hardy [34] introduced multiquadrics in the analysis of scattered geographical data. In the 1990's Kansa [6] used multiquadrics for the solution of partial differential equations.

Considering N distinct interpolations, and given $u(x_j), j = 1,2,\ldots,N$, we find α_i by the solution of a $N \times N$ linear system

$$\mathbf{A}\underline{\alpha} = \mathbf{u} \tag{4}$$

where $\mathbf{A} = [\phi(\|x - y_i\|_2)]_{N\times N}$, $\underline{\alpha} = [\alpha_1, \alpha_2, \ldots, \alpha_N]^T$ and $\mathbf{u} = [u(x_1), u(x_2), \ldots, u(x_N)]^T$. The RBF interpolation matrix A is positive definite for some RBFs [35], but in general provides ill-conditioned systems.

2.5. Solution of the static problem

The solution of a static problem by radial basis functions considers N_I nodes in the domain and N_B nodes on the boundary, with total number of nodes $N = N_I + N_B$.

We denote the sampling points by $x_i \in \Omega, i = 1,\ldots,N_I$ and $x_i \in \partial\Omega$, $i = N_I + 1,\ldots,N$. At the points in the domain we solve the following system of equations

$$\sum_{i=1}^{N} \alpha_i \mathscr{L}\phi(\|x - y_i\|_2) = \mathbf{f}(x_j), \quad j = 1,2,\ldots,N_I \tag{5}$$

or

$$\mathscr{L}^I\underline{\alpha} = \mathbf{F} \tag{6}$$

where

$$\mathscr{L}^I = [\mathscr{L}\phi(\|x - y_i\|_2)]_{N_I\times N} \tag{7}$$

For the boundary conditions we have

$$\sum_{i=1}^{N} \alpha_i \mathscr{L}_B\phi(\|x - y_i\|_2) = \mathbf{g}(x_j), \quad j = N_I + 1,\ldots,N \tag{8}$$

or

$$\mathbf{B}\underline{\alpha} = \mathbf{G} \tag{9}$$

Therefore we can write a finite-dimensional static problem as

$$\begin{bmatrix} \mathscr{L}^I \\ \mathbf{B} \end{bmatrix} \underline{\alpha} = \begin{bmatrix} \mathbf{F} \\ \mathbf{G} \end{bmatrix} \tag{10}$$

where

$$\mathscr{L}^I = L\phi\left[\left(\|x_{N_I} - y_j\|_2\right)\right]_{N_I\times N}, \quad \mathbf{B} = L_B\phi\left[\left(\|x_{N_I+1} - y_j\|_2\right)\right]_{N_B\times N}$$

By inverting the system (10), we obtain the vector of parameters $\underline{\alpha}$. We then proceed to the solution by the interpolation Eq. (3).

2.6. Solution of the eigenproblem

We consider N_I nodes in the interior of the domain and N_B nodes on the boundary, with $N = N_I + N_B$.

We denote interpolation points by $x_i \in \Omega$, $i = 1,\ldots,N_I$ and $x_i \in \partial\Omega$, $i = N_I + 1,\ldots,N$. For the points in the domain, the following problem is defined

$$\sum_{i=1}^{N} \alpha_i \mathscr{L}\phi(\|x - y_i\|_2) = \lambda\widetilde{\mathbf{u}}(x_j), \quad j = 1,2,\ldots,N_I \tag{11}$$

or

$$\mathscr{L}^I\underline{\alpha} = \lambda\widetilde{\mathbf{u}}^I \tag{12}$$

where

$$\mathscr{L}^I = [\mathscr{L}\phi(\|x - y_i\|_2)]_{N_I\times N} \tag{13}$$

For the boundary conditions we have

$$\sum_{i=1}^{N} \alpha_i \mathscr{L}_B\phi(\|x - y_i\|_2) = 0, \quad j = N_I + 1,\ldots,N \tag{14}$$

or

$$\mathbf{B}\underline{\alpha} = 0 \quad (15)$$

Therefore we can write a finite-dimensional problem as a generalized eigenvalue problem

$$\begin{bmatrix} \mathscr{L}^I \\ \mathbf{B} \end{bmatrix} \underline{\alpha} = \lambda \begin{bmatrix} \mathbf{A}^I \\ \mathbf{0} \end{bmatrix} \underline{\alpha} \quad (16)$$

where

$$\mathbf{A}^I = \phi\left[(\|x_{N_I} - y_j\|_2)\right]_{N_I \times N}, \quad \mathbf{B} = \mathscr{L}_B \phi\left[(\|x_{N_I+1} - y_j\|_2)\right]_{N_B \times N}$$

We seek the generalized eigenvalues and eigenvectors of these matrices.

3. Free vibration analysis

Based on the first-order shear deformation theory (FSDT), the transverse displacement $w(x, y)$ and the rotations $\theta_x(x, y)$ and $\theta_y(x, y)$ about the $y-$ and $x-$ axes are independently interpolated due to uncoupling between in-plane displacements and bending displacements for plates. For free vibration analysis we consider the following equations of motion:

$$D_{11}\frac{\partial^2\theta_x}{\partial x^2} + D_{16}\frac{\partial^2\theta_y}{\partial x^2} + (D_{12} + D_{66})\frac{\partial^2\theta_y}{\partial x\partial y} + 2D_{16}\frac{\partial^2\theta_x}{\partial x\partial y} + D_{66}\frac{\partial^2\theta_x}{\partial y^2} + D_{26}\frac{\partial^2\theta_y}{\partial y^2} + -kA_{45}\left(\theta_y + \frac{\partial w}{\partial y}\right) - kA_{55}\left(\theta_x + \frac{\partial w}{\partial x}\right) = I_2\frac{\partial^2\theta_x}{\partial t^2} \quad (17)$$

Table 1
Natural frequencies of a CCCC square Mindlin/Reissner plate with $h/a = 0.1$, $k = 0.8601$, $\nu = 0.3$.

Mode no.	m	n	13×13	17×17	21×21	Rayleygh–Ritz [42]	Liew et al. [26]
1	1	1	1.5911	1.5911	1.5911	1.5940	1.5582
2	2	1	3.0393	3.0389	3.0393	3.0390	3.0182
3	1	2	3.0393	3.0389	3.0395	3.0390	3.0182
4	2	2	4.2641	4.2624	4.2607	4.2650	4.1711
5	3	1	5.0290	5.0249	5.0247	5.0350	5.1218
6	1	3	5.0756	5.0724	5.0687	5.0780	5.1594
7	3	2	6.0890	6.0800	6.0784		6.0178
8	2	3	6.0890	6.0801	6.0786		6.0178

Table 2
Natural frequencies of a CCCC square Mindlin/Reissner plate with $h/a = 0.01$, $k = 0.8601$, $\nu = 0.3$.

Mode no.	m	n	13×13	17×17	21×21	Rayleygh–Ritz [42]	Liew et al. [26]
1	1	1	0.1846	0.1753	0.1754	0.1754	0.1743
2	2	1	0.3787	0.3575	0.3577	0.3576	0.3576
3	1	2	0.3787	0.3575	0.3577	0.3576	0.3576
4	2	2	0.5615	0.5280	0.5250	0.5274	0.5240
5	3	1	0.6525	0.6433	0.6403	0.6402	0.6465
6	1	3	0.6596	0.6463	0.6403	0.6432	0.6505
7	3	2	0.7722	0.8137	0.7997		0.8015
8	2	3	0.7722	0.8138	0.8001		0.8015

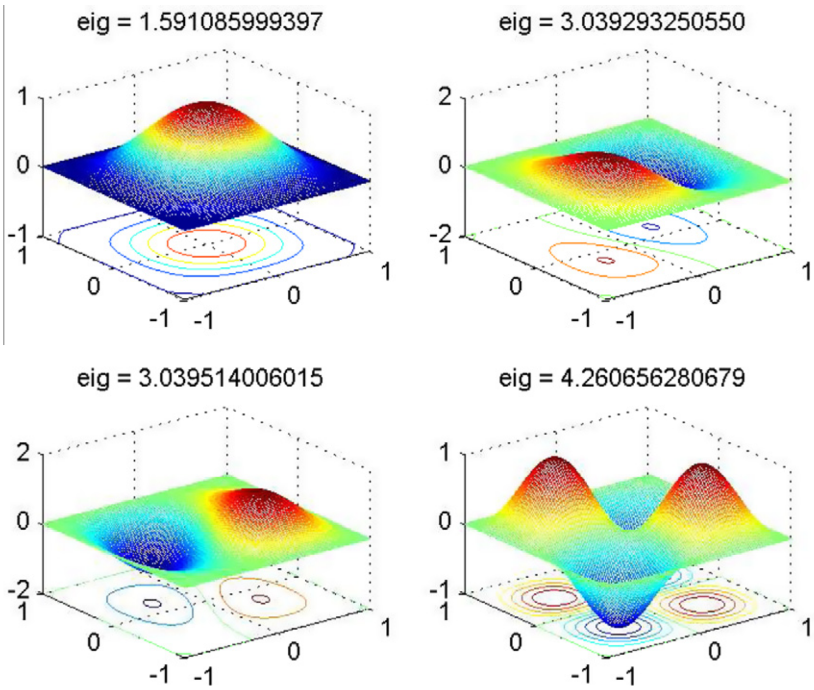

Fig. 1. Mode shapes (1–4) for CCCC plate with $h/a = 0.1$.

$$D_{16}\frac{\partial^2\theta_x}{\partial x^2}+D_{66}\frac{\partial^2\theta_y}{\partial x^2}+(D_{12}+D_{66})\frac{\partial^2\theta_x}{\partial x\partial y}+2D_{26}\frac{\partial^2\theta_y}{\partial x\partial y}+D_{26}\frac{\partial^2\theta_x}{\partial y^2}+D_{22}\frac{\partial^2\theta_y}{\partial y^2}+-kA_{44}\left(\theta_y+\frac{\partial w}{\partial y}\right)-kA_{45}\left(\theta_x+\frac{\partial w}{\partial x}\right)=I_2\frac{\partial^2\theta_y}{\partial t^2} \quad (18)$$

$$\frac{\partial}{\partial x}\left[kA_{45}\left(\theta_y+\frac{\partial w}{\partial y}\right)+kA_{55}\left(\theta_x+\frac{\partial w}{\partial x}\right)\right]+\frac{\partial}{\partial y}\left[kA_{44}\left(\theta_y+\frac{\partial w}{\partial y}\right)+kA_{45}\left(\theta_x+\frac{\partial w}{\partial x}\right)\right]=I_0\frac{\partial^2 w}{\partial t^2} \quad (19)$$

where D_{ij} and A_{ij} are the bending and shear stiffness components, k is the shear correction factor, and I_i are the mass inertias defined as [36]

$$I_0=\int_{-\frac{h}{2}}^{\frac{h}{2}}\rho dz,\quad I_2=\int_{-\frac{h}{2}}^{\frac{h}{2}}\rho z^2 dz \quad (20)$$

Here ρ and h denote the density and the total thickness of the plate, respectively.

For free vibration problems we set $p = 0$, and assume harmonic solution in terms of displacements w, θ_x, θ_y in the form

$$w(x,y,t)=W(w,y)e^{i\omega t} \quad (21)$$

$$\theta_x(x,y,t)=\Psi_x(w,y)e^{i\omega t} \quad (22)$$

$$\theta_y(x,y,t)=\Psi_y(w,y)e^{i\omega t} \quad (23)$$

where ω is the frequency of natural vibration.

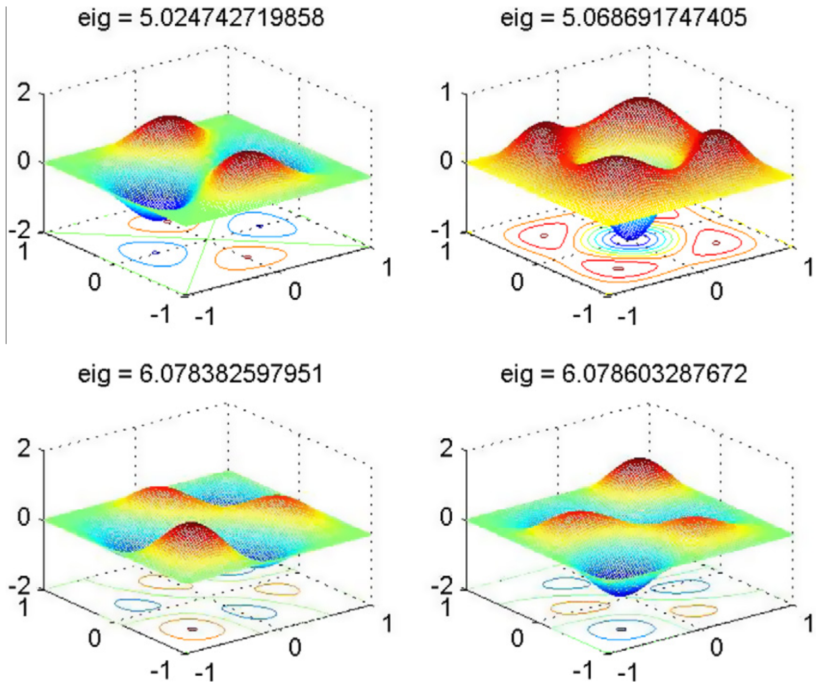

Fig. 2. Mode shapes (5–8) for CCCC plate with $h/a = 0.1$.

Table 3
Natural frequencies of a SSSS square Mindlin/Reissner plate with $h/a = 0.1$, $k = 0.833$, $\nu = 0.3$ (* - closed form).

Mode no.	m	n	13 × 13	17 × 17	21 × 21	3D* [43]	Mindlin [43]	Liew et al. [26]
1	1	1	0.930	0.930	0.930	0.932	0.930	0.922
2	2	1	2.219	2.219	2.219	2.226	2.219	2.205
3	1	2	2.219	2.219	2.219	2.226	2.219	2.205
4	2	2	3.406	3.406	3.406	3.421	3.406	3.377
5	3	1	4.151	4.149	4.149	4.171	4.149	4.139
6	1	3	4.151	4.149	4.149	4.171	4.149	4.139
7	3	2	5.209	5.206	5.205	5.239	5.206	5.170
8	2	3	5.209	5.206	5.205	5.239	5.206	5.170

Table 4
Natural frequencies of a SSSS square Mindlin/Reissner plate with $h/a = 0.01$, $k = 0.833$, $\nu = 0.3$.

Mode no.	m	n	13 × 13	17 × 17	21 × 21	Mindlin [43]	Liew et al. [26]
1	1	1	0.0965	0.0963	0.0963	0.0963	0.0961
2	2	1	0.2417	0.2407	0.2401	0.2406	0.2419
3	1	2	0.2417	0.2407	0.2403	0.2406	0.2419
4	2	2	0.3884	0.3851	0.3846	0.3848	0.3860
5	3	1	0.4775	0.4818	0.4802	0.4809	0.4898
6	1	3	0.4788	0.4819	0.4808	0.4809	0.4898
7	3	2	0.6290	0.6267	0.6253	0.6249	0.6315
8	2	3	0.6290	0.6268	0.6255	0.6249	0.6315

Substituting the harmonic expansion (21)–(23) into the equations of motion (17)–(19) we obtain the following equations in terms of the amplitudes W, Ψ_x, Ψ_y

$$D_{11}\frac{\partial^2\Psi_x}{\partial x^2}+D_{16}\frac{\partial^2\Psi_y}{\partial x^2}+(D_{12}+D_{66})\frac{\partial^2\Psi_y}{\partial x\partial y}+2D_{16}\frac{\partial^2\Psi_x}{\partial x\partial y}+D_{66}\frac{\partial^2\Psi_x}{\partial y^2}+D_{26}\frac{\partial^2\Psi_y}{\partial y^2}-kA_{45}\left(\Psi_y+\frac{\partial W}{\partial y}\right)-kA_{55}\left(\Psi_x+\frac{\partial W}{\partial x}\right)=-I_2\omega^2\Psi_x \quad (24)$$

$$D_{16}\frac{\partial^2\Psi_x}{\partial x^2}+D_{66}\frac{\partial^2\Psi_y}{\partial x^2}+(D_{12}+D_{66})\frac{\partial^2\Psi_x}{\partial x\partial y}+2D_{26}\frac{\partial^2\Psi_y}{\partial x\partial y}+D_{26}\frac{\partial^2\Psi_x}{\partial y^2}+D_{22}\frac{\partial^2\Psi_y}{\partial y^2}-kA_{44}\left(\Psi_y+\frac{\partial W}{\partial y}\right)-kA_{45}\left(\Psi_x+\frac{\partial W}{\partial x}\right)=-I_2\omega^2\Psi_y \quad (25)$$

$$\frac{\partial}{\partial x}\left[kA_{45}\left(\Psi_y+\frac{\partial W}{\partial y}\right)+kA_{55}\left(\Psi_x+\frac{\partial W}{\partial x}\right)\right]+\frac{\partial}{\partial y}\left[kA_{44}\left(\Psi_y+\frac{\partial W}{\partial y}\right)+kA_{45}\left(\Psi_x+\frac{\partial W}{\partial x}\right)\right]=-I_0\omega^2W \quad (26)$$

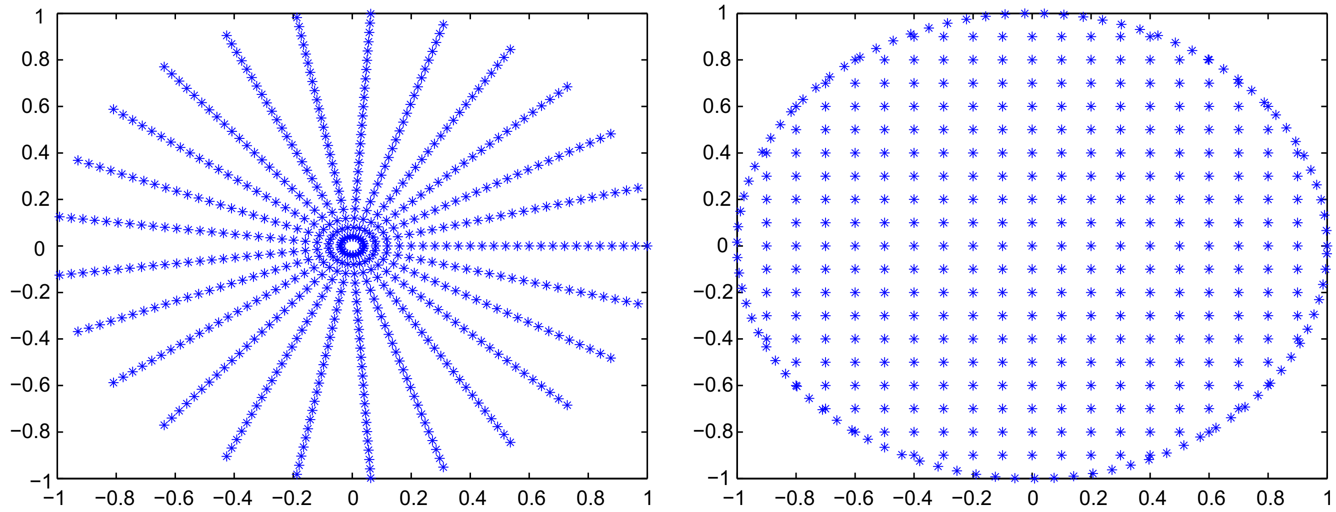

Fig. 3. Two grids for circular plates, Grids 1 and 2.

Table 5
The normalized frequency parameters ($\bar{\omega}=\omega R^2\sqrt{\rho h/D}$, k = 0.833) for a clamped circular Mindlin/Reissner plate with thickness to radius ratio: h/R = 0.1, Grid 1.

n	s	Present (400 nodes)	Present (625 nodes)	Exact [44]	Mesh-free [26]
0	1	9.9410	9.9409	9.941	9.931
	2	36.4745	36.4778	36.479	36.665
	3	75.6468	75.6600	75.664	76.531
	4	123.3820	123.3389	123.32	122.46
1	1	20.1761	20.1765	20.232	20.194
	2	53.8346	53.8441	53.890	54.257
	3	97.8753	97.8766	97.907	99.207
2	0	32.2005	32.2042	32.406	32.353
	1	72.2032	72.2172	72.368	72.669
	2	120.5482	120.4776	120.55	121.94
3	0	45.7592	45.7711	46.178	45.827
	1	91.4528	91.4367	91.712	92.267
4	0	60.6319	60.6378	61.272	60.6595
	1	111.5998	111.3795	111.74	110.68
5	0	76.7997	76.6216	77.454	76.5343
6	0	95.0694	93.6460	94.527	93.285

Table 6
The normalized frequency parameters ($\bar{\omega}=\omega R^2\sqrt{\rho h/D}$, k = 0.833) for a clamped circular Mindlin/Reissner plate with thickness to radius ratio: h/R = 0.01, Grid 1.

n	s	Present (400 nodes)	Present (625 nodes)	Finite element [43]	Mesh-free [26]
0	1	10.2317	10.2221	10.2158	10.2661
	2	39.6223	39.6946	39.771	40.2905
1	1	21.2684	21.2614	21.26	21.4488
	2	60.8731	60.7231	60.82	62.1455
2	0	34.9802	34.9171	34.88	35.2556
	1	86.8181	84.9762	84.58	86.3649
3	0	52.1268	51.3888	51.04	51.6626
	1	121.4737	113.7459	111.01	113.594
4	0	76.3506	71.4766	69.6659	70.4145
	1	121.6326	138.1215	140.108	142.119

The eigenproblem associated to Eqs. (24)–(26) is defined as

$$[\mathscr{L} - \omega^2 \mathscr{G}]\mathbf{X} = \mathbf{0} \tag{27}$$

where $\mathscr{L}$ collects all stiffness terms and $\mathscr{G}$ collects all inertial terms. In (27) $\mathbf{X}$ are the vibrational modes associated with the natural frequencies defined as ω.

4. Buckling analysis

The buckling analysis considers the following equations of motion [37–39]:

$$D_{11}\frac{\partial^2\theta_x}{\partial x^2} + D_{16}\frac{\partial^2\theta_y}{\partial x^2} + (D_{12}+D_{66})\frac{\partial^2\theta_y}{\partial x\partial y} + 2D_{16}\frac{\partial^2\theta_x}{\partial x\partial y} + D_{66}\frac{\partial^2\theta_x}{\partial y^2} + D_{26}\frac{\partial^2\theta_y}{\partial y^2} + -kA_{45}\left(\theta_y + \frac{\partial w}{\partial y}\right) - kA_{55}\left(\theta_x + \frac{\partial w}{\partial x}\right) = 0 \tag{28}$$

$$D_{16}\frac{\partial^2\theta_x}{\partial x^2} + D_{66}\frac{\partial^2\theta_y}{\partial x^2} + (D_{12}+D_{66})\frac{\partial^2\theta_x}{\partial x\partial y} + 2D_{26}\frac{\partial^2\theta_y}{\partial x\partial y} + D_{26}\frac{\partial^2\theta_x}{\partial y^2} + D_{22}\frac{\partial^2\theta_y}{\partial y^2} + -kA_{44}\left(\theta_y + \frac{\partial w}{\partial y}\right) - kA_{45}\left(\theta_x + \frac{\partial w}{\partial x}\right) = 0 \tag{29}$$

$$\frac{\partial}{\partial x}\left[kA_{45}\left(\theta_y + \frac{\partial w}{\partial y}\right) + kA_{55}\left(\theta_x + \frac{\partial w}{\partial x}\right)\right] + \frac{\partial}{\partial y}\left[kA_{44}\left(\theta_y + \frac{\partial w}{\partial y}\right) + kA_{45}\left(\theta_x + \frac{\partial w}{\partial x}\right)\right] + \bar{N}_{xx}\frac{\partial^2 w}{\partial x^2} + 2\bar{N}_{xy}\frac{\partial^2 w}{\partial x\partial y} + \bar{N}_{yy}\frac{\partial^2 w}{\partial y^2} = 0 \tag{30}$$

In (30), $\overline{N_{xx}}, \bar{N}_{xy}$, and $\bar{N}_{yy}$ are the in-plane applied forces. In order to determine the critical buckling load of the laminated plate, the transverse load is set to zero.

The eigenproblem associated with (28)–(30) is defined as

$$[\mathscr{L} - \lambda\mathscr{G}]\mathbf{X} = \mathbf{0} \tag{31}$$

where $\mathscr{L}$ collects all stiffness terms and $\mathscr{G}$ collects all terms related to the in-plane forces. In (31) $\mathbf{X}$ are the buckling modes associated with the buckling loads defined as λ.

5. Resultants and boundary conditions

The bending moments and shear forces are expressed as functions of the displacement gradients and the material constitutive equations by

$$M_x = D_{11}\frac{\partial\theta_x}{\partial x} + D_{12}\frac{\partial\theta_y}{\partial y} + D_{16}\left(\frac{\partial\theta_x}{\partial y} + \frac{\partial\theta_y}{\partial x}\right) \tag{32}$$

$$M_y = D_{12}\frac{\partial\theta_x}{\partial x} + D_{22}\frac{\partial\theta_y}{\partial y} + D_{26}\left(\frac{\partial\theta_x}{\partial y} + \frac{\partial\theta_y}{\partial x}\right) \tag{33}$$

$$M_{xy} = D_{16}\frac{\partial\theta_x}{\partial x} + D_{26}\frac{\partial\theta_y}{\partial y} + D_{66}\left(\frac{\partial\theta_x}{\partial y} + \frac{\partial\theta_y}{\partial x}\right) \tag{34}$$

$$Q_x = kA_{55}\left(\theta_x + \frac{\partial w}{\partial x}\right) + kA_{45}\left(\theta_y + \frac{\partial w}{\partial y}\right) \tag{35}$$

$$Q_y = kA_{45}\left(\theta_x + \frac{\partial w}{\partial x}\right) + kA_{55}\left(\theta_y + \frac{\partial w}{\partial y}\right) \tag{36}$$

The boundary conditions for an arbitrary edge with simply-supported, clamped and free edge conditions are defined as follows [40]:

(a) Simply-supported
- SS1, $w = 0; M_n = 0; M_{ns} = 0$
- SS2, $w = 0; M_n = 0; \theta_s = 0$

(b) Clamped, $w = 0; \theta_n = 0; \theta_s = 0$
(c) Free, $Q_n = 0; M_n = 0; M_{ns} = 0$

Table 7
The normalized frequency parameters ($\bar{\omega} = \omega R^2\sqrt{\rho h/D}$, $k = 0.833$) for a clamped circular Mindlin/Reissner plate with thickness to radius ratio: $h/R = 0.1$, Grid 2.

n	s	Present (408 nodes)	Present (647 nodes)	Exact [44]	Mesh-free [26]
0	1	9.9442	9.9444	9.941	9.931
	2	36.5086	36.5085	36.479	36.665
	3	75.7558	75.7143	75.664	76.531
	4	123.4944	123.3491	123.32	122.46
1	1	20.1884	20.1772	20.232	20.194
	2	53.9028	53.8757	53.890	54.257
	3	97.9955	97.8664	97.907	99.207
2	0	32.2313	32.2314	32.406	32.353
	1	72.3012	72.2894	72.368	72.669
	2	120.5391	120.5039	120.55	121.94
3	0	45.8353	45.7803	46.178	45.827
	1	91.5885	91.3558	91.712	92.267
4	0	60.7466	60.7932	61.272	60.6595
	1	111.4686	111.3841	111.74	110.68
5	0	76.7763	76.6476	77.454	76.5343
6	0	93.7642	93.5409	94.527	93.285

Table 8
The normalized frequency parameters ($\bar{\omega} = \omega R^2\sqrt{\rho h/D}$, $k = 0.833$) for a clamped circular Mindlin/Reissner plate with thickness to radius ratio: $h/R = 0.01$, Grid 2.

n	s	Present (408 nodes)	Present (647 nodes)	Finite element [43]	Mesh-free [26]
0	1	10.2283	10.2281	10.2158	10.2661
	2	39.7735	39.8084	39.771	40.2905
1	1	21.2825	21.2861	21.26	21.4488
	2	60.9426	60.8979	60.82	62.1455
2	0	34.9849	34.9316	34.88	35.2556
	1	85.2664	84.6716	84.58	86.3649
3	0	51.8594	51.2085	51.04	51.6626
	1	121.3689	111.4787	111.01	113.594
4	0	70.4856	70.0040	69.6659	70.4145
	1	143.3500	141.0533	140.108	142.119

In previous equations, the subscripts n and s refer to the normal and tangencial directions of the edge, respectively; M_n, M_{ns} and Q_n represent the normal bending moment, twisting moment and shear force on the plate edge; θ_n and θ_s represent the rotations about the tangencial and normal coordinates at the plate edge.

The stress resultants on an edge whose normal is represented by $\mathbf{n} = (n_x, n_y)$ can be expressed as

$$M_n = n_x^2 M_x + 2 n_x n_y M_{xy} + n_y^2 M_y \tag{37}$$

$$M_{ns} = (n_x^2 - n_y^2) M_{xy} - n_x n_y (My - Mx) \tag{38}$$

$$Q_n = n_x Q_x + n_y Q_y \tag{39}$$

$$\theta_n = n_x \theta_x + n_y \theta_y \tag{40}$$

$$\theta_s = n_x \theta_y - n_y \theta_x \tag{41}$$

where n_x and n_y are the direction cosines of a unit normal vector at a point at the laminated plate boundary [36,40].

6. Discretization of the equations of motion and boundary conditions

The radial basis collocation method follows a simple implementation procedure. Taking Eq. (13), we compute

$$\boldsymbol{\alpha} = \begin{bmatrix} L^I \\ \mathbf{B} \end{bmatrix}^{-1} \begin{bmatrix} \mathbf{F} \\ \mathbf{G} \end{bmatrix} \tag{42}$$

This $\boldsymbol{\alpha}$ vector is then used to obtain solution $\tilde{\mathbf{u}}$, by Eq. (7). If derivatives of $\tilde{\mathbf{u}}$ are needed, such derivatives are computed as

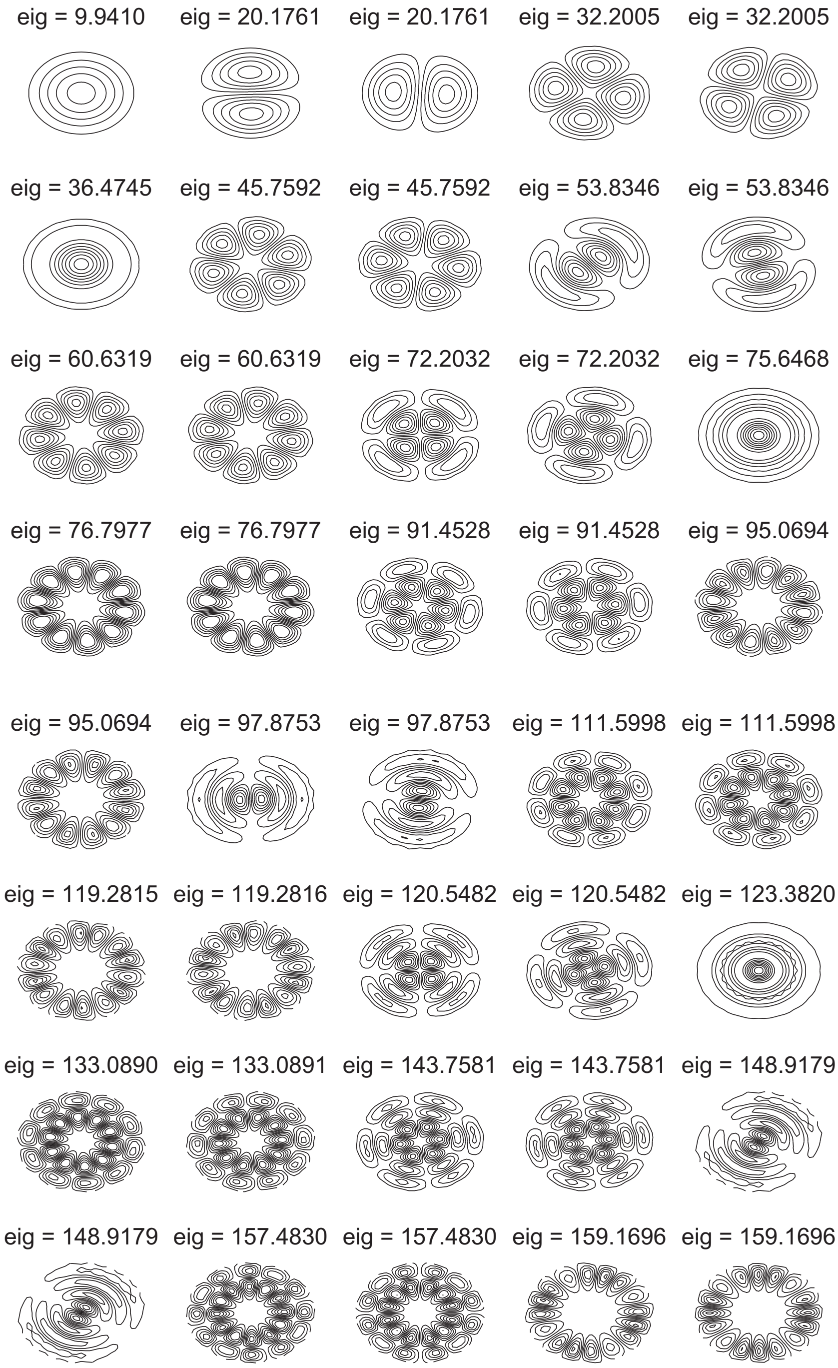

Fig. 4. First 40 vibration modes of the clamped isotropic plate ($h/R = 0.1$), using 400 nodes.

$$\frac{\partial \tilde{\mathbf{u}}}{\partial x} = \sum_{j=1}^{N} \alpha_j \frac{\partial \phi_j}{\partial x} \tag{43}$$

$$\frac{\partial^2 \tilde{\mathbf{u}}}{\partial x^2} = \sum_{j=1}^{N} \alpha_j \frac{\partial^2 \phi_j}{\partial x^2}, \quad \text{etc.} \tag{44}$$

As an example of discretization by RBF's, let's consider the buckling problem. The equations of motion and the boundary conditions can now be discretized according to the radial basis function collocation, as

$$D_{11} \sum_{j=1}^{N} \alpha_j^{\Psi_x} \frac{\partial^2 \phi_j}{\partial x^2} + D_{16} \sum_{j=1}^{N} \alpha_j^{\Psi_y} \frac{\partial^2 \phi_j}{\partial x^2} + (D_{12} + D_{66}) \sum_{j=1}^{N} \alpha_j^{\Psi_y} \frac{\partial^2 \phi_j}{\partial x \partial y} + 2D_{16} \sum_{j=1}^{N} \alpha_j^{\Psi_x} \frac{\partial^2 \phi_j}{\partial x \partial y} + D_{66} \sum_{j=1}^{N} \alpha_j^{\Psi_x} \frac{\partial^2 \phi_j}{\partial y^2} + D_{26} \sum_{j=1}^{N} \alpha_j^{\Psi_y} \frac{\partial^2 \phi_j}{\partial y^2} - kA_{45} \left(\sum_{j=1}^{N} \alpha_j^{\Psi_y} \phi_j + \sum_{j=1}^{N} \alpha_j^{W} \frac{\partial \phi_j}{\partial y} \right) - kA_{55} \left(\sum_{j=1}^{N} \alpha_j^{\Psi_x} \phi_j + \sum_{j=1}^{N} \alpha_j^{W} \frac{\partial \phi_j}{\partial x} \right) = 0 \tag{45}$$

$$D_{16} \sum j = 1^N \alpha_j^{\Psi_x} \frac{\partial^2 \phi_j}{\partial x^2} + D_{66} \sum_{j=1}^{N} \alpha_j^{\Psi_y} \frac{\partial^2 \phi_j}{\partial x^2} + (D_{12} + D_{66}) \sum_{j=1}^{N} \alpha_j^{\Psi_x} \frac{\partial^2 \phi_j}{\partial x \partial y} + 2D_{26} \sum_{j=1}^{N} \alpha_j^{\Psi_y} \frac{\partial^2 \phi_j}{\partial x \partial y} + D_{26} \sum_{j=1}^{N} \alpha_j^{\Psi_x} \frac{\partial^2 \phi_j}{\partial y^2} + D_{22} \sum_{j=1}^{N} \alpha_j^{\Psi_y} \frac{\partial^2 \phi_j}{\partial y^2} - kA_{44} \left(\sum_{j=1}^{N} \alpha_j^{\Psi_y} \phi_j + \sum_{j=1}^{N} \alpha_j^{W} \frac{\partial \phi_j}{\partial y} \right) - kA_{45} \left(\sum_{j=1}^{N} \alpha_j^{\Psi_x} \phi_j + \sum_{j=1}^{N} \alpha_j^{W} \frac{\partial \phi_j}{\partial x} \right) = 0 \tag{46}$$

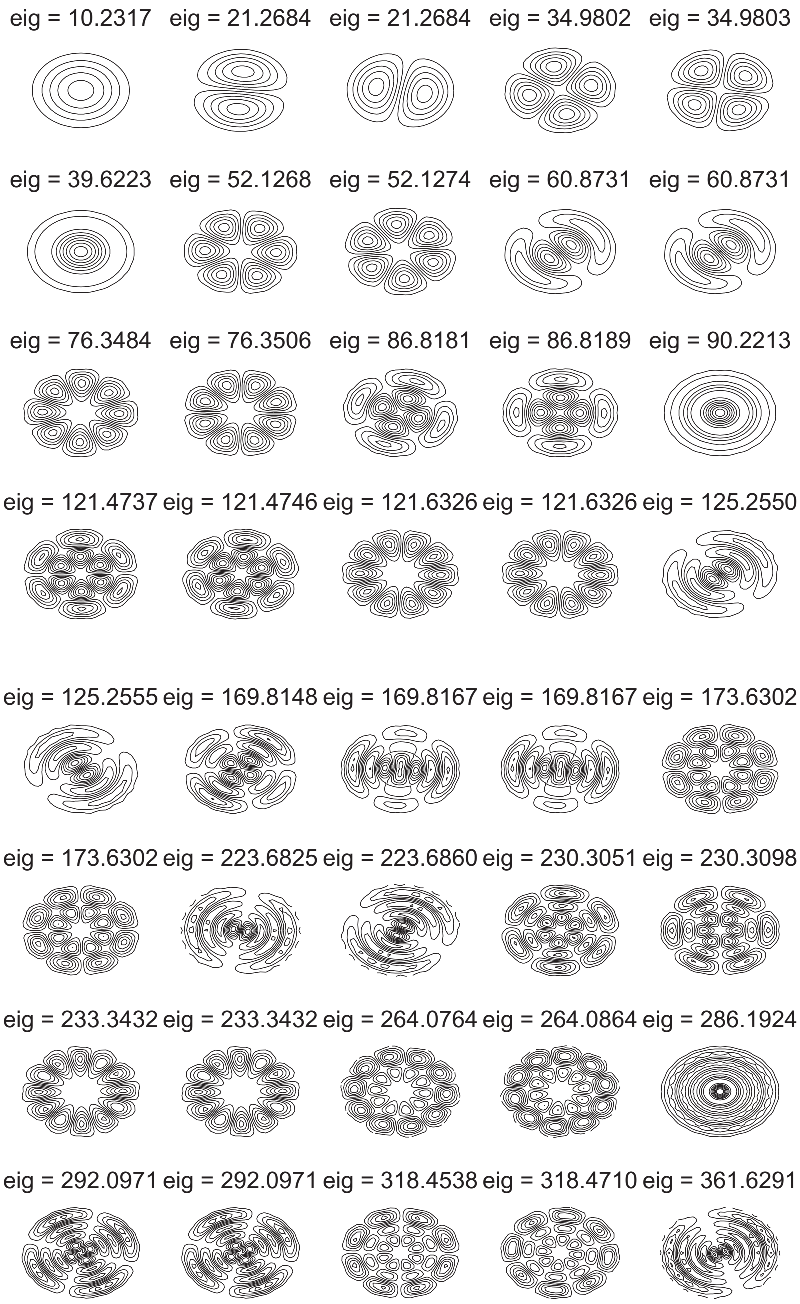

Fig. 5. First 40 vibration modes of the clamped isotropic plate ($h/R = 0.01$), using 400 nodes.

$$\begin{aligned}&\frac{\partial}{\partial x}\left[kA_{45}\left(\sum_{j=1}^{N}\alpha_j^{\Psi_y}\phi_j+\sum_{j=1}^{N}\alpha_j^{W}\frac{\partial\phi_j}{\partial y}\right)+kA_{55}\left(\sum_{j=1}^{N}\alpha_j^{\Psi_x}\phi_j+\sum_{j=1}^{N}\alpha_j^{W}\frac{\partial\phi_j}{\partial x}\right)\right]\\&\quad+\frac{\partial}{\partial y}\left[kA_{44}\left(\sum_{j=1}^{N}\alpha_j^{\Psi_y}\phi_j+\sum_{j=1}^{N}\alpha_j^{W}\frac{\partial\phi_j}{\partial y}\right)+kA_{45}\left(\sum_{j=1}^{N}\alpha_j^{\Psi_x}\phi_j+\sum_{j=1}^{N}\alpha_j^{W}\frac{\partial\phi_j}{\partial x}\right)\right]\\&\quad-\bar{N}_{xx}\sum_{j=1}^{N}\alpha_j^{W}\frac{\partial^2\phi_j}{\partial x^2}+2\bar{N}_{xy}\sum_{j=1}^{N}\alpha_j^{W}\frac{\partial^2\phi_j}{\partial x\partial y}+\overline{N_{yy}}\sum_{j=1}^{N}\alpha_j^{W}\frac{\partial^2\phi_j}{\partial y^2}=0\end{aligned}\tag{47}$$

where N represents the total number of points of the structure. The vector $\alpha^W, \alpha^{\Psi_x}, \alpha^{\Psi_y}$ corresponds to the vector of unknowns related to generalized displacements W, Ψ_x, Ψ_y.

Boundary conditions can be discretized as follows. For a simply-supported plate, along the perimeter we enforce the SS2 conditions as

$$w=0\rightarrow\sum_{j=1}^{N}\alpha_j^{W}\phi_j=0\tag{48}$$

$$\begin{aligned}M_n=0\rightarrow\ &n_x^2\left(D_{11}\sum_{j=1}^{N}\alpha_j^{\Psi_x}\frac{\partial\phi_j}{\partial x}+D_{12}\sum_{j=1}^{N}\alpha_j^{\Psi_y}\frac{\partial\phi_j}{\partial x}\right.\\&\left.+D_{16}\sum_{j=1}^{N}\left(\alpha_j^{\Psi_y}\frac{\partial\phi_j}{\partial x}+\alpha_j^{\Psi_x}\frac{\partial\phi_j}{\partial y}\right)\right)+2n_xn_y\left(D_{12}\sum_{j=1}^{N}\alpha_j^{\Psi_x}\frac{\partial\phi_j}{\partial x}\right.\\&\left.+D_{22}\sum_{j=1}^{N}\alpha_j^{\Psi_y}\frac{\partial\phi_j}{\partial x}+D_{26}\sum_{j=1}^{N}\left(\alpha_j^{\Psi_y}\frac{\partial\phi_j}{\partial x}+\alpha_j^{\Psi_x}\frac{\partial\phi_j}{\partial y}\right)\right)\\&+n_y^2\left(D_{16}\sum_{j=1}^{N}\alpha_j^{\Psi_x}\frac{\partial\phi_j}{\partial x}+D_{26}\sum_{j=1}^{N}\alpha_j^{\Psi_y}\frac{\partial\phi_j}{\partial x}\right.\\&\left.+D_{66}\sum_{j=1}^{N}\left(\alpha_j^{\Psi_y}\frac{\partial\phi_j}{\partial x}+\alpha_j^{\Psi_x}\frac{\partial\phi_j}{\partial y}\right)\right)=0\end{aligned}\tag{49}$$

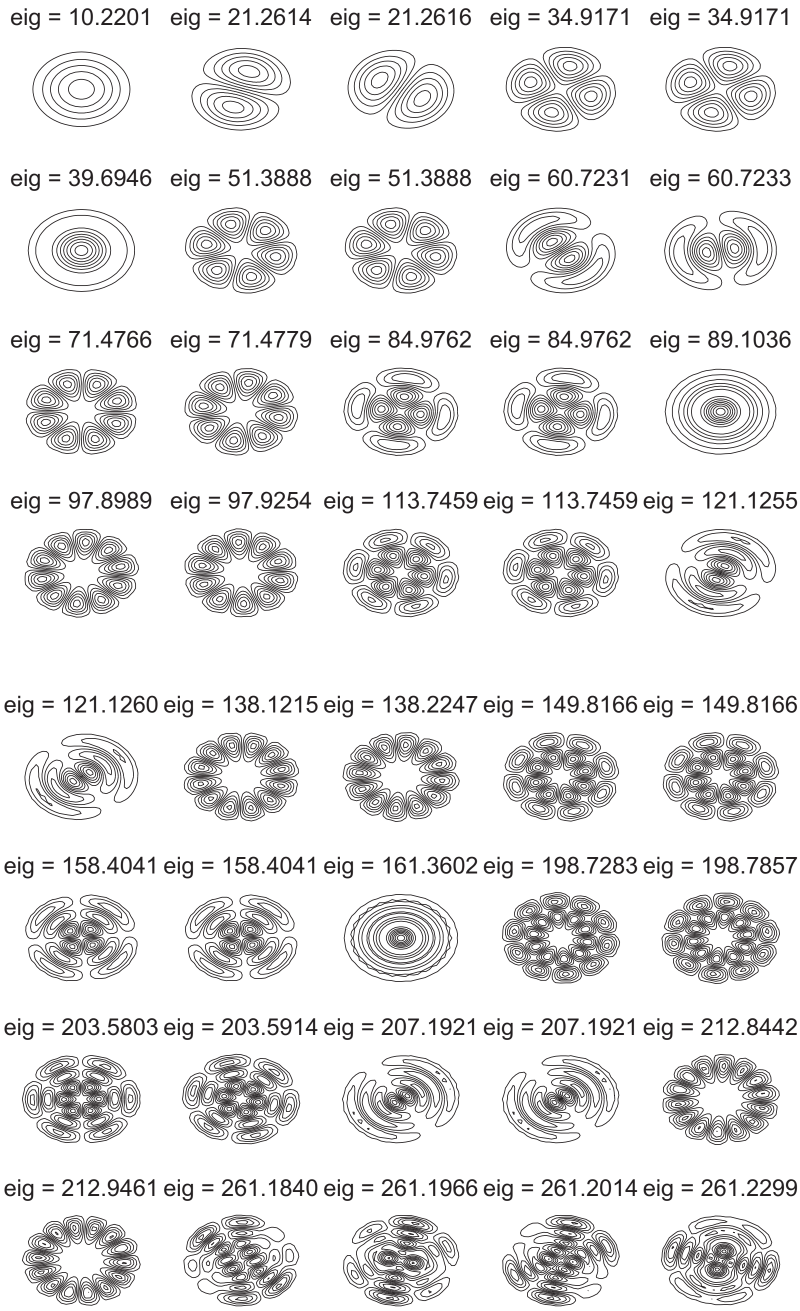

Fig. 6. First 40 vibration modes of the clamped isotropic plate ($h/R = 0.01$), using 625 nodes.

$$\theta_s = 0 \rightarrow n_x \sum_{j=1}^{N} \alpha_j^{\Psi_y} \phi_j + n_y \sum_{j=1}^{N} \alpha_j^{\Psi_x} \phi_j = 0 \tag{50}$$

7. Vibration examples

Unless otherwise stated, a Chebyshev grid was used. For all examples, the following Wendland function was considered:

$$\phi(r) = (1 - cr)_+^8 \left(32(cr)^3 + 25(cr)^2 + 8cr + 1\right). \tag{51}$$

where the shape parameter c is taken as 0.1. This value was previously obtained by an optimization technique by Ferreira and Fasshauer [41].

7.1. Isotropic square plates

We consider a square plate, where the length of the plate is a and we study the effect of two thickness-to-side ratios $h/a = 0.01$ and *0.1*. The effects of shear deformation are considered and the shear correction factors are employed accordingly in order to compare with the corresponding results from other analyses. A non-dimensional frequency parameter is defined as

$$\bar{\omega} = \omega_{mn} a \sqrt{\frac{\rho}{G}},$$

where ω is the frequency, ρ is the mass density per unit volume, G is the shear modulus – $G = E/(2(1 + v))$, E the Young's modulus and v the Poisson ratio. The subscripts m and n denote the number of half-waves in the modal shapes in the x and y directions, respectively.

We compute results for an isotropic plate with different clamped (CCCC-k = 0.8601) and simply-supported (SSSS-k = 0.833) boundary conditions. Firstly, two fully clamped (CCCC) Mindlin/Reissner square plates with different thickness-to-side ratios are considered. The plates are clamped at all boundary edges. The first modes of vibration for both plates are computed (shear correction factor is 0.8601). Two cases of thickness-to-side ratios $h/a = 0.01$ and 0.1 are considered. The comparison of frequency parameters with the Rayleigh-Ritz solutions [42] and results by Liew et al. [26], using a reproducing kernel particle approximation, for each plate is listed in Tables 1 and 2. Excellent agreement is obtained even for a small number of nodes. In Figs. 1 and 2 the first eight modal shapes of the CCCC plate ($h/a = 0.1$) are presented.

Secondly, fully simply-supported (SSSS) Mindlin/Reissner square plates with different thickness-to-side ratios are considered. The first modes of vibration are computed for two cases of thickness-to-side ratios $h/a = 0.01$ and *0.1*. Results are compared with 3d-Elasticity and Mindlin closed form solutions [43], and results by Liew et al. [26]. Results are listed in Tables 3 and 4 and show excellent agreement with closed form solutions.

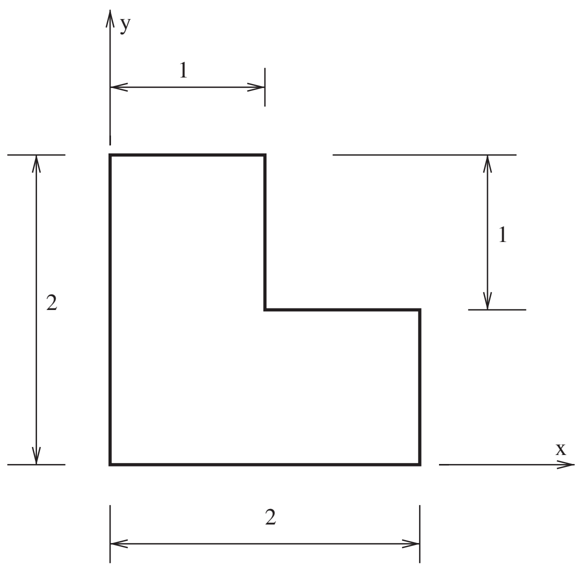

Fig. 7. Geometry for L-shaped CCCC plate.

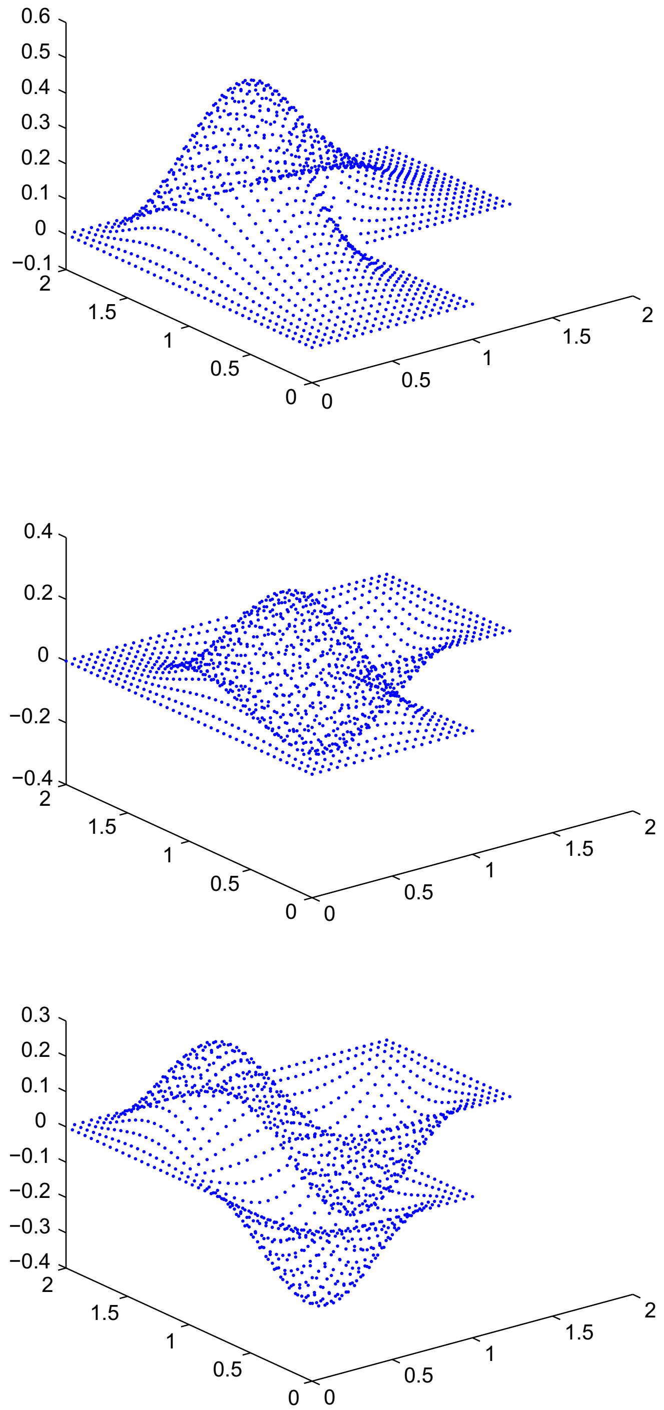

Fig. 8. First three modes of vibration for the L-shaped CCCC plate, $h/a = 0.1$.

Table 9
Natural frequencies of a CCCC L-shaped plate with $h/a = 0.1, \nu = 0.3$.

Number of nodes	Mode no.	Present	Finite elements [45]
121	1	2.0909	2.0042
	2	2.6245	2.6156
	3	2.9775	2.9642
	4	3.8161	3.9978
441	1	1.9088	1.8782
	2	2.4280	2.4273
	3	2.7884	2.7931
	4	3.6181	3.6754
961	1	1.8785	1.8557
	2	2.4019	2.3952
	3	2.7654	2.7637
	4	3.5969	3.6210

7.2. Isotropic circular plates

In this problem we consider isotropic ($\nu = 0.3$, $k = 0.833$) clamped circular plates. The adimensional frequency parameters are given by

$$\bar{\omega} = \omega R^2 \sqrt{\rho h / D}$$

where D is the flexural stiffness. Two grids were considered, as illustrated in Fig. 3. Grid 1 is regularly spaced in both radial and tangential directions, while Grid 2 is initially generated as a square plate, later nodes outside the circle are removed. The boundary nodes are finally placed on the boundary. Both thick ($h/R = 0.1$) and thin ($h/R = 0.01$) plates are considered.

The results obtained from the present method are compared with exact solutions by Liew et al. [44], a mesh-free method based on the reproducing kernel particle technique by Liew et al. [26] and finite element results by Hinton [43]. Results obtained are shown in Tables 5–8 for both grids, and are in excellent agreement with those in [43] and [44]. The first 40 modes of vibration for the thick plate are illustrated in Fig. 4 while in Figs. 5 and 6 the modes are illustrated for thinner plate. As can be seen, the modes of vibration are very smooth. No significant different is visible for the two grids considered in this example.

7.3. Isotropic L-shaped plate

In order to demonstrate the ability of the present method to analyse irregular geometries, this example considers the free vibrations of a clamped L-shape plate. The Poisson's ratio is 0.3 and the adimensional natural frequency is given by $\bar{\omega} = \omega a \sqrt{\rho / G}$. Given the geometry of the plate (see Fig. 7), there are no analytical solutions available. We compare the present solution with an independently computed finite element solution by the authors [45]. We used a 4 node, Lagrangian Mindlin plate element, based on 3 degrees of freedom. The present results are in very good agreement with the finite element solution. The modes of vibration shapes are illustrated in Fig. 8, using 441 nodes. As can be seen, the modes of vibration are again very smooth.

7.4. Composite plates

Unless otherwise stated, all layers of the laminate are assumed to be of the same thickness, density and made of the same linearly elastic composite material. The following material parameters of a layer are used:

$$\frac{E_1}{E_2} = 10, 20, 30 \quad \text{or} \quad 40; \quad G_{12} = G_{13} = 0.6E_2; G_3 = 0.5E_2;$$
$$\nu_{12} = 0.25$$

The subscripts 1 and 2 denote the directions normal and transverse to the fiber direction in a lamina, which may be oriented at an angle to the plate axes. The ply angle of each layer is measured from the global x-axis to the fiber direction. The simply-supported boundary condition is taken to be the hard type SS2 condition. In all examples we use a shear correction factor $k = \pi^2/12$, as proposed in [40] (see Table 9).

The example considered is a simply-supported square plate of the cross-ply lamination [0°/90°/90°/0°]. The thickness and length of the plate are denoted by h and a, respectively. The thickness-to-span ratio $h/a = 0.2$ is employed in the computation. Table 10 lists the fundamental frequency of the simply-supported laminate made of various modulus ratios of E_1/E_2. It is found that the results are in very close agreement with the values of [36,46] and the mesh-free results of Liew [40] based on the FSDT. The relative errors between the analytical and present solutions are shown in brackets. For all E_1/E_2 ratios errors are below 0.5%. Results for all E_1/E_2 ratios converge quite well. In Fig. 9 the first eight modes are illustrated, for $E_1/E_2 = 20$, using 13 × 13 nodes, showing a very smooth shape.

8. Buckling examples

In all following examples a Chebyshev grid was used. The Wendland function used was

$$\phi(r) = (1 - cr)_+^8 \left(32(cr)^3 + 25(cr)^2 + 8cr + 1\right). \tag{52}$$

where the shape parameter c is taken as 0.1.

8.1. Effect of orthotropy and number of layers

The following typical dimensionless high-modulus graphite–epoxy material properties are used:

$$E_1/E_2 = 10, 20, 30, 40; \quad G_{12}/E_2 = G_{13}/E_2 = 0.6; \quad G_{23}/E_2 = 0.5; \nu_{12} = 0.25$$

The effect of degree of orthotropy of the individual layers and the number of layers on the critical buckling loads is investigated for simply-supported square bidirectional composite plates, with

Table 10
The normalized fundamental frequency of the simply-supported cross-ply laminated square plate [0°/90°/90°/0°] ($\bar{w} = (wa^2/h)\sqrt{\rho/E_2}, h/a = 0.2$).

Method	Grid	E_1/E_2			
		10	20	30	40
Liew [40]		8.2924	9.5613	10.320	10.849
Exact (Reddy, Khdeir)[36,46]		8.2982	9.5671	10.326	10.854
Present	13 × 13	8.2670	9.5297	10.2835	10.8077
	17 × 17	8.2669	9.5296	10.2833	10.8076
	21 × 21	8.2668	9.5296	10.2833	10.8076
	Error in % w.r.t.[36,46]	(0.38)	(0.39)	(0.41)	(0.43)

$a/h = 10$, under uni-axial buckling load ($\overline{N} = \overline{N}_{xx}a^2/(E_2h^3)$, $\overline{N}_{xy} = 0, \overline{N}_{yy} = 0$). All layers are assumed to be of the same thickness and material properties. In Table 11, results are compared with the 3D elasticity solutions by Noor [47], and a mixed finite element solution by Reddy and Phan [30]. In Fig. 10 it is illustrated the buckling modes. It can be seen that the present meshless solution agrees very well with the elasticity and the finite element solutions.

8.2. Effect of boundary conditions

Three-layer [0°/90°/0°] and four-layer [0°/90°/90°0°] square cross-ply laminates are chosen to compute the uni- and bi-axial buckling loads. The plate has width a and thickness h. The span-to-thickness ratio a/h is taken to be 10. All layers are assumed to be of the same thickness and material properties:

$$E_1/E_2 = 40; \quad G_{12}/E_2 = G_{13}/E_2 = 0.6; \quad G_{23}/E_2 = 0.5; \nu_{12} = 0.25$$

Table 12 lists the uni-axial buckling loads of the four-layer simply-supported laminated plate discretized with a regular grid. Exact solutions by Khdeir and Librescu [23] and differential quadrature results by Liew and Huang [27] based on the FSDT are also presented for comparison. It is found that the critical buckling load is obtained with a few grid points. The present results are in excellent correlation with those of Khdeir and Librescu [23], and those of Liew and Huang [27].

Table 13 tabulates the bi-axial buckling loads of the [0°/90°/0°] laminated plate. The laminated plate is simply-supported along the edges parallel to the x-axis while the other two edges may be

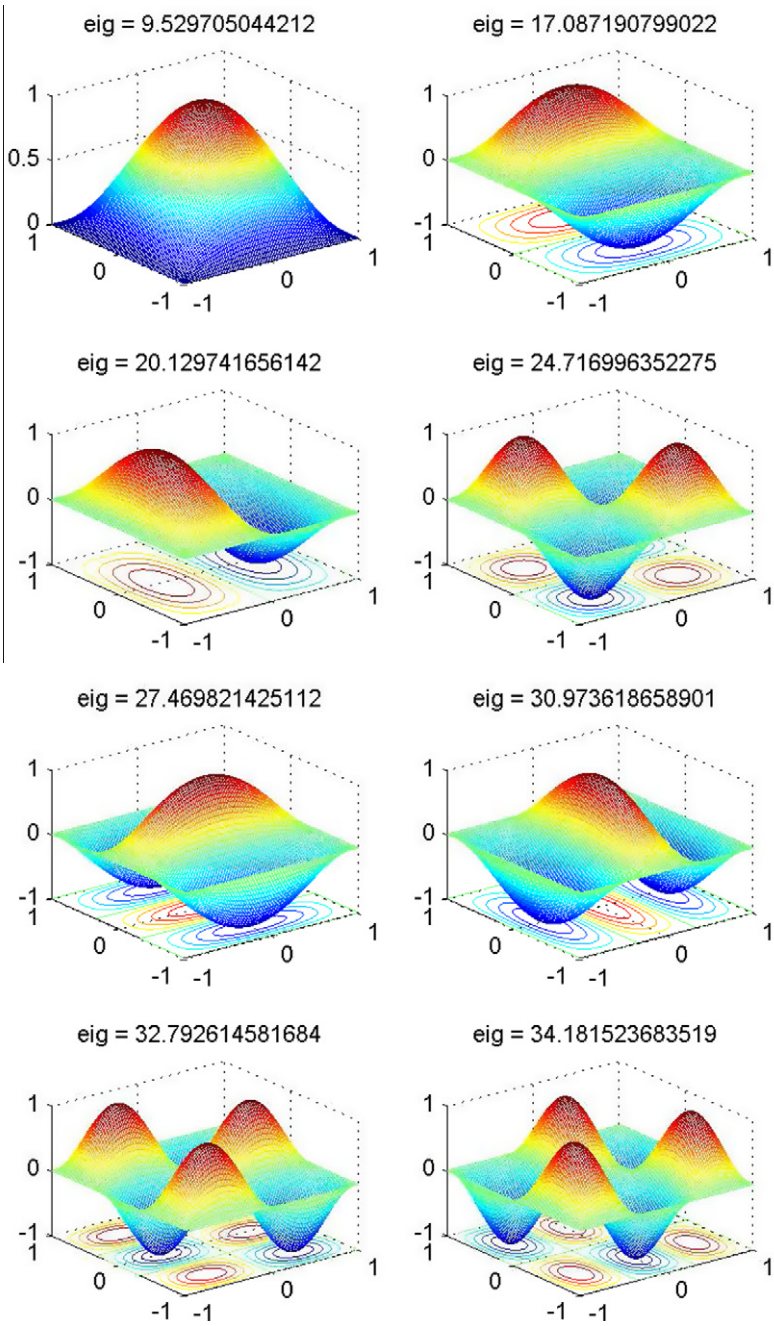

Fig. 9. First eight vibration modes of the simply-supported cross-ply laminated square plate [0°/90°/90°/0°], $E_1/E_2 = 20$, 13 × 13 nodes.

Table 11
Effect of degree of orthotropy of the individual layers on the buckling loads of simply-supported square bidirectional composite plates, with $a/h = 10$, under uni-axial buckling load ($\overline{N} = \overline{N}_{xx}a^2/(E_2h^3),\ \overline{N}_{xy} = 0,\ \overline{N}_{yy} = 0$).

Source	Laminate	E_1/E_2				
		3	10	20	30	40
Noor [47]	[0°/90°/0°]	5.3044	9.7621	15.0191	19.3040	22.8807
Reddy (HSDT) [30]		5.3933	9.9406	15.2980	19.6740	23.3400
Reddy (FSDT)[30]		5.3931	9.9652	15.3510	19.7560	23.4530
Present 11 × 11		5.3904	9.9036	15.0514	19.1134	22.4138
Present 15 × 15		5.3952	9.8815	15.0052	19.0529	22.3450
Present 19 × 19		5.3960	9.8751	14.9922	19.0362	22.3261
CPT		5.7538	11.4920	19.7120	27.9630	36.160
Noor [47]	[0°/90°/0°/90°/0°]	5.3255	9.9603	15.6527	20.4663	24.5929
Reddy (HSDT)[30]		5.4096	10.1500	16.0080	20.9990	25.3080
Reddy (FSDT)[30]		5.4093	10.1360	15.9560	20.9080	25.1850
Present 11 × 11		5.4010	10.1117	15.8143	20.5922	24.6748
Present 15 × 15		5.4059	10.0876	15.7601	20.5173	24.5852
Present 19 × 19		5.4067	10.0805	15.7450	20.4966	24.5608
CPT		5.7538	11.4920	19.7120	27.9630	36.160
Noor [47]	[0°/90°/0°/90°/0°/90°/0 °/90 °/0°]	5.3352	10.0417	15.9153	20.9614	25.3436
Reddy (HSDT)[30]		5.4313	10.1970	16.1720	21.3150	25.7900
Reddy (FSDT)[30]		5.4126	10.1890	16.1460	21.2650	25.7150
Present 11 × 11		5.4059	10.2051	16.1513	21.2332	25.6345
Present 15 × 15		5.4108	10.1800	16.0936	21.1523	25.5368
Present 19 × 19		5.4117	10.1729	16.0776	21.1300	25.5110
CPT		5.7538	11.4920	19.7120	27.9630	36.160

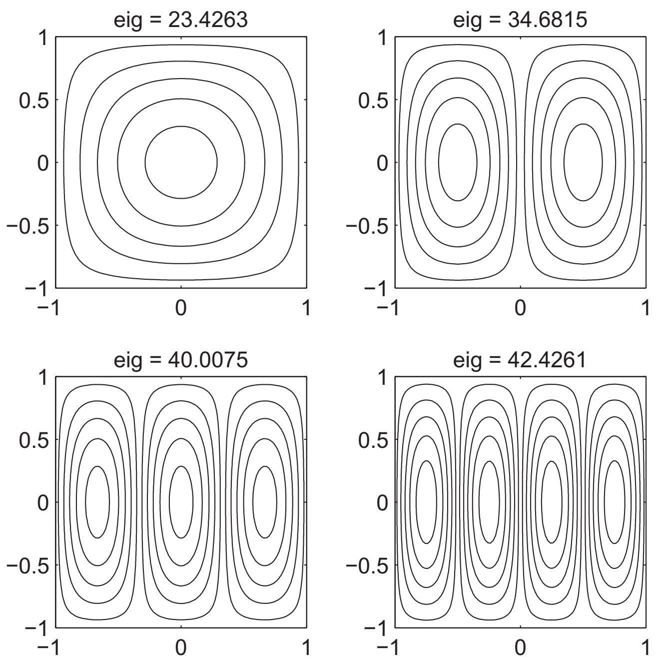

Fig. 10. First 4 buckling modes: Uni-axial buckling load of four-layer [0°/90°/90°/0°] simply-supported laminated plate ($\overline{N} = \overline{N}_{xx}a^2/(E_2h^3), \overline{N}_{xy} = 0, \overline{N}_{yy} = 0$), grid 17 × 17 points.

Table 12
Uni-axial buckling load of four-layer [0°/90°/90°/0°] simply-supported laminated plate ($\overline{N} = \overline{N}_{xx}a^2/(E_2h^3), \overline{N}_{xy} = 0, \overline{N}_{yy} = 0$).

Grid	Present	Liew and Huang [27]	Khdeir and Librescu [23]
13 × 13	23.4271	23.463	23.453
17 × 17	23.4263		
21 × 21	23.4261		
25 × 25	23.4261		

Table 13
Bi-axial buckling load of three-layer [0°/90°/0°] simply-supported laminated plate ($\overline{N} = \overline{N}_{xx}a^2/(E_2h^3), \overline{N}_{xy} = 0, \overline{N}_{yy} = \overline{N}_{xx}$).

Grid	SS	SC	CC
13 × 13	10.1979	11.5984	13.2884
17 × 17	10.1970	11.5976	13.2877
21 × 21	10.1969	11.5972	13.2919
Liew and Huang [27]	10.178	11.575	13.260
Khdeir and Librescu [23]	10.202	11.602	13.290

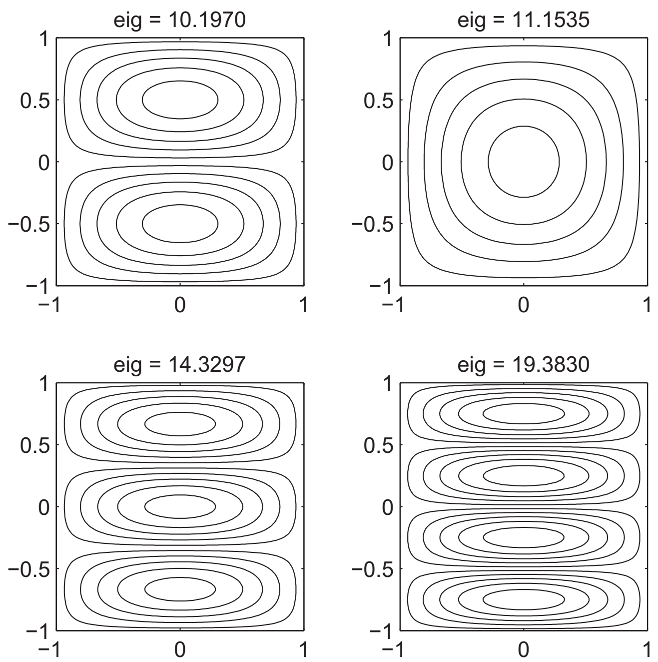

Fig. 11. First four buckling modes: Bi-axial buckling load of three-layer [0°/90°/0°] simply-supported laminated plate ($\overline{N} = \overline{N}_{xx}a^2/(E_2h^3), \overline{N}_{xy} = 0, \overline{N}_{yy} = \overline{N}_{xx}$), grid 17 × 17 points.

simply-supported (S), or clamped (C). The notations SS, SC, and CC refer to the boundary conditions of the two edges parallel to the y-axis only.

In Fig. 11 it is illustrated the first four buckling modes for bi-axial buckling load of three-layer [0°/90°/0°] simply-supported laminated plate ($\overline{N} = \overline{N}_{xx}a^2/(E_2h^3), \overline{N}_{xy} = 0, \overline{N}_{yy} = \overline{N}_{xx}$), using a grid of 17×17 points.

In Fig. 12 it is illustrated the first 4 buckling modes for bi-axial buckling load of three-layer [0°/90°/0°] SCSC laminated plate ($\overline{N} = \overline{N}_{xx}a^2/(E_2h^3), \overline{N}_{xy} = 0, \overline{N}_{yy} = \overline{N}_{xx}$, using a grid of 17×17 points.

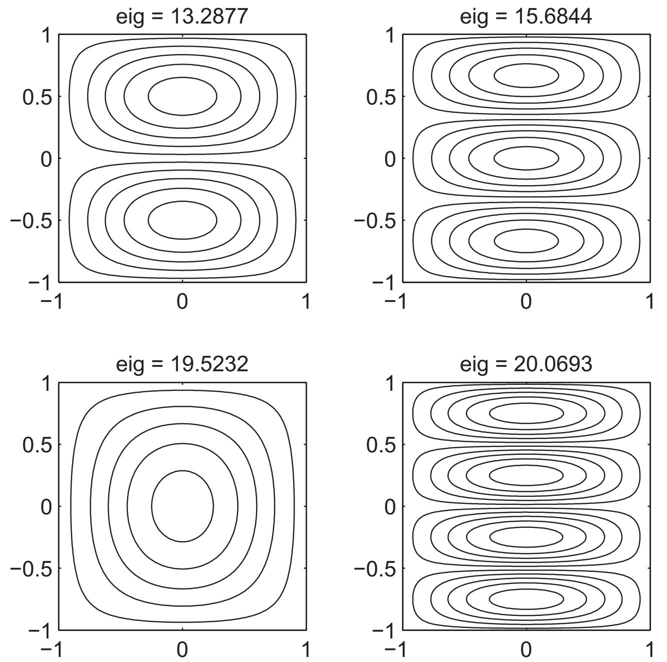

Fig. 12. First four buckling modes: Bi-axial buckling load of three-layer [0°/90°/0°] SCSC laminated plate ($\overline{N} = \overline{N}_{xx}a^2/(E_2h^3), \overline{N}_{xy} = 0, \overline{N}_{yy} = \overline{N}_{xx}$), grid 17×17 points.

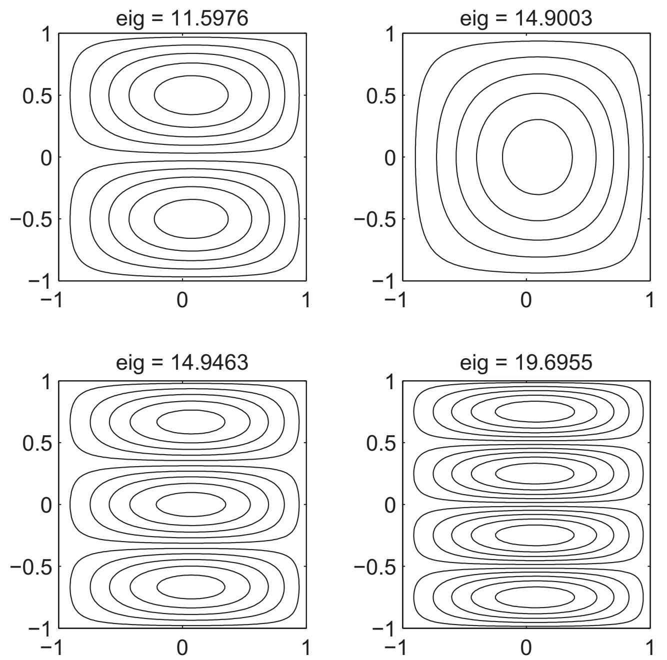

Fig. 13. First 4 buckling modes: Bi-axial buckling load of three-layer [0°/90°/0°] SSSC laminated plate ($\overline{N} = \overline{N}_{xx}a^2/(E_2h^3), \overline{N}_{xy} = 0, \overline{N}_{yy} = \overline{N}_{xx}$), grid 17×17 points.

In Fig. 13 it is illustrated the first 4 buckling modes for bi-axial buckling load of three-layer [0°/90°/0°] SSSC laminated plate ($\overline{N} = \overline{N}_{xx}a^2/(E_2h^3), \overline{N}_{xy} = 0, \overline{N}_{yy} = \overline{N}_{xx}$)), using a grid of 17×17 points.

It is found that excellent agreement is achieved for all edge conditions considered when comparing the results obtained by the present radial basis function approach with the FSDT solutions by Khdeir and Librescu [23], and those of Liew and Huang [27], who use a MLSDQ approach.

9. Conclusions

In this paper we used the radial basis function collocation method to analyse buckling loads and free vibrations of isotropic and laminated plates. The first-order shear deformation theory set of equations of motion define a eigenproblem where the eigenvalues are the buckling loads or the natural frequencies, and the eigenvectors are either the buckling modes or the vibrational modes. We showed how the equations of motion and the boundary conditions can be discretized by radial basis functions.

We presented free vibration and buckling examples, considering isotropic and laminated composite plates, of various geometries, boundary conditions, and laminations.

The present results were compared with existing analytical solutions, or finite element schemes and are in very good agreement with reference solutions. The buckling and vibrational modes are smooth and illustrate the flexibility of the method to analyse irregular geometries and boundary conditions.

The present method is a simple yet powerful alternative to other finite element or meshless methods in the buckling and free vibration analysis of plates.

Acknowledgement

The financial support of the National Foundation for Science and Technology (FCT) to LAETA is gratefully acknowledged.

References

[1] Reissner E, Stavsky Y. Bending and stretching of certain types of aelotropic elastic plates. J Appl Mech 1961;28:402–8.
[2] Mindlin RD. Influence of rotary inertia and shear in flexural motions of isotropic elastic plates. J Appl Mech 1951;18:31–8.
[3] Reissner E. The effect of transverse shear deformations on the bending of elastic plates. J Appl Mech 1945;12:A69–77.
[4] Kant T. Numerical analysis of thick plates. Comput Methods Appl Mech Eng 1982;31:1–18.
[5] Reddy JN. A simple higher-order theory for laminated composite plates. J Appl Mech 1984;51:745–52.
[6] Kansa EJ. Multiquadrics – a scattered data approximation scheme with applications to computational fluid dynamics. I: surface approximations and partial derivative estimates. Comput Math Appl 1990;19(8/9):127–45.
[7] Hon YC, Lu MW, Xue WM, Zhu YM. Multiquadric method for the numerical solution of byphasic mixture model. Appl Math Comput 1997;88:153–75.
[8] Hon YC, Cheung KF, Mao XZ, Kansa EJ. A multiquadric solution for the shallow water equation. ASCE J Hydraul Eng 1999;125(5):524–33.
[9] Wang JG, Liu GR, Lin P. Numerical analysis of biot's consolidation process by radial point interpolation method. Int J Solids Struct 2002;39(6):1557–73.
[10] Liu GR, Gu YT. A local radial point interpolation method (lrpim) for free vibration analyses of 2-d solids. J Sound Vib 2001;246(1):29–46.
[11] Liu GR, Wang JG. A point interpolation meshless method based on radial basis functions. Int J Num Methods Eng 2002;54:1623–48.
[12] Wang JG, Liu GR. On the optimal shape parameters of radial basis functions used for 2-d meshless methods. Comput Meth Appl Mech Eng 2002;191:2611–30.
[13] Chen XL, Liu GR, Lim SP. An element free galerkin method for the free vibration analysis of composite laminates of complicated shape. Compos Struct 2003;59:279–89.
[14] Dai KY, Liu GR, Lim SP, Chen XL. An element free galerkin method for static and free vibration analysis of shear-deformable laminated composite plates. J Sound Vib 2004;269:633–52.

[15] Liu GR, Chen XL. Buckling of symmetrically laminated composite plates using the element-free galerkin method. Int J Struct Stabil Dyn 2002;2: 281–94.
[16] Liew KM, Chen XL, Reddy JN. Mesh-free radial basis function method for buckling analysis of non-uniformity loaded arbitrarily shaped shear deformable plates. Comput Methods Appl Mech Eng 2004;193: 205–25.
[17] Huang YQ, Li QS. Bending and buckling analysis of antisymmetric laminates using the moving least square differential quadrature method. Comput Methods Appl Mech Eng 2004;193:3471–92.
[18] Liu L, Liu GR, Tan VCB. Element free method for static and free vibration analysis of spatial thin shell structures. Comput Methods Appl Mech Eng 2002;191:5923–42.
[19] Ferreira AJM. A formulation of the multiquadric radial basis function method for the analysis of laminated composite plates. Compos Struct 2003;59:385–92.
[20] Ferreira AJM. Thick composite beam analysis using a global meshless approximation based on radial basis functions. Mech Adv Mater Struct 2003;10:271–84.
[21] Ferreira AJM, Roque CMC, Martins PALS. Analysis of composite plates using higher-order shear deformation theory and a finite point formulation based on the multiquadric radial basis function method. Composites: Part B 2003;34:627–36.
[22] Wang CM, Liew KM, Xiang Y, Kipornchai S. Buckling of rectangular Mindlin plates with internal line supports. Int J Solid Struct 1993;30(1):1–17.
[23] Khdeir AA, Librescu L. Analysis of symmetric cross-ply elastic plates using a higher-order theory. Part ii: buckling and free vibration. Compos Struct 1988;9:259–77.
[24] Bhimaraddi A. Free vibration analysis of doubly curved shallow shells on rectangular planform using three-dimensional elasticity theory. Int J Solids Struct 1991;27(7):897–913.
[25] Kitipornchai S, Xiang Y, Wang CM, Liew KM. Buckling of thick skew plates. Int J Num Meth Eng 1993;36:1299–310.
[26] Liew KM, Wang J, Ng TY, Tan MJ. Free vibration and buckling analyses of shear-deformable plates based on fsdt meshfree method. J Sound Vib 2004;276:997–1017.
[27] Liew KM, Huang YQ. Bending and buckling of thick symmetric rectangular laminates using the moving least-squeares differential quadrature method. Int J Mech Sci 2003;45:95–114.
[28] Liew KM, Huang YQ, Reddy JN. Vibration analysis of symmetrically laminated plates based on fsdt using the moving least squares differential quadrature method. Comput Methods Appl Mech Eng 2003;192(19):2203–22.
[29] Putcha NS, Reddy JN. Stability and natural vibration analysis of laminated plates by using a mixed element based on a refined plate theory. J. Sound Vib 1986;104(2):285–300.
[30] Reddy JN, Phan ND. Stability and vibration of isotropic, orthotropic and laminated plates according to a higher-order shear deformation theory. J. Sound Vib 1985;98(2):157–70.
[31] Carrera E. Historical review of zig-zag theories for multilayered plates and shells. Appl Mech Rev 2003(56):287–308.
[32] Madich WR, Nelson SA. Multivariate interpolation and conditionally positive definite functions. ii. Math Comp 1990;54(189):211–30.
[33] Yoon J. Spectral approximation orders of radial basis function interpolation on the sobolev space. SIAM J Math Anal 2001;33(4):946–58.
[34] Hardy RL. Multiquadric equations of topography and other irregular surfaces. Geophys Res 1971;176:1905–15.
[35] Buhmann MD. Radial basis functions. Acta Numer 2000;9:1–38.
[36] Reddy JN. Mechanics of laminated composite plates: theory and analysis. Boca Raton: CRC Press; 1997.
[37] Liew KM, Teo TM. Differential cubature method for analysis of shear deformable rectangular plates on pasternak foundations. Int J Mech Sci 2002;44:1179–94.
[38] Liew KM, Han JB, Xiao ZM, Du H. Differential quadrature method for Mindlin plates on winkler foundations. Int J Mech Sci 1996;38:405–21.
[39] Han JB, Liew KM. Numerical differential quadrature method for Reissner–Mindlin plates on two-parameter foundations. Int J Mech Sci 1997;39:977–89.
[40] Liew KM, Huang YQ, Reddy JN. Vibration analysis of symmetrically laminated plates based on fsdt using the moving least squares differential quadrature method. Comput Meth Appl Mech Eng 2003;192:2203–22.
[41] Ferreira AJM, Fasshauer GE. Computation of natural frequencies of shear deformable beams and plates by a rbf-pseudospectral method. Comput Methods Appl Mech Eng 2006;196:134–46.
[42] Dawe DJ, Roufaeil OL. Rayleigh–Ritz vibration analysis of Mindlin plates. J Sound Vib 1980;69(3):345–59.
[43] Hinton E. Numerical methods and software for dynamic analysis of plates and shells. Pineridge Press; 1988.
[44] Liew KM, Wang CM, Xiang Y, Kitipornchai S. Vibration of Mindlin plates. Amsterdam: Elsevier; 1998.
[45] Ferreira AJM. MATLAB codes for finite element analysis: solids and structures. Springer; 2008.
[46] Khdeir AA, Librescu L. Analysis of symmetric cross-ply elastic plates using a higher-order theory, part ii: buckling and free vibration. Compos Struct 1988;9:259–77.
[47] Noor AK. Free vibration of multilayered plates. AIAA J 1973;11:1038–9.

3.1.5 Buckling analysis of isotropic and laminated plates by radial basis functions according to a higher-order shear deformation theory

A. J. M. Ferreira, C. M. C. Roque, Ana M. A. Neves, R. M. N. Jorge, C. M. M. Soares, J. N. Reddy, Buckling analysis of isotropic and laminated plates by radial basis functions according to a higher-order shear deformation theory, Thin-Walled Structures, Volume 49, Issue 7, 2011, pages 804-811.

Thin-Walled Structures 49 (2011) 804–811

Contents lists available at ScienceDirect

Thin-Walled Structures

journal homepage: www.elsevier.com/locate/tws

Buckling analysis of isotropic and laminated plates by radial basis functions according to a higher-order shear deformation theory

A.J.M. Ferreira [a,*], C.M.C. Roque [b], A.M.A. Neves [a], R.M.N. Jorge [a], C.M.M. Soares [c], J.N. Reddy [d]

[a] Departamento de Engenharia Mecânica, Faculdade de Engenharia da Universidade do Porto, Rua Dr. Roberto Frias, 4200-465 Porto, Portugal
[b] INEGI, Faculdade de Engenharia da Universidade do Porto, Rua Dr. Roberto Frias, 4200-465 Porto, Portugal
[c] Departamento de Engenharia Mecânica, Instituto Superior Técnico, Av. Rovisco Pais, Lisboa, Portugal
[d] Department of Mechanical Engineering, Texas A & M University, College Station, TX 77843-3123, USA

ARTICLE INFO

Article history:
Received 26 May 2010
Received in revised form
2 February 2011
Accepted 11 February 2011
Available online 11 March 2011

Keywords:
Radial basis functions
Buckling
Meshless methods
Composite materials

ABSTRACT

The third-order shear deformation theory of Reddy and collocation with radial basis functions is used to predict the buckling loads of elastic plates. The theory accounts for parabolic distribution of the transverse strains through the thickness of the plate. It is shown that the collocation method with radial basis functions produces highly accurate critical buckling loads and modes.

1. Introduction

Laminated composite plates have been widely used in various applications, from military to civilian systems, due to their high strength-to-weight ratio and flexibility in design. It is well known that the classical laminated plate theory (CLPT) based on the Kirchhoff hypothesis yields acceptable results only for thin laminates [1]. Composite structures designed based on the CLPT may be unsafe because the CLPT underestimates the deflections and overestimates buckling loads. Therefore, the first-order shear deformation theory (FSDT) [1–3] and higher-order [1,4,5] shear deformation theories (HSDTs) have been developed to account for the transverse shear strains.

Recently, radial basis functions (RBFs) have enjoyed considerable success and research as a technique for interpolating data and functions. A radial basis function, $\phi(\|x-x_j\|)$ is a spline that depends on the Euclidian distance between distinct data centers $x_j, j=1,2,\ldots,N \in \mathbb{R}^n$, also called nodal or collocation points.

Although most of the work to date on RBFs relate to scattered data approximation and in general to interpolation theory, there has recently been an increased interest in their use for solving partial differential equations (PDEs). This approach, which approximates the whole solution of the PDE directly using RBFs, is very attractive due to the fact that this is truly a mesh-free technique. Kansa [6] introduced the concept of solving PDEs using RBFs. Kansa's method is an unsymmetric RBF collocation method based upon the multiquadrics (MQ) interpolation functions, in which the shape parameter is considered to be variable across the problem domain. The distribution of the shape parameter is obtained by an optimization approach, in which the value of the shape parameter is assumed to be proportional to the curvature of the unknown solution of the original partial differential equation. In this way, it is possible to reduce the condition number of the matrix at the expense of implementing an additional iterative algorithm. In the present work, we will implement the unsymmetric collocation method in its simpler form, without any optimization of the interpolation functions and the collocation points.

The analysis of plates by finite element methods is now fully established. The use of alternative methods such as the meshless methods based on radial basis functions is attractive due to the absence of a mesh and the ease of collocation methods. The use of radial basis function for the analysis of structures and materials has been previously studied by numerous authors [7–18]. More recently the authors have applied RBFs to the static deformations of composite beams and plates [19–21].

Some relevant works on buckling of thick plates include those of Wang et al. [22], Kitipornchai et al. [23], Liew et al. [24,25], and Reddy et al. [26,27]. The objective of this paper is to determine the elastic buckling loads of thick plates that are subjected to partial in-plane edge loads by collocation with radial basis functions, according to the higher-order shear deformation theory of Reddy [1,5].

* Corresponding author.
E-mail address: ferreira@fe.up.pt (A.J.M. Ferreira).

0263-8231/$ - see front matter
doi:10.1016/j.tws.2011.02.005

2. The radial basis function method

2.1. The static problem

Radial basis functions' (RBFs) approximations are grid-free numerical schemes that can exploit accurate representations of the boundary, are easy to implement and can be spectrally accurate [28,29]. In this section the formulation of a global unsymmetrical collocation RBF-based method to compute eigenvalues of elliptic operators is presented.

Consider a linear elliptic partial differential operator L and a bounded region Ω in $\mathbb{R}^n$ with some boundary $\partial\Omega$. The static problems aims the computation of displacements (primary variables) ($\mathbf{u}$) from the global system of equations:

$$L\mathbf{u} = \mathbf{f} \quad \text{in } \Omega \tag{1}$$

$$L_B\mathbf{u} = \mathbf{g} \quad \text{on } \partial\Omega \tag{2}$$

where L, L_B are linear operators in the domain and on the boundary, respectively. The right-hand side of (1) and (2) represent the external forces applied on the plate and the boundary conditions applied along the perimeter of the plate, respectively. The continuum problem defined in (1) and (2) will be replaced by a discrete problem, defined by an algebraic system of equations, after the radial basis expansions.

2.2. The eigenproblem

The eigenproblem looks for eigenvalues (λ) and eigenvectors ($\mathbf{u}$) that satisfy

$$L\mathbf{u} + \lambda\mathbf{u} = 0 \quad \text{in } \Omega, \tag{3}$$

$$L_B\mathbf{u} = 0 \quad \text{on } \partial\Omega. \tag{4}$$

As in the static problem, the eigenproblem defined in (3) and (4) is replaced by a finite-dimensional eigenvalue problem, based on RBF approximations.

2.3. Radial basis functions

The radial basis function (ϕ) approximation of a function ($\mathbf{u}$) is given by

$$\tilde{\mathbf{u}}(\mathbf{x}) = \sum_{i=1}^{N} \alpha_i \phi(\|x - y_i\|_2), \quad \mathbf{x} \in \mathbb{R}^n, \tag{5}$$

where $y_i, i = 1, \ldots, N$ is a finite set of distinct points (centers) in $\mathbb{R}^n$. The coefficients α_i are chosen so that $\tilde{\mathbf{u}}$ satisfies some boundary conditions. The most common RBFs are

$$\phi(r) = r^3, \quad \text{cubic},$$

$$\phi(r) = r^2 \log(r), \quad \text{thin plate splines},$$

$$\phi(r) = (1-r)_+^m p(r), \quad \text{Wendland functions},$$

$$\phi(r) = e^{-(cr)^2}, \quad \text{Gaussian},$$

$$\phi(r) = \sqrt{c^2 + r^2}, \quad \text{multiquadrics},$$

$$\phi(r) = (c^2 + r^2)^{-1/2}, \quad \text{inverse multiquadrics},$$

where the Euclidian distance r is real and non-negative and c is a shape parameter, a positive constant. In the following, the radial basis function used was a compact-support Wendland function in the form:

$$\phi(r) = (1 - cr)_+^8 (32(cr)^3 + 25(cr)^2 + 8cr + 1). \tag{6}$$

2.4. Solution of the interpolation problem

Hardy [30] introduced multiquadrics in the analysis of scattered geographical data. In the 1990s Kansa [6] used multiquadrics for the solution of partial differential equations.

Considering N distinct interpolations, and knowing $u(x_j), j = 1, 2, \ldots, N$, we find α_i by the solution of a $N \times N$ linear system:

$$\mathbf{A}\underline{\alpha} = \mathbf{u}, \tag{7}$$

where $\mathbf{A} = [\phi(\|x - y_i\|_2)]_{N \times N}$, $\underline{\alpha} = [\alpha_1, \alpha_2, \ldots, \alpha_N]^T$ and $\mathbf{u} = [u(x_1), u(x_2), \ldots, u(x_N)]^T$. The RBF interpolation matrix A is positive definite for some RBFs [31], but in general provides ill-conditioned systems.

2.5. Solution of the static problem

The solution of a static problem by radial basis functions considers N_I nodes in the domain and N_B nodes on the boundary, with total number of nodes $N = N_I + N_B$. We denote the sampling points by $x_i \in \Omega, i = 1, \ldots, N_I$ and $x_i \in \partial\Omega, i = N_I + 1, \ldots, N$. At the domain points we solve the following system of equations:

$$\sum_{i=1}^{N} \alpha_i L\phi(\|x - y_i\|_2) = \mathbf{f}(x_j), \quad j = 1, 2, \ldots, N_I \tag{8}$$

or

$$L^I \underline{\alpha} = \mathbf{F}, \tag{9}$$

where

$$L^I = [L\phi(\|x - y_i\|_2)]_{N_I \times N}. \tag{10}$$

For the boundary conditions we have

$$\sum_{i=1}^{N} \alpha_i L_B \phi(\|x - y_i\|_2) = \mathbf{g}(x_j), \quad j = N_I + 1, \ldots, N \tag{11}$$

or

$$\mathbf{B}\underline{\alpha} = \mathbf{G}. \tag{12}$$

Therefore we can write a finite-dimensional static problem as

$$\begin{bmatrix} L^I \\ \mathbf{B} \end{bmatrix} \underline{\alpha} = \begin{bmatrix} \mathbf{F}^I \\ \mathbf{G}^I \end{bmatrix} \tag{13}$$

where

$$\mathbf{L}^I = L\phi[(\|x_{N_I} - y_j\|_2)]_{N_I \times N}, \quad \mathbf{B} = L_B\phi[(\|x_{N_I+1} - y_j\|_2)]_{N_B \times N}.$$

By inverting the system (13), we obtain the vector of $\underline{\alpha}$. We then proceed to the solution by the interpolation equation (5).

2.6. Solution of the eigenproblem

We consider N_I nodes in the interior of the domain and N_B nodes on the boundary, with $N = N_I + N_B$. We denote interpolation points by $x_i \in \Omega, i = 1, \ldots, N_I$ and $x_i \in \partial\Omega$, $i = N_I + 1, \ldots, N$. For the interior points we have that

$$\sum_{i=1}^{N} \alpha_i L\phi(\|x - y_i\|_2) = \lambda \tilde{\mathbf{u}}(x_j), \quad j = 1, 2, \ldots, N_I \tag{14}$$

or

$$L^I \underline{\alpha} = \lambda \tilde{\mathbf{u}}^I, \tag{15}$$

where

$$L^I = [L\phi(\|x - y_i\|_2)]_{N_I \times N}. \tag{16}$$

For the boundary conditions we have

$$\sum_{i=1}^{N} \alpha_i L_B \phi(\|x-y_i\|_2)=0, \quad j=N_I+1,\ldots,N \tag{17}$$

or

$$\mathbf{B}\underline{\alpha}=0. \tag{18}$$

Therefore we can write a finite-dimensional problem as a generalized eigenvalue problem:

$$\begin{bmatrix} L^I \\ \mathbf{B} \end{bmatrix}\underline{\alpha}=\lambda\begin{bmatrix} \mathbf{A}^I \\ \mathbf{0} \end{bmatrix}\underline{\alpha u} \tag{19}$$

where

$$\mathbf{A}^I=\phi[(\|x_{N_I}-y_j\|_2)]_{N_I\times N}, \quad \mathbf{B}^I=L_B\phi[(\|x_{N_I+1}-y_j\|_2)]_{N_B\times N}.$$

We seek the generalized eigenvalues and eigenvectors of these matrices.

3. Buckling analysis of elastic plates

Consider a rectangular plate of plan-form dimensions a and b and thickness h. The co-ordinate system is taken such that the x–y plane coincides with the midplane of the plate, and the origin of the co-ordinate system is taken at the lower left corner of the plate. The plate is composed of uniform thickness layers of orthotropic material.

Following the higher-order theory of Reddy [1,5], the following displacement field is chosen, which satisfies the stress-free boundary condition, and gives parabolic distribution of transverse shear strains through the plate thickness:

$$u=u_0+z\left[\theta_x-\frac{4}{3}\left(\frac{z}{h}\right)^2\left(\theta_x+\frac{\partial w}{\partial x}\right)\right], \tag{20}$$

$$v=v_0+z\left[\theta_y-\frac{4}{3}\left(\frac{z}{h}\right)^2\left(\theta_y+\frac{\partial w}{\partial y}\right)\right], \tag{21}$$

$$w=w_0. \tag{22}$$

The strains associated with the small-displacement theory of elasticity become

$$\varepsilon_1\equiv\varepsilon_{11}=\varepsilon_1^0+z(k_1^0+z^2k_1^2); \quad \varepsilon_2\equiv\varepsilon_{22}=\varepsilon_2^0+z(k_2^0+z^2k_2^2);$$
$$\varepsilon_3\equiv\varepsilon_{33}=0; \tag{23}$$

$$\varepsilon_4\equiv 2\varepsilon_{23}=\varepsilon_4^0+z^2k_4^2; \quad \varepsilon_5\equiv 2\varepsilon_{13}=\varepsilon_5^0+z^2k_5^2; \tag{24}$$

$$\varepsilon_6\equiv 2\varepsilon_{12}=\varepsilon_6^0+z(k_6^0+z^2k_6^2), \tag{25}$$

where

$$\varepsilon_1^0=\frac{\partial u_0}{\partial x}; \quad k_1^0=\frac{\partial\theta_x}{\partial x}; \quad k_1^2=-\left(\frac{4}{3h^2}\right)\left(\frac{\partial\theta_x}{\partial x}+\frac{\partial^2 w}{\partial x^2}\right); \tag{26}$$

$$\varepsilon_2^0=\frac{\partial v_0}{\partial y}; \quad k_2^0=\frac{\partial\theta_y}{\partial y}; \quad k_2^2=-\left(\frac{4}{3h^2}\right)\left(\frac{\partial\theta_y}{\partial y}+\frac{\partial^2 w}{\partial y^2}\right); \tag{27}$$

$$\varepsilon_4^0=\theta_y+\frac{\partial w}{\partial y}; \quad k_4^2=-\left(\frac{4}{h^2}\right)\left(\theta_y+\frac{\partial w}{\partial y}\right); \tag{28}$$

$$\varepsilon_5^0=\theta_x+\frac{\partial w}{\partial x}; \quad k_5^2=-\left(\frac{4}{h^2}\right)\left(\theta_x+\frac{\partial w}{\partial x}\right); \tag{29}$$

$$\varepsilon_6^0=\frac{\partial u_0}{\partial y}+\frac{\partial v_0}{\partial x}; \quad k_6^0=\frac{\partial\theta_x}{\partial y}+\frac{\partial\theta_y}{\partial x}; \tag{30}$$

$$k_6^2=-\left(\frac{4}{3h^2}\right)\left(\frac{\partial\theta_x}{\partial y}+\frac{\partial\theta_y}{\partial x}+2\frac{\partial^2 w}{\partial x\partial y}\right). \tag{31}$$

The constitutive equations of an orthotropic layer, in material axes, are given by

$$\begin{Bmatrix}\sigma_1\\ \sigma_2\\ \sigma_6\end{Bmatrix}=\begin{bmatrix} Q_{11} & Q_{12} & 0\\ Q_{12} & Q_{22} & 0\\ 0 & 0 & Q_{66}\end{bmatrix}\begin{Bmatrix}\varepsilon_1\\ \varepsilon_2\\ \varepsilon_6\end{Bmatrix}, \quad \begin{Bmatrix}\sigma_4\\ \sigma_5\end{Bmatrix}=\begin{bmatrix} Q_{44} & 0\\ 0 & Q_{55}\end{bmatrix}\begin{Bmatrix}\varepsilon_4\\ \varepsilon_5\end{Bmatrix} \tag{32}$$

where Q_{ij} are the plane-stress reduced elastic constants (due to $\varepsilon_3=0$) in the material axes of the plate:

$$Q_{11}=\frac{E_1}{1-\nu_{12}\nu_{21}}, \quad Q_{12}=\nu_{21}\frac{E_1}{1-\nu_{12}\nu_{21}}, \quad Q_{22}=\frac{E_2}{1-\nu_{12}\nu_{21}}, \tag{33}$$

$$Q_{44}=G_{23}, \quad Q_{55}=G_{13}, \quad Q_{66}=G_{12}. \tag{34}$$

It is interesting to note that this theory does not consider the use of shear-correction factors, as in the FSDT. The equations of motion for this theory were derived by Reddy [1,5,27] using Hamilton's principle. They are repeated here for convenience:

$$\delta u_0: \frac{\partial N_1}{\partial x}+\frac{\partial N_6}{\partial y}=I_1\ddot{u}_0+\bar{I}_2\ddot{\theta}_x-\frac{4}{3h^2}I_4\frac{\partial\ddot{w}_0}{\partial x},$$

$$\delta v_0: \frac{\partial N_6}{\partial x}+\frac{\partial N_2}{\partial y}=I_1\ddot{v}_0+\bar{I}_2\ddot{\theta}_y-\frac{4}{3h^2}I_4\frac{\partial\ddot{w}_0}{\partial y},$$

$$\begin{aligned}\delta w_0: &\frac{\partial Q_1}{\partial x}+\frac{\partial Q_2}{\partial y}+\left(\frac{\partial}{\partial x}\right)\left(\overline{N}_{xx}\frac{\partial w}{\partial x}\right)+\left(\frac{\partial}{\partial y}\right)\left(\overline{N}_{yy}\frac{\partial w}{\partial y}\right)\\ &+q-\frac{4}{h^2}\left(\frac{\partial R_1}{\partial x}+\frac{\partial R_2}{\partial y}\right)+\frac{4}{3h^2}\left(\frac{\partial^2 P_1}{\partial x^2}+2\frac{\partial^2 P_6}{\partial x\partial y}+\frac{\partial^2 P_2}{\partial y^2}\right)\\ &=I_1\ddot{w}_0-\left(\frac{4}{3h^2}\right)^2 I_7\left(\frac{\partial^2\ddot{w}_0}{\partial x^2}+\frac{\partial^2\ddot{w}_0}{\partial y^2}\right)\\ &+\left(\frac{4}{3h^2}\right)I_4\left(\frac{\partial\ddot{u}_0}{\partial x}+\frac{\partial\ddot{v}_0}{\partial y}\right)+\left(\frac{4}{3h^2}\right)\bar{I}_5\left(\frac{\partial\ddot{\theta}_x}{\partial x}+\frac{\partial\ddot{\theta}_y}{\partial y}\right),\end{aligned}$$

$$\begin{aligned}\delta\theta_x: &\frac{\partial M_1}{\partial x}+\frac{\partial M_6}{\partial y}-Q_1+\left(\frac{4}{h^2}\right)R_1-\left(\frac{4}{3h^2}\right)\left(\frac{\partial P_1}{\partial x}+\frac{\partial P_6}{\partial y}\right)\\ &=\bar{I}_2\ddot{u}_0+\bar{I}_3\ddot{\theta}_x-\frac{4}{3h^2}\bar{I}_5\frac{\partial\ddot{w}_0}{\partial x},\end{aligned}$$

$$\begin{aligned}\delta\theta_y: &\frac{\partial M_6}{\partial x}+\frac{\partial M_2}{\partial y}-Q_2+\left(\frac{4}{h^2}\right)R_2-\left(\frac{4}{3h^2}\right)\left(\frac{\partial P_6}{\partial x}+\frac{\partial P_2}{\partial y}\right)\\ &=\bar{I}_2\ddot{v}_0+\bar{I}_3\ddot{\theta}_y-\frac{4}{3h^2}\bar{I}_5\frac{\partial\ddot{w}_0}{\partial y},\end{aligned} \tag{35}$$

$$\bar{I}_2=I_2-\frac{4}{3h^2}I_4, \quad \bar{I}_5=I_5-\frac{4}{3h^2}I_7, \quad \bar{I}_3=I_3-\frac{8}{3h^2}I_5+\frac{16}{9h^4}I_7 \tag{36}$$

The stress resultants N_i,M_i,P_i,Q_i and R_i are defined by

$$(N_i,M_i,P_i)=\int_{-h/2}^{h/2}\sigma_i(1,z,z^3)\,dz, \quad (i=1,2,6), \tag{37}$$

$$(Q_2,R_2)=\int_{-h/2}^{h/2}\sigma_4(1,z^2)\,dz, \quad (Q_1,R_1)=\int_{-h/2}^{h/2}\sigma_5(1,z^2)\,dz, \tag{38}$$

and the inertias $I_i(i=1,2,3,4,5,7)$ by

$$(I_1,I_2,I_3,I_4,I_5,I_7)=\int_{-h/2}^{h/2}\rho(1,z,z^2,z^3,z^4,z^6)\,dz \tag{39}$$

being ρ the material density. An interesting feature of this theory is that it considers the same number of degrees of freedom of the FSDT. In Eq. (35), $\overline{N}_{xx}$ and $\overline{N}_{yy}$ denote the in-plane loads perpendicular to the edges $x=0$ and $y=0$, respectively. For free vibrations, one sets $\overline{N}_{xx}=\overline{N}_{yy}=0$, and for buckling analysis one sets all inertias to zero.

The resultants defined in Eq. (37) can be related to the total strains in Eq. (23) by the following equations:

$$\left\{\begin{array}{c}\left\{\begin{array}{c}N_1\\N_2\\N_6\end{array}\right\}\\\left\{\begin{array}{c}M_1\\M_2\\M_6\end{array}\right\}\\\left\{\begin{array}{c}P_1\\P_2\\P_6\end{array}\right\}\end{array}\right\} = \left[\begin{array}{ccc}\begin{bmatrix}A_{11} & A_{12} & A_{16}\\ & A_{22} & A_{26}\\ symm. & & A_{66}\end{bmatrix} & \begin{bmatrix}B_{11} & B_{12} & B_{16}\\ & B_{22} & B_{26}\\ symm. & & B_{66}\end{bmatrix} & \begin{bmatrix}E_{11} & E_{12} & E_{16}\\ & E_{22} & E_{26}\\ symm. & & E_{66}\end{bmatrix}\\ & \begin{bmatrix}D_{11} & D_{12} & D_{16}\\ & D_{22} & D_{26}\\ symm. & & D_{66}\end{bmatrix} & \begin{bmatrix}F_{11} & F_{12} & F_{16}\\ & F_{22} & F_{26}\\ symm. & & F_{66}\end{bmatrix}\\ symmetric & & \begin{bmatrix}H_{11} & H_{12} & H_{16}\\ & H_{22} & H_{26}\\ symm. & & H_{66}\end{bmatrix}\end{array}\right]\left\{\begin{array}{c}\left\{\begin{array}{c}\varepsilon_1^0\\\varepsilon_2^0\\\varepsilon_6^0\end{array}\right\}\\\left\{\begin{array}{c}k_1^0\\k_2^0\\k_6^0\end{array}\right\}\\\left\{\begin{array}{c}k_1^2\\k_2^2\\k_6^2\end{array}\right\}\end{array}\right\} \quad (40)$$

$$\left\{\begin{array}{c}\left\{\begin{array}{c}Q_2\\Q_1\end{array}\right\}\\\left\{\begin{array}{c}R_2\\R_1\end{array}\right\}\end{array}\right\} = \left[\begin{array}{cc}\begin{bmatrix}A_{44} & A_{45}\\A_{45} & A_{55}\end{bmatrix} & \begin{bmatrix}D_{44} & D_{45}\\D_{45} & D_{55}\end{bmatrix}\\ symm. & \begin{bmatrix}F_{45} & F_{45}\\F_{45} & F_{55}\end{bmatrix}\end{array}\right]\left\{\begin{array}{c}\left\{\begin{array}{c}\varepsilon_4^0\\\varepsilon_5^0\end{array}\right\}\\\left\{\begin{array}{c}k_4^2\\k_5^2\end{array}\right\}\end{array}\right\} \quad (41)$$

Here A_{ij}, B_{ij}, etc., denote the plate stiffnesses:

$$(A_{ij},B_{ij},D_{ij},E_{ij},F_{ij},H_{ij}) = \int_{-h/2}^{h/2} \overline{Q}_{ij}(1,z,z^2,z^3,z^4,z^6)\,dz \quad (i,j=1,2,6),$$

$$(A_{ij},D_{ij},F_{ij}) = \int_{-h/2}^{h/2} \overline{Q}_{ij}(1,z^2,z^4)\,dz \quad (i,j=4,5), \quad (42)$$

where $\overline{Q}_{ij}$ are the transformed elastic stiffness coefficients.

The eigenproblem associated to the equations of motion is defined as

$$[\mathcal{L}-\lambda\mathcal{G}]\mathbf{X}=\mathbf{0} \quad (43)$$

where $\mathcal{L}$ collects all stiffness terms and $\mathcal{G}$ collects all terms related to the in-plane forces. In (43) $\mathbf{X}$ are the buckling modes associated with the buckling loads defined as λ.

Table 1
Uniaxial buckling load of simply supported isotropic rectangular plates ($\overline{N}=\overline{N}_{xx}b^2/(\pi^2 D),\overline{N}_{xy}=0,\overline{N}_{yy}=0$), CLPT solution in parenthesis.

$a/b=$	0.4 (8.410)	1.0 (4.000)	1.4 (4.470)
$a/h=5$			
11×11	4.6477	3.2641	3.7982
15×15	4.6479	3.2650	3.8104
19×19	4.6468	3.2654	3.8160
Reddy and Phan [27] (HSDT)	4.6466	3.2653	3.8206
$a/h=10$			
11×11	6.9808	3.7710	4.1809
15×15	7.0042	3.7811	4.2581
19×19	6.9840	3.7744	4.2737
Reddy and Phan [27] (HSDT)	6.9853	3.7865	4.2876
$a/h=100$			
11×11	8.1393	3.5707	3.2793
15×15	8.3195	3.8579	4.0637
19×19	8.3666	3.9411	4.2859
Reddy and Phan [27] (HSDT)	8.3928	3.9977	4.4682

4. Numerical examples

In all following examples a regular grid was used. The multiquadric function was considered, with the shape parameter c taken as $2/\sqrt{N}$, unless otherwise stated.

4.1. Buckling of isotropic plates

In this section, isotropic rectangular plates with three different aspect ratios $a/b=0.4,1.0,1.4$ ($\nu=0.3$) are chosen to compute the buckling loads for uniaxially and biaxially loaded plates. Here a and b denote the plate in-plane dimensions and h denotes the plate thickness. We consider three side-to-thickness a/h ratios and perform a convergence study using 11×11, 15×15, and 19×19 points.

Table 1 lists the uniaxial buckling loads $\overline{N}=\overline{N}_{xx}b^2/(\pi^2 D)$, $\overline{N}_{xy}=0,\overline{N}_{yy}=0$) of the simply supported rectangular plate.

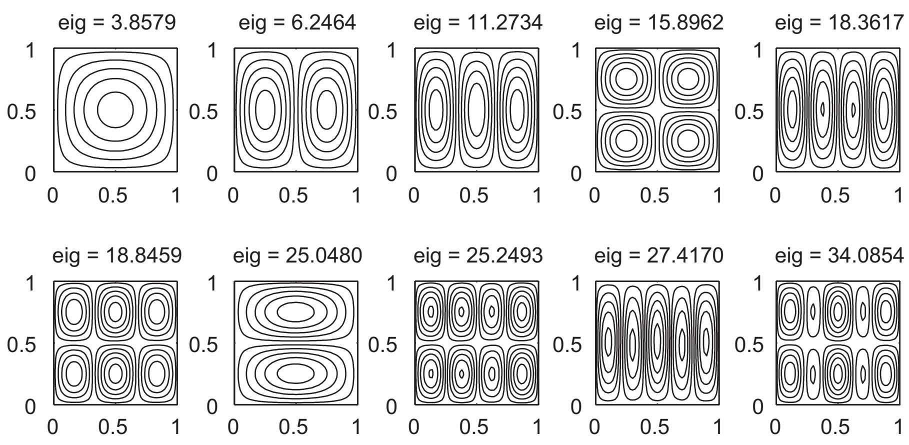

Fig. 1. First 10 buckling modes: uniaxial buckling load of simply supported isotropic plate ($\overline{N}=\overline{N}_{xx}a^2/(E_2h^3),\overline{N}_{xy}=0,\overline{N}_{yy}=0$), grid 15×15 points.

Table 2
Effect of degree of orthotropy of the individual layers on the buckling loads of simply supported square bidirectional composite plates, with $a/h=10$, under uniaxial buckling load ($\overline{N}=\overline{N}_{xx}a^2/(E_2h^3)$,$\overline{N}_{xy}=0$,$\overline{N}_{yy}=0$).

Source	Laminate	E_1/E_2				
		3	10	20	30	40
Noor [32]	[0◦/90◦/0◦]	5.3044	9.7621	15.0191	19.3040	22.8807
Reddy (HSDT) [26]		5.3933	9.9406	15.2980	19.6740	23.3400
Reddy (FSDT)[26]		5.3931	9.9652	15.3510	19.7560	23.4530
Present 11 × 11		5.3706	9.8241	14.9012	18.9118	22.1793
Present 15 × 15		5.3830	9.8309	14.8995	18.9013	22.1604
Present 19 × 19		5.3872	9.8331	14.8975	18.8942	22.1513
CLPT		5.7538	11.4920	19.7120	27.9630	36.160
Noor [32]	[0◦/90◦/0◦/90◦/0◦]	5.3255	9.9603	15.6527	20.4663	24.5929
Reddy (HSDT)[26]		5.4096	10.1500	16.0080	20.9990	25.3080
Reddy (FSDT)[26]		5.4093	10.1360	15.9560	20.9080	25.1850
Present 11 × 11		5.3871	10.0794	15.7956	20.6057	24.7228
Present 15 × 15		5.3996	10.0861	15.7927	20.5919	24.6988
Present 19 × 19		5.4041	10.0888	15.7913	20.5914	24.6901
CLPT		5.7538	11.4920	19.7120	27.9630	36.160
Noor [32]	[0◦/90◦/0◦/90◦/0◦/90◦/0◦/90◦/0◦]	5.3352	10.0417	15.9153	20.9614	25.3436
Reddy (HSDT) [26]		5.4313	10.1970	16.1720	21.3150	25.7900
Reddy (FSDT) [26]		5.4126	10.1890	16.1460	21.2650	25.7150
Present 11 × 11		5.3925	10.1673	16.1093	21.2078	25.6369
Present 15 × 15		5.4050	10.1737	16.1069	21.1963	25.6169
Present 19 × 19		5.4092	10.1767	16.1063	21.1918	25.6088
CLPT		5.7538	11.4920	19.7120	27.9630	36.160

Table 3
Uniaxial buckling load of simply supported cross-ply square plates ($\overline{N}=\overline{N}_{xx}b^2/(E_2h^3)$,$\overline{N}_{xy}=0$,$\overline{N}_{yy}=0$,$E_1/E_2=40$), CLPT solution in parenthesis.

a/h	[0/90] (12.628)	[0/90/0] (35.831)	[0/90/90/0] (35.831)
5			
11 × 11	8.8466	11.0794	12.1897
15 × 15	8.8231	11.0718	12.1976
19 × 19	8.8128	11.0798	12.2086
Reddy and Phan [27] (HSDT)	8.628	11.008	12.444
10			
11 × 11	11.5776	22.1793	23.3946
15 × 15	11.5795	22.1604	23.3703
19 × 19	11.5762	22.1513	23.2444
Reddy and Phan [27] (HSDT)	11.305	22.160	23.849
100			
11 × 11	11.5358	34.3982	34.1887
15 × 15	12.5226	35.4604	35.4194
19 × 19	12.7724	35.7484	35.9746
Reddy and Phan [27] (HSDT)	12.614	35.602	35.645

Table 4
Uniaxial loading for $(45/-45)_p p=1,3 : c=2/\sqrt{N}$.

	N	$a/h=5$	$a/h=10$	$a/h=20$	$a/h=100$
$p=1$	9	10.9264	18.1412	20.5039	19.2893
	11	10.8903	18.1495	20.5988	20.5920
	13	10.8762	18.1547	20.6412	21.0916
	15	10.8709	18.1573	20.6627	21.3308
	17	10.8693	18.1583	20.6742	21.4919
	19	10.8691	18.1588	20.6816	21.5562
	21	10.8696	18.1583	20.6875	21.6215
	25	10.8720	18.1580	20.6893	21.6168
	Reddy [33]	10.881	18.154	20.691	21.666
	Error (%)	0.08	0.02	0.01	0.23
$p=3$	9	12.3087	32.6258	53.1283	58.3766
	11	12.2508	32.5067	53.1516	60.3705
	13	12.2229	32.4542	53.1676	61.1577
	15	12.2076	32.4293	53.1782	61.5510
	17	12.1989	32.4169	53.1852	61.7196
	19	12.1940	32.4104	53.1962	61.8400
	21	12.1915	32.4080	53.1947	61.9253
	25	12.1905	32.4036	53.1966	61.9858
	Reddy [33]	12.1690	32.4050	53.1980	62.0220
	Error(%)	0.177	0.004	0.003	0.058

In Fig. 1 the first 10 buckling modes are illustrated. The present radial basis functions' results are compared with those of Reddy and Phan [27] and the classical laminate plate (CLPT) solution, and show excellent correlation with those of Reddy. Clearly, the CLPT solution is inadequate for thicker plates.

4.2. Buckling of cross-ply laminated plates

The effect of degree of orthotropy of the individual layers and the number of layers on the critical buckling loads are investigated for simply supported square bidirectional composite plates, with $a/h=10$, under uniaxial buckling load ($\overline{N}=\overline{N}_{xx}a^2/(E_2h^3)$, $\overline{N}_{xy}=0$,$\overline{N}_{yy}=0$).

The following dimensionless high-modulus graphite–epoxy material properties are used:

$$E_1/E_2=10,20,30,40;\;\; G_{12}/E_2=G_{13}/E_2=0.6; G_{23}/E_2=0.5;\;\; \nu_{12}=0.25.$$

In Table 2, results are compared with the 3D elasticity solutions by Noor [32], and a mixed finite element solution by Putcha and Reddy [26]. It can be seen that the present meshless solution agrees very well with the elasticity and the finite element solutions.

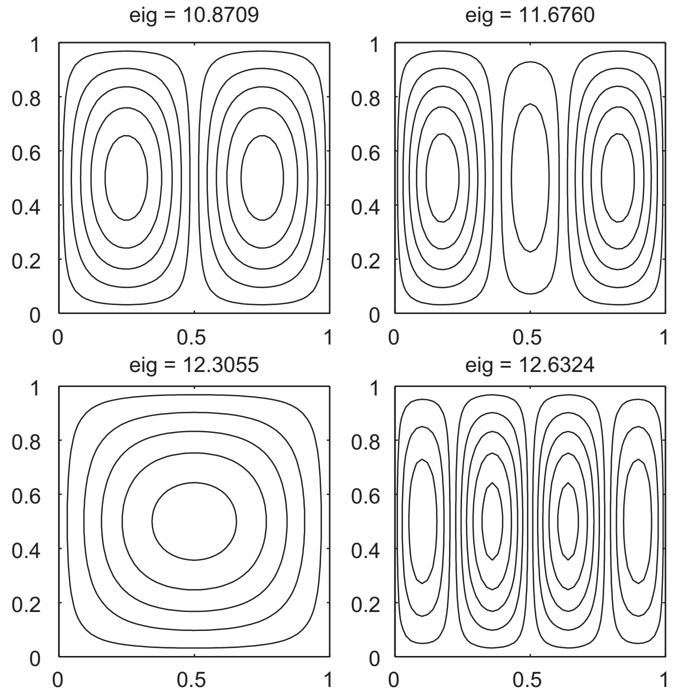

Fig. 2. Uniaxial loading $(45/-45)$, $a/h=5$, $c=2/\sqrt{N}$, $N=15$.

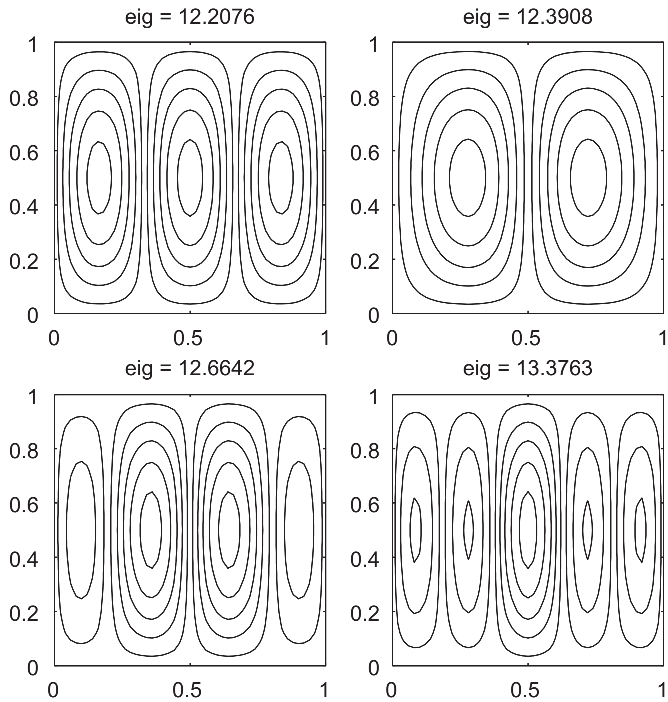

Fig. 4. Uniaxial loading $(45/-45)_3$, $a/h=5$, $c=1/\sqrt{N}$, $N=15$.

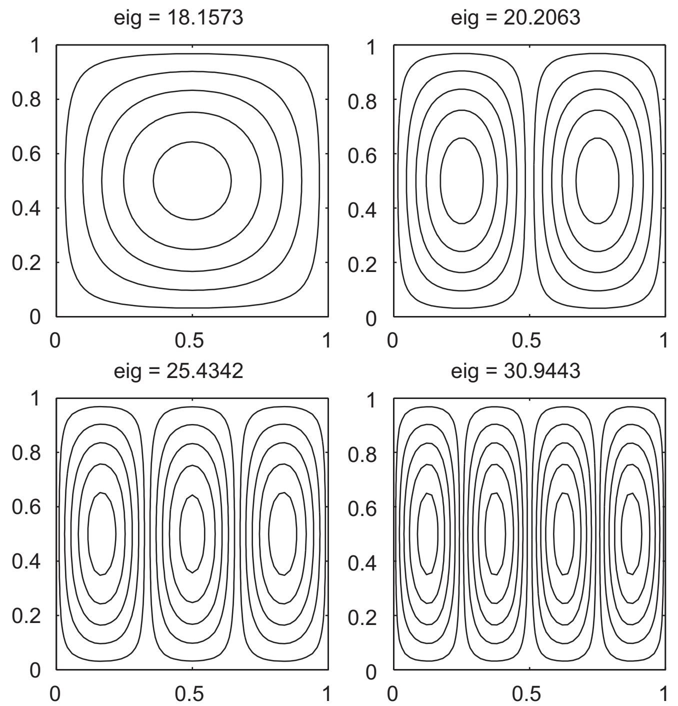

Fig. 3. Uniaxial loading $(45/-45)$, $a/h=10$, $c=2/\sqrt{N}$, $N=15$.

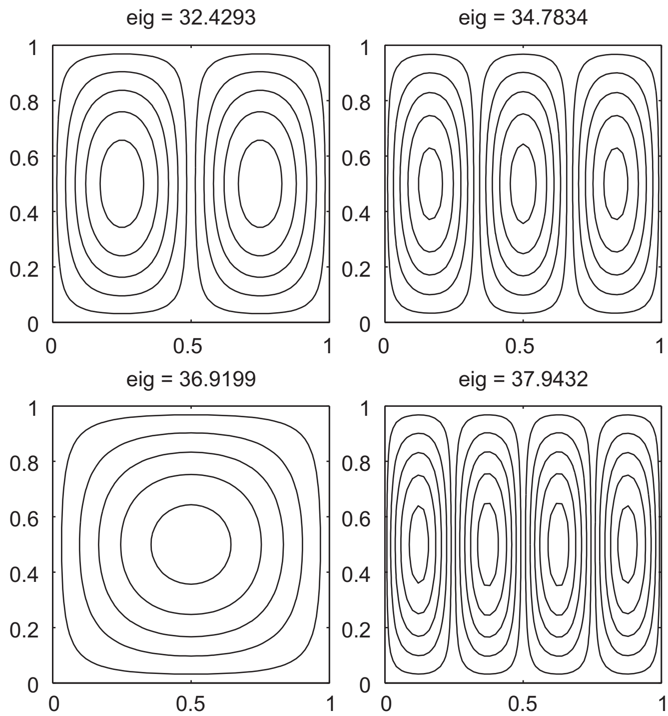

Fig. 5. Uniaxial loading $(45/-45)_3$, $a/h=10$, $c=2/\sqrt{N}$, $N=15$.

The non-dimensional critical buckling loads for cross-ply laminated plates are presented in Table 3, where the present solution is compared with analytical results by Reddy and Phan [27]. Three laminates are considered: ([0/90], [0/90/0], [0/90/90/0]. The effect of the shear deformation on the buckling parameters is very significant. Our results compare quite well with those of Reddy and Phan.

In order to discuss the applicability of the present approach to other laminate configurations, uniaxial numerical tests were performed on unsymmetric angle-ply $(45/-45)_p$ ($p=1$ or 3) laminates. The shape parameter is set as $c=2/\sqrt{N}$. For various side-to-thickness (a/h) ratios, we present in Table 4 the critical buckling loads. Results are compared with those of Reddy [1], and show excellent comparison (difference to Reddy's results are

Table 5
Uniaxial and biaxial loading for (45/−45/−45/45), $c=1/\sqrt{N}$.

	N	$a/h=5$	$a/h=10$	$a/h=20$	$a/h=100$
Biaxial	9	7.0071	14.3164	19.4202	19.2613
	11	6.9997	14.3773	19.6510	17.9303
	13	6.9968	14.4353	19.8547	18.6447
	15	6.9951	14.4818	20.0153	19.6692
	17	6.9937	14.5173	20.1403	20.5724
	19	6.9924	14.5439	20.2380	21.2881
	21	6.9912	14.5638	20.3149	21.8390
	25	6.9890	14.5900	20.4246	22.5857
Uniaxial	9	10.5523	26.7978	38.5430	38.2611
	11	10.4995	26.6363	39.0618	35.7013
	13	10.4775	26.5558	39.5003	37.1731
	15	10.4651	26.5092	39.8397	39.2442
	17	10.4575	26.4796	40.1009	41.0625
	19	10.4525	26.4597	40.3033	42.5005
	21	10.4491	26.4454	40.4615	43.6052
	25	10.4453	26.4266	40.6858	45.0994

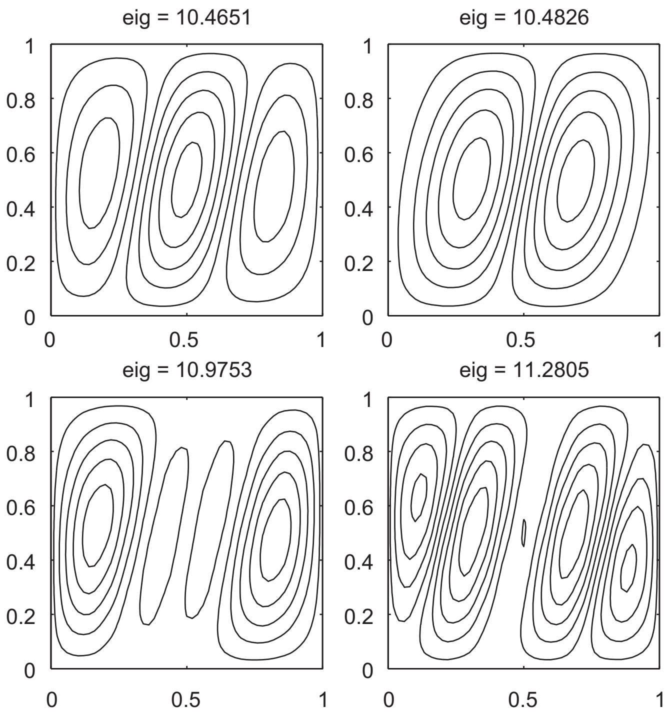

Fig. 6. Uniaxial loading (45/−45/−45/45), $a/h=5$, $c=1/\sqrt{N}$, $N=15$.

below 0.25% for all cases). In Figs. 2–5 the first four modes of buckling are illustrated, for several side-to-thickness ratios, using $N=15$, where N is the number of nodes per side (total number of nodes is $N\times N$).

Uniaxial and biaxial buckling loadings in symmetric (45/−45/−45/45) angle-ply laminates are considered next in Table 5, using $c=1/\sqrt{N}$. The results show good convergence with the increasing number of nodes.

Figs. 6–8 illustrate the mode shapes for uniaxial loading of (45/−45/−45/45) laminates, using various a/h ratios, and $N=15$. It is clear the difference in mode shapes when compared with those of previous figures for unsymmetric laminates.

5. Conclusions

In this paper we used the radial basis function collocation method to analyze buckling loads of isotropic and laminated plates. The higher-order shear deformation theory of Reddy defines a set of equations of motion and boundary conditions as an eigenvalue problem where the eigenvalues are the buckling loads. The present results were compared with existing analytical solutions, or finite element schemes and are in very good agreement. The collocation method with radial basis functions according to a higher-order shear deformation theory is a simple yet powerful alternative to other finite element or meshless methods for buckling analysis of plates.

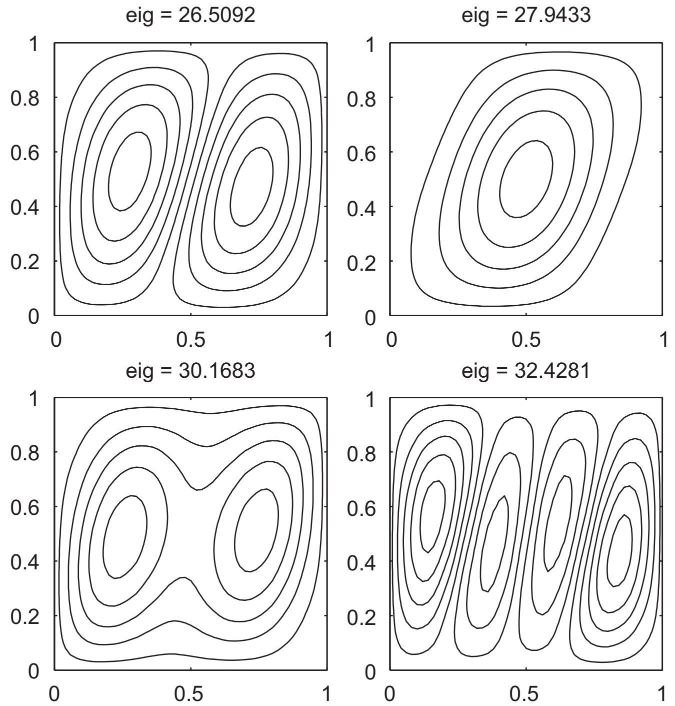

Fig. 7. Uniaxial loading (45/−45/−45/45), $a/h=10$, $c=1/\sqrt{N}$, $N=15$.

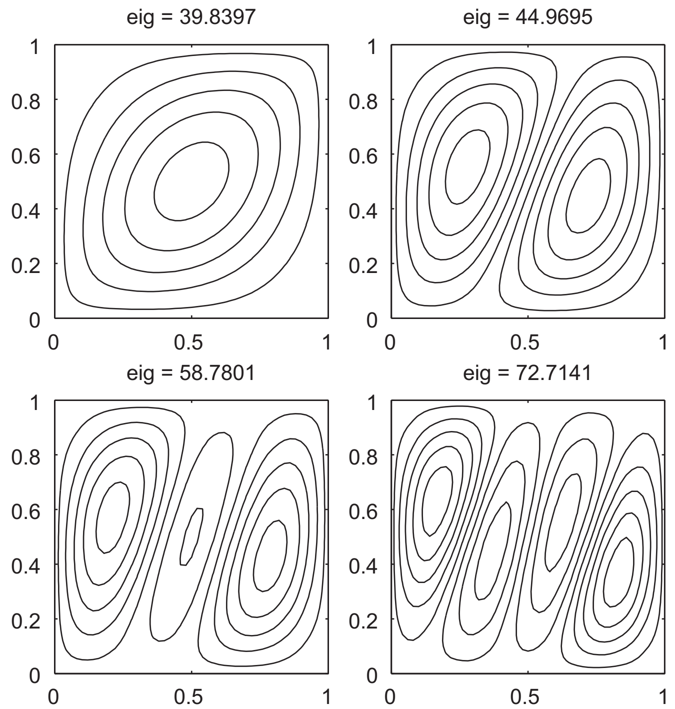

Fig. 8. Uniaxial loading (45/−45/−45/45), $a/h=20$, $c=1/\sqrt{N}$, $N=15$.

References

[1] Reddy JN. Bending of laminated anisotropic shells by a shear deformable finite element. Fibre Science and Technology 1982;17:9–24.
[2] Mindlin RD. Influence of rotary inertia and shear in flexural motions of isotropic elastic plates. Journal of Applied Mechanics 1951;18:31–8.
[3] Reissner E. The effect of transverse shear deformations on the bending of elastic plates. Journal of Applied Mechanics 1945;12:A69–77.
[4] Kant T. Numerical analysis of thick plates. Computer Methods in Applied Mechanics and Engineering 1982;31:1–18.
[5] Reddy JN. A simple higher-order theory for laminated composite plates. Journal of Applied Mechanics 1984;51:745–52.
[6] Kansa EJ. Multiquadrics—a scattered data approximation scheme with applications to computational fluid dynamics. I: Surface approximations and partial derivative estimates. Computers and Mathematics with Applications 1990;19(8/9):127–45.
[7] Hon YC, Lu MW, Xue WM, Zhu YM. Multiquadric method for the numerical solution of biphasic mixture model. Applied Mathematics and Computation 1997;88:153–75.
[8] Hon YC, Cheung KF, Mao XZ, Kansa EJ. A multiquadric solution for the shallow water equation. ASCE Journal of Hydraulic Engineering 1999;125(5):524–33.
[9] Wang JG, Liu GR, Lin P. Numerical analysis of biot's consolidation process by radial point interpolation method. International Journal of Solids and Structures 2002;39(6):1557–73.
[10] Liu GR, Gu YT. A local radial point interpolation method (lrpim) for free vibration analyses of 2-d solids. Journal of Sound and Vibration 2001;246(1):29–46.
[11] Liu GR, Wang JG. A point interpolation meshless method based on radial basis functions. International Journal of Numerical Methods and Engineering 2002;54:1623–48.
[12] Wang JG, Liu GR. On the optimal shape parameters of radial basis functions used for 2-d meshless methods. Computation Methods in Applied Mechanics and Engineering 2002;191:2611–30.
[13] Chen XL, Liu GR, Lim SP. An element free Galerkin method for the free vibration analysis of composite laminates of complicated shape. Composite Structures 2003;59:279–89.
[14] Dai KY, Liu GR, Lim SP, Chen XL. An element free Galerkin method for static and free vibration analysis of shear-deformable laminated composite plates. Journal of Sound and Vibration 2004;269:633–52.
[15] Liu GR, Chen XL. Buckling of symmetrically laminated composite plates using the element-free Galerkin method. International Journal of Structural Stability and Dynamics 2002;2:281–94.
[16] Liew KM, Chen XL, Reddy JN. Mesh-free radial basis function method for buckling analysis of non-uniformity loaded arbitrarily shaped shear deformable plates. Computer Methods in Applied Mechanics and Engineering 2004;193:205–25.
[17] Q Huang Y, Li QS. Bending and buckling analysis of antisymmetric laminates using the moving least square differential quadrature method. Computer Methods in Applied Mechanics and Engineering 2004;193:3471–92.
[18] Liu L, Liu GR, Tan VCB. Element free method for static and free vibration analysis of spatial thin shell structures. Computer Methods in Applied Mechanics and Engineering 2002;191:5923–42.
[19] Ferreira AJM. A formulation of the multiquadric radial basis function method for the analysis of laminated composite plates. Composite Structures 2003;59:385–92.
[20] Ferreira AJM. Thick composite beam analysis using a global meshless approximation based on radial basis functions. Mechanics of Advanced Materials and Structures 2003;10:271–84.
[21] Ferreira AJM, Roque CMC, Martins PALS. Analysis of composite plates using higher-order shear deformation theory and a finite point formulation based on the multiquadric radial basis function method. Composites: Part B 2003;34:627–36.
[22] Wang CM, Liew KM, Xiang Y, Kipornchai S. Buckling of rectangular mindlin plates with internal line supports. International Journal of Solid Structures 1993;30(1):1–17.
[23] Kitipornchai S, Xiang Y, Wang CM, Liew KM. Buckling of thick skew plates. International Journal of Numerical Methods and Engineering 1993;36: 1299–310.
[24] Liew KM, Wang J, Ng TY, Tan MJ. Free vibration and buckling analyses of shear-deformable plates based on FSDT meshfree method. Journal of Sound and Vibration 2004;276:997–1017.
[25] Liew KM, Huang YQ. Bending and buckling of thick symmetric rectangular laminates using the moving least-squares differential quadrature method. International Journal of Mechanical Sciences 2003;45:95–114.
[26] Putcha NS, Reddy JN. Stability and natural vibration analysis of laminated plates by using a mixed element based on a refined plate theory. Journal of Sound and Vibration 1986;104(2):285–300.
[27] Reddy JN, Phan ND. Stability and vibration of isotropic, orthotropic and laminated plates according to a higher-order shear deformation theory. Journal of Sound and Vibration 1985;98(2):157–70.
[28] Madich WR, Nelson SA. Multivariate interpolation and conditionally positive definite functions. ii. Mathematics of Computation 1990;54(189): 211–30.
[29] Yoon J. Spectral approximation orders of radial basis function interpolation on the Sobolev space. SIAM Journal of Mathematical Analysis 2001;33(4):946–58.
[30] Hardy RL. Multiquadric equations of topography and other irregular surfaces. Geophysical Research 1971;176:1905–15.
[31] Buhmann MD. Radial basis functions. Acta Numerica 2000;9:1–38.
[32] Noor AK. Free vibration of multilayered plates. AIAA Journal 1973;11:1038–9.
[33] Reddy JN. Mechanics of laminated composite plates and shells. New York: CRC Press; 2004.

3.2 On the RBF-PS method

3.2.1 Solving time-dependent problems by an RBF-PS method with an optimal shape parameter

A. M. A. Neves, C. M. C. Roque, A. J. M. Ferreira, C. M. M. Soares, R. M. N. Jorge, Solving time-dependent problems by an RBF-PS method with an optimal shape parameter, Journal of Physics: Conference Series, volume 181, number 1, 012053, 2009.

Journal of Physics: Conference Series **181** (2009) 012053 doi:10.1088/1742-6596/181/1/012053

Solving time-dependent problems by an RBF-PS method with an optimal shape parameter

Ana M. A. Neves[1], **C. M. C. Roque**[1], **A. J. M. Ferreira**[1], **C. M. M. Soares**[2], **R. M. N. Jorge**[1]

[1] Departamento de Engenharia Mecânica e Gestão Industrial, Faculdade de Engenharia da Universidade do Porto,
Rua Dr. Roberto Frias, 4200-465 Porto, Portugal

[2] IDMEC - Instituto de Engenharia Mecânica - Instituto Superior Técnico, Av. Rovisco Pais, 1096 Lisboa Codex, Portugal

E-mail: ana.m.neves@fe.up.pt,croque@fe.up.pt,ferreira@fe.up.pt, cristovao.mota.soares@dem.ist.utl.pt,rnatal@fe.up.pt

Abstract. An hybrid technique is used for the solutions of static and time-dependent problems. The idea is to combine the radial basis function (RBF) collocation method and the pseudospectal (PS) method getting to the RBF-PS method. The approach presented in this paper includes a shape parameter optimization and produces highly accurate results.

Different examples of the procedure are presented and different radial basis functions are used. One and two-dimensional problems are considered with various boundary and initial conditions. We consider generic problems, but also results on beams and plates. The displacement and the stress analysis are conducted for static and transient dynamic situations. Results obtained are in good agreement with exact solutions or references considered.

1. Introduction

Both pseudospectral (PS) method ([1, 2]) and radial basis function (RBF) method ([3] to [7]) are good solvers for PDEs. Combining the two methods we can extend the high accuracy of the results to complex geometries and keep it simple to implement.

Ferreira and colleagues used the multiquadrics RBF ([8]) to solve time-dependent problems including structural problems. Fasshauer, Ferreira, and colleagues ([9] to [14]) have already used with success the RBF-PS method for the solution of some problems. This paper extends the application of the RBF-PS method to the transient analysis of structural problems including an optimization of the shape parameter for the radial basis functions, allowing an user-independent analysis.

2. RBF-PS method for time-dependent problems

Suppose you want to approximate a function that you want to differentiate or to approximate the solution $u(x)$ or $u(x,t)$ of a given a differential equation with boundary conditions. The approximation considered is a finite sum of very smooth and global basis functions,

$$u(x) = \sum_{k=0}^{N} \lambda_k \phi_k(x), \text{ in the case of static problems} \tag{1}$$

Journal of Physics: Conference Series **181** (2009) 012053 doi:10.1088/1742-6596/181/1/012053

$$\text{or} \quad u(x,t) = \sum_{k=0}^{N} \lambda_k(t)\phi_k(x), \text{ for time-dependent problems} \tag{2}$$

where the basis functions $\phi_k(x)$ can be for example trigonometric functions or polynomials, such as Chebyshev polynomials. Then, you differentiate these functions exactly ([2]).

When using pseudospectral method, if you are given a set of grid points x_i and corresponding function values $u_i = u(x_i)$, you can use this data to approximate the derivative of u via *differentiation matrices*. Writing u as a column vector, you can find a square matrix D such that, at x_i, you have

$$u' = D.u. \tag{3}$$

Finding the derivative of a vector of data becomes a $matrix \times vector$ multiplication. We just need some manipulations to get to D.

You must evaluate (1) at the grid points x_i and get

$$u(x_i) = \sum_{k=0}^{N} \lambda_k \phi_k(x_i), \tag{4}$$

or in matrix-vector notation

$$u = A\lambda, \tag{5}$$

where λ is the column vector of the coefficients λ_k, matrix A has entries $A_{ik} = \phi_k(x_i)$, and u is as before. If you ensure that A is invertible, you get

$$\lambda = A^{-1}.u. \tag{6}$$

Recall that the invertibility of matrix A depends both on the basis function chosen and the location of the points x_i. For univariate polynomials with a set of distinct points invertibility is ensured.

On the other hand, differentiating both sides of (1), you get

$$\frac{d}{dx}u(x) = \sum_{k=1}^{N} \lambda_k \frac{d}{dx}\phi_k(x) \tag{7}$$

Evaluating at the grid points x_i we get in matrix-vector notation

$$u' = M\lambda, \tag{8}$$

where λ is the column vector of the coefficients λ_k, matrix M has entries $M_{ik} = \frac{d}{dx}\phi_k(x_i)$, and u is as before.

So, using (6) in (8), we obtain $u' = M.A^{-1}.u$ so that the differentiation matrix D we were looking for in (3) is

$$D = M.A^{-1}. \tag{9}$$

D_{ij} is the derivative of the j^{th} curve at x_i.

In this paper we use (infinitely smooth) radial basis functions in a spectral framework. The basis function expansion $\phi_k(x)$ in (1) will take the form $\phi_k(x) = g(||x - x_k||, \epsilon) = g(r, \epsilon)$, chosen from a list more extense than the following ([14] among others), e.g.:

$$g(r,\epsilon) = e^{-(\epsilon r)^2}; \quad \text{gaussian} \tag{10}$$

$$g(r,\epsilon) = 1/\sqrt{(1+(\epsilon r)^2)}; \quad \text{inverse multiquadric} \tag{11}$$

$$g(r,\epsilon) = e^{-\epsilon r}(15 + 15\epsilon r + 6(\epsilon r)^2 + (\epsilon r)^3); \quad \text{cubic matérn} \tag{12}$$

$$g(r,\epsilon) = \sqrt{1+(\epsilon r)^2}; \quad \text{multiquadric} \tag{13}$$

$$g(r,\epsilon) = max(1-\epsilon r, 0)^8(32(\epsilon r)^3 + 25(\epsilon r)^2 + 8\epsilon r + 1) \quad \text{Wendland's } \varphi_{3,3} \tag{14}$$

being r the (Euclidean) distance and ϵ a free parameter.

For the RBF-PS technique, matrix A in (5) and (9) has entries

$$A_{ij} = g(r_j, \epsilon)_{|x=x_i} = g(||x_i - x_j||, \epsilon). \tag{15}$$

Furthermore, the entries of M in (8) become $\frac{d}{dx}g(r, \epsilon)_{|x=x_i}$.

In all dynamic problems, depending on the nature of the problem, at each time t we can approximate $u(x,t)$ or $u(x,y,t)$ considering the *forward Euler method* or the *leap frog method*, for example:

$$\frac{\partial u}{\partial t} \approx \frac{u(x,t_{n+1}) - u(x,t_n)}{\Delta t} \tag{16}$$

$$\frac{\partial u}{\partial t} \approx \frac{u(x,t_{n+1}) - u(x,t_{n-1})}{2\Delta t} \tag{17}$$

$$\frac{\partial^2 u}{\partial t^2} = \frac{\partial}{\partial t}\left(\frac{\partial u}{\partial t}\right) \approx \frac{u(x,t_{n+1}) - 2u(x,t_n) + u(x,t_{n-1})}{(\Delta t)^2} \tag{18}$$

being $\Delta t = t_{n+1} - t_n$. This allows us to march in time. The key to the solution of the problems is the approximation of the spatial derivative, both in dynamic or static problems.

To solve a PDE like

$$\frac{\partial}{\partial t}u(x,t) + \frac{\partial}{\partial x}u(x,t) = 0 \tag{19}$$

using the rbf-spectral differentiation matrix D to express the spatial derivative and (16) leads to

$$u(x,t_{n+1}) = u(x,t_n) - \Delta t.D.u(x,t_n) \tag{20}$$

The procedure just described can be generalized to more complex linear differential operators. In this paper we are interested in those such as the ones involved in the following PDE's

$$\frac{\partial}{\partial t}u(x,t) = \frac{\partial^2}{\partial x^2}u(x,t) \tag{21}$$

$$\frac{\partial^2}{\partial t^2}u(x,t) = \frac{\partial^2}{\partial x^2}u(x,t) \tag{22}$$

If we use (16) for the time derivative and the second order rbf-spectral differential matrix D^2 for the spatial derivative, (21) leads to

$$u(x,t_{n+1}) = u(x,t_n) + \Delta t.D^2.u(x,t_n) \tag{23}$$

and if we use (18) for the time derivative and the second order rbf-spectral differential matrix D^2 for the spatial derivative, (22) leads to

$$u(x,t_{n+1}) = 2 * u(x,t_n) - u(x,t_{n-1}) + (\Delta t)^2 * D^2 * u(x,t_n); \tag{24}$$

where D^2 is defined as $D^2 = M^2.A^{-1}$ being $M^2_{ik} = \frac{d^2}{dx^2}g(||x_i - x_k||, \epsilon)$.

In general, D^p_{ij} is the p^{th} derivative of curve number j at x_i:

$$D^p = M^p.A^{-1} \tag{25}$$

being $M^p_{ik} = \frac{d^p}{dx^p}g(||x_i - x_k||, \epsilon)$.

Table 1. Solution errors (%) for problem 3.1.1 with 11 Chebyshev points, $\Delta t = 0.001$, and Wendland C6 RBF

time	$E_{x_0=1}$	E_{x_1}	E_{x_2}	E_{x_3}	E_{x_4}	E_{x_5}
0.1	1.169e-1	1.167e-1	1.125e-1	9.735e-2	6.853e-2	3.477e-2
0.2	8.727e-2	8.716e-2	8.505e-2	7.722e-2	6.102e-2	3.898e-2
0.3	6.484e-2	6.478e-2	6.369e-2	5.959e-2	5.102e-2	3.909e-2
0.4	5.170e-2	5.166e-2	5.113e-2	4.914e-2	4.496e-2	3.913e-2
0.5	4.498e-2	4.496e-2	4.472e-2	4.379e-2	4.185e-2	3.917e-2

For the solution of a two-dimensional problem involving $\frac{\partial}{\partial x}u(x,y,t)$, $\frac{\partial}{\partial y}u(x,y,t)$, $\frac{\partial^2}{\partial x^2}u(x,y,t)$, $\frac{\partial^2}{\partial x \partial y}u(x,y,t)$, or $\frac{\partial^2}{\partial y^2}u(x,y,t)$ we can use the same approximation of the time derivative but we must use different differentiation matrix for the approximation of each spatial derivative. We consider the following approximations, e.g.:

$$\frac{\partial}{\partial x}u(x,y,t) \approx D_x.u(x,y,t) \qquad D_x = \frac{\partial}{\partial x}g(r,\epsilon)_{|(x,y)=(x_i,y_i)}.A^{-1} \tag{26}$$

$$\frac{\partial^2}{\partial x^2}u(x,y,t) \approx D_{xx}.u(x,y,t) \qquad D_{xx} = \frac{\partial^2}{\partial x^2}g(r,\epsilon)_{|(x,y)=(x_i,y_i)}.A^{-1} \tag{27}$$

$$\frac{\partial^2}{\partial x \partial y}u(x,y,t) \approx D_{xy}.u(x,y,t) \qquad D_{xy} = \frac{\partial^2}{\partial x \partial y}g(r,\epsilon)_{|(x,y)=(x_i,y_i)}.A^{-1} \tag{28}$$

$$\tag{29}$$

being $g(r,\epsilon)$ the chosen RBF and A as in (15).

The question of the invertibility of the matrix A remains unsolved for some cases. Fasshauer presents detailed information on the subject in his book [14].

The optimization of the RBF shape parameter is the same used in [12, 13, 14] and a fairly detailed exposition is available in these references.

3. Numerical examples

3.1. One-dimensional problems

3.1.1. Initial-boundary-value problem 1

$$\begin{cases} \text{PDE} & \frac{\partial u}{\partial t} = \frac{\partial^2 u}{\partial x^2},\ 0 \le x \le 1,\ t \ge 0 \\ \text{BC} & \frac{\partial u}{\partial x}(0,t) = \frac{\partial u}{\partial x}(1,t) = 0,\ t \ge 0 \\ \text{IC} & u(x,0) = 9 + 3\cos(\pi x) + 5\cos(4\pi x),\ 0 \le x \le 1 \end{cases} \tag{30}$$

The PDE was implemented for the RBF-PS method as $u_{t+1} = u_t + \Delta t.D2.u_t$.

In tables 1-2 we present the results obtained with present method. We compare with the exact solution $u(x,t) = 9 + 3e^{-\pi^2 t}\cos(\pi x) + 5e^{-16\pi^2 t}\cos(4\pi x)$. Results are in good agreement, the biggest error being approximately 0.2%.

Using 11 Chebyshev points, $\Delta t = 0.001$, and Wendland C6 RBF, the optimized shape parameter is $\epsilon = 0.100064$. For the same RBF but using 21 Chebyshev points and $\Delta t = 0.0001$, we get $\epsilon = 0.160453$. If we use 11 Chebyshev points, $\Delta t = 0.001$, and the Matérn Cubic RBF, we obtain $\epsilon = 0.276603$. Using 21 Chebyshev points, the Matérn Cubic RBF, and $\Delta t = 0.0001$, we get $\epsilon = 1.250831$.

Using 21 Chebyshev points the error achieves a value smaller than $5 * 10^{-5}$%.

Table 2. Solution errors (%) for problem 3.1.1 with 11 Chebyshev points, $\Delta t = 0.001$, and Matérn Cubic RBF

time	$E_{x_0=1}$	E_{x_1}	E_{x_2}	E_{x_3}	E_{x_4}	E_{x_5}
0.1	1.175e-1	1.173e-1	1.132e-1	9.823e-2	6.971e-2	3.611e-2
0.2	8.809e-2	8.800e-2	8.594e-2	7.824e-2	6.225e-2	4.038e-2
0.3	6.590e-2	6.584e-2	6.477e-2	6.075e-2	5.229e-2	4.046e-2
0.4	5.286e-2	5.283e-2	5.231e-2	5.036e-2	4.625e-2	4.046e-2
0.5	4.618e-2	4.617e-2	4.593e-2	4.503e-2	4.313e-2	4.046e-2

3.1.2. Initial-boundary-value problem 2

$$\begin{cases} \text{PDE} & \frac{\partial^2 u}{\partial t^2} = \frac{\partial^2 u}{\partial x^2},\ 0 \le x \le \pi,\ t \ge 0 \\ \text{BC} & u(0,t) = u(\pi,t) = 0,\ t \ge 0 \\ \text{IC} & \begin{cases} u(x,0) = \pi x - x^2,\ 0 \le x \le \pi \\ \frac{\partial u}{\partial t}(x,0) = 0,\ 0 \le x \le \pi \end{cases} \end{cases} \tag{31}$$

To solve this problem we considered $\Delta t = 1.5625 * 10^{-5}$ and 81 Chebyshev points for $t \in [0,4]$. Results obtained with the RBF-PS method, with an optimized shape parameter, both for Matérn Cubic and Wendland C6 RBF are in good agreement with the exact solution, which is $u(x,t) = \frac{8}{\pi}\sum_{odd\ n} n^{-3}\sin(nx)\cos(nt)$. The error is lower than 1% except for the boundary as the exact solution here is equal to zero for every t and around $t = 1.6$ which corresponds to values near zero for the exact solution.

The values for the shape parameter are quite different as we change the RBF: for the Matérn Cubic RBF the optimal shape parameter obtained was $\epsilon = 4.142739$ and for the Wendland C6 was $\epsilon = 0.962844$.

3.1.3. Transient analysis of a beam For the transient dynamic study of a beam in bending we are using the first-order shear deformation theory (FSDT) ([15]), with shear correction factor $K = 5/6$. When applied to beams, the equations of motion are

$$KGbh\left(\frac{\partial^2 w_0}{\partial x^2} + \frac{\partial \theta_x}{\partial x}\right) + bq = bI_0\frac{\partial^2 w_0}{\partial t^2} \tag{32}$$

$$EI\frac{\partial^2 \theta_x}{\partial x^2} - KGbh\left(\frac{\partial w_0}{\partial x} + \theta_x\right) = bI_2\frac{\partial^2 \theta_x}{\partial t^2} \tag{33}$$

Here, $w = w(x,t)$ is the transverse displacement, $\theta_x = \theta_x(x,t)$ is the rotation about the x axis, $K = 5/6$ is the shear correction coefficient, and q is the total transverse load. The remaining terms are obtained from given constants that characterize both the material properties and the structural properties of the beam.

We use the static solution of bending equilibrium as the initial conditions.

For the time-steping procedure we considered equations (32) and (33) divided by bI_0 and bI_2, respectively, and used the *forward Euler method*.

We consider an isotropic beam with both ends simply-supported and material properties $E = 10920$; $\rho = 1$; $\nu = 0.25$. The dimensions of the beam are $a = 1$, $b = 1$, $h = 0.1$, being a the length, h the thickness, and $b * h$ the cross section dimensions.

We used 11 Chebyshev points along the beam, $x \in [0,1]$, the Cubic Matérn RBF (see (12)), and $\Delta t = 5 * 10^{-5}$. The optimal RBF shape parameter obtained was $\epsilon = 0.276603$.

In figure 1 we present the transverse displacement of the central point of the beam for $t \in [0,1]$.

3.2. Transient analysis of a plate

Consider now an isotropic square plate in bending, clamped at all edges. Length of each side is $a = 2$ and side-over-thickness ratio is $a/h = 10$. The material properties are $\rho = 1$, $E = 10920$, and $\nu = 0.3$.

In the present study the First-Order Shear Deformation Theory (FSDT) is used ([15]). When applied to plates, the equations of motion are

$$D_{11}\frac{\partial^2\theta_x}{\partial x^2} + D_{16}\frac{\partial^2\theta_y}{\partial x^2} + (D_{12}+D_{66})\frac{\partial^2\theta_y}{\partial x\partial y} + 2D_{16}\frac{\partial^2\theta_x}{\partial x\partial y} + D_{66}\frac{\partial^2\theta_x}{\partial y^2} + D_{26}\frac{\partial^2\theta_y}{\partial y^2} + \\ - kA_{45}\left(\theta_y + \frac{\partial w}{\partial y}\right) - kA_{55}\left(\theta_x + \frac{\partial w}{\partial x}\right) = I_2\frac{\partial^2\theta_x}{\partial t^2} \quad (34)$$

$$D_{16}\frac{\partial^2\theta_x}{\partial x^2} + D_{66}\frac{\partial^2\theta_y}{\partial x^2} + (D_{12}+D_{66})\frac{\partial^2\theta_x}{\partial x\partial y} + 2D_{26}\frac{\partial^2\theta_y}{\partial x\partial y} + D_{26}\frac{\partial^2\theta_x}{\partial y^2} + D_{22}\frac{\partial^2\theta_y}{\partial y^2} + \\ - kA_{44}\left(\theta_y + \frac{\partial w}{\partial y}\right) - kA_{45}\left(\theta_x + \frac{\partial w}{\partial x}\right) = I_2\frac{\partial^2\theta_y}{\partial t^2} \quad (35)$$

$$\frac{\partial}{\partial x}\left[kA_{45}\left(\theta_y + \frac{\partial w}{\partial y}\right) + kA_{55}\left(\theta_x + \frac{\partial w}{\partial x}\right)\right] + \\ \frac{\partial}{\partial y}\left[kA_{44}\left(\theta_y + \frac{\partial w}{\partial y}\right) + kA_{45}\left(\theta_x + \frac{\partial w}{\partial x}\right)\right] + q = I_0\frac{\partial^2 w}{\partial t^2}, \quad (36)$$

where $w = w(x,y,t)$ is the transverse displacement, $\theta_x = \theta_x(x,y,t)$ and $\theta_y = \theta_y(x,y,t)$ are the rotations about the x and y axis, respectively, $K = 5/6$ is the shear correction coefficient, and q is the total transverse load.

The initial conditions are the static solution of bending equilibrium. A mesh of 81 points was used, corresponding to 9 equally spaced points per side, in [-1,1], and $\Delta t = 10^{-5}$. The RBF used was the Matérn Cubic (see (12)) and the optimal RBF shape parameter obtained was $\epsilon = 0.104817$.

In figure 2 we present the transverse displacement of the central point of the plate considered along the time $t \in [0, 1]$.

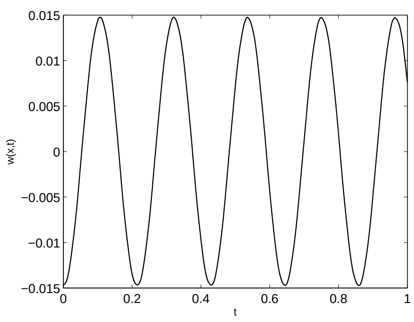

Figure 1. Central displacement of the beam

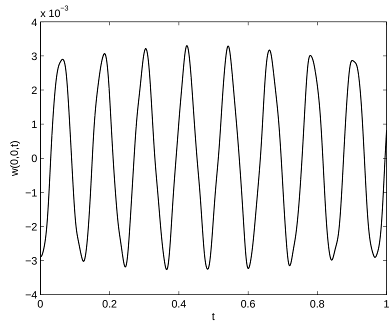

Figure 2. Central displacement of the plate

4. Conclusions

This paper addresses the solution of several PDE problems using a technique that combines the radial basis function (RBF) collocation technique and the pseudospectal (PS) method with the optimization of the RBF shape parameter. This allows the extension of the accurate results to complex geometries, keeping it simple to implement.

Several numerical tests were performed using some radial basis functions, boundary conditions, and initial conditions, for both one and two-dimensional problems. We extended previous work to the transient analysis of a beam and a plate.

Results obtained demonstrate that the method produces good results which are in good agreement with exact solutions or references considered.

Further studies, including the application of the method to composite structures and with more complex geometries are to be made.

References

[1] Trefethen L N 2000 *Spectral Methods in Matlab* (Philadelphia: SIAM)
[2] Fornberg B 1998 *A Practical Guide to Pseudospectral Methods* (Cambridge: Cambridge University Press)
[3] Kansa E J 1990 *Computers & mathematics with applications*, **19(8-9)** 127–145
[4] Kansa E J 1990 *Computers & mathematics with applications*, **19(8-9)** 147–161
[5] Larsson E and Fornberg B 2003 *Computers & Mathematics with Applications*, **46 (5-6)** 891–902
[6] Fasshauer G E 1997 *Proc. of the 3rd Int. Conf. on Curves and Surfaces* **2** 131–138
[7] Sarra S A 2005 *Applied Numerical Mathematics* **54 (11)** 79–94.
[8] Ferreira A J M, Martins P A L S and Roque C M C 2005 *Journal of Sound and Vibration* **280** 595–610
[9] Ferreira A J M and Fasshauer G E 2007 *Composite Structures* **79** 202–210
[10] Ferreira A J M and Fasshauer G E 2006 *Computer Methods in Applied Mechanics and Engineering* **196** 134–146
[11] Fasshauer G E 2005 *Boundary Elements XXVII* 47–56
[12] Ferreira A J M and Fasshauer G E 2007 *Advances in Meshfree Techniques* 283–310
[13] Ferreira A J M, Fasshauer G E, Batra R C and Rodrigues J D 2008 *Composite Structures* **86** 328–343
[14] Fasshauer G E 2007 *Meshfree Approximation Methods with Matlab* (Singapore: World Scientific Publishers)
[15] Reddy J N 1997 *Mechanics of laminated composite plates* (New York: CRC Press)

3.2.2 Transient analysis of composite plates by radial basis functions in a pseudospectral framework

C. M. C. Roque, A. J. M. Ferreira, Ana M. A. Neves, C. M. M. Soares, J. N. Reddy, R. M. N. Jorge, Transient analysis of composite plates by radial basis functions in a pseudospectral framework, Computers & Structures, Volume 89, Issues 1-2, 2011, pages 161-169.

Computers and Structures 89 (2011) 161–169

Contents lists available at ScienceDirect

Computers and Structures

journal homepage: www.elsevier.com/locate/compstruc

Transient analysis of composite plates by radial basis functions in a pseudospectral framework

C.M.C. Roque [a], A.J.M. Ferreira [b,*], A.M.A. Neves [b], C.M.M. Soares [c], J.N. Reddy [d], R.M.N. Jorge [b]

[a] INEGI, Faculdade de Engenharia da Universidade do Porto, Rua Dr. Roberto Frias, 4200-465 Porto, Portugal
[b] Departamento de Engenharia Mecânica, Faculdade de Engenharia da Universidade do Porto, Rua Dr. Roberto Frias, 4200-465 Porto, Portugal
[c] Departamento de Engenharia Mecânica, Instituto Superior Técnico, Av. Rovisco Pais, Lisboa, Portugal
[d] Department of Mechanical Engineering, Texas A & M University, College Station, Texas 77843-3123, USA

ARTICLE INFO

Article history:
Received 30 March 2010
Accepted 25 August 2010
Available online 20 September 2010

Keywords:
Transient analysis
Dynamics
Composite plates
Radial basis functions
Collocation

ABSTRACT

This paper presents a study of the linear transient response of composite plates using radial basis functions and collocation method in a pseudospectral framework. The first-order shear deformation plate theory is used to define a set of algebraic equations from the equations of motion and boundary conditions. The transient analysis is performed by a Newmark algorithm. In order to assess the quality of the present numerical method, an analytical solution was also developed. Numerical tests on square and rectangular cross-ply laminated plates demonstrate that the present method produces highly accurate displacements and stresses when compared with the available results.

1. Introduction

Recently, radial basis functions (RBFs) have enjoyed considerable success as a technique for interpolating data and functions. A radial basis function, $\phi(\|x - x_j\|)$ is a spline that depends on the Euclidian distance between distinct data centers $x_j, j = 1, 2, \ldots, N \in \mathbb{R}^n$, also called nodal or collocation points.

Although most work to date on RBFs relates to scattered data approximation and in general to interpolation theory, there has recently been an increased interest in their use for solving partial differential equations (PDEs). This approach, which approximates the whole solution of a PDE directly using RBFs is very attractive due to the fact that this is truly a mesh-free technique. Kansa [1] introduced the concept of solving PDEs using RBFs.

The analysis of plates using the finite element method is now fully established. The use of alternative methods such as the meshless methods based on radial basis functions is attractive due to the absence of a mesh (hence element interfaces where the solution derivatives may be discontinuous) and the ease of using the collocation method. The use of radial basis function for the analysis of structures and materials has been previously studied by numerous authors [2–13]. More recently the authors have applied RBFs to the static deformations of composite beams, plates and shells [14–18].

The radial basis function collocation method, proposed by Kansa [1], has one small drawback in transient analysis: for every time step, an extra computation is needed to obtain the final solution. To overcome such problem, here we propose the use of radial basis functions in a pseudospectral framework, as proposed by Ferreira and Fasshauer [19]. The advantage is that the method produces the direct solution in every time step by solving a linearized system of equations.

For transient analysis, the Newmark time-integration algorithm is used. The Newmark scheme was used by Reddy with a first-order shear deformation theory to analyze the dynamic response of anisotropic composite plates [20]. It was also used by Liu et al. [21] with the radial basis function collocation method to analyze the dynamic behavior of electroactuated beams and by Kirby and Yosibash [22] with a pseudospectral method for the dynamic non-linear analysis of plates.

Because there are few results in tabular form, we independently developed an analytical solution (see Reddy's book [23]) to compare with the present meshless method.

As it will be shown in the examples, the present method yields excellent results when compared with the analytical solutions. This paper shows for the first time an application of the RBF-PS method to analyze the transient response of composite plates in bending.

* Corresponding author.
E-mail address: ferreira@fe.up.pt (A.J.M. Ferreira).

0045-7949/$ - see front matter © 2010 Elsevier Ltd. All rights reserved.
doi:10.1016/j.compstruc.2010.08.012

2. The RBF-pseudospectral method

One way to implement the pseudospectral method is via so-called differentiation matrices, i.e., one finds a matrix D such that at the grid points x_i we have

$$\mathbf{u}' = D\mathbf{u}. \tag{1}$$

Here $\mathbf{u} = [u^h(x_1), \ldots, u^h(x_N)]^T$ is the vector of values of u^h at the grid points. Below we will illustrate how to follow this approach for the RBF collocation method.

As mentioned above, traditional PS methods employ polynomials (such as Chebyshev polynomials) as basis functions. Radial basis functions are composed with the Euclidean norm to make it a radial function, i.e., $\phi_j(x) = \Phi(\|x - x_j\|)$. In the theory of radial basis functions one usually takes (conditionally) positive definite basic functions Φ. The inverse multiquadric we will be using below is of the form

$$\Phi(r) = \frac{1}{\sqrt{1 + (cr)^2}}. \tag{2}$$

This function is infinitely smooth and positive definite on $\mathbb{R}^d$. Here we consider a modified version of the inverse multiquadric, given by:

$$\phi_j(x_i) = \Phi(r) = \left[1 + c^2\left((x_i - x_j)^2 + \frac{(y_i - y_j)^2}{(b/a)^2}\right)\right]^{-1}, \tag{3}$$

where r is the euclidian norm between grid points of coordinates (x,y), a, b are the length of the plate along x and y axis respectively and c is a (positive) shape parameter. It should be mentioned that the RBF function is modified to accommodate the a/b ratio. This is not seen elsewhere in the literature and proved to be more accurate than the usual inverse multiquadric functions, in our computations.

Other popular choices include, e.g., the multiquadrics

$$\Phi(r) = \sqrt{1 + (cr)^2} \tag{4}$$

and Gaussians

$$\Phi(r) = e^{-(cr)^2}. \tag{5}$$

Both of these functions are also infinitely differentiable. The Gaussian is positive definite, while the multiquadric is conditionally negative definite. As explained above, we use r to denote the radial variable, i.e., $r = \|x\|$. Moreover, all of our examples contain a spositive shape parameter c.

The shape parameter c can be used to influence the accuracy of the numerical method. One approach to finding a good value of the shape parameter is the use of leave-one-out cross validation (see Ferreira and Fasshauer [19] and Roque and Ferreira [24] for details).

The spatial part of the approximate solution u^h of a given PDE is represented by a linear combination of certain basis functions ϕ_j, $j = 1, \ldots, N$, i.e.,

$$u^h(x) = \sum_{j=1}^{N} c_j \phi_j(x), \quad x \in \mathbb{R}. \tag{6}$$

Let ϕ_j, $j = 1, \ldots, N$, be an arbitrary linearly independent set of smooth functions that will serve as our basis functions. In order to obtain a formulation for the differentiation matrix $\mathbf{D}$ of (1) we evaluate (6) at the grid points x_i, $i = 1, \ldots, N$. This results in

$$u^h(x_i) = \sum_{j=1}^{N} c_j \phi_j(x_i), \quad i = 1, \ldots, N \tag{7}$$

or in matrix–vector notation

$$\mathbf{u} = \mathbf{A}\mathbf{c}, \tag{8}$$

where $\mathbf{c} = [c_1, \ldots, c_N]^T$ is the coefficient vector, the evaluation matrix $A_{ij} = \phi_j(x_i)$, and $\mathbf{u}$ is as before.

We compute the derivative of u^h by differentiating the basis functions, i.e.,

$$\frac{d}{dx} u^h(x) = \sum_{j=1}^{N} c_j \frac{d}{dx} \phi_j(x). \tag{9}$$

If we again evaluate at the grid points x_i then we get in matrix–vector notation

$$\mathbf{u}' = \mathbf{A}_x \mathbf{c}, \tag{10}$$

where $\mathbf{u}$ and $\mathbf{c}$ are as above, and the matrix $\mathbf{A}_x$ has entries $\frac{d}{dx}\phi_j(x_i)$, or, in the case of radial functions, $\frac{d}{dx}\Phi(\|x - x_j\|)_{x=x_i}$.

It is now easy to obtain the desired formula for $\mathbf{D}$. We simply solve Eq. (8) for $\mathbf{c}$ and substitute the result into (10). This gives us

$$\mathbf{u}' = \mathbf{A}_x \mathbf{A}^{-1} \mathbf{u}, \tag{11}$$

so that the differentiation matrix $\mathbf{D}$ corresponding to (1) is of the form

$$\mathbf{D} = \mathbf{A}_x \mathbf{A}^{-1}. \tag{12}$$

The procedure described above can be followed for more complex linear differential operators $\mathcal{L}$ operating on functions of several variables such as the operators in our examples below. This leads to a discretized differential operator (differentiation matrix)

$$\mathbf{L} = \mathbf{A}_{\mathcal{L}} \mathbf{A}^{-1}, \tag{13}$$

where the matrix $\mathbf{A}_{\mathcal{L}}$ has entries $\mathbf{A}_{\mathcal{L},ij} = \mathcal{L}\phi_j(x_i)$. If we use radial basis functions then these entries are of the form $\mathbf{A}_{\mathcal{L},ij} = \mathcal{L}\Phi(\|x - x_j\|)_{x=x_i}$.

In order to see how the matrix L changes when we add boundary conditions we consider how the linear elliptic PDE

$$\mathcal{L}\mathbf{u} = \mathbf{f} \quad \text{in } \Omega, \tag{14}$$

with boundary condition

$$\mathcal{L}_B = \mathbf{g} \quad \text{on } \Gamma = \partial\Omega \tag{15}$$

can be solved using pseudospectral methods. In order to satisfy the boundary conditions we take the differentiation matrix $\mathbf{L}$ based on all grid points x_i, and then replace the rows of $\mathbf{L}$ corresponding to collocation at boundary points with unit vectors that have a one in the position corresponding to the diagonal of $\mathbf{L}$. Thus, the condition $\mathcal{L}_B = \mathbf{g}$ is explicitly enforced at this point.

3. First-order shear deformation theory

In this section, we briefly present the basic equations for the first-order shear deformation theory (FSDT) for plates. A more detailed review can be found in Reddy [23]. We seek the equations of motion and the discretization of such equations, and the boundary conditions, by the RBF-PS interpolation.

The displacement field for the first-order shear deformation theory is:

$$\begin{aligned} u(x,y,z,t) &= u_0(x,y,t) + z\theta_x(x,y,t), \\ v(x,y,z,t) &= v_0(x,y,t) + z\theta_y(x,y,t), \\ w(x,y,z,t) &= w_0(x,y,t), \end{aligned} \tag{16}$$

where u and v are the in-plane displacements at any point (x,y,z), u_0 and v_0 denote the in-plane displacement of the point $(x,y,0)$ on the midplane, w is the deflection, θ_x and θ_y are the rotations of the normals to the midplane about the y and x axes, respectively. The thickness of the plate is denoted as h.

The strain–displacement relationships are given as

$$\begin{Bmatrix} \epsilon_{xx} \\ \epsilon_{yy} \\ \gamma_{xy} \\ \gamma_{xz} \\ \gamma_{yz} \end{Bmatrix} = \begin{Bmatrix} \frac{\partial u}{\partial x} \\ \frac{\partial v}{\partial y} \\ \frac{\partial u}{\partial y} + \frac{\partial v}{\partial x} \\ \frac{\partial u}{\partial z} + \frac{\partial w}{\partial x} \\ \frac{\partial v}{\partial z} + \frac{\partial w}{\partial y} \end{Bmatrix} \tag{17}$$

Therefore strains can be expressed as

$$\begin{Bmatrix} \epsilon_{xx} \\ \epsilon_{yy} \\ \gamma_{xy} \\ \gamma_{xz} \\ \gamma_{yz} \end{Bmatrix} = \begin{Bmatrix} \epsilon_{xx}^{(0)} \\ \epsilon_{yy}^{(0)} \\ \gamma_{xy}^{(0)} \\ \gamma_{xz}^{(0)} \\ \gamma_{yz}^{(0)} \end{Bmatrix} + z \begin{Bmatrix} \epsilon_{xx}^{(1)} \\ \epsilon_{yy}^{(1)} \\ \gamma_{xy}^{(1)} \\ \gamma_{xz}^{(1)} \\ \gamma_{yz}^{(1)} \end{Bmatrix}, \tag{18}$$

where

$$\begin{Bmatrix} \epsilon_{xx}^{(0)} \\ \epsilon_{yy}^{(0)} \\ \gamma_{xy}^{(0)} \\ \gamma_{xz}^{(0)} \\ \gamma_{yz}^{(0)} \end{Bmatrix} = \begin{Bmatrix} \frac{\partial u_0}{\partial x} \\ \frac{\partial v_0}{\partial y} \\ \frac{\partial u_0}{\partial y} + \frac{\partial v_0}{\partial x} \\ \frac{\partial w_0}{\partial x} + \theta_x \\ \frac{\partial w_0}{\partial y} + \theta_y \end{Bmatrix}; \quad \begin{Bmatrix} \epsilon_{xx}^{(1)} \\ \epsilon_{yy}^{(1)} \\ \gamma_{xy}^{(1)} \\ \gamma_{xz}^{(1)} \\ \gamma_{yz}^{(1)} \end{Bmatrix} = \begin{Bmatrix} \frac{\partial \theta_x}{\partial x} \\ \frac{\partial \theta_y}{\partial y} \\ \frac{\partial \theta_x}{\partial y} + \frac{\partial \theta_y}{\partial x} \\ 0 \\ 0 \end{Bmatrix}. \tag{19}$$

A laminate can be manufactured from orthotropic layers (or plies) of unidirectional fibrous composite materials. The plane-stress-reduced stress–strain relations in the fiber local coordinate system can be expressed as

$$\begin{Bmatrix} \sigma_1 \\ \sigma_2 \\ \tau_{12} \\ \tau_{23} \\ \tau_{31} \end{Bmatrix} = \begin{bmatrix} Q_{11} & Q_{12} & 0 & 0 & 0 \\ Q_{12} & Q_{22} & 0 & 0 & 0 \\ 0 & 0 & Q_{33} & 0 & 0 \\ 0 & 0 & 0 & Q_{44} & 0 \\ 0 & 0 & 0 & 0 & Q_{55} \end{bmatrix} \begin{Bmatrix} \varepsilon_1 \\ \varepsilon_2 \\ \gamma_{12} \\ \gamma_{23} \\ \gamma_{31} \end{Bmatrix}, \tag{20}$$

where subscripts 1 and 2 are respectively the fiber and the normal to fiber in-plane directions, 3 is the direction normal to the plate, and the reduced stiffness components, Q_{ij} are given by

$$Q_{11} = \frac{E_1}{1-\nu_{12}\nu_{21}}; \quad Q_{22} = \frac{E_2}{1-\nu_{12}\nu_{21}}; \quad Q_{12} = \nu_{21} Q_{11};$$
$$Q_{33} = G_{12}; \quad Q_{44} = G_{23}; \quad Q_{55} = G_{31}; \quad \nu_{21} = \nu_{12}\frac{E_2}{E_1}$$

in which E_1, E_2, ν_{12}, G_{12}, G_{23} and G_{31} are material properties of the lamina [23].

By performing adequate coordinate transformation, the stress–strain relations in the global xyz-coordinate system can be obtained as

$$\begin{Bmatrix} \sigma_{xx} \\ \sigma_{yy} \\ \tau_{xy} \\ \tau_{yz} \\ \tau_{zx} \end{Bmatrix} = \begin{bmatrix} \overline{Q}_{11} & \overline{Q}_{12} & \overline{Q}_{16} & 0 & 0 \\ \overline{Q}_{12} & \overline{Q}_{22} & \overline{Q}_{26} & 0 & 0 \\ \overline{Q}_{16} & \overline{Q}_{26} & \overline{Q}_{66} & 0 & 0 \\ 0 & 0 & 0 & \overline{Q}_{44} & \overline{Q}_{45} \\ 0 & 0 & 0 & \overline{Q}_{45} & \overline{Q}_{55} \end{bmatrix} \begin{Bmatrix} \varepsilon_{xx} \\ \varepsilon_{yy} \\ \gamma_{xy} \\ \gamma_{yz} \\ \gamma_{zx} \end{Bmatrix}, \tag{21}$$

where $\overline{Q}_{ij}$ are the components of the constitutive matrix in laminate axes [23].

The equations of motion of the first-order theory are derived from the principle of virtual displacements [23]. The virtual strain energy (δU), virtual kinetic energy (δK), and the virtual work done by applied forces (δV) are given by

$$\begin{aligned} \delta U &= \int_{\Omega_0} \left\{ \int_{-h/2}^{h/2} \left[\sigma_{xx}\left(\delta\epsilon_{xx}^{(0)} + z\delta\epsilon_{xx}^{(1)}\right) + \sigma_{yy}\left(\delta\epsilon_{yy}^{(0)} + z\delta\epsilon_{yy}^{(1)}\right) \right.\right. \\ &\quad \left.\left. + \tau_{xy}\left(\delta\gamma_{xy}^{(0)} + z\delta\gamma_{xy}^{(1)}\right) + \tau_{xz}\left(\delta\gamma_{xz}^{(0)}\right) + \tau_{yz}\left(\delta\gamma_{yz}^{(0)}\right)\right] dz \right\} dx\,dy \\ &= \int_{\Omega_0} \left(N_{xx}\delta\epsilon_{xx}^{(0)} + M_{xx}\delta\epsilon_{xx}^{(1)} + N_{yy}\delta\epsilon_{yy}^{(0)} + M_{yy}\delta\epsilon_{yy}^{(1)} + N_{xy}\delta\gamma_{xy}^{(0)} \right. \\ &\quad \left. + M_{xy}\delta\gamma_{xy}^{(1)} + Q_x\delta\gamma_{xz}^{(0)} + Q_y\delta\gamma_{yz}^{(0)} \right) dx\,dy, \end{aligned}$$

$$\begin{aligned} \delta K &= \int_{\Omega_0} \left\{ \int_{-h/2}^{h/2} \rho \left[\left(\dot{u}_0 + z\dot{\theta}_x\right)\left(\delta\dot{u}_0 + z\delta\dot{\theta}_x\right) \right.\right. \\ &\quad \left.\left. + \left(\dot{v}_0 + z\dot{\theta}_y\right)\left(\delta\dot{v}_0 + z\delta\dot{\theta}_y\right) + \dot{w}_0\delta\dot{w}_0 \right] dz\,dx\,dy \right. \\ &= \int_{\Omega_0} \left[-I_0(\dot{u}_0\delta\dot{u}_0 + \dot{v}_0\delta\dot{v}_0 + \dot{w}_0\delta\dot{w}_0) \right. \\ &\quad - I_1\left(\dot{\theta}_x\delta\dot{u}_0 + \dot{\theta}_y\delta\dot{v}_0 + \dot{\theta}_x\delta\dot{u}_0 + \dot{\theta}_y\delta\dot{v}_0\right) \\ &\quad \left. - I_2\left(\dot{\theta}_x\delta\dot{\theta}_x + \dot{\theta}_y\delta\dot{\theta}_y\right) dx\,dy \right] \end{aligned} \tag{22}$$

and

$$\delta V = -\int_{\Omega_0} q\,\delta w_0\,dx\,dy, \tag{23}$$

where Ω_0 denotes the midplane of the laminate, q is the external distributed load and

$$\begin{Bmatrix} N_{\alpha\beta} \\ M_{\alpha\beta} \end{Bmatrix} = \int_{-h/2}^{h/2} \sigma_{\alpha\beta} \begin{Bmatrix} 1 \\ z \end{Bmatrix} dz; \quad \{Q_\alpha\} = K \int_{-h/2}^{h/2} \sigma_{\alpha z}\,dz, \tag{24}$$

where α, β take the symbols x, y and K is a shear corrector factor (here taken as 5/6 due to the monolithic laminate configuration). It is relevant to note that the use of the shear correction factor in the first-order shear deformation theories is an approximation to match exact and assumed transverse shear stresses.

Substituting for δU, δV and δK into the virtual work statement, noting that the virtual strains can be expressed in terms of the generalized displacements, integrating by parts to relieve from any derivatives of the generalized displacements and using the fundamental lemma of the calculus of variations, we obtain the following Euler–Lagrange equations [23]:

$$\frac{\partial N_{xx}}{\partial x} + \frac{\partial N_{xy}}{\partial y} = I_0\ddot{u}_0 + I_1\ddot{\theta}_x, \tag{25}$$

$$\frac{\partial N_{xy}}{\partial x} + \frac{\partial N_{yy}}{\partial y} = I_0\ddot{v}_0 + I_1\ddot{\theta}_y, \tag{26}$$

$$\frac{\partial Q_x}{\partial x} + \frac{\partial Q_y}{\partial y} + q = I_0\ddot{w}_0, \tag{27}$$

$$\frac{\partial M_{xx}}{\partial x} + \frac{\partial M_{xy}}{\partial y} - Q_x = I_1\ddot{u}_0 + I_2\ddot{\theta}_x, \tag{28}$$

$$\frac{\partial M_{xy}}{\partial x} + \frac{\partial M_{yy}}{\partial y} - Q_y = I_1\ddot{v}_0 + I_2\ddot{\theta}_y, \tag{29}$$

with

$$I_i = \sum_{k=1}^{nc} \int_{z_k}^{z_{k+1}} \rho^k z^i\,dz. \tag{30}$$

In this paper, the Newmark method is used [23] for the numerical time integration. The Euler–Lagrange equations can be written in terms of the displacements by substituting strains and stress resultants in (25)–(29). The resulting system of equations can be written in the form:

$$\mathbf{M}\ddot{\mathbf{u}} + \mathbf{K}\mathbf{u} = \mathbf{F}. \tag{31}$$

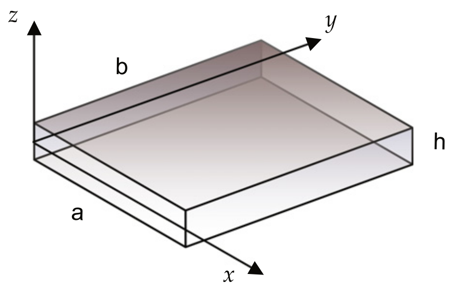

Fig. 1. Composite plate of thickness h, lengths a, b and reference axes xyz.

Time derivatives in equation (31) are approximated using Taylor's series

$$\ddot{u}_{t+\Delta t} = a_3(u_{t+\Delta t} - u_t) - a_4\dot{u}_t - a_5\ddot{u}_t, \tag{32}$$

$$\dot{u}_{t+\Delta t} = \dot{u}_t + a_1\ddot{u}_t + a_2\ddot{u}_{t+\Delta t}, \tag{33}$$

with $\alpha = 3/2,\ \gamma = 8/5,\ a_1 = (1-\alpha)\Delta t;\ a_2 = \alpha\Delta t;\ a_3 = \frac{2}{\gamma(\Delta t)^2};\ a_4 = a_3\Delta t;\ a_5 = \frac{1-\gamma}{\gamma}$.

Substituting Eqs. (32), (33) in equation (31), the latter can be written as:

$$\widehat{\mathbf{K}}\mathbf{u} = \widehat{\mathbf{F}}, \tag{34}$$

with

$$\widehat{\mathbf{K}}_{t+\Delta t} = \mathbf{K}_{t+\Delta t} + a_3\mathbf{M}_{t+\Delta t}, \tag{35}$$

$$\widehat{\mathbf{F}}_{t+\Delta t} = \mathbf{F}_{t+\Delta t} + \mathbf{M}_{t+\Delta t}(a_3u_t + a_4\dot{u}_t + a_5\ddot{u}_t). \tag{36}$$

Initial values for u_0 and $\dot{u}_0$ are set to zero and $\ddot{u}_0$ is given by $\ddot{u}_0 = \mathbf{M}^{-1}(\mathbf{F} - \mathbf{Ku})$.

4. Analytical solution

Because there are few results in tabular form, we developed an analytical solution (see Reddy's book [23]) to compare with the present meshless method.

Table 1
Cross-ply 0/90 square plate $b = a, p = 0, c = \sqrt{n+1}/50$.

$t \times 10^{-4}$	$\bar{w}$		$\bar{\sigma}_{xx}$		$\bar{\sigma}_{xy}$	
	RBF-PS	Analytical	RBF-PS	Analytical	RBF-PS	Analytical
0.5	4.8073×10^{-1}	4.8064×10^{-1}	3.2357×10^{-2}	3.2324×10^{-2}	1.9981×10^{-2}	2.0212×10^{-2}
1.0	1.5466	1.5466	1.0555×10^{-1}	1.0548×10^{-1}	6.4815×10^{-2}	6.5622×10^{-2}
1.5	2.3695	2.3711	1.6224×10^{-1}	1.6219×10^{-1}	9.9505×10^{-2}	1.0081×10^{-1}
2.0	2.3112	2.3157	1.5783×10^{-1}	1.5799×10^{-1}	9.6930×10^{-2}	9.8314×10^{-2}
2.5	1.4182	1.4243	9.6886×10^{-2}	9.7239×10^{-2}	5.9466×10^{-2}	6.0474×10^{-2}
3.0	3.8521×10^{-1}	3.8963×10^{-1}	2.6091×10^{-2}	2.6351×10^{-2}	1.6058×10^{-2}	1.6431×10^{-2}
3.5	1.4196×10^{-2}	1.3614×10^{-2}	4.2258×10^{-4}	3.9694×10^{-4}	3.8897×10^{-4}	3.6027×10^{-4}
4.0	5.9191×10^{-1}	5.8642×10^{-1}	4.0291×10^{-2}	3.9892×10^{-2}	2.4749×10^{-2}	2.4828×10^{-2}
4.5	1.6684	1.6628	1.1396×10^{-1}	1.1345×10^{-1}	6.9972×10^{-2}	7.0585×10^{-2}
5.0	2.4075	2.4076	1.6454×10^{-1}	1.6443×10^{-1}	1.0100×10^{-1}	1.0227×10^{-1}
5.5	2.2358	2.2441	1.5297×10^{-1}	1.5339×10^{-1}	9.3847×10^{-2}	9.5368×10^{-2}
6.0	1.2883	1.3007	8.7862×10^{-2}	8.8614×10^{-2}	5.3982×10^{-2}	5.5159×10^{-2}
6.5	3.0170×10^{-1}	3.0961×10^{-1}	2.0261×10^{-2}	2.0812×10^{-2}	1.2505×10^{-2}	1.3006×10^{-2}
7.0	4.1666×10^{-2}	3.9164×10^{-2}	2.5264×10^{-3}	2.3449×10^{-3}	1.6128×10^{-3}	1.5147×10^{-3}
7.5	7.0901×10^{-1}	6.9775×10^{-1}	4.8142×10^{-2}	4.7327×10^{-2}	2.9625×10^{-2}	2.9502×10^{-2}
8.0	1.7841	1.7733	1.2192×10^{-1}	1.2109×10^{-1}	7.4830×10^{-2}	7.5310×10^{-2}
8.5	2.4318	2.4317	1.6633×10^{-1}	1.6615×10^{-1}	1.0207×10^{-1}	1.0332×10^{-1}
9.0	2.1502	2.1633	1.4695×10^{-1}	1.4772×10^{-1}	9.0208×10^{-2}	9.1881×10^{-2}
9.5	1.1593	1.1777	7.9103×10^{-2}	8.0300×10^{-2}	4.8575×10^{-2}	4.9962×10^{-2}
10	2.2942×10^{-1}	2.3989×10^{-1}	1.5330×10^{-2}	1.6022×10^{-2}	9.4878×10^{-3}	1.0033×10^{-2}

Table 2
Cross-ply 0/90 rectangular plate $b = 2a$, $p = 0, c = \sqrt{n+1}/50$.

$t \times 10^{-4}$	$\bar{w}$		$\bar{\sigma}_{xx}$		$\bar{\sigma}_{xy}$	
	RBF-PS	Analytical	RBF-PS	Analytical	RBF-PS	Analytical
0.5	3.1338×10^{-2}	3.1335×10^{-2}	8.0283×10^{-3}	8.0206×10^{-3}	2.8698×10^{-3}	2.8981×10^{-3}
1.0	1.1271×10^{-1}	1.1271×10^{-1}	2.9284×10^{-2}	2.9261×10^{-2}	1.0308×10^{-2}	1.0413×10^{-2}
1.5	2.1170×10^{-1}	2.1174×10^{-1}	5.5218×10^{-2}	5.5175×10^{-2}	1.9359×10^{-2}	1.9559×10^{-2}
2.0	2.8892×10^{-1}	2.8905×10^{-1}	7.5266×10^{-2}	7.5229×10^{-2}	2.6435×10^{-2}	2.6714×10^{-2}
2.5	3.1367×10^{-1}	3.1393×10^{-1}	8.1757×10^{-2}	8.1754×10^{-2}	2.8688×10^{-2}	2.9000×10^{-2}
3.0	2.7613×10^{-1}	2.7652×10^{-1}	7.2012×10^{-2}	7.2045×10^{-2}	2.5236×10^{-2}	2.5526×10^{-2}
3.5	1.9131×10^{-1}	1.9175×10^{-1}	4.9798×10^{-2}	4.9865×10^{-2}	1.7469×10^{-2}	1.7686×10^{-2}
4.0	9.2967×10^{-2}	9.3357×10^{-2}	2.4165×10^{-2}	2.4252×10^{-2}	8.4548×10^{-3}	8.5733×10^{-3}
4.5	2.0255×10^{-2}	2.0464×10^{-2}	5.2140×10^{-3}	5.2622×10^{-3}	1.7904×10^{-3}	1.8227×10^{-3}
5.0	2.0894×10^{-3}	2.0284×10^{-3}	4.2097×10^{-4}	4.0285×10^{-4}	1.2665×10^{-4}	1.1694×10^{-4}
5.5	4.5635×10^{-2}	4.5328×10^{-2}	1.1817×10^{-2}	1.1735×10^{-2}	4.1054×10^{-3}	4.1115×10^{-3}
6.0	1.3352×10^{-1}	1.3311×10^{-1}	3.4769×10^{-2}	3.4624×10^{-2}	1.2147×10^{-2}	1.2226×10^{-2}
6.5	2.3075×10^{-1}	2.3043×10^{-1}	6.0110×10^{-2}	5.9969×10^{-2}	2.1049×10^{-2}	2.1228×10^{-2}
7.0	2.9864×10^{-1}	2.9860×10^{-1}	7.7852×10^{-2}	7.7780×10^{-2}	2.7257×10^{-2}	2.7528×10^{-2}
7.5	3.1019×10^{-1}	3.1055×10^{-1}	8.0873×10^{-2}	8.0888×10^{-2}	2.8309×10^{-2}	2.8635×10^{-2}
8.0	2.6085×10^{-1}	2.6157×10^{-1}	6.7970×10^{-2}	6.8097×10^{-2}	2.3796×10^{-2}	2.4110×10^{-2}
8.5	1.7031×10^{-1}	1.7118×10^{-1}	4.4360×10^{-2}	4.4553×10^{-2}	1.5507×10^{-2}	1.5751×10^{-2}
9.0	7.4630×10^{-2}	7.5352×10^{-2}	1.9388×10^{-2}	1.9552×10^{-2}	6.7517×10^{-3}	6.8933×10^{-3}
9.5	1.1868×10^{-2}	1.2175×10^{-2}	2.9876×10^{-3}	3.0685×10^{-3}	1.0125×10^{-3}	1.0564×10^{-3}
10	6.9711×10^{-3}	6.7393×10^{-3}	1.7284×10^{-3}	1.6693×10^{-3}	5.6894×10^{-4}	5.5678×10^{-4}

Table 3
Relative error for cross-ply 0/90 square plate $b = a$.

$t \times 10^{-4}$	Relative error (%)		
	$\bar{w}$	$\bar{\sigma}_{xx}$	$\bar{\sigma}_{xy}$
0.5	0.02	0.10	1.16
1.0	0.00	0.07	1.25
1.5	0.07	0.03	1.31
2.0	0.19	0.11	1.43
2.5	0.43	0.36	1.70
3.0	1.13	0.99	2.32
3.5	4.27	6.46	7.38
4.0	0.94	1.00	0.32
4.5	0.34	0.45	0.88
5.0	0.00	0.07	1.25
5.5	0.37	0.28	1.62
6.0	0.95	0.85	2.18
6.5	2.56	2.65	4.00
7.0	6.39	7.74	6.08
7.5	1.61	1.72	0.42
8.0	0.61	0.69	0.64
8.5	0.01	0.11	1.22
9.0	0.60	0.52	1.86
9.5	1.56	1.49	2.85
10	4.36	4.32	5.75

Table 4
Relative error for cross-ply 0/90 rectangular plate $b = 2a$.

$t \times 10^{-4}$	Relative error (%)		
	$\bar{w}$	$\bar{\sigma}_{xx}$	$\bar{\sigma}_{xy}$
0.5	0.01	0.10	0.97
1.0	0.00	0.08	1.00
1.5	0.02	0.08	1.02
2.0	0.04	0.05	1.04
2.5	0.08	0.00	1.08
3.0	0.14	0.05	1.14
3.5	0.23	0.13	1.23
4.0	0.42	0.36	1.38
4.5	1.02	0.92	1.77
5.0	3.01	4.50	8.30
5.5	0.68	0.70	0.15
6.0	0.31	0.42	0.65
6.5	0.14	0.23	0.84
7.0	0.01	0.09	0.99
7.5	0.12	0.02	1.14
8.0	0.27	0.19	1.30
8.5	0.51	0.43	1.55
9.0	0.96	0.84	2.05
9.5	2.52	2.64	4.16
1.0	3.44	3.54	2.18

The analytical solution is computed by assuming a spatial variation of the displacements and reducing the differential equations to a set of differential equations in time (see Reddy's book [23] for details).

The solution of Eq. (31) is assumed to be of the form

$$u(x,y,t) = \sum_{m=1}^{\infty}\sum_{n=1}^{\infty} T_{mn}(t)U_{mn}(x,y). \quad (37)$$

The Navier solution procedure is used to determine the spatial variation and the Newmark method is used to solve the resulting ordinary differential equations in time.

As an example, for a simply supported (SS1-type) cross-ply rectangular plate of length a, b, the boundary conditions are imposed as:

$$\text{in } x = 0, \quad a : v = w = \theta_y = N_x = M_x = 0, \quad (38)$$

$$\text{in } y = 0, \quad b : u = w = \theta_x = N_y = M_y = 0. \quad (39)$$

The boundary conditions in (38) and (39) are satisfied by the following expansions of the displacements (Eq. (37)) and applied load [23]:

$$u_0(x,y,t) = \sum_{n=1}^{\infty}\sum_{m=1}^{\infty} U_{nm}(t)\cos(\alpha x)\sin(\beta y), \quad (40)$$

$$v_0(x,y,t) = \sum_{n=1}^{\infty}\sum_{m=1}^{\infty} V_{nm}(t)\sin(\alpha x)\cos(\beta y), \quad (41)$$

$$w_0(x,y,t) = \sum_{n=1}^{\infty}\sum_{m=1}^{\infty} W_{nm}(t)\sin(\alpha x)\sin(\beta y), \quad (42)$$

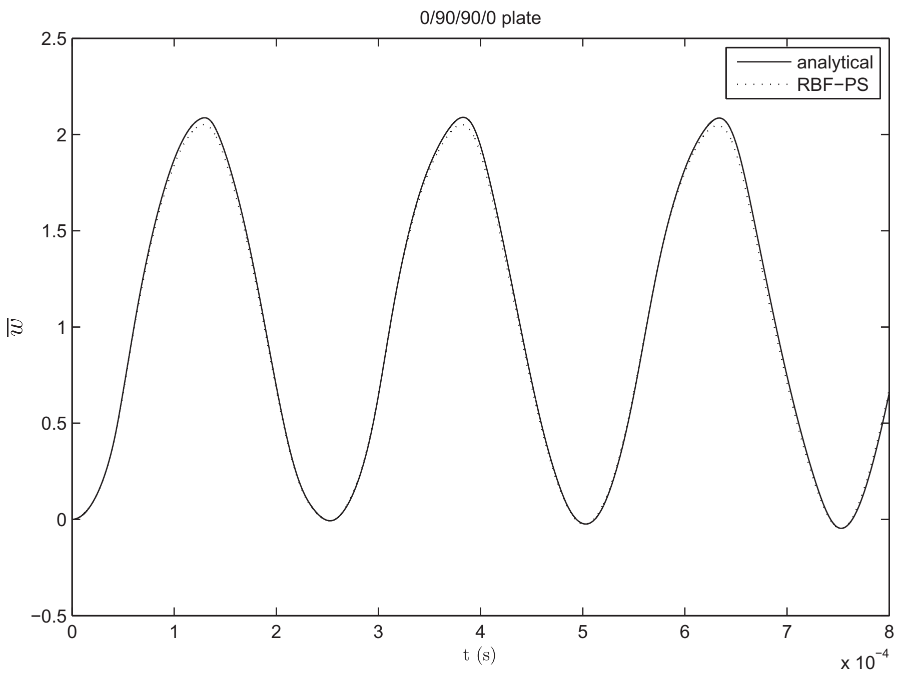

Fig. 2. Present and analytical solutions for central deflection $\bar{w}$ for cross-ply 0/90/90/0 square plate.

$$\theta_x(x,y,t) = \sum_{n=1}^{\infty}\sum_{m=1}^{\infty} \Theta x_{nm}(t)\cos(\alpha x)\sin(\beta y), \tag{43}$$

$$\theta_y(x,y,t) = \sum_{n=1}^{\infty}\sum_{m=1}^{\infty} \Theta y_{nm}(t)\sin(\alpha x)\cos(\beta y), \tag{44}$$

$$q(x,y,t) = \sum_{n=1}^{\infty}\sum_{m=1}^{\infty} Q_{nm}(t)\sin(\alpha x)\sin(\beta y), \tag{45}$$

with

$$\alpha = \frac{m\pi}{a}; \quad \beta = \frac{n\pi}{b}, \tag{46}$$

$$Q_{nm}(t) = \frac{4}{ab}\int_0^a\int_0^b q(x,y,t)\sin\frac{m\pi x}{a}\sin\frac{n\pi y}{b}\,dx\,dy. \tag{47}$$

It should be mentioned that Eqs. (45), (47) represent a Fourier series expansion of the applied load. Substituting Eqs. (40)–(45) in (31) we can write

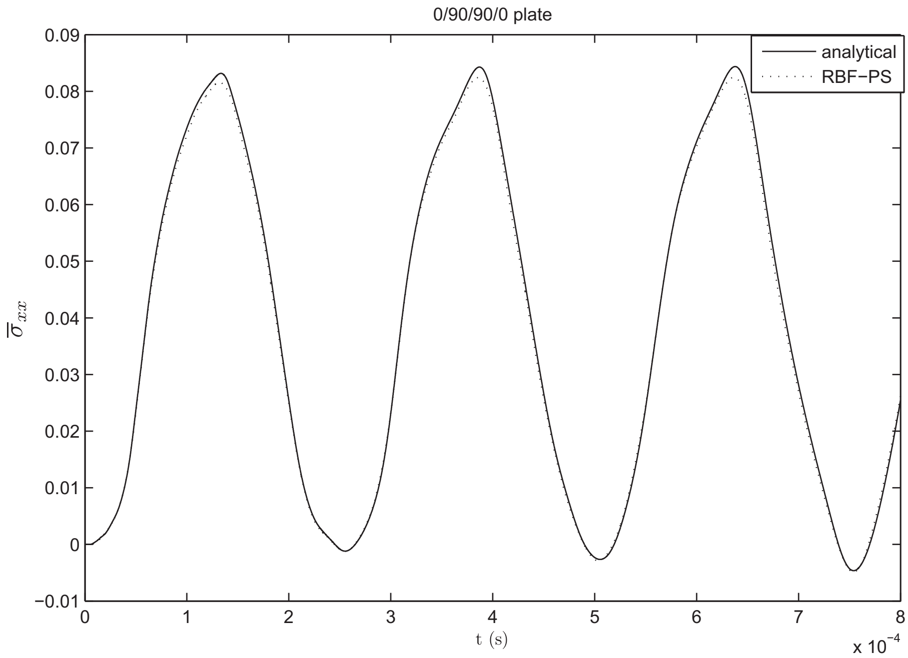

Fig. 3. Present and analytical solutions for in-plane stress $\bar{\sigma}_{xx}$ for cross-ply 0/90/90/0 square plate.

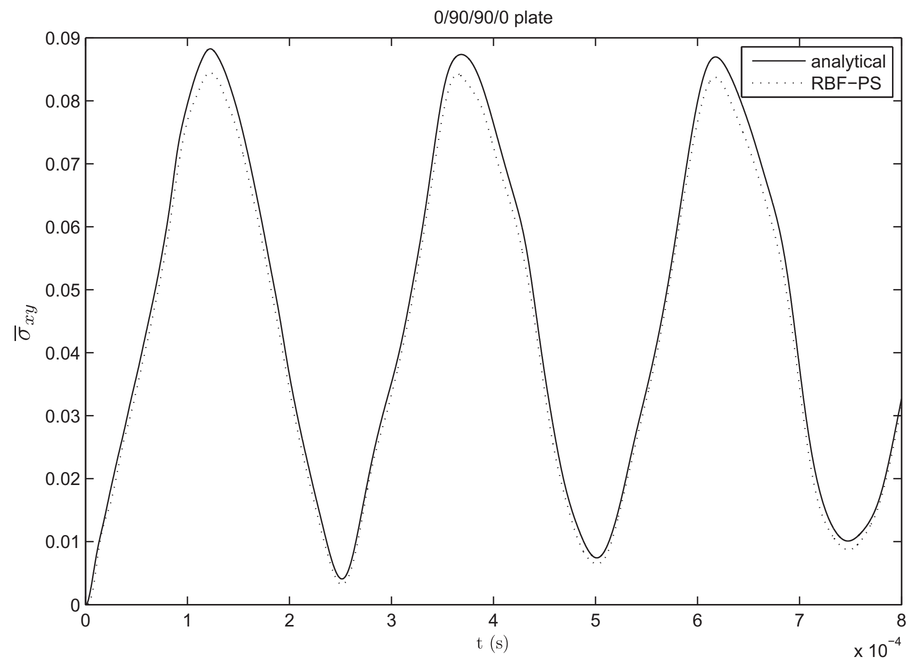

Fig. 4. Present and analytical solutions for in-plane shear stress $\bar{\sigma}_{xy}$ for cross-ply 0/90/90/0 square plate.

$$\mathbf{M}\ddot{\boldsymbol{\Delta}} + \mathbf{K}\boldsymbol{\Delta} = \mathbf{F}, \tag{48}$$

where $\boldsymbol{\Delta} = (\mathbf{U}_{mn}, \mathbf{V}_{mn}, \mathbf{W}_{mn}, \boldsymbol{\Theta}\mathbf{x}_{mn}, \boldsymbol{\Theta}\mathbf{y}_{mn})^T$.

Eq. (48) can then be solved numerically by the Newmark method.

5. Numerical examples

Two examples are presented. We consider simply supported square ($b = a$) and rectangular ($b = 2a$) composite plates with thickness h and length a, b under suddenly applied transverse uniform load ($q_0 = 1$) (see Fig. 1 for basic geometry). A length/thickness ratio of $a/h = 10$ is considered for all plates ($a = 25$).

The material properties for each lamina are given as:

$$E_1 = 25E_2; \quad E_2 = 2.1 \times 10^6; \quad G_{12} = G_{13} = 0.5E_2;$$
$$G_{23} = 0.2E_2; \quad \nu_{12} = 0.25; \quad \rho = 8 \times 10^{-6}.$$

For each example, the analytical Navier and numerical RBF-PS solutions are computed and compared. The number of terms used to

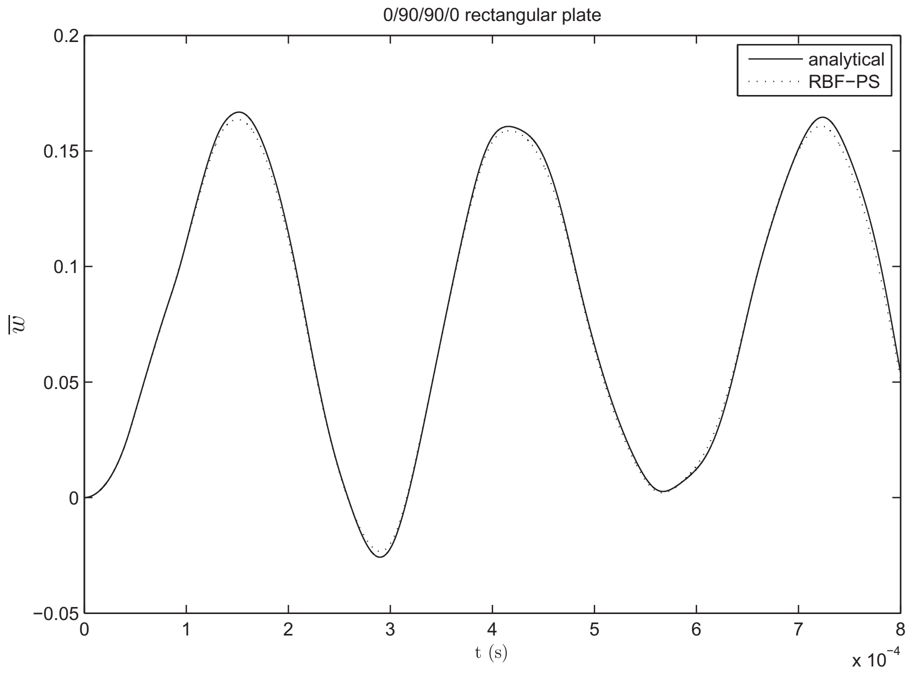

Fig. 5. Present and analytical solutions for central deflection $\bar{w}$ for cross-ply 0/90/90/0 rectangular plate.

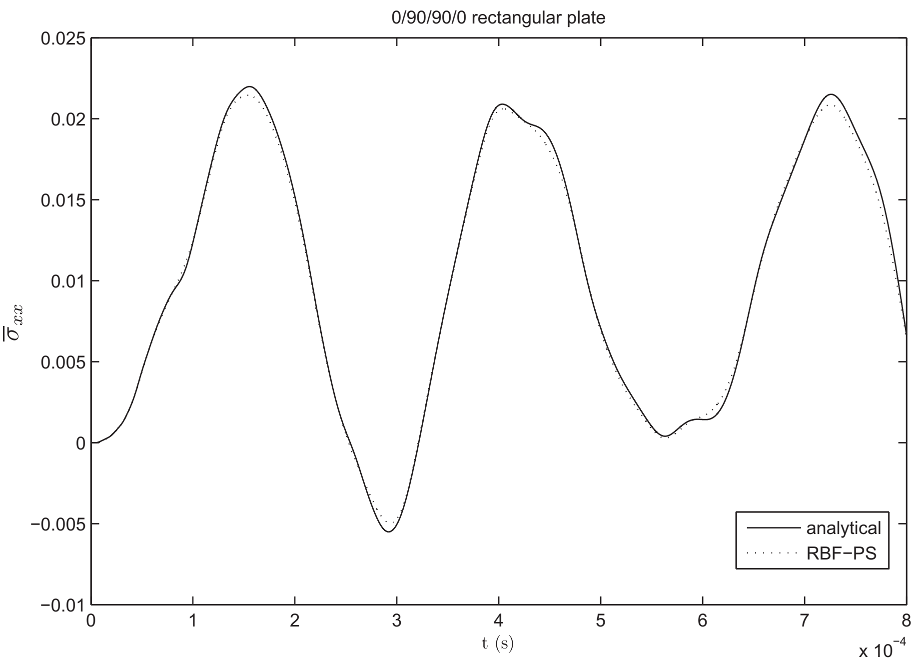

Fig. 6. Present and analytical solutions for in-plane stress $\bar{\sigma}_{xx}$ for cross-ply 0/90/90/0 rectangular plate.

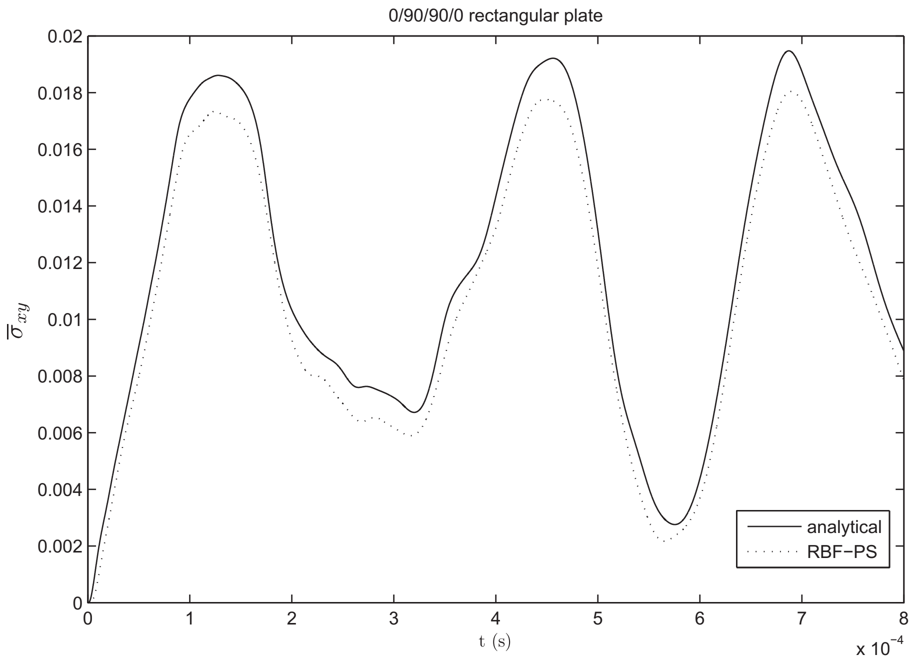

Fig. 7. Present and analytical solutions for in-plane shear stress $\bar{\sigma}_{xy}$ for cross-ply 0/90/90/0 rectangular plate.

find the Navier solutions (in Eqs. (40)–(45)) is set to 35. For the Newmark scheme, initial conditions for displacements Δ and velocities $\dot{\Delta}$ are set to zero, $\alpha = 3/2$, $\gamma = 8/5$ and time step $\Delta t = 10^{-7}$. The time step was selected in order to obtain a stable Navier solution, using the largest possible time step.

The RBF-PS method considers a shape parameter $c = \sqrt{14}/50$. A grid of 13×13 uniformly spaced points is used in all examples.

Results for central deflection and stresses are normalized as:

$$\overline{w}(a/2, b/2) = \frac{w10^2 E_2 h^3}{q_0 b^4};$$
$$\overline{\sigma}_{xx}(a/2, b/2, h/2) = \frac{\sigma_{xx} h^2}{q_0 b^2};$$
$$\overline{\sigma}_{xy}(a, b, -h/2) = \frac{\sigma_{xy} h^2}{q_0 b^2}.$$

5.1. Composite cross-ply *0/90* plate

The transverse central displacement $\bar{w}$, in-plane stress $\bar{\sigma}_{xx}$ and shear in-plane stress $\bar{\sigma}_{xy}$ are listed in Table 1 for a square plate and in Table 2 for a rectangular plate. Relative errors for $\bar{w}, \bar{\sigma}_{xx}$ and $\bar{\sigma}_{xy}$ are presented in Tables 3 and 4 and range from 0.01% to 8%. The results are found to be in very good agreement with the analytical solution. Results are excellent for transverse displacement as well as normal stresses. A reasonable correlation for shear stresses is also found.

5.2. Composite cross-ply *0/90/90/0* plate

Figs. 2–4 and Figs. 5–7 show the plot of numerical (RBF-PS) and analytical (Navier) solutions for transverse central displacement $\bar{w}$, in-plane stress $\bar{\sigma}_{xx}$ and shear in plane stress $\bar{\sigma}_{xy}$ for cross-ply [0/90/90/0] square and rectangular plate, respectively.

Numerical results are in excellent agreement with analytical solutions for central displacement and in-plane stress $\bar{\sigma}_{xx}$. Results for in-plane shear stresses are in good agreement with the analytical solutions. One explanation for this small discrepancy can be due to the in-plane stress being computed at points where degrees of freedom u_0, v_0, θ_x, θ_y are very close to zero, due to imposed boundary conditions. This may produce rounding errors, affecting the final result.

6. Conclusions

For the first time, a combination of radial basis functions and a pseudospectral method was used to study the transient response of composite plates. The Newmark time-integration algorithm was chosen to approximate the ordinary differential equations in time. The shape parameter in the radial basis function was found to be a very important factor in maintaining the stability of the Newmark scheme. Also, the use of a modified radial basis function allowed us to maintain the same shape parameter in square and rectangular domains. Overall, the method provides very accurate solutions for deflections as well as for stresses, and it is simple to implement.

Acknowledgements

The support of Ministério da Ciência Tecnologia e do Ensino superior and Fundo Social Europeu (MCTES and FSE) under programs POPH-QREN are gratefully acknowledged.

References

[1] Kansa EJ. Multiquadrics – A scattered data approximation scheme with applications to computational fluid dynamics. i: Surface approximations and partial derivative estimates. Comput Math Appl 1990;19(8/9):127–45.
[2] Hon YC, Lu MW, Xue WM, Zhu YM. Multiquadric method for the numerical solution of byphasic mixture model. Appl Math Comput 1997;88:153–75.
[3] Hon YC, Cheung KF, Mao XZ, Kansa EJ. A multiquadric solution for the shallow water equation. ASCE J Hydr Engrg 1999;125(5):524–33.
[4] Wang JG, Liu GR, Lin P. Numerical analysis of biot's consolidation process by radial point interpolation method. Int J Solids Struct 2002;39(6):1557–73.
[5] Liu GR, Gu YT. A local radial point interpolation method (lrpim) for free vibration analyses of 2-d solids. J Sound Vib 2001;246(1):29–46.
[6] Liu GR, Wang JG. A point interpolation meshless method based on radial basis functions. Int J Num Meth Engrg 2002;54:1623–48.

[7] Wang JG, Liu GR. On the optimal shape parameters of radial basis functions used for 2-d meshless methods. Comp Meth Appl Mech Engrg 2002;191:2611–30.
[8] Chen XL, Liu GR, Lim SP. An element free galerkin method for the free vibration analysis of composite laminates of complicated shape. Compos Struct 2003;59:279–89.
[9] Dai KY, Liu GR, Lim SP, Chen XL. An element free galerkin method for static and free vibration analysis of shear-deformable laminated composite plates. J Sound Vib 2004;269:633–52.
[10] Liu GR, Chen XL. Buckling of symmetrically laminated composite plates using the element-free galerkin method. Int J Struct Stabil Dyn 2002;2:281–94.
[11] Liew KM, Chen XL, Reddy JN. Mesh-free radial basis function method for buckling analysis of non-uniformity loaded arbitrarily shaped shear deformable plates. Comput Meth Appl Mech Engrg 2004;193:205–25.
[12] Huang YQ, Li QS. Bending and buckling analysis of antisymmetric laminates using the moving least square differential quadrature method. Comput Meth Appl Mech Engrg 2004;193:3471–92.
[13] Liu L, Liu GR, Tan VCB. Element free method for static and free vibration analysis of spatial thin shell structures. Comput Meth Appl Mech Engrg 2002;191:5923–42.
[14] Ferreira AJM. A formulation of the multiquadric radial basis function method for the analysis of laminated composite plates. Compos Struct 2003;59:385–92.
[15] Ferreira AJM. Thick composite beam analysis using a global meshless approximation based on radial basis functions. Mech Adv Mater Struct 2003;10:271–84.
[16] Ferreira AJM, Roque CMC, Martins PALS. Analysis of composite plates using higher-order shear deformation theory and a finite point formulation based on the multiquadric radial basis function method. Composites: Part B 2003;34:627–36.
[17] Ferreira AJM, Roque CMC, Jorge RMN. Modelling cross-ply laminated elastic shells by a higher-order theory and multiquadrics. Comput Struct 2005;83(27):2225–37.
[18] Ferreira AJM, Roque CMC, Jorge RMN. Modelling cross-ply laminated elastic shells by a higher-order theory and multiquadrics. Comput Struct 2006;84(19–20):1288–99.
[19] Ferreira AJM, Fasshauer GE. Analysis of natural frequencies of symmetric composite plates by a rbf-pseudospectral method. Compos Struct 2007;79:202–10.
[20] Reddy JN. Dynamic (transient) analysis of layered anisotropic composite-material plates. Int J Num Meth Engrg 1983;19(2):237–55.
[21] Liu Y, Liew KM, Hon YC, Zhang X. Numerical simulation and analysis of an electroactuated beam using a radial basis function. Smart Mater Struct 2005;14(6):1163–71.
[22] Kirby RM, Yosibash Z. Solution of von-karman dynamic non-linear plate equations using a pseudo-spectral method. Comput Meth Appl Mech Engrg 2004;193(6-8):575–99.
[23] Reddy JN. Mechanics of Laminated Composite Plates and Shells. CRC Press; 2004.
[24] Roque CMC, Ferreira AJM. Numerical experiments on optimal shape parameters for radial basis functions. Num Meth Partial Diff Eqn 2010;26(3):675–89.

3.2.3 Transient analysis of composite and sandwich plates by radial basis functions

C. M. C. Roque, A. J. M. Ferreira, Ana M. A. Neves, C. M. M. Soares, J. N. Reddy, R. M. N. Jorge, Transient analysis of composite and sandwich plates by radial basis functions, Journal of Sandwich Structures and Materials, Volume 13, 2011, pages 681-704.

Original Article

JOURNAL OF SANDWICH STRUCTURES & MATERIALS

Journal of Sandwich Structures and Materials
13(6) 681–704

DOI: 10.1177/1099636211419132
jsm.sagepub.com
SAGE

Transient analysis of composite and sandwich plates by radial basis functions*

C. M. C. Roque[1], A. J. M. Ferreira[2], A. M. A. Neves[2], C. M. M. Soares[3], J. N. Reddy[4] and R. M. N. Jorge[2]

Abstract

This article presents a study of the linear transient response of composite plates using radial basis functions and collocation method. We use the Kansa method and radial basis functions in a pseudo-spectral framework. The first-order and a third-order shear deformation plate theories are used. It is shown that the present method produces highly accurate displacements and stresses when compared with the available results in the literature.

Keywords

meshless methods, plates, sandwich plates, radial basis functions

Introduction

Recently, radial basis functions (RBFs) have enjoyed considerable success as a technique for interpolating data and functions. A radial basis function, $\phi(\|x - x_j\|)$ is a spline that depends on the Euclidian distance between distinct data centers x_j, $j = 1, 2, \ldots, N \in \mathbb{R}^n$, also called nodal or collocation points.

[1]Faculdade de Engenharia da Universidade do Porto, INEGI, Rua Dr. Roberto Frias, 4200-465 Porto, Portugal.
[2]Departamento de Engenharia Mecânica, Faculdade de Engenharia da Universidade do Porto, Rua Dr. Roberto Frias, 4200-465 Porto, Portugal.
[3]Departamento de Engenharia Mecânica, Instituto Superior Técnico, Av. Rovisco Pais, Lisboa, Portugal.
[4]Department of Mechanical Engineering, Texas A&M University, College Station, USA.
*This paper is dedicated to the memory of Professor Vitaly Skvortsov.

Corresponding author:
A. J. M. Ferreira, Departamento de Engenharia Mecânica, Faculdade de Engenharia da Universidade do Porto, Rua Dr. Roberto Frias, 4200-465 Porto, Portugal
Email: ferreira@fe.up.pt

Although most work to date on RBFs relates to scattered data approximation and, in general, to interpolation theory, there has recently been an increased interest in their use for solving partial differential equations (PDEs). This approach, which approximates the complete solution of a PDE directly using RBFs is very attractive due to the fact that this is truly a mesh-free technique. Kansa [1] introduced the concept of solving PDEs using RBFs.

The analysis of plates using the finite element method is now fully established [2]. The use of alternative methods such as the meshless methods based on radial basis functions is attractive due to the absence of a mesh (hence element interfaces where the solution derivatives may be discontinuous) and the ease of using the collocation method. The use of radial basis function for the analysis of structures and materials has been previously studied by numerous authors [3–14]. More recently, the authors have applied RBFs to the static deformations of composite beams, plates and shells [15–19]. A good review on collocation methods using RBFs was given in [20].

The radial basis function collocation method, proposed by Kansa [1], has one small drawback in transient analysis: for every time step, an extra computation is needed to obtain the final solution. To overcome such problem, here we propose the use of radial basis functions in a pseudo-spectral framework, as proposed by Ferreira and Fasshauer [21]. The advantage is that the method produces the direct solution in every time step by solving a linearized system of equations.

For transient analysis, the Newmark time-integration algorithm is used. The Newmark scheme was used by Reddy with a first-order shear deformation theory (FSDT) to analyze the dynamic response of anisotropic composite plates [22]. It was also used by Liu et al. [23] with the radial basis function collocation method to analyze the dynamic behavior of electro-actuated beams and by Kirby and Yosibash [24] with a pseudo-spectral method for the dynamic nonlinear analysis of plates. Because there are few results in tabular form, we independently computed an analytical solution (see Reddy's book [2]) to compare with the present meshless method.

As it will be shown in the examples, the present method yields excellent results when compared with the analytical solutions. This article shows for the first time an application of the RBF-PS method to study the transient response of composite plates in bending.

The radial basis function method

Consider a linear elliptic partial differential operator L and a bounded region Ω in $\mathbb{R}^n$ with some boundary $\partial\Omega$. The static problems aim the computation of displacements (primary variables) ($\boldsymbol{u}$) from the global system of equations

$$L\mathbf{u} = \mathbf{f} \text{ in } \Omega \tag{1}$$

$$L_B\mathbf{u} = \mathbf{g} \text{ on } \partial\Omega \tag{2}$$

where L, L_B are linear operators in the domain and on the boundary, respectively. The right-hand side of (1) and (2) represent the external forces applied on the plate and the boundary conditions applied along the perimeter of the plate, respectively. The PDE problem defined in (1) and (2) will be replaced by a finite problem, defined by an algebraic system of equations, after the radial basis expansions.

The radial basis function (ϕ) approximation of a function ($\boldsymbol{u}$) is given by

$$\widetilde{\mathbf{u}}(\mathbf{x}) = \sum_{i=1}^{N} \alpha_i \phi(\|x - y_i\|_2), \mathbf{x} \in \mathbb{R}^n \tag{3}$$

where y_i, $i = 1,.., N$ is a finite set of distinct points (centers) in $\mathbb{R}^n$. The coefficients α_i are chosen so that $\tilde{\mathbf{u}}$ satisfies some boundary conditions. The most common RBFs are

$$\begin{array}{ll} \phi(r) = r^3, & \text{cubic} \\ \phi(r) = r^2 \log(r), & \text{thin plate splines} \\ \phi(r) = (1-r)_+^m p(r), & \text{Wendland functions} \\ \phi(r) = e^{-(cr)^2}, & \text{Gaussian} \\ \phi(r) = \sqrt{c^2 + r^2}, & \text{Multiquadrics} \\ \phi(r) = (c^2 + r^2)^{-1/2}, & \text{Inverse Multiquadrics} \end{array}$$

where the Euclidian distance r is real and non-negative and c is a shape parameter, a positive constant. In the following, the radial basis functions used were both the multiquadric and the inverse multiquadric functions.

Solution of the interpolation problem

Hardy [25] introduced multiquadrics in the analysis of scattered geographical data. In the 1990s, Kansa [1] used multiquadrics for the solution of partial differential equations.

Considering N distinct interpolations, and knowing $u(x_j)$, $j = 1, 2,\ldots, N$, we find α_i by the solution of a $N \times N$ linear system

$$\mathbf{A}\underline{\alpha} = \mathbf{u} \tag{4}$$

where $\mathbf{A} = [\phi\ (\|x - y_i\|_2)]_{N\times N}$, $\underline{\alpha} = [\alpha_1, \alpha_2,\ldots, \alpha_N]^T$ and $\mathbf{u} = [u(x_1), u(x_2),\ldots, u(x_N)]^T$. The RBF interpolation matrix A is positive definite for some RBFs [26], but in general provides ill-conditioned systems.

Solution of the static problem

The solution of a static problem by radial basis functions considers N_I nodes in the domain and N_B nodes on the boundary, with total number of nodes $N = N_I + N_B$. We denote the sampling points by $x_i \in \Omega$, $i = 1,\ldots, N_I$ and $x_i \in \partial\Omega$, $i = N_I + 1,\ldots, N$. At the domain points, we solve the following system of equations

$$\sum_{i=1}^{N} \alpha_i L\phi(\|x - y_i\|_2) = \mathbf{f}(x_j), \quad j = 1, 2, \ldots, , N_I \tag{5}$$

or

$$\mathcal{L}^I \underline{\alpha} = \mathbf{F} \tag{6}$$

where

$$\mathcal{L}^I = [L\phi(\|x - y_i\|_2)]_{N_I \times N} \tag{7}$$

For the boundary conditions, we have

$$\sum_{i=1}^{N} \alpha_i \mathcal{L}_B \phi(\|x - y_i\|_2) = \mathbf{g}(x_j), \quad j = N_I + 1, \ldots,, N \tag{8}$$

or

$$\mathbf{B}\underline{\alpha} = \mathbf{G} \tag{9}$$

Therefore, we can write a finite-dimensional static problem as

$$\begin{bmatrix} \mathcal{L}^I \\ \mathbf{B} \end{bmatrix} \underline{\alpha} = \begin{bmatrix} \mathbf{F} \\ \mathbf{G} \end{bmatrix} \tag{10}$$

where

$$\mathcal{L}^I = L\phi\big[\big(\|x_{N_I} - y_j\|_2\big)\big]_{N_I \times N}, \mathbf{B} = \mathcal{L}_B\phi\big[\big(\|x_{N_I+1} - y_j\|_2\big)\big]_{N_B \times N}$$

By inverting the system (10), we obtain the vector of $\underline{\alpha}$. We then proceed to the solution by the interpolation equation (3).

The RBF-pseudospectral method

Pseudo-spectral (PS) methods (see [27] for an introduction to the subject) are known as highly accurate solvers for PDEs. Generally speaking, one represents the spatial part of the approximate solution of a given PDE by a linear combination of certain smooth basis functions (i, j represents the N grid points)

$$u^h(x_i) = \sum_{j=1}^{N} \alpha_j \phi_j(x_i), i = 1, \ldots,, N \tag{11}$$

or in matrix–vector notation

$$\mathbf{u} = \mathbf{A}\alpha \tag{12}$$

where $A(i, j) = \phi(i, j)$. Applying linear operator $\mathcal{L}$ to equation (11), we obtain

$$\mathbf{u}_{\mathcal{L}} = \mathbf{A}_{\mathcal{L}}\alpha \tag{13}$$

with $\alpha = [\alpha_1, \ldots, \alpha_x]$ and $A_{\mathcal{L}} = \mathcal{L}\phi_j(x_i)$. Solving Equation (12) for α and substituting in Equation (13), we can write

$$\mathbf{u}_{\mathcal{L}} = \mathbf{A}_{\mathcal{L}}\mathbf{A}^{-1}\mathbf{u} \equiv \mathbf{D}_{\mathcal{L}}\mathbf{u} \tag{14}$$

The derivatives of 14 are easily computed. For example,

$$\mathbf{u}' = \mathbf{A_x}\alpha = \mathbf{D_x}\mathbf{u} \tag{15}$$

with $A_x = \frac{d}{dx}\phi_j(x_i)$. In the case of a boundary value problem with linear operator $\mathcal{L}$ applied on the domain and operator $\mathcal{L}_B$ applied on boundary points, the system of equations to be solved can be organized as follows:

$$\begin{bmatrix} (D_{\mathcal{L}})_{N_k \times N} \\ (D_{\mathcal{L}_B})_{N_b \times N} \end{bmatrix} \begin{bmatrix} \mathbf{u} \end{bmatrix} = \begin{bmatrix} f_k \\ q_b \end{bmatrix} \tag{16}$$

where N_k and N_b are domain and boundary nodes and f_k, q_b are external conditions in domain and boundary, respectively (see [21] for more details). In (16), $D_{\mathcal{L}}$, $D_{\mathcal{L}_B}$ represent the derivative matrices obtained from (14) and (15).

Traditionally, polynomial basis functions are used. In this article, however, we will use both multiquadric and inverse multiquadric functions. For rectangular plates, we change the functions to accommodate the ratio a/b. The inverse multiquadric function is then given by:

$$\phi_j(x_i) = \Phi(r) = \left[1 + c^2\left((x_i - x_j)^2 + \frac{(y_i - y_j)^2}{(b/a)^2}\right)\right]^{-1} \tag{17}$$

where r is the euclidian norm between grid points of coordinates (x, y), a, b the length of the plate along x and y axis, respectively, and c a (positive) shape parameter. The shape parameter is user defined and works as a fine tuner for some radial basis functions. It should be mentioned that the RBF function is modified to accommodate the a/b ratio. This is not seen elsewhere in the literature and proved to be more accurate than the usual inverse multi-quadric functions, in our computations.

Third-order plate theory of Reddy

Equations of motion and boundary conditions

Consider a rectangular plate of planform dimensions a and b and thickness h (Figure 1). The coordinate system is taken such that the xy-plane coincides with the midplane of the plate, and the origin of the coordinate system is taken at the lower left corner of the plate. The plate is composed of uniform thickness layers of orthotropic material.

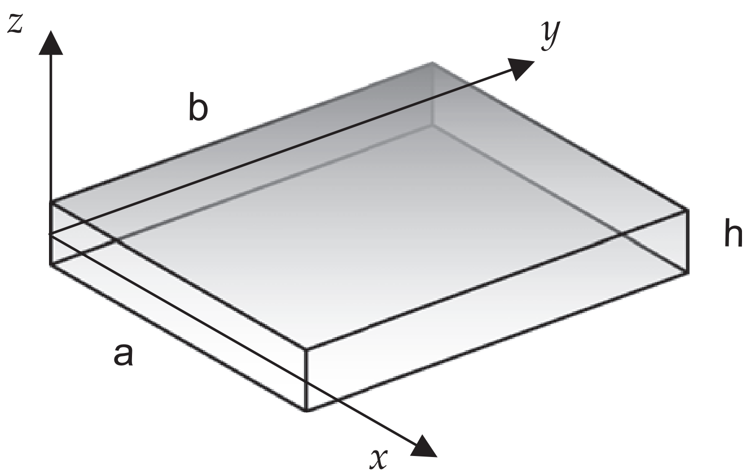

Figure 1. Composite plate of thickness *h*, lengths *a*, *b*, and reference axes *xyz*.

Following the third-order theory of Reddy [2,28,29], the following displacement field is chosen, which satisfies the stress-free boundary conditions on the top and bottom surfaces of the plate and gives parabolic distribution of transverse shear strains through the plate thickness:

$$u = u_0 + z\left[\theta_x - \frac{4}{3}\left(\frac{z}{h}\right)^2\left(\theta_x + \frac{\partial w}{\partial x}\right)\right] \tag{18}$$

$$v = v_0 + z\left[\theta_y - \frac{4}{3}\left(\frac{z}{h}\right)^2\left(\theta_y + \frac{\partial w}{\partial y}\right)\right] \tag{19}$$

$$w = w_0 \tag{20}$$

Note that the first-order theory can be fully recovered in the following, just by setting $c_1 = -\frac{4}{3}\left(\frac{z}{h}\right)^2 = 0$.

The infinitesimal strains associated with the displacement field are

$$\epsilon_1 \equiv \epsilon_{11} = \epsilon_1^0 + z\left(k_1^0 + z^2 k_1^2\right);\ \epsilon_2 \equiv \epsilon_{22} = \epsilon_2^0 + z\left(k_2^0 + z^2 k_2^2\right);\ \epsilon_3 \equiv \epsilon_{33} = 0; \tag{21}$$

$$\epsilon_4 \equiv 2\epsilon_{23} = \epsilon_4^0 + z^2 k_4^2;\ \epsilon_5 \equiv 2\epsilon_{13} = \epsilon_5^0 + z^2 k_5^2; \tag{22}$$

$$\epsilon_6 \equiv 2\epsilon_{12} = \epsilon_6^0 + z\left(k_6^0 + z^2 k_6^2\right), \tag{23}$$

where

$$\epsilon_1^0 = \frac{\partial u_0}{\partial x};\quad k_1^0 = \frac{\partial \theta_x}{\partial x};\quad k_1^2 = -\left(\frac{4}{3h^2}\right)\left(\frac{\partial \theta_x}{\partial x} + \frac{\partial^2 w}{\partial x^2}\right); \tag{24}$$

$$\epsilon_2^0 = \frac{\partial v_0}{\partial y};\quad k_2^0 = \frac{\partial \theta_y}{\partial y};\quad k_2^2 = -\left(\frac{4}{3h^2}\right)\left(\frac{\partial \theta_y}{\partial y} + \frac{\partial^2 w}{\partial y^2}\right); \tag{25}$$

$$\epsilon_4^0 = \theta_y + \frac{\partial w}{\partial y}; \quad k_4^2 = -\left(\frac{4}{h^2}\right)\left(\theta_y + \frac{\partial w}{\partial y}\right); \tag{26}$$

$$\epsilon_5^0 = \theta_x + \frac{\partial w}{\partial x}; \quad k_5^2 = -\left(\frac{4}{h^2}\right)\left(\theta_x + \frac{\partial w}{\partial x}\right); \tag{27}$$

$$\epsilon_6^0 = \frac{\partial u_0}{\partial y} + \frac{\partial v_0}{\partial x}; \quad k_6^0 = \frac{\partial \theta_x}{\partial y} + \frac{\partial \theta_y}{\partial x}; \tag{28}$$

$$k_6^2 = -\left(\frac{4}{3h^2}\right)\left(\frac{\partial \theta_x}{\partial y} + \frac{\partial \theta_y}{\partial x} + 2\frac{\partial^2 w}{\partial x \partial y}\right) \tag{29}$$

The constitutive equations of an orthotropic layer, in material axes, are given by

$$\begin{Bmatrix} \sigma_1 \\ \sigma_2 \\ \sigma_6 \end{Bmatrix} = \begin{bmatrix} Q_{11} & Q_{12} & 0 \\ Q_{12} & Q_{22} & 0 \\ 0 & 0 & Q_{66} \end{bmatrix} \begin{Bmatrix} \epsilon_1 \\ \epsilon_2 \\ \epsilon_6 \end{Bmatrix}, \quad \begin{Bmatrix} \sigma_4 \\ \sigma_5 \end{Bmatrix} = \begin{bmatrix} Q_{44} & 0 \\ 0 & Q_{55} \end{bmatrix} \begin{Bmatrix} \epsilon_4 \\ \epsilon_5 \end{Bmatrix} \tag{30}$$

where Q_{ij} are the plane-stress reduced elastic constants (due to $\varepsilon_3 = 0$) in the material axes of the plate [2]

$$Q_{11} = \frac{E_1}{1 - \nu_{12}\nu_{21}}, \quad Q_{12} = \nu_{21}\frac{E_1}{1 - \nu_{12}\nu_{21}}, \quad Q_{22} = \frac{E_2}{1 - \nu_{12}\nu_{21}}, \tag{31}$$

$$Q_{44} = KG_{23}, \quad Q_{55} = KG_{13}, \quad Q_{66} = G_{12} \tag{32}$$

The third-order plate theory does not use shear correction factors (K); therefore, we set $K = 1$. In the first-order shear theory, we use $K = 5/6$ for isotropic or monolithic laminates. For sandwich or generic laminates, the FSDT needs a procedure for the computation of shear correction factors. This will be dealt later in the paper.

The equations of motion for this theory were derived by Reddy [28–30] using Hamilton's principle. They are repeated here for ready reference

$$\delta u_0: \quad \frac{\partial N_1}{\partial x} + \frac{\partial N_6}{\partial y} = I_1 \ddot{u}_0 + \bar{I}_2 \ddot{\theta}_x - \frac{4}{3h^2} I_4 \frac{\partial \ddot{w}_0}{\partial x}, \tag{33}$$

$$\delta v_0: \quad \frac{\partial N_6}{\partial x} + \frac{\partial N_2}{\partial y} = I_1 \ddot{v}_0 + \bar{I}_2 \ddot{\theta}_y - \frac{4}{3h^2} I_4 \frac{\partial \ddot{w}_0}{\partial y}, \tag{34}$$

$$\delta w_0: \quad \frac{\partial Q_1}{\partial x} + \frac{\partial Q_2}{\partial y} + \left(\frac{\partial}{\partial x}\right)\left(\bar{N}_{xx}\frac{\partial w}{\partial x}\right) + \left(\frac{\partial}{\partial y}\right)\left(\bar{N}_{yy}\frac{\partial w}{\partial y} + 2\left(\frac{\partial}{\partial x}\right)\left(\bar{N}_{xy}\frac{\partial w}{\partial y}\right)\right) \tag{35}$$

$$+ q - \frac{4}{h^2}\left(\frac{\partial R_1}{\partial x} + \frac{\partial R_2}{\partial y}\right) + \frac{4}{3h^2}\left(\frac{\partial^2 P_1}{\partial x^2} + 2\frac{\partial^2 P_6}{\partial x \partial y} + \frac{\partial^2 P_2}{\partial y^2}\right) \tag{36}$$
$$= I_1 \ddot{w}_0 - \left(\frac{4}{3h^2}\right)^2 I_7 \left(\frac{\partial^2 \ddot{w}_0}{\partial x^2} + \frac{\partial^2 \ddot{w}_0}{\partial y^2}\right) + \left(\frac{4}{3h^2}\right) I_4 \left(\frac{\partial \ddot{u}_0}{\partial x} + \frac{\partial \ddot{v}_0}{\partial y}\right)$$
$$+ \left(\frac{4}{3h^2}\right) \bar{I}_5 \left(\frac{\partial \ddot{\theta}_x}{\partial x} + \frac{\partial \ddot{\theta}_y}{\partial y}\right),$$

$$\delta\theta_x : \quad \frac{\partial M_1}{\partial x} + \frac{\partial M_6}{\partial y} - Q_1 + \left(\frac{4}{h^2}\right) R_1 - \left(\frac{4}{3h^2}\right)\left(\frac{\partial P_1}{\partial x} + \frac{\partial P_6}{\partial y}\right)$$
$$= \bar{I}_2 \ddot{u}_0 + \bar{I}_3 \ddot{\theta}_x - \frac{4}{3h^2} \bar{I}_5 \frac{\partial \ddot{w}_0}{\partial x}, \tag{37}$$

$$\delta\theta_y : \quad \frac{\partial M_6}{\partial x} + \frac{\partial M_2}{\partial y} - Q_2 + \left(\frac{4}{h^2}\right) R_2 - \left(\frac{4}{3h^2}\right)\left(\frac{\partial P_6}{\partial x} + \frac{\partial P_2}{\partial y}\right)$$
$$= \bar{I}_2 \ddot{v}_0 + \bar{I}_3 \ddot{\theta}_y - \frac{4}{3h^2} \bar{I}_5 \frac{\partial \ddot{w}_0}{\partial y} \tag{38}$$

$$\bar{I}_2 = I_2 - \frac{4}{3h^2} I_4, \quad \bar{I}_5 = I_5 - \frac{4}{3h^2} I_7, \quad \bar{I}_3 = I_3 - \frac{8}{3h^2} I_5 + \frac{16}{9h^4} I_7 \tag{39}$$

The stress resultants N_i, M_i, P_i, Q_i, and R_i are defined by

$$(N_i, M_i, P_i) = \int_{-h/2}^{h/2} \sigma_i\left(1, z, z^3\right) dz, \quad (i = 1, 2, 6), \tag{40}$$

$$(Q_2, R_2) = \int_{-h/2}^{h/2} \sigma_4\left(1, z^2\right) dz, \quad (Q_1, R_1) = \int_{-h/2}^{h/2} \sigma_5\left(1, z^2\right) dz, \tag{41}$$

and the inertias I_i (i = 1, 2, 3, 4, 5, 7) by

$$(I_1, I_2, I_3, I_4, I_5, I_7) = \int_{-h/2}^{h/2} \rho\left(1, z, z^2, z^3, z^4, z^6\right) dz \tag{42}$$

ρ being the material density. An interesting feature of this higher order (HSDT) theory is that it considers the same number of degrees of freedom as in the FSDT. In equation (33), $\bar{N}_{xx}$, $\bar{N}_{yy}$, and $\bar{N}_{xy}$ denote the in-plane loads perpendicular to the edges $x = 0$ and $y = 0$, and in-plane shear buckling loads, respectively. For free vibrations, one sets $\bar{N}_{xx} = \bar{N}_{yy} = \bar{N}_{xy} = 0$, and for buckling analysis one sets all inertial terms to zero.

The stress resultants defined in Equation (40) can be related to the total strains in Equation (21) by the following equations [2]:

$$\left\{\begin{array}{c}\left\{\begin{array}{c}N_1\\N_2\\N_6\end{array}\right\}\\\left\{\begin{array}{c}M_1\\M_2\\M_6\end{array}\right\}\\\left\{\begin{array}{c}P_1\\P_2\\P_6\end{array}\right\}\end{array}\right\}=\left[\begin{array}{ccc}\begin{bmatrix}A_{11}&A_{12}&A_{16}\\&A_{22}&A_{26}\\symm.&&A_{66}\end{bmatrix}&\begin{bmatrix}B_{11}&B_{12}&B_{16}\\&B_{22}&B_{26}\\symm.&&B_{66}\end{bmatrix}&\begin{bmatrix}E_{11}&E_{12}&E_{16}\\&E_{22}&E_{26}\\symm.&&E_{66}\end{bmatrix}\\&\begin{bmatrix}D_{11}&D_{12}&D_{16}\\&D_{22}&D_{26}\\symm.&&D_{66}\end{bmatrix}&\begin{bmatrix}F_{11}&F_{12}&F_{16}\\&F_{22}&F_{26}\\symm.&&F_{66}\end{bmatrix}\\symmetric&&\begin{bmatrix}H_{11}&H_{12}&H_{16}\\&H_{22}&H_{26}\\symm.&&H_{66}\end{bmatrix}\end{array}\right]\left\{\begin{array}{c}\left\{\begin{array}{c}\epsilon_1^0\\\epsilon_2^0\\\epsilon_6^0\end{array}\right\}\\\left\{\begin{array}{c}k_1^0\\k_2^0\\k_6^0\end{array}\right\}\\\left\{\begin{array}{c}k_1^2\\k_2^2\\k_6^2\end{array}\right\}\end{array}\right\} \tag{43}$$

$$\left\{\begin{array}{c}\left\{\begin{array}{c}Q_2\\Q_1\end{array}\right\}\\\left\{\begin{array}{c}R_2\\R_1\end{array}\right\}\end{array}\right\}=\left[\begin{array}{cc}\begin{bmatrix}A_{44}&A_{45}\\A_{45}&A_{55}\end{bmatrix}&\begin{bmatrix}D_{44}&D_{45}\\D_{45}&D_{55}\end{bmatrix}\\symm.&\begin{bmatrix}F_{45}&F_{45}\\F_{45}&F_{55}\end{bmatrix}\end{array}\right]\left\{\begin{array}{c}\left\{\begin{array}{c}\epsilon_4^0\\\epsilon_5^0\end{array}\right\}\\\left\{\begin{array}{c}k_4^2\\k_5^2\end{array}\right\}\end{array}\right\} \tag{44}$$

Here, A_{ij}, B_{ij}, etc., denote the plate stiffnesses

$$\begin{aligned}&\left(A_{ij},B_{ij},D_{ij},E_{ij},F_{ij},H_{ij}\right)=\int_{-h/2}^{h/2}\bar{Q}_{ij}\left(1,z,z^2,z^3,z^4,z^6\right)dz \quad (i,j=1,2,6),\\&\left(A_{ij},D_{ij},F_{ij}\right)=\int_{-h/2}^{h/2}\bar{Q}_{ij}\left(1,z^2,z^4\right)dz \quad (i,j=4,5),\end{aligned} \tag{45}$$

where $\bar{Q}_{ij}$ are the transformed elastic stiffness coefficients.

Shear correction factors

In case one wishes to use the FSDT, the shear correction factors should be computed for a general laminate. At layer interfaces, continuity of transverse shear stresses is required, for laminates with distinct materials across the thickness direction. According to the FSDT assumptions, the transverse shear deformation is constant through the thickness, which is a coarse approximation to the actual variation even for a homogeneous cross-section. For homogeneous cross-sections, the shear deformation is commonly accepted to be a parabolic function of z. Therefore, a shear correction factor k must be introduced to approximate on an average basis the transverse deformation energy. Assuming a heterogeneous plate free of tangential tractions, the equilibrium equation in the x direction can be expressed as

$$\frac{\partial \sigma_x}{\partial x} + \frac{\partial \tau_{xy}}{\partial y} + \frac{\partial \tau_{xz}}{\partial z} = 0 \tag{46}$$

Assuming, for simplicity, cylindrical bending, then

$$\tau_{xz} = -\int_{-h/2}^{z} \frac{\partial \sigma_x}{\partial x} \mathrm{d}z = -\int_{-h/2}^{z} \frac{\partial M_x}{\partial x} \frac{D_1(z)}{R_1} z\mathrm{d}z = -\frac{Q_x}{R_1}\int_{-h/2}^{z} D_1(z)z\mathrm{d}z = \frac{Q_x}{R_1} g(z) \tag{47}$$

where Q_x is the shear force on the xz plane; $R_1 = \int_{-h/2}^{h/2} D_1(z)z^2\mathrm{d}z$ the flexural plate stiffness in the x direction; z the coordinate through the thickness; $g(z) = -\int_{-h/2}^{z} D_1(z)z\mathrm{d}z$ is the shear shape function.

The function $g(z)$ that shapes the shear stress diagram is independent of loadings, becoming the well-known parabolic function $g(z) = [D_1\mathrm{h}^2/8][1 - 4(z/h)^2]$ for the case of a homogeneous cross-section. The strain energy component is given as

$$w_s = \int_{-h/2}^{h/2} \frac{\tau_{xz}^2}{G_{13}(z)} \mathrm{d}z = \frac{Q_x^2}{R_1^2}\int_{-h/2}^{h/2} \frac{g^2(z)}{G_{13}(z)} \mathrm{d}z \tag{48}$$

where $G_{13}(z)$ is the shear modulus, variable through the thickness, in the xz plane. The strain energy component, under the assumption of constant shear strain, is given as

$$\overline{w}_s = \int_{-h/2}^{h/2} \overline{\gamma}_{xz} G_{13}(z) \overline{\gamma}_{xz} \mathrm{d}z = \frac{Q_x^2}{h^2\overline{G}_1^2} h\overline{G}_1 = \frac{Q_x^2}{h\overline{G}_1} \tag{49}$$

where

$$h\overline{G}_1 = \int_{-h/2}^{h/2} G_{13}(z)\mathrm{d}z \tag{50}$$

and $\overline{\gamma}_{xz}$ is the mean value of the shear strains. Therefore, it is now possible to evaluate the correction factor k_1 in the xz plane to be

$$k_1 = \frac{\overline{w}_s}{w_s} = \frac{R_1^2}{h\overline{G}_1 \displaystyle\int_{-h/2}^{h/2} g^2(z)/G_{13}(z)\mathrm{d}z} \tag{51}$$

For k_2, we proceed the same way. This can be applied to symmetric or non-symmetric cross-sections. Here, we use the same correction factor ($k = k_1 = k_2$).

For numerical implementation, all integrals are replaced by summation over the layer thicknesses in the case of composite laminated structures with different material layers.

Numerical time integration

In this article, the Newmark method is used [2] for the numerical time integration. The resulting system of equations of motion (33) can be written in the form:

$$M\ddot{u} + Ku = F \tag{52}$$

Time derivatives in Equation (52) are approximated using Taylor's series

$$\ddot{u}_{t+\Delta t} = a_3(u_{t+\Delta t} - u_t) - a_4\dot{u}_t - a_5\ddot{u}_t \tag{53}$$

$$\dot{u}_{t+\Delta t} = \dot{u}_t + a_1\ddot{u}_t + a_2\ddot{u}_{t+\Delta t} \tag{54}$$

with $a_1 = (1-\alpha)\Delta t$; $a_2 = \alpha\Delta t$; $a_3 = \frac{2}{\gamma(\Delta t)^2}$; $a_4 = a_3\Delta t$; $a_5 = \frac{1-\gamma}{\gamma}$

Substituting equations (53), (54) in equation (52), the later can be written as:

$$\hat{K}u = \hat{F} \tag{55}$$

with

$$\hat{K}_{t+\Delta t} = K_{t+\Delta t} + a_3 M_{t+\Delta t} \tag{56}$$

$$\hat{F}_{t+\Delta t} = F_{t+\Delta t} + M_{t+\Delta t}(a_3 u_t + a_4\dot{u}_t + a_5\ddot{u}_t) \tag{57}$$

Initial values for u_0 and $\dot{u}_0$ are set to zero and $\ddot{u}_0$ is given by $\ddot{u}_0 = M^{-1}(F - Ku)$.

Analytical solution

Because there are few results in tabular form, we implemented an analytical solution (see Reddy's book [2]) to compare with the present meshless method.

The analytical solution is computed by assuming a spacial variation of the displacements and reducing the differential equations to a set of differential equations in time (see Reddy's book [2] for details).

The solution of Equation (52) is assumed to be of the form

$$u(x, y, t) = \sum_{m=1}^{\infty}\sum_{n=1}^{\infty} T_{mn}(t)U_{mn}(x, y) \tag{58}$$

The Navier solution procedure is used to determine the spatial variation and the Newmark method is used to solve the resulting ordinary differential equations in time.

As an example, for a simply supported cross-ply rectangular plate of lengths a and b, the boundary conditions are imposed as:

$$\text{in } x = 0, a : v = w = \theta_y = N_x = M_x = 0 \tag{59}$$

$$\text{in } y = 0, b : u = w = \theta_x = N_y = M_y = 0 \tag{60}$$

The boundary conditions in (59) and (60) are satisfied by the following expansions of the displacements and applied load [2]:

$$u_0(x, y, t) = \sum_{n=1}^{\infty}\sum_{m=1}^{\infty} U_{nm}(t)\cos(\alpha x)\sin(\beta y) \tag{61}$$

$$v_0(x, y, t) = \sum_{n=1}^{\infty}\sum_{m=1}^{\infty} V_{nm}(t)\sin(\alpha x)\cos(\beta y) \tag{62}$$

$$w_0(x, y, t) = \sum_{n=1}^{\infty}\sum_{m=1}^{\infty} W_{nm}(t)\sin(\alpha x)\sin(\beta y) \tag{63}$$

$$\theta_x(x, y, t) = \sum_{n=1}^{\infty}\sum_{m=1}^{\infty} \Theta x_{nm}(t)\cos(\alpha x)\sin(\beta y) \tag{64}$$

$$\theta_y(x, y, t) = \sum_{n=1}^{\infty}\sum_{m=1}^{\infty} \Theta y_{nm}(t)\sin(\alpha x)\cos(\beta y) \tag{65}$$

$$q(x, y, t) = \sum_{n=1}^{\infty}\sum_{m=1}^{\infty} Q_{nm}(t)\sin(\alpha x)\sin(\beta y) \tag{66}$$

with

$$\alpha = \frac{m\pi}{a};\ \beta = \frac{n\pi}{b} \tag{67}$$

$$Q_{nm}(t) = \frac{4}{ab}\int_0^a \int_0^b q(x, y, t)\sin\frac{m\pi x}{a}\sin\frac{n\pi y}{b}\,\mathrm{d}x\,\mathrm{d}y \tag{68}$$

Substituting Equations (61)–(66) in (52), we can write

$$\mathbf{M}\ddot{\Delta} + \mathbf{K}\Delta = \mathbf{F} \tag{69}$$

where $\Delta = (U_{mn}, V_{mn}, W_{mn}, \Theta x_{mn}, \Theta y_{mn})^T$, and $\mathbf{M}$, $\mathbf{K}$ are the mass and stiffness matrices, respectively. The source vector is denoted by $\mathbf{F}$. Equation (69) can then be solved numerically by the Newmark method.

Numerical examples

Three examples are presented (cross-ply 0/90, 0/90/90/0 and sandwich plates). ($b = 2a$) composite plates with thickness h and length a, b under suddenly applied transverse uniform load ($q_0 = 1$) for cross-ply plates and uniform and sinusoidal load for sandwich plates.

The RBF-PS method is used with the inverse multiquadric to model the cross-ply plates and Kansa's unsymmetrical version with multiquadrics is used to model sandwich plates.

For each example, the analytical Navier and numerical RBF-PS solutions are computed and compared. The number of terms used to find the Navier solutions (in Equations (61)–(66)) is set to 35. For the Newmark scheme, initial conditions for displacements Δ and velocities $\dot{\Delta}$ are set to zero, $\alpha = 3/2$, $\gamma = 8/5$ and time step $\Delta t = 10^{-7}$ for cross-ply plates and $\Delta t = 10^{-3}$ for sandwich plates. The time step was selected in order to obtain a stable Navier solution, using the largest possible time step.

For cross-ply plates, a length-to-thickness ratio of $a/h = 10$ is considered ($a = 25$). Also, the material properties for each lamina are given as:

$$E_1 = 25E_2;\ E_2 = 2.1 \times 10^6;\ G_{12} = G_{13} = 0.5E_2;$$
$$G_{23} = 0.2E_2;\ \nu_{12} = 0.25;\ \rho = 8 \times 10^{-6}$$

Composite cross-ply 0/90 plate

The RBF-PS method considers a shape parameter $c = \sqrt{14}/50$. A grid of 13×13 uniformly spaced points is used in all examples. Results for central deflection and stresses are normalized as:

$$\overline{w}_{(a/2,\,b/2)} = w10^2(E_2h^3)/q_0b^4;$$
$$\overline{\sigma}_{xx(a/2,\,b/2,\,h/2)} = \sigma_{xx}h^2/(q_0b^2);$$
$$\overline{\sigma}_{xy(a,\,b,\,-h/2)} = \sigma_{xy}h^2/(q_0b^2);$$

The transverse central displacement $\overline{w}$, in-plane stress $\overline{\sigma}_{xx}$ and shear in-plane stress $\overline{\sigma}_{xy}$ are listed in Table 1 for a square plate and in Table 2 for a rectangular plate. Relative errors for $\overline{w}$, $\overline{\sigma}_{xx}$ and $\overline{\sigma}_{xy}$ are presented in Tables 3 and 4 and range from 0.01% to 8%. The results are found to be in very good agreement with the analytical solution. Results are excellent for transverse displacement as well as normal stresses. A reasonable correlation for shear stresses is also found.

Table 1. Cross-ply 0/90 square plate $b = a$, $p = 0$, $c = \sqrt{n+1}/50$.

$t \times 10^{-4}$	$\overline{w}$		$\overline{\sigma}_{xx}$		$\overline{\sigma}_{xy}$	
	RBF-PS	Analytical	RBF-PS	Analytical	RBF-PS	Analytical
0.5	4.8073×10^{-1}	4.8064×10^{-1}	3.2357×10^{-2}	3.2324×10^{-2}	1.9981×10^{-2}	2.0212×10^{-2}
1.0	1.5466	1.5466	1.0555×10^{-1}	1.0548×10^{-1}	6.4815×10^{-2}	6.5622×10^{-2}
1.5	2.3695	2.3711	1.6224×10^{-1}	1.6219×10^{-1}	9.9505×10^{-2}	1.0081×10^{-1}
2.0	2.3112	2.3157	1.5783×10^{-1}	1.5799×10^{-1}	9.6930×10^{-2}	9.8314×10^{-2}
2.5	1.4182	1.4243	9.6886×10^{-2}	9.7239×10^{-2}	5.9466×10^{-2}	6.0474×10^{-2}
3.0	3.8521×10^{-1}	3.8963×10^{-1}	2.6091×10^{-2}	2.6351×10^{-2}	1.6058×10^{-2}	1.6431×10^{-2}
3.5	1.4196×10^{-2}	1.3614×10^{-2}	4.2258×10^{-4}	3.9694×10^{-4}	3.8897×10^{-4}	3.6027×10^{-4}
4.0	5.9191×10^{-1}	5.8642×10^{-1}	4.0291×10^{-2}	3.9892×10^{-2}	2.4749×10^{-2}	2.4828×10^{-2}
4.5	1.6684	1.6628	1.1396×10^{-1}	1.1345×10^{-1}	6.9972×10^{-2}	7.0585×10^{-2}
5.0	2.4075	2.4076	1.6454×10^{-1}	1.6443×10^{-1}	1.0100×10^{-1}	1.0227×10^{-1}
5.5	2.2358	2.2441	1.5297×10^{-1}	1.5339×10^{-1}	9.3847×10^{-2}	9.5368×10^{-2}
6.0	1.2883	1.3007	8.7862×10^{-2}	8.8614×10^{-2}	5.3982×10^{-2}	5.5159×10^{-2}
6.5	3.0170×10^{-1}	3.0961×10^{-1}	2.0261×10^{-2}	2.0812×10^{-2}	1.2505×10^{-2}	1.3006×10^{-2}
7.0	4.1666×10^{-2}	3.9164×10^{-2}	2.5264×10^{-3}	2.3449×10^{-3}	1.6128×10^{-3}	1.5147×10^{-3}
7.5	7.0901×10^{-1}	6.9775×10^{-1}	4.8142×10^{-2}	4.7327×10^{-2}	2.9625×10^{-2}	2.9502×10^{-2}
8.0	1.7841	1.7733	1.2192×10^{-1}	1.2109×10^{-1}	7.4830×10^{-2}	7.5310×10^{-2}
8.5	2.4318	2.4317	1.6633×10^{-1}	1.6615×10^{-1}	1.0207×10^{-1}	1.0332×10^{-1}
9.0	2.1502	2.1633	1.4695×10^{-1}	1.4772×10^{-1}	9.0208×10^{-2}	9.1881×10^{-2}
9.5	1.1593	1.1777	7.9103×10^{-2}	8.0300×10^{-2}	4.8575×10^{-2}	4.9962×10^{-2}
10	2.2942×10^{-1}	2.3989×10^{-1}	1.5330×10^{-2}	1.6022×10^{-2}	9.4878×10^{-3}	1.0033×10^{-2}

Table 2. Cross-ply 0/90 rectangular plate $b = 2a$ $p = 0$, $c = \sqrt{n+1}/50$.

$t \times 10^{-4}$	$\overline{w}$ RBF-PS	$\overline{w}$ Analytical	$\overline{\sigma}_{xx}$ RBF-PS	$\overline{\sigma}_{xx}$ Analytical	$\overline{\sigma}_{xy}$ RBF-PS	$\overline{\sigma}_{xy}$ Analytical
0.5	3.1338×10^{-2}	3.1335×10^{-2}	8.0283×10^{-3}	8.0206×10^{-3}	2.8698×10^{-3}	2.8981×10^{-3}
1.0	1.1271×10^{-1}	1.1271×10^{-1}	2.9284×10^{-2}	2.9261×10^{-2}	1.0308×10^{-2}	1.0413×10^{-2}
1.5	2.1170×10^{-1}	2.1174×10^{-1}	5.5218×10^{-2}	5.5175×10^{-2}	1.9359×10^{-2}	1.9559×10^{-2}
2.0	2.8892×10^{-1}	2.8905×10^{-1}	7.5266×10^{-2}	7.5229×10^{-2}	2.6435×10^{-2}	2.6714×10^{-2}
2.5	3.1367×10^{-1}	3.1393×10^{-1}	8.1757×10^{-2}	8.1754×10^{-2}	2.8688×10^{-2}	2.9000×10^{-2}
3.0	2.7613×10^{-1}	2.7652×10^{-1}	7.2012×10^{-2}	7.2045×10^{-2}	2.5236×10^{-2}	2.5526×10^{-2}
3.5	1.9131×10^{-1}	1.9175×10^{-1}	4.9798×10^{-2}	4.9865×10^{-2}	1.7469×10^{-2}	1.7686×10^{-2}
4.0	9.2967×10^{-2}	9.3357×10^{-2}	2.4165×10^{-2}	2.4252×10^{-2}	8.4548×10^{-3}	8.5733×10^{-3}
4.5	2.0255×10^{-2}	2.0464×10^{-2}	5.2140×10^{-3}	5.2622×10^{-3}	1.7904×10^{-3}	1.8227×10^{-3}
5.0	2.0894×10^{-3}	2.0284×10^{-3}	4.2097×10^{-4}	4.0285×10^{-4}	1.2665×10^{-4}	1.1694×10^{-4}
5.5	4.5635×10^{-2}	4.5328×10^{-2}	1.1817×10^{-2}	1.1735×10^{-2}	4.1054×10^{-3}	4.1115×10^{-3}
6.0	1.3352×10^{-1}	1.3311×10^{-1}	3.4769×10^{-2}	3.4624×10^{-2}	1.2147×10^{-2}	1.2226×10^{-2}
6.5	2.3075×10^{-1}	2.3043×10^{-1}	6.0110×10^{-2}	5.9969×10^{-2}	2.1049×10^{-2}	2.1228×10^{-2}
7.0	2.9864×10^{-1}	2.9860×10^{-1}	7.7852×10^{-2}	7.7780×10^{-2}	2.7257×10^{-2}	2.7528×10^{-2}
7.5	3.1019×10^{-1}	3.1055×10^{-1}	8.0873×10^{-2}	8.0888×10^{-2}	2.8309×10^{-2}	2.8635×10^{-2}
8.0	2.6085×10^{-1}	2.6157×10^{-1}	6.7970×10^{-2}	6.8097×10^{-2}	2.3796×10^{-2}	2.4110×10^{-2}
8.5	1.7031×10^{-1}	1.7118×10^{-1}	4.4360×10^{-2}	4.4553×10^{-2}	1.5507×10^{-2}	1.5751×10^{-2}
9.0	7.4630×10^{-2}	7.5352×10^{-2}	1.9388×10^{-2}	1.9552×10^{-2}	6.7517×10^{-3}	6.8933×10^{-3}
9.5	1.1868×10^{-2}	1.2175×10^{-2}	2.9876×10^{-3}	3.0685×10^{-3}	1.0125×10^{-3}	1.0564×10^{-3}
10	6.9711×10^{-3}	6.7393×10^{-3}	1.7284×10^{-3}	1.6693×10^{-3}	5.6894×10^{-4}	5.5678×10^{-4}

Table 3. Relative error for cross-ply 0/90 square plate $b = a$.

	Relative error (%)		
$t \times 10^{-4}$	$\overline{w}$	$\overline{\sigma}_{xx}$	$\overline{\sigma}_{xy}$
0.5	0.02	0.10	1.16
1.0	0.00	0.07	1.25
1.5	0.07	0.03	1.31
2.0	0.19	0.11	1.43
2.5	0.43	0.36	1.70
3.0	1.13	0.99	2.32
3.5	4.27	6.46	7.38
4.0	0.94	1.00	0.32
4.5	0.34	0.45	0.88
5.0	0.00	0.07	1.25
5.5	0.37	0.28	1.62
6.0	0.95	0.85	2.18
6.5	2.56	2.65	4.00
7.0	6.39	7.74	6.08
7.5	1.61	1.72	0.42
8.0	0.61	0.69	0.64
8.5	0.01	0.11	1.22
9.0	0.60	0.52	1.86
9.5	1.56	1.49	2.85
10	4.36	4.32	5.75

Composite cross-ply 0/90/90/0 plate

The RBF-PS method considers a shape parameter $c = \sqrt{14}/50$. A grid of 13×13 uniformly spaced points is used in all examples. Results for central deflection and stresses are normalized as:

$$\overline{w}_{(a/2,\,b/2)} = w10^2(E_2h^3)/q_0b^4;$$
$$\overline{\sigma}_{xx(a/2,\,b/2,\,h/2)} = \sigma_{xx}h^2/(q_0b^2);$$
$$\overline{\sigma}_{xy(a,\,b,\,-h/2)} = \sigma_{xy}h^2/(q_0b^2);$$

Figures 2–4 and 5–7 show the plot of numerical (RBF-PS) and analytical (Navier) solutions for transverse central displacement $\overline{w}$, in plane stress $\overline{\sigma}_{xx}$ and shear in plane stress $\overline{\sigma}_{xy}$ for cross-ply [0/90/90/0] square and rectangular plate, respectively.

Numerical results are in excellent agreement with analytical solutions for central displacement and in-plane stress $\overline{\sigma}_{xx}$. Results for in-plane shear stresses are in good agreement with the analytical solutions. One explanation for this small discrepancy

Table 4. Relative error for cross-ply 0/90 rectangular plate $b = 2a$.

$t \times 10^{-4}$	Relative error (%)		
	$\overline{w}$	$\overline{\sigma}_{xx}$	$\overline{\sigma}_{xy}$
0.5	0.01	0.10	0.97
1.0	0.00	0.08	1.00
1.5	0.02	0.08	1.02
2.0	0.04	0.05	1.04
2.5	0.08	0.00	1.08
3.0	0.14	0.05	1.14
3.5	0.23	0.13	1.23
4.0	0.42	0.36	1.38
4.5	1.02	0.92	1.77
5.0	3.01	4.50	8.30
5.5	0.68	0.70	0.15
6.0	0.31	0.42	0.65
6.5	0.14	0.23	0.84
7.0	0.01	0.09	0.99
7.5	0.12	0.02	1.14
8.0	0.27	0.19	1.30
8.5	0.51	0.43	1.55
9.0	0.96	0.84	2.05
9.5	2.52	2.64	4.16
1.0	3.44	3.54	2.18

can be due to the in-plane stress being computed at points, where degrees of freedom u_0, v_0, θ_x, θ_y are very close to zero, due to imposed boundary conditions. This may produce rounding errors, affecting the final result.

Three-layer square sandwich plate

A simply supported sandwich square plate, under uniform and sinusoidal transverse load is considered. The material properties of the sandwich core are expressed in the stiffness matrix, $\overline{Q}_{core}$ as:

$$\overline{Q}_{core} = \begin{bmatrix} 0.999781 & 0.231192 & 0 & 0 & 0 \\ 0.231192 & 0.524886 & 0 & 0 & 0 \\ 0 & 0 & 0.262931 & 0 & 0 \\ 0 & 0 & 0 & 0.266810 & 0 \\ 0 & 0 & 0 & 0 & 0.159914 \end{bmatrix}$$

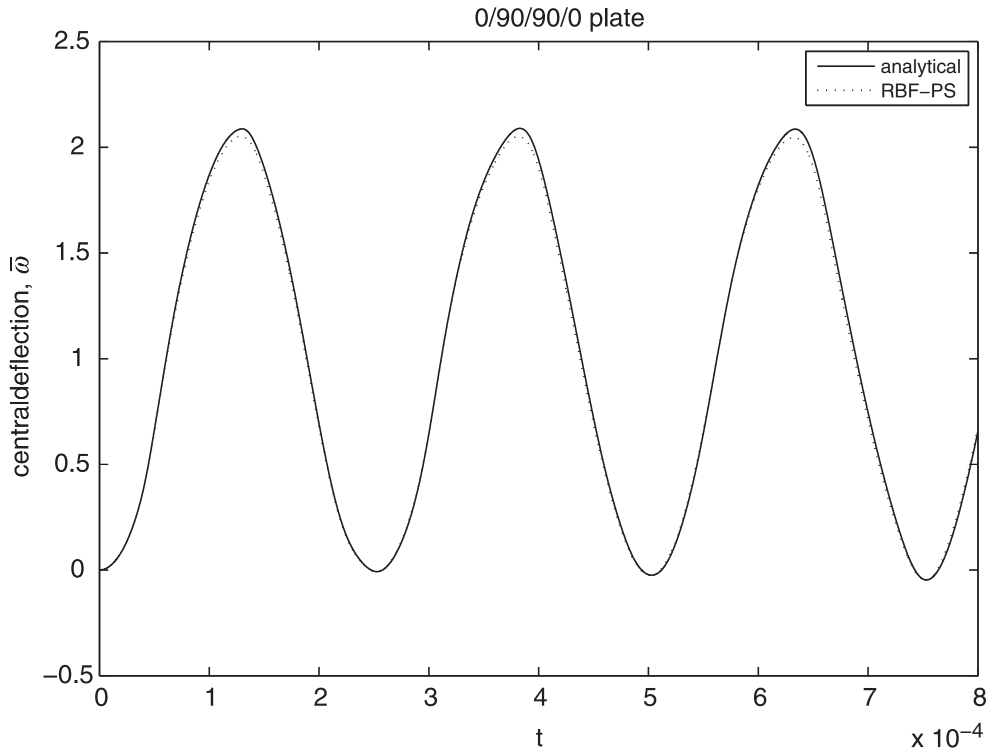

Figure 2. Present and analytical solutions for central deflection $\overline{w}$ for cross-ply 0/90/90/0 square plate.

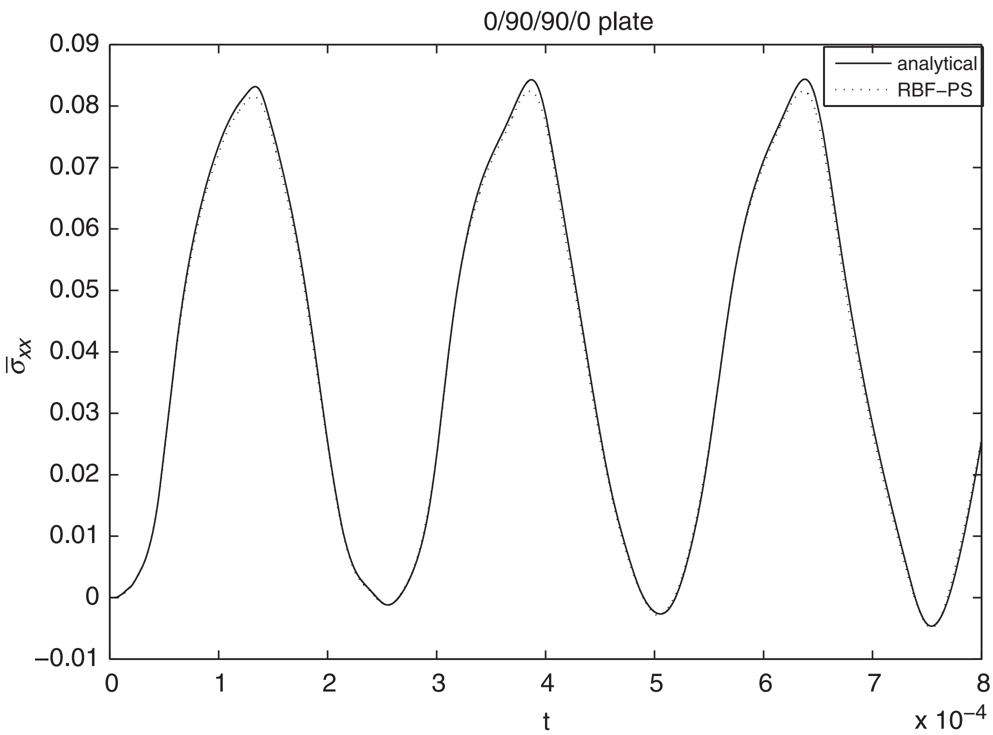

Figure 3. Present and analytical solutions for in-plane stress $\overline{\sigma}_{xx}$ for cross-ply 0/90/90/0 square plate.

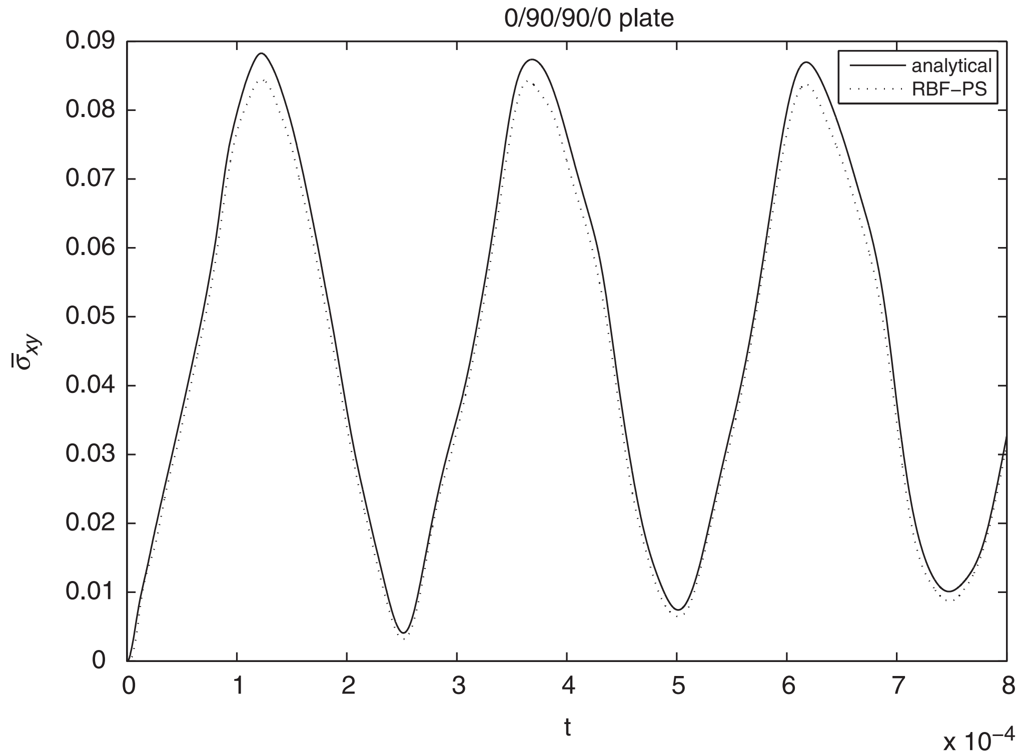

Figure 4. Present and analytical solutions for in-plane shear stress $\bar{\sigma}_{xy}$ for cross-ply 0/90/90/0 square plate.

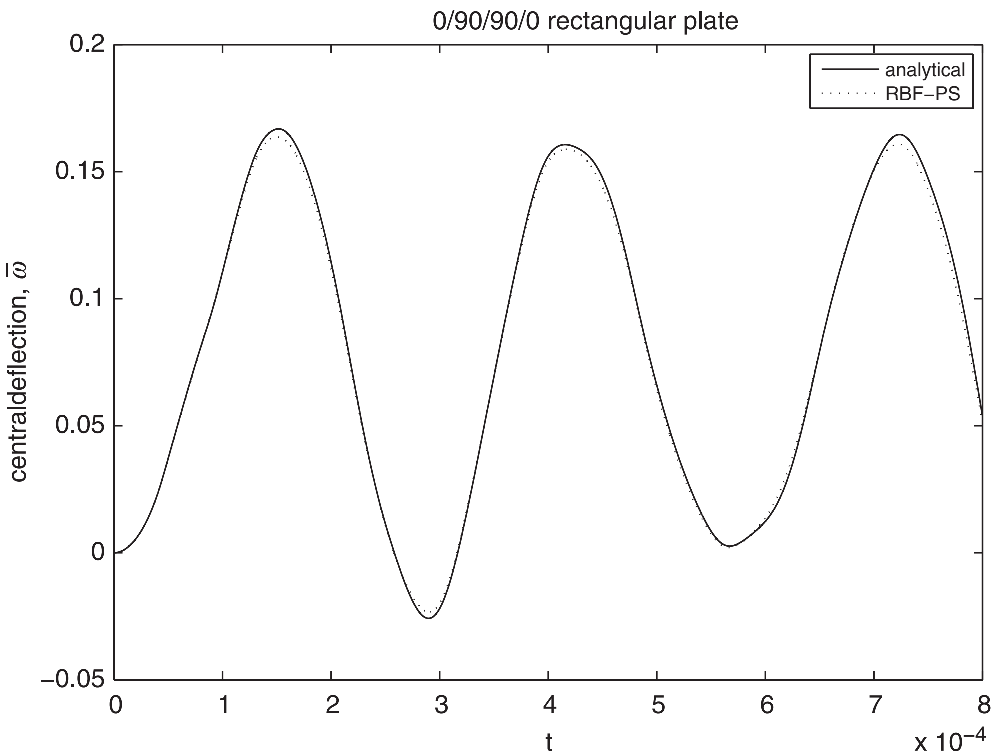

Figure 5. Present and analytical solutions for central deflection $\overline{w}$ for cross-ply 0/90/90/0 rectangular plate.

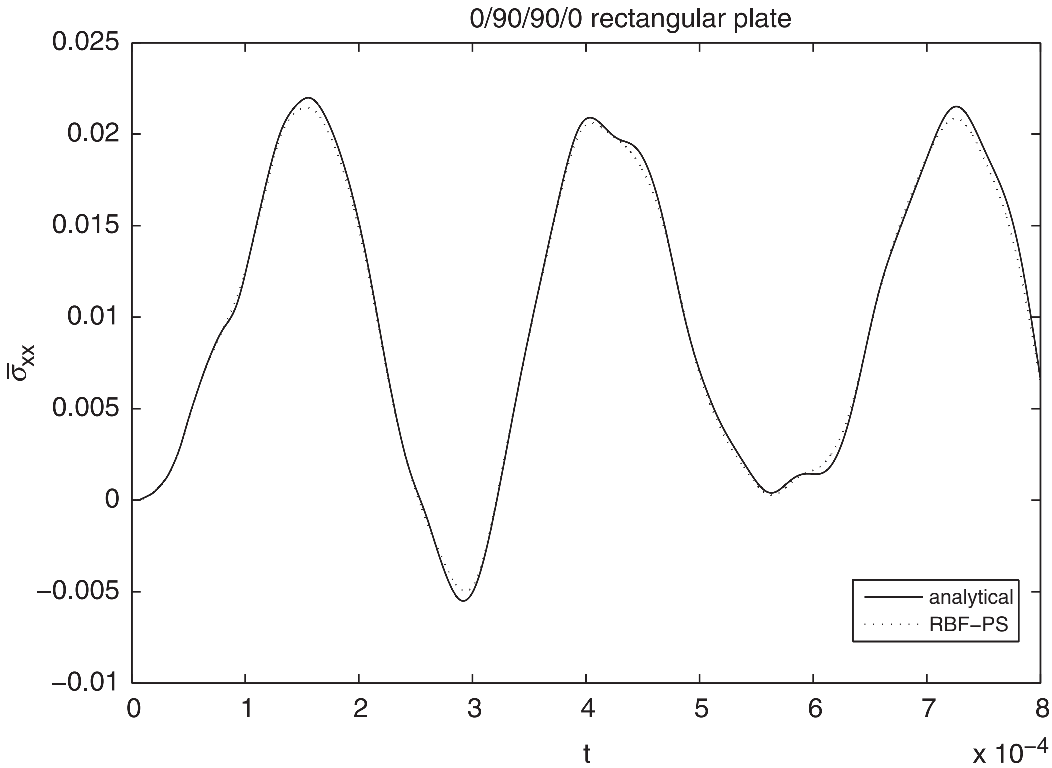

Figure 6. Present and analytical solutions for in-plane stress $\overline{\sigma}_{xx}$ for cross-ply 0/90/90/0 rectangular plate.

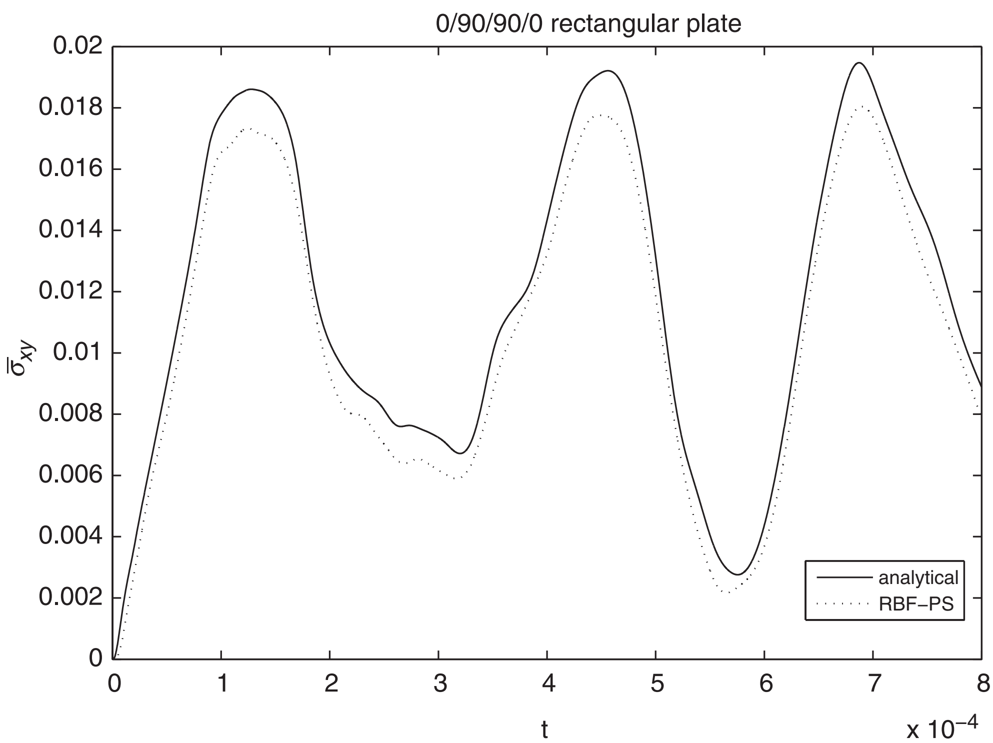

Figure 7. Present and analytical solutions for in-plane shear stress $\overline{\sigma}_{xy}$ for cross-ply 0/90/90/0 rectangular plate.

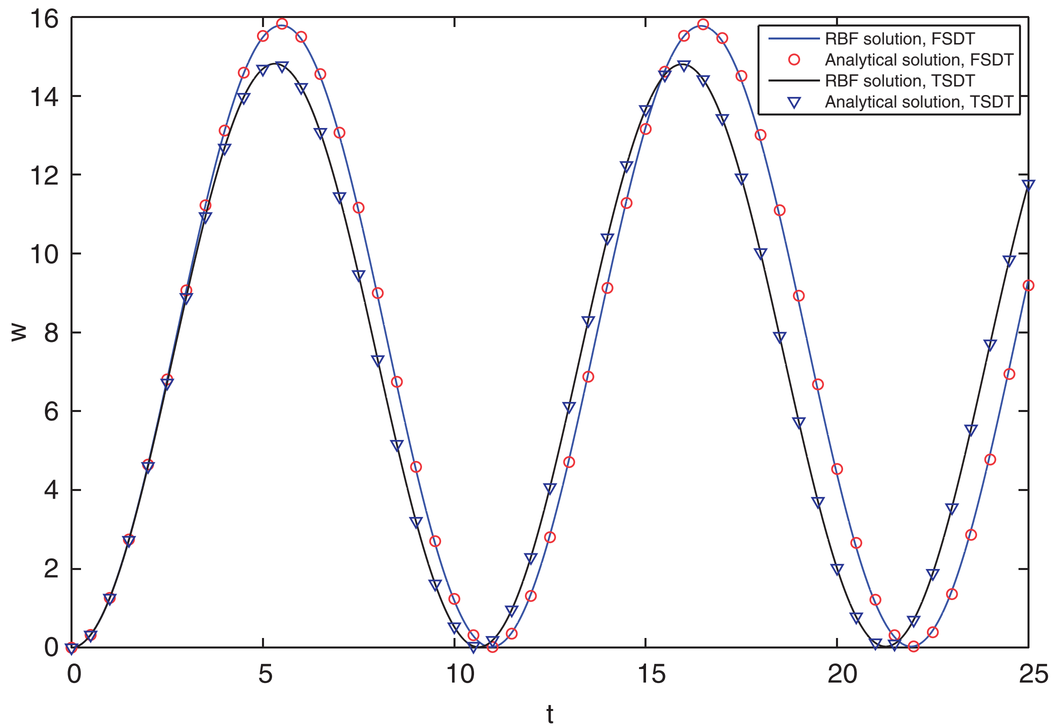

Figure 8. Sandwich plate under sinusoidal load.

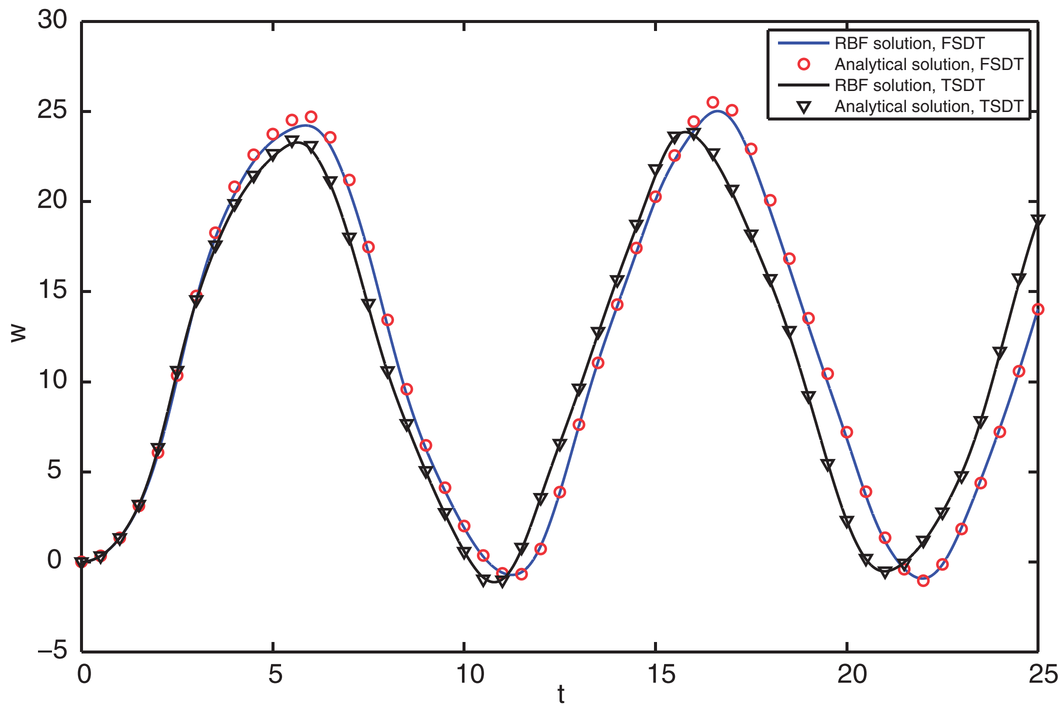

Figure 9. Sandwich plate under uniform load.

and $\rho_{core} = 1$. The skins material properties are related with the core properties by $R = 15$:

$$\overline{Q}_{skin} = R\overline{Q}_{core};\ \rho_{skin} = R\rho_{core}$$

For all sandwich plates, time step for Newmark iteration algorithm is $\Delta t = 10^{-3}$. Unlike the previous examples, where we used the RBF formulation in a pseudo-spectral framework, here we use the RBF formulation in Kansa's unsymmetrical version, with the multiquadric function with $c = 2/\sqrt{n}$.

First- and third-order shear deformation plate theories are used to study the transient analysis of sandwich plates. The third-order shear deformation theory (TSDT) does not need shear correction factors. For FSDT, a shear correction factor of $k = 0.2625$ is used. Figures 8 and 9 show the evolution of central deflection, w with time t. RBF and analytical (Navier) solutions are plotted for comparison. It can be seen an excellent correlation between Navier solutions and the solutions of the present meshless formulation.

Conclusions

In this article, we presented a transient analysis of composite and sandwich plates using radial basis functions and collocation method. Two collocations techniques were used: the Kansa's unsymmetrical collocation and radial basis functions on a pseudospectral framework. Both approaches provide identical results. However, the use of RBF-PS method is computationally less expensive, as it does not need the interpolation of displacements at each time step. The Newmark time-integration algorithm was chosen to approximate the ordinary differential equations in time. The first-order and the third-order shear deformation plate theories were used.

The shape parameter in the radial basis function was found to be a very important factor in maintaining the stability of the Newmark scheme. Also, the use of a modified radial basis function allowed us to maintain the same shape parameter in square and rectangular domains. Overall, both methods provide very accurate solutions for deflections as well as for stresses, and it is simple to implement.

Acknowledgment

The support of under programs POPH-QREN are gratefully acknowledged.

Funding

This work was supported by Ministério da Ciência Tecnologia e do Ensino superior and Fundo Social Europeu (MCTES and FSE).

References

1. Kansa EJ. Multiquadrics- a scattered data approximation scheme with applications to computational fluid dynamics. i: Surface approximations and partial derivative estimates. *Comput Math Appl* 1990; 19(8/9): 127–145.

2. Reddy JN. *Mechanics of laminated composite plates and shells*. Boca Raton, FL: CRC Press, 2004.
3. Hon YC, Lu MW, Xue WM and Zhu YM. Multiquadric method for the numerical solution of biphasic mixture model. *Appl Math Comput* 1997; 88: 153–175.
4. Hon YC, Cheung KF, Mao XZ and Kansa EJ. A multiquadric solution for the shallow water equation. *ASCE J Hydr Eng* 1999; 125(5): 524–533.
5. Wang JG, Liu GR and Lin P. Numerical analysis of biot's consolidation process by radial point interpolation method. *Int J Solids Struct* 2002; 39(6): 1557–1573.
6. Liu GR and Gu YT. A local radial point interpolation method (lrpim) for free vibration analyses of 2-d solids. *J Sound Vib* 2001; 246(1): 29–46.
7. Liu GR and Wang JG. A point interpolation meshless method based on radial basis functions. *Int J Numer Methods Eng* 2002; 54: 1623–1648.
8. Wang JG and Liu GR. On the optimal shape parameters of radial basis functions used for 2-d meshless methods. *Comp Meth Appl Mech Eng* 2002; 191: 2611–2630.
9. Chen XL, Liu GR and Lim SP. An element free galerkin method for the free vibration analysis of composite laminates of complicated shape. *Compos Struct* 2003; 59: 279–289.
10. Dai KY, Liu GR, Lim SP and Chen XL. An element free galerkin method for static and free vibration analysis of shear-deformable laminated composite plates. *J Sound Vib* 2004; 269: 633–652.
11. Liu GR and Chen XL. Buckling of symmetrically laminated composite plates using the element-free galerkin method. *Int J Struct Stab Dyn* 2002; 2: 281–294.
12. Liew KM, Chen XL and Reddy JN. Mesh-free radial basis function method for buckling analysis of non-uniformity loaded arbitrarily shaped shear deformable plates. *Comput Meth Appl Mech Eng* 2004; 193: 205–225.
13. Huang YQ and Li QS. Bending and buckling analysis of antisymmetric laminates using the moving least square differential quadrature method. *Comput Meth Appl Mech Eng* 2004; 193: 3471–3492.
14. Liu L, Liu GR and Tan VCB. Element free method for static and free vibration analysis of spatial thin shell structures. *Comput Meth Appl Mech Eng* 2002; 191: 5923–5942.
15. Ferreira AJM. A formulation of the multiquadric radial basis function method for the analysis of laminated composite plates. *Compos Struct* 2003; 59: 385–392.
16. Ferreira AJM. Thick composite beam analysis using a global meshless approximation based on radial basis functions. *Mech Adv Mater Struct* 2003; 10: 271–284.
17. Ferreira AJM, Roque CMC and Martins PALS. Analysis of composite plates using higher-order shear deformation theory and a finite point formulation based on the multiquadric radial basis function method. *Composites Part B* 2003; 34: 627–636.
18. Ferreira AJM, Roque CMC and Jorge RMN. Modelling cross-ply laminated elastic shells by a higher-order theory and multiquadrics. *Comput Struct* 2005; 83(27): 2225–2237.
19. Ferreira AJM, Roque CMC and Jorge RMN. Modelling cross-ply laminated elastic shells by a higher-order theory and multiquadricss. *Comput Struct* 2006; 84(19-20): 1288–1299.
20. Chen W. New rbf collocation schemes and kernel rbfs with applications. *Lecture Notes in Computational Science and Engineering* 2002; 26: 75–86.
21. Ferreira AJM and Fasshauer GE. Analysis of natural frequencies of symmetric composite plates by a rbf-pseudospectral method. *Composite Structures* 2007; 79: 202–210.
22. Reddy JN. Dynamic (transient) analysis of layered anisotropic composite-material plates. *Int J Numer Methods Eng* 1983; 19(2): 237–255.

23. Liu Y, Liew KM, Hon YC and Zhang X. Numerical simulation and analysis of an electroactuated beam using a radial basis function. *Smart Mater Struct* 2005; 14(6): 1163–1171.
24. Kirby RM and Yosibash Z. Solution of von-Karman dynamic non-linear plate equations using a pseudo-spectral method. *Comput Meth Appl Mech Eng* 2004; 193(6-8): 575–599.
25. Hardy RL. Multiquadric equations of topography and other irregular surfaces. *Geophys Res* 1971; 176: 1905–1915.
26. Buhmann MD. Radial basis functions. *Acta Numer* 2000; 9: 1–38.
27. Trefethen LN. *Spectral methods in MATLAB*. Philadelphia, PA: Siam, 2000.
28. Reddy JN. Bending of laminated anisotropic shells by a shear deformable finite element. *Fibre Sci Technol* 1982; 17: 9–24.
29. Reddy JN. A simple higher-order theory for laminated composite plates. *J Appl Mech* 1984; 51: 745–752.
30. Reddy JN and Phan ND. Stability and vibration of isotropic, orthotropic and laminated plates according to a higher-order shear deformation theory. *J Sound Vib* 1985; 98(2): 157–170.

3.2.4 Dynamic analysis of functionally graded plates and shells by radial basis functions

C. M. C. Roque, A. J. M. Ferreira, Ana M. A. Neves, G. E. Fasshauer, C. M. M. Soares e R. M. N. Jorge, Dynamic analysis of functionally graded plates and shells by radial basis functions, Mechanics of Advanced Materials and Structures, Volume 17, Issue 8, 2010, pages 636-652.

Mechanics of Advanced Materials and Structures, 17:636–652, 2010

ISSN: 1537-6494 print / 1537-6532 online
DOI: 10.1080/15376494.2010.518932

Dynamic Analysis of Functionally Graded Plates and Shells by Radial Basis Functions

Carla M. C. Roque,[1] António J. M. Ferreira,[1] Ana M. A. Neves,[1] Greg E. Fasshauer,[2] Cristóvão M. M. Soares[3] and Renato M. N Jorge[1]
[1]*Departamento de Engenharia Mecânica, Universidade do Porto, Porto, Portugal*
[2]*Department of Applied Mathematics, Illinois Institute of Technology, Chicago, Illinois, USA*
[3]*IDMEC -Instituto de Engenharia Mecânica -Instituto Superior Técnico, Portugal*

A meshless numerical method with a first-order shear deformation theory is used to study the linear transient response of functionally graded plates and shells. The present meshless method is based on the combination of pseudospectral methods and a collocation method with radial basis functions. A Newmark algoritm is used to advance the analysis in time. Results obtained are compared with analytical solutions.

Keywords meshless, shear deformation, functionally graded plates, functionally graded shells, radial basis

1. INTRODUCTION

A first-order shear deformation theory [1] is used to study the linear transient response of functionally graded plates and shells. The first order theory generates a system of five partial differential equations (PDEs) with five boundary conditions. To solve the system of PDEs, a method that combines radial basis functions with pseudospectrals is used. Pseudospectral (PS) methods are known as highly accurate solvers for PDEs [2]. Generally speaking, the spatial part of the approximate solution of a partial differential equation can be given by a linear combination of radial basis functions, i.e., the inverse multiquadric. The present method allows the analysis of irregular geometries, making it a possible alternative to more established methods, such as finite elements.

For the analysis in time, a Newmark algorithm is used. The Newmark scheme was used by Reddy with a first order shear deformation theory to analyze the dynamic response of anisotropic composite plates [3]. It was also used by Liu et al. [4] with the radial basis function collocation method to analyze the dynamic behavior of electroactuated beams and by Kirby and Yosibash [5] with a pseudospectral method for the dynamic non-linear analysis of plates.

A collocation method with radial basis functions was used by the authors for the analysis of static and free vibration of composite plates and shells and functionally graded plates [6–8].

Functionally graded materials (FGM) were first proposed by Bever and Duwez [9] in 1972. The computational modelling of functionally graded materials is an important tool to the understanding of static and dynamic behavior, and has been the target of intense research, from micro to macro mechanics [10–13]. In functionally graded materials (FGMs), material properties vary continuously as opposed to those in laminated composites where such variation is discontinuous at layer interfaces. In an FGM the material properties are varied by changing the volume fractions of the constituents. An example of such materials is an NFG coating deposited on top of a metallic substrate [14, 15].

The static and dynamic analysis of shallow FGM shells using a meshless method based in local Petrov-Galerkin weak-form was performed by Sladek et al. [16].

This paper presents, for the first time, the transient dynamical analysis of functionally graded plates and shells, using a pseudo-spectral/radial basis function method.

2. THE RBF-PSEUDOSPECTRAL METHOD

Pseudospectral (PS) methods (see [2] for an introduction to the subject) are known as highly accurate solvers for PDEs. Generally speaking, one represents the spatial part of the approximate solution of a given PDE by a linear combination of certain smooth basis functions, (i, j represents the N grid points).

$$u^h(x_i)\sum_{j=1}^{N}\alpha_j\phi_j(x_i),\, i=1,\dots N \tag{1}$$

Address correspondence to Carla Roque, Departmento de Engenharia Mecânica faculdade de Engenharia de Universidade do Porto Rua Dr. Roberto frias, 4200-465, Porto, Portugal. E-mail: croque@fe.up.pt

or in matrix-vector notation

$$\mathbf{u} = \mathbf{A}\alpha \tag{2}$$

with $\alpha = [\alpha_1, \ldots \alpha_x]$ and $A_{i,i} = \phi_i(x_i)$

Traditionally, polynomial basis functions are used. In this paper, however, we will use radial basis functions (RBFs). In this paper, we use an inverse multiquadric, defined as:

$$\phi_j(x_i) = \Phi(r) = 1/\sqrt{1 + c^2\left((x_i - x_j)^2 + \frac{(y_i - y_j)^2}{(b/a)^2}\right)} \tag{3}$$

where r is the euclidian norm between grid points of coordinates (x, y), a, b are the length of the plate along x and y axis, respectively and c is a user defined shape parameter.

Note that in Eq. (3) the radial basis function depends on the direction it is being computed and is sometimes called anisotropic radial basis function [17].

The derivatives are easily computed. For example,

$$\mathbf{u}' = A_x\alpha = \mathbf{D}\mathbf{u} \tag{4}$$

with $A_x = \frac{d}{xd}\phi_j(x_i)$ where the matrix is the differentiation matrix.

The use of PS and RBF combined for the analysis of structures was first presented by Ferreira and Fasshauer [18]. Its application for laminated structures was then presented by Ferreira et al. [19].

3. FIRST ORDER SHEAR DEFORMATION THEORIES

First-order theories are adequate for modeling moderately thick plates and shells and are of simpler physical interpretation than higher order shear deformation theories [1]. In this section the first-order shear deformation theories for plates and shells are presented. In both theories a small displacement/small rotation field is assumed. Using strain-displacement relationships and the principle of virtual displacements the equilibrium equations can be written [1].

3.1. First-Order Shear Deformation Plate Theory

The displacement field for the first order shear deformation plate theory is [1]:

$$\begin{aligned} u(x, y, z, t) &= u_{0(}x, y, t) + z\phi_x(x, y, t) \\ v(x, y, z, t) &= v_{0(}x, y, t) + z\phi_y(x, y, t) \\ w(x, y, z, t) &= w_{0(}x, y, t) \end{aligned} \tag{5}$$

where u and v are the inplane displacements at any point (x, y, z), u_0 and v_0 denote the inplane displacement of the point $(x, y, 0)$ on the midplane, w is the deflection, ϕ_x and ϕ_y are the rotations of the normals to the midplane about the y and x axes, respectively. The thickness of the plate is denoted as h.

The strain-displacement relationships are given as:

$$\left\{\begin{array}{c} \epsilon_{xx} \\ \epsilon_{yy} \\ \gamma_{xy} \\ \gamma_{xz} \\ \gamma_{yz} \end{array}\right\} = \left\{\begin{array}{c} \frac{\partial u}{\partial x} \\ \frac{\partial v}{\partial y} \\ \frac{\partial u}{\partial z} + \frac{\partial u}{\partial x} \\ \frac{\partial u}{\partial z} + \frac{\partial w}{\partial x} \\ \frac{\partial v}{\partial z} + \frac{\partial w}{\partial y} \end{array}\right\} \tag{6}$$

Therefore strains can be expressed as

$$\left\{\begin{array}{c} \epsilon_{xx} \\ \epsilon_{yy} \\ \gamma_{xy} \\ \gamma_{xz} \\ \gamma_{yz} \end{array}\right\} = \left\{\begin{array}{c} \epsilon_{xx}^{(0)} \\ \epsilon_{yy}^{(0)} \\ \gamma_{xy}^{(0)} \\ \gamma_{xz}^{(0)} \\ \gamma_{yz}^{(0)} \end{array}\right\} + z\left\{\begin{array}{c} \epsilon_{xx}^{(1)} \\ \epsilon_{yy}^{1)} \\ \gamma_{xy}^{(1)} \\ \gamma_{xz}^{(1)} \\ \gamma_{yz}^{(1)} \end{array}\right\} \tag{7}$$

where

$$\left\{\begin{array}{c} \epsilon_{xx}^{(0)} \\ \epsilon_{yy}^{(0)} \\ \gamma_{xy}^{(0)} \\ \gamma_{xz}^{(0)} \\ \gamma_{yz}^{(0)} \end{array}\right\} = \left\{\begin{array}{c} \frac{\partial u_o}{\partial x} \\ \frac{\partial v_o}{\partial y} \\ \frac{\partial u_o}{\partial y} + \frac{\partial u_o}{\partial x} \\ \frac{\partial u_o}{\partial x} + \phi x \\ \frac{\partial u_o}{\partial y} + \phi y \end{array}\right\} \quad \left\{\begin{array}{c} \epsilon_{xx}^{(1)} \\ \epsilon_{yy}^{(1)} \\ \gamma_{xy}^{(1)} \\ \gamma_{xz}^{(1)} \\ \gamma_{yz}^{(1)} \end{array}\right\} = \left\{\begin{array}{c} \frac{\partial \phi_x}{\partial x} \\ \frac{\partial \phi_y}{\partial y} \\ \frac{\partial \phi_x}{\partial y} + \frac{\partial \phi_y}{\partial x} \\ 0 \\ 0 \end{array}\right\} \tag{8}$$

A laminate can be manufactured from orthotropic layers (or plies) of pre-impregnated unidirectional fibrous composite materials. Neglecting σ_z for each layer, the stress-strain relations in the fiber local coordinate system can be expressed as

$$\left\{\begin{array}{c} \sigma_1 \\ \sigma_2 \\ \tau_{12} \\ \tau_{23} \\ \tau_{31} \end{array}\right\} = \left[\begin{array}{ccccc} Q_{11} & Q_{12} & 0 & 0 & 0 \\ Q_{12} & Q_{22} & 0 & 0 & 0 \\ 0 & 0 & Q_{33} & 0 & 0 \\ 0 & 0 & 0 & Q_{44} & 0 \\ 0 & 0 & 0 & 0 & Q_{55} \end{array}\right] \left\{\begin{array}{c} \epsilon_1 \\ \epsilon_2 \\ \gamma_{12} \\ \gamma_{23} \\ \gamma_{31} \end{array}\right\} \tag{9}$$

where subscripts 1 and 2 are respectively the fiber and the normal to fiber inplane directions, 3 is the direction normal to the plate, and the reduced stiffness components, Q_{ij} are given by

$$Q_{11} = \frac{E_1}{1 - v_{12}v_{21}};\ Q_{22} = \frac{E_2}{1 - v_{12}v_{21}};\ Q_{12} = v_{12}Q_{11};$$
$$Q_{33} = G_{12};\qquad Q_{44} = G_{23};\quad Q_{55} = G_{31};\quad v_{21} = v_{12}\frac{E_2}{E_1}$$

in which E_1, E_2, ν_{12}, G_{12}, G_{23} and G_{31} are materials properties of the lamina.

By performing adequate coordinate transformation, the stress-strain relations in the global x-y-z coordinate system can be obtained as

$$\begin{Bmatrix} \sigma_{xx} \\ \sigma_{yy} \\ \tau_{xy} \\ \tau_{yz} \\ \tau_{zx} \end{Bmatrix} = \begin{bmatrix} \bar{Q}_{11} & \bar{Q}_{12} & \bar{Q}_{16} & 0 & 0 \\ \bar{Q}_{12} & \bar{Q}_{22} & \bar{Q}_{26} & 0 & 0 \\ \bar{Q}_{16} & \bar{Q}_{26} & \bar{Q}_{66} & 0 & 0 \\ 0 & 0 & 0 & \bar{Q}_{44} & \bar{Q}_{45} \\ 0 & 0 & 0 & \bar{Q}_{45} & \bar{Q}_{55} \end{bmatrix} \begin{Bmatrix} \varepsilon_{xx} \\ \varepsilon_{yy} \\ \gamma_{xy} \\ \gamma_{yz} \\ \gamma_{zx} \end{Bmatrix} \tag{10}$$

The equations of motion of the first-order theory are derived from the principle of virtual displacements. The virtual strain energy (δU), the virtual inertial terms (δK), the virtual work done by applied forces (δV) are given by

$$\begin{aligned}
\delta U &= \int_{\Omega_0} \left\{ \int_{-h/2}^{h/2} \left[\sigma_{xx}\left(\delta\varepsilon_{xx}^{(0)} + z\delta\varepsilon_{xx}^{(1)}\right) + \sigma_{yy}\left(\delta\varepsilon_{yy}^{(0)} + z\delta\varepsilon_{yy}^{(1)}\right) \right.\right. \\
&\quad \left.\left. + \tau_{xy}\left(\delta\gamma_{xy}^{(0)} + z\delta\gamma_{xy}^{(1)}\right) + \tau_{xz}\left(\delta\gamma_{xz}^{(0)}\right) + \tau_{yz}\left(\delta\gamma_{yz}^{(0)}\right)\right] dz \right\} \\
&\quad dx\,dy \\
&= \int_{\Omega_0} \left(N_{xx}\delta\varepsilon_{xx}^{(0)} + M_{xx}\delta\varepsilon_{xx}^{(1)} + N_{yy}\delta\varepsilon_{yy}^{(0)} + M_{yy}\delta\varepsilon_{yy}^{(1)} \right. \\
&\quad \left. + N_{xy}\delta\gamma_{xy}^{(0)} + M_{xy}\delta\gamma_{xy}^{(1)} + Q_x\delta\gamma_{xz}^{(0)} + Q_y\delta\gamma_{yz}^{(0)} \right) dx\,dy \\
\delta K &= \int_{\Omega_0} \left\{ \int_{-h/2}^{h/2} p\left[\left(\dot{u}_0 + z\dot{\phi}_x\right)\left(\delta\dot{u}_0 + z\delta\dot{\phi}_x\right) + \left(\dot{v}_0 + z\dot{\phi}_y\right) \right.\right. \\
&\quad \left.\left. \times \left(\delta\dot{v}_0 + z\delta\dot{\phi}_y\right) + \dot{w}_0\delta\dot{w}_0 \right] dz\,dx\,dy \right. \\
&= \int_{\Omega_0} \left[-I_0\left(\dot{u}_0\delta\dot{u}_0 + \dot{v}_0\delta\dot{v}_0 + \dot{w}_0\delta\dot{w}_0\right) \right. \\
&\quad - I_1\left(\dot{\phi}_x\delta\dot{u}_0 + \dot{\phi}_y\delta\dot{v}_0 + \dot{\phi}_x\delta\dot{u}_0 + \dot{\phi}_y\delta\dot{v}_0\right) \\
&\quad \left. - I_2\left(\dot{\phi}_x\delta\dot{\phi}_x + \dot{\phi}_y\delta\dot{\phi}_y\right) dx\,dy \right]
\end{aligned} \tag{11}$$

and

$$\delta V = -\int_{\Omega_0} q\delta w_0\,dx\,dy \tag{12}$$

where $\dot{()}$ represents derivative w.r.t. time, Ω_0 denotes the mid-plane of the laminate, q is the external distributed load and

$$\begin{Bmatrix} N_{\alpha\beta} \\ M_{\alpha\beta} \end{Bmatrix} = \int_{-h/2}^{h/2} \sigma_{\alpha 3} \begin{Bmatrix} 1 \\ z \end{Bmatrix} dz; \quad \{Q_\alpha\} = K\int_{-h/2}^{h/2} \sigma_{\alpha z}\,dz \tag{13}$$

where α, β take the symbols x, y and K is a shear corrector factor.

Substituting for δU, δV and δK into the virtual work statement, noting that the virtual strains can be expressed in terms of the generalized displacements, integrating by parts to relieve from any derivatives of the generalized displacements and using the fundamental lemma of the calculus of variations, we obtain the following Euler-Lagrange equations [1]:

$$\frac{\partial N_{xx}}{\partial x} + \frac{\partial N_{xy}}{\partial y} = I_0\ddot{u}_0 + I_1\ddot{\phi}_x \tag{14}$$
$$\frac{\partial N_{xy}}{\partial x} + \frac{\partial N_{yy}}{\partial y} = I_0\ddot{v}_0 + I_1\ddot{\phi}_y \tag{15}$$
$$\frac{\partial Q_x}{\partial x} + \frac{\partial Q_y}{\partial y} + q = I_0\ddot{w}_0 \tag{16}$$
$$\frac{\partial M_{xx}}{\partial x} + \frac{\partial M_{xy}}{\partial y} - Q_x = I_0\ddot{u}_0 + I_2\ddot{\phi}_x \tag{17}$$
$$\frac{\partial M_{xY}}{\partial x} + \frac{\partial M_{yy}}{\partial y} - Q_y = I_1\ddot{v}_0 + I_2\ddot{\phi}_y \tag{18}$$

with

$$I_i = \int_{-h/2}^{h/2} \rho z^i dz;\ i = 0, 1, 2 \tag{19}$$

3.2. First-order Shear Deformation Shell Theory

Let (ξ_1, ξ_2, ζ) denote the orthogonal curvilinear coordinates (or shell coordinates) such that the ξ_1-and ξ_2-curves are lines of curvature on the middle surface $\zeta = 0$, and ζ-curves are straight lines perpendicular to the surface $\zeta = 0$. For cylindrical and spherical shells the lines of principal curvature coincide with the coordinate lines. The values of the principal radii of curvature are denoted by R_1 and R_2. The displacement field for the first-order shear deformation shell theory is [1]:

$$\begin{aligned}
u(x, y, z, t) &= \left(1 + \frac{\zeta}{R_1}\right)u_0(x, y, t) + \zeta\phi_x(x, y, t) \\
v(x, y, z, t) &= \left(1 + \frac{\zeta}{R_2}\right)v_0(x, y, t) + \zeta\phi_y(x, y, t) \\
w(x, y, z, t) &= w_0(x, y, t)
\end{aligned} \tag{20}$$

The strain-displacement relations referred to an orthogonal curvilinear coordinate system leads to the following deformation field, where x_i denote the cartesian coordinates ($dx_1 = \alpha_i d\xi_i$),

$i = 1, 2$.

$$\begin{aligned} \varepsilon_1 &= \varepsilon_1^{(0)} + \zeta k_1^{(0)} \\ \varepsilon_2 &= \varepsilon_2^{(0)} + \zeta k_2^{(0)} \\ \varepsilon_4 &= \varepsilon_4^{(0)} \\ \varepsilon_5 &= \varepsilon_5^{(0)} \\ \varepsilon_6 &= \varepsilon_6^{(0)} + \zeta k_6^{(0)} \end{aligned} \tag{21}$$

where

$$\begin{aligned} \varepsilon_1^{(0)} &= \frac{\partial u_0}{\partial x_1} + \frac{w}{R_1} \\ \varepsilon_2^{(0)} &= \frac{\partial v_0}{\partial x_2} + \frac{w}{R_2} \\ \varepsilon_4^{(0)} &= \frac{\partial w_0}{\partial x_2} + \theta_2 \\ \varepsilon_5^{(0)} &= \frac{\partial w_0}{\partial x_1} + \theta_1 \\ \varepsilon_6^{(0)} &= \frac{\partial u_0}{\partial x_2} + \frac{\partial v_0}{\partial x_1} \\ k_1^{(0)} &= \frac{\partial \theta_1}{\partial x_1} \\ k_2^{(0)} &= \frac{\partial \theta_2}{\partial x_2} \\ k_6^{(0)} &= \frac{\partial \theta_2}{\partial x_1} + \frac{\partial \theta_1}{\partial x_2} \end{aligned} \tag{22}$$

Using the same procedure as in the plate theory, the following equilibrium equations are obtained:

$$\frac{\partial N_{xx}}{\partial x} + \frac{\partial N_{xy}}{\partial y} = I_0 \ddot{u}_0 + I_1 \ddot{\phi}_x \tag{23}$$

$$\frac{\partial N_{xy}}{\partial x} + \frac{\partial N_{yy}}{\partial y} = I_0 \ddot{v}_0 + I_1 \ddot{\phi}_y \tag{24}$$

$$\frac{\partial Q_x}{\partial x} + \frac{\partial Q_y}{\partial y} - \frac{N_{xx}}{R_1} - \frac{N_{yy}}{R_2} + q = I_0 \ddot{w}_0 \tag{25}$$

$$\frac{\partial M_{xx}}{\partial x} + \frac{\partial M_{xy}}{\partial y} - Q_x = I_1 \ddot{u}_0 + I_2 \ddot{\phi}_x \tag{26}$$

$$\frac{\partial M_{xy}}{\partial x} + \frac{\partial M_{yy}}{\partial y} - Q_y = I_0 \ddot{v}_0 + I_2 \ddot{\phi}_y \tag{27}$$

where q is the distributed transverse load, N_i, M_I, etc. are the stress resultants, given by

$$\begin{aligned} (N_i, M_i) &= \int_{\zeta_{k-1}}^{\zeta_k} \sigma_i(1, \zeta)\, d\zeta, (i = xx, yy, xy) \\ (Q_x, Q_y) &= \int_{\zeta_{k-1}}^{\zeta_k} (\sigma_{xz}, \sigma_{yz})\, d\zeta; \\ I_i &= \int_{\zeta_{k-1}}^{\zeta_k} \rho z\, d\zeta,\ (i = 0, 1, 2) \end{aligned} \tag{28}$$

4. NUMERICAL INTEGRATION

For the numerical time integration, the Newmark method is used [1]. The Euler-Lagrange equations can be written in terms of the displacements by substituting strains and stress resultants in Eqs. (14)–(18) (i.e., for the plate theory). The resulting system of equations can be written as:

$$M\ddot{u} + Ku = F \tag{29}$$

where M represents the matrix of inertial terms, K the stiffness matrix and F the vector related to external forces.

Time derivatives in Eq. (29) are approximated using Taylor's series:

$$\ddot{u}_{t+\Delta t} = a_3(u_{t+\Delta t} - u_t) - a_4\dot{u}_t - a_5\ddot{u}_t \tag{30}$$

$$\dot{u}_{t+\Delta t} = \dot{u}_t + a_1\ddot{u}_t + a_2\ddot{u}_{t+\Delta t} \tag{31}$$

with

$$a_1 = (1-\alpha)\Delta t;\ a_2 = \alpha\Delta t;\ a_3 = \frac{2}{\gamma(\Delta t)^2};\ a_4 = a_3\Delta t;\ a_5 = \frac{1-\gamma}{\gamma}$$

Substituting Eqs. (30, 31) in Eq. (29), the later can be written in the form:

$$\hat{K}u = \hat{F} \tag{32}$$

with

$$\hat{K}_{t+\Delta t} = K_{t+\Delta t} + a_3 M_{t+\Delta t} \tag{33}$$

$$\hat{F}_{t+\Delta t} = F_{t+\Delta t} + M_{i+\Delta t}\,(a_3 u_t + a_4\dot{u}_t + a_5\ddot{u}_t) \tag{34}$$

Initial values for displacements u_0 and velocities $\dot{u}_0$ are set to zero, while accelerations $\ddot{u}_0$ are set as $\ddot{u}_0 = M^{-1}(F - Ku)$.

5. HOMOGENIZATION TECHNIQUE

The FGM equivalent material properties E and ν at a point are determined by the Mori-Tanaka homogenization technique. For a random distribution of isotropic particles in an isotropic matrix, the bulk modulus K, and the shear modulus G, of the FGM material at a given thickness coordinate, are given by

$$\frac{K - K_1}{K_2 - K_1} = \frac{V_2}{1 + (1 - V_2)\,\frac{K_2 - K_1}{K_1 + \frac{4}{3}G_1}} \tag{35}$$

$$\frac{G - G_1}{G_2 - G_1} = \frac{V_2}{1 + (1 - V_2)\,\frac{G_2 - G_1}{G_1 + f_1}} \tag{36}$$

where $f_1 = \frac{G_1(9K_1 + 8G_1)}{6(K_1 + 2G_1)}$ and subscripts 1 and 2 represent the ceramic and the metal phases respectively. Young's modulus and Poisson's ratio are related to the bulk and the shear moduli

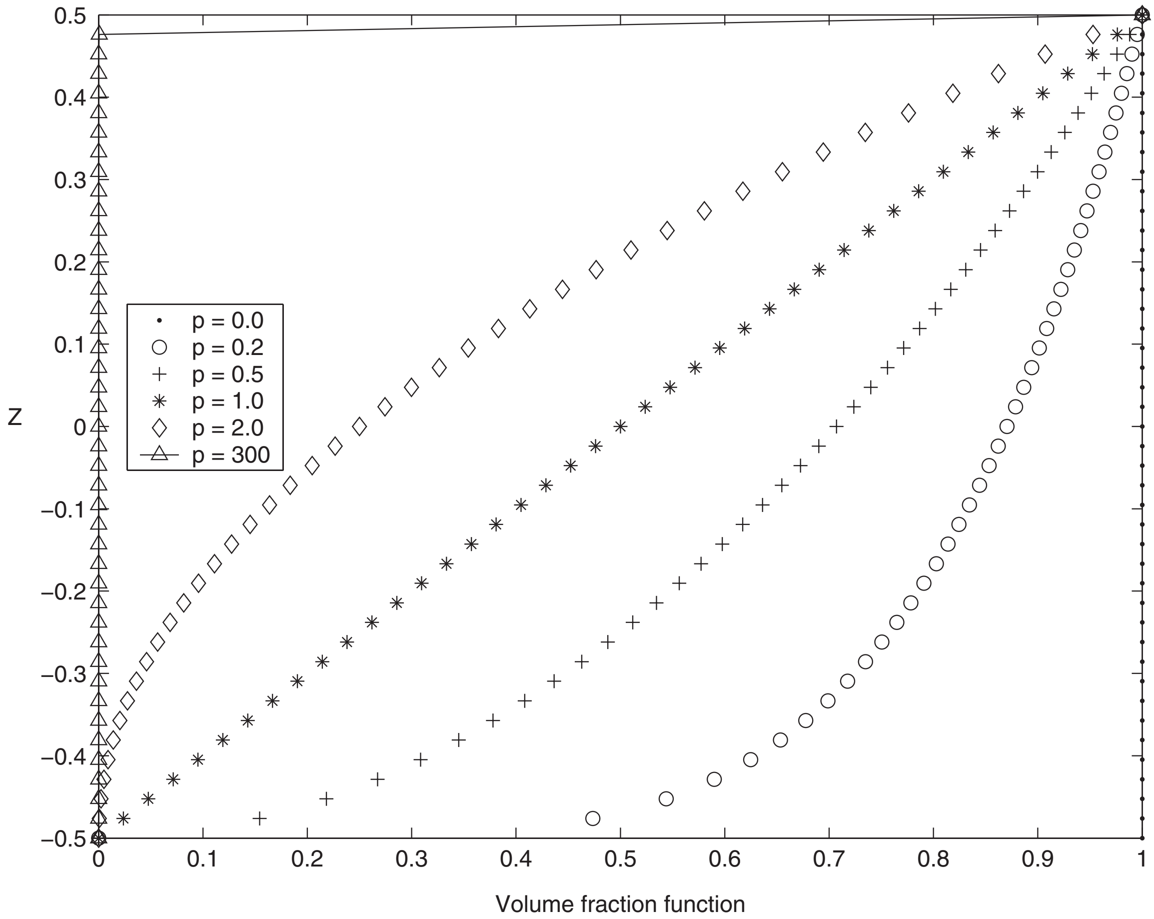

FIG. 1. Variation of volume fraction of the ceramic phase along the thickness z for various values of p.

by

$$K = \frac{E}{3(1-2\nu)} \tag{37}$$

$$G = \frac{E}{2(1-\nu)} \tag{38}$$

It is assumed that the volume fraction of the ceramic phase varies only in the thickness direction according to the relation

$$V_1 = \left(\frac{1}{2} + \frac{z}{h}\right)^p \tag{39}$$

where p is an exponent factor, h the plate thickness, and $-h/2 \leq z \leq h/2$.

6. ANALYTICAL SOLUTION

In order to assess the quality of our numerical approach, an analytical solution was independently computed by assuming a spacial variation of the displacements and reducing the differential equations to a set of differential equations in time [1].

The solution of Eq. (29) is assumed to be of the form:

$$u(x, y, t) = \sum_{m=1}^{\infty}\sum_{n=1}^{\infty} T_{mn}(t)U_{mn}(x, y) \tag{40}$$

The Navier procedure is used to determine the spatial variation and the Newmark method is used to solve the differential equations in time.

As an example, for a simply supported cross-ply rectangular plate of length a, b the boundary conditions are imposed as:

$$\text{in } x = 0, a{:}\, v = w = \phi_y = N_x = M_x = 0 \tag{41}$$

$$\text{in } y = 0, b{:}\, u = w = \phi_x = N_y = M_y = 0 \tag{42}$$

The boundary conditions in Eq. (41) and Eq. (42) are satisfied by the following expansions of the displacements and applied

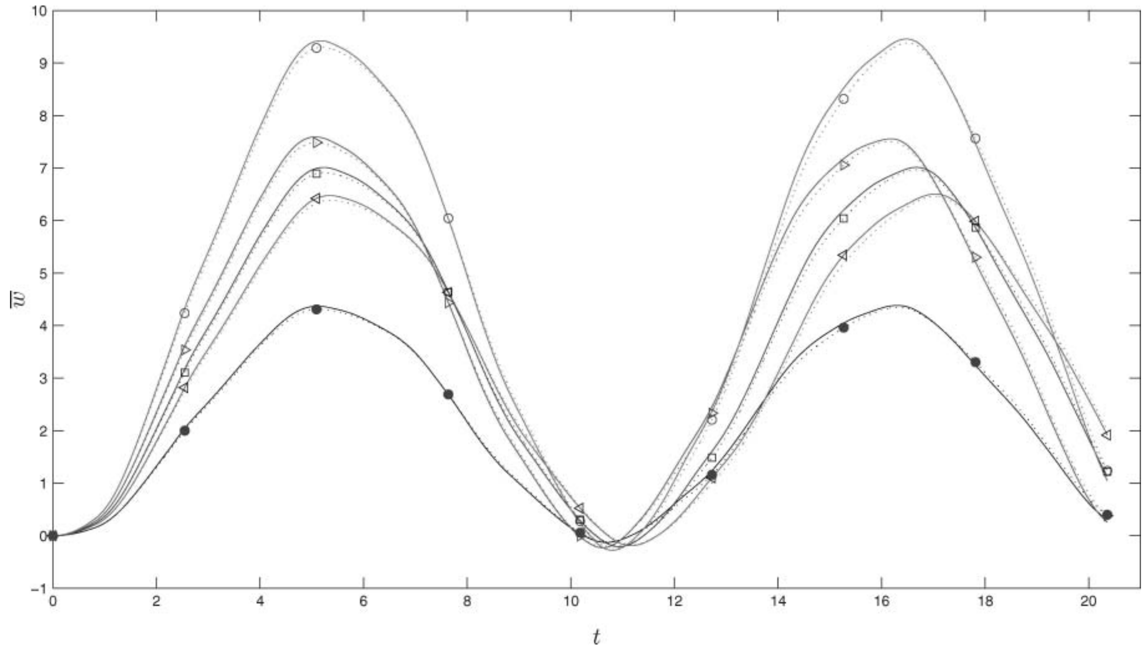

FIG. 2. Present and analytical solutions for central deformation $\bar{w}$ of an FGM square plate, uniform force, $c = \sqrt{n+1}/2$. Legend: — analytical solution (p = 0, 1, 2, 5, ∞); ● present, p = 0 (ceramic); ◁ present, p = 1; □ present, p=2; ▷ present, p=5; ○ present, p = ∞ (metal).

load:

$$u_0(x, y, t) = \sum_{n=1}^{\infty}\sum_{m=1}^{\infty} U_{nm}(t)\cos(\alpha x)\sin(\beta y) \tag{43}$$

$$v_0(x, y, t) = \sum_{n=1}^{\infty}\sum_{m=1}^{\infty} V_{nm}(t)\sin(\alpha x)\cos(\beta y) \tag{44}$$

$$w_0(x, y, t) = \sum_{n=1}^{\infty}\sum_{m=1}^{\infty} W_{nm}(t)\sin(\alpha x)\cos(\beta y) \tag{45}$$

$$\phi_x(x, y, t) = \sum_{n=1}^{\infty}\sum_{m=1}^{\infty} \Phi x_{nm}(t)\cos(\alpha x)\sin(\beta y) \tag{46}$$

$$\phi_y(x, y, t) = \sum_{n=1}^{\infty}\sum_{m=1}^{\infty} \Phi y_{nm}(t)\sin(\alpha x)\cos(\beta y) \tag{47}$$

$$q(x, y, t) = \sum_{n=1}^{\infty}\sum_{m=1}^{\infty} Q_{nm}(t)\sin(\alpha x)\sin(\beta y) \tag{48}$$

with

$$\alpha = \frac{m\pi}{a};\ \beta = \frac{n\pi}{b} \tag{49}$$

$$Q_{nm}(t) = \frac{4}{ab}\int_0^a\int_0^b q(x, y, t)\sin\frac{m\pi x}{a} \times \sin\frac{m\pi y}{b}dx\,dy \tag{50}$$

Substituting Eqs. (43–48) in Eq. (29) we can write:

$$M\ddot{\Delta} + K\Delta = F \tag{51}$$

where $\Delta = (U_{mn}, V_{mn}, W_{mn}, x_{mn}, y_{mn})^T$ croque Eq. (51) can then be solved numerically by the Newmark method.

7. NUMERICAL EXAMPLES

Results for simply supported FGM plates and shells of length a and b composed of aluminum/ceramic phases are presented.

Square ($b = a$) and rectangular ($b = 2a$) simply supported FGM plates under suddenly applied transverse uniform load and rectangular ($b = 2a$) simply supported FGM shells under suddenly applied transverse uniform and sinusoidal loads are considered.

A shear correction factor K of 5/6 is used for all examples. Although this is not the most correct value [13], many authors use it for the analysis of isotropic, composite and functionally graded plates [1, 20], so the same value is used here for comparison purposes.

The values of both n and m in Eqs. (43–48) is 35. For the Newmark scheme, initial conditions for displacements Δ and velocities Δ are set to zero, $\alpha = 3/2$, $\gamma = 8/5$ and time step $\Delta t = 10^{-7}$.

All plates and shells have the ratio length/thickness $a/h = 10$ and the grid used has 13×13 uniformly spaced points. A ratio $R/a = 5$ for all shells is considered.

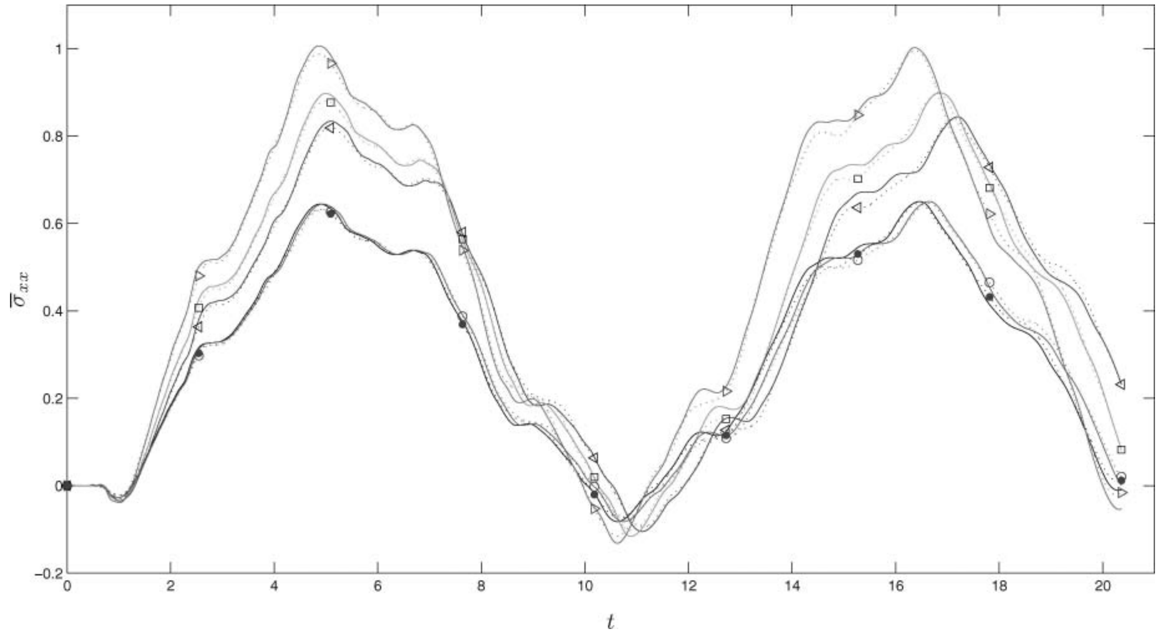

FIG. 3. Present and analytical solutions for in-plane stress $\bar{\sigma}_{xx}$ of an FGM square plate, uniform force, $c = \sqrt{n+1}/2$. Legend: — analytical solution (p = 0, 1, 2, 5, ∞); ● present, p = 0 (ceramic); ◁ present, p = 1; □ present, p = 2; ▷ present, p = 5; ○ present, p = ∞ (metal).

For each example three figures are presented, showing the evolution in time of the central deformation $\overline{w}$, in-plane stress $\bar{\sigma}_{xx}$ and in-plane shear stress $\bar{\sigma}_{xy}$ in points $(a/2, b/2)$, $(a/2, b/2, h/2)$ and $(a, b, -h/2)$ respectively.

For each figure results for various values of p in Eq. (39) are presented. Considered values of p are 0 (ceramic plate), 1, 2, 5 and ∞ (metal plate) (see Figure 1). The analytical solutions are computed and presented in the same plot for all examples.

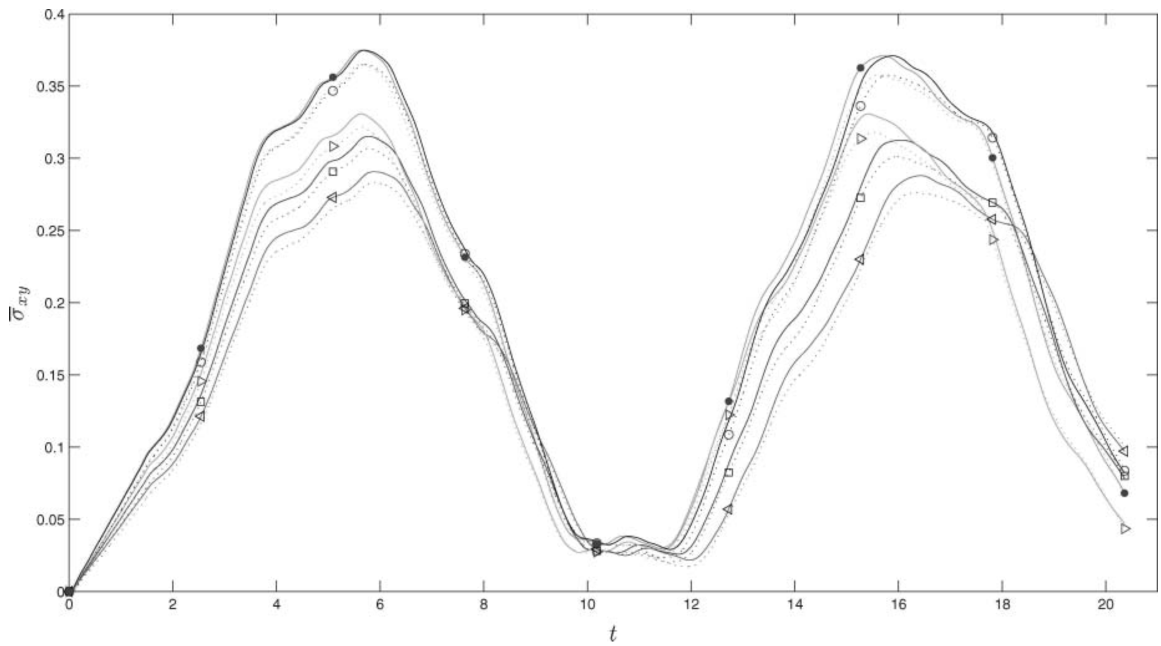

FIG. 4. Present and analytical solutions for in-plane shear stress $\bar{\sigma}_{xy}$ of an FGM square plate, uniform force, $c = \sqrt{n+1}/2$. Legend: — analytical solution (p = 0, 1, 2, 5, ∞); ● present, p = 0 (ceramic); ◁ present, p = 1; □ present, p = 2; ▷ present, p = 5; ○ present, p= ∞ (metal).

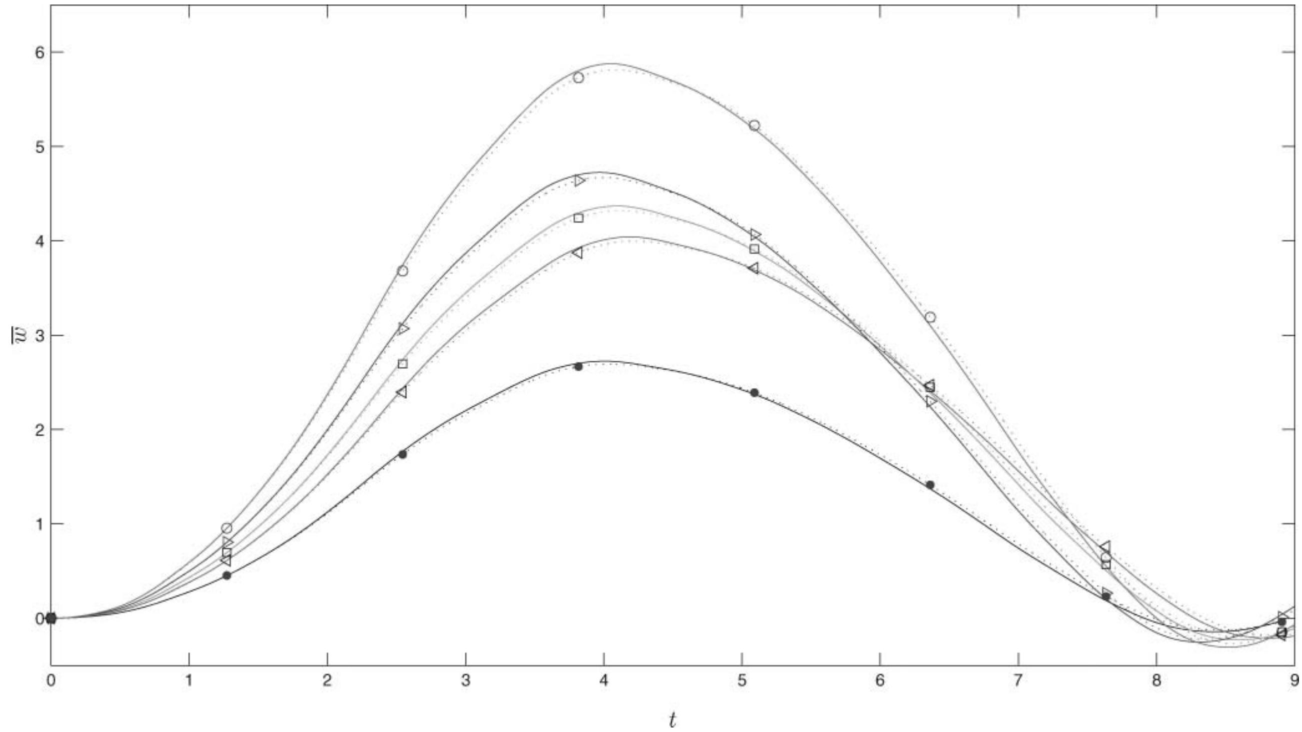

FIG. 5. Present and analytical solutions for central deformation $\bar{w}$ of an FGM rectangular plate, uniform force, $c = \sqrt{n+1}/2$. Legend: — analytical solution (p = 0, 1, 2, 5, ∞); ● present, p = 0 (ceramic); ◁ present, p = 1; □ present, p = 2; ▷ present, p = 5; ○ present, p= ∞ (metal).

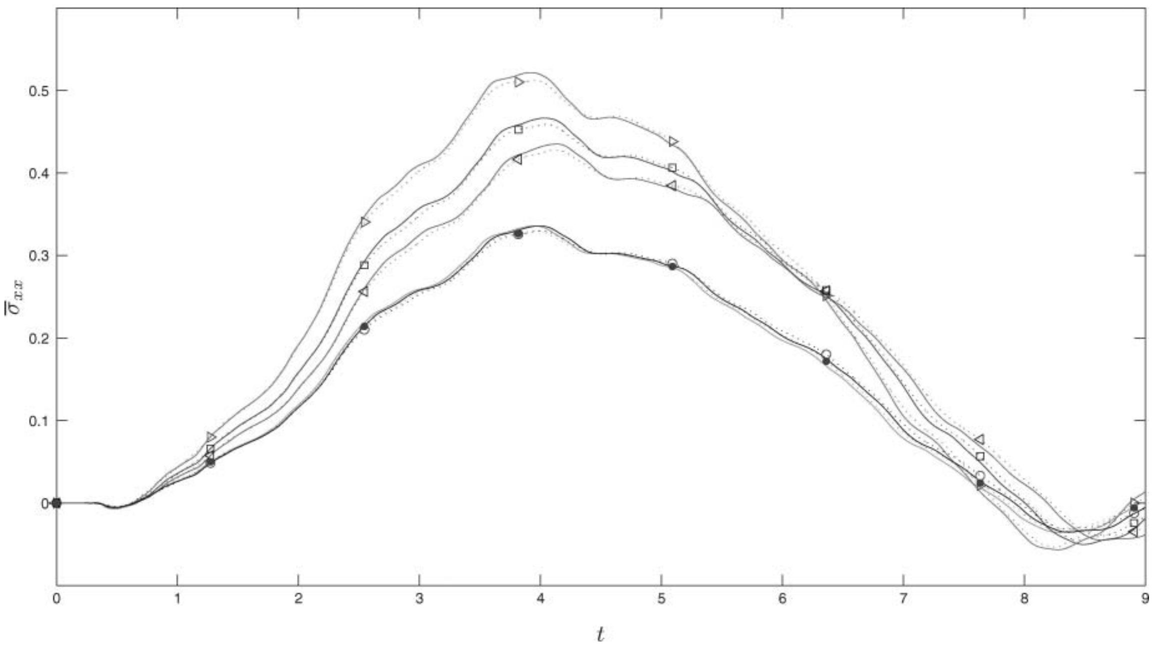

FIG. 6. Present and analytical solutions for in-plane stress $\bar{\sigma}_{xx}$ of an FGM rectangular plate, uniform force, $c = \sqrt{n+1}/2$. Legend: — analytical solution (p = 0, 1, 2, 5, ∞); ● present, p = 0 (ceramic); ◁ present, p = 1; □ present, p = 2; ▷ present, p = 5; ○ present, p = ∞ (metal).

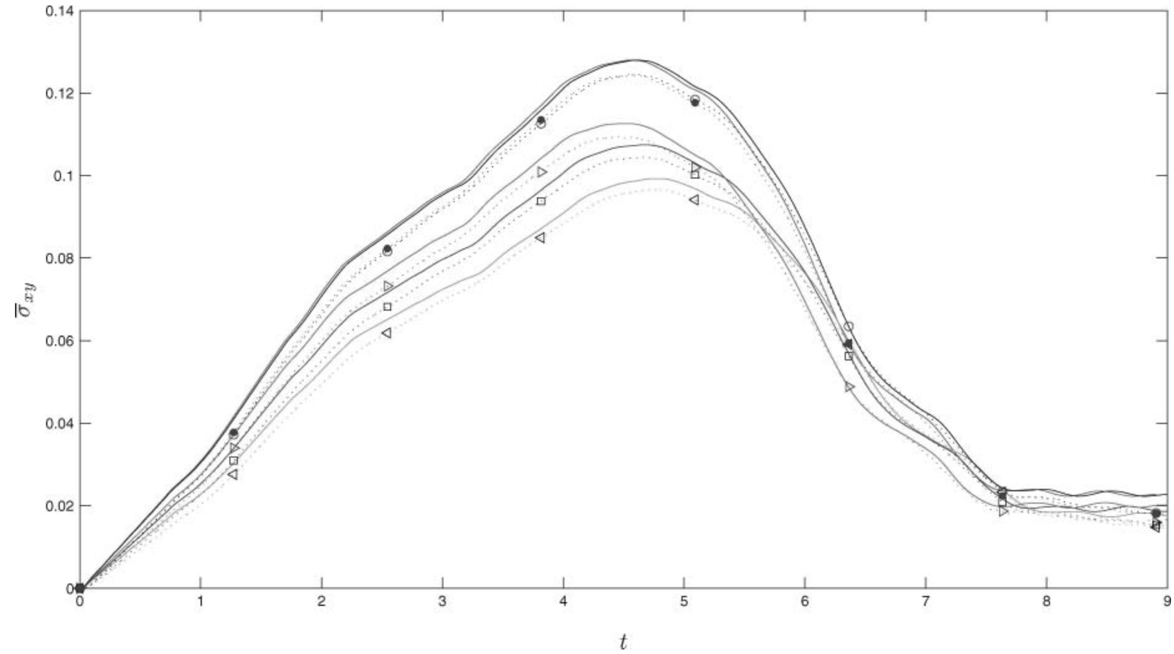

FIG. 7. Present and analytical solutions for in-plane shear stress $\bar{\sigma}_{xy}$ of an FGM rectangular plate, uniform force, $c = \sqrt{n+1}/2$. Legend: — analytical solution (p = 0, 1, 2, 5, ∞); ● present, p = 0 (ceramic); ◁ present, p = 1; □ present, p = 2; ▷ present, p = 5; ○ present, p = ∞ (metal).

The same legend is maintained for all examples (except in Figure 1). The numerical solutions are plotted in a dashed line and different markers are added according to the value of p. Since the analytical solutions are always very close to the respective numerical solutions, they are simply plotted with a full line.

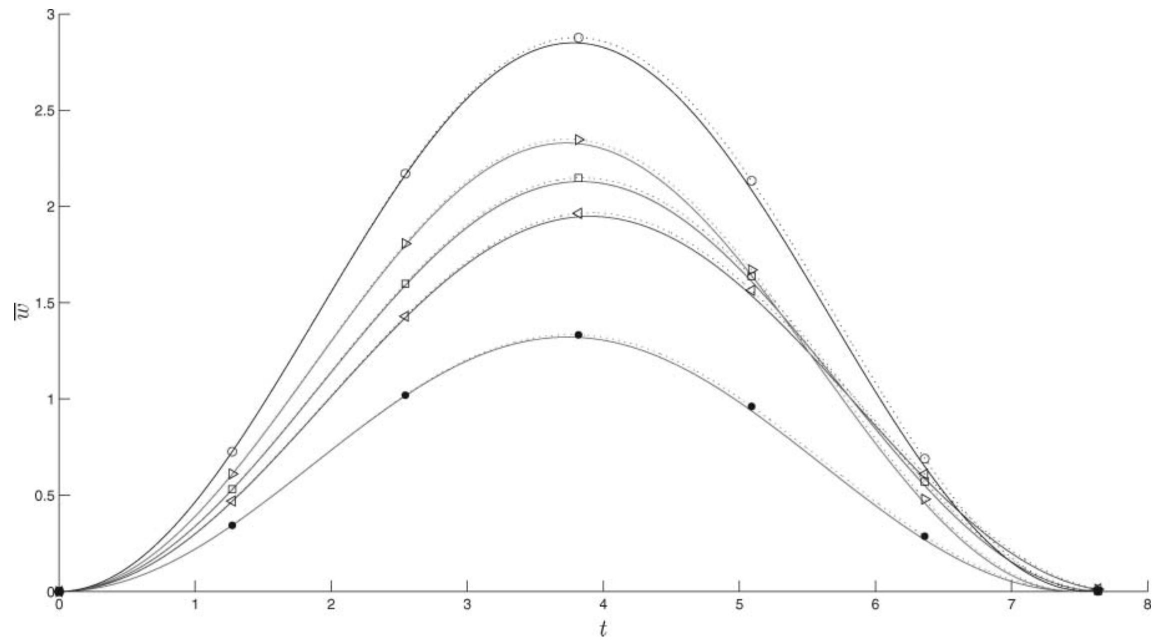

FIG. 8. Present and analytical solutions for central deformation $\bar{w}$ of an FGM rectangular shell, sinusoidal force, $c = \sqrt{n+1}/2$. Legend: — analytical solution (p = 0, 1, 2, 5, ∞); ● present, p = 0 (ceramic); ◁ present, p = 1; □ present, p = 2; ▷ present, p = 5; ○ present, p = ∞ (metal).

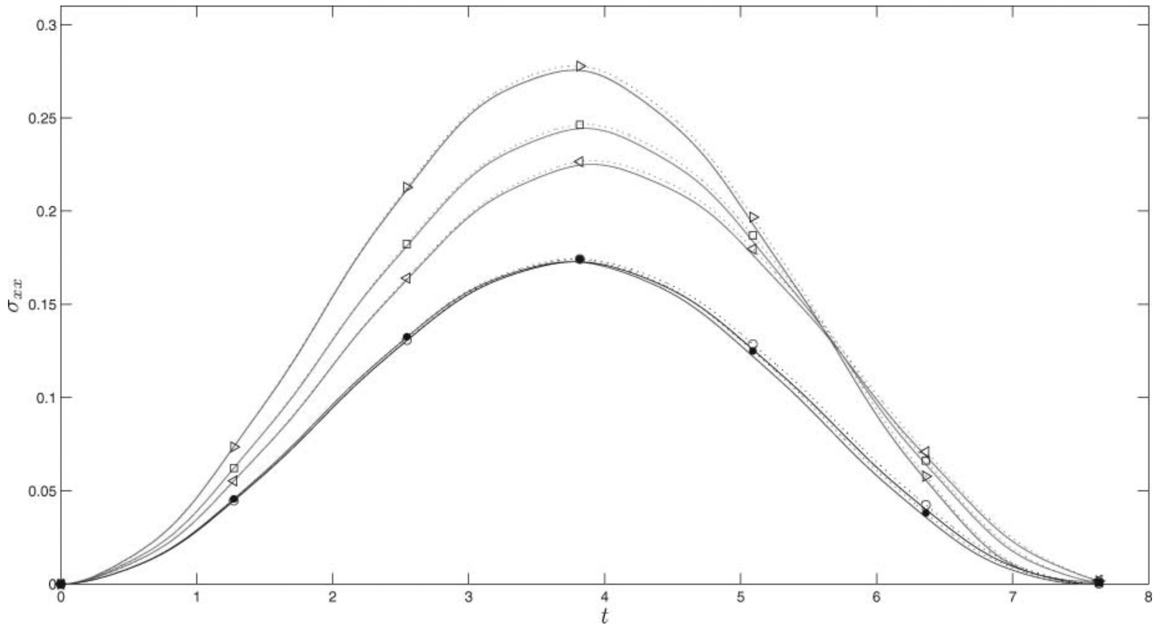

FIG. 9. Present and analytical solutions for in-plane stress $\bar{\sigma}_{xx}$ of an FGM rectangular shell, sinusoidal force, $c = \sqrt{n+1}/2$. Legend: — analytical solution (p = 0, 1, 2, 5, ∞); • present, p = 0 (ceramic); ◁ present, p = 1; □ present, p = 2; ▷ present, p = 5; ○ present, p = ∞ (metal).

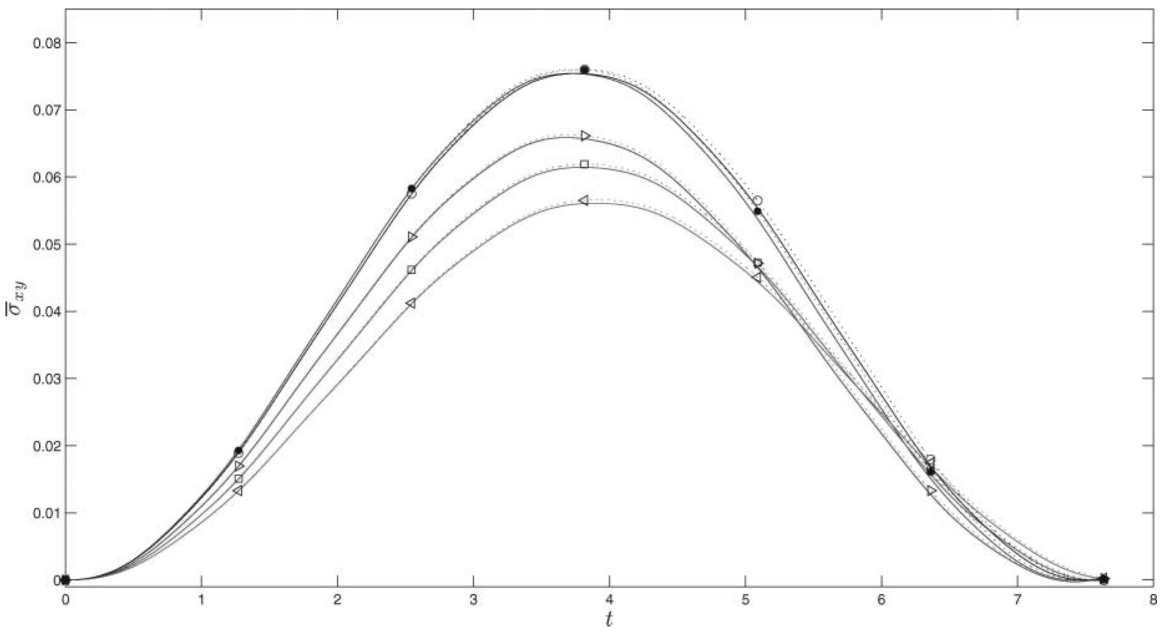

FIG. 10. Present and analytical solutions for in-plane stress $\bar{\sigma}_{xy}$ of an FGM rectangular shell, sinusoidal force, $c = \sqrt{n+1}/2$ Legend: – analytical solution (p = 0, 1, 2, 5, ∞); • present, p = 0 (ceramic); ◁ present, p = 1; □ present, p =2 ; ▷ present, p = 5; ○ present, p = ∞ (metal).

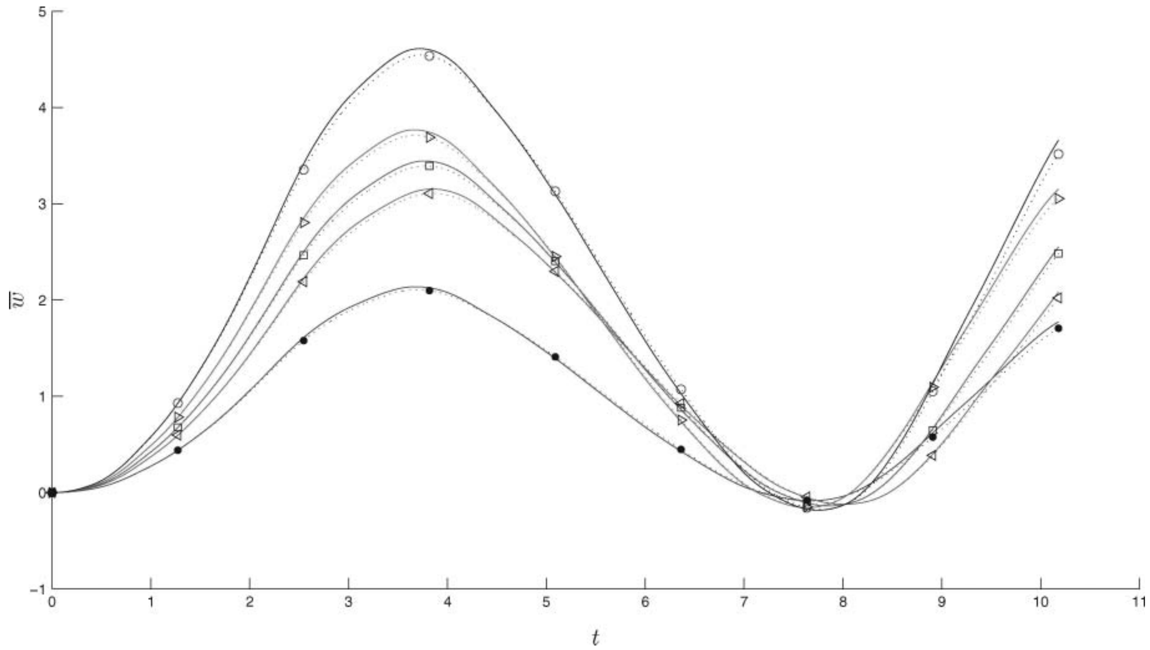

FIG. 11. Present and analytical solutions for central deformation $\bar{w}_{xy}$ of an FGM rectangular shell, uniform force, $c = \sqrt{n+1}/2$. Legend: — analytical solution (p = 0, 1, 2, 5, ∞); $\bullet$ present, p = 0 (ceramic); $\triangleleft$ present, p = 1; $\square$ present, p = 2; $\triangleright$ present, p = 5; $\circ$ present, p = ∞ (metal).

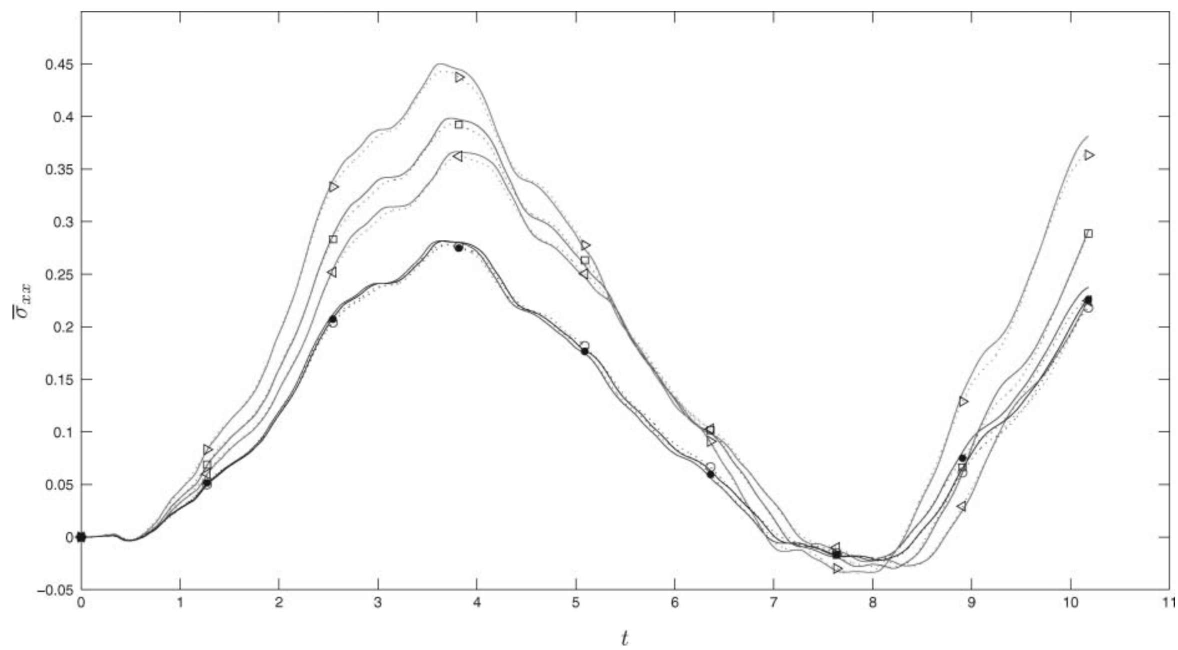

FIG. 12. Present and analytical solutions for in-planeshear stress $\bar{\sigma}_{xx}$ of an FGM rectangular shell, uniform force, $c = \sqrt{n+1}/2$. Legend: – analytical solution (p = 0, 1, 2, 5, ∞); $\bullet$ present, p = 0 (ceramic); $\triangleleft$ present, p = 1; $\square$ present, p = 2; $\triangleright$ present, p = 5; $\circ$ present, p = ∞ (metal).

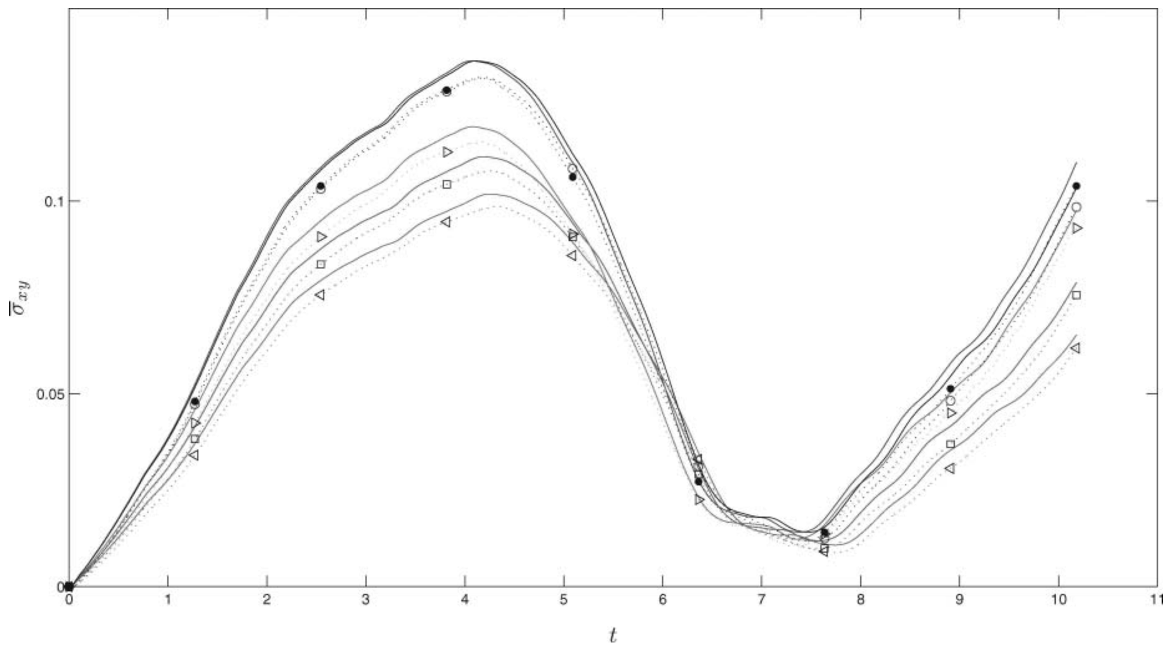

FIG. 13. Present and analytical solutions for in-planeshear stress $\bar{\sigma}_{xy}$ of an FGM rectangular shell, uniform force, $c = \sqrt{n+1}/2$. Legend: – analytical solution (p = 0, 1, 2, 5, ∞); • present, p = 0 (ceramic); ◁ present, p = 1; □ present, p = 2; ▷ present, p = 5; ○ present, p = ∞ (metal).

TABLE 1
Present numerical solution for central deformation $\bar{w}$ of an FGM rectangular shell, sinusoidal force, $c = \sqrt{n+1}/2$

	$\bar{w}$									
	p = 0		p = 1		p = 2		p = 5		p = ∞	
t	rbf	analytical	rbf	analytical	rbf	analytical	rbf	analytical	rbf	analytical
0.51	0.0597	0.0597	0.0811	0.0809	0.0920	0.0917	0.1062	0.1059	0.1259	0.1259
1.02	0.2276	0.2276	0.3104	0.3092	0.3515	0.3500	0.4048	0.4035	0.4808	0.4807
1.53	0.4740	0.4736	0.6505	0.6479	0.7345	0.7312	0.8424	0.8393	1.0030	1.0022
2.04	0.7546	0.7534	1.0451	1.0405	1.1754	1.1697	1.3396	1.3342	1.6009	1.5984
2.54	1.0194	1.0163	1.4294	1.4219	1.5987	1.5898	1.8069	1.7980	2.1701	2.1637
3.05	1.2216	1.2153	1.7407	1.7296	1.9328	1.9202	2.1607	2.1475	2.6120	2.5990
3.56	1.3247	1.3141	1.9275	1.9119	2.1203	2.1032	2.3367	2.3183	2.8491	2.8271
4.07	1.3107	1.2952	1.9596	1.9394	2.1297	2.1082	2.3038	2.2802	2.8404	2.8080
4.58	1.1819	1.1619	1.8314	1.8070	1.9591	1.9339	2.0675	2.0398	2.5874	2.5451
5.09	0.9611	0.9382	1.5638	1.5367	1.6373	1.6102	1.6702	1.6407	2.1334	2.0845
5.60	0.6878	0.6646	1.2010	1.1737	1.2195	1.1933	1.1837	1.1556	1.5583	1.5080
6.11	0.4108	0.3903	0.8021	0.7773	0.7767	0.7539	0.6955	0.6719	0.9622	0.9167
6.62	0.1795	0.1647	0.4335	0.4140	0.3851	0.3682	0.2941	0.2779	0.4495	0.4153
7.13	0.0355	0.0287	0.1553	0.1431	0.1112	0.1019	0.0516	0.0447	0.1098	0.0921
7.63	0.0041	0.0065	0.0135	0.0100	0.0020	0.0010	0.0117	0.0146	0.0021	0.0039

TABLE 2
Present numerical solution for central deformation $\bar{\sigma}_{xx}$ of an FGM rectangular shell, sinusoidal force, $c = \sqrt{n+1}/2$

	$\bar{\sigma}_{xx}$									
	p = 0		p = 1		p = 2		p = 5		p = ∞	
t	rbf	analytical	rbf	analytical	rbf	analytical	rbf	analytical	rbf	analytical
0.51	0.0085	0.0085	0.0105	0.0107	0.0118	0.0121	0.0139	0.0143	0.0084	0.0084
1.02	0.0299	0.0299	0.0360	0.0359	0.0405	0.0404	0.0481	0.0480	0.0293	0.0293
1.53	0.0619	0.0619	0.0753	0.0750	0.0844	0.0842	0.0999	0.0996	0.0608	0.0608
2.04	0.0990	0.0989	0.1210	0.1206	0.1352	0.1347	0.1590	0.1585	0.0973	0.0972
2.54	0.1326	0.1323	0.1641	0.1631	0.1824	0.1812	0.2127	0.2114	0.1308	0.1305
3.05	0.1596	0.1589	0.2010	0.2000	0.2219	0.2206	0.2559	0.2545	0.1582	0.1576
3.56	0.1727	0.1714	0.2213	0.2194	0.2420	0.2398	0.2753	0.2729	0.1720	0.1708
4.07	0.1706	0.1688	0.2257	0.2235	0.2438	0.2414	0.2721	0.2692	0.1715	0.1697
4.58	0.1546	0.1521	0.2110	0.2081	0.2244	0.2214	0.2446	0.2413	0.1568	0.1543
5.09	0.1250	0.1221	0.1797	0.1765	0.1870	0.1837	0.1967	0.1931	0.1286	0.1258
5.60	0.0901	0.0872	0.1391	0.1362	0.1405	0.1377	0.1409	0.1379	0.0948	0.0918
6.11	0.0539	0.0512	0.0921	0.0892	0.0886	0.0859	0.0820	0.0792	0.0583	0.0555
6.62	0.0234	0.0216	0.0508	0.0489	0.0450	0.0435	0.0357	0.0341	0.0274	0.0254
7.13	0.0055	0.0046	0.0183	0.0170	0.0133	0.0123	0.0070	0.0064	0.0074	0.0063
7.63	0.0006	0.0009	0.0020	0.0017	0.0006	0.0007	0.0016	0.0020	0.0001	0.0002

TABLE 3
Present numerical solution for central deformation $\bar{\sigma}_{xy}$ of an FGM rectangular shell, sinusoidal force, $c = \sqrt{n+1}/2$

	$\bar{\sigma}_{xy}$									
	p = 0		p = 1		p = 2		p = 5		p = ∞	
t	rbf	analytical	rbf	analytical	rbf	analytical	rbf	analytical	rbf	analytical
0.51	0.0031	0.0031	0.0021	0.0021	0.0024	0.0024	0.0027	0.0027	0.0030	0.0031
1.02	0.0129	0.0129	0.0089	0.0089	0.0101	0.0101	0.0113	0.0113	0.0126	0.0127
1.53	0.0269	0.0270	0.0186	0.0186	0.0211	0.0210	0.0237	0.0237	0.0264	0.0265
2.04	0.0428	0.0429	0.0300	0.0299	0.0338	0.0337	0.0376	0.0376	0.0421	0.0422
2.54	0.0583	0.0582	0.0412	0.0411	0.0462	0.0461	0.0511	0.0510	0.0575	0.0574
3.05	0.0696	0.0693	0.0500	0.0498	0.0557	0.0553	0.0609	0.0606	0.0690	0.0687
3.56	0.0756	0.0751	0.0556	0.0552	0.0613	0.0609	0.0660	0.0657	0.0754	0.0750
4.07	0.0749	0.0741	0.0564	0.0559	0.0614	0.0609	0.0650	0.0645	0.0752	0.0744
4.58	0.0673	0.0663	0.0527	0.0521	0.0565	0.0559	0.0582	0.0576	0.0683	0.0673
5.09	0.0549	0.0537	0.0451	0.0444	0.0472	0.0466	0.0472	0.0465	0.0565	0.0553
5.60	0.0391	0.0378	0.0344	0.0337	0.0350	0.0343	0.0332	0.0325	0.0410	0.0398
6.11	0.0233	0.0222	0.0231	0.0225	0.0224	0.0218	0.0196	0.0190	0.0254	0.0242
6.62	0.0102	0.0094	0.0123	0.0117	0.0109	0.0104	0.0081	0.0077	0.0118	0.0109
7.13	0.0017	0.0013	0.0044	0.0040	0.0031	0.0028	0.0013	0.0011	0.0026	0.0022
7.63	0.0001	0.0003	0.0003	0.0002	−0.0001	−0.0001	0.0002	0.0003	0.0000	0.0001

TABLE 4
Present numerical solution for central deformation $\bar{w}$ of an FGM rectangular shell, uniform force, $c = \sqrt{n+1}/2$

	$\bar{w}$									
	p = 0		p = 1		p = 2		p = 5		p = ∞	
t	rbf	analytical	rbf	analytical	rbf	analytical	rbf	analytical	rbf	analytical
0.51	0.0619	0.0616	0.0833	0.0827	0.0950	0.0942	0.1104	0.1097	0.1303	0.1297
1.02	0.2829	0.2844	0.3836	0.3858	0.4358	0.4375	0.5041	0.5053	0.5968	0.6006
1.53	0.6260	0.6288	0.8524	0.8519	0.9666	0.9663	1.1153	1.1172	1.3220	1.3274
2.04	1.0829	1.0959	1.4757	1.4862	1.6737	1.6857	1.9301	1.9474	2.2878	2.3146
2.54	1.5784	1.6082	2.1911	2.2225	2.4649	2.5009	2.8041	2.8501	3.3526	3.4147
3.05	1.9132	1.9442	2.7251	2.7706	3.0279	3.0754	3.3870	3.4375	4.0913	4.1593
3.56	2.0961	2.1287	3.0402	3.0826	3.3510	3.3987	3.6982	3.7545	4.5059	4.5763
4.07	2.0258	2.0474	3.0702	3.1126	3.3176	3.3634	3.5517	3.5964	4.4092	4.4597
4.58	1.7524	1.7506	2.7428	2.7564	2.9172	2.9300	3.0627	3.0704	3.8436	3.8444
5.09	1.4089	1.3941	2.2979	2.2875	2.4045	2.3942	2.4524	2.4412	3.1296	3.0966
5.60	1.0111	0.9919	1.7541	1.7396	1.7865	1.7742	1.7483	1.7323	2.2848	2.2458
6.11	0.6253	0.6023	1.1922	1.1714	1.1682	1.1480	1.0669	1.0437	1.4540	1.4039
6.62	0.2832	0.2673	0.6763	0.6577	0.6070	0.5951	0.4614	0.4500	0.7097	0.6752
7.13	0.0244	0.0145	0.2296	0.2177	0.1412	0.1307	0.0151	0.0059	0.1165	0.0903
7.63	−0.0797	−0.0847	−0.0459	−0.0524	−0.1003	−0.1069	−0.1484	−0.1569	−0.1575	−0.1723
8.14	0.0100	0.0184	−0.1098	−0.1119	−0.0814	−0.0857	0.0539	0.0554	−0.0525	−0.0440
8.65	0.3523	0.3781	0.1349	0.1409	0.3255	0.3327	0.6955	0.7163	0.5909	0.6376
9.16	0.8044	0.8587	0.6890	0.7159	1.0039	1.0442	1.4999	1.5685	1.5390	1.6495
9.67	1.2837	1.3410	1.3371	1.3965	1.7370	1.7932	2.3496	2.4180	2.5466	2.6682
10.18	1.7057	1.7736	2.0223	2.0818	2.4833	2.5512	3.0538	3.1522	3.5161	3.6598

TABLE 5
Present numerical solution for central deformation $\bar{\sigma}_{xx}$ of an FGM rectangular shell, uniform force, $c = \sqrt{n+1}/2$

	$\bar{\sigma}_{xx}$									
	p = 0		p = 1		p = 2		p = 5		p = ∞	
t	rbf	analytical	rbf	analytical	rbf	analytical	rbf	analytical	rbf	analytical
0.51	−0.0023	−0.0032	−0.0029	−0.0036	−0.0029	−0.0034	−0.0030	−0.0036	−0.0024	−0.0033
1.02	0.0289	0.0286	0.0334	0.0340	0.0383	0.0386	0.0467	0.0464	0.0280	0.0280
1.53	0.0701	0.0701	0.0860	0.0854	0.0961	0.0959	0.1131	0.1133	0.0691	0.0690
2.04	0.1250	0.1241	0.1467	0.1464	0.1674	0.1663	0.2029	0.2011	0.1217	0.1211
2.54	0.2072	0.2118	0.2519	0.2545	0.2832	0.2867	0.3332	0.3392	0.2040	0.2083
3.05	0.2393	0.2412	0.3057	0.3126	0.3362	0.3417	0.3846	0.3877	0.2388	0.2412
3.56	0.2743	0.2800	0.3414	0.3422	0.3793	0.3818	0.4386	0.4459	0.2717	0.2772
4.07	0.2590	0.2631	0.3548	0.3612	0.3790	0.3858	0.4103	0.4176	0.2644	0.2689
4.58	0.2130	0.2116	0.2884	0.2863	0.3055	0.3035	0.3374	0.3358	0.2144	0.2139
5.09	0.1765	0.1745	0.2504	0.2471	0.2632	0.2585	0.2776	0.2738	0.1818	0.1778
5.60	0.1196	0.1169	0.1847	0.1829	0.1838	0.1822	0.1879	0.1852	0.1241	0.1222
6.11	0.0783	0.0746	0.1225	0.1192	0.1222	0.1162	0.1214	0.1157	0.0821	0.0772
6.62	0.0340	0.0326	0.0791	0.0761	0.0683	0.0683	0.0493	0.0512	0.0406	0.0401
7.13	−0.0051	−0.0058	0.0168	0.0173	0.0025	−0.0006	−0.0113	−0.0138	−0.0026	−0.0056
7.63	−0.0169	−0.0187	−0.0100	−0.0130	−0.0171	−0.0189	−0.0299	−0.0321	−0.0152	−0.0177
8.14	−0.0188	−0.0179	−0.0237	−0.0219	−0.0285	−0.0284	−0.0247	−0.0246	−0.0201	−0.0208
8.65	0.0384	0.0375	−0.0088	−0.0110	0.0176	0.0153	0.0714	0.0668	0.0244	0.0232
9.16	0.0967	0.1064	0.0755	0.0758	0.1152	0.1202	0.1647	0.1788	0.0905	0.0996
9.67	0.1592	0.1634	0.1385	0.1479	0.1795	0.1846	0.2679	0.2686	0.1429	0.1473
10.18	0.2259	0.2375	0.2247	0.2261	0.2886	0.2917	0.3634	0.3813	0.2181	0.2277

Values of material properties are listed below:

$$E_1 = 70\,\text{GPa},\ \nu_1 = 0.3;\ \rho_1 = 2702$$
$$E_2 = 151\,\text{GPa},\ \nu_2 = 0.3;\ \rho_2 = 5700$$
$$q_0 = 1\times 10^6;\ a = 1;$$

The time, central deflection and stress are normalized by:

$$t = t\sqrt{\frac{E_1}{\rho_1 b^2}}$$
$$\bar{w}(a/2, b/2) = w\frac{E_1 h}{q_0 b^2};$$
$$\bar{\sigma}_{xx}(a/2, b/2, h/2) = \sigma_{xx}\frac{h^2}{q_0 b^2};$$
$$\bar{\sigma}_{xy}(a, b, -h/2) = \sigma_{xy}\frac{h^2}{q_0 b^2};$$

Figures 2, 3, and 4 show the transverse central displacement $\bar{w}$, in-plane stress $\bar{\sigma}_{xx}$ and shear in-plane stress $\bar{\sigma}_{xy}$ for a square plate, under suddenly applied uniform load. Results are in good agreement with analytical solutions. The shape parameter is $c = \sqrt{n+1}/2$. From the three computed quantities, the in-plane shear stress $\bar{\sigma}_{xy}$ is the one that presents a larger difference to analytical solutions. This occurs in all examples in this paper.

In Figures 5, 6, and 7 the transient analysis of a rectangular plate under suddenly applied uniform load is presented. The use of an anisotropic radial basis function allowed to maintain the same shape parameter regardless of the geometry of the plate.

A rectangular shell ($b = 2a$) under suddenly applied sinusoidal force is considered in Figures 8, 9, and 10. Results for a rectangular shell under suddenly applied uniform force is shown in Figures 11, 12, and 13. The same shape parameter ($c = \sqrt{n+1}/2$) is used for the analysis of rectangular shells.

For all examples, numerical and analytical results are in very good agreement as shown in Tables 1–6 for an FGM shell.

Given the ability to analyze irregular geometries, the present method may represent a viable alternative to finite element methods.

8. CONCLUSIONS

A combination of radial basis functions and a pseudospectral method is used to study the transient response of functionally graded plates and shells. A Newmark algorithm is used to

TABLE 6
Present numerical solution for central deformation $\bar{\sigma}_{xy}$ of an FGM rectangular shell, uniform force, $c = \sqrt{n+1}/2$

	$\bar{\sigma}_{xy}$									
	p = 0		p = 1		p = 2		p = 5		p = ∞	
t	rbf	analytical	rbf	analytical	rbf	analytical	rbf	analytical	rbf	analytical
0.51	0.0152	0.0181	0.0110	0.0130	0.0122	0.0144	0.0134	0.0158	0.0150	0.0178
1.02	0.0356	0.0394	0.0255	0.0282	0.0285	0.0315	0.0314	0.0346	0.0351	0.0389
1.53	0.0624	0.0671	0.0443	0.0476	0.0497	0.0533	0.0549	0.0588	0.0616	0.0661
2.04	0.0871	0.0927	0.0623	0.0662	0.0694	0.0738	0.0762	0.0810	0.0860	0.0916
2.54	0.1040	0.1087	0.0757	0.0794	0.0836	0.0876	0.0907	0.0949	0.1032	0.1081
3.05	0.1145	0.1186	0.0839	0.0869	0.0924	0.0957	0.1000	0.1034	0.1138	0.1181
3.56	0.1256	0.1293	0.0916	0.0944	0.1015	0.1045	0.1101	0.1134	0.1250	0.1287
4.07	0.1317	0.1364	0.0970	0.1004	0.1068	0.1108	0.1150	0.1193	0.1314	0.1363
4.58	0.1253	0.1297	0.0964	0.0997	0.1042	0.1080	0.1089	0.1131	0.1265	0.1310
5.09	0.1062	0.1100	0.0859	0.0893	0.0906	0.0943	0.0915	0.0952	0.1084	0.1123
5.60	0.0785	0.0810	0.0692	0.0720	0.0704	0.0733	0.0662	0.0692	0.0822	0.0849
6.11	0.0436	0.0448	0.0462	0.0490	0.0435	0.0464	0.0362	0.0378	0.0485	0.0502
6.62	0.0197	0.0200	0.0210	0.0217	0.0188	0.0191	0.0167	0.0171	0.0212	0.0212
7.13	0.0137	0.0166	0.0129	0.0135	0.0133	0.0148	0.0119	0.0151	0.0148	0.0176
7.63	0.0141	0.0175	0.0091	0.0110	0.0099	0.0120	0.0137	0.0160	0.0125	0.0154
8.14	0.0286	0.0330	0.0148	0.0171	0.0199	0.0230	0.0262	0.0297	0.0261	0.0305
8.65	0.0436	0.0498	0.0253	0.0292	0.0318	0.0366	0.0388	0.0441	0.0412	0.0476
9.16	0.0591	0.0642	0.0359	0.0403	0.0431	0.0479	0.0521	0.0560	0.0560	0.0618
9.67	0.0779	0.0836	0.0470	0.0505	0.0562	0.0606	0.0705	0.0743	0.0731	0.0792
10.18	0.1039	0.1100	0.0619	0.0653	0.0756	0.0789	0.0930	0.0976	0.0985	0.1035

advance the analysis in time. The method is very sensitive to the shape parameter. The use of an anisotropic radial basis function simplified the task of choosing a shape parameter, contributing to the stability of the Newmark method.

REFERENCES

1. J.N. Reddy, Mechanics of Laminated Composite Plates and Shells, CRC Press, 2004.
2. L.N. Trefethen, Spectral Methods in MATLAB, Siam, Philadelphia, PA., 2000.
3. J.N. Reddy, Dynamic (Transient) Analysis of Layered Anisotropic Composite-Material Plates, Int. J. Numer. Meth. Eng. vol. 19, no. 2, pp. 237–255, 1983.
4. Y. Liu, K.M. Liew, Y.C. Hon, et al., Numerical Simulation and Analysis of an Electroactuated Beam Using a Radial Basis Function, Smart Mat. Struct., vol. 14, no. 6, pp. 1163–1171, 2005.
5. R.M. Kirby and Z. Yosibash, Solution of Von-Karman Dynamic Non-Linear Plate Equations Using a Pseudo-Spectral Method, Comput. Method. Appl. M.,vol. 193, no 68, pp. 575–599, 2004.
6. C.M.C. Roque, A.J.M. Ferreira, and R.M.N. Jorge, Free Vibration Analysis of Composite and Sandwich Plates by a Trigonometric Layerwise Deformation Theory and Radial Basis Functions, J. Sandw. Struct. Mater., vol. 8, no. 6, pp. 497–515, 2006.
7. A.J.M. Ferreira, C.M.C. Roque, and R.M.N. Jorge, Natural Frequencies of FSDT Cross-Ply Composite Shells by Multiquadrics, Compos. Struct., vol. 77, no 3, pp. 296–305, 2007.
8. A.J.M. Ferreira, C.M.C. Roque, R.M.N. Jorge, et al., Analysis of Functionally Graded Plates by a Robust Meshless Method, Mech. Ad. Mater. Struct., vol. 14, no 8, pp. 577–587, 2007.
9. M.B. Bever and P.E. Duwez, Gradients in Composite Materials, Mate. Sci. Eng., vol. 10, pp. 1–8, 1972.
10. F.J. Ferrante and L.L. Graham-Brady, Stochastic Simulation of Non-Gaussian/Non-Stationary Properties in a Functionally Graded Plate, Comput. Method. Appl. M., vol. 194, no. 12–16, pp. 1675–1692, 2005.
11. H.M. Yin, L.Z. Sun, and G.H. Paulino, Micromechanics-Based Elastic Model for Functionally Graded Materials with Particle Interactions, Acta Materialia, vol. 52, no. 12, pp. 3535–3543, 2004.
12. Z. Zhong and E. Shang, Closed-form Solutions of Three-Dimensional Functionally Graded Plates, Mech. Adv. Mater. Struc., vol. 15, no 5, pp. 355–363, 2008.
13. T.K. Nguyen, K. Sab, and G. Bonnet, Shear Correction Factors for Functionally Graded Plates, Mech. Adv. Mater. Struc., vol. 14, no. 8, pp. 567–575, 2007.
14. K.-L. Choy and E. Felix, Functionally Graded Diamond-Like Carbon Coatings on Metallic Substrates, Mater. Sci. Eng. A, vol. 278, pp. 162–169, 2000.
15. K.A. Khor and Y.W. Gu, Effects of Residual Stress on the Performance of Plasma Sprayed Functionally Graded zro2/Nicocraly Coatings. Mater, Sci. Eng. A, vol. 277, pp. 64–76, 2000.
16. J. Sladek, V. Sladek, Ch. Zhang, et al., Static and Dynamic Analysis of Shallow Shells with Functionally Graded and Orthotropic Material Properties, Mech. Adv. Mater. Struc, vol. 15, no. 2, pp. 142–156, 2008.
17. G. Casciola, D. Lazzaro, L.B. Montefusco, et al., Shape Preserving Surface Reconstruction Using Locally Anisotropic Radial Basis Function Interpolants, Comput. Math. Appl, vol. 51, no. 8, pp. 1185–1198, 2006.

18. A.J.M. Ferreira and G.E. Fasshauer, Computation of Natural Frequencies of Shear Deformable Beams and Plates by a RBF-Pseudospectral Method, Comput. Method. Appl. M, vol. 196, pp.134–146, 2006.
19. A.J.M. Ferreira, G.E. Fasshauer, R.C. Batra, et al., Static Deformations and Vibrations Analysis of Composite and Sandwich Plates Using a Layer-wise Theory and RBF-ps Discretizations with Optimal Shape Parameters, Compos. Struct, vol. 86, pp. 328–343, 2008.
20. He X.Q. Ng T.Y. Sivashanker S, et al., Active Control of FGM Plates Subjected to a Temperature Gradient: Modelling via Finite Element Method Based on FSDT. Int. J. Numeri. Meth. Eng, vol. 52, no. 11, pp. 1253–1271, 2001.

4

Conclusions and suggestions for future work

4.1 Conclusions

This thesis comprehends a numerical study on the analysis (static, free vibration and buckling) of laminated and functionally graded plates and shells. The numerical study is based on collocation with radial basis functions. In 1.3 the definition of meshless methods was introduced and the need of such methods was justified. Classifications and examples of different meshless methods were given. The global collocation technique with radial basis functions and its combination with pseudospectral method were discussed in detail, as these are the numerical methods for the study of plates and shells used in this thesis.

The global collocation with radial basis functions needs the explicit governing equations for its conversion to algebraic system of equations. In the present thesis the governing equations are automatically derived and implemented in a MATLAB code by the Carrera's Unified Formulation (CUF). The CUF allows the use of any C^0 shear deformation theory, including the through-the-thickness deformation. In this thesis several new theories were implemented using CUF, namely polynomial, sinusoidal, hyperbolic sine and zig-zag theories. The new deformation theories implemented in the present thesis asked for a generalization of the original CUF, by introducing different displacement fields for in-plane and out-of-plane displacements. Carrera's Unified Formulation and its application to the analysis of functionally graded plates and shells was presented in 1.4 focusing on functionally graded structures because studies on the combination of carrera's Unified Formulation and meshless methods were performed for the first time for such structures in this thesis.

The combination of CUF and meshless methods was already performed for laminated plates and shells. In the present thesis the combination of CUF and meshless methods was generalized for FG plates and shells which forces to consider virtual layers. The combination of CUF and RBFs for FG plates and shells proved to still extremely accurate and easily implemented. The present approach was able to capture the exact results that can be found in many literature analytical results.

A novel application of CUF was proposed in this thesis. The explicit governing equations and boundary conditions in terms of displacements of the static, free vibration or buckling problems were obtained using symbolic computation. The combination of CUF and the symbolic calculations performed in MATLAB can be seen as a time-saving and error reducer and was used for the first time in this thesis with this purpose.

Regarding the influence of the through-the-tickness deformation, the work developed and presented in this thesis lead us to the following conclusions: irrespective of the nature of the mechanical problem (bending, free vibration or buckling), there is an influence on the solutions by considering or neglecting the transverse normal deformations σ_{zz}. These effect is more significative in thicker structures. In the case of shells, it seems independent of the curvature radius. In the numerical tests performed, the influence of the warping effects in the mechanical behaviour of FG plates is stronger than the zig-zag effects.

4.2 Suggestions for future work

Although the thesis covered a lot of topic we wished to study, some areas were left for post-doc work.

This thesis deals only with structures with regular geometry. Further studies on structures with arbitrary geometry are to be done in the future.

The use of layerwise approach in CUF is important for FGM sandwich plates and shells.

The analysis of FGM sandwich plates and shells using Reissner-Mixed variational theory (RMVT) can also be an interesting topic to obtain directly the transverse shear stresses at the sandwich interfaces.

The thesis used global collocation only. It would have been interesting to use local collocation schemes, such as the RBF-FD (Finite differences) or the RBF-DQ (differential quadrature) local schemes, wich improves the ill-conditioning of the present global collocation.

Although we have appplied CUF only to static, free vibration and buckling problems, the transient dynamic behaviour of FGM plates and shells is an important structural aspect that can be easily analysed by some step-marching schemes.